BINDING SERVICES
Tel +44 (0)29 2087 4949
Fax.+44 (0)29 2037 1921
E-Mail Bindery@Cardiff.ac.uk

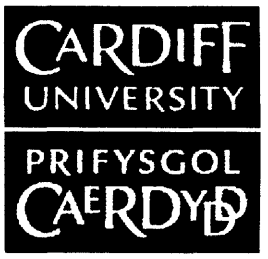

3D SEISMIC ANALYSIS OF SEDIMENTARY PROCESSES ON DEEPWATER CONTINENTAL MARGINS

PÄIVI TUULI HEINIÖ

Cardiff University

July 2007

UMI Number: U585448

All rights reserved

INFORMATION TO ALL USERS
The quality of this reproduction is dependent upon the quality of the copy submitted.

In the unlikely event that the author did not send a complete manuscript
and there are missing pages, these will be noted. Also, if material had to be removed,
a note will indicate the deletion.

UMI U585448
Published by ProQuest LLC 2013. Copyright in the Dissertation held by the Author.
Microform Edition © ProQuest LLC.
All rights reserved. This work is protected against
unauthorized copying under Title 17, United States Code.

ProQuest LLC
789 East Eisenhower Parkway
P.O. Box 1346
Ann Arbor, MI 48106-1346

SUMMARY

Two 3D seismic reflection datasets from the West African and Brazilian continental margins were analysed to determine their architectural elements and to further the understanding of the sedimentary processes that control their morphology. The results suggest a strong influence of local slope variations on the sedimentary processes and depositional and erosional products within these complex deepwater settings.

The Niger Delta dataset is characterised by large channel-levee systems and thrust-related folds. The folds degrade by channel erosion and slope failure, which creates laterally discontinuous erosional surfaces on the crests and flanks of the anticlines and chaotic deposits at their bases. The type of slope failure depends on the length and morphology of the local slope, sediment properties and the presence of anisotropies, such as faults.

The location and morphology of the channel-levee systems on the Niger Delta are affected by topographical effects associated with thrust-related folding. Fold-induced local changes in gradient cause turbidity currents to deposit sediment upstream of the folds and erode the seafloor downstream of them. This results in the formation of knickpoints along the present-day thalweg of a channel-levee system. A model for the formation and evolution of the knickpoints predicts that they migrate upstream and leave internal erosion surfaces and terraces with coarse sediments in the sedimentary record. They may be an important process by which channels cut through uplifting fold belts.

The Espirito Santo Basin dataset is characterised by salt diapirs, slope failures, channels and canyons. Interaction of turbidity currents with variations in topography has led to the formation of large depressions, which occur above abrupt breaks in slope and in trails that follow underlying erosional channels. They are inferred to form by Froude-supercritical currents that become unstable as they encounter topographical irregularities, such as scarps and knickpoints. This leads to the formation of erosional scours and deposits similar to sediment waves, which, when confined within channels, appear as roughly circular depressions.

AUTHOR'S NOTE

Chapters 3, 4 and 5 of the thesis have been published or submitted for publication in different international scientific journals. The status of these publications at the time of the submission of the thesis is as follows:

- Chapter 3 has been published as:

Heiniö, P. and Davies, R.J. 2006. Degradation of compressional fold belts: Deep-water Niger Delta. *AAPG Bulletin* 90(5), 753-770. Doi: 10.1306/11210505090

- Chapter 4 has been published as:

Heiniö, P. and Davies, R.J. 2007. Knickpoint migration in submarine channels in response to fold growth, western Niger Delta. *Marine and Petroleum Geology.* Doi: 10.1016/j.marpetgeo.2006.09.002

- Chapter 5 has been accepted for publication as:

Heiniö, P. and Davies, R.J. Current-generated giant depressions along submarine channels on the continental margin of the Espirito Santo Basin, Brazil. *GSA Bulletin.*

ACKNOWLEDGEMENTS

A much greater number of people than can be mentioned here deserve my thanks for making this PhD project possible, better and more enjoyable. Firstly, I'd like to thank my supervisor Richard Davies for giving me the opportunity to undertake this research. His enthusiasm and constant encouragement helped me in so many aspects of the project. I am grateful for CGGVeritas and Richard Morgan for providing data and Cardiff University, The Finnish Cultural Foundation and Helsingin Sanomat Centennial Foundation for funding. Steve Corfield and Martin Gee are thanked for recommending me for this PhD.

I'd like to thank the reviewers of my papers: Art Saller, Bill Brumbaugh, Jeff Peakall, Mark Deptuck and Russell Wynn and also Neil Mitchell, Dorthe Hansen, Joe Cartwright, and Simon Higgins for improving the quality of the papers. I am grateful for all the feedback and discussions I had with numerous people in Cardiff and at conferences, including Joe, Dorthe, Mads Huuse and David James. I thank David Mohrig and Kyle Straub for introducing turbidity currents and flume tank experiments to me. Gwen Pettigrew, Andrew Wiltshire, Derek John and Neil Ferguson are thanked for sorting out so many computer-related issues. Thanks are also due to Jeff Peakall and Paul Wright who examined this thesis.

Many people have made my life in Cardiff fun and enjoyable and are kindly thanked for this. Catherine Baudon and Simon Higgins deserve special thanks for being such tolerant and lovely officemates and making the office a nice place with good music, inspirational discussions and lots of coffee. I've been really lucky to have such fantastic bunch of people to share my life with in Cardiff. The numerous pints of beer and glasses of wine consumed at pubs, parks and house parties, and the trips to the beach, countryside and Africa in such good company kept me more or less sane during my time here and gave me fond memories. So thank you Cat, Bryan, Wendy, Lizzie, Sarah, Julia, Dave, Alan, Ruth, Mostyn, Cathal, Dan, Anna, Helena, Christian, Rich, Simon, Jess, Rob, Suzy, Marcus, Martin, Katrien, Shanshan, Cat, Mairi, Chloe, Simon S., Aggie and everybody else. I also want to thank friends outside Cardiff for keeping in touch and helping me remember another kind of life out there.

Finally I'd like to thank all my family, especially my parents Ulla and Ari, sisters Laura and Jonna, brother-in-law Paavo, little nephews Okko and Aki and my grandparents, who all have been a great source of motivation, inspiration and support.

TABLE OF CONTENTS

LIST OF FIGURES

Chapter 1. Introduction

Chapter 2. Geological setting and architectural elements of the study areas

Chapter 3. Degradation of compressional fold belts: deepwater Niger Delta

Chapter 4. Knickpoint migration in submarine channels in response to fold growth, western Niger Delta

Chapter 5. Current-generated giant depressions along submarine channels on the continental margin of the Espirito Santo Basin, Brazil

Chapter 6. Discussion

LIST OF TABLES

Chapter 3. Degradation of compressional fold belts: deepwater Niger Delta

Chapter 4. Knickpoint migration in submarine channels in response to fold growth, western Niger Delta

Chapter 5. Current-generated giant depressions along submarine channels on the continental margin of the Espirito Santo Basin, Brazil

Chapter 1

1 INTRODUCTION

This chapter provides the background and the rationale for this thesis. The aims, objectives and scope of this project are given and the thesis layout is explained. This chapter also introduces the 3D seismic method and sedimentary processes in the deepwater setting.

1.1 AIMS AND RATIONALE

This PhD project seeks to understand a range of deepwater sedimentary processes and their products in a novel way through the use of 3D seismic data from the African and Brazilian continental margins. The aim is to improve the understanding of the fundamental processes that control the morphology and the architecture of depositional and erosional features in deepwater settings.

Deepwater and ultra-deepwater (>1.5 km) areas of continental margins are of major scientific interest, because they are one of the least understood sedimentary environments. The analysis of the common architectural elements, and the understanding of the processes controlling these environments, are less advanced compared to subaerial and shallow marine systems, due to previous lack of data coverage and the difficulty of obtaining direct observations. Research of continental margins has also wider implications, because their overall architecture, morphology and the spatial and temporal distribution of sediment deposits provide a record of past changes in relative sea level, climatic and oceanic conditions and tectonic events.

The study of deep-sea sediments started in the early 20th century (see Stow, 1986), and the first channels formed by turbidity currents were discovered in the late 1940s and early 1950s on the continental margins of North America (Menard, 1955). The interest in the deep marine environment has been increasing since. Between the 1960's and 1980's, deepwater depositional systems were studied using outcrops, bathymetric swath and side-scan sonar data and 2D seismic lines (Posamentier and Kolla, 2003). Recently, the interpretation of submarine systems from 3D seismic data has become more common, because these datasets have been made available by the hydrocarbon industry, which is interested in these settings (e.g. Mayall and Stewart, 2000; Abreu et al., 2003; Fonnesu, 2003; Morgan, 2003; Mayall et al., 2006). 3D seismic surveys have proven deepwater fans to have much more complex architecture and internal structures than what was interpreted from 2D surveys (Eschard, 2001). They have

enabled the establishment of the true 3D morphology of depositional elements (Mayall and Stewart, 2000; Abreu et al., 2003; Deptuck et al., 2003; Fonnesu, 2003; Posamentier, 2003; Posamentier and Kolla, 2003; Mayall et al., 2006) and excellent imaging of hydrocarbon reservoir architecture (Mayall and Stewart, 2000; Fonnesu, 2003; Samuel et al., 2003; Mayall et al., 2006). The study of deepwater sedimentary systems and especially turbidite channels has indeed been driven by hydrocarbon industry, and the quantity and quality of 3D seismic datasets have increased while the cost has decreased (Posamentier and Kolla, 2003; Mayall et al., 2006). Despite this increase in data and methods, the deep marine realm is still one of the least well understood depositional environments (Wonham et al., 2000; Eschard, 2001).

This PhD project aims to further the understanding of deepwater sedimentary processes and products from 3D seismic reflection data. The analysis of deposits and erosional features and the inference of what processes led to their development and control their distribution have wider significance for sedimentary basin analysis, including basin modelling, hydrocarbon exploration, fluid dynamics and turbidity current studies.

1.2 OBJECTIVES

This thesis will:

- Depict the architectural elements of confined deepwater channel-levee systems and debris flows on the western Niger Delta.
- Develop a better understanding of some of the processes involved in the formation of sinuous channels and associated features, such as levees.
- Analyse the distribution of depositional and erosional elements relative to structures that create seafloor topography.
- Analyse evidence for sediment remobilisation and recycling in the deepwater setting, especially the degradation of submarine folds.
- Develop a better understanding of the erosional and depositional patterns and processes along continental margins and establish models for their formation.
- Demonstrate how 3D seismic data can be used to understand a range of deepwater sedimentary processes.

1.3 METHODS – 3D SEISMIC INTERPRETATION

The interpretation of the 3D seismic reflection data was done by Unix-run Sun workstations using Schlumberger's Geoframe IESX and GeoViz software. This section gives a brief introduction to 3D seismic data, interpretation and visualisation, and the nature of seismic reflections.

1.3.1 Introduction to 3D seismic method

The 3D seismic method was initiated in the 1960s, but it was not until the 1990s for it to be commonly used by industry and academia (Hart, 1999). 3D seismic data have also increased the understanding of subsurface geology and the controls of local processes and proved many interpretations based on 2D seismic to be wrong (Hart, 1999). Although 2D seismic data commonly have higher resolution than 3D data, 3D seismic data are better for determining the 3D geometry of many features, such as sediment deposits, because of denser seismic grid and 3D, rather than 2D migration process (Hart, 1999; Stewart, 1999; Bacon et al., 2003). The method has significantly enhanced drilling success and thus has been of enormous importance to the petroleum industry.

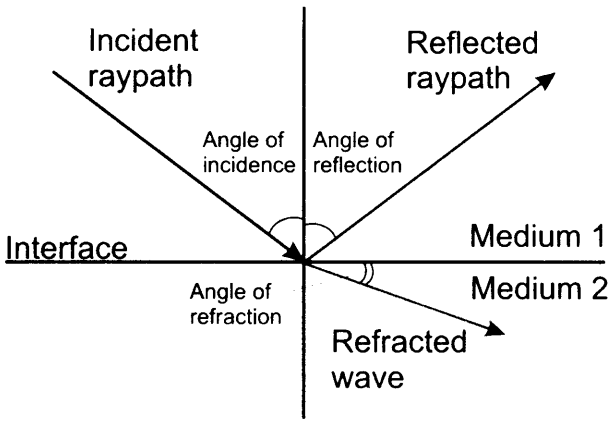

Figure 1.1. The behaviour of a wavefront as it meets an interface of two media with contrasting acoustic impedances. The angle of the incident wave is the same to the reflected wave in an isotropic media. The angle of refraction depends on the seismic velocity of the medium. Modified from Kearey and Brooks (1991).

Marine 3D seismic data are acquired by generating an acoustic pulse near the sea surface, normally by airgun arrays (Hart, 1999; Bacon et al., 2003). Some of the energy is reflected from subsurface interfaces, where there are changes in acoustic velocity and density (Fig. 1.1). This reflected energy is detected by hydrophones. The time a seismic wave takes to travel from the source to the receiver is measured in seconds or milliseconds two-way time (TWT), also sometimes referred to as two-way travel time or twtt. The data have to be

processed and migrated to place all the reflection points in the right location, get rid of unwanted features and increase the quality of the data. A fuller account of seismic acquisition and processing is given in Sheriff and Geldart (1995).

1.3.2 Nature and nomenclature of seismic waves and reflections

Seismic waves are waves of elastic energy that propagate outwards from a seismic source (Kearey and Brooks, 1991). Marine seismic data acquisition is mainly concerned with the detection of compressional P-waves (Kearey and Brooks, 1991; Hart, 1999). The most important parameters of seismic waves are their velocity and frequency. The velocity (v) with which seismic waves travel through rocks vary depending on composition, texture, porosity, fluid content, elastic modulus and the density of the rocks (Kearey and Brooks, 1991). Seismic velocity increases with depth as rocks become more compacted (Brown, 1999). Frequency (f) is defined by the number of peaks passing one point per second (Brown, 1999). It decreases with depth because higher frequencies are attenuated as the waves propagate through rock.

Seismic reflections record changes in the acoustic impedance of the subsurface. Acoustic Impedance (Z) is defined by density (ρ) and seismic velocity (v) of the rocks ($Z=\rho v$) (Kearey and Brooks, 1991; Brown, 1999). As a seismic wave meets an interface of two layers with contrasting acoustic impedance, some of the energy is reflected upwards and some is refracted downwards (Fig. 1.1) (Kearey and Brooks, 1991; Brown, 1999). The changes in acoustic impedance across the interface are recorded as wavelets (Fig. 1.2). The size of a wavelet measured normal to the propagation direction of the wave is given as amplitude. The distance between two peaks is wavelength (λ) (Fig. 1.2), and is proportional to velocity and frequency of the wave ($\lambda=v/f$) (Brown, 1999). The greater the difference between acoustic impedances of two layers, the greater proportion of energy is transmitted through the interface (Kearey and Brooks, 1991). Furthermore, if a geologically significant interface does not have a difference in acoustic impedance, it will not be visible on seismic data (Bacon et al., 2003).

An increase in the acoustic impedance downwards is referred to as a positive amplitude or 'peak' and a decrease is referred to as a negative amplitude or a 'trough'. This is called the 'SEG (Society of Exploration Geologists) normal polarity' (Sheriff and Geldart, 1995). Some

data are displayed as 'SEG reverse polarity', which shows negative values for increases in acoustic impedance. Peaks and troughs are normally displayed in different colours (Fig. 1.2).

The motion of periodic waves is described by phase. Seismic surveys can be of maximum, minimum or zero phase. Most surveys are zero phase, which means that the wavelet is symmetrical, with the majority of the energy being concentrated in the central lobe which also coincides with the interface (Brown, 1999) (Fig. 1.2).

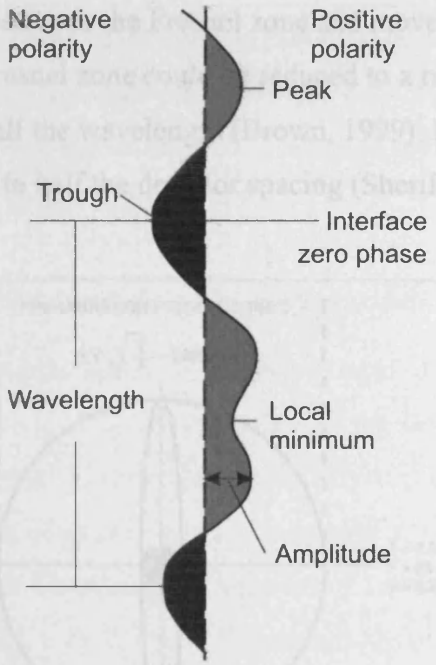

Figure 1.2. Nomenclature of a seismic wavelet of SEG normal polarity zero phase data, in which positive amplitudes (peaks) are displayed in red and negative amplitudes (troughs) in black. Amplitude is the size of the wavelet, and wavelength measures the distance from crest to crest.

1.3.3 Resolution

Vertical resolution defines the potential for the seismic data to distinguish individual layers. It is measured in terms of wavelength. As frequency decreases with depth, vertical resolution deteriorates. A typical wavelength in the shallow part of the seismic data (top 1-2 seconds TWT below seafloor) is approximately 40 m (for a velocity of 2000 ms^{-1} and frequency of 50 Hz) and approximately 250 m in deep section (velocity of 5000 ms^{-1} and frequency of 20 Hz) (Brown, 1999). Maximum resolution of a wavelet in terms of a quarter of a wavelength would thus be approximately 10 m and 63 m respectively. When layer thickness is one quarter of the wavelength, constructive interference called tuning occurs (Sheriff and Geldart, 1995; Brown, 1999). This means that amplitude can be boosted as the bed thins. As beds become thinner,

they get attenuated until invisible. However, even beds with a thickness of $\lambda/30$ can be detected, but their thicknesses cannot be determined (Sheriff and Geldart, 1995).

Horizontal resolution is more complex to quantify. Seismic waves travel in three dimensions from their source and thus the seismic reflection comes from an area rather than a point. This area defining the horizontal resolution is called the Fresnel zone and it is a function of velocity and frequency of the wave and the TWT to the reflector (Fig. 1.3) (Sheriff and Geldart, 1995; Brown, 1999). The migration process improves horizontal resolution by concentrating the energy spread over the Fresnel zone and moves reflections to their right position. Theoretically, the Fresnel zone could be reduced to a radius of quarter wavelength, but in reality this is only to half the wavelength (Brown, 1999). For a flat-lying reflector the horizontal resolution is equal to half the detector spacing (Sheriff and Geldart, 1995).

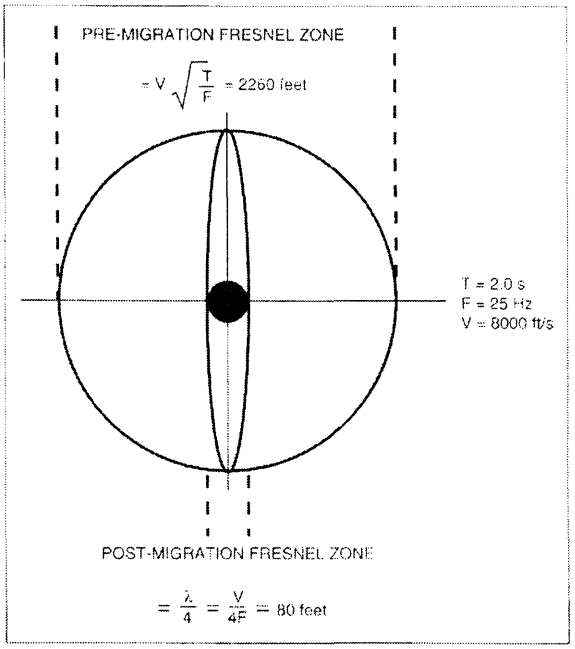

Figure 1.3. The Fresnel zone defines the area from which a reflection is received. The large circle represents the Fresnel zone before migration, the oval is the Fresnel zone after 2D migration. Ideally, Fresnel zone could be reduced to the radius of 1/4 of the wavelength, represented by the black dot in the middle. From Brown (1999).

The issue of resolution is illustrated by Abreu et al. (2003), who compared conventional resolution (35 Hz) seismic data with high-resolution (65 Hz) seismic data, and observed that evidence for lateral migration of a deepwater channel can only be seen in the high-resolution data.

1.3.4 Artefacts and pitfalls

Seismic energy can, and commonly is, reflected more than once from strong reflectors (Brown, 1999). This positions reflections in a false location and causes 'multiples', however, they can normally be removed by seismic processing (Kearey and Brooks, 1991).

Velocity anomalies are caused by lateral variations in lithology or fluid content. For example, a high-velocity channel-fill can cause the underlying reflections to be pulled up causing apparent but non-existing anticlinal fold (velocity pull-up) (Brown, 1999). Velocity push-down can occur below low velocity zones and gas accumulations. The seismic interpreter needs to be aware of this phenomenon, as well as other issues, such as the problem of interpreting onlapping and toplapping reflections. Truncated reflections may seem to continue as the reflections that truncate them (Brown, 1999).

1.3.5 3D seismic interpretation and visualisation approach

The purpose of 3D seismic visualisation is to produce images of numerical data to aid in the interpretation and communication of the interpretation of the data (Hart, 1999). The objectives are to define subsurface stratigraphy, structure and the physical properties of rocks.
3D seismic data can be thought of as consisting of bins with x, y and z dimensions which represent a single seismic trace. These units of volume are called voxels and they have an individual amplitude value (Fig. 1.4). X and y dimensions are measured in metres and z in milliseconds (Bacon et al., 2003).

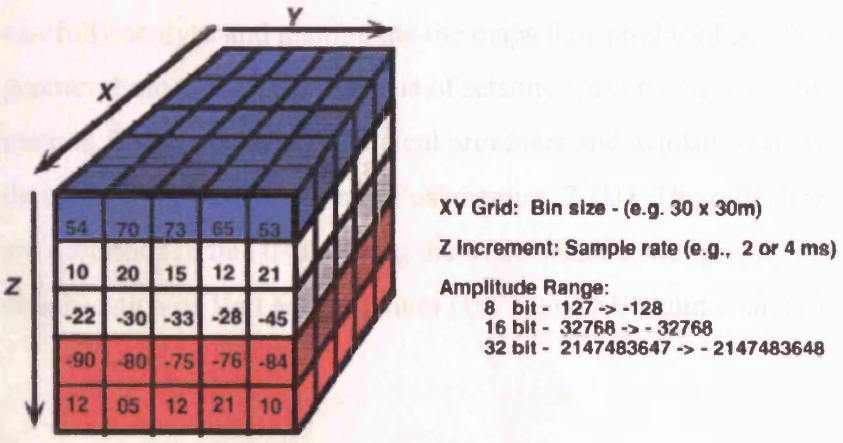

Figure 1.4. Diagram representing 3D seismic data volume from Hart (1999). Each voxel is characterised by x, y and z coordinates and an amplitude value. The x and y values represent the bin size and the z value is the sampling interval, determined by acquisition parameters. The colours given to the negative and positive amplitude values are determined by the interpreter.

3D seismic data can be manipulated in many ways. Only the approach and methods used in this project are outlined here. The line of section to be viewed can be chosen as inlines (vertical section in the direction of data acquisition), crosslines or arbitrary lines (traverse) through the data. Horizontal sections, or timeslices (xy in Fig. 1.4), can also be viewed. They show the stratigraphy intersection on a plane of constant two-way time. Slicing of the data can also be made along arbitrary planes and interpreted horizons. Volumes of data and interpreted horizons can also be viewed in 3D space.

3D seismic interpretation involves horizon picking, which produces a structure map, or a horizon that can be converted to true depth if velocity data is available. An attribute is a derivate of a seismic measurement, such as time, amplitude, frequency and azimuth. Attribute maps provide structural and stratigraphic information that is not so obvious on other means of interpretation (Brown, 1999). The most commonly used attributes in this thesis are dip magnitude and seismic amplitude. Dip magnitude measures the local dip of the horizon surface. It compares time values of voxels with their neighbours and forms a plane between these values to illustrate the attribute dip. Dip maps can reveal very subtle features (even sub-sampling resolution), such as faults and flexures. Seismic amplitude shows the amplitude value at a horizon or two-way time. Amplitude extractions can also be made within an assigned window of time or with reference to interpreted horizons within the data. They are useful when studying subtle stratigraphic features that have anomalous amplitude values, such as channels.

The technique used to carry out this research is to map seismic reflections of interest and carefully analyse and manipulate the maps thus produced and to combine seismic geomorphology with the analysis of seismic sections. Seismic geomorphology is a fairly new method for determining geological processes and depositional systems from plan view images derived from 3D seismic data (Posamentier, 2003). The reflection patterns and characteristics are described in this thesis using the basic seismic stratigraphy nomenclature and classification of Vail and Mitchum (1977) and Mitchum et al. (1977) where applicable.

1.4 SEDIMENTARY PROCESSES IN CONTINENTAL MARGINS

1.4.1 Deepwater sedimentary processes

1.4.1.1 The nature of passive continental margins and their sedimentary processes

Continental margins cover large areas of the Earth and include shelf, slope, rise and abyssal plain (Fig. 1.5). Shelves dip typically at gradients of approximately 0.5°, and the slope and rise commonly have gradients around 1-10° (Stow, 1986). Continental margins can have very variable geometries, affected by many factors, such as regional tectonics, climate, relative sea levels and different depositional environments. For example, mud-dominated margins generally have lower slope angles (Reading and Richards, 1994; Adams and Schlager, 2000). Slope systems are classified into 12 classes based on grain size and sediment feeder system and the nature and controls of each type are discussed thoroughly in Reading and Richards (1994).

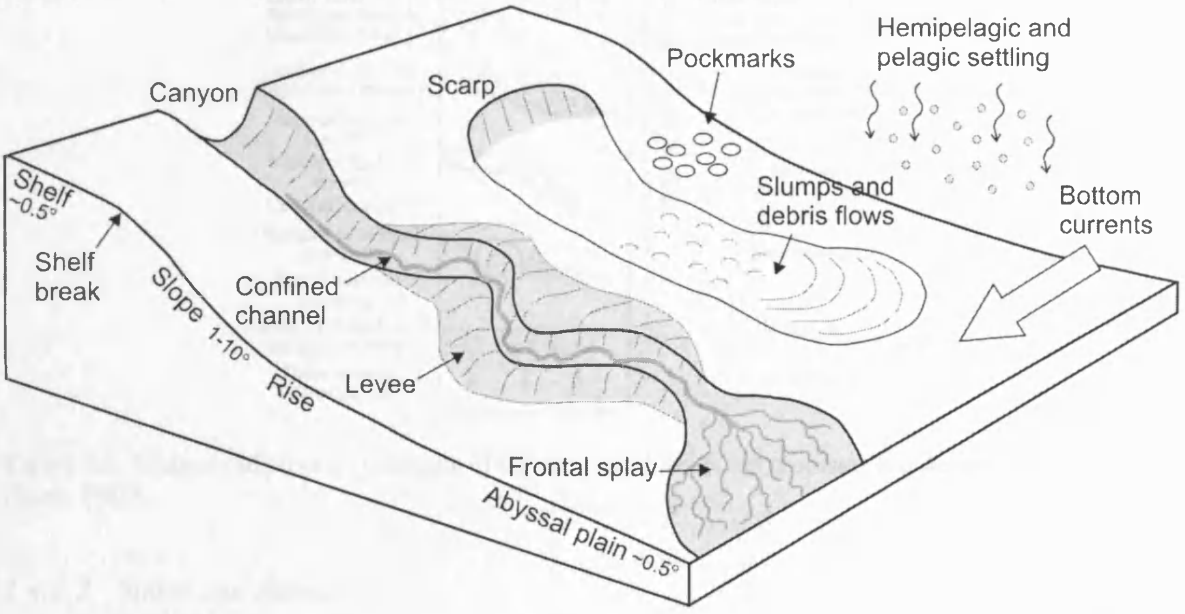

Figure 1.5. A schematic of a passive continental margin and the main sedimentary processes and architectural elements that occur along it and are of interest to this research. Not to scale.

Continental margins are important sites of clastic sediment transport from continents into deep water. Clastic material can be transported over hundreds of kilometres even where the gradient is very low (Eschard, 2001). Downslope processes that deliver sediment into deep water are varied and complex (Stow and Mayall, 2000), and many classification schemes exist (e.g. Mulder and Cochonat, 1996; Locat, 2001). Stow (1986) classifies deepwater processes according to the mechanical behaviour of flow, transport mechanism and sediment

support system. They form a continuum of behaviour from elastic to plastic to viscous fluid and settling (Fig. 1.6). All processes driven by gravitational forces that move sediment to deep water are called 'resedimentation processes'. These, together with normal bottom currents and pelagic and hemipelagic settling, are the main processes capable of transporting and depositing sediment in the deep sea (Stow, 1986). The processes important in this thesis are described briefly below.

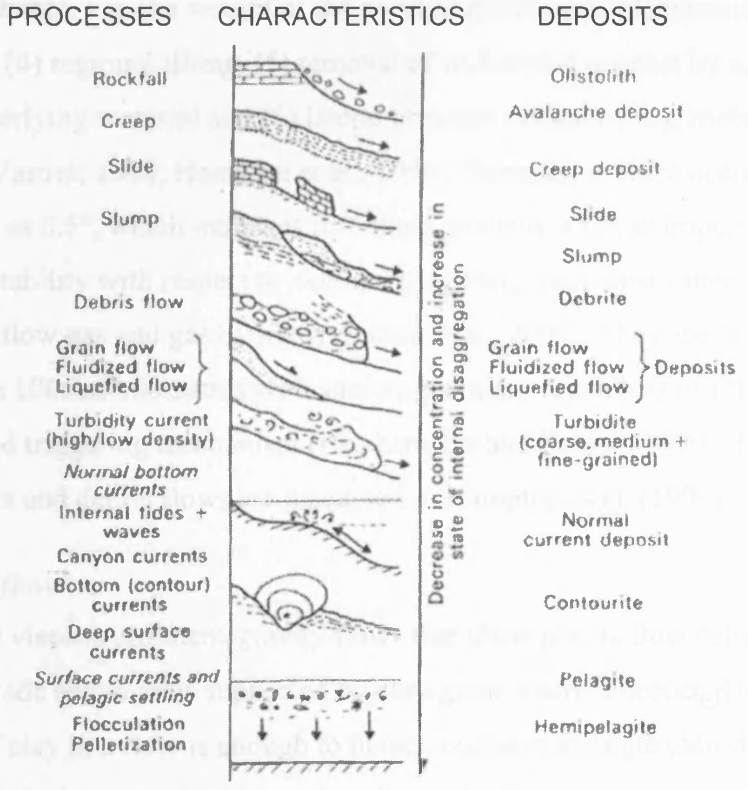

Figure 1.6. Summary of process continuum of the main resedimentation processes and deposits in the deep sea (Stow, 1986).

1.4.1.2 Slides and slumps

Slides and slumps are defined as semi-consolidated, internally coherent sediment masses that are displaced along a basal shear plane (Stow, 1986). A slide can be described as a shear strain with movement along one or several planar surfaces, whereas a slump is a rotational, commonly spoon-shaped slide (Varnes, 1978). A typical slump deposit has (1) a head with extensional faults, scars and sediment deficiency, (2) a relatively undisturbed body and (3) a toe area characterised by compressional structures such as thrusting and overriding of beds (Varnes, 1978; Stow, 1986). They can disintegrate into debris flows and turbidity currents. The transition from a slide to a debris flow to a turbidity current has been observed in nature,

for example in the Nice airport event in 1979 (Mulder et al., 1997) and in Grand Banks in 1929 (Heezen and Ewing, 1955).

Submarine sediment failure, such as slumping and sliding can be initiated if shear stress exceeds the shear strength of sediment. Shear strength is a function of the cohesion between the grains and the intergranular friction (Stow, 1986). Shear stress can be increased by several means, for example by (1) removal of lateral support by e.g. erosion by channels or previous failures, (2) surcharge, e.g. the weight of the overlying sediment, (3) transitory earth stresses, i.e. earthquakes, (4) regional tilting, (5) removal of underlying support by e.g. losing strength or failure of underlying material and (6) lateral pressure caused by e.g. mobilisation of residual stress (Varnes, 1978; Hampton et al., 1996). Submarine slides occur on slopes with gradients as low as 0.5°, which indicates that slope gradient is not as important a factor in marine slope instability with respect to external triggering mechanism such as fluid flow, earthquakes, shallow gas and gas hydrates (Sultan et al., 2004). They are found at scales of less than 1 cm to 100s of kilometres with similar geometry regardless of lithology, degree of consolidation and triggering mechanism (Hesthammer and Fossen, 1999). The dynamics of submarine failure and debris flows are discussed in Hampton et al. (1996).

1.4.1.3 Debris flows

Debris flows are viscous sediment-gravity flows that show plastic flow behaviour (Stow, 1986). Mixed-grade sediment is supported by clay-grade matrix (Leeder, 1999). A 5 % concentration of clay in a flow is enough to induce cohesive strength (Mulder and Cochonat, 1996). Many debris flows contain so much sediment that the water component is interstitial (Mohrig and Marr, 2003). Unlike turbidity currents, debris flows conserve their density when travelling down slopes (Pratson et al., 2000). The high density and clay content prevent settling of sediment from flows and cause poorly-sorted 'en masse' deposition (Kneller and McCaffrey, 2003). Debris flow deposits commonly exhibit pressure ridges at the toe of the deposit. Longitudinal grooves at the base of the deposits and blocky top surfaces indicate the presence of cohesive blocks transported within the debris flow (Prior et al., 1984).

1.4.1.4 Turbidity currents

Turbidity currents are relatively dilute sediment suspension-driven sediment-gravity flows that occur in subaqueous environment (e.g. Kneller, 1995; Kolla et al., 2001). They transport clastic material over hundreds of kilometres from continents to deep ocean over very low slope gradients (Eschard, 2001; Deptuck et al., 2003; Mohrig and Marr, 2003). Sediment is

kept in suspension by the upward component of fluid turbulence (Stow, 1986; Middleton, 1993; Leeder, 1999; Mohrig and Marr, 2003), however, substantial amounts of sediment can also be transported as bedload (Normark et al., 1993). Turbulence is largely the result of friction at the boundaries of the flow with seafloor and ambient water (Stow, 1986).

Turbidity currents are density stratified (Peakall et al., 2000b), and most consist of a dense laminar bottom flow and a turbulent upper plume, so strictly speaking they are gravity flows (Mulder et al., 1997). The term 'turbidity current' has become a general term applied to many sediment gravity flows, even if they cannot be determined to be turbidity currents, and terms like density current or gravity current should probably be used instead (Kneller and Buckee, 2000). Further classification of subaqueous density flows is given in Mulder and Alexander (2001).

Turbidity currents develop a typical anatomy consisting of a head, neck, body and tail (Fig. 1.7) (Stow, 1986; Kneller and Buckee, 2000). They change their density constantly through erosion, deposition and entrainment (Pratson et al., 2000). Most of the erosion and entrainment of ambient fluid occurs at the head. Billows are formed at the upper boundary behind the head where ambient fluid is mixed with the current (Middleton, 1993; Kneller and Buckee, 2000). The body moves faster than the head, and consequently the height of the head increases (Kneller and Buckee, 2000).

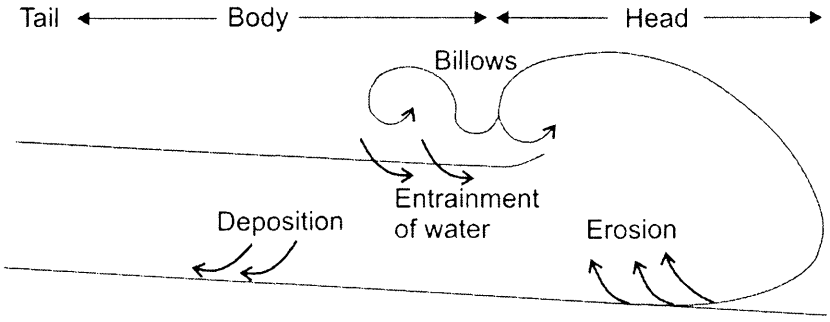

Figure 1.7. The simplified anatomy of a turbidity current. Most erosion occurs at the head and deposition along the body. A mixing vortex of sediment and ambient water occurs at the back of the head causing billows.

Deposition from turbidity currents occurs progressively by settling from a steady or waxing flow (Kneller and McCaffrey, 2003). Turbidity current deposits, i.e. turbidites, can be a few millimetres to 10 m thick and commonly exhibit components of the Bouma sequence or Lowe sequence (e.g. Kneller, 1995). Differences in deposits due to complex flow structures are described in Kneller and McCaffrey (2003) and Kneller (1995).

Deposition and erosion by turbidity currents is controlled by density and velocity of the current (Parker et al., 1986). Currents accelerate as slope gradient increases because of greater effect of gravity on steeper slopes (Parker et al., 1986; Leeder, 1999). As they accelerate, more energy is available for erosion (Parker et al., 1986). Similarly, the currents are likely to deposit as they decelerate (Leeder, 1999). A swift turbidity current can have enough power to erode and incorporate sediment into the flow even without a gradient increase. This increases its density and weight, and as a result the current can accelerate and erode more sediment (Parker et al., 1986). This is called self-acceleration or ignition. Accelerations during transport and deposition affect the character and distribution of turbidite sandstones (Kneller, 1995).

Changes in bottom topography influence erosion and deposition by turbidity currents. Obstacles and changes in slope affect velocity and thus deposition from turbidity currents (Kneller, 1995). The effects of topography depend on the velocity of the current, obstacle height, current density and density stratification (Kneller and Buckee, 2000). Partial blocking of currents causes them to undergo a rapid decrease in both competence and capacity to carry sediment in suspension, and sedimentation is likely to occur as a result (Hiscott, 1994; Kneller and Buckee, 2000).

Turbidity currents are thought to be mainly short-lived surge type flows that last about up to a few tens of hours and do not have a permanent sediment supply (i.e. are often sourced by sediment failures), but where a canyon is connected to a river, quasi-steady flows lasting from hours to months can form (Mulder and Alexander, 2001). Most direct observations of turbidity currents come from cable break data (e.g. Heezen and Ewing, 1955; Krause et al., 1970; Mulder et al., 1997), with suggested velocities of approximately 20-60 km h^{-1}. Direct measurements have been done at least once, however. Khripounoff et al. (2003) measured velocities and turbulence and collected sediment samples before and during a turbidity current on Zaire submarine valley at water depths of 4000 m and also on a levee 13 km away from the channel axis. Although some of their equipment were damaged or broken, they measured a velocity change from a normal 2.8 cm s^{-1} to over 121 cm s^{-1} 150 m above channel. Normal velocity at the base of the channel was 3.4 cm s^{-1}, but the meter broke when the turbidity current hit it. Sediment traps trapped coarse sand and plant debris 40 m above the channel. The current was approximately 400 m thick, but the thickness of the overflow current on the levee was less than 40 m. The duration of the turbidity current was 10 days.

Due to the difficulty in observing and measuring natural turbidity currents and submarine debris flows, most knowledge is gained from interpreting erosional and depositional features from outcrops and subsurface data (Kneller, 2003), and also from laboratory experiments (e.g. Kneller, 1995; Mulder and Cochonat, 1996; Mohrig et al., 1999; Bursik and Woods, 2000; Peakall et al., 2000b; Marr et al., 2002; Mohrig and Marr, 2003) and numerical modelling (e.g. Pratson et al., 2000). These studies give valuable quantitative information of fluid dynamics, characters and the effect of changes in their controlling parameters, such as density, discharge, velocity and structure.

Turbidity currents can be characterised by many dimensioless parameters, most commonly Reynolds, Richardson and Froude numbers (e.g. Kneller and Buckee, 2000). Reynolds number reflects the ratio of inertial to viscous forces acting on a fluid flow. It is the criterion for turbulence in Newtonian fluids and needs to be over 2000 for a fully turbulent flow (Kneller and Buckee, 2000). Turbulence depends on the concentration, velocity and thickness of the flow. Richardson number describes the ability of the current to entrain. Froude number reflects the ratio of inertial to gravitational forces acting on a fluid flow (Kneller and Buckee, 2000). The densimetric Froude number, which is probably most used for describing turbidity currents, is defined by

$$Fr_d = U/(RCgh)^{1/2},$$

in which U is the depth-averaged flow velocity, R is the submerged specific gravity of the sediment, C is the layer-averaged volume of sediment in concentration, g is the gravitational acceleration and h is the flow depth (e.g. Fildani et al., 2006). When $Fr_d > 1$, flows are supercritical and when $Fr_d < 1$, they are subcritical. Supercritical flows are swift, thin and more likely to be capable of eroding seafloor because of higher flow velocities (Nemec, 1990; Kubo and Nakajima, 2002; Fagherazzi and Sun, 2003). Subcritical flows are slow and thick and promote sediment deposition. However, flow regime alone does not determine whether erosion or deposition occurs, but other factors, such as slope gradient and velocity of the currents affect sedimentation rate, too (e.g. Nakajima and Satoh, 2001; Ercilla et al., 2002).

Turbidity currents can be formed from slides, slumps, debris flows (Mulder and Cochonat, 1996; Mohrig and Marr, 2003), but have also been interpreted to be generated by e.g. storms (Parker et al., 1986) and hyperpycnal plumes from river effluent, commonly associated with

flooding events (Leeder, 1999; Kneller and Buckee, 2000; Mulder and Alexander, 2001). However, Khripounoff et al. (2003) observed that although flooding provided the material to the turbidity current, there was no other connection between them, i.e. the timing of flooding did not coincide with the onset of the turbidity current. The dynamic evolution of offshore slope processes and various origins of turbidity currents are discussed in Mulder and Cochonat (1996) and Mulder and Alexander (2001).

1.4.1.5 Bottom currents

Bottom currents are caused by thermohaline circulation and are not gravity-controlled or driven by sediment suspension (Stow, 1986). They are able to erode, transport and deposit sediment on the seafloor and create furrows and construct large elongate sediment drifts and contourites (Stow, 1986).

1.4.1.6 Pelagic and hemipelagic settling

Pelagic sediments are composed of planktonic organisms and related organic matter, whereas hemipelagic sediments are terrigenous elements transported mainly by winds and surface currents (Stow, 1986). Pelagic and hemipelagic sedimentation form commonly drapes because they are settled down through the water column.

1.4.1.7 Other processes

Several other processes that affect the architecture of deepwater environments occur in continental margins. These include structural deformation, for example faulting, folding and mud and salt diapirism, which all are able to create topography and slope instabilities. Diagenesis and compaction can cause overpressure and fluid flow. This can result, for example, in pockmark formation and the development of mud volcanoes, which are common components of continental margins.

1.4.1.8 Controls on continental margin sedimentation

Several factors contribute to the style of sediment transport on continental margins. The main controls are sediment supply, tectonics and sea level fluctuations, but there are also numerous secondary controls (Stow, 1986). These are for example basin size and configuration, slope length and gradient, seafloor rugosity, amount and type of resedimentation, deposition rate, local tectonics, bottom currents and relative sea level variations (Posamentier and Kolla, 2003). The nature of the hinterland affects the source material, and shelf width and the presence of canyons incising the margin affect the ease of sediment bypass into deep water. Slope instability and faulting may lead to resedimentation downslope and processes like salt

CARDIFF UNIVERSITY

tectonics and sub-basin formation may trap sediments and divert flows (Normark et al., 1993; Reading and Richards, 1994; Richards et al., 1998; Eschard, 2001). The nature of sediment supply can also be an important factor in determining the nature of the deposit. Decreasing grain size causes a decrease in the slope gradient and the tendency of channel-levee systems to develop, whereas slumping and meandering increase (Stow and Mayall, 2000).

There is still some controversy in reaching a consensus on models of deepwater processes and deposits. To understand ancient systems, it is important to map the architecture and stacking patterns of the present day examples (Stow and Mayall, 2000). However, modern submarine fans, such as Amazon, Nile and Mississippi, only exhibit processes occurring during relative sea level highstand with low sediment supply rates, which may cause some limitations in applying models derived from recent systems to ancient deepwater basins (Eschard, 2001).

1.5 THE SCOPE AND LAYOUT OF THE THESIS

This thesis contains seven chapters, of which Chapters 2-5 are the main result chapters. Chapters 3-5 are written for publication in scientific journals, which has affected their style and caused some repetition. At the time of submission of this thesis, Chapter 3 has been published, Chapter 4 is in press and Chapter 5 is in review. The specific topics of the chapters were chosen with the intent to produce new, topical and exciting science. Therefore the general architectural elements are not discussed in detail here, but more emphasis is given on rather narrower topics instead.

The work is based on 3D seismic reflection data. No specific lithological or well log data were available from the areas of the 3D seismic surveys, but general information could be gleaned from limited published sources. The main limitations for the work were the data available and limitations within, such as resolution, interpretational uncertainties and errors.

Chapter 2 gives the geological background of the Niger Delta and the Espirito Santo Basin and introduces the two datasets that this research is based on. The chapter focuses on the common deepwater depositional and erosional elements that are found in these datasets. Together with Chapter 1, it provides the context for the Chapters 3-5. Chapter 3 concentrates on the resedimentation phenomena and the degradation of structural highs, namely the toe-of-slope thrust and fold belt folds on the Niger Delta. Chapter 4 focuses on the present day thalweg of a submarine channel-levee system on the Niger Delta, and the formation and

evolution of knickpoints as a result of uplift associated with the thrust and fold belt. Chapter 5 examines peculiar, large depressions that form individually or in trails along underlying erosional channels in the Espirito Santo Basin and that are interpreted to have been formed by erosion and deposition by unstable gravity flows. The key results of the Chapters 2-5 are drawn together in Chapter 6, and selected topics, such as the effects of slope variation to the sedimentary processes are discussed further. The results and shortcomings of this research are discussed in the context of other analytical methods. The conclusions of this PhD project are drawn in Chapter 7.

Chapter 2

2 GEOLOGICAL SETTING AND ARCHITECTURAL ELEMENTS OF THE STUDY AREAS

2.1 INTRODUCTION

This chapter provides the background information on architectural elements that are common on continental margins, concentrating on depositional and erosional features, especially on channels and mass transport complexes. It gives an overview of the geological settings of the Niger Delta and Espirito Santo Basin on both sides of the Atlantic Ocean and describes the different sedimentary elements that characterise the shallow parts of the studied datasets. The datasets differ from each other, as the data from Espirito Santo Basin are located just beneath the shelf break at water depths of 0.5-2 km and the area is dominated by salt diapirs, whereas the data from the Niger Delta have a more distal location at water depths of 2.2-3.4 km, dominated by toe-of-slope thrust and fold belt.

2.1.1 Architectural elements in deepwater settings

Depositional elements are the basic components that are mappable in all scales from field to subsurface studies (Posamentier and Kolla, 2003). Morphological elements in deepwater environments include for example canyons, channels, levees, lobes, mounds, drifts, slumps, debris flows and mass transport complexes (Stow, 1986; Stow and Mayall, 2000; Posamentier and Kolla, 2003; Mayall et al., 2006) (Fig. 2.1). These occur mainly in specific areas within continental margins, for example, shelf edge areas are commonly dominated by large-scale erosional features, such as failures and canyons, slopes are sites for the development of channels and the distal basin is dominated by hemipelagites (Normark et al., 1993).

Much of the previous work on deepwater architectural elements has concentrated on the submarine channels and channel-levee complexes, the architectural complexities of which are described and classified by many authors (e.g. Clark and Pickering, 1996; Galloway, 1998; Deptuck et al., 2003; Posamentier and Kolla, 2003). The terminology is still somewhat confusing, because the study of deep marine sedimentary processes and products is still relatively young. In this thesis, the terminology and classification of Deptuck et al. (2003) is used where applicable. They define a channel-levee system (CLS) as "a single channel-belt, bordered by outer levees" and a channel-levee complex (CLC) as "a series of stacked channel-levee systems that are fed by the same canyon".

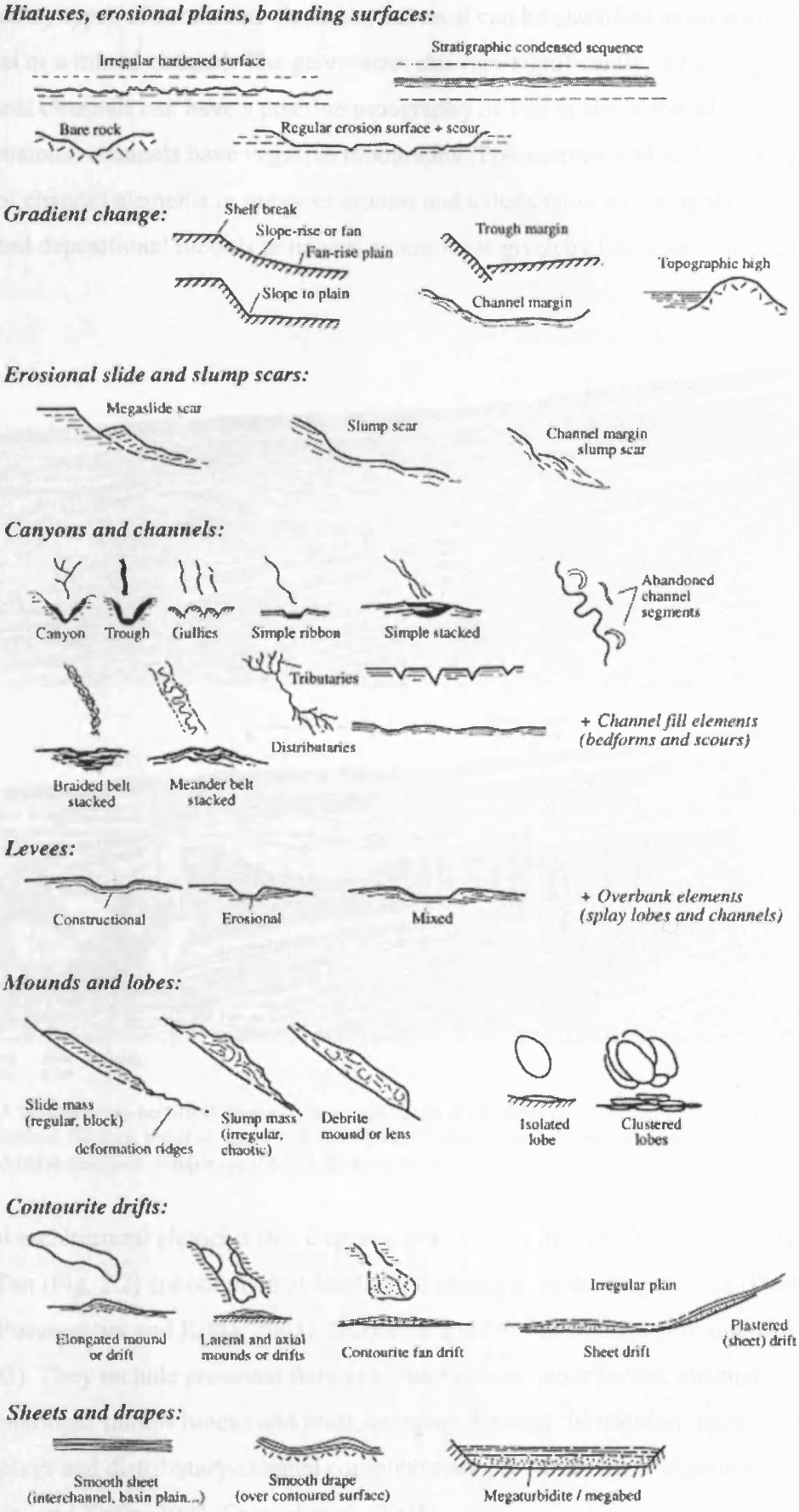

Figure 2.1. The principal architectural elements in deepwater sedimentary systems (Stow and Mayall, 2000).

There are many types of submarine channels, but most can be classified as an erosional, depositional or a mixed channel. The geometries can vary significantly, for example, aggradational channels can have a positive topography of 100 m above the adjacent seafloor, whereas erosional channels have negative topography (Posamentier and Kolla, 2003). A gooc summary of channel elements in previous studies and a discussion on the application of erosional and depositional models to natural examples is given by Clark and Pickering (1996).

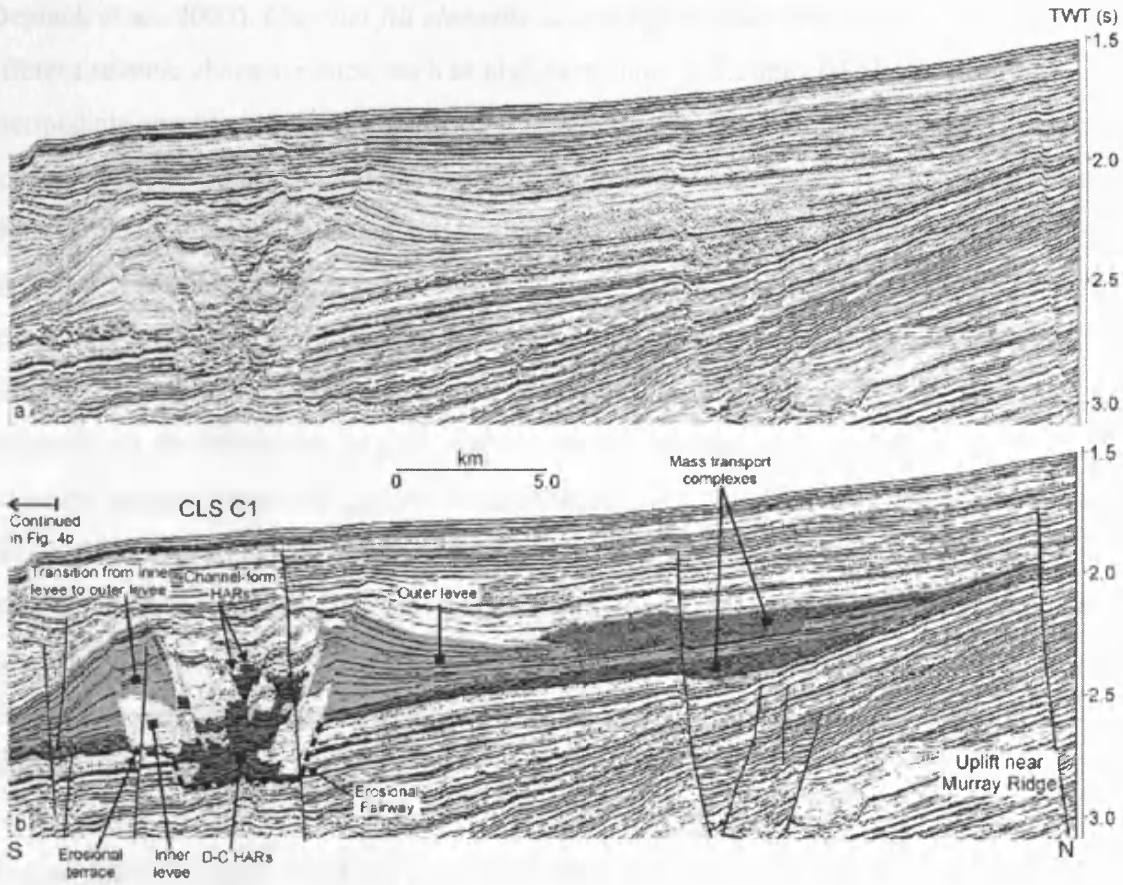

Figure 2.2. A typical cross-sectional geometry and architectural elements of a channel-levee system (CLS) including erosional fairway, terraces, inner and outer levees, channel-axis deposits (channel-form HARs and D-C HARs) and mass transport complexes (MTC) (Deptuck et al, 2003).

The typical architectural elements that Deptuck et al. (2003) defined from seismic data from the Indus Fan (Fig. 2.2) are common at least in the channels on the Niger Delta (Deptuck et al., 2003; Posamentier and Kolla, 2003), Indonesia and Gulf of Mexico (Posamentier and Kolla, 2003). They include erosional fairways, outer levees, inner levees, channel-axis deposits, rotational slumps blocks and mass transport deposits. In addition, frontal splays, crevasse splays and distributary-channel complexes are present in some channels (Posamentier and Kolla, 2003; Samuel et al., 2003).

Following the classification of Deptuck et al. (2003), a channel-levee system (CLS) is characterised by a channel-belt, where channel-axis deposits and inner levees, together with mass transport deposits and slump blocks, are the dominant architectural elements. The channel-belt is bordered by a basal erosional fairway and outer levees of varying thickness (Deptuck et al., 2003).

Erosional fairways are canyon-like incisions that can be up to hundreds of metres deep (Deptuck et al., 2003). *Channel-fill elements* can comprise of several types of deposits with different seismic characteristics, such as high-amplitude reflections (HARs), parallel intermediate amplitude reflections and low-amplitude chaotic reflections. HARs within channel-belts are usually interpreted to be coarse-grained sediments (e.g. Kastens and Shor, 1986; Deptuck et al., 2003; Posamentier and Kolla, 2003). The term channel-axis deposit is used here to distinguish the deposits on the floor of the channel near its axis, disregarding the further division of them into three distinct seismic types according to their width, acoustic character and vertical stacking by Deptuck et al. (2003). Channel-axis deposits are often partly eroded, but the preserved parts commonly show evidence that helps to reveal channel evolution, such as channel migration, which is further described and discussed by Abreu et al. (2003). Parallel, horizontal reflections within the channel-fill that show no evidence for channelisation are referred to as 'passive fill' after Posamentier and Kolla (2003) *or inner levees*, if they form bench-like terraces within the channel-belt (Deptuck et al., 2003). Chaotic low-amplitude seismic facies is often interpreted as debris flow and other mass transport deposits.

Mass transport complex (MTC) is a general term that includes slumps, slides and debris flows. Mass transport deposits are recognised on seismic data by contorted, chaotic low-amplitude reflections. They commonly occur between channel-levee systems (Lopez, 2001; Popescu et al., 2001; Deptuck et al., 2003) and can be up to 150 m thick and tens of kilometres wide (Posamentier and Kolla, 2003). Debris flows have various morphologies, such as sheets, lobes and channels (Posamentier and Kolla, 2003) and form commonly mounds with steep margins (3-4°), but also some of them thin gradually. Individual debris flow deposits can be 80 m thick and reach as far into the basin as turbidites (Posamentier and Kolla, 2003). Erosional scours and long linear grooves at the base of debris flows and irregular top surfaces suggest the presence of large cohesive blocks of sediment within the flow (Prior et al., 1984; Posamentier and Kolla, 2003).

Outer levees are the result of channel overbank deposition and form wedge-shaped cross-sectional geometries (Deptuck et al., 2003). They can be hundreds of metres high and thin away over distances of approximately 10 km. Outer levees are typically an order of magnitude wider than their channels (Posamentier and Kolla, 2003), and commonly interbedded with pelagic sediments and may therefore record changes in global climate (Clark and Pickering, 1996). In highly erosional systems, levees can be completely absent (Posamentier and Kolla, 2003). Levee height decreases down-CLS due to flow stripping and overspill (Peakall et al., 2000b; Posamentier and Kolla, 2003).

Some levees are characterised by sediment waves. They can have a height of 1-70 m, a wavelength of 0.1-6 km and the wave crests can be 60 km long (Wynn et al., 2000b). Sediment waves are orientated roughly perpendicular to the transport direction and they migrate upslope (Wynn et al., 2000b). They occur normally on slopes with a slope <2° (Wynn et al., 2000a).

Frontal splays are the lobe-shaped depositional elements at the termini of channel-levee systems (Posamentier and Kolla, 2003). Frontal splays commonly occur at a significant break in slope where channels are reduced in width, depth and sinuosity (Posamentier and Kolla, 2003). The transition from confined to unconfined flow and the location of the frontal splays is also a function of the sand-to-mud ratio and of slope curvature (Posamentier and Kolla, 2003). Frontal splays and lobes are further discussed by Droz et al. (2003) and Posamentier and Kolla (2003).

Much work is still required to characterise and quantify the architectural elements of deepwater systems. Lateral and vertical connectivity of submarine channel-fill elements and transitional features are still not well characterised (Stow and Mayall, 2000). Understanding stacking patterns is important for the hydrocarbon industry for determining reservoir distribution (Mayall et al., 2006). However, each channel is different, because there are so many parameters that control their formation and final geometries, e.g. sediment type and supply rate, tectonic setting and activity, climate and sea level variations (Bouma, 2004).

2.2 NIGER DELTA

2.2.1 Geological setting

The Niger Delta is a large, up to 12 km thick delta on the Gulf of Guinea on the West African passive continental margin (Fig. 2.3). The delta has formed in the southern culmination of the Benue Trough, a failed arm of a triple junction that formed during the opening of the Atlantic in the Late Cretaceous (Doust and Omatsola, 1990). The Niger and Benue rivers have delivered sediment to the delta at least since the Eocene (Morgan, 2003). The present day annual sediment discharge of the Niger River upstream of the point where the distributary system fans out is 19 million m^3 (Doust and Omatsola, 1990).

The delta is divided into three main stratigraphic formations: Akata, Agbada and Benin (e.g. Knox and Omatsola, 1989; Doust and Omatsola, 1990; Damuth, 1994; Cohen and McClay, 1996; Morgan, 2004). The Late Cretaceous-Palaeocene Akata Formation overlies the continental and oceanic crust and is 2-7 km thick (Corredor et al., 2005). It consists of a succession of overpressured shales, clays and silts (Doust and Omatsola, 1990; Damuth, 1994; Morgan, 2003). Overlying the Akata Formation, the mixed clastic Agbada Formation, consisting of sands, silts and clays (Doust and Omatsola, 1990; Damuth, 1994), can reach a thickness of 5 km (Corredor et al., 2005). The topmost, largely fluvial Benin Formation is the thinnest (up to 2.5 km) and laterally the least extensive formation (Cohen and McClay, 1996) (Fig. 2.3B). The Akata Formation is the distal equivalent of the Agbada Formation, which is the marine equivalent to the nonmarine Benin Formation. The stratigraphic division is made based on differences in seismic character and velocity (Morgan, 2003) (Fig. 2.4). Overall, the delta is dominated by mudstone (>80 %) interbedded with channel-laid sands and has a high sedimentation rate (Davies, 2003).

The Niger Delta can be divided into three broad structural domains: (1) an extensional domain characterised by growth faults, (2) a translational domain with shale diapirs and (3) a compressional domain dominated by imbricated toe-of-slope thrusts (Fig. 2.3B). This division is due to gravity tectonics, caused by rapid progradation of the delta (Knox and Omatsola, 1989; Doust and Omatsola, 1990; Damuth, 1994; Cohen and McClay, 1996; Hooper et al., 2002; Morgan, 2003). Corredor et al. (2005) divide the delta into 5 structural zones: extensional mud diapir, inner fold and thrust belt (with imbricate, basinward-verging thrusts), transitional detachment fold zone, and outer fold and thrust belt (with thrusts verging both

land- and basinward), and give further description of different structural styles of the fault-related folds.

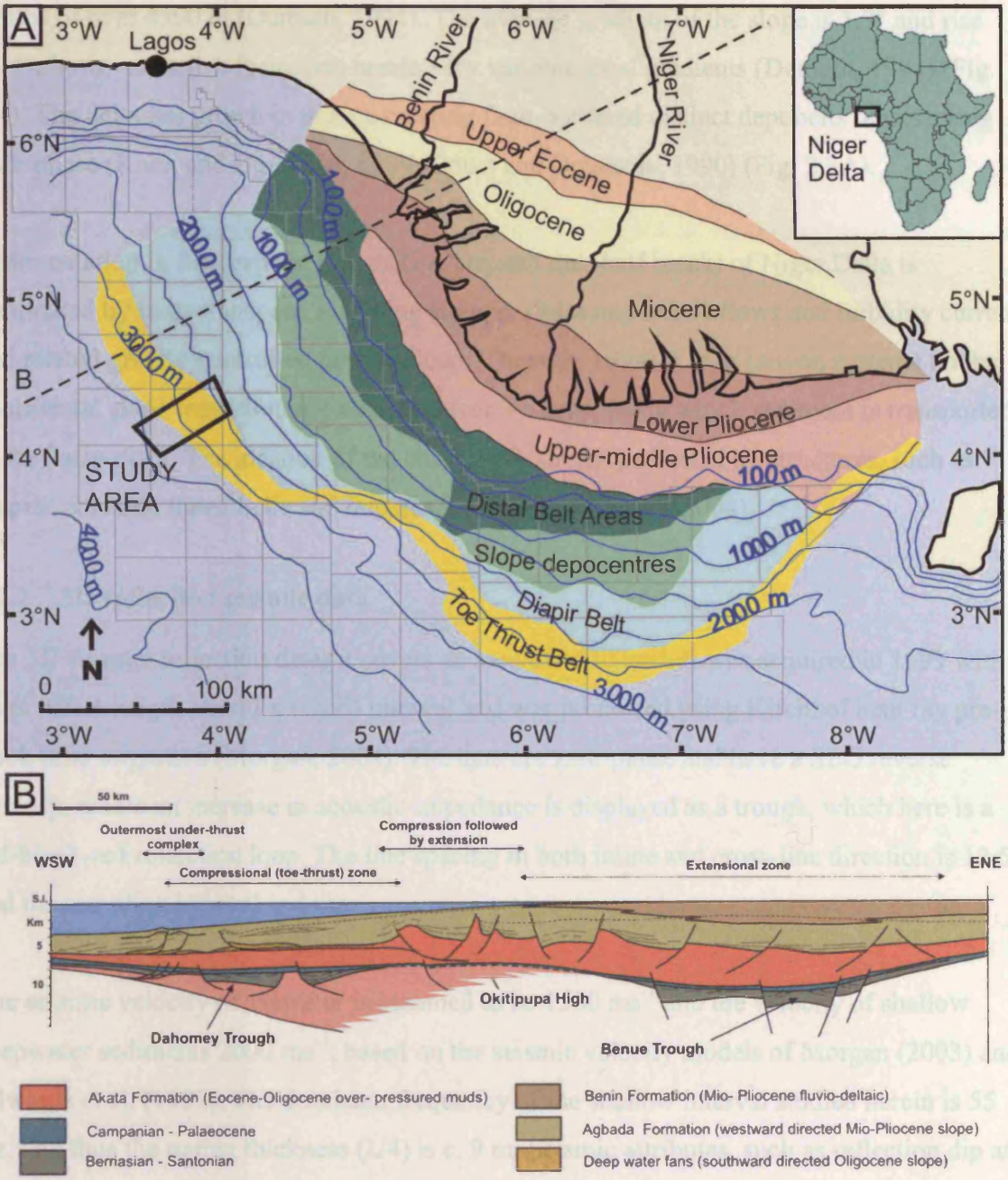

Figure 2.3. Location of the 3D seismic data on the Niger Delta, western Africa. (A) A map of the Niger Delta and its main onshore depobelts and offshore tectonic areas (after Knox and Omatsola, 1989; Doust and Omatsola, 1990; Armentrout et al., 2000). The grey grid marks the location of deepwater hydrocarbon industry licence blocks. (B) A simplified line drawing showing a cross section of the delta with extensional faults at the proximal end, translational zone with mud diapirs and distal compressional zone with toe-thrust and fold belt (Morgan, 2004).

Hydrocarbon exploration and production in the Niger Delta area is prolific, with increasing interest in the deep and ultradeepwater (1500-4000 m) parts of the delta (e.g. Morgan, 2003). The shelf break occurs at the water depth of 150-210 m, and the abyssal plain is reached at depths of over 4500 m (Damuth, 1994). The average gradient of the slope is 1.7° and rise 0.16°, however, active tectonism create very variable local gradients (Damuth, 1994) (Fig. 2.4). The delta has grown in phases creating fault-bordered distinct depobelts representing each phase (Knox and Omatsola, 1989; Doust and Omatsola, 1990) (Fig. 2.3A).

Sedimentation in the deepwater parts (i.e. beneath the shelf break) of Niger Delta is dominated by mass transport, including slumps, slides and debris flows and turbidity currents and related gravity-controlled density flows (Damuth, 1994). Large canyon systems on the continental slope transition into channel-levee systems, along which sediment is transported to the basin plain. The location of the channels is strongly affected by structures, such as diapirs, fold and thrust belts and transfer fault zones (Morgan, 2004).

2.2.2 3D reflection seismic data

The 3D seismic reflection dataset covers an area of 1630 km^2. It was acquired in 1999 with a 6 km offset length and 12 s record interval and was processed using Kirchhof bent ray pre-stack time migration (Morgan, 2004). The data are zero-phase and have a SEG reverse polarity, where an increase in acoustic impedance is displayed as a trough, which here is a red-black-red reflection loop. The line spacing in both inline and cross-line direction is 12.5 m and the sampling interval is 4 ms.

The seismic velocity of seawater is assumed to be 1500 ms^{-1} and the velocity of shallow deepwater sediments 2000 ms^{-1}, based on the seismic velocity models of Morgan (2003) and Edwards et al. (1997). The dominant frequency of the shallow interval studied herein is 55 Hz, and thus the tuning thickness ($\lambda/4$) is c. 9 m. Seismic attributes, such as reflection dip and amplitude were used to reveal depositional and deformational features. Lithological interpretations follow earlier work done by Deptuck et al. (2003) and Posamentier and Kolla (2003), and is based on the recognition of seismic reflection character, amplitude and geometry.

2.2.3 Overview of the architectural elements

The data are located on the western lobe of the Niger Delta, c. 150 km away from the shoreline (Fig. 2.3A). This area is dominated by thrust-cored anticlines and large channel-levee systems, which are also the main features visible on the seafloor (Figs. 2.4 and 2.5). Other common features include slope failures, mass-transport complexes and sediment waves (Fig. 2.5). The failure scars and depositional lobes that characterise the anticline limbs are described and analysed in Chapter 3 and sediment waves are discussed further in Chapter 5. This chapter concentrates on the other features, especially the channel-levee systems and the architectural elements associated with them. A description of each architectural element and a brief discussion of its significance and formation are given below.

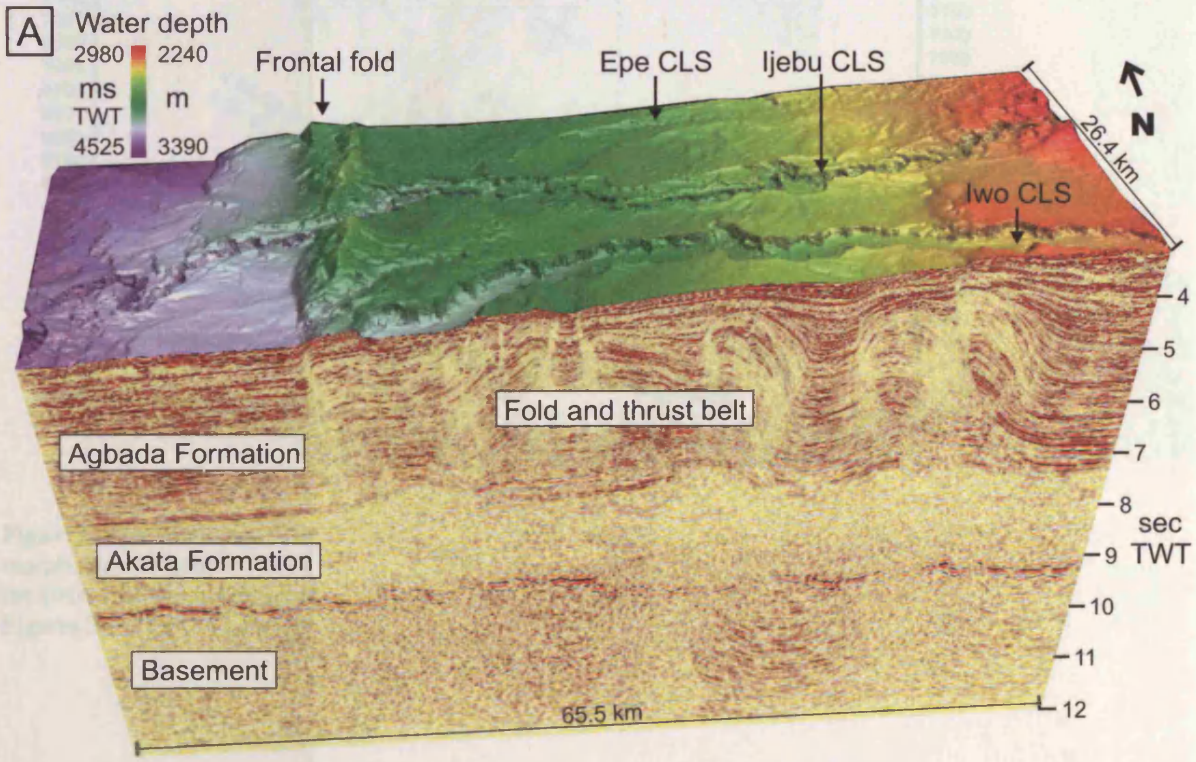

Figure 2.4. (A) A 3D view of the seismic data showing the extent of the data and the main structural and stratigraphic features that characterize it. Thrust-related folds have topography on the seafloor, on which the three main channel-levee systems (CLS) are the dominant features. Continues on next page.

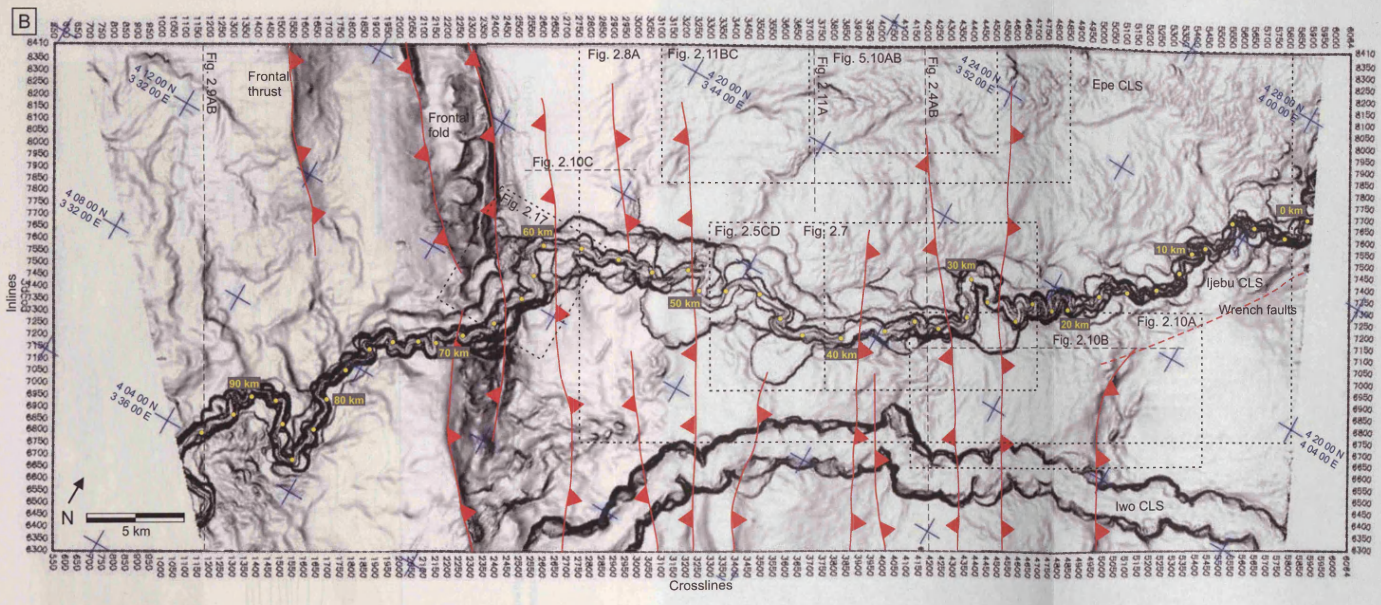

Figure 2.4 (continued) (B) A dip map of the seafloor of the Niger Delta dataset showing the main morphological features. The locations of the main thrusts are traced in red. The yellow dots and numbers along the Ijebu CLS are the datapoints from which the measurements of Figures 2.6 and 4.4 were taken. Locations of Figures 2.5-2.11, 2.17 and 5.10 are shown.

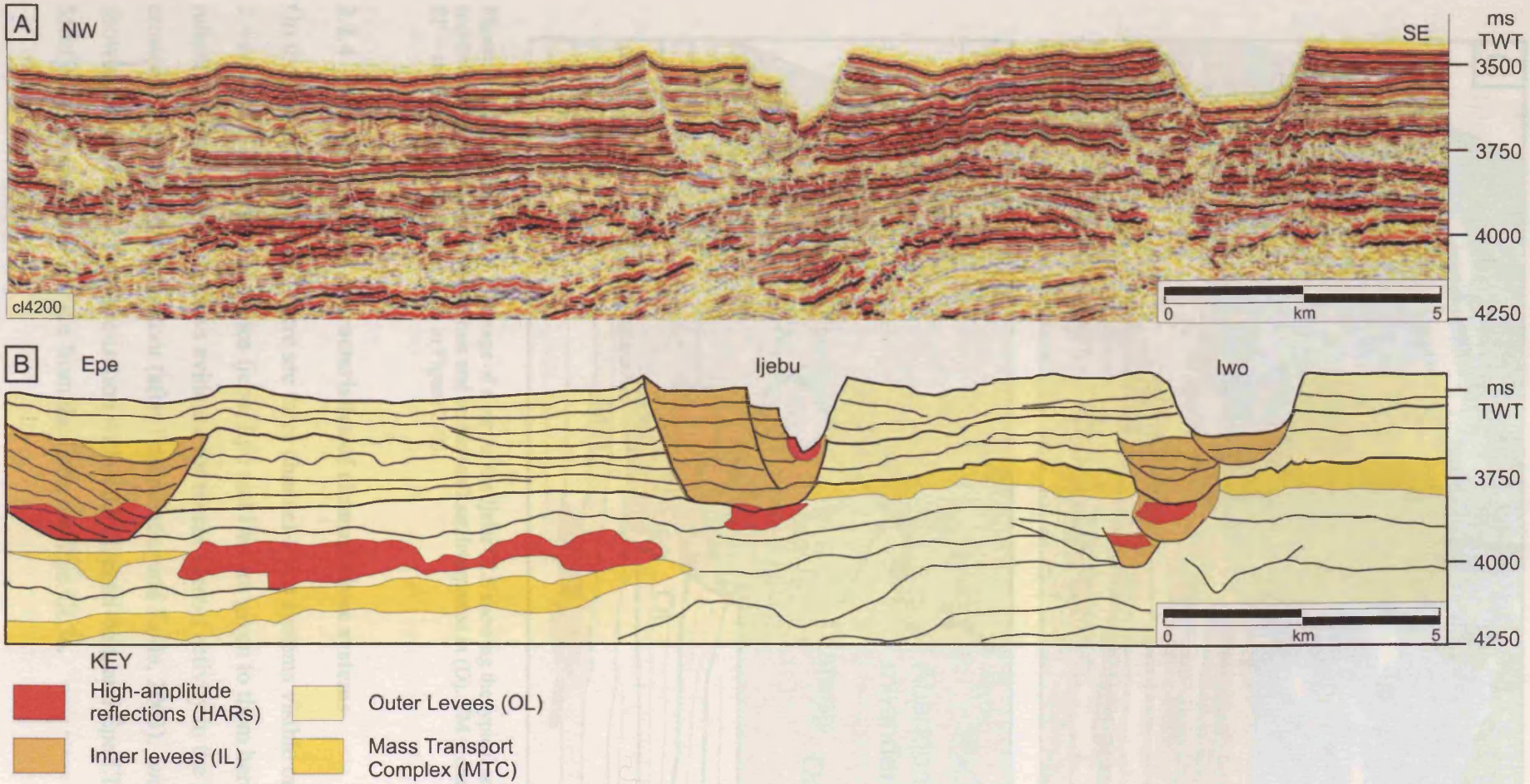

Figure 2.5. (A) A representative seismic line across the data showing three channel-levee systems in the shallow section. For more seismic lines, see Appendix 2. (B) A line drawing with the interpretation of the main seismic facies and architectural elements important for this project. See location in Figure 2.4B. (C) and (D) on next page.

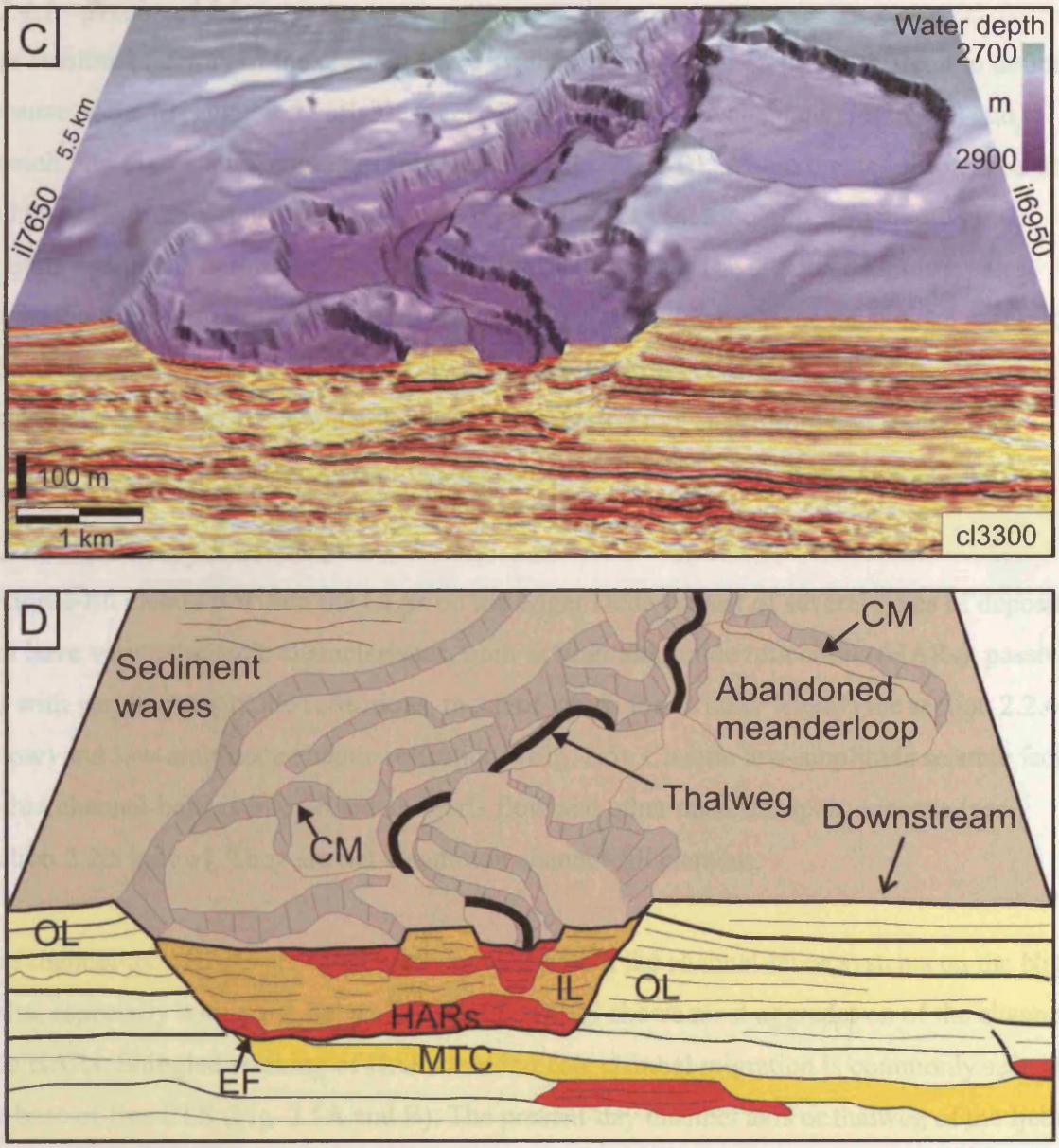

Figure 2.5. (Continued) (C) A 3D image of a part of the Ijebu CLS showing the typical seismic facies and architectural elements in seismic section and on the seafloor, interpreted in (D). CM = channel-margin collapse. EF = erosional fairway. See location in Figure 2.4B.

2.2.4 Morphology and characteristics of channel-levee systems

On the Niger Delta dataset, there are three channel-levee systems visible on the seafloor (Figs. 2.4 and 2.5). The informal names Ijebu, Epe and Iwo are given to them here for the ease of reference. The Ijebu CLS shows evidence for recent current activity in the form of presence of erosional channels on the seafloor (after Posamentier and Kolla, 2003), Iwo CLS is inactive, showing no evidence of channelisation within the channel-belt, and Epe CLS is almost buried. Most of the examples below are from the Ijebu and Epe CLSs.

2.2.4.1 Erosional fairway

The erosional fairway of the channel-levee systems on the Niger Delta are difficult to define, because of the irregular and variable level of incision along the channels (Fig. 2.6F) and erosion into pre-existing channel-levee systems (Fig. 2.5A-B). Where the definition is easier and the measurements are more accurate, they indicate an incision of c. 150 m into pre-existing sediments before the base of extensive outer levees. The erosion depth is greatest across the folds with greatest uplift of the seafloor and shallowest at the most distal part of the CLS (Fig. 2.6F). These results are likely to be slightly exaggerated, however, because small wedge-shaped levees are found at lower levels occasionally, suggesting that some levee-building occurred before the start of the deposition of the extensive levees (Fig. 2.5A-B).

2.2.4.2 Channel-fill elements

Channel-fill elements within the CLSs on the Niger Delta consist of several types of deposits that have various seismic characteristics, such as high-amplitude reflections (HARs), passive fill with variable amplitude reflections, much of which forms inner levees (see section 2.2.4.3 below) and low-amplitude chaotic reflections (Fig. 2.5). Chaotic low-amplitude seismic facies within channel-belts is interpreted as debris flow and other mass transport deposits (see section 2.2.5 below). They are not a common channel-fill element.

The channel-axis HARs are often partly eroded within the channel-levee systems on the Niger Delta, especially within the Ijebu CLS. The Epe CLS shows most aggradation of the channel-axis HARs. Shingled stacking of HARs that indicate channel migration is commonly seen at the base of Epe CLS (Fig. 2.5A and B). The present-day channel axis or thalweg of the Ijebu CLS is c. 80 m wide (Figs. 2.5D and 2.6C). Figure 2.7 reveals that this is a common width for channel-axes deposits throughout the evolution of the channel-levee system. It also illustrates the process of meander bend cutoff. The present day thalweg is further described and discussed in Chapter 4.

2.2.4.3 Inner levees

The Ijebu CLS has several levels of terraces, the elevation of which is highly variable with respect to the thalweg (Fig. 2.5C and D). The seismic character of the inner levees varies from low to high-amplitude continuous to chaotic reflections and they can be very different to outer levees (Fig. 2.5). This suggests a different composition and origin for inner and outer levees (Deptuck et al., 2003). Inner levees are commonly bordered by erosive surfaces inclined less than 25° (Deptuck et al., 2003), however, on the Niger Delta these surfaces can be up to 35°.

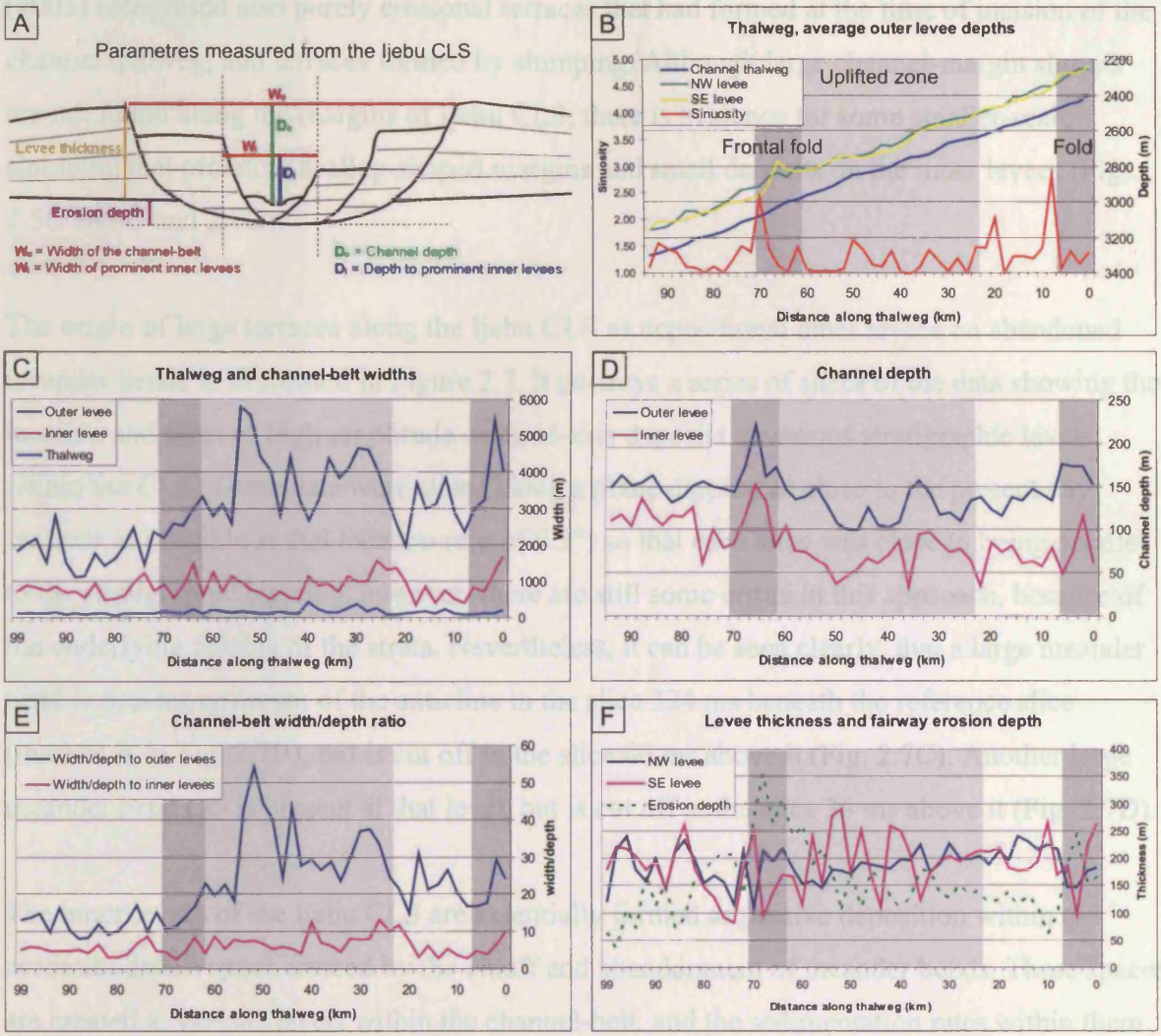

Figure 2.6. Quantification of morphological features of the Ijebu channel-levee system. The measurements of the parameters shown in (A) are recorded along the present day Ijebu thalweg every 2 km. (B) A graph showing the water depth along the course of the Ijebu thalweg and the crest of the outer levees, plotted together with sinuosity values from the thalweg. (C) Width of the channel-belt, prominent inner levees and thalweg. The width of the channel-belt decrease dramatically inboard of the frontal fold. (D) The depth of channel shows increase half way down the system. (E) Channel width/depth ratio. (F) Measurements of the levee thicknesses and the depth of erosion of the fairway. Quality of the measurements is lower where thrusts are present. Depth to the most prominent inner levees does not change. Datapoints located in Figure 2.4B.

Similar terraces to what are observed on the Niger Delta are recognised in the channels of many fans, such as the Indus (McHargue and Webb, 1986; von Rad and Tahir, 1997; Deptuck et al., 2003), Zaire (Droz et al., 1996; Babonneau et al., 2002; Droz et al., 2003; Babonneau et al., 2004), Bengal (Hübscher et al., 1997), Sao Tomé (Viana et al., 2003) and Rhône (Torres et al., 1997) fans. They have been interpreted as levee margin growth faults (Clark and Pickering, 1996), slumped levees and channel margins, depositional terraces and confined inner levees. Recent interpretation of 3D seismic data has proved their origin as inner levees deposited on the space created by channel erosion (Babonneau et al., 2004). Deptuck et al.

(2003) recognised also purely erosional terraces that had formed at the time of incision of the channel thalweg, and terraces formed by slumping. Although large channel-margin slumps are not found along the margins of Ijebu CLS, there is evidence for some smaller-scale slumping that produces scallop-shaped margins and small deposits on the inner levees (Figs. 2.5C and D and 2.7G).

The origin of large terraces along the Ijebu CLS as depositional inner levees on abandoned meander bends is illustrated in Figure 2.7. It portrays a series of slices of the data showing the location and form of high-amplitude channel-axis deposits at various stratigraphic levels within the CLS. These data were sliced along a plane dipping as close to the present day seafloor as possible at that location (dip of 0.3°) so that each slice was close to being parallel to the stratigraphic layering, however, there are still some errors in this approach, because of the underlying folding of the strata. Nevertheless, it can be seen clearly, that a large meander bend is present upstream of the anticline in the slice 324 ms beneath the reference slice (marked Y in Fig. 2.7B), but is cut off in the slice 60 ms above it (Fig. 2.7C). Another large meander bend (X) is present at that level, but is cut off in the slice 36 ms above it (Fig. 2.7D).

The inner levees of the Ijebu CLS are essentially formed as passive deposition within the accommodation space created by the cutoff and abandonment of meander bends. These spaces are created at various levels within the channel-belt, and the sedimentation rates within them are variable. Therefore the thickness of an inner levee does not necessarily reflect its age, and the terraces cannot be correlated based on their height above the channel thalweg alone.

2.2.4.4 Outer levees

The large outer levees that border Ijebu channel-belt are wedge-shaped, exhibit both high and low-amplitude reflections and are approximately 5 km wide (Fig. 2.5A and B). The levees on both sides are typically c. 200 m thick (Fig. 2.6F). However, as pointed out above, small wedge-shaped deposits are found locally at lower stratigraphic levels, and therefore the levees could be much thicker.

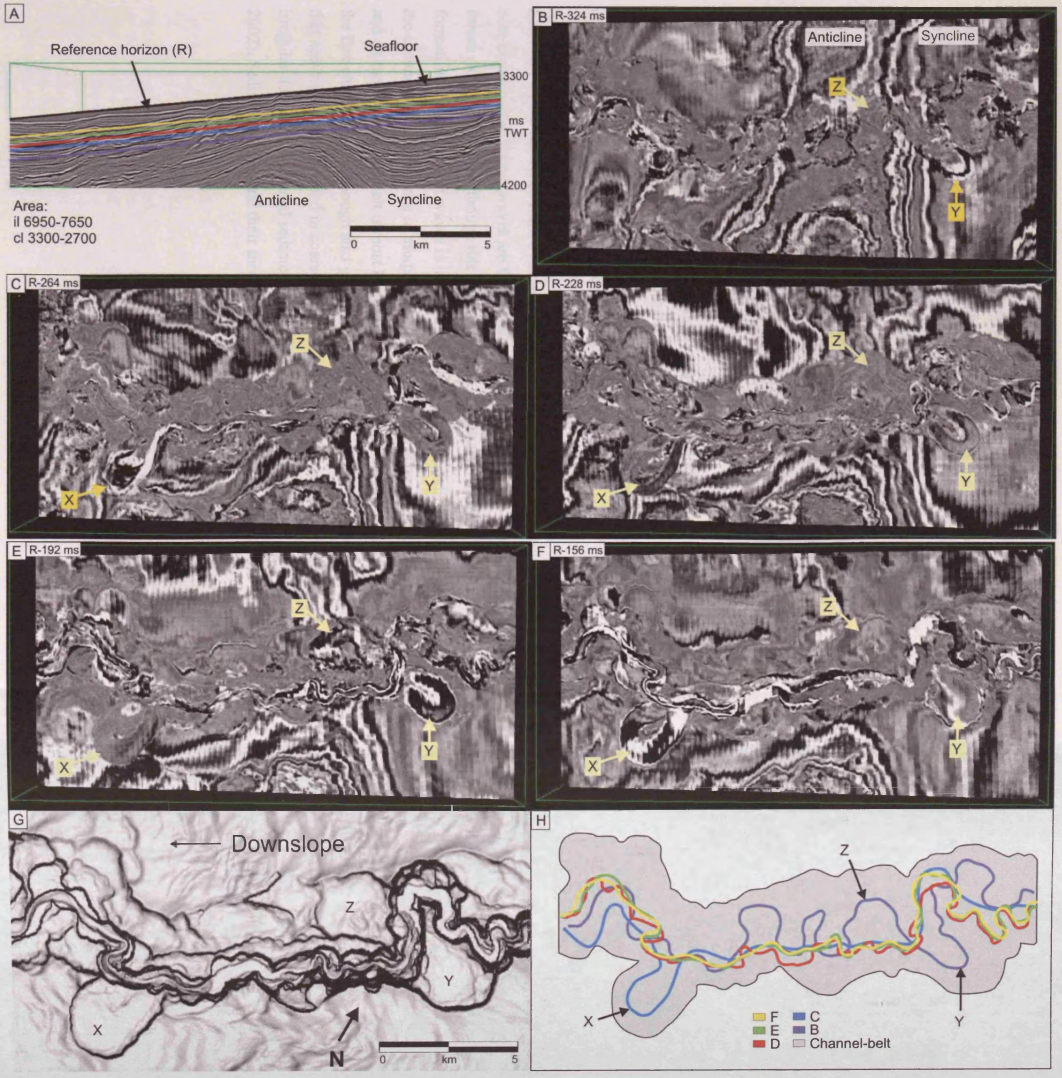

Figure 2.7. (continues to next page) Formation of terraces by channel thalweg migration and meander bend cutoff. (A) A cross section of the seismic volume, which is sliced along an arbitrary plane (R). This reference slice inclined to dip 0.3° to match the approximate seafloor dip. (B-F) Slices of the seismic data showing the variation in the location of the channel-axis deposits, shown in bright colours (high amplitudes) and the evolution of meander bend cutoffs into large terraces (X, Y and Z) within the channel-belt. (G) Seafloor dip map of the same are showing the large terraces (X, Y and Z). (H) A line drawing, in which the most prominent channel-axis deposits from each slice and the limits of the present day channel-belt are superimposed. See locations in Figure 2.4B.

2.2.4.5 Sediment waves

Sediment waves are a prominent feature on the levees of the Ijebu CLS (Fig. 2.8). The linear and arcuate crests of the waves are typically several kilometres long and orientated oblique to the channel-belt. A typical crest to crest distance is approximately 1 km and the waves are up to 20 m high (Fig. 2.8B). An azimuth map that shows the direction of dip of the local seafloor slopes reveals that most stoss flanks dip upslope (Fig. 2.8A). A seismic section across some of the waves on the levees shows evidence for the growth and upstream migration of the waves by preferential deposition on the stoss flanks (Fig. 2.8B). Some of the reflections have a high seismic amplitude signal on the stoss flanks, suggesting the presence of relatively coarse sediment (Fig. 2.8B; see also Fig. 2.9).

Sediment waves are also found on the seafloor overlying the buried channel-belt of the Epe CLS (Fig. 2.8C). These waves have more irregular morphology and are more closely spaced than the waves on the levees. They have developed above a passive channel-fill and do not occur below the level of 130 ms below the present seafloor.

Sediment waves on levees form by flow-stripping from turbidity currents within channels and best-developed sediment waves are found outboard of the outer bends due to centrifugal forces (Komar, 1969). Although this phenomenon is not observed on the Niger Delta, the formation of the sediment waves is likely to be related to the turbidity currents flowing down the channels. The difference in morphology of sediment waves on the intra-channel seafloor and on the Epe channel-belt is most likely due to the weak confinement of the flows within the Epe channel-belt, although also grain-size can affect the sediment wave morphology so that sediment waves formed in coarse-grained sediments are commonly smaller and more irregular than in fine-grained sediment and associated with erosional scours (Wynn and Stow, 2002). Sediment waves and their formation are further discussed in Chapter 5.

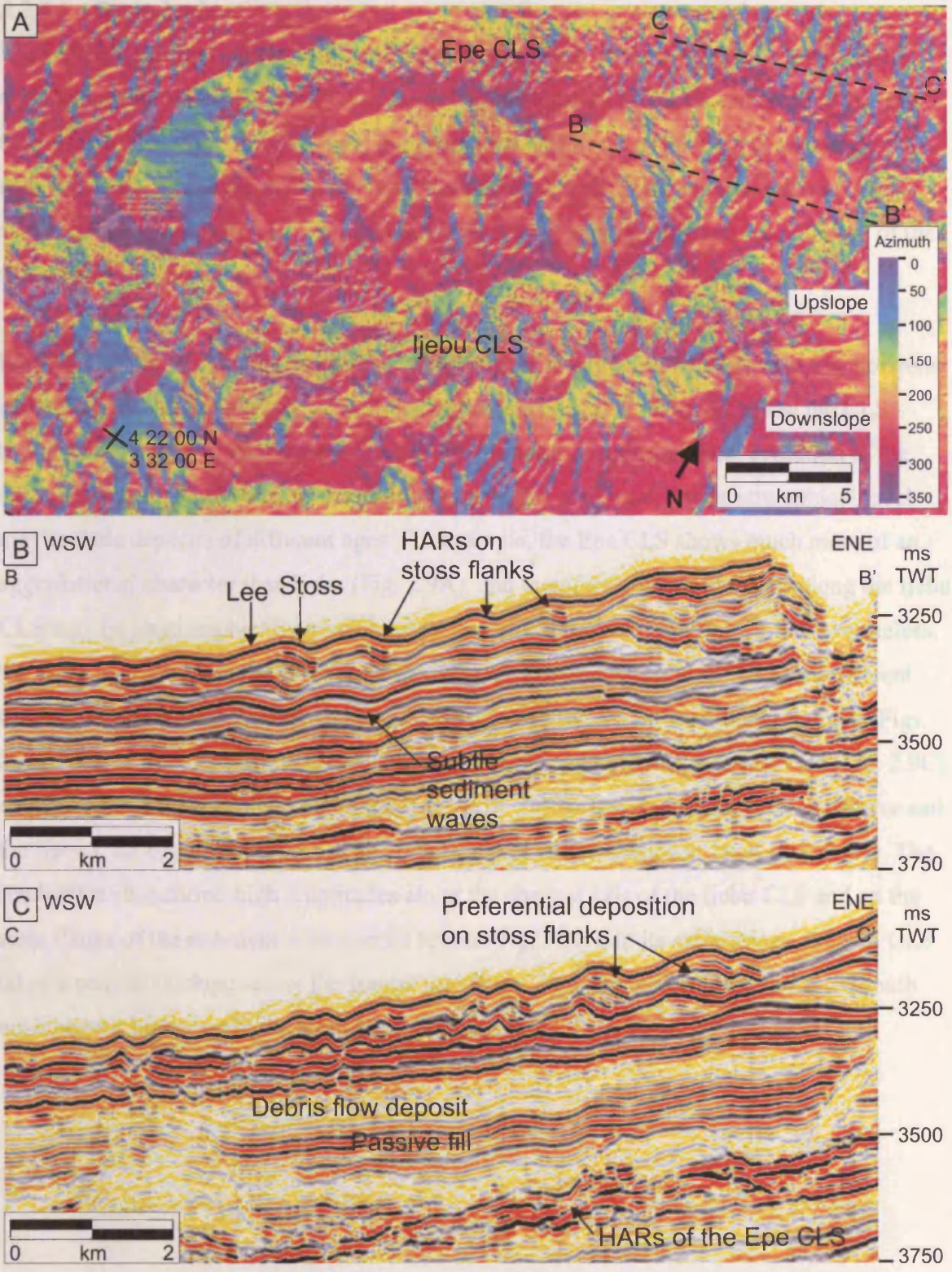

Figure 2.8. Sediment waves on the levees of Ijebu and on the channel-belt of Epe. (A) A dip azimuth map showing the direction, into which the local seafloor slopes are dipping. The sediment waves on both sides of Ijebu CLS have upslope-dipping stoss flanks. The wave crests are up to 4 km long and have a wavelength of c. 1 km. The sediment waves on Epe CLS are slightly smaller and less regular. See location in Figure 2.4B. (B) Sediment waves on a levee, crests approximately parallel to slope. Waves are subtle c. 250 ms below the seafloor but become larger up-section with much more deposition on the upslope (stoss) flanks. (C) Sediment waves along the Epe channel-belt occur on the top c. 100 ms and are very irregular. The traverse shows an along-section channel-fill of the Epe CLS.

2.2.4.6 Frontal splays

The extensive frontal splays of the channel-levee systems on the Niger Delta are located outside the data area (Morgan, 2004). However, the location of the frontal splay of the Epe CLS used to lie within the data area, but prograded basinward as the CLS grew longer. The splay is visible as a layer of chaotic HARs at the base of the Epe CLS on a seismic cross-section (Fig. 2.9A) and as a high-amplitude fan-shaped area that spreads out outboard of the frontal fold in plan view (Fig. 2.9C).

Figure 2.9 shows maximum amplitude extractions of seismic volumes between two horizons created by combining various proportions of the seabed and the horizon below the CLS (horizon BC in Fig. 2.9B) in order to establish the seismic stratigraphical evolution of the CLSs. However, since some of the channels are highly erosional, one stratigraphical level may include deposits of different ages. For example, the Epe CLS shows much more of an aggradational character than Ijebu (Fig. 2.9A), and therefore younger deposits along the Ijebu CLS may lie stratigraphically much lower than older deposits of the Epe CLS. Nevertheless, the gross evolution and the location of the channel-axis deposits and the CLSs at different levels can be established. At lower levels, the Epe and Iwo CLSs are most prominent (Figs. 2.9C-D). The Epe CLS transitions into a frontal splay outboard of the frontal fold (Fig. 2.9C), and sinuous CLS is developed onto the splay (Fig. 2.9E). The Epe CLS becomes passive and the Ijebu CLS becomes the CLS with strongest imprint at a shallower level (Fig. 2.9G). The shallowest slice shows high amplitudes along the channel axis of the Ijebu CLS and on the stoss flanks of the sediment waves on its levees (Fig. 2.9H). In its early stages, the Iwo CLS takes a path downslope across the frontal fold (Figs. 2.9C-E), but becomes deflected south upslope of it higher up in the stratigraphy (Fig. 2.9H).

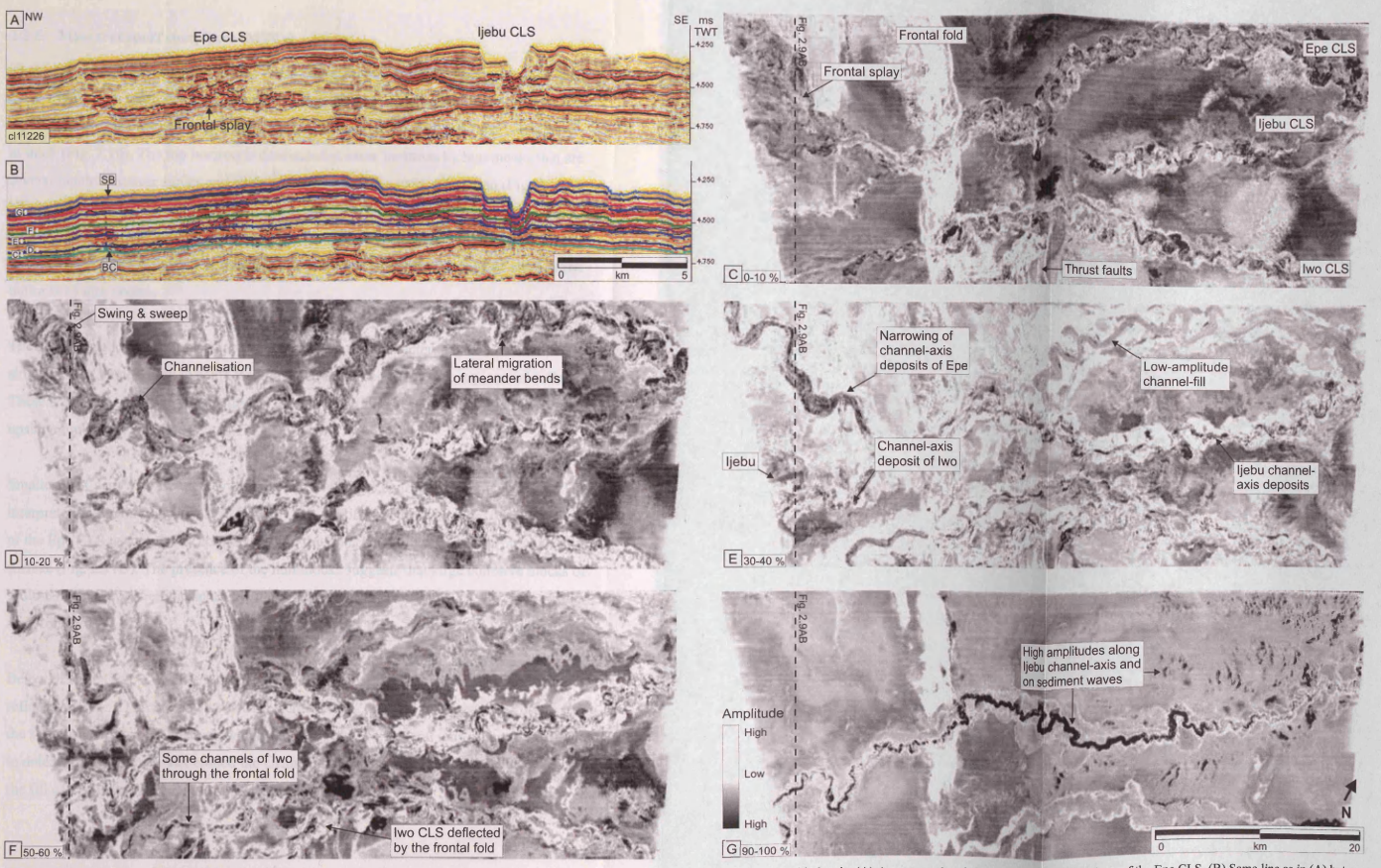

Figure 2.9. A series of maximum amplitude extractions between isoproportional slices showing the seismic facies of the CLSs at different stratigraphic levels. (A) A cross section showing a frontal splay at the base of the Epe CLS. (B) Same line as in (A) but with the isoproportional slices between the green horizon (BC) and the seabed (SB) superimposed on it. The percentage of seafloor used is shown on (C-G). (C) Maximum amplitude extraction between BC and the lowest slice. It shows the depositional frontal splay outboard of the frontal fold. (D) Channels of the Epe CLS showing both swing and sweep become confined on the splay. The path of the Iwo CLS is roughly straight outboard and across the frontal fold, better seen in (E) with a single channel clearly visible. Sinuous channel-axis deposits are seen also along the Epe and Ijebu CLSs at this level. (F) The imprint of the Ijebu CLS becomes stronger at this level. The path of Iwo CLS is deflected south before the frontal thrust. Epe CLS is passive. (G) High amplitudes are seen along Ijebu thalweg and low terraces, and also on upslope flanks of sediment waves on the levees in the extraction between seafloor and the topmost slice.

2.2.5 Mass transport complexes (MTCs)

There are several MTC deposits on the Niger Delta, mainly in the shallow part of the data (top 1-2 s TWT below seafloor). One particularly extensive MTC that extends almost across the whole data area is located beneath the 3 channel-levee systems (Fig. 2.5) and is typically c. 60 m thick (Fig. 2.10). The top horizon is dominated at some locations by hummocks that are several hundred metres across and slightly elongate in a downslope direction (Fig. 2.10A). The onlap of reflections onto the hummocks (Fig. 2.10B) indicates that they were present at the time of the deposition of the MTC, and are thus interpreted as coherent blocks that were transported within the mass flow. Some preferential deposition on the upslope sides of the hummocks also occurs.

The MTC has a low-amplitude chaotic seismic reflection character, however, some internal structures can be observed in some locations, for example steeply dipping internal reflections. These are interpreted as imbricate thrusts formed within the MTC, typically found on the upslope limb of an anticline (Fig. 2.10C).

Smaller MTCs are also frequent within the data. Some are confined within channels and interpreted as debris flow deposits (Fig. 2.11). A debris flow deposit on top of the passive fill of the Epe CLS is completely confined within the Epe channel-belt and has a hummocky top surface (Fig. 2.11B). The presence of the hummocks suggests that large cohesive blocks of sediment may have been transported within the debris flow (Prior et al., 1984; Posamentier and Kolla, 2003).

Below the Epe CLS, a distinct u-shaped channel scour is filled with low-amplitude chaotic reflections (Fig. 2.11A). This channel-fill element has a constant thickness of c. 110 m along the sinuous course of the channel, which can be traced over several tens of km. It is difficult to determine the process that eroded the channel, but based on the reflection characteristics, the fill can be identified as a debris flow deposit.

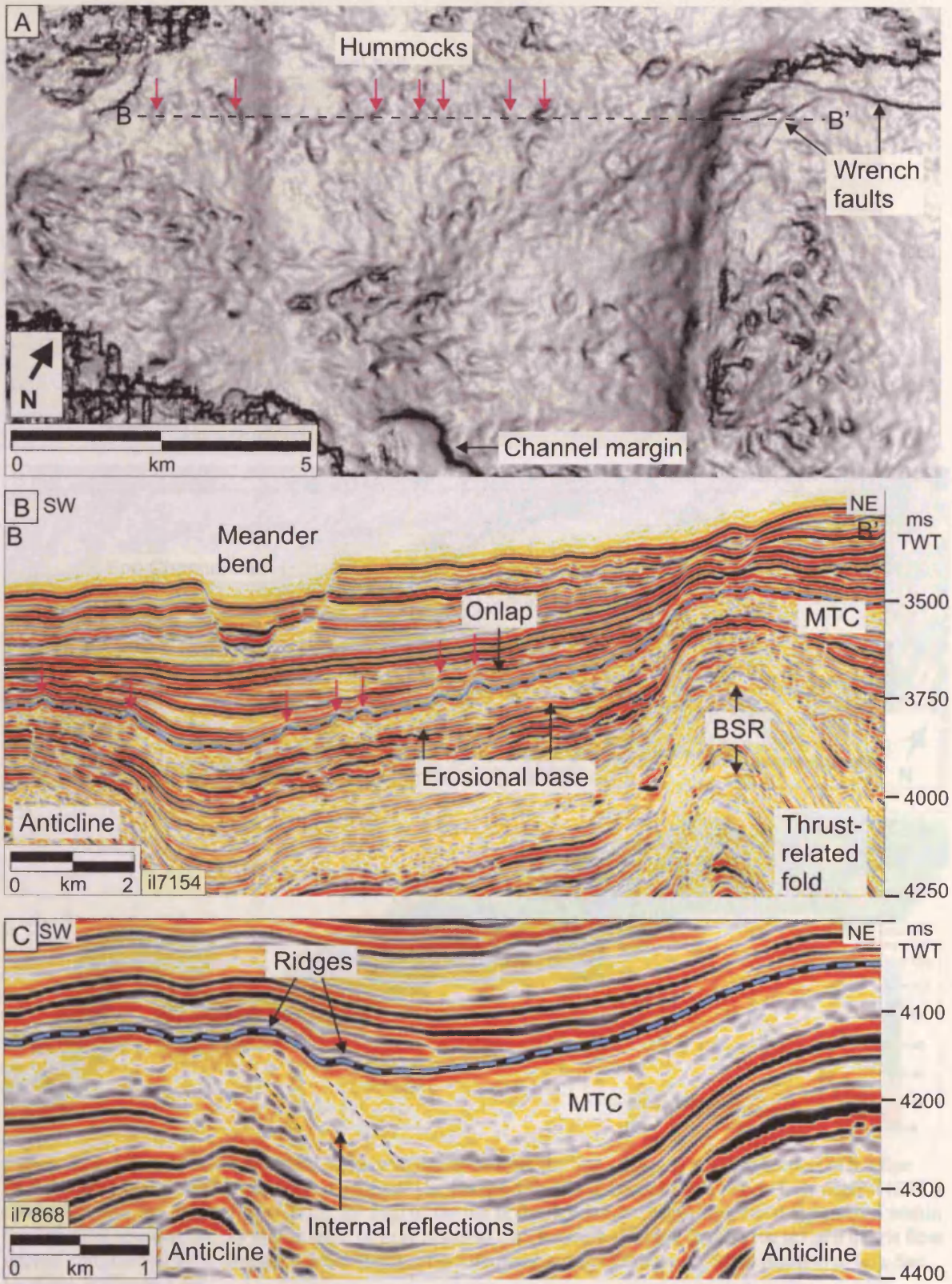

Figure 2.10. Seismic characteristics of an extensive mass transport complex (MTC) on the Niger Delta. (A) A dip map displaying a part of the top surface of the MTC and showing hummocks that are slightly elongate in the downslope direction. (B) A cross-section showing the typical low-amplitude chaotic seismic character of the MTC. The MTC is approximately 60 m thick and has an erosional base and hummocks on its top surface (blue dashed line). These hummocks are onlapped by subsequent reflections with preferential deposition on the upslope sides. (C) An example of internal structures within the MTC (dashed lines) that are interpreted as imbricate thrusts. See locations in Figure 2.4B.

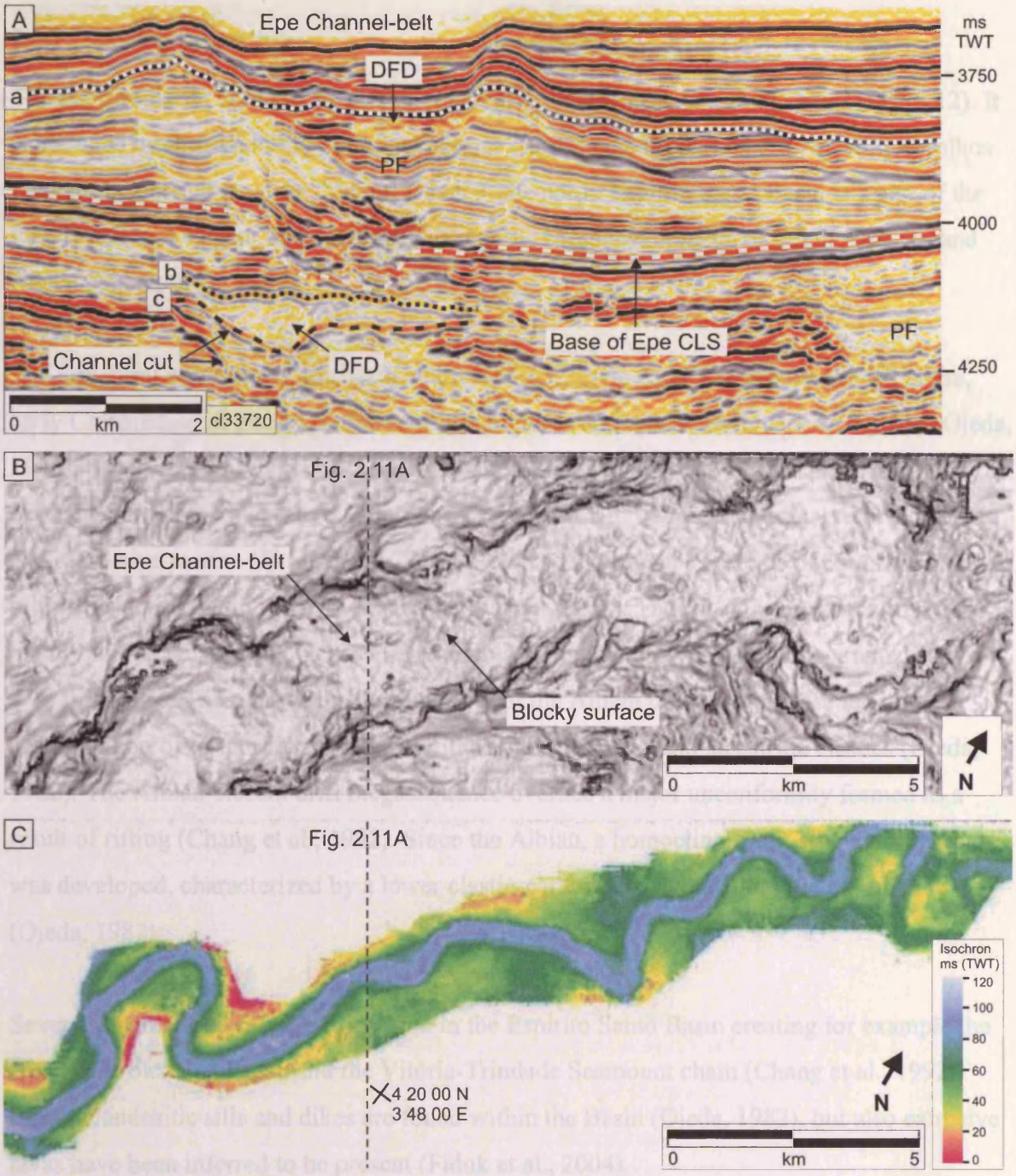

Figure 2.11. Channel-confined debris flows within and beneath the Epe CLS. (A) A cross-section of the Epe CLS showing lateral shift towards the southeast. The passive fill (PF) is overlain by a debris flow deposit (DFD) confined within the channel-belt. (B) A dip map of the top of the debris flow deposit (horizon a) confined within the Epe CLS showing blocky appearance. (C) An isochron map between the base (b) and top (c) of a debris flow deposit confined within a channel beneath the Epe CLS showing constant thickness. Same location as (B). See locations in Figure 2.4B.

2.3 ESPIRITO SANTO BASIN

2.3.1 Geological setting

The Espirito Santo Basin is located on the passive continental margin of Brazil (Fig. 2.12). It is bounded by the structurally similar Campos Basin to the south, and the volcanic Abrolhos Plateau separates it from the Mucuri Basin to the north. Espirito Santo Basin is a part of the East Brazil Rift system that developed during the Mesozoic breakup of South America and Africa (Chang et al., 1992).

The structural evolution of the basin includes late Jurassic-early Cretaceous pre-rift phase, early Cretaceous rift phase, Aptian transitional phase and Albian to Recent drift phase (Ojeda, 1982). Stratigraphically, the basin is divided into five depositional megasequences that correspond to the structural evolution phases: pre-rift, rift, transitional, transgressive marine and regressive marine (Fiduk et al., 2004). The pre-rift sequence consists of continental sediments deposited in intracratonic basins (Ojeda, 1982). The rift-phase sediments are mainly fluvial, deltaic and lacustrine sediments, dominated by fine to coarse-grained sands, silts and shales. The relative tectonic stability of the Albian transitional phase led to the accumulation of evaporitic succession with some carbonates and lacustrine clastics (Ojeda, 1982). The Albian-Recent drift megasequence overlies a major unconformity formed as a result of rifting (Chang et al., 1992). Since the Albian, a homoclinal shelf-slope morphology was developed, characterized by a lower clastic-carbonate unit and an upper clastic unit (Ojeda, 1982).

Several magmatic events have occurred in the Espirito Santo Basin creating for example the Abrolhos volcanic plateau and the Vitória-Trindade Seamount chain (Chang et al., 1992). Basaltic/andesitic sills and dikes are found within the Basin (Ojeda, 1982), but also extrusive lavas have been inferred to be present (Fiduk et al., 2004).

The basin has been deformed by salt tectonics, growth faulting and inversion along its margin since the Albian (Ojeda, 1982). Aptian-age salt has been deformed into pillow structures, diapirs, rollers, canopies and thrusts (Ojeda, 1982; Jackson et al., 1994). This deformation is ongoing and mainly driven by gravity gliding (Fiduk et al., 2004). Since the Eocene, the Espirito Santo Basin has been a prograding shelf and slope environment (Fiduk et al., 2004). Several canyons have incised into the basin slope and modified the geometry and depositional

evolution of the basin during its development. Today, the Doce River supplies sediment to the basin from the Mantiqueira and Espinhaço mountain chains.

2.3.2 3D seismic reflection data

The 3D seismic reflection data of the Espirito Santo Basin cover an area of 1600 km^2, where the present day water depth is between 35 and 1800 m (Fig. 2.12). The data was collected using 12.5x25 m bin spacing (Fiduk et al., 2004). The sample interval is 2 ms and the record interval is 4 s TWT. The data are zero-phase migrated and displayed with SEG normal polarity so that an increase in acoustic impedance is a black-red-black reflection loop. Lithological or well data were not availablefor this work. Seismic velocities of 1500 ms^{-1} for seawater and 1800 ms^{-1} for the shallow succession were suggested by the data provider (Schultz, CGGVeritas, personal communication) and are used when calculating thicknesses of sediment packages and dips of horizons. The prevailing frequency of the studied, shallow interval is c. 40 Hz. Using the average velocity of 1800 ms^{-1}, the dominant wavelength is c. 45 m and thus vertical resolution in the context of tuning thickness ($\lambda 4^{-1}$) is c. 11 m.

2.3.3 Overview of the data

The dataset is located immediately downstream of the present day shelf break and is dominated by salt diapirs, incised canyons, channels, slumps and debris flows (Fig. 2.12). The shelf break occurs at present day water depth of 100 m. The proximal slope angles are up to 15° and shallow to 1-2° more distally. The salt diapirs deform the seafloor and modify local slopes.

The sub-division of the strata is based on seismic character and the work of Fiduk et al. (2004). A representative seismic traverse across the slope shows the typical seismic facies observed within the dataset, and the division of the stratigraphy into 4 units according to seismic character (Fig. 2.12B).

The Unit 1 is a Palaeocene-Eocene-age, low-amplitude, continuous reflection package that overlies the Cretaceous deposits. The Horizon E/O marking the change from low-amplitude to high-amplitude reflection character between Units 1 and 2 is inferred to be the post middle Eocene or Oligocene unconformity (Fiduk et al., 2004). The high-amplitude character of the reflections of Unit 2 is caused by volcaniclastic material derived from the Abrolhos Plateau

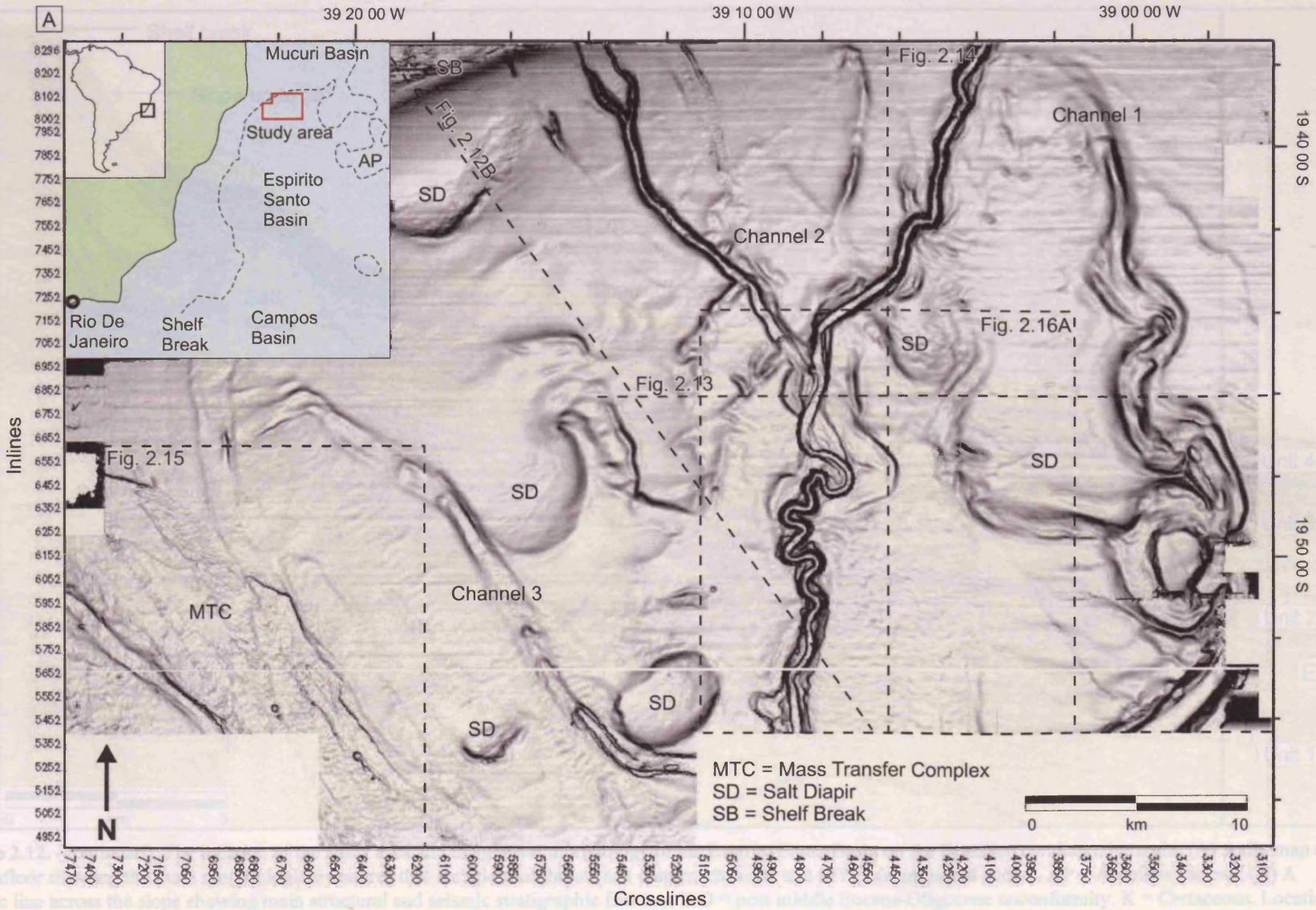

Figure 2.12. (continues to next page).

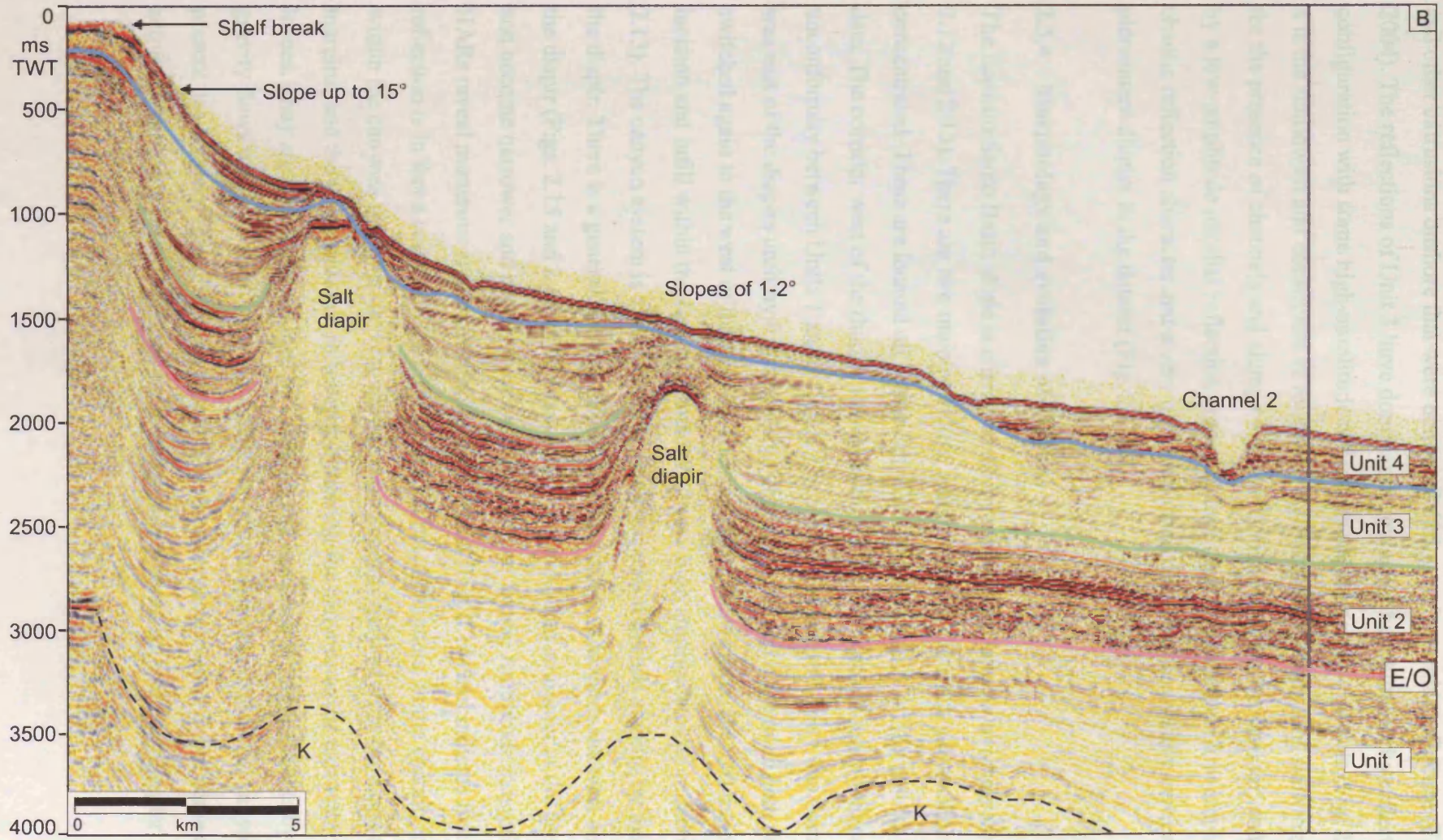

Figure 2.12. (continued). The location of the study area and the general morphology of the Espirito Santo Basin on the Brazilian continental margin. (A) A dip map of the seafloor showing the main morphological features that include shelf break, salt diapirs, channels and MTCs (slumps and slides). AP = Abrolhos Plateau. (B) A seismic line across the slope showing main structural and seismic stratigraphic features. E/O = post middle Eocene-Oligocene unconformity. K = Cretaceous. Location of the Cretaceous-Cenozoic boundary is uncertain.

and other extrusions onshore that were emplaced during early to middle Eocene (Fiduk et al., 2004). The reflections of Unit 3 have dominantly low-amplitude hummocky reflection configuration with some high-amplitude reflections and numerous channels (Fig. 2.12B). Unit 4 is the shallowest and constitutes of relatively high-amplitude reflections showing evidence for the presence of channels and slumps within c. 300 ms beneath the seafloor, and is capped by a low-amplitude parallel reflection drape package. Salt diapirs have a low-amplitude chaotic reflection character and a very high amplitude cap. They are mainly vertical piercement diapirs in the dataset (Fig. 2.12B).

2.3.4 Morphology and evolution of canyons

The Espirito Santo Basin slope is characterised by numerous channels and canyons (Figs. 2.12 and 2.13). There are two main corridors, along which the canyons and channels are concentrated. These are located on both sides of the two salt diapirs on the eastern part of the data. The corridor west of the diapirs was dominant prior to the post Eocene-Oligocene unconformity between Units 1 and 2 (Fig. 2.13). Above the unconformity, the dominant path was east of the diapirs until by the time of the deposition of Unit 4 the main path was switched again to the west of the diapirs. The succession shows more than 10 major phases of incision and infill within the canyon system with very high amplitude basal reflections (Fig. 2.13). The canyon system is almost 1 km in thickness and deformed slightly by the uplift of the diapir. There is a general trend of migration of the canyons towards the west and towards the diapir (Figs. 2.13 and 2.14). The basal HARs are wider and straighter at the deeper level, and become narrower and more sinuous at the shallower levels. Amplitude extractions of the HARs reveal numerous channels within one reflection (Fig. 2.14) and indicate that each reflection is in fact a composite of several, amalgamated channels. Some chaotic reflections within the canyons are most likely mass-transport deposits derived from the slope and canyon margins, and the low-amplitude reflections bordering the canyons to the east resemble inner levees. They are most likely formed by overspill and modification of sediments by sediment-gravity flows within the canyons (Fig. 2.13). The rounded appearance of the canyon on the present day seafloor (Fig. 2.12) suggests that no erosion occurs along it, but some current activity is probably present to form the rounded scours on its surface (see Chapter 5).

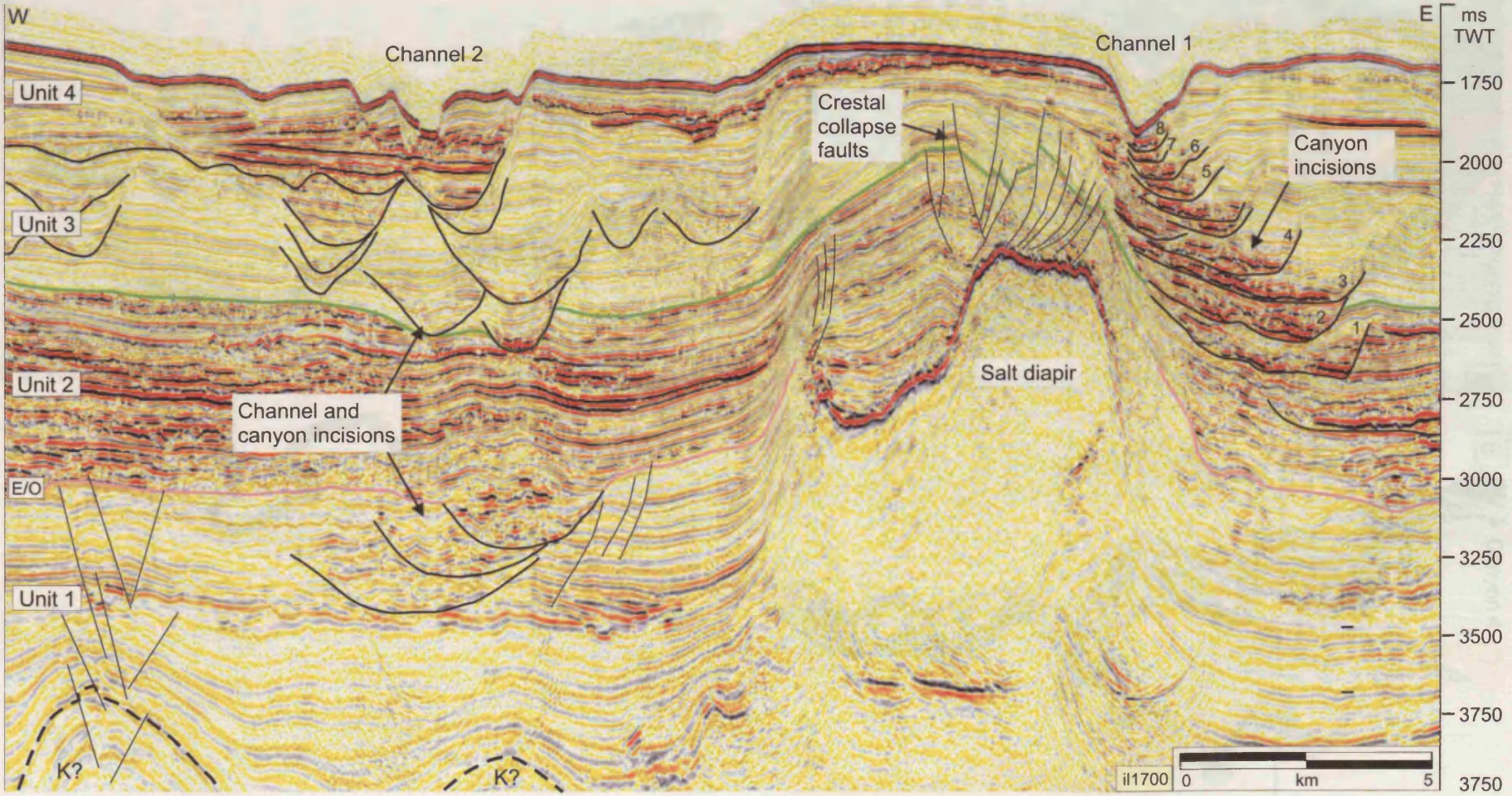

Figure 2.13. A seismic traverse showing the cross-sectional seismic character of the channels and canyons on the Espirito Santo Basin. The canyon system has several phases of incision and infill and has migrated westward. The present day channel 2 shows lateral shift of channel-axis HARs and formation of inner levees. Location of the line in Fig. 2.12A.

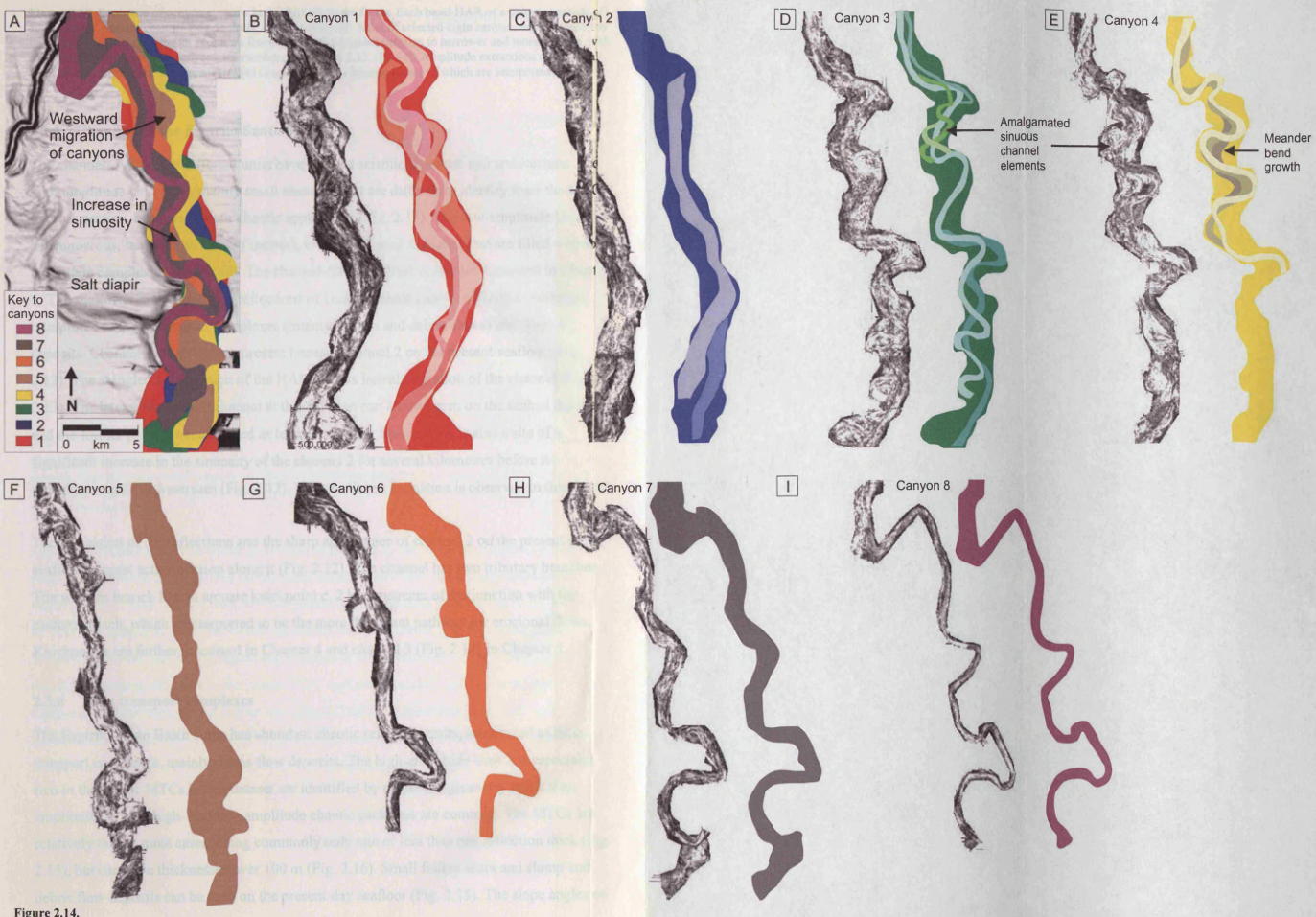
A
Westward migration of canyons
Increase in sinuosity
Salt diapir
Key to canyons
8
7
6
5
4
3
2
1
N
0 km 5
B
Canyon 1
C
Canyon 2
D
Canyon 3
Amalgamated sinuous channel elements
E
Canyon 4
Meander bend growth
F
Canyon 5
G
Canyon 6
H
Canyon 7
I
Canyon 8

Figure 2.14.

Figure 2.14. Evolution of canyon systems in the Espirito Santo Basin. Each basal HAR of a canyon consists of amalgamated sinuous channel-axis deposits. (A) The erosional bases of selected eight canyons superimposed to the seabed dip map showing an evolution from wider and straighter canyons to narrower and more sinuous, with some lateral migration. The canyons are numbered in Figure 2.13. (B) – (I) Amplitude extractions of the basal HAR of the canyons showing amalgamated sinuous channel elements, some of which are interpreted.

2.3.5 Channels in the Espirito Santo Basin

The channels within the different units have various seismic character and architecture. The high-amplitude Unit 2 has mainly small channels that are difficult to identify from the MTCs in cross section, because of their chaotic appearance (Fig. 2.13). The low-amplitude Unit 3 has numerous, large (up to 100s of metres), v- and u-shaped incisions that are filled with low-amplitude complex or chaotic fill. The channel-fill of this unit is further discussed in Chapter 5. The shallower high-amplitude reflections of Unit 4 include chaotic reflection packages, interpreted as mass transport complexes (mainly slumps and debris flows) and channel deposits. Channel-axis HARs are present beneath channel 2 on the present seafloor (Fig. 2.12). The shingled organisation of the HARs shows lateral migration of the channel (Fig. 2.13). The lateral shift of the channel at this location can also be seen on the seabed dip map, and the former paths are manifested as terraces or inner levees. This is also a site of a significant increase in the sinuosity of the channel 2 for several kilometres before it straightens again downstream (Fig. 2.12). No outer levee formation is observed in this dataset.

The truncation of the reflections and the sharp appearance of channel 2 on the present day seafloor suggest active erosion along it (Fig. 2.12). The channel has two tributary branches. The western branch has an arcuate knickpoint c. 2 km upstream of the junction with the eastern branch, which is interpreted to be the more dominant pathway for erosional flows. Knickpoints are further discussed in Chapter 4 and channel 3 (Fig. 2.12) in Chapter 5.

2.3.6 Mass transport complexes

The Espirito Santo Basin slope has abundant chaotic reflection units, interpreted as mass transport complexes, mainly debris flow deposits. The high-amplitude Unit 2 is especially rich in them. The MTCs in this dataset are identified by reflection geometry rather than amplitude, as both high- and low-amplitude chaotic packages are common. The MTCs are relatively thin in most cases, being commonly only one or less than one reflection thick (Fig. 2.15), but can have thicknesses over 100 m (Fig. 2.16). Small failure scars and slump and debris flow deposits can be seen on the present day seafloor (Fig. 2.15). The slope angles on

this part of the seafloor shallow from approximately 2.5° to 1.7°, suggesting the slope angle is not an important factor for failures to occur in the study area.

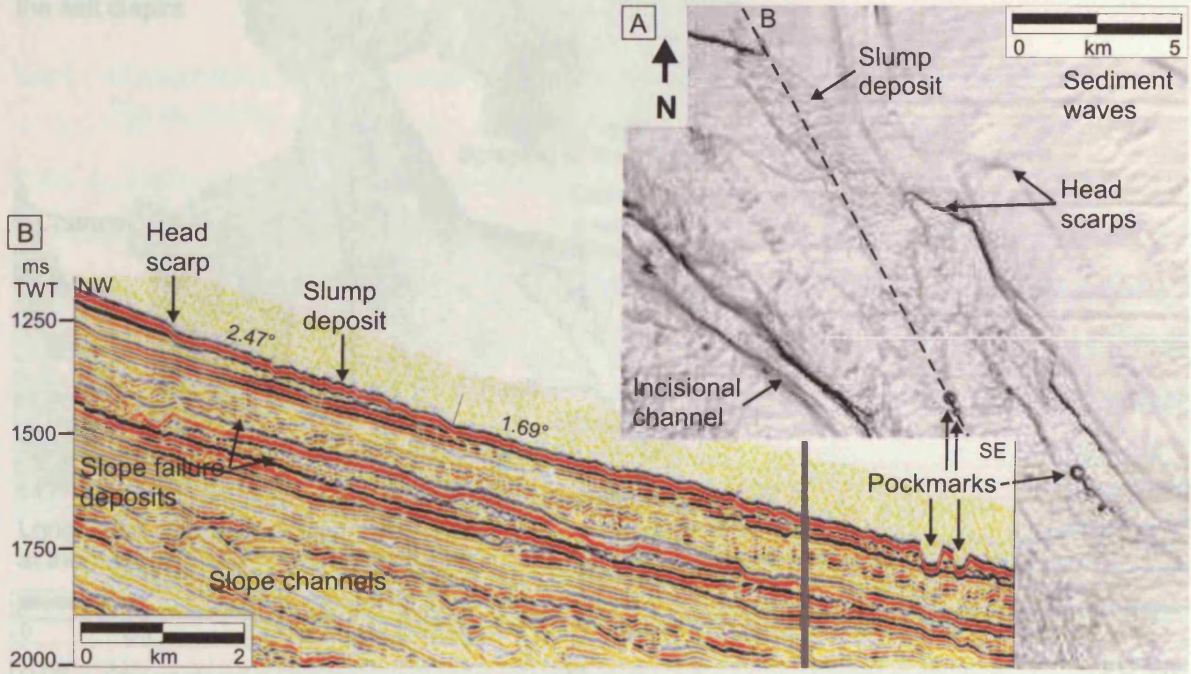

Figure 2.15. Slope failure features near the seafloor on the slope of Espirito Santo Basin. (A) Sea floor dip map showing steep head scarps and irregular surface of MTCs (slump deposits). See location in Figure 2.14A. (B) A seismic traverse showing the cross-sectional expression of a slope failure with a head scarp and a thin deposit with an irregular top surface.

The transport paths of some of the MTCs are controlled by the slope structure. The transport path can be indicated by grooves on the basal surface that curve around and between the salt diapirs (Fig. 2.16A). The grooves are interpreted to have formed by scouring of the seafloor by coherent blocks of sediment within the debris flow. A seismic line across the deposit shows the grooves and also irregular top surfaces of the debris flows (Fig. 2.16B). The parallel reflections adjacent to the lowest MTC unit are truncated, and that truncation may represent a lateral margin of a failure scar (Fig. 2.16B). All the subsequent high- and moderate-amplitude reflections and the MTCs are confined within this corridor, and the strata is undisturbed to the east of it, as if in the 'lee' of the large salt diapir.

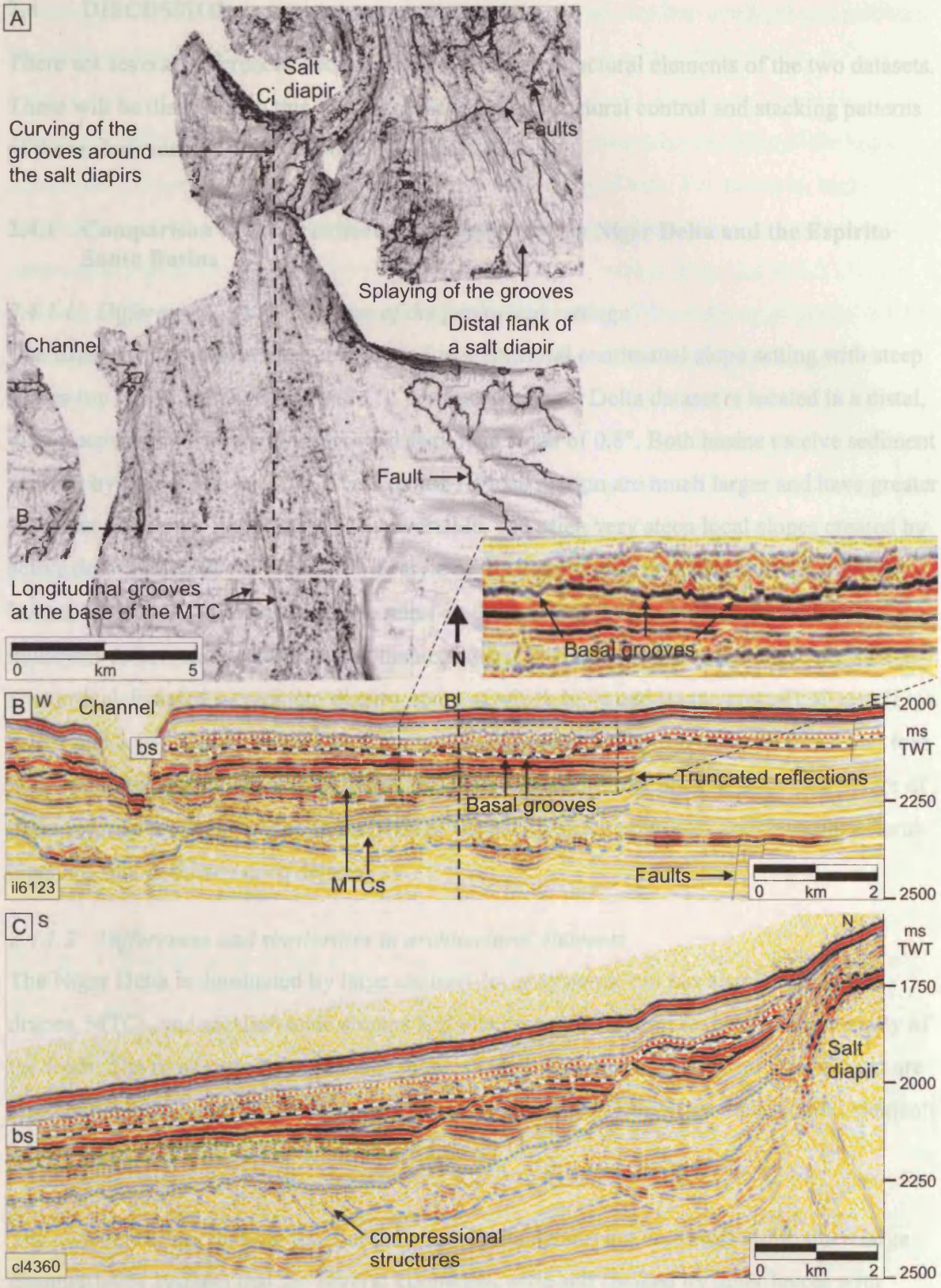

Figure 2.16. Mass transport complexes on the slope of the Espirito Santo Basin. (A) A dip map of a basal surface of a MTC (marked bs in B and C) showing longitudinal grooves that curve around the salt diapirs. See location in Figure 2.14A. (B) Seismic line across the MTC showing the grooves at its base in cross-section. Several MTCs are confined within this corridor. (C) A seismic line showing the cross section along the MTCs. The lowest one shows some internal compressional structures.

2.4 DISCUSSION

There are several differences and similarities in the architectural elements of the two datasets. These will be discussed in this section, as well as the structural control and stacking patterns of these elements and the sinuosity of the channels.

2.4.1 Comparison of the architectural elements of the Niger Delta and the Espirito Santo Basins

2.4.1.1 Differences and similarities of the geological settings

The Espirito Santo Basin dataset is located in a proximal continental slope setting with steep slopes (up to 15° but shallowing to 1°), whereas the Niger Delta dataset is located in a distal, ultra-deepwater delta environment with shallower slope of 0.8°. Both basins receive sediment sourced by rivers, however, the rivers on the African margin are much larger and have greater sediment discharge. Both datasets have variable, and often very steep local slopes created by active deformation of the seafloor. The style of the deformation is different in the different basins, but both styles create positive relief on the seafloor. In the Espirito Santo Basin, the dominant deformation process is salt diapirism, and the majority of the diapirs in the dataset are vertical, isolated piercement diapirs, some of which have undergone crestal collapse (Figs. 2.12B and 2.14). On the Niger Delta, the seafloor is deformed by toe-of-slope thrust and fold belt, which creates ridges normal to the sediment transport direction (Fig. 2.5). The nature of these settings has significance to the style of the sedimentary processes and the architectural elements that dominate each dataset.

2.4.1.2 Differences and similarities in architectural elements

The Niger Delta is dominated by large channel-levee systems, but has also hemipelagic drapes, MTCs, and smaller-scale slumps and other resedimentation features in the vicinity of the folds. The most prominent features in the shallow section of the Espirito Santo Basin are also channels, however, slope failures and MTCs are equally important architectural elements in this dataset, as well as are hemipelagic drapes.

The channels at the shallow level of the Niger Delta dataset are confined within three large channel-levee systems that are several kilometres wide and flanked by outer levees with sediment waves (Figs. 2.4 and 2.5). The channel-fill elements are complex, and include channel-axis HARs, chaotic and passive fill facies, and a number of inner levees. In the Espirito Santo Basin, many small gullies and tributary channels dominate, due to the

proximity of the shelf break and the steep slope. The channels are less confined and no outer levees have developed.

There are some similarities between the channel 2 on the present day seafloor of the Espirito Santo Basin (Figs. 2.12 and 2.13) and the CLSs on the Niger Delta. For example, high-amplitude channel-axis deposits show lateral migration of the channel locally, and inner levee terraces have been formed above previous incisions of the channel (Figs. 2.4 and 2.13). The thalweg of the channel 2 is c. 100 m wide, whereas the width of the thalweg of the Ijebu CLS on the Niger Delta is c. 80 m. Both datasets show evidence of several phases of channel incision and infill.

Although the smaller channels in the Espirito Santo Basin are not confined within levees as on the Niger Delta, some confinement also occurs, and channelised deposits form stacks hundreds of metres thick (Fig. 2.13). The best example of these very long-term sediment transport pathways, active from at least the Oligocene to the Present, is the canyon system on the eastern part of the dataset that has over 10 major phases of incision and erosion. The high-amplitude basal reflections are several kilometres wide and consist of amalgamated ribbons of channel-axis deposits. Mass transport deposits also fill parts of these canyons. This architectural element is found only within the steep slopes of the Espirito Santo Basin, although the basal HARs within the CLSs of the Niger Delta are similar in scale and seismic character.

The mass transport complexes have similar, low-amplitude chaotic seismic character in both datasets, however, also high-amplitude MTCs are identified in the Espirito Santo Basin. The MTCs on the Niger Delta are tens of metres thick and not very common. They occur as extensive sheets or are channelised, most likely plugging existing channel scours within the CLSs (Figs. 2.10 and 2.11). In the Espirito Santo Basin, the MTCs are in general much thinner, although some deposits of several tens of metres thickness are also found. The areal extent of the MTCs in the Espirito Santo Basin is much smaller than on the Niger Delta, but the frequency of their occurrence is much higher (Figs. 2.13, 2.15 and 2.16). They can be defined more easily with more features clearly visible, such as erosional grooves on their basal surfaces. In many cases, the whole feature including slump scar and the related deposit can be identified (Fig. 2.15). Small slope failures like this occur also in the Niger Delta dataset, but they are restricted to the fold limbs (see Chapter 3). The MTCs in both datasets

exhibit some internal structures, interpreted as imbricate thrusts and pressure ridges, and have erosional bases and blocky top surfaces. Therefore it can be suggested, that the processes that formed them are similar, regardless of the differences in settings and scales. The more proximal location and steep slopes of the Espirito Santo Basin make slope failure more likely, and the features better defined due to shorter transport distances.

2.4.2 Structural control on sedimentary systems

Both pre-existing and actively deforming structures have an influence on sediment dispersal patterns and style. The data described in this chapter reveal several examples, where sedimentation is controlled by structure. On the Niger Delta, the Ijebu and Epe CLSs appear to breach through the middle of the frontal fold and the Iwo CLS is deflected southward away from it (Fig. 2.5). The location of the CLSs is not coincidental, however. A transfer zone that coincides with the major Chain Fracture Zone has affected the positioning of the CLSs in the dataset (Morgan, 2004). Furthermore, the location, where the fold is breached by the channels, is the location where the underlying thrust faults change vergence (see Fig. 4.2), and was therefore likely a weak or a low point in the early growth history of the fold, and thus a preferred path for the channels to be positioned. The isoproportional slicing through the CLSs revealed that the deflection of the Iwo CLS by the fold occurred at a late stage of its evolution (Fig. 2.9), and this is interpreted to be as a response of higher uplift rate of the northern part of the fold. The location of the frontal splay was also most likely controlled by structure, based on the observation that in the early stages of the Epe CLS evolution, it was located immediately outboard of the frontal fold, where there was likely a significant break in slope.

Some of the sediment pathways in the Espirito Santo Basin are also clearly influenced by structure. The salt diapirs themselves are located on anticlinal ridges that are orientated in the downslope direction. The channels and the canyon system have been concentrated within the structural lows between these ridges at least since the Eocene (Fig. 2.14). Sediment-gravity flows preferably travel down the path where the slope is steepest. This is well illustrated by the scours at the base of a MTC that curve around the salt diapirs (Fig. 2.15A).

Although minibasin development and ponding of sediment within them is not prominent in either of the datasets, the highest accumulation of sediments is concentrated in the accommodation space created by the structures on both datasets. The synclines between the anticlines on the Niger Delta can have very thick accumulations of sediment (Fig. 2.5 and

Chapter 3), and the development of salt-cored ridges in the Espirito Santo Basin most likely also resulted in the formation of synclines due to salt withdrawal between them, which concentrated the sediment-gravity flows within these structural lows.

2.4.3 Sinuosity of the submarine channels in the study areas

The mechanisms by which sinuosity is established in submarine channels are still being discussed in the literature (Eschard, 2001). The observations of channel sinuosity from the two datasets are discussed below in the context of (1) slope gradients, (2) types of sinuosity and (3) sinuosity evolution. The observations from the Espirito Santo Basin are mainly qualitative, but quantitative observations were made in the Niger Delta dataset.

2.4.3.1 The effect of slope gradients on sinuosity

Deepwater channel migration and sinuosity evolution are complex and sometimes related to sea floor topography. Generally, straight and low sinuosity channels suggest an originally steep slope gradient, whereas higher sinuosity channels form on lower gradients (Fonnesu, 2003; Posamentier and Kolla, 2003).

The effect of slope gradients on sinuosity can be best observed in the Espirito Santo Basin, where the slope gradients change dramatically within the data area. The channels exhibit low sinuosities, where the slope gradients are several degrees, but when the gradient shallows to 1-2°, several prominent meander loops develop along the Channel 2 (Fig. 2.12).

On the Niger Delta, the slope gradient does not appear to affect the present day thalweg sinuosity. The measurements of the sinuosity of the thalweg show no real correlation with slope angles (Fig. 2.6). Two peaks of high sinuosity occur just outboard of folds that have moderate or high topography on the present day seafloor, however, this is more likely to be a coincidence rather than a real relationship, because the rest of the data does not exhibit predicted relationships. The slope gradient may have had some effect on the sinuosity of the channels in the Niger Delta in the earlier stages of their development. The terraces formed on abandoned meander bends are most abundant and largest within the uplifted part of the Ijebu channel-belt, suggesting that the lower gradients caused by the uplift affected the development of high sinuosity at earlier stages of the CLS, when the channels were less confined (e.g. Fig. 2.7).

2.4.3.2 Types of sinuosity

Sinuosity is not just a function of gradient, but it is due to a combination of factors including erosion from turbidity currents, lateral shifting and stacking of channels due to channel filling and incision (Mayall and Stewart, 2000; Mayall et al., 2006). There are several different types of sinuosity, and they have impact on sand distribution within channels (Mayall et al., 2006). Mayall et al. (2006) recognise four categories of sinuosity: (1) initial erosional base, (2) lateral shifting, (3) lateral accretion and (4) sinuosity caused by seafloor topography, e.g. faults and folds.

The erosional fairways of the channel-levee systems on the Niger Delta exhibit low sinuosity, however, the channel-axis deposits within them have high sinuosities (Fig. 2.9). Similar observations can be made from the canyon systems in the Espirito Santo Basin (Fig. 2.14). The sinuosity of the canyons increase as they become younger, however, the channels within the canyons are sinuous throughout the evolution of the canyon system. The sinuosity of these channels and the channels within the CLSs of the Niger Delta seem to be mainly increased by lateral migration and shifting of the channels. Meander bend cutoff decreases sinuosity and produces accommodation space for terraces and inner levees (Fig. 2.7). Meander bend cutoffs are not as common in submarine channels as in their subaerial counterparts (Peakall et al., 2000b; Posamentier and Kolla, 2003). They may have been more common within the Ijebu CLS during times when the channels were less confined, however, evidence of meander bend cutoff can also be observed on the present day seafloor (Fig. 2.17).

The seafloor topography affects the sinuosity of the channels to some extent in both of the datasets. The morphology of the Ijebu CLS changes above the thrust and fold belt (Fig. 2.6). That region has more and larger terraces that were formed by abandonment of large meander bends (Fig. 2.7). Their formation may have been due to the increase in sinuosity on lower gradients that were created by the uplift of the fold belt, or the channel location may have been affected by the emerging folds on the seafloor. This kind of correlation between the seafloor topography and the quantitative measurements of the present day thalweg cannot be made, neither do the present day meander bends correlate to any underlying folds or faults. Some meander bends on a near-seafloor channel of the Espirito Santo Basin appear to be controlled by the location of the salt diapirs, however (Fig. 2.12).

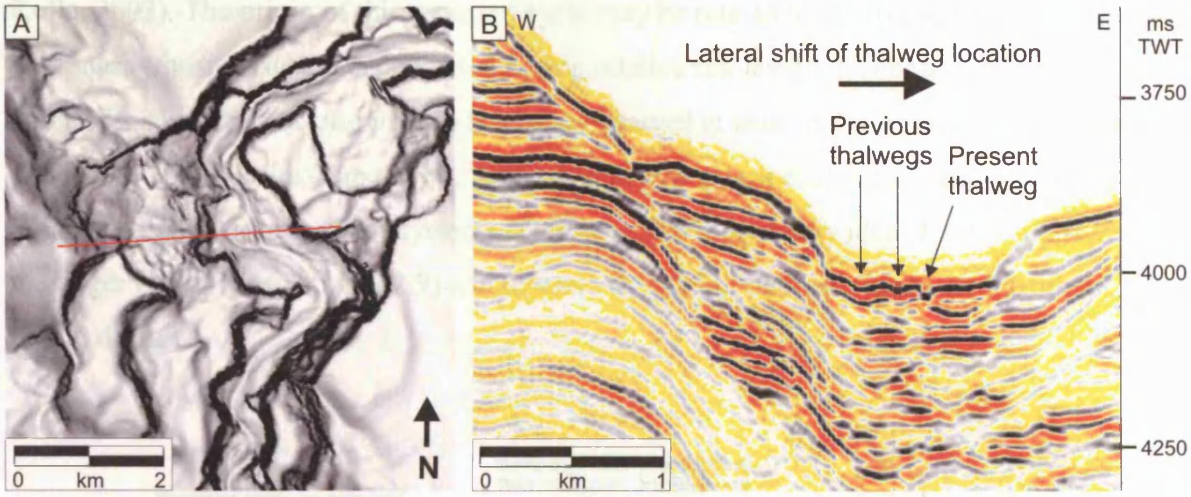

Figure 2.17. Meander bend cutoff at the present day thalweg of the Ijebu CLS, Niger Delta. (A) A dipmap of the seafloor showing the straightening of the present day thalweg in two steps moving eastward. See location in Figure 2.4B. (B) A seismic traverse across the thalweg showing the present course of the thalweg being deeper than the abandoned ones.

2.4.3.3 Sinuosity evolution

The evolution from straight to sinuous is common in submarine channels that have an aggradational history (Kastens and Shor, 1986; Clark and Pickering, 1996; Peakall et al., 2000a; Wonham et al., 2000; Kolla et al., 2001; Deptuck et al., 2003). Peakall et al. (2000a) proposed a three-stage model for the evolution of high-sinuosity aggradational submarine channels. In this model, lateral accumulation and bend growth occurs, until an equilibrium phase is reached. The channel then has a stable planform geometry aggrading nearly vertically until abandonment. As Peakall et al. (2000a) anticipated, this process model may not apply to all submarine channels, as it was derived from aggradational channels, and this kind of evolution is indeed not observed in the channels of the Niger Delta or Espirito Santo basins, except for perhaps in the large scale evolution of the canyon system in the Espirito Santo Basin (Fig. 2.14). It evolves from straight and wide to narrow and sinuous, however, this may be more analogous to the typical evolution of channel-levee systems from wide, erosional fairways to narrow, confined channels, which is also observed in the Niger Delta CLSs, and which Deptuck et al. (2003) interpreted to reflect the changes in gravity flow character, such as velocity and magnitude (Posamentier and Kolla, 2003).

2.4.4 Stacking patterns and facies prediction

Deep-water successions have commonly predictable stacking patterns with mass-transport deposits at the base, overlain by frontal splay deposits and leveed-channel deposits, and finally draped by condensed-section deposits (hemipelagites and pelagites) (Posamentier and

Kolla, 2003). The origin of this repeated cycle may be related to relative sea-level changes with mass-transport deposits deposited during relative sea-level fall (Posamentier and Kolla, 2003). This kind of stacking pattern has been observed at least in the Amazon (Posamentier and Kolla, 2003), Zaire (Droz et al., 2003), Danube (Popescu et al., 2001) and Sao Tomé (Viana et al., 2003) deepwater systems. This pattern is also clearly identifiable on Epe CLS of the Niger Delta (Figs. 2.5 and 2.9) and to some extent, but not completely, by the other CLSs in that dataset.

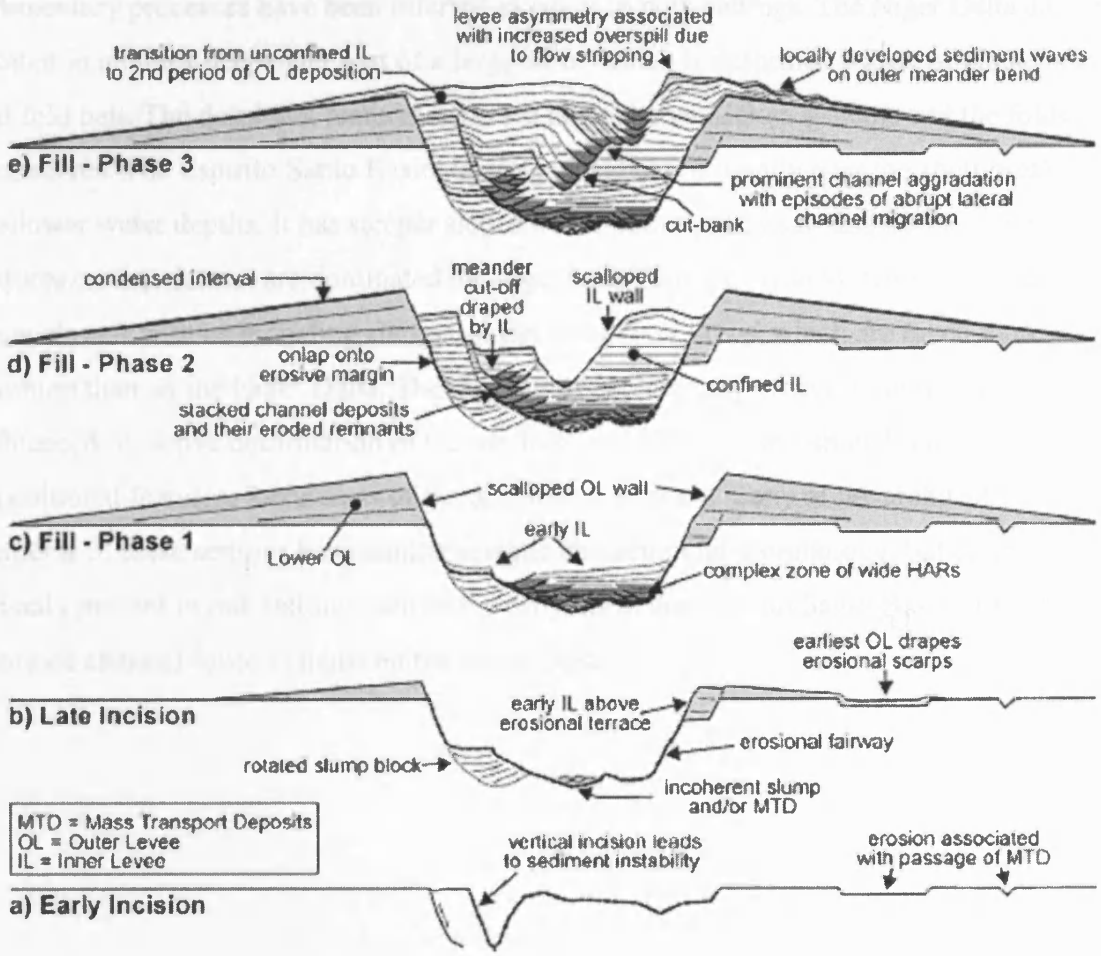

Figure 2.18. Evolutionary stages of Benin-major channel-levee system showing several phases of incision and infill (Deptuck et al., 2003).

The key characteristic of the Ijebu CLS is that it has undergone several phases of incision and infill that have produced a complex stacking pattern within the channel-belt. Erosion, infill and abandonment is a typical evolution path of submarine channels and occurs repeatedly (e.g. Hübscher et al., 1997; Posamentier and Kolla, 2003). The evolution of a submarine channel-levee system with both erosional and depositional components and that is comparable

to the CLSs on the Niger Delta, is described by Deptuck et al. (2003) (Fig. 2.18). The evolution of the CLS starts with the incision of a channel fairway, continues with levee building and infilling of the channel-belt with channel-axis deposits and inner levees until abandonment by a mass transport deposit plugging the remaining depositional relief.

2.5 CONCLUSIONS

The two 3D seismic datasets from opposite margins of the Atlantic Ocean are located in differing structural, stratigraphic and slope-morphological settings, however, similar sedimentary processes have been inferred to occur in both settings. The Niger Delta dataset is located in an ultra-deepwater part of a large delta, which is deformed by toe-of-slope thrust and fold belt. The dominant features there are large channel-levee systems and the folds themselves. The Espirito Santo Basin dataset is located proximally near the shelf break at shallower water depths. It has steeper slopes and is deformed by salt diapirs. Sedimentary features on that dataset are dominated by large, long-lasting canyon systems and small slope channels and failures including slumps, slides and debris flows, which are much more common than on the Niger Delta. The downslope sedimentary processes in both datasets are influenced by active deformation of the seafloor, and both datasets show both erosional and depositional features. Regardless of the differences in scale, many of the architectural elements of these settings have similar seismic character and morphology, but certain features are only present in one setting, such as the canyons in the Espirito Santo Basin or the large, confined channel-levee systems on the Niger Delta.

Chapter 3

3 DEGRADATION OF COMPRESSIONAL FOLD BELTS: DEEPWATER NIGER DELTA

3.1 ABSTRACT

3D seismic interpretation of the toe-of-slope region of the western Niger Delta reveals a range of erosional and depositional features that are the result of the degradation of thrust-propagation folds and include (1) backlimb and forelimb failures that cause debris flows and deposits no more than a few tens of metres thick, (2) large slumps with evidence for internal deformation, (3) more enigmatic ovoid depressions, probably formed as a result of slumping and bottom current erosion and (4) degradation by deepwater channel erosion and channel margin slumping. Thrust-propagation folds in the study area have up to 200 m of relief on the seafloor and are at various stages of degradation and burial. The dominant style of degradation of these folds occurs as retrogradational, small volume failures that form thin deposits at or below seismic resolution. Slope morphology, sedimentology and the presence of anisotropies affect the type of failure that occurs. The backlimb is long and shallow (6°), and the failed sediment masses have longer runout distances than on the forelimb, which has a steeper slope (15°), which abruptly shallows causing the flow velocity to drop. A generic model for fold degradation in this submarine setting is synthesised, and it is predicted that a significant proportion of the sediment deposited in adjacent minibasins has been recycled from the fold crests and is a non-reservoir. Stratigraphic variability means that along-strike and across-fault correlation of deposits and erosional surfaces is difficult at shallow level and highly problematic in buried, potentially prospective, degraded folds.

3.2 INTRODUCTION

Compressional fold belts that typify foreland basins, accretionary wedges and the toe-of-slopes of deltas are a fundamental component of many sedimentary basins. These basins undergo significant modification during fold growth as folds create local relief, and slopes with increased gradients become prone to failure. Fold and thrust belts in deepwater continental passive margins are the focus of recent hydrocarbon exploration, e.g. in Nigeria (Morgan, 2003), Angola (Cramez and Jackson, 2000), Gulf of Mexico (Grando and McClay, 2004), northwestern Borneo (Demyttenaere et al., 2000; McClay et al., 2000; Ingram et al., 2004) and East Kalimantan (Saller et al., 2004). Compressional anticlines are targets for exploration boreholes, and therefore the seismic-based recognition of unconformities formed

by fold degradation and remobilised sediment deposits adjacent to the fold limbs is important. Furthermore, submarine landslides and other types of slope failure are potential hazards for offshore installations.

In submarine slope settings, there is a continuum of gravity-driven resedimentation processes, ranging from rock falls to slumps and slides to viscous debris flows and dilute turbidity currents to pelagic settling (Stow, 1986). Several authors have described and classified these processes (Varnes, 1978; Stow, 1986; Mulder and Alexander, 2001; Lastras et al., 2004). The shear strength of the slope sediment is a function of the cohesion between the grains and the intergranular friction (Stow, 1986), with failure occurring once the shear stress exceeds it. Sediment properties, such as chemical composition, cohesion, and angle of internal friction and the presence of free gas or gas hydrates also affect slope stability (Nigro and Renda, 2004).

Submarine slope failures have common features that are independent of scale. Arcuate headwall scarps commonly form at the upslope reach of a failure and often grade or transform abruptly into a listric shear surface (Varnes, 1978; Prior and Coleman, 1982; Lastras et al., 2004). These shear surfaces often have a lower dip than the seafloor and therefore intersect it (Mello and Pratson, 1999). A scar is left behind if the failed sediment mass is mobilised post-failure and moved downslope. The failed mass, if coherent, commonly exhibits evidence for extensional deformation near the scarp and compressional deformation, such as pressure ridges, near the toe of the deposit. In some cases, blocks of sediment become detached from the main mass of failed sediment and glide further down the slope, forming outrunner blocks (e.g. Lastras et al., 2004). Failed sediment masses are identified from seismic data on the basis of their low-amplitude chaotic reflection pattern (Lastras et al., 2004; Frey Martinez et al., 2005).

Three-dimensional seismic data acquired by the hydrocarbon industry over the compressional domain of the deepwater West Niger Delta allow for the first detailed analysis of the seafloor and subsurface expression of degradation complexes associated with submarine folds. The term "degradation complex" has been used to describe the collapse of footwalls of extensional fault scarps in the North Sea, United Kingdom (Underhill et al., 1997; Berger and Roberts, 1999; McLeod and Underhill, 1999). Given the difficulty in objectively defining the actual

process or processes from seismic data, this term is adopted here, as it encapsulates all modes of sediment failure, transport and deposition in these settings.

The aims of this chapter are to (1) define and describe a range of features that form during fold degradation, (2) illustrate their three-dimensional complexity and the variety of resedimentation styles, (3) demonstrate the role of pre-existing structure and slope morphology in degradation complex development, (4) speculate on the transport mechanism on the basis of specific, objective observations, such as seismic geometry and a general knowledge of sediment properties and (5) synthesize a general model for the evolution of fold degradation phenomena in this geological setting. Subsequently, the chapter provides information essential for understanding the stratigraphic results of to-be-drilled exploration, development and production boreholes that target deepwater compressional folds.

3.3 PREVIOUS STUDIES OF FOLD DEGRADATION

Submarine failures have been widely studied on continental slopes (Prior and Coleman, 1982; Hampton et al., 1996; Locat and Lee, 2002; Canals et al., 2004; Lastras et al., 2004; Sultan et al., 2004; Frey Martinez et al., 2005). Degradation of growing folds, however, has been studied mostly in subaerial depositional settings, where the sedimentary processes can be observed and the key variables measured (Burbank and Raynolds, 1988; Steidtmann and Schmitt, 1988). Folds in subaerial settings are commonly lithified and predominantly degraded by stream erosion and are thus not comparable to submarine settings. Submarine fold degradation has been recognised by previous workers, who have proposed a number of geometric and numerical models to quantify the evolution of compressional structures and the associated syntectonic growth strata that develop on their flanks (Hardy and Poblet, 1995; Storti and Poblet, 1997; Rafini and Mercier, 2002). Many of these models, however, concentrate on fold kinematics and simplify sedimentation and erosion processes and the depositional products. Outcrop analysis of slope degradation and resedimentation caused by fold growth generally allow for a detailed understanding of these depositional products (Nigro and Renda, 2004), but is generally limited by the two-dimensional nature and limited scale of the exposures. Evidence for slumping and other mass wasting of submarine growth folds have been identified e.g. in North Sea (Cartwright, 1989) and northwestern Borneo (Ingram et al., 2004). Nevertheless, to our knowledge, the three-dimensional morphology and stratal geometries created by the degradation of compressional folds in submarine settings at scales from tens of metres to kilometres, have not been described elsewhere.

3.4 GEOLOGICAL SETTING

The Niger Delta is a 12 km thick, regressive Cenozoic delta on the West African passive margin. It is a prolific hydrocarbon exploration and production area, generating increasing interest in the deepwater and the ultradeepwater domains of the delta slope in the past 5-10 years. The Akata, Agbada and Benin Formations (e.g. Doust and Omatsola, 1990; Damuth, 1994; Morgan, 2004) overlie stretched continental and oceanic crust. This article focuses on the ultradeepwater compressional domain of the western Niger Delta (Fig. 3.1A), where the Agbada Formation comprises deepwater channel-levee systems, mass transport complexes and hemipelagic sediments (Deptuck et al., 2003). The delta is divided into three structural domains: (1) an extensional domain dominated by growth faults, (2) a translational domain characterised by mud diapirism and (3) a compressional domain dominated by toe-of-slope thrusts (Fig. 3.1B). This structural configuration is caused by gravitationally-driven delta tectonics, where the Agbada Formation is collapsing on a detachment within the Akata Formation (e.g. Damuth, 1994; Cohen and McClay, 1996; Morgan, 2004).

3.5 DATA AND METHODS

The 3D seismic dataset covers an area of 1630 km^2. It is zero-phase migrated and displayed so that an increase in acoustic impedance is a red-black-red reflection loop. The line spacing is 12.5 m in both inline and crossline direction. For the conversion of two-way-travel time (TWT) to depth, a velocity of 1480 ms^{-1} is used for seawater and 2000 ms^{-1} for sediment. The frequency of the studied shallow section is 55 Hz, and thus the tuning thickness (and thus the maximum vertical resolution) is c. 9 m. It is important to note that the frequency changes with depth, thus buried and older structures would have different geometry. The succession is subdivided using seismic reflections that define units that have distinct internal seismic facies. Seismic attributes, including reflection dip and amplitude, were used to reveal depositional and deformational features.

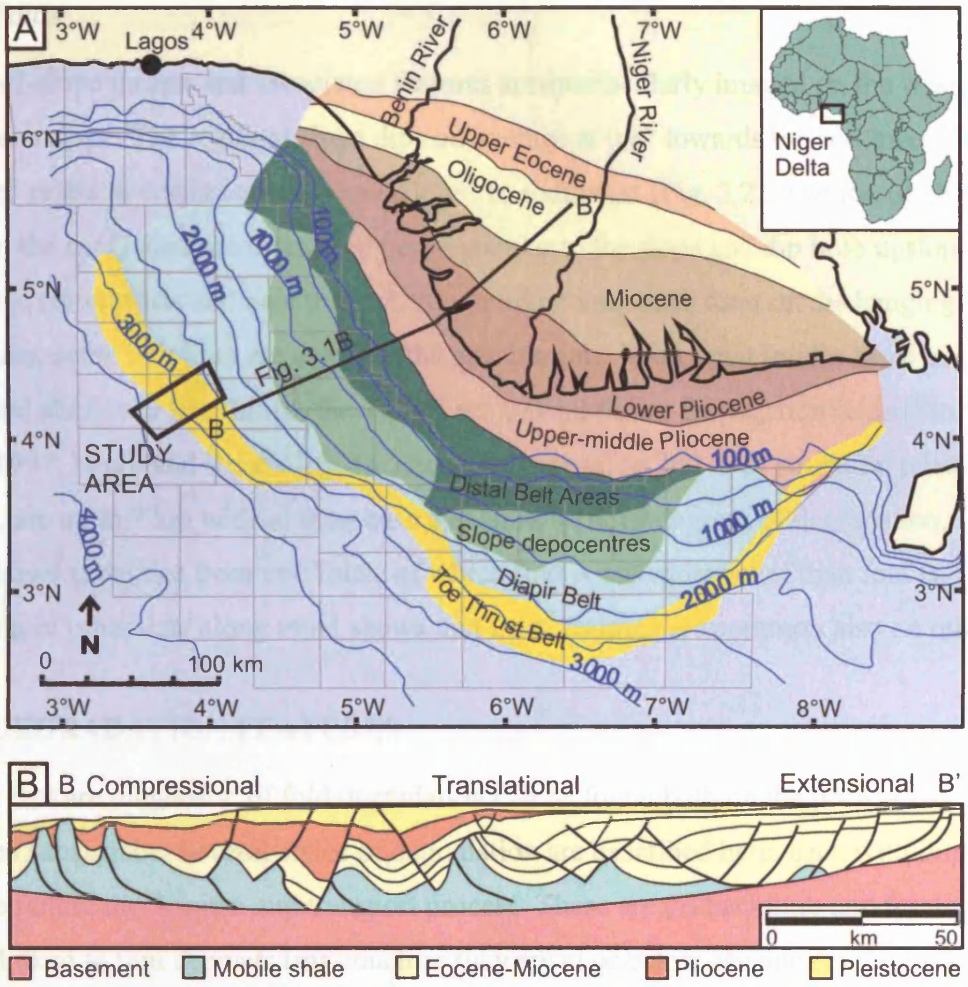

Figure 3.1. (A) Location of the study area in the compressional toe-of-slope thrust belt of western Niger Delta. Depobelts from Armentrout et al. (2000) and Hooper et al. (2002). (B) Simplified schematic cross-section from delta-top to deepwater, after Haack et al. (2000). Vertical exaggeration = 2.

3.6 SEISMIC FACIES AND ARCHITECTURAL ELEMENTS

Typical architectural elements and seismic facies of submarine slopes have been described elsewhere (Deptuck et al., 2003; Posamentier and Kolla, 2003). The lithological interpretation of the seismic facies in this article follows this earlier work and is based on the recognition of seismic reflection character and geometry, as well as unpublished well calibrations within the deepwater domain. The main seismic facies and architectural elements relevant to this study are: (1) low- to high-amplitude, continuous reflections, which can have subparallel, hummocky or divergent geometry and are interpreted as levee deposits and hemipelagic drape and (2) low-amplitude chaotic reflection packages, which are typical of mass transport complexes. High-amplitude channel-fill elements are also very common. A high-amplitude reflection that cross-cuts stratal reflections is noted in the dataset. This bottom simulating reflection (BSR) is considered to be caused by the base of gas hydrate.

3.6.1 Folds

The toe-of-slope thrusts and associated features are spectacularly imaged on the western Niger Delta slope. The regional slope dips on average at 0.8° towards the southwest, therefore "upslope" refers to northeast and "downslope" to southwest (Fig. 3.2). The toe-of-slope thrusts in the study area are orientated perpendicular to the slope and dip both upslope and downslope (forethrusts and backthrusts). Asymmetric anticlines form on the hangingwalls of these faults, some of which are active at the present time. With steep forelimbs adjacent to the thrusts and shallower backlimbs, these folds are typical thrust-propagation folds (Storti and Poblet, 1997; Nigro and Renda, 2004). The folds have up to 200 m of structural relief on the seafloor, are up to 7 km wide at their base and show various degrees of degradation. This article shows examples from two folds, of which fold A has more relief than fold B. Inspection of other data along trend shows that these features are common also on other folds.

3.7 DEGRADATION FEATURES

Features that are diagnostic of fold degradation can be found both on the present day seafloor and in the subsurface. Several styles of degradation are described here, each with implications for slope failure mechanism and transport process. These are (a) backlimb and forelimb failures linked to thin deposits (inasmuch as they are at or below seismic resolution and up to 50 m thick), (b) slumps that show clear evidence for internal deformation and relatively short transport distances, (c) failures associated with ovoid depressions, the interpretation of which remains enigmatic and (d) degradation by deepwater channel erosion and associated channel margin collapse. The creation of erosional truncation surfaces is common to all styles.

3.7.1 Truncation surfaces in folds

Growing folds commonly have truncation surfaces on their crests and limbs (Cartwright, 1989; Hardy and Poblet, 1995; Storti and Poblet, 1997; Rafini and Mercier, 2002). These submarine erosional surfaces can be extensive and indicate that a substantial amount of material has been removed. Degradation of folds A and B (Fig. 3.2) results in the formation of distinct erosional surfaces (Fig. 3.3C). In these examples, the reflections are truncated down to 100 m (Fig. 3.3C). These erosional surfaces are only 300-2000 m wide along strike, and therefore laterally discontinuous. This is caused by their formation mechanism as single small events or a laterally restricted process, e.g. channel erosion instead of a uniform erosional

process across the whole structure. Nevertheless, these erosional surfaces indicate that a large amount of sediment has been removed from the structural highs.

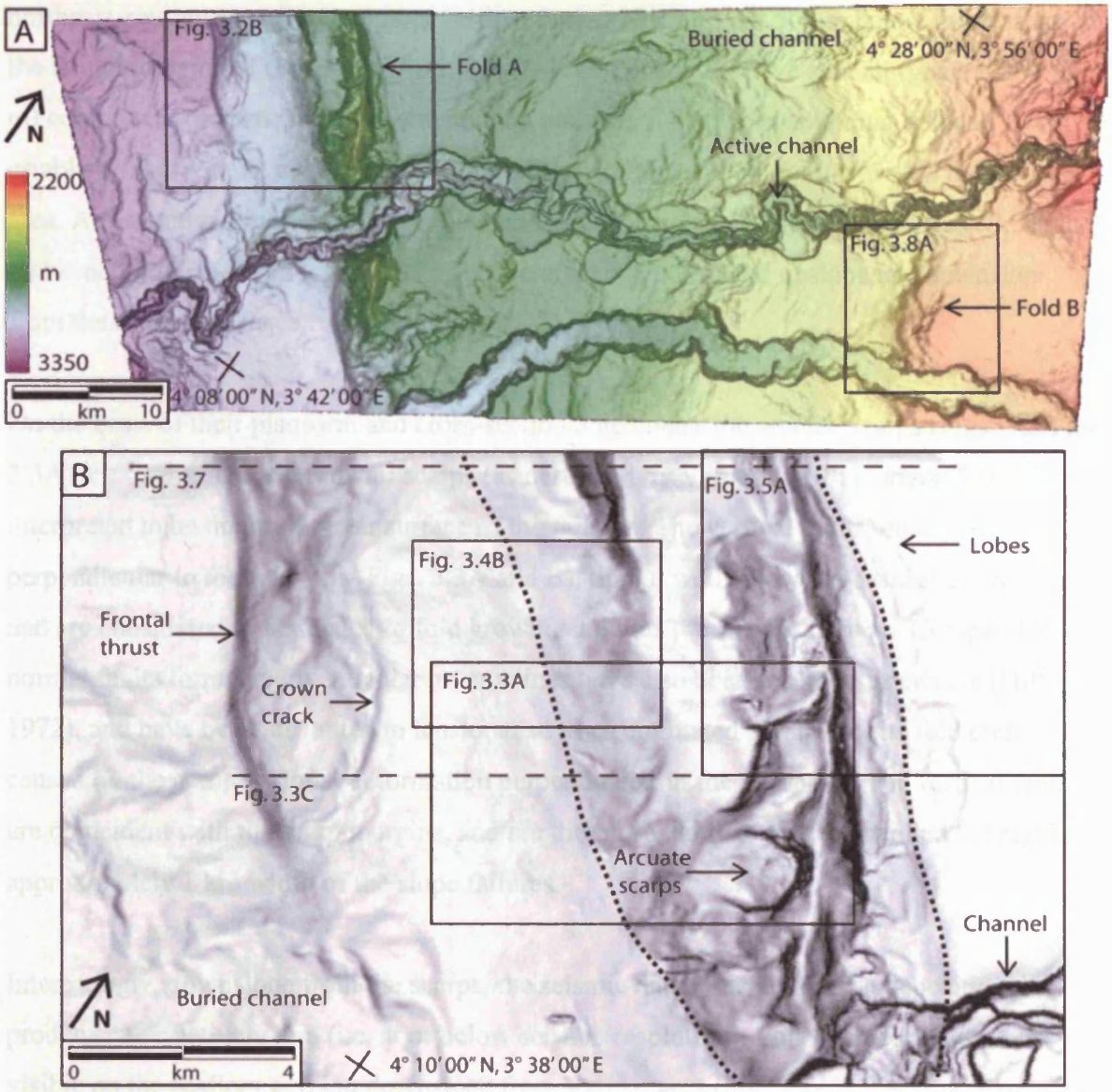

Figure 3.2. Seabed dip magnitude maps showing locations of Figures and folds A and B. (A) Seabed map showing turbidite channels and thrust-propagation folds. The slope dips towards the southwest. (B) Seabed dip magnitude map of the area in which the study is concentrated. Darker colours mean greater dip. Fold A is outlined by a dotted line. Note the arcuate scarps on the southwestern side and lobe-shaped features on the northeastern side.

3.7.2 Backlimb failures linked to thin deposits

The backlimb of fold A is dipping c. 6° towards the abyssal plain. It is dominated by arcuate scarps with thin deposits found downdip of them. The scarps and characteristic deposits are described below.

Arcuate scarps occur on the backlimb of the fold A (Figs. 3.2-3.5). A typical scarp is c. 700-1700 m wide, 10-19° steep and cuts through approximately 100 m of stratigraphy (Figs. 3.3 and 3.4). A cross section parallel to the fold axis dissects the scarps (Fig. 3.3B) revealing northeast-southwest striking, almost vertical faults, which tip out 500 m below the seafloor at the lateral margins of the scarps (Figs. 3.3A and B). The faults have a small (generally < 10 m) component of vertical displacement, with any lateral displacement being difficult to establish. These faults occur only on the backlimb of this and other folds within the study area. A distinctive high-amplitude reflection 50-200 m below the seabed (S in Figs. 3.3B and C) borders truncated reflection packages laterally (Fig. 3.3B) and upslope and downslope from the scarp (packages A and B in Fig. 3.3C).

On the basis of their planform and cross-sectional geometry the arcuate scarps (Figs. 3.2B and 3.3A) are interpreted as headwall scarps (as described by Varnes 1978). Horizon S is interpreted to be the basal shear surface of the failures. The vertical faults, observed perpendicular to the fold axis (Figs. 3.3A and B), tip out well below the basal shear surface and are considered to be related to fold growth, and thus predate the failures. Comparable normal faults formed perpendicular to anticlines have also been recorded elsewhere (Hills, 1972), and have been attributed to tensional stresses orientated parallel to the fold crest caused by the compressional deformation perpendicular to the fold crest. The vertical faults are coincident with the scarp margins, and are therefore likely to have controlled the regular approximately 1 km width of the slope failures.

Interestingly, downslope from the scarps, the seismic data indicate that the depositional products are relatively thin (i.e. at or below seismic resolution). Lobe-shaped features are visible on the seafloor c. 6 km downslope from some scarps (Fig. 3.3A). They correlate with a slight thickening and lowering of amplitude of a reflection near the seafloor (Fig. 3.3D). They are interpreted as thin (<10 m) deposits of sediment that failed on the fold and were then transported as a debris flow. The limited thickness with respect to seismic resolution of these deposits makes it difficult to correlate lobes with scarps, and many thin deposits are probably unresolved by the seismic data. Although the above interpretation is preferred, the absence of obvious depositional products could also be caused by erosion or very long transport distances (>20 km), so that the failed sediments now lie outside the area covered by the dataset.

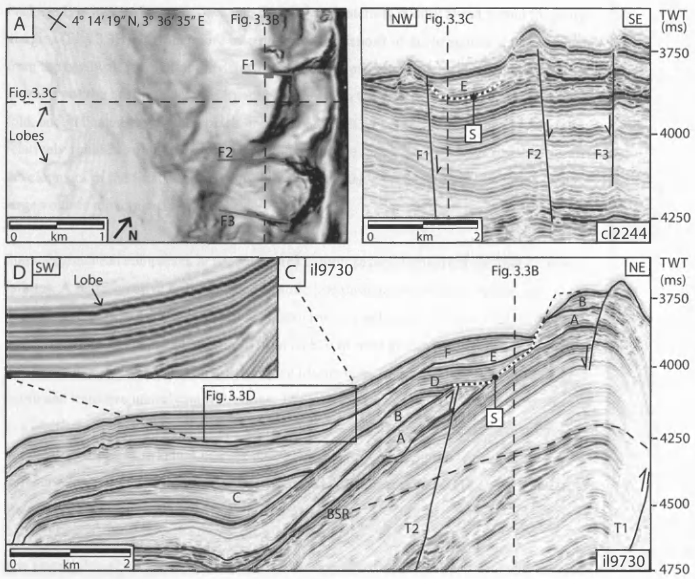

Figure 3.3. Degradation of a backlimb. (A) Dip magnitude map of seabed showing arcuate scarps on the backlimb and lobe-shaped features downslope from them. Darker colours mean greater dip (0-20°). F1-F3 = faults. (B) A section across the scarps showing subvertical faults at the margins of scarps, also marked in (A). Horizon S, marked with white dashed line, is the basal shear surface of failure. (C) A dip-orientated seismic line across a scarp. The wedge-shaped chaotic package E is the deposit of a degraded headwall scarp (also visible in B), the original geometry of which is interpreted in a black dashed line. The packages A and B are truncated by the basal shear surface S and subsequently onlapped by packages D and F. The reflection geometry at the intersection of A and S is repeated in many places in the stratigraphy, e.g. in package C. BSR = bottom simulating reflection, T1 and T2 = thrusts. (D) Thin deposit of failed sediment is represented as a slight thickening and lowering of amplitude at seabed. It correlates with a lobe-shaped feature visible on seabed (A). See location in Fig. 3.2B.

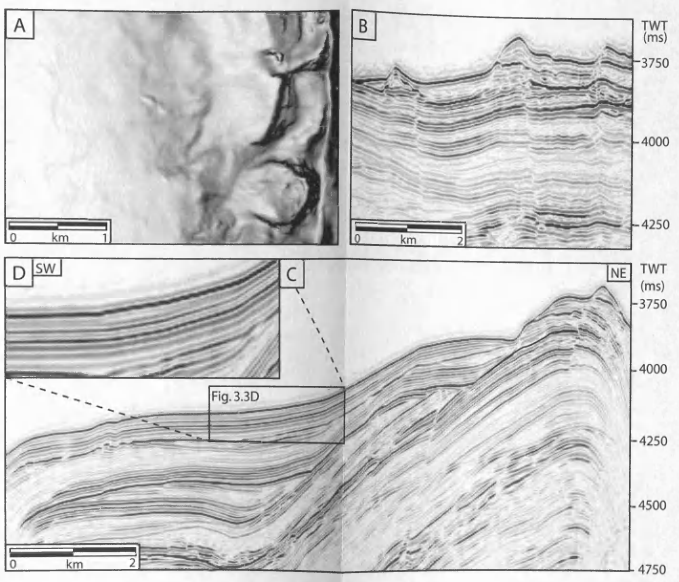

Figure 3.3. Uninterpreted.

Other examples of thin failure deposits on the backlimb consist of low-amplitude, chaotic wedge-shaped seismic reflection packages. For instance, seismic package E (Figs. 3.3B and C), which has a maximum thickness of 30 m and volume of 6 x 10^7 m^3, is located at the foot of the headwall scarp. The basal shear surface of previous failures (horizon S) is onlapped by packages D and F, which are interpreted as levee and hemipelagic deposits respectively.

Package E is located between packages D and F and laterally is only found within the scarp margins (Fig. 3.3B). It is therefore interpreted as the deposit of failed sediment that originated from the headwall scarp after the deposition of D and prior to the deposition of F. The original geometry of the headwall scarp is interpreted based on the geometry of other scarps on the fold, and indicated as a dashed black line in Figure 3.3C. Failures from the head scarp are relatively small in volume relative to the volume of the final scar, which suggests a protracted development of the final scar due to multiple retrogressive failure events, instead of a single large volume movement.

Some degradation complexes in the study area exhibit several typical characteristics of slope failures. A representative dip-orientated seismic line through one of them reveals an approximately 55 m thick low-amplitude discontinuous reflection package 80 m below the seabed (Fig. 3.4). It is located downdip from an 850 m wide arcuate headwall scarp with a maximum dip of about 19°. The basal surface (dashed line in Fig. 3.4A) of the deposit is listric and truncates underlying reflections. The package thins downdip, where it corresponds to a high-amplitude reflection with a 'corrugated' cross-sectional geometry. In planform, these corrugations form ridges that are clearly visible on a dip magnitude map of the top reflection (dotted line in Fig. 3.4B). The ridges exhibit a maximum height of 11 m and have a crest-crest wavelength of approximately 100 m.

The feature described above is interpreted as the deposit of a mass failure, probably a debris flow, mudflow or slump, with the ridges being pressure ridges comparable to those described by Prior and Coleman (1982) and Nemec (1990). Ridges occur in some but not all examples of thin backlimb failure deposits in the study area.

The types of failure on backlimbs described in this section result in a distinctive reflection configuration, which comprises of reflection packages that are truncated upslope at an almost horizontal angle (A and B in Fig. 3.3C). Subsequent reflections are draped on this truncation. This pattern is repeated throughout the stratigraphy of the backlimb, e.g. in package C (Fig. 3.3C), which is truncated both upslope and downslope. These geometries are not laterally continuous and are thus significantly different from the typical models of growth stratal geometries.

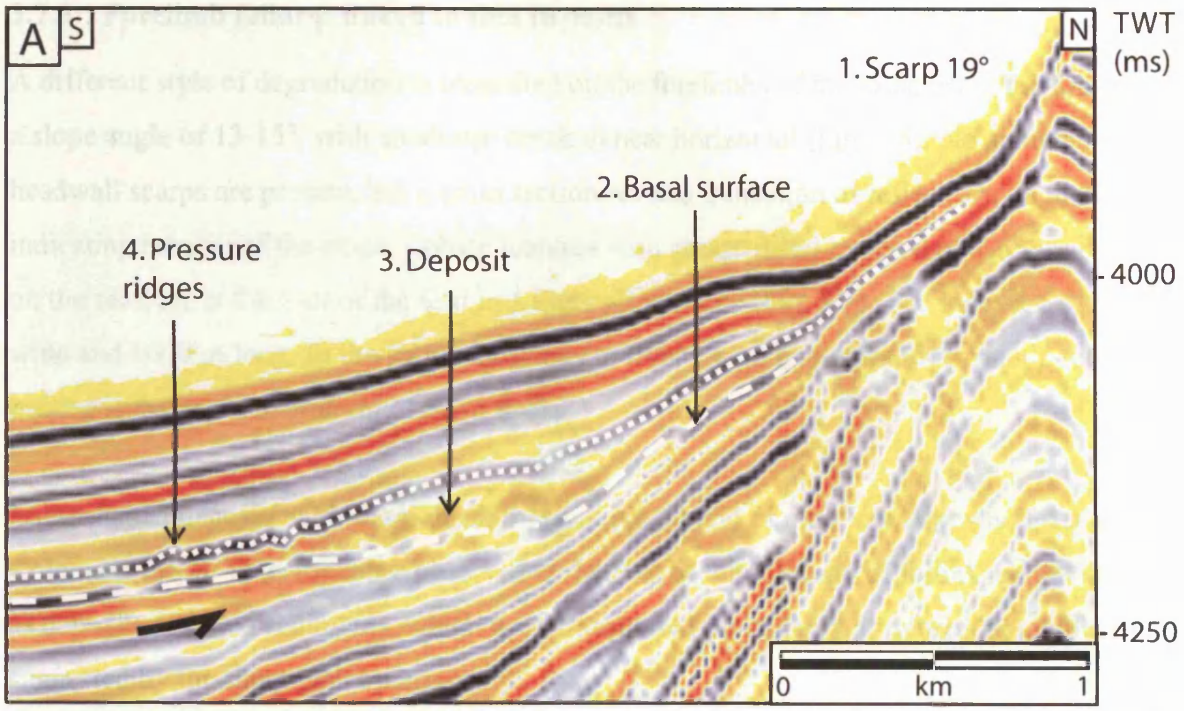

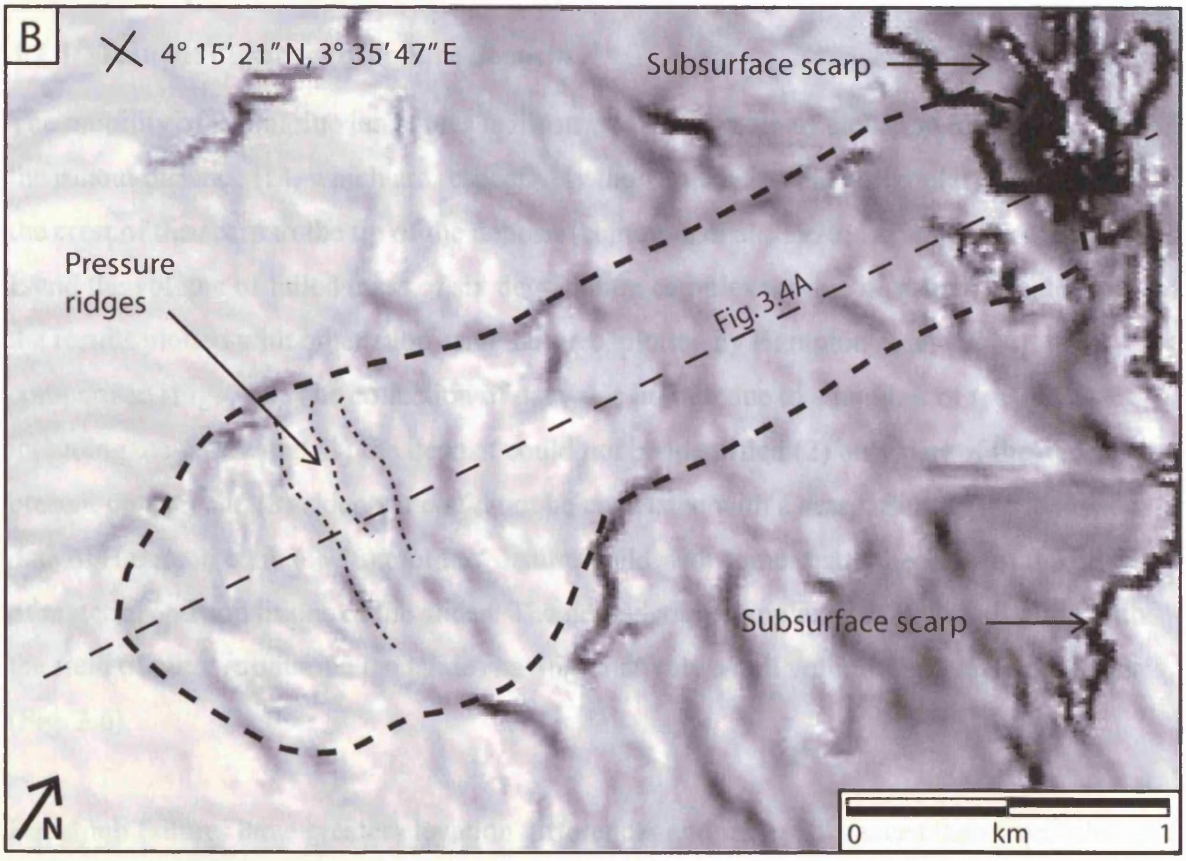

Figure 3.4. (A) A representative seismic line along the middle of a degradation complex showing all typical features: (1) arcuate headwall scarp, (2) listric basal surface truncating reflections beneath it (dashed line), (3) chaotic, low-amplitude deposit buried under 80 m of levee and hemipelagic sediments (between dashed and dotted line) and (4) pressure ridges, visible as corrugations in the top horizon (dotted line). TWT = two-way travel time. (B) A dip magnitude map of the top horizon of the deposit showing pressure ridges at the toe of the deposit. The deposit is outlined with a dashed line. See location in Fig. 3.2B.

3.7.3 Forelimb failures linked to thin deposits

A different style of degradation is identified on the forelimbs of the folds. Here the fold A has a slope angle of 13-15°, with an abrupt break to near horizontal (Fig. 3.5). No arcuate headwall scarps are present, but a cross section reveals truncation of reflections on the fold indicating erosion of the slope. Lobate features with abrupt distal margins of 2-6° are present on the seafloor at the foot of the fold in a footwall syncline (Fig. 3.5). The lobes are c. 2000 m wide and 1000 m long. In the subsurface, they correlate with low-amplitude chaotic reflection packages that are a maximum of 30 m thick.

Lobe-shaped deposits with sharp distal margins are typical of mudflow deposits (Prior and Coleman, 1982). Thus the lobes observed at the foot of the forelimb of fold A are interpreted as deposits of failed sediments, which were transported most likely as debris- or mudflows, as suggested by the sharp distal margins.

3.7.4 Runout distances of failure deposits

The mobility of submarine landslides is illustrated by the ratio of elevation difference (H) and the runout distance (L), which are respectively the vertical and the horizontal distances from the crest of the scarp to the tip of the deposit (Hampton et al., 1996; Locat and Lee, 2002). H, L and the volume of failed mass of six degradation complexes were measured (Table 3.1) and the results plotted with other submarine failures, plotted by Hampton et al. (1996), for comparison (Fig. 3.6). The collection of data was limited due to a number of reasons including the following: (1) the deposit could not be identified (2) only part of the deposit was present on data and (3) a deposit could not be correlated with a scarp. Submarine landslide data of Hampton et al. (1996) plot in a distinct field with some scatter because of the diversity of material and conditions of the slides. The degradation complexes of this study fit in with the field of other submarine landslides having relatively small volumes and high H/L ratios (Fig. 3.6).

Backlimb failures have greater elevation differences and runout distances than forelimb failures (Table 3.1). The H/L ratio is also higher for backlimb failures (0.1) than forelimb failures (0.07), and they plot higher on the graph (Fig. 3.6). It has been suggested that H/L ratio can be used to distinguish the transport mechanism from translational slides (< 0.15) and rotational slumps (> 0.33) (Mulder and Alexander, 2001). The data (Table 3.1, Fig. 3.6)

suggests that the degradation complexes measured for this work are translational slides. However, if the failed sediment mass have transformed into plastic flows (e.g. debris flows), that classification would be inappropriate.

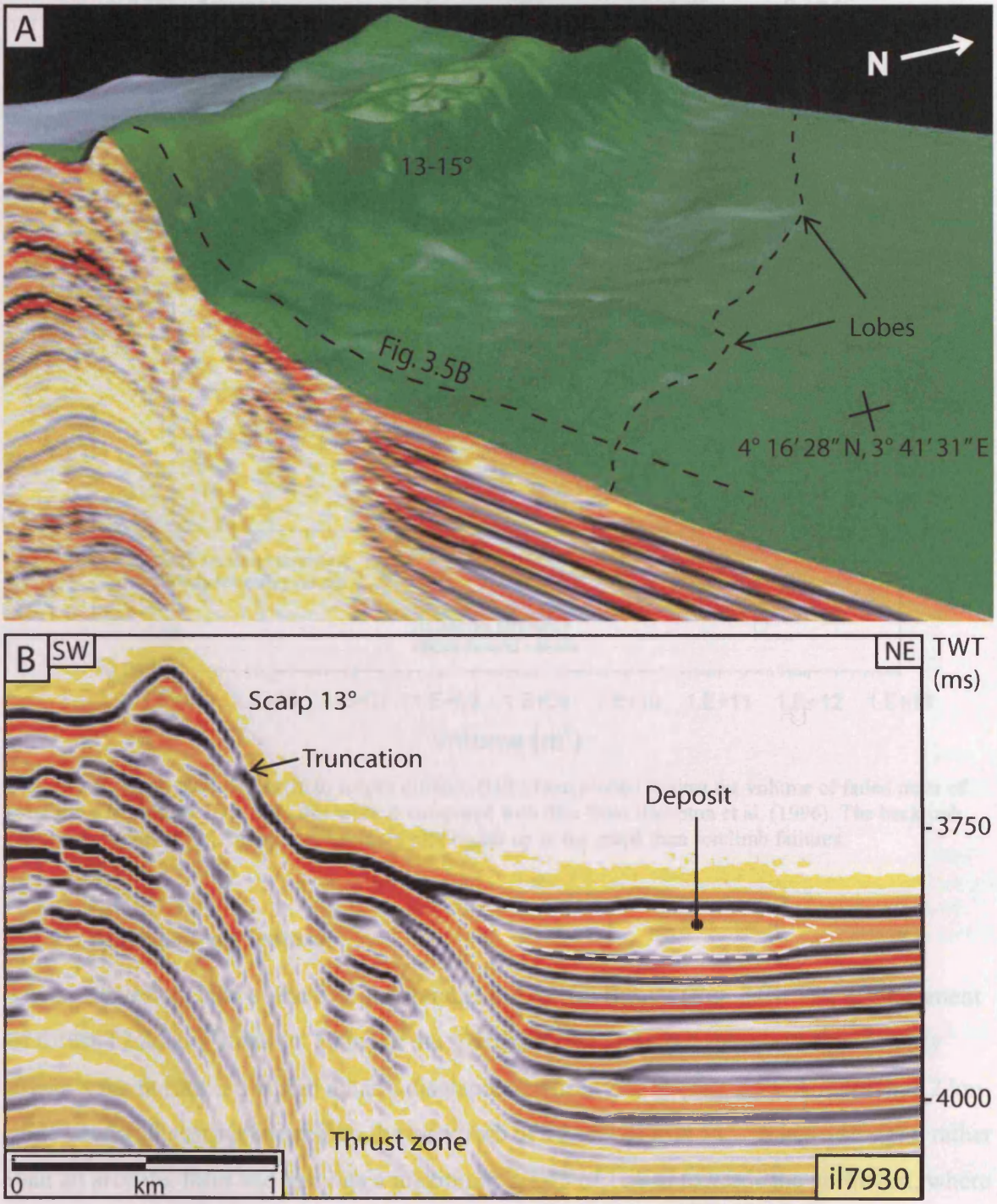

Figure 3.5. Degradation of a forelimb. (A) Oblique view of the seabed on the forelimb side showing the 170 m high fold, which is dipping 13-15°. The lobes at the foot of the fold are wide and short (2 by 1 km). (B) A representative seismic line across the forelimb. The reflections are truncated at the scarp. The low-amplitude package at the foot of the fold (outlined by dashed line) is the deposit of failed sediment. In the subsurface the reflections are disturbed due to steep angle of strata and fracturing by thrust. TWT = two-way travel time.

Table 3.1. Height, runout distance and volume of some degradation complexes of this study.

	H (m)	L (m)	Volume (m^3)	H/L ratio
backlimb 1	227	1950	$6.00*10^7$	0.1163
backlimb 2	365	3125	$6.16*10^7$	0.1166
backlimb 3	508	6300	$2.82*10^7$	0.0806
Average	***366***	***3792***	***$4.99*10^7$***	***0.1045***
forelimb 1	172	2275	$4.01*10^7$	0.0756
forelimb 2	178	2425	$6.23*10^7$	0.0735
forelimb 3	227	3600	$1.95*10^7$	0.0631
Average	***192***	***2767***	***$4.06*10^7$***	***0.0707***

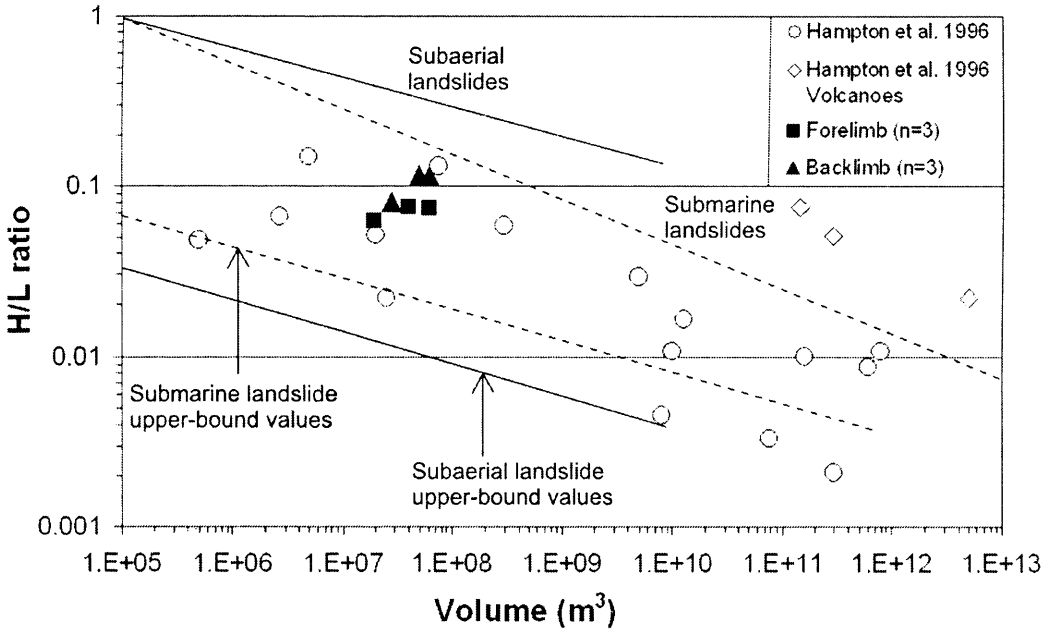

Figure 3.6. Graph showing height to runout distance (H/L) ratio plotted against the volume of failed mass of submarine landslides. Data from this work is compared with data from Hampton et al. (1996). The backlimb failures have higher H/L ratios, and therefore plot higher up in the graph than forelimb failures.

3.7.5 Buried slump feature

The northwestern part of the fold A is comprised of two thrusts (Fig. 3.7). The displacement of thrust T2 is very small (c. 10 m) in the southeast (Fig. 3.3), but increases significantly towards the northwest, where it has a displacement of c. 200 m (Fig. 3.7). A more than 2 km wide headwall scarp is located on the backlimb of T2 and dips at 11°. It has a straight, rather than an arcuate, form and exhibits a maximum height of 165 m towards the northwest, where it meets the outer extent of the data coverage.

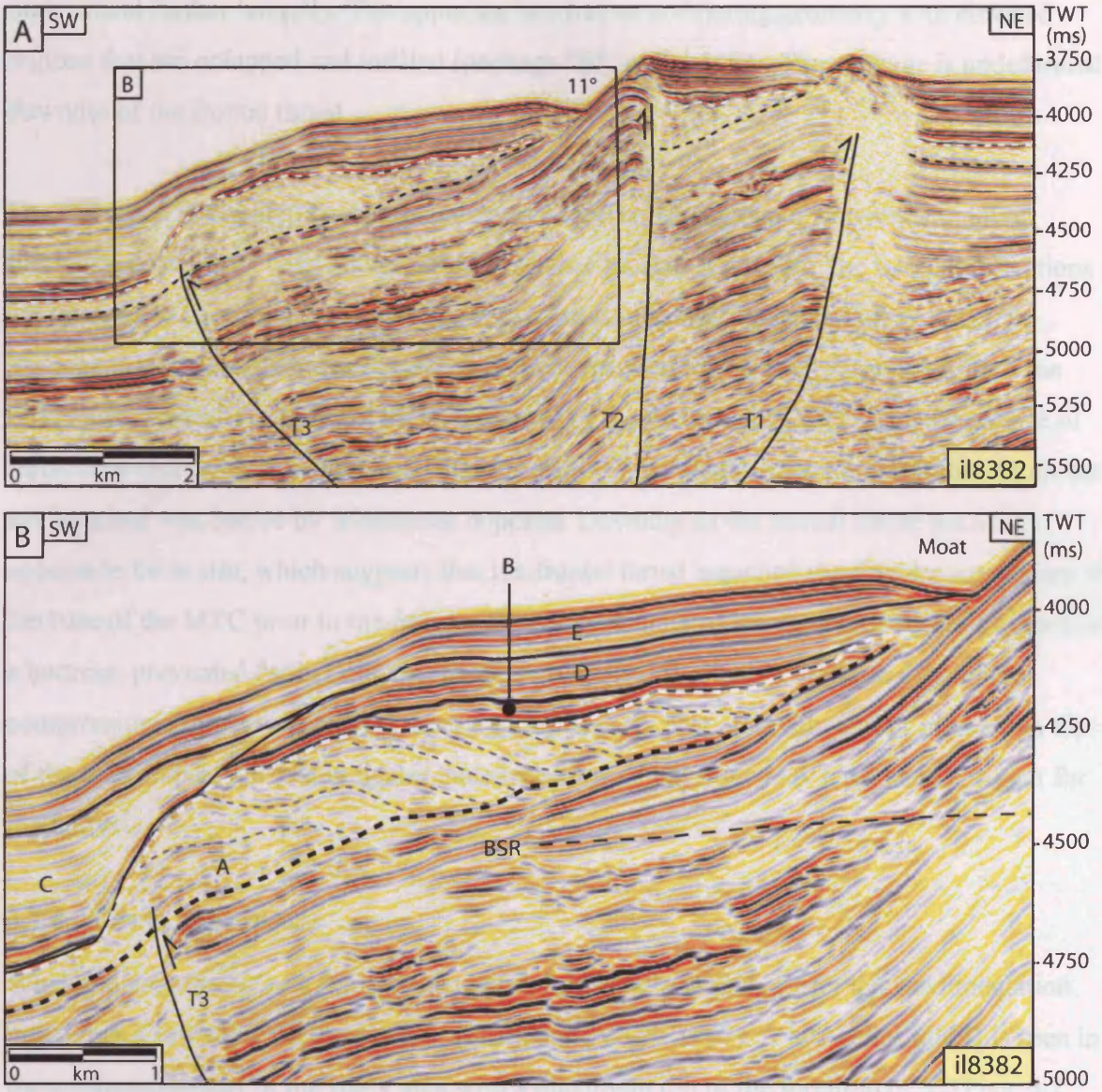

Figure 3.7. Degradation by slumping. (A) A representative seismic line across the fold A composed of two backthrusts T1 and T2 and a frontal thrust T3. The base of the MTC is marked with black dashed line, the top with a white dashed line. The slump is located between T3 and T2 and buried underneath levee and hemipelagic deposits. (B) Slumped unit A showing internal reflections interpreted as thrusts that formed as the movement along basal surface ceased. Subsequent reflections infill and smooth out the geometry (B-E). The moat adjacent to the scarp is thought to have formed by bottom current activity. TWT = two-way travel time.

Seismic package A has a distinctive, low-amplitude chaotic reflection character and it can be traced over most of the seismic volume (Fig. 3.7). Its spatial extent and seismic facies is consistent with it originally being a much more extensive mass transport complex that was deposited on this part of the delta slope. It is generally 60-70 m thick and buried under c. 260-380 m of sediment. Downdip of the scarp, however, its thickness increases to a maximum of 220 m between the frontal thrust and T2 (Fig. 3.7). Here the package shows internal upslope-dipping reflections, which have a regular spacing of c. 60 m and form an imbricate duplex geometry. The feature is at least 1 km wide, but because it is located at the edge of the data, it

may extend further laterally. The upper surface has an undulating geometry with elevated regions that are onlapped and infilled (package "B" in Fig. 3.7B). The package is undeformed downdip of the frontal thrust.

The feature is interpreted as a mass transport complex deposit that underwent slumping following deposition, with the detachment surface located at its base. The internal reflections are interpreted as imbricate thrusts that formed as downslope movement of the sediment package on the detachment surface ceased. This is supported by the c. 60 m spacing of the reflections, which is equivalent to the thickness of the undeformed MTC. The occurrence of reflections that onlap the undulating upper surface of the slump suggests that it formed on the seafloor and was buried by subsequent deposits. Downdip of the frontal thrust the MTC appears to be *in situ*, which suggests that the frontal thrust breached the detachment surface at the base of the MTC prior to the failure. This discontinuity of the detachment surface acted as a buttress, prevented further downslope movement, and resulted in the formation of the compressional thrust structures at the toe of the deposit. The relatively abrupt increase in dip of the backlimb of the fold indicates that steepening of the slope may have been a trigger for the failure.

3.7.6 Ovoid depressions

When the growth rate of a thrust-propagation fold is only slightly faster than sedimentation rate, it has a low relief on the seafloor (Storti and Poblet, 1997). A low-relief fold B is seen in the northeastern part of the study area with a maximum dip of the forelimb of 5° (Figs. 3.2 and 3.8). Its degradation character is different to that of the fold A. Localised low-amplitude zones of disruption radiate upwards in the core of the fold (Figs. 3.8B and C). These are interpreted as radial faults that formed due to extension caused by the fold growth and are common in other submarine growth folds (e.g. Ingram et al., 2004). Wrench faults at the lateral margin of the thrust reach the seafloor indicating recent movement on the thrust (Fig. 3.8A).

Several 300-700 m long oval depressions are found on the seafloor above the fold B with small seafloor expression (Fig. 3.8). The depressions occur above the crest or on the backlimb (upslope) of the fold. They have rounded appearance and are elongate parallel to the fold axis. Some depressions have walls truncating stratigraphy to about 100 m at a maximum angle of 16° (X in Fig. 3.8C). Similar reflection truncations are found in the subsurface (Z in Fig.

3.8C). Other seabed depressions are much shallower and located above listric zones of reflection truncations in the subsurface (Y in Fig. 3.8C). The shaded reflection package in Figure 3.8C consists of continuous parallel reflections to the east of fold B and divergent reflections showing offlap to the west. Between depressions X and Y the package forms a small upslope-dipping wedge (M) that consists of chaotic reflections.

The ovoid depressions may have formed by several processes. They may be (1) rotational failures on a listric decollement, (2) a result of bottom current activity, (3) possibly a combination of both processes, or (4) pockmarks associated with escaping gas. The depth, down to which reflections are cut by the depressions, is in all cases 100 m, therefore it can be assumed that this is a critical depth for a failure. A weak layer may exist at that depth e.g. because of dewatering and overpressure generation. The low-amplitude wedge M is interpreted as a deposit of mass failure. Depression Y is thus the seafloor expression of a buried headwall scarp at depth. Alternatively, the depressions may have been formed by current activity. This is supported by the roundedness of the depressions and evidence of current activity in the form of sediment waves on the seafloor (Fig. 3.8A). In addition, depression X does not have any detectable deposit downdip from the scarp, which may suggest it formed as a result of current scouring. Bottom currents are known to erode steep scarps on their path e.g. in Judd Deeps in the Faeroe-Shetland Channel (Smallwood, 2004). Currents may accelerate locally and scour more effectively when they encounter an obstacle in their path or the slope flattens (Nemec, 1990). Fold B would be such an obstacle.

Pockmarks on the seafloor above toe-thrust anticlines in northwest Borneo have been attributed to upward migration of thermogenic gas (Demyttenaere et al., 2000). During fold growth the outer arc of the fold experienced tensional stresses that are manifested by fold-crest faults that have an upward radiating geometry in cross section. These faults could provide migration paths for gas (Ingram et al., 2004) and cause pockmarks on the seafloor. However, in this case, the geometries of depressions X and Y are more consistent for the ovoid depressions to be the result of a combination of mechanical failure and bottom current activity.

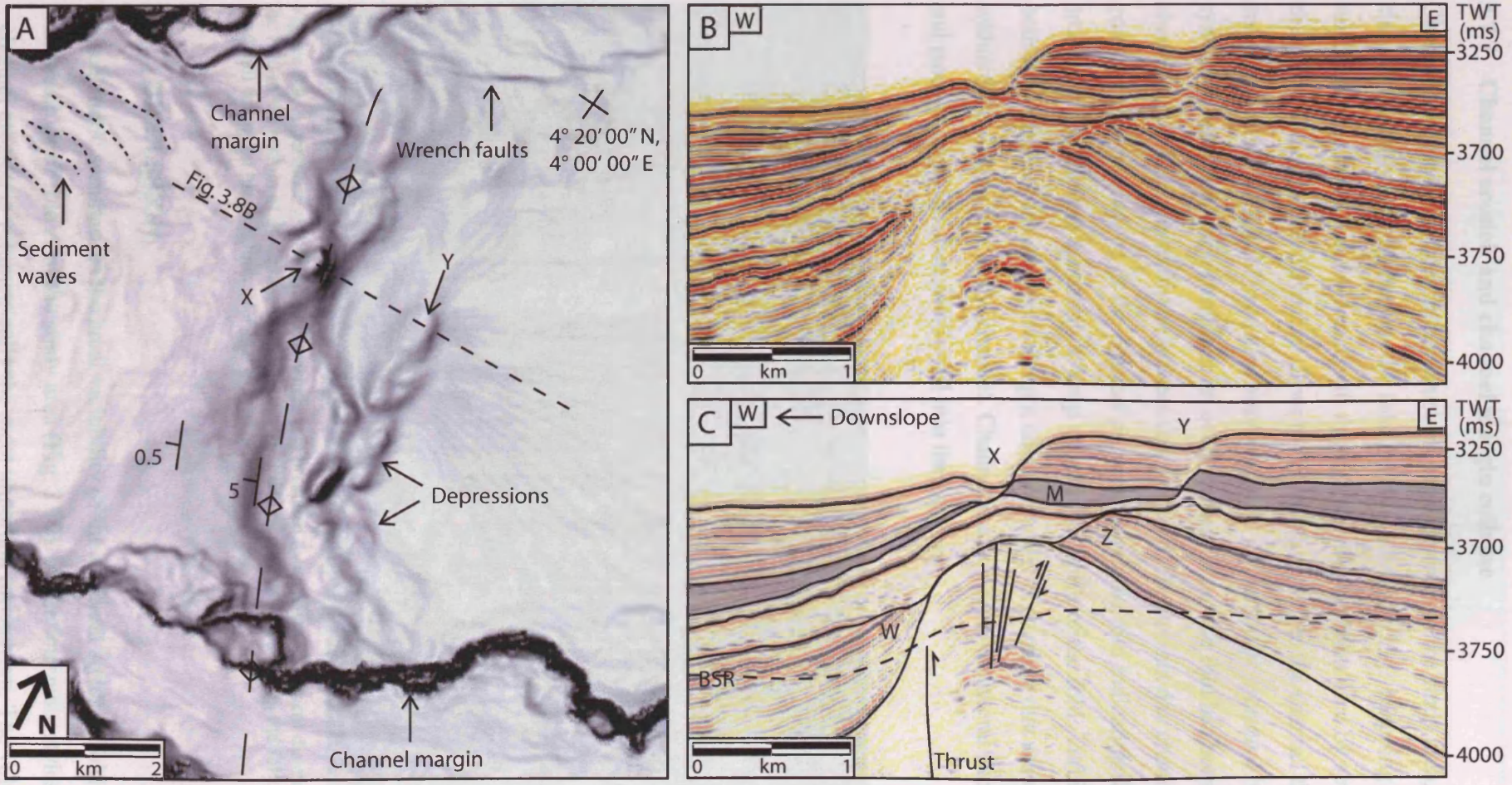

Figure 3.8. Degradation of fold B with only minor seafloor expression. (A) Seabed dip magnitude map showing oval depressions that occur on and upslope of a fold crest. Note the sediment waves near the active channel and wrench faulting caused by thrusting. (B) Representative seismic line with interpretation (C) across two oval-shaped depressions (X and Y). Reflections are truncated down to 100 m at X. The depression Y is located above a listric zone of reflection truncation at subsurface. Similar geometry can be found deeper in the section (Z). The package M (shaded grey) is interpreted to have failed with a buried headwall scarp below Y and deposit of failed sediment between X and Y. BSR = bottom simulating reflection. Note also radial faults in the core of the fold. TWT = two-way travel time.

3.7.7 Channel erosion and channel margin collapse

Channel-levee systems breach the thrust-propagation folds in the study area, with an active channel currently cutting through the fold A (Figs. 3.2A and 3.9). Mapping of channels in the subsurface indicates that the same path through the fold has been used by several buried channels. The elevation difference from the crest of the fold to the channel thalweg is 420 m and the volume of the fold eroded is approximately 1.3 km^3. The erosional base of the channel system is, however, buried and thus an even greater part of the fold has been eroded by channels than is apparent on the present day seafloor. The present day channel thalweg gradient does not change as the channel passes through the fold indicating that the rate of erosion of the channel is enough to keep up with the uplift of the fold. Turbidity currents can both erode and deposit sediment along a channel, and it is possible that erosion occurs mainly within the uplifting part of the channel. Channel erosion removes lateral support for sediment and parts of the fold subsequently fail into the channel.

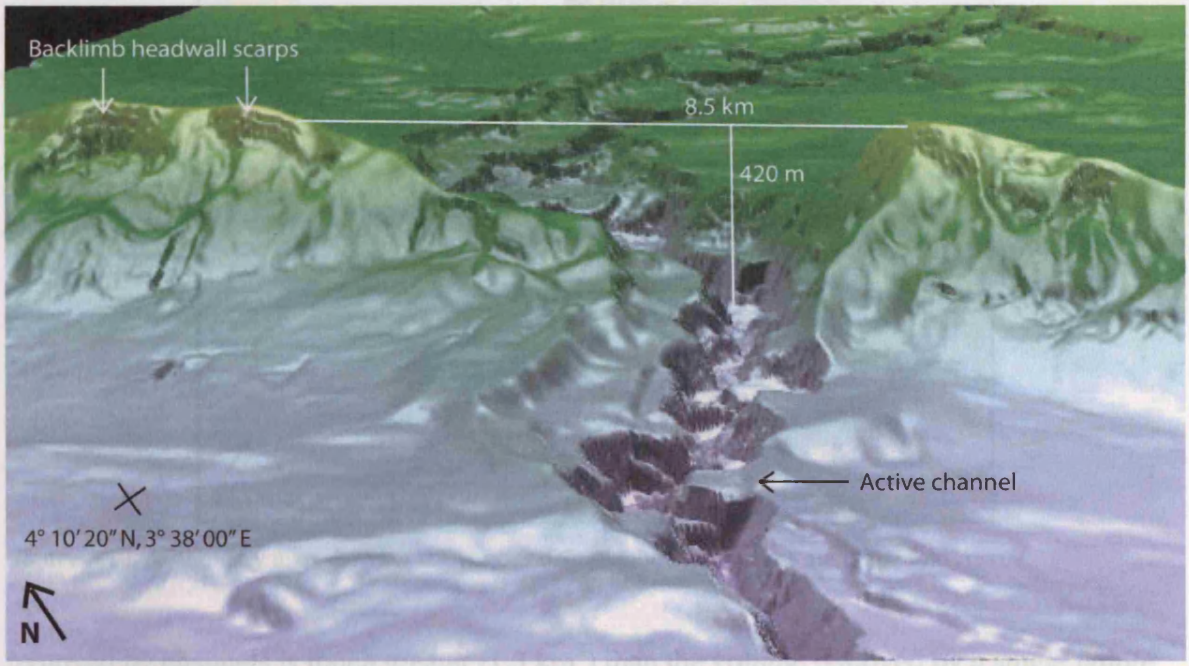

Figure 3.9. A perspective view of fold A where it is breached by a channel. Vertical distance from the crest of the fold to the bottom of the active channel is 420 m. Field of view is 15 km along the fold. Note the arcuate headwall scarps on the backlimb. Vertical exaggeration is c. 2.5.

3.8 DISCUSSION

A schematic summarises the areal variability of the different styles of fold degradation near the seafloor of fold A of the study area (Fig. 3.10). Of the four main styles of degradation, channel erosion is volumetrically the most important mechanism. The volume of sediment

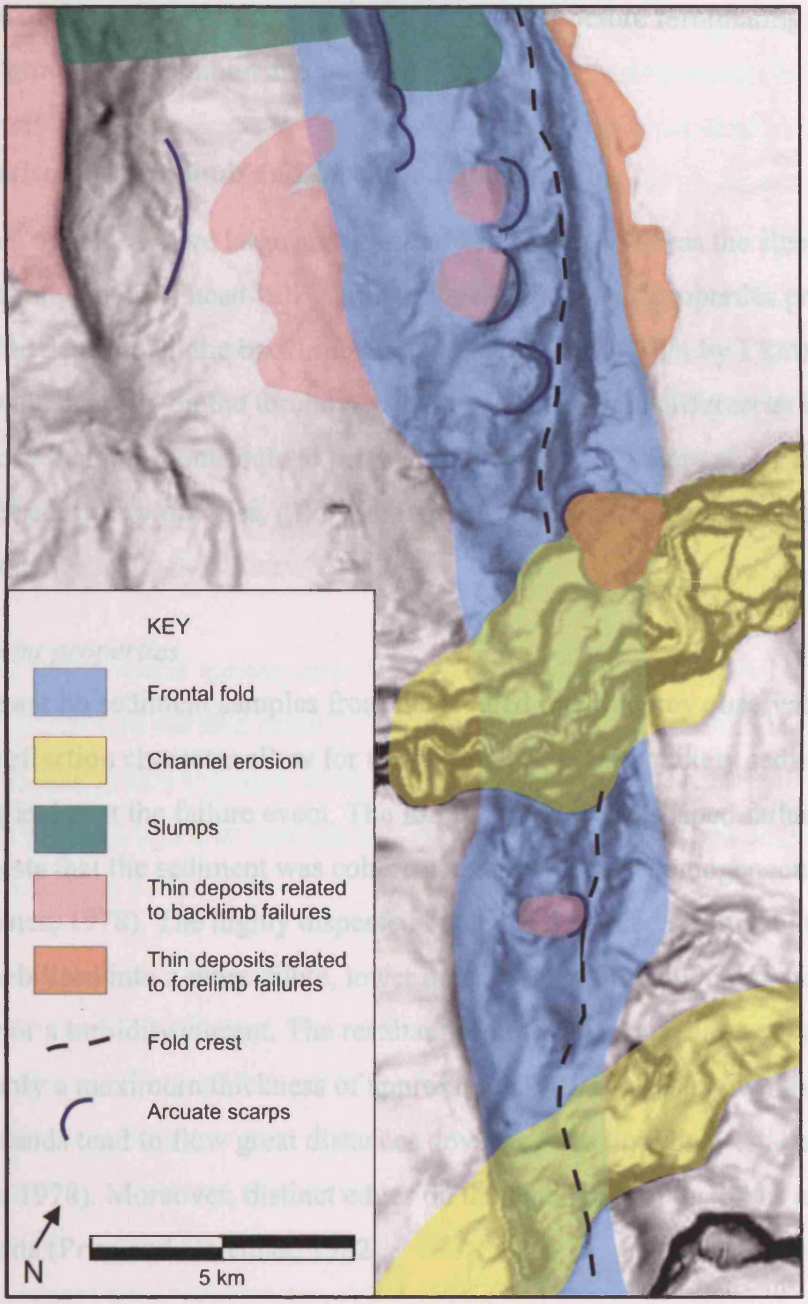

Figure 3.10. A summary map showing the various degradation mechanisms along the fold A.

removed by channels is much greater (1.3 km^3) than the volume removed by a single failure (up to 0.062 km^3, Table 3.1). Channel erosion can be considered as a continuous process and thus differs from the other degradation mechanisms, which are considered as individual, repetitive failure events. The backlimb and forelimb failures associated with thin, almost seismically indiscernible sedimentary deposits downdip are by far the most common types of degradation in the study area and have been identified within other 3D seismic datasets in this part of the Niger Delta, and therefore are the focus in this discussion. The main controls on

the architecture of these types of failure are considered first before formulating a generic model for fold growth, degradation and burial.

3.8.1 Comparison of backlimb and forelimb failures

Backlimb slopes of fold A have large arcuate headwall scarps, whereas the steeper forelimb does not exhibit any obvious headwall scarps despite the sediment properties probably being very similar. The deposits on the backlimb are long and narrow (3 km by 1 km) compared to the short and wide deposits on the forelimb (1 km by 2 km). Some differences in the pre-failure conditions that may contribute to producing the different failure styles and depositional features are (1) sediment properties, (2) the presence and orientation of anisotropies and (3) slope morphology.

3.8.1.1 Sediment properties

Although there are no sediment samples from the studied interval, key observations of deposit geometry and reflection character allow for the consideration of the likely sediment properties prior to, during and post the failure event. The formation of scoop-shaped failures on the backlimb suggests that the sediment was coherent and most likely homogeneous at the time of the failure (Varnes, 1978). The highly dispersed nature of the failed sediment mass suggests that it was remobilised into a more dilute, lower density flow, probably in the form of a debris flow, mudflow or a turbidity current. The resultant sediment package has a very low aspect ratio and probably a maximum thickness of approximately 10 m. It is known that soft clays and loose fine sands tend to flow great distances downslope as liquid material even on gentle slopes (Varnes, 1978). Moreover, distinct edges on the distal part of the lobes are typical of mudflow deposits (Prior and Coleman, 1982).

The presence of slumps with internal slip planes indicates that movement could also occur as more coherent and viscous sediment bodies. The slump described in this paper (Fig. 3.8) occurred due to the remobilisation of a mass transport complex deposit. This more coherent style of sediment transport could be a coincidental relationship, but may also suggest that the mass transport complexes had different sediment properties prior to failure than levee and hemipelagic sediments and this affected the type of failure that occurred.

3.8.1.2 Anisotropies

The presence and orientation of stratigraphic and structural anisotropies can influence mass wasting processes (e.g. Stewart and Reeds, 2003). Planes of weakness reduce the shear strength of sediment and enable failure to occur with lower imposed shear stresses. The main anisotropies in the study area are bedding planes and the sub-vertical faults associated with fold growth (Fig. 3.3). The dip of the strata is greater in the forelimb than on the backlimb, which may result in more slab-like failures along bedding planes on the steeper forelimbs. However, close inspection of the forelimb failures shows that there is no evidence for bedding-parallel detachment surfaces. Instead, the strata are clearly truncated (Fig. 3.5). This means that the failure plane is steeper than the dip of the strata of the forelimbs, and thus unlikely to be controlled by bedding-parallel slip.

The sub-vertical faults, which are perpendicular to the fold axes, are present on the backlimbs but do not continue across the fold crests to the forelimbs. The faults coincide with the lateral margins of the failure scarps and most likely control the width of the scarps. Forelimbs lack these planes of weakness and also lack arcuate failure scarps, indicating a possible relationship between the two.

3.8.1.3 Slope morphology

The backlimb and forelimb of fold A have different slope morphologies. The forelimb is steep (15°) and short, and the slope gradient reduces abruptly, whereas the backlimb is shallower (6°), longer and has no abrupt changes in dip. Slope morphology may determine the type of slope degradation that occurs, because it determines the failure plane geometry and affects the runout distance. The orientation of slip plane is controlled by the distribution of principal stresses on the slope (Mello and Pratson, 1999). The orientation of stress field rotates within a slope, because the upper part is under an extensional stress regime, whereas the lower part is in a compressional stress regime simply due to gravitational force. This means that the direction of the slip planes will rotate producing listric surfaces in shallow slopes and more planar and slope-parallel as the slope steepens. Mello and Pratson (1999) predict that sediments fail when the slope inclination is $\geq 2/3$ of the friction angle. In marine sediments this should be approximately 13° (Mello and Pratson, 1999), however, other factors (e.g. high pore pressures) will contribute to the failure of shallower slopes. The arcuate headwall scarps on the backlimb and the forelimb slope with truncated reflections have an angle of 13-15°. This fits in well with the prediction of the angle of failure initiation.

Submarine slides occur on slopes with gradients as low as 0.5°, and slope gradient is thus not always considered an important factor in marine slope instability (Sultan et al., 2004). However, the gravitational shear stress and the weight of the overlying sediment increase if a slope steepens. Therefore, steeper slopes are predicted to be more prone to failures. Also increased transport velocities can be attained on steeper slopes. An abrupt break in slope causes increased basal friction, deceleration and deposition of the failed sediment mass, resulting in relatively thick deposits (Nemec, 1990). On a longer, more uniform slope, the failed sediment mass has more time and space to dilute by the entrainment of ambient water and hence disintegrate. This increase sediment transport distance and dispersal, leading to the formation of thin, widespread deposits, because both basal and internal friction are reduced. The observations of the degradation complexes in the study area match perfectly with these predictions.

3.8.2 Model for fold degradation

Several mechanisms for fold degradation were described above. Here a general synoptic model that accounts for the dominant style of degradation observed in the study area is synthesised (Fig. 3.11).

An asymmetric fold forms on the hangingwall of an underlying thrust (Fig. 3.11A). During folding, normal faults may form perpendicular to the fold axis on the backlimb of the fold. Initial slope failure occurs once the stresses become large enough for compressional failure on the lower part of the slope (Mello and Pratson, 1999) (Fig. 3.11B). This may be triggered by several factors, e.g. slope steepening or earthquakes. The headwall scarps on the backlimb are arcuate in plan view, which is typical of homogeneous materials with a relatively shallow slope dip (Varnes, 1978). The width of the scarps is most likely controlled by the pre-existing normal faults that act as planes of weakness. On the forelimb there are no arcuate scarps because the slope is steeper, which causes the slip plane to have an orientation parallel to the slope surface (Mello and Pratson, 1999). The sediment mass that fails disintegrates after failure during transport. It is transported down the slope as a debris/mudflow or a turbidity current as more ambient water is entrained by it and dilutes it. The transport distance is great enough that the failure scar is completely evacuated. The deposits are widespread thin lobes on the long shallow backlimb (<10 x 3000 m), whereas on the forelimb that has an abrupt break in slope, the sediment is deposited at the foot of the fold in thicker and shorter deposits (30 m x 1000 m).

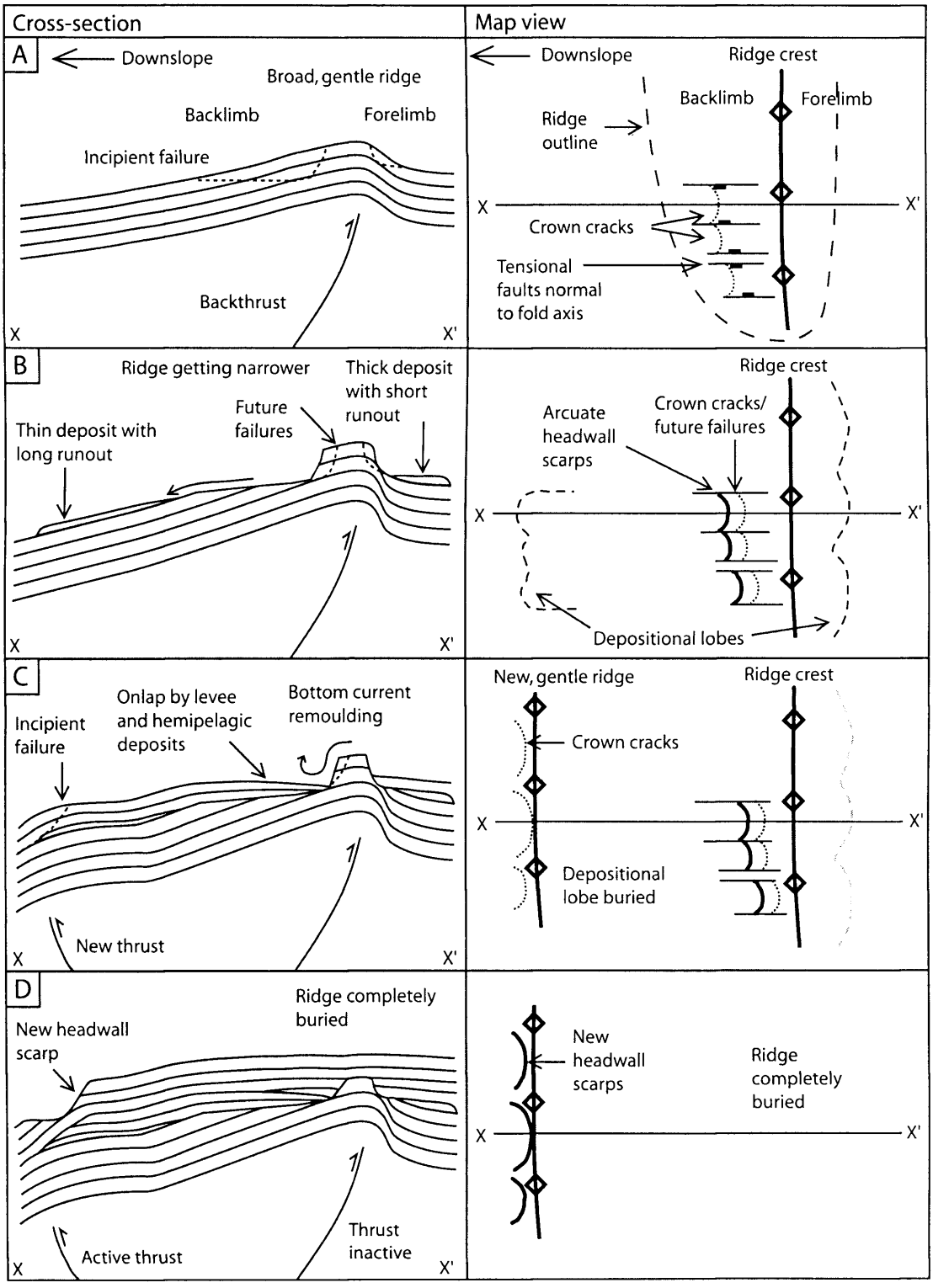

Figure 3.11. A simplified cartoon showing the formation of stratal geometry observed repeatedly on the folds in cross-section and plan view. Not to scale. (A) A thrust-propagation fold at pre-failure stage forming a broad and gentle fold on the seafloor. Tensional faults normal to the fold axis are formed on the backlimb. Incipient failures are listric in shape. (B) Fold at an early stage of degradation. Part of the fold fails and produces thin deposits with a long runout distances on the gentle backlimb and a short runout distances on the forelimb with an abrupt break in slope. The deposits form lobe-shaped features in plan view. Crown cracks form upslope of previous headwall scarps. (C) Fold at a later stage of failure. The fold is getting narrower due to repeated retrogradation of the headwall scarps. Levee and hemipelagic deposits onlap the fold and the failure scars. Bottom currents may modify the stratal geometries. A new frontal thrust starts to develop and causes a new fold to be uplifted. (D) The fold has been completely degraded and buried. New fold has continued to be uplifted and is now the centre of degradation.

Upslope of the scarps, new crown cracks develop as a result of the removal of lateral support and mark the location of subsequent failures (Fig. 3.11B). The scarp retrogrades upslope as a result of multiple small volume failures. Subsequently, levee and hemipelagic deposits onlap the empty failure scar (Fig. 3.11C) and bottom currents modify the stratal geometries. When a new thrust forms basinward of the previous thrust, less displacement occurs on the older thrust. A new fold starts to form on the seafloor and failure occurs above it (Figs. 3.11C and D). The old fold is eventually degraded and buried completely as erosion and sedimentation rates outpace the rate of uplift.

3.8.3 Initiation mechanisms

It is well established that shear stress can be increased or shear strength decreased by (1) earthquake shaking, (2) imposing a tilt, (3) high sedimentation rate and the weight of overlying sediment, (4) removal of underlying or lateral support (for example, erosion by channels or previous failures), (5) presence of gas or destabilisation of gas hydrates and (6) lateral pressure caused by e.g. mobilisation of residual stress (e.g. Varnes et al. 1978, Hampton et al., 1996). The most common trigger mechanisms for slope failure are earthquake shaking (Canals et al., 2004) and gas seepage (Lastras et al., 2004; Sultan et al., 2004).

Dewatering and pore fluid migration caused by folding and burial may contribute to the destabilisation of sediments on slopes. Elevated pore fluid pressures can create permeable extensional fracture networks (Ingram et al., 2004). These and the extensional faults on fold crests caused by folding can act as pathways for pore fluid and hydrocarbon migration. No pore pressure or sediment strength information from the study area was available for this work, and it is therefore difficult to be unequivocal about trigger mechanisms. The BSR (Fig. 3.3) indicates the presence of gas hydrates in the study area, however, there is no evidence for dissociation or seepage in the seismic data, suggesting that gas seepage is an unlikely trigger of the failures. The area is tectonically quiescent, with only a few earthquakes with greater than magnitude 4 recorded in historical times (c. 200 years) (Ambraseys, 1988). However, larger earthquakes may be less frequent and thus not recorded. Moreover, thrust propagation may have produced small earthquakes, which are capable of triggering sediment failures. All the failures in this study occur on slopes with increased inclination (6-15°) and no similar failures are found where the slope is 0.8°. This suggests that slope inclination is an important factor contributing to failure generation here. In addition, the sedimentation rate is high on the Niger Delta, and overpressure is likely to be generated due to disequilibrium compaction.

This could explain the similar heights of many headwall scarps, suggesting that effective stress is reduced sufficiently at c. 100 m burial depth. High sedimentation rates also lead to thick piles of unlithified sediment, which fail more easily than thin piles or lithified rock (Schnellmann et al., 2005).

Other failures are triggered by removal of lateral support. Channel erosion removes lateral support and as a result parts of the fold failed into the channel. The same principle can be applied to the retrogradational failure process as each failure will result in the removal of lateral support.

3.9 IMPLICATIONS FOR HYDROCARBON EXPLORATION

This study highlights the formation of erosional surfaces on fold crests and limbs and the deposition of degradation products on the margins of the folds. It is likely that both of these phenomena will be penetrated by exploration, development and production wells in the future, and therefore the recognition of unconformities and deposits of failed and remobilised sediments is important for predicting stratigraphy prior to drilling. The failed sediment deposits are not likely to be of good reservoir quality as this part of Niger Delta is extremely mud-prone. Even in sandier systems, debris-flow deposits are commonly too poorly sorted to be a good hydrocarbon reservoir. Furthermore, although not considered here, uplift and erosion of folds may have implications for seal integrity (Ingram et al., 2004), and accurate estimation of the amount of unroofing is therefore important. Although the degradation complexes described in this paper are relatively small, unloading the fold crest by larger failures could lead to depressurising of gas hydrates. Gas and fluid derived from the gas hydrates or from escaping free gas trapped beneath the gas hydrates could contribute to the destabilisation of sediments and the degradation of the fold.

Based on the seismic interpretation of the study area, it is evident that different styles of degradation occur along the same structure, separated by only a few hundreds of metres. This results in significant along-strike variability in the erosional and depositional features and means that unconformities and individual seismic reflections can only be traced locally (Fig. 3.10). In addition, it was shown that the dominant degradation products are thin debris flows or turbidites, many of which are probably not seismically resolvable even close to the seabed. Their function in filling minibasins that developed between the folds is easily underestimated, particularly where seismic resolution is reduced. The complexity associated with fold growth

and degradation will therefore be further amplified in buried examples making the correct correlation of reflections across and along fold structures difficult and accurate stratigraphic predictions highly challenging.

Deepwater compressional fold and thrust belts are important hydrocarbon exploration targets throughout the world. Hangingwall anticlines host major hydrocarbon accumulations offshore East Kalimantan (Saller et al., 2004) and northwestern Borneo (Demyttenaere et al., 2000; Ingram et al., 2004). In addition, other deepwater compressional structures, such as shale and salt diapirs and ridges that dominate other major hydrocarbon provinces, e.g. Gulf of Mexico (Winker and Booth, 2000; Grando and McClay, 2004) and Angola (Corredor et al., 2005) may have similar degradational patterns that influence reservoir geology. Slumps have been observed near anticlines in deepwater Borneo (Ingram et al., 2004) and on basin inversion anticlines in the North Sea (Cartwright, 1989). Inspection of other three-dimensional datasets along trend on the Niger Delta shows that the styles of degradation described here are common on fold-related highs. It is also likely that these styles of degradation complexes are not unique but will typify other compressional settings.

3.10 CONCLUSIONS

This paper describes several different styles of submarine fold degradation complexes that are the result of various failure and transport processes and produce laterally discontinuous erosional surfaces and deposits that have impact on reservoir prediction. A significant amount of sediment is removed from folds and thick deposits of non-reservoir accumulated in minibasins adjacent to folds. In this particular dataset, channel erosion is volumetrically the most important degradation mechanism. The dominant style in this part of the western Niger Delta, however, is that of multiple, retrogressive, small volume failures that can have a common locus, if pre-existing planes of weakness are present. The difference in the geometries of the backlimbs and forelimbs of thrust propagation folds is a fundamental control on the style of degradation and the runout distance of such failures. The abrupt break in slope on forelimbs reduces the velocity of the failed sediment mass and causes deposition resulting in relatively thick, short and wide deposits, whereas the longer but shallower slope of the backlimb leads into disintegration of failed sediment mass into debris flows or turbidity currents that produce widespread, thin deposits with longer runout distances. Both backlimb and forelimb failures are likely to form deposits that are below seismic resolution. They are therefore difficult, if not impossible, to identify adjacent to buried folds where the seismic

resolution is reduced. These deposits are likely to be muddy and even in sandier systems poorly sorted and therefore not good reservoir.

Other degradation styles have also been observed in the study area. Sediments with higher internal shear strength form more coherent downslope mass movements on a basal detachment and shortening by internal imbricate thrusting. More enigmatic ovoid depressions are considered to represent small scale slumping that are modified by bottom currents. This style shows that folds that have only a minor relief on the seafloor degrade differently to folds with greater relief, i.e. through a combination of brittle failure and bottom current erosion. Given the variety and three-dimensional complexity of these degradation complexes, comparison with other seismic volumes would be essential to fully characterise degradation in compressional submarine settings.

Chapter 4

4 KNICKPOINT MIGRATION IN SUBMARINE CHANNELS IN RESPONSE TO FOLD GROWTH, WESTERN NIGER DELTA

4.1 ABSTRACT

Several knickpoints have been identified along the present day thalweg of a sinuous submarine channel on the slope of the western Niger Delta using 3D seismic data. The knickpoints form as a result of gradient changes caused by the uplift of a thrust and fold belt orthogonal to the channel. The channel gradient is lower locally upstream of folds causing turbidity currents within the channel to decelerate and deposit the coarsest sediment load. The basinward dipping fold limb causes local steepening of the gradient, which leads to increased flow velocity and turbulence within the turbidity currents. This enhances erosion at the base of the channel and leads to the formation of a knickpoint. If preserved, e.g. as a result of channel avulsion or abandonment, the deposits upstream of the knickpoints could constitute an important hydrocarbon reservoir element. They can, however, also be partially eroded by headward-migrating knickpoints, as the channel strives to regain its equilibrium profile, leaving remnant sand pockets preserved on channel margins. Although knickpoints are difficult to recognise from subsurface seismic or outcrop data, it is anticipated that they can form at any stage of the evolution of a channel-levee system and may be particularly important in controlling 3D channel architecture where channels intersect dynamically changing seabed topography.

4.2 INTRODUCTION

Deepwater channels have been a focus of significant research effort since their discovery in the 1940s on the continental margins of North America (Menard, 1955) and more recently since they have been recognised as important hydrocarbon reservoirs. Channel-fill elements, together with terminal and intraslope fans and crevasse splays, are exploration targets in buried turbidite systems. Many of the reservoirs in recent discoveries off West Africa consist of sinuous shoe-string, ribbon- and pod-shaped sand bodies deposited within canyons and valleys (Prather, 2003). Outcrop analysis, seismic data, borehole and hydrocarbon production data all show that many deepwater channels have complex internal fills, with multiple phases of erosion, bypass and fill (e.g. Deptuck et al., 2003; Posamentier and Kolla, 2003). This complexity could be the result of external factors, such as changes in sediment supply from

the shelf, climate and relative sea level (e.g. Posamentier and Kolla, 2003). It could also be due to the dynamic nature of slopes, which are complicated by active, growing structures such as faults, folds, salt or mud diapirs and withdrawal basins.

Deepwater channels act as conduits for sediment to be transported by gravity flows, such as turbidity currents and debris flows, into the deep sea (Deptuck et al., 2003). Gravity flows travelling down slopes react in various ways to changes in topography. This depends on several factors, such as rate of seafloor deformation and the type, grain size and density of the flows (Pirmez et al., 2000; Kneller, 2003). Some channels are diverted around structures on the seafloor (Kukowski et al., 2001; Smith, 2004) or dammed by growing structures leading to abandonment (Demyttenaere et al., 2000; Huyghe et al., 2004). In other cases, however, compressional structures orthogonal to channels have apparently little effect on the channel location, but along with some changes in planform morphology they mainly cause changes in channel profile, e.g. steepening of gradient across the thrust front of the Barbados accretionary prism (Huyghe et al., 2004). This is also characteristic of the channel of this paper.

Channels constantly adjust their profiles towards equilibrium, i.e. a profile that sustains little aggradation or degradation along the channel with prevailing sediment discharge conditions (Pirmez et al., 2000). This is achieved mainly by erosional and depositional processes of turbidity currents, including changes in channel sinuosity and development of distributary channels and aggradational sheets (Pirmez et al., 2000; Kneller, 2003; Adeogba et al., 2005). Despite complex seafloor topography, many submarine channels form concave-up equilibrium profiles (Pirmez et al., 2000).

Submarine channels may also adjust their profiles towards equilibrium via the formation of knickpoints, a process that is well known in fluvial settings. The role of this process in determining the internal architecture of deepwater channel complexes in regions of evolving topography has received much less attention until very recently (Pirmez et al., 2000; Mitchell, 2006). This paper presents an analysis of knickpoints on the ultra-deepwater Niger Delta using 3D seismic data. The knickpoints formed along a present day channel thalweg due to fold growth. Detailed analysis of knickpoints shows how a confined submarine channel evolves as it traverses across an uplifting thrust and fold belt and suggests that knickpoint migration plays a significant role in controlling the architecture of channel-levee complexes.

4.2.1 Knickpoints

A knickpoint is defined in fluvial systems as a steep gradient section between lower gradient sections along a river course (Howard et al., 1994) and thus represents a disruption in equilibrium profile. Knickpoints and rapids form in fluvial systems as a result of changes in base level (i.e. sea level), sediment flux, bedrock resistance and tectonic deformation across the river course (e.g. Howard et al., 1994). Stream power increases along the steep gradient causing enhancement of sediment or bedrock erosion. The increased erosion increases sediment flux downstream (Burbank and Anderson, 2001 p. 162) leading to enhanced deposition.

Knickpoints will, in certain conditions, migrate upstream retaining the morphology (parallel retreat) leaving cut terraces behind, but they can also be smoothed out with or without upstream-migration by gradual decrease of the knickpoint lip gradient (slope replacement) (Gardner, 1983; Howard et al., 1994). The type of knickpoint evolution depends on the relationship between bottom shear stress (τ_o) and critical shear stress needed to initiate motion (τ_c), bed-load transport discontinuities and spatial variability of bed resistance (Gardner, 1983). Knickpoint retreat is most likely to occur if there is a resistant caprock where $\tau_c > \tau_o$ overlying a non-resistant layer, but retreat can also occur in homogeneous rock if the knickpoint has a height to flow depth ratio greater than 1 and the flow is sufficient to transport material away from the base (Burbank and Anderson, 2001). Knickpoint replacement occurs in uniformly resistant material where $\tau_c > \tau_o$ within the knickpoint reach, such as cohesive silts, clay and alluvial channels. Knickpoints can be formed due to differential erosion due to variation in resistance to erosion along channel (Burbank and Anderson, 2001). In the numerical models of Howard et al. (1994), knickpoints migrate when erosion rate is proportional to stream power but become rounded and smoothed out when erosion rate is proportional to bed shear stress.

Knickpoints have been identified along several submarine channels and canyons and can have various origins (Table 4.1). Although formed in a different environment, submarine knickpoints have many similar characteristics to their fluvial counterparts. Submarine channels are cut mainly by turbidity current scouring (Pratson and Coakley, 1996). According to Pirmez et al. (2000), turbidity currents can erode several tens of metres of seafloor in a few thousand years. Incision at the base of a flow increases when velocity increases (Mulder and

Cochonat, 1996) and velocity increases when slope steepens, therefore the incision rate increases when slope steepens (Pirmez et al., 2000; Kneller, 2003). Velocity reduction, flow spreading and deposition occur in topographically unconfined areas, areas of lower gradient and downslope from abrupt reductions in gradient (Nemec, 1990; Demyttenaere et al., 2000; Pirmez et al., 2000; Prather, 2003; Smith, 2004). The adjustment to the equilibrium profile across many knickpoints occurs by erosion and deposition as summarised in the model of Pirmez et al. (2000), in which erosion occurs along the channel upstream of the knickpoint and deposition of sediments occurs downstream, where the channel profile is lower than the equilibrium profile, until the equilibrium profile is restored.

Table 4.1. Submarine knickpoints in the literature

Origin of knickpoint	**System**	**Reference**
Avulsion	The Amazon	(Pirmez et al., 2000)
	The Rhone	(Pirmez et al., 2000)
	The Zaire	(Babonneau et al., 2002)
	The Magdalena	(Estrada et al., 2005)
Tributary confluences i.e. hanging valleys	The East Breaks (the Gulf of Mexico)	(Pirmez et al., 2000)
Normal faulting	The East Breaks (the Gulf of Mexico)	(Pirmez et al., 2000)
	The Niger Delta	(Pirmez et al., 2000; Adeogba et al., 2005)
Transition from one sub-basin to another	The East Breaks (the Gulf of Mexico)	(Pirmez et al., 2000)
	The Niger Delta	(Pirmez et al., 2000; Prather, 2003; Smith, 2004; Adeogba et al., 2005)
Diapirism	The Niger Delta	(Adeogba et al., 2005)
Variability in substrate properties	The Central Atlantic USA Margin	(Mitchell, 2004)
Folding in convergent plate margins	The Barbados Ridge Complex, the Caribbean	(Huyghe et al., 2004; Mitchell, 2006)
	The Makran accretionary wedge, Pakistan	(Kukowski et al., 2001)
	The Tenryu Canyon, Tokai Prism, Japan	(Soh and Tokuyama, 2002)
	Astoria Canyon, USA	(Mitchell, 2006)
	Alaskan slope, USA	(Mitchell, 2006)
? Canyon - channel transition	The Danube Canyon, Black Sea	(Popescu et al., 2004)
? Landslide headwalls	New Jersey continental Slope, USA	(Mitchell, 2006)
? Slope retreat	San Antonio Canyon, Chile	(Mitchell, 2006)
? Break of slope	Angola	(Gee and Gawthorpe, 2006)
Not specified	Monterey Channel, Western USA	(Masson et al., 1995)

Knickpoint evolution and morphology is influenced by various factors. Mitchell (2006) used numerical modelling of advection (migration) and diffusion (smoothing out) to replicate the morphology of knickpoints in the Barbados Canyon. The model reveals that advection sharpens knickpoint lips and diffusion rounds them, but when a boundary condition of nondeposition or erosion is applied at the base of the knickpoint, the diffusion only model can produce knickpoint morphology similar to the advection model.

The term knickpoint is used somewhat loosely here to describe a reach with a higher gradient than the adjacent reaches. Knickpoint terminology is adapted from Gardner (1983), where the knickpoint lip is the break in slope where the channel becomes oversteepened and the knickpoint face is the steep reach between the lip and the base of the knickpoint.

4.3 GEOLOGICAL SETTING AND DATABASE

The Niger Delta on the West African continental margin (Fig. 4.1) is a prolific hydrocarbon province. The delta is undergoing gravitational downslope collapse and this results in three structural domains: (1) an extensional domain dominated by growth faults, (2) a translational domain characterised by mud diapirism and (3) a compressional domain dominated by toe-of-slope thrusts (Damuth, 1994; Cohen and McClay, 1996; Morgan, 2004). This case study focuses on the ultra-deep-water compressional domain of the western Niger Delta, where the regional slope dips on average at 0.8° towards the southwest (Fig. 4.1). The toe-of-slope thrusts are orientated perpendicular to the slope and dip both upslope and downslope (forethrusts and backthrusts) (Fig. 4.2). Anticlines on the hangingwalls of these faults have up to 200 m of positive relief on the seafloor and are up to 7 km wide (Heiniö and Davies, 2006). This paper considers the response of the thalweg of an active channel-levee system (CLS) to growing folds orthogonal to its path.

The 3D seismic data cover an area of 1630 km^2 of the western Niger Delta (Fig. 4.1). It is zero-phase migrated and displayed so that an increase in acoustic impedance is a red-black-red reflection loop (see Brown, 1999 p. 35-47). The line spacing is 12.5 m in both the inline and crossline direction. For the conversion of two-way-travel time (TWT) to depth a velocity of 1480 ms^{-1} is used for seawater and 2000 ms^{-1} is used for sediment. The dominant frequency of the studied shallow section is 55 Hz and thus the tuning thickness ($\lambda/4$) is c. 9 m. The succession is subdivided using seismic reflections that define units with distinct internal seismic facies. Seismic attributes, including reflection dip and amplitude were used to reveal

depositional and deformational features. There are very few publicly available boreholes in this part of the Niger Delta. Lithological interpretation of the seismic facies in this paper follows earlier work done by Posamentier and Kolla (2003) and Deptuck et al. (2003), and is based on the recognition of seismic reflection character, amplitude and geometry, as well as the knowledge of unpublished well calibrations within the deepwater domain.

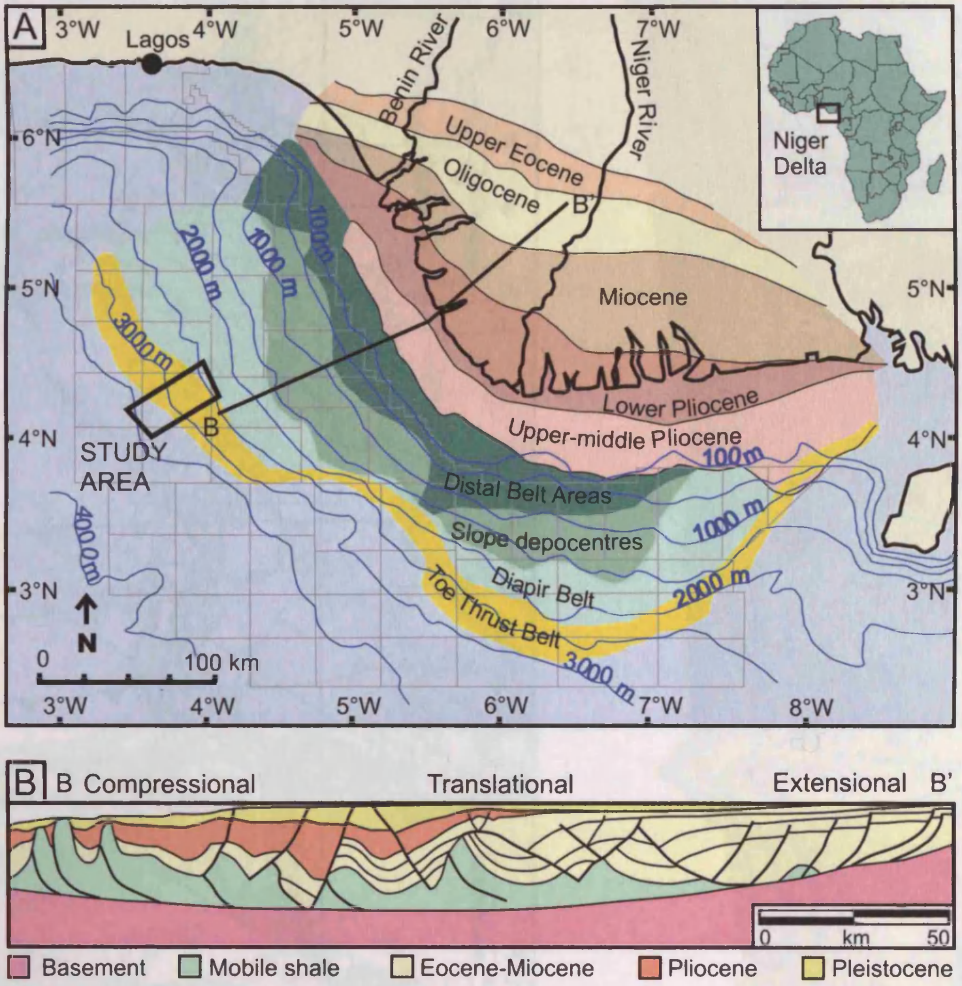

Figure 4.1. (A) Location of the study area at the outer thrust belt of western Niger Delta. Depobelts from Armentrout et al. (2000) and Hooper et al. (2002). Boxes outline offshore licence blocks. (B) Schematic cross section through the delta. Modified after Haack et al. (2000). Vertical exaggeration = 2.

4.4 CHANNEL-LEVEE SYSTEM (CLS)

4.4.1 Architectural elements

Two active channel-levee systems and a partially buried one are clearly visible on the seafloor of the study area (Fig. 4.2A). The CLS analysed here has a 1.5-6 km wide channel-belt, in which inner levees and channel-axis deposits are the dominant architectural elements (Fig. 4.3). The channel-belt is underlain by a basal erosional fairway and bordered by wedge-

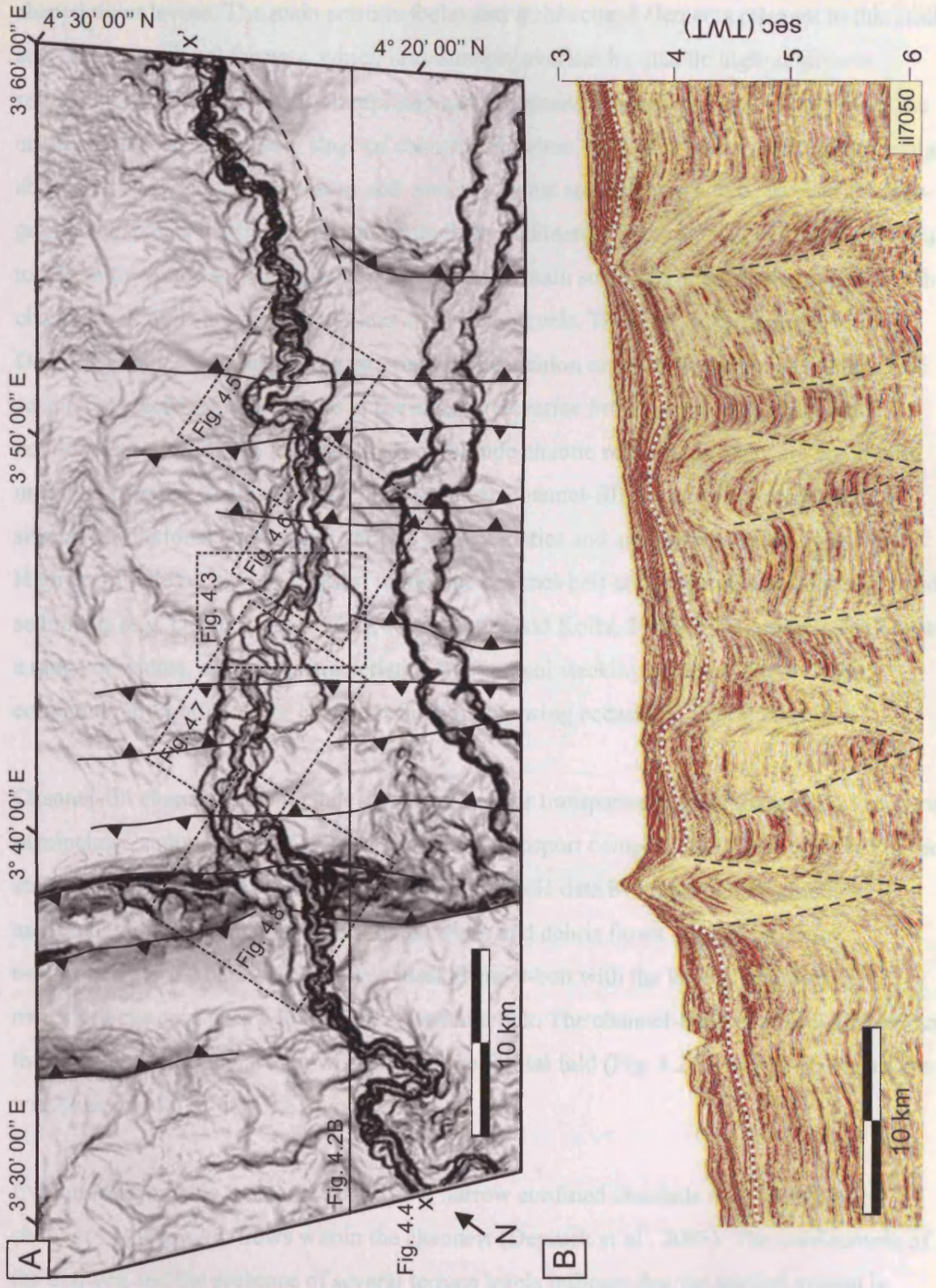

Figure 4.2. (A) Seabed dip magnitude map of the study area with the main thrusts in the subsurface traced and locations of Figures 4.5-4.8 indicated (dashed boxes). X-x' = location of end points of profiles shown in Fig. 4.4 along the studied channel. Darker shading means higher angle of dip. Maximum dip is c. 35° at some channel margins. Flow direction is from right to left. Location of area shown on Fig. 4.1A. (B) Downslope-orientated seismic line with main thrust faults traced. Dotted line marks the top of a mass transport complex, which is commonly incised by the studied CLS. Sec TWT = seconds two-way-travel time.

shaped outer levees. The main seismic facies and architectural elements relevant to this study are: (1) An erosional fairway, which is commonly overlain by chaotic high-amplitude reflections (HARs), which are interpreted as the deposits of semi-confined flows within the erosional fairway at an early stage of channel formation. (2) Outer levees, which form wedge-shaped cross-sectional geometries and consist of what are interpreted to be overspilled fine-grained turbidites interbedded with hemipelagic sediments. In the studied system they are up to 250 m thick and several kilometres wide and contain some sediment waves. (3) Within the channel-belt there are arcuate terraces at multiple levels. These are called inner levees by Deptuck et al. (2003) suggesting an origin by deposition on abandoned meander loops. The seismic character of inner levees in the study area varies from low- to high-amplitude continuous reflections to low- and high-amplitude chaotic reflections. They are commonly modified by small-scale slumping (Fig. 4.3). (4) Channel-fill elements are comprised of several depositional bodies with various characteristics and are commonly partly eroded. High-amplitude reflections (HARs) within the channel-belt are interpreted as coarse-grained sediments (e.g. Deptuck et al., 2003; Posamentier and Kolla, 2003). Channel-axis HARs show a range of widths, acoustic characteristics and vertical stacking patterns, but are most commonly discontinuous or chaotic reflections showing occasional lateral migration.

Channel-fill elements also include low-amplitude or transparent facies interpreted as mud-rich hemipelagic sediments. (5) One extensive mass transport complex (MTC) is identified in the study area (Fig. 4.3). MTCs are recognised on seismic data by contorted, chaotic low-amplitude reflections and include slumps, slides and debris flows. They contribute occasionally to the channel-fill. The widest channel-belt with the largest abandoned meanderloops coincides with the thrust and fold belt. The channel-belt becomes narrower and the channel depth increases downstream of the frontal fold (Fig. 4.2A), which decreases the width/depth ratio of the CLS significantly.

Evolution from wide erosional fairways to narrow confined channels may be caused by changes in the gravity flows within the channels (Deptuck et al., 2003). The confinement of the thalweg and the presence of several terrace levels indicate that the studied system is dominated by erosional flows but has a complex history involving several phases of incision and aggradation. Present day deposition occurs dominantly on inner levees and occasionally by overspilling on outer levees, as suggested by the wedge-shaped morphology and the presence of sediment waves on some parts of the outer levees (Fig. 4.3).

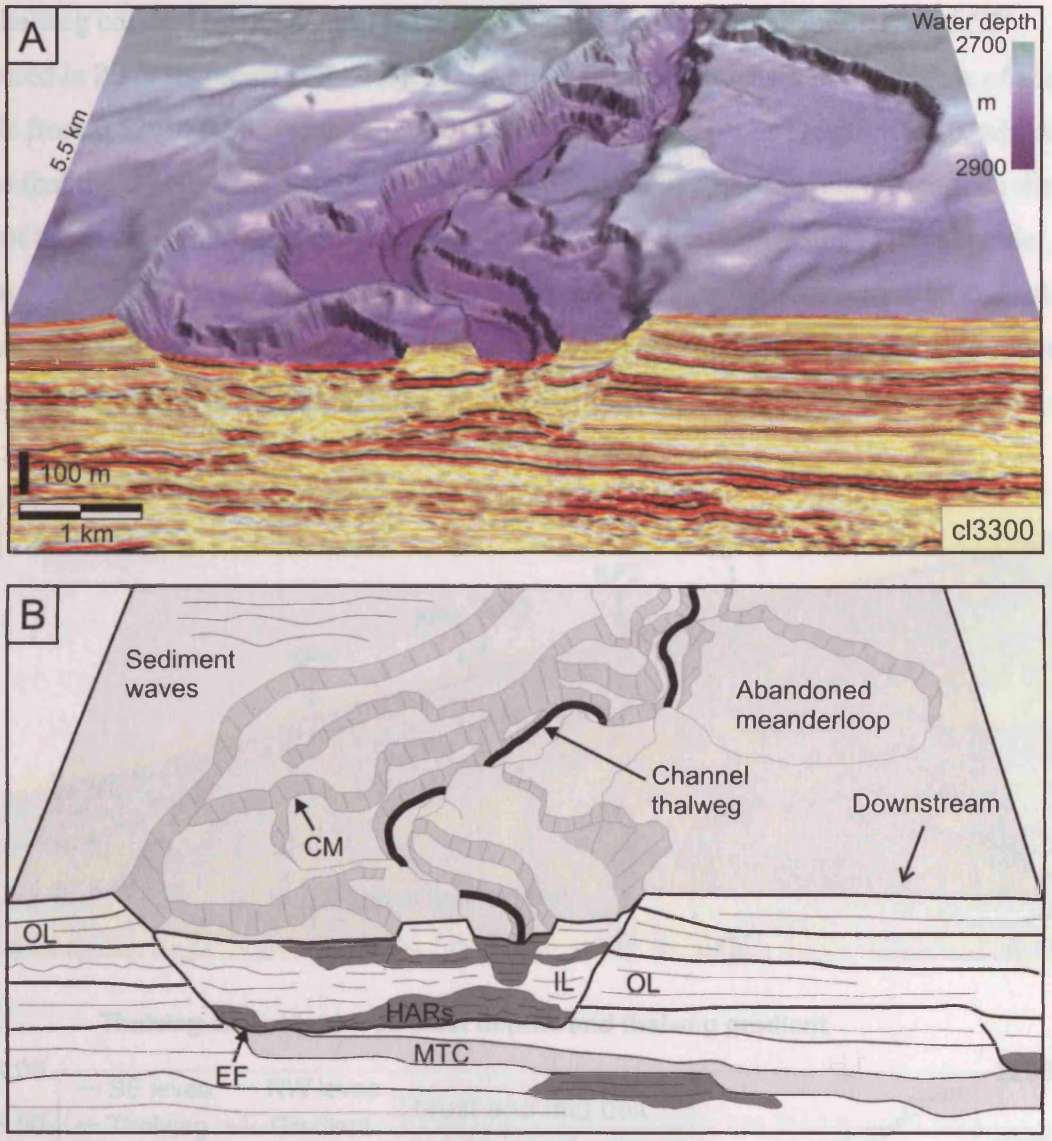

Figure 4.3. Seismic facies and architectural elements of the channel-levee system (CLS). (A) Seismic line with seabed structure map. Vertical exaggeration = 2.5. Location shown in Fig. 4.2A. (B) Line drawing of (A). EF = erosional fairway of the channel-belt, overlain by chaotic high-amplitude reflections (HARs). OL = outer levees, which confine the channel-belt. IL = inner levees. CM = collapsed margin. MTC = mass transport complex.

4.4.2 Present day channel thalweg

The present day channel thalweg is located 100-220 m below the outer levee crests. The channel walls can have slopes up to 36°. Channel wall morphology is most likely to be determined by the activity of turbidity currents within the channel. Centrifugal forces cause increased flow stripping onto levees and erosion at the base of outer bends. This results in higher and steeper walls on the outer bends and gentler walls on inner bends (Babonneau et al., 2004). In plan view the channel thalweg is c. 80 m wide. Measured in 2 km segments, the average sinuosity of the thalweg is 1.3, ranging from 1.0 to 2.8 and the mean radius of curvature measured from best-fit circles at each bend (Morisawa, 1985) is c. 350 m.

The thalweg covered by the dataset is 95 km long and has an average gradient of 0.55° measured in 2 km segments (Fig. 4.4). The average gradient increases in the middle of the profile from 0.52° to 0.59° (with ranges of 0.08-1.14° and 0.32-0.89° respectively), which means that the channel has a slightly convex-up profile. The convexity correlates with the zone of thrusts and folds across the channel and indicates that the thalweg is not at grade (sensu Prather, 2003), but has been uplifted above grade due to thrust propagation and fold growth. The right and left levee crest profiles are relatively similar to each other and record some of the uplift by convex-up flexure of the profiles (Fig. 4.4B).

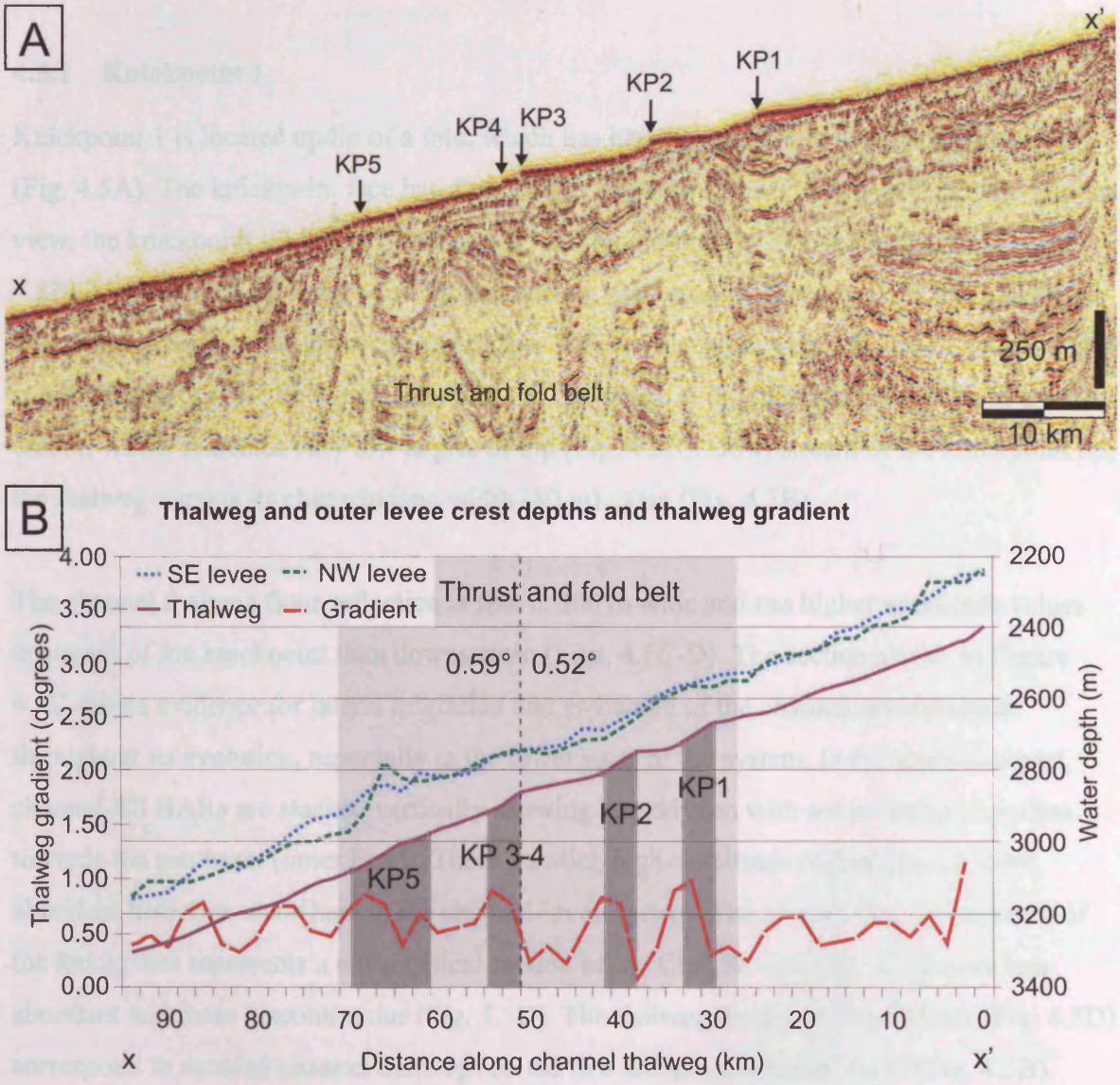

Figure 4.4. Present day channel thalweg profile. The knickpoints described in this paper are marked as KP1-KP5. (A) Seismic line along the sinuous channel thalweg. Location of x-x' shown on Fig. 4.2A. The thrusts and folds are not clearly imaged due to the sinuous course of the seismic line. (B) Graph showing the thalweg profile and gradient and levee profiles measured in 2 km increments. Note the increase of the gradient values in the middle of the uplifted thrust and fold belt (shaded). Datapoints shown in Figure 2.4B.

4.5 KNICKPOINTS 1-5

The present day channel has several knickpoints along its thalweg. The largest knickpoints occur above the thrust and fold belt, and are clearly identified from the thalweg profile because of their high gradients (Fig. 4.4). In addition, some knickpoints are characterised by very low gradient reaches upstream of them. Three types of knickpoints are distinguished according to their size, morphology and maturity. Five representative examples (KP 1-5) are described below. Knickpoints 1 and 2 represent the largest and the least mature Type I, knickpoints 3 and 4 the intermediate Type II and knickpoint 5 the most mature and smallest knickpoint Type III.

4.5.1 Knickpoint 1

Knickpoint 1 is located updip of a fold, which has bathymetric effect on adjacent seafloor (Fig. 4.5A). The knickpoint face has a maximum gradient of 4.86° and is 200 m long. In plan view, the knickpoint lip forms two arcs c. 850 m long obliquely across the channel (Fig. 4.5B). Upstream of the knickpoint lip the thalweg gradient is reduced to 0.30° for a distance of c. 5 km. This reach is characterised by a c. 500 m wide zone, where the 80 m wide thalweg is not defined (i.e. the thalweg becomes c. 500 m wide). A dip map represents this as a white colour, which indicates very low angles of dip (Fig. 4.5B). Downstream of the knickpoint lip, the thalweg regains its characteristic width (80 m) again (Fig. 4.5B).

The channel thalweg floor reflection is flat, c. 500 m wide and has higher amplitude values upstream of the knickpoint than downstream (Figs. 4.5C-D). The section shown in Figure 4.5C shows evidence for lateral migration and switching of the channel several times throughout its evolution, especially in the lower parts of the system. In the shallower part, channel-fill HARs are stacked vertically showing aggradation with some lateral migration towards the southeast (inner bend). These parallel, high-amplitude reflections are more abundant here than elsewhere in the channel-levee system. The seismic line downstream of the knickpoint represents a more typical section of the CLS, in which the HARs are less abundant and more discontinuous (Fig. 4.5D). The thalweg scours on the seafloor (Fig. 4.5D) correspond to scoured channel thalwegs on the two arcuate knickpoint faces (Fig. 4.5B).

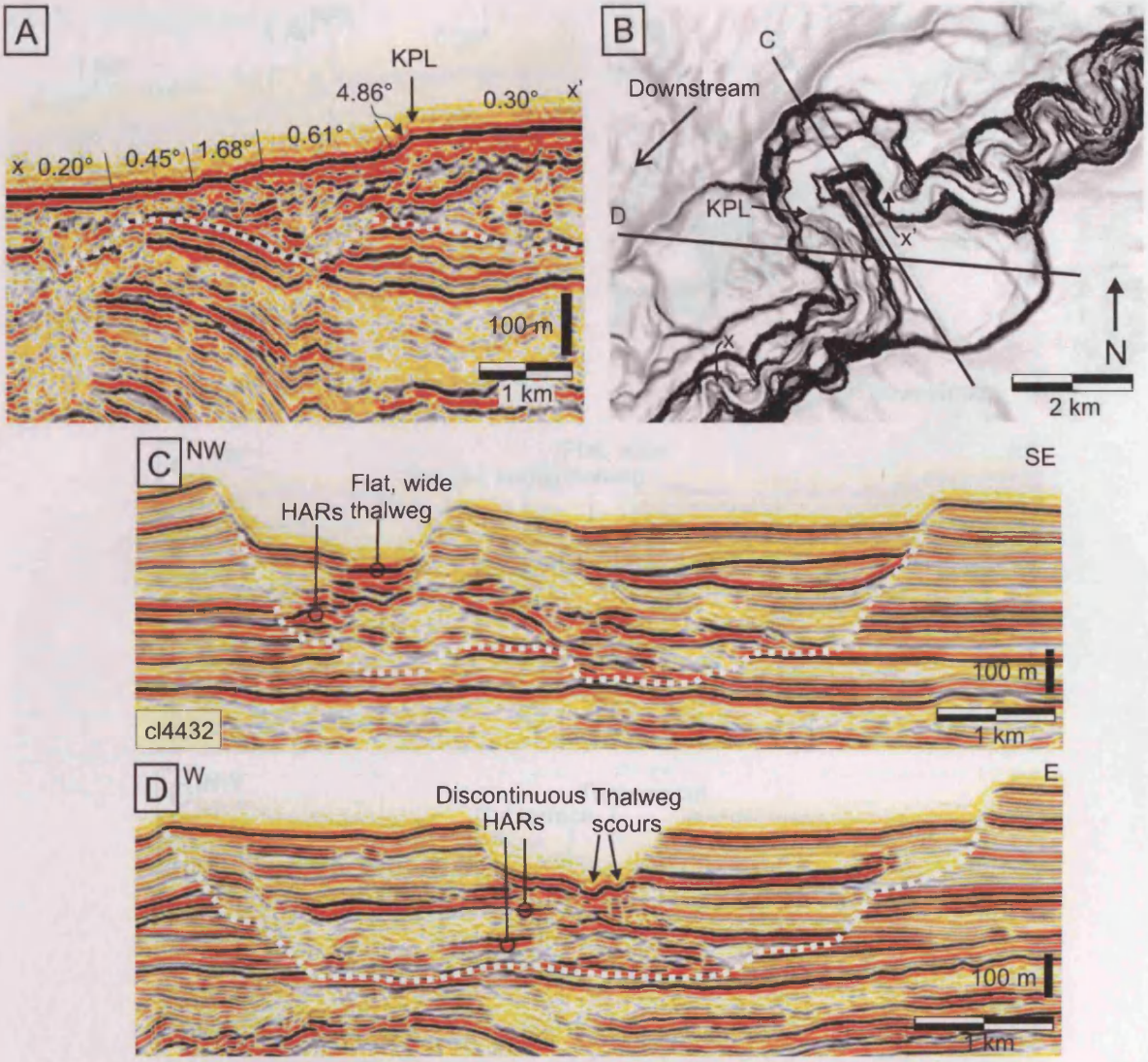

Figure 4.5. Morphology of knickpoint 1. (A) Thalweg profile across knickpoint 1. KPL = knickpoint lip in this and subsequent Figures. (B) Seabed dip map showing planform morphology of knickpoint 1. Note how knickpoint lip comprises two arcs. X-x' marks the location of (A) along thalweg. Location shown in Fig. 4.2A. (C) Seismic line across the channel-levee system upstream of knickpoint 1. (D) Seismic line across the CLS downstream of knickpoint 1. Dotted line on all cross sections marks the base of the CLS.

4.5.2 Knickpoint 2

Knickpoint 2 is located above the forelimb of a thrust-propagation fold and has a similar morphology to knickpoint 1 (Fig. 4.6). The maximum gradient of the knickpoint face is 4.74° for a distance of 300 m, after which the gradient gradually decreases to 0.42° going downstream. Upstream of the knickpoint lip the gradient is 0.20° for c. 2.5 km. This low-gradient reach also correlates to widening of the thalweg from 80 m to 500 m (Fig. 4.6B). The knickpoint lip is arc-shaped in plan view and c. 570 m long. Downstream the thalweg is 80 m wide again.

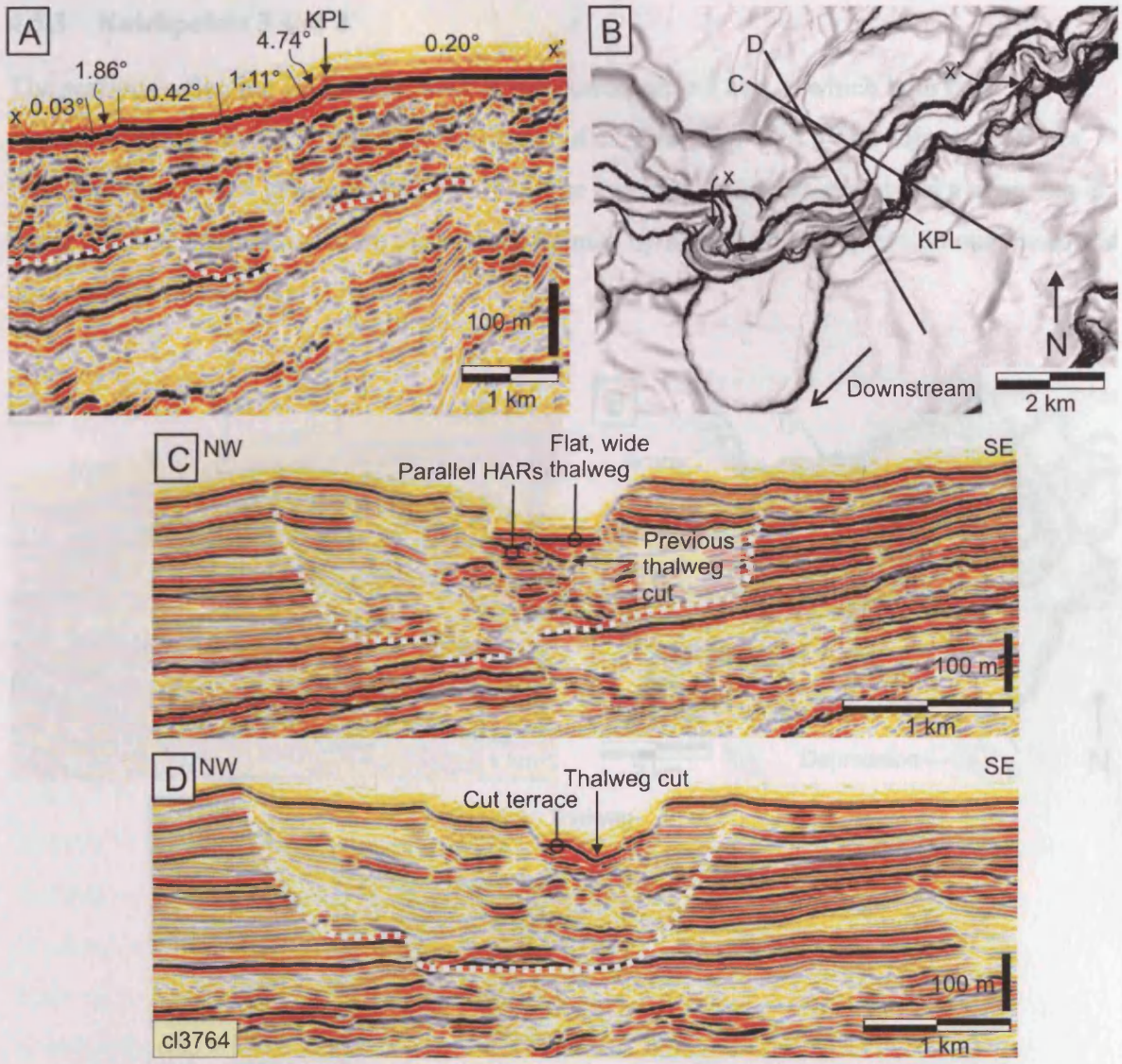

Figure 4.6. Morphology of knickpoint 2. (A) Thalweg profile across knickpoint 2. (B) Seabed dip map showing planform morphology of knickpoint 2. Location shown in Fig. 4.2A. (C) Seismic line across the channel-levee system upstream of knickpoint 2. Note the previous thalweg cut below the present day 400 m wide thalweg reflection. (D) Seismic line across channel downstream of knickpoint 2 showing v-shaped morphology. The terrace on the north-western side is interpreted as a remnant deposit cut by the thalweg. Dotted line on all cross sections marks the base of the CLS.

The cross section upstream of knickpoint 2 shows continuous parallel HARs in the channel-fill (Fig. 4.6C). The present day thalweg is 400 m wide in the section. It is flat and has very high amplitude. Directly beneath it, a reflection dips towards the southeast before flattening to a c. 80 m wide horizontal reflection. 1.2 km downstream, the channel-levee system has a different architecture with fewer HARs. The channel is v-shaped and the thalweg is 80 m wide (Fig. 4.6D).

4.5.3 Knickpoints 3 and 4

The seafloor reflection is discontinuous across knickpoints 3 and 4, which both have maximum angles of c. 25° and a vertical relief of c. 25 m (Fig. 4.7A). The adjacent reaches have low to very low gradients (0.30-0.03°). The knickpoints are located above a zone that is being uplifted, as manifested on the seabed dip map by a scarp and a depression outside of the channel-belt (Fig. 4.7B).

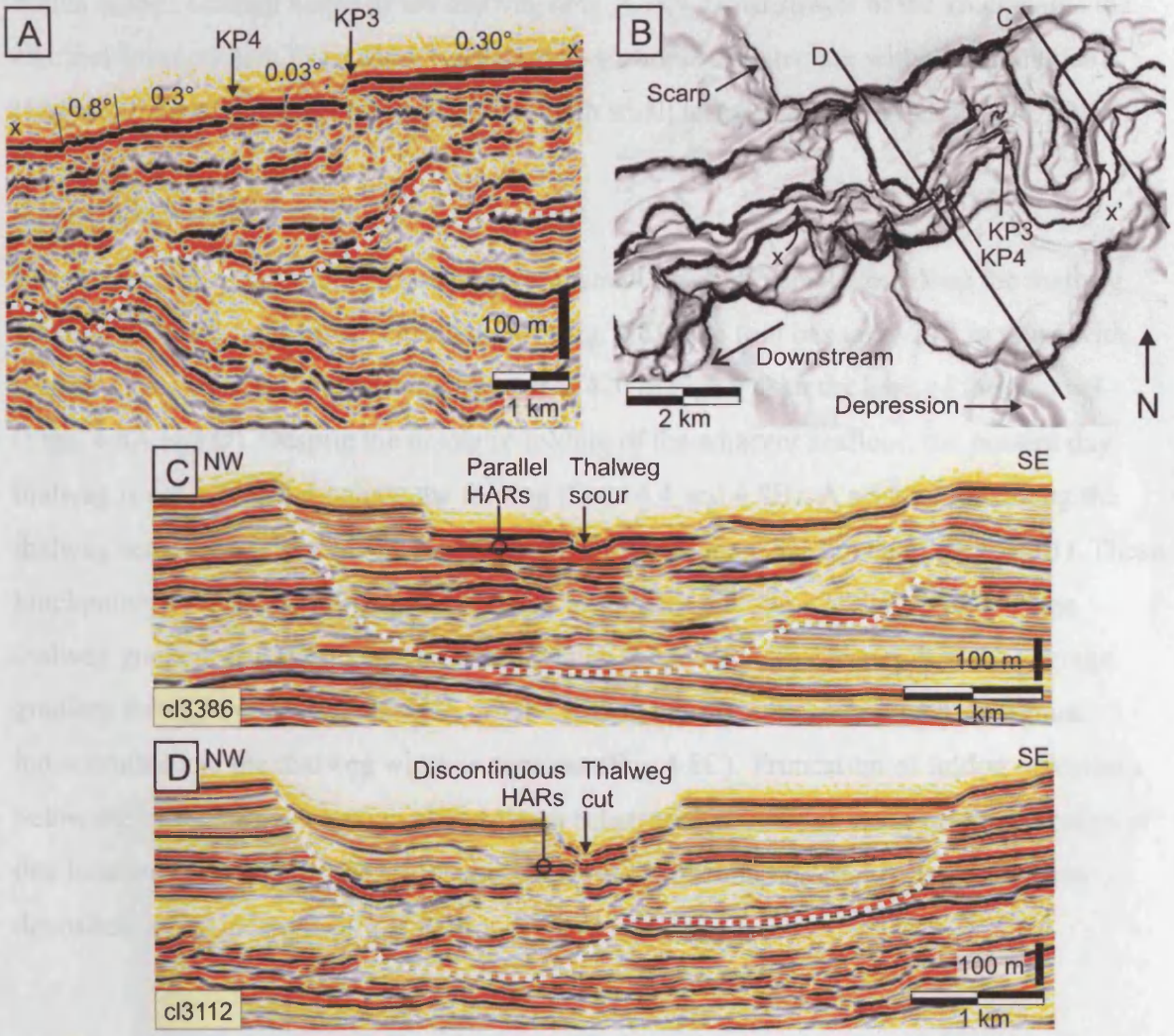

Figure 4.7. Morphology of knickpoints 3 and 4 (KP3 and KP4). (A) Thalweg profile across knickpoints 3 and 4 showing discontinuous seabed reflection with stepped appearance across the knickpoints. (B) Seabed dip map showing the planform morphology of knickpoints 3 and 4. The knickpoint lips are as wide as the thalweg, which can be traced upstream of them in contrast to knickpoints 1 and 2. The scarp and the depression are formed above the uplifting anticline. Location shown in Fig. 4.2A. (C) Seismic line across the CLS upstream of knickpoint 3. Thalweg scour is c. 20 m below the high-amplitude terraces. Note dominant parallel continuous HARs in the channel-fill. (D) Seismic line across channel downstream of knickpoint 4. Note the lack of parallel HARs. Dotted line on all cross sections marks the base of the CLS.

Knickpoints 3 and 4 can be identified on the seabed dip map as abrupt deeper incisions of the thalweg, which appear as darker outlines of the thalweg (Fig. 4.7B). The knickpoint lips are thus as wide as the thalweg. The gradient is low upstream of the knickpoint lips, but unlike in knickpoints 1 and 2, the 80 m wide thalweg can be traced throughout the uplifted zone. This can also be seen in the cross section of the channel upstream of knickpoint 3 (Fig. 4.7C). The most recent part of the system is dominated by continuous parallel HARs that are incised by the thalweg to a depth of c. 20 m. The scour is 280 m wide but its flat base is 80 m wide, which is the common width of the thalweg (Fig. 4.7C). Downstream of the knickpoints the channel-levee system has a more typical cross-sectional architecture with discontinuous HARs and deeply incised, narrow thalweg with small terraces adjacent to it (Fig. 4.7D).

4.5.4 Knickpoint 5

The last example comprises a zone of several small knickpoints located along the thalweg where it passes through a large frontal fold (Fig. 4.8). The fold has up to 200 m relief with respect to the adjacent seafloor and its crest is 420 m higher than the base of the channel (Figs. 4.8A and D). Despite the dramatic folding of the adjacent seafloor, the present day thalweg is not affected much by the folding (Figs. 4.4 and 4.8B). A seismic line along the thalweg across the fold shows a series of small knickpoints 0.5-1 km apart (Fig. 4.8B). These knickpoints have 6-10 m high and 50-100 m long faces with dips of 4-7°. The average thalweg gradient is 0.68° along this reach, which is considerably steeper than the average gradient throughout the data (0.55°). On the seabed dip map the knickpoints are almost indiscernible and the thalweg width is constant (Fig. 4.8C). Truncation of folded reflections below the channel-levee system shows that a substantial amount of strata has been eroded at this location (Fig. 4.8B). The CLS is only c. 100 m thick and no outer levees have been deposited at this location (Fig. 4.8D).

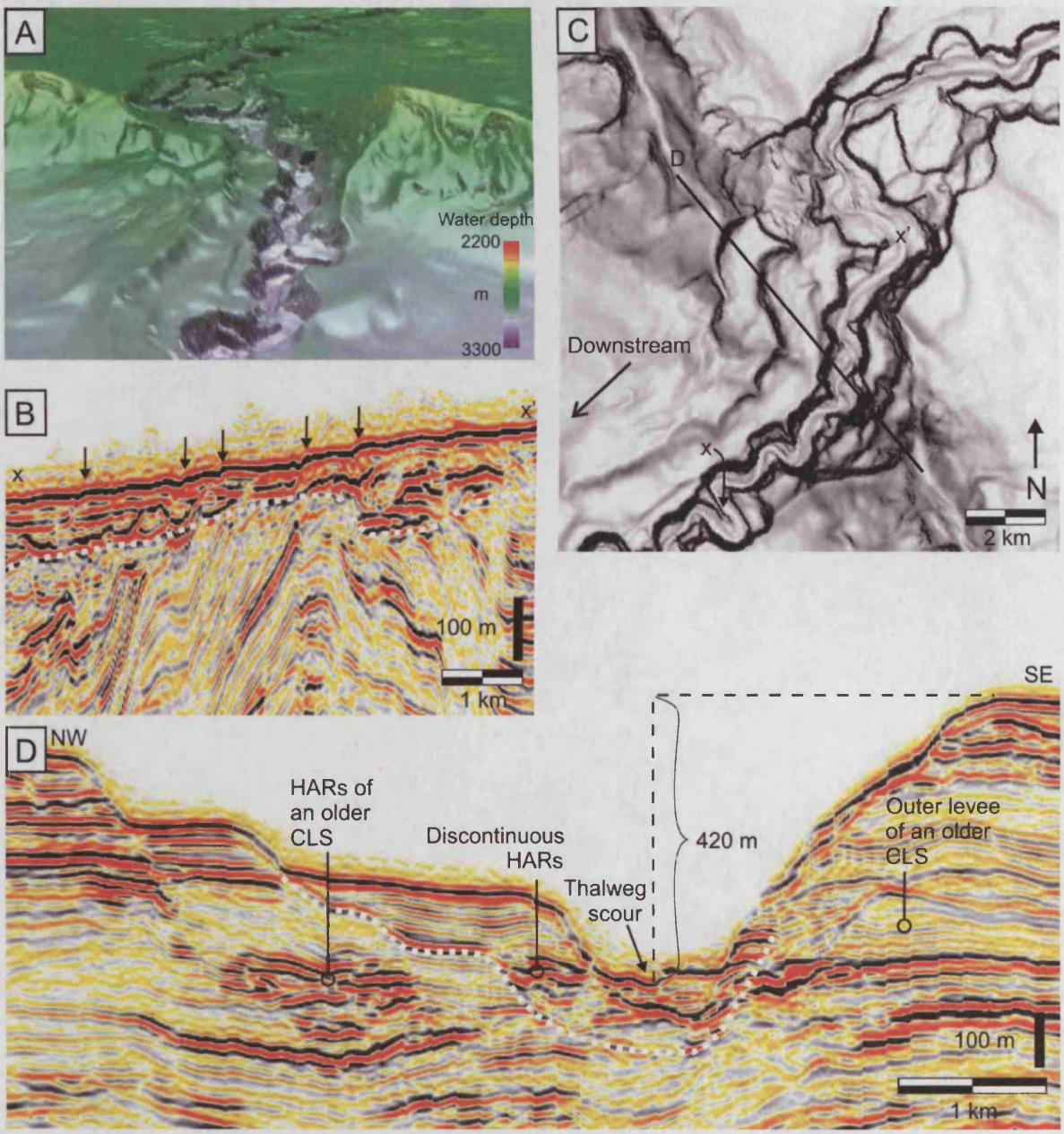

Figure 4.8. Morphology of the channel across the frontal fold (knickpoint 5). (A) 3D perspective view of seabed showing the channel as it breaches through the frontal fold. (B) Seismic section along the sinuous thalweg showing its profile and truncation of underlying folded reflections. Small knickpoints, 6-10 m high and 4-7° steep, are marked with arrows. Location of x-x' shown in (C). (C) Seabed dip magnitude map with present day thalweg imaged as a white line and locations of (B) and (D) indicated. Location shown in Fig. 4.2A. (D) Seismic line across the CLS at frontal fold. Parts of older channel systems are preserved on both sides of the present day channel. Dotted line on all cross sections marks the base of the CLS.

4.5.5 Reflection amplitude

The amplitude patterns of the seabed reflection in the vicinity of knickpoints are shown in Figure 4.9. The inter-channel seabed and most terraces are dominated by low-amplitude values shown in purple. The terraces closest to the thalweg commonly exhibit intermediate amplitude values shown in green. These terraces are no more than 30 m above the thalweg.

The highest values are shown in red and yellow and are found mainly in several kilometres long elongate zones within the channel upstream of knickpoints 1 and 2, where the thalweg is widened 6-fold and has a low gradient (Figs. 4.9A and B), and on the terraces upstream of knickpoint 3 (Fig. 4.9C). The high-amplitude (red and yellow) terraces upstream of knickpoint 3 are found in a c. 500 m wide and c. 5 km long zone, very similar to knickpoints 1 and 2 (Fig. 4.9C). The terraces are separated by the c. 80 m wide thalweg, which is entrenched 6-20 m below them. Small terraces with only intermediate amplitudes are observed adjacent to the thalweg across the frontal fold, no high-amplitude values are observed upstream of the fold (Fig. 4.9D).

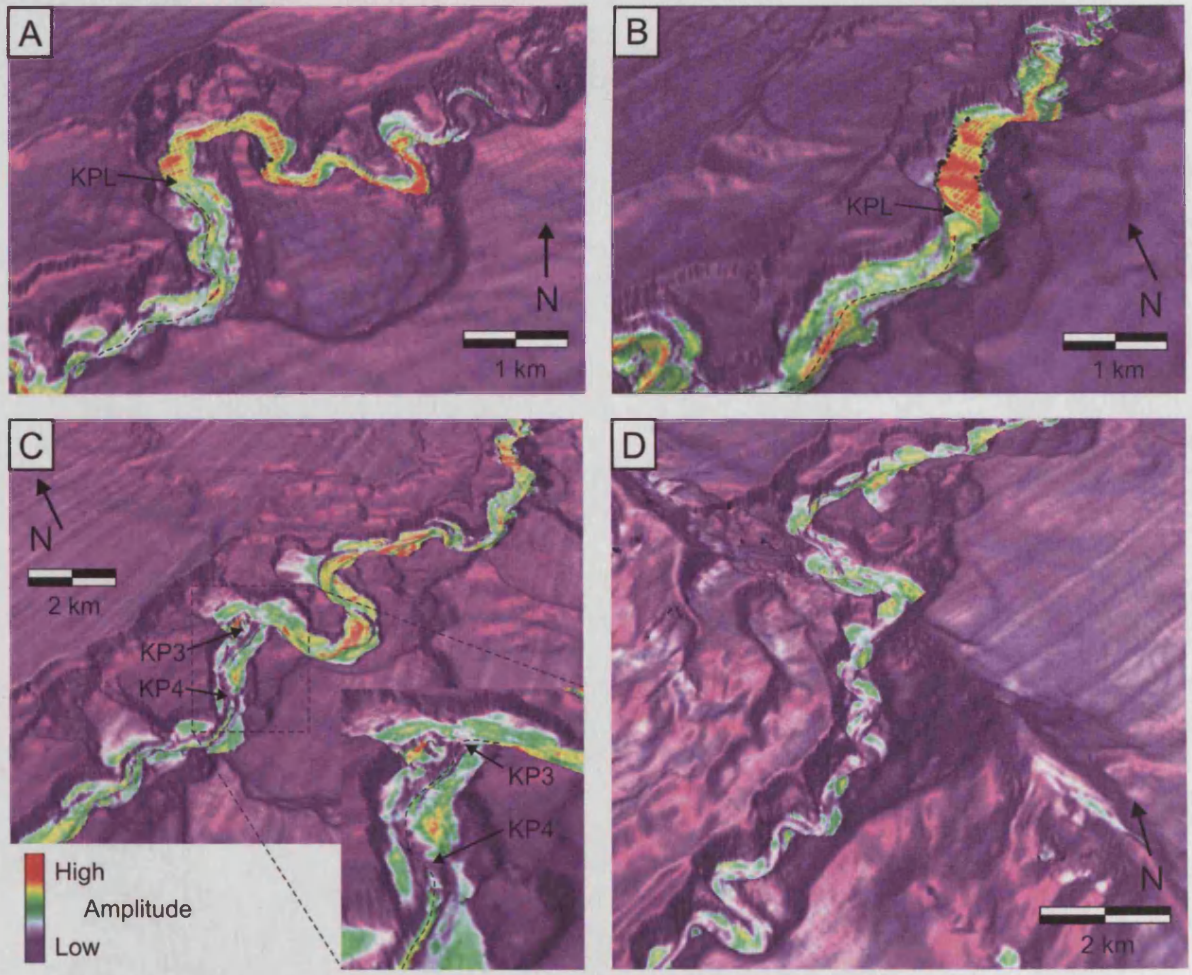

Figure 4.9. Perspective views of knickpoints with acoustic amplitude values of the seabed reflection shown. (A) Knickpoint 1 with high amplitudes shown in red and yellow concentrated on wide low-angle zone upstream of the arcuate knickpoint lip (KPL). (B) Knickpoint 2 with high amplitudes upstream of knickpoint lip. (C) High amplitude values on terraces several kilometres upstream of knickpoint 3. (D) Terraces and channel floor across the frontal fold and upstream of it show moderate amplitude values (green).

4.6 INTERPRETATION OF SEISMIC DATA

The amplitude value of a reflection can give clues about grain size, with high amplitudes commonly corresponding to coarse-grained sediments (Deptuck et al., 2003; Posamentier and Kolla, 2003). Therefore the high amplitudes of some terraces and along the thalweg upstream of knickpoints 1-3 are interpreted as deposits of the coarsest load of turbidity currents. Although no information on real grain size is available, these deposits are referred to as "coarse deposits" below. The low-amplitude values on higher terraces and the inter-channel seabed are interpreted to correspond to fine-grained sediments derived from the turbidity current plume and hemipelagic sedimentation.

The high-amplitude reflections are interpreted to have a recent depositional origin based on the reflection geometry and thalweg morphology. The dipping reflection beneath the present day thalweg reflection upstream of knickpoint 2 (Fig. 4.6C) is interpreted as a previous channel cut that has been subsequently filled by coarse deposits manifested by flat HARs. The v-shaped geometry of the channel cross section downstream of knickpoint 2 (Fig. 4.6D) suggests less deposition and more dominant bypass or erosion by turbidity currents at this location and the channel is interpreted to be empty of coarse deposits. A high-amplitude terrace located on the northwest side of the thalweg in Figure 4.6 is interpreted as a cut terrace, i.e. an erosional remnant of high-amplitude channel-fill left behind after knickpoint migration. Truncation of folded reflections beneath the CLS and the low thickness of the CLS deposits across the frontal fold (Fig. 4.8) suggest that it has been a zone of erosion and bypass for a long time. However, it is difficult to assess the relative timing of phases of fold growth, channel erosion and fill. It is likely that both fold amplification and erosion have occurred episodically and that several knickpoints have already migrated through the entire frontal fold bringing the channel profile closer to equilibrium. Thus knickpoint 5 represents a more mature stage of knickpoint migration.

4.7 MODEL FOR KNICKPOINT FORMATION AND MIGRATION

The knickpoints in the studied channel-levee system are interpreted to have formed in response to gradient changes along the thalweg, brought about by the growth of the folds (Fig. 4.10). Although knickpoints could form as a response to changes in gravity flows, the location of knickpoints above the thrust and fold belt suggests structural control for their formation. Gradient changes can cause changes in sinuosity in some submarine channels (Pirmez et al.,

2000; Adeogba et al., 2005), however, the high degree of confinement of the studied thalweg within its levees (100-220 m deep) prevents major avulsion or sinuosity changes. Instead, flows passing through the channel respond to the uplift by depositing and eroding in specific areas. The uplift of an anticline across the channel causes local reduction of gradient and concavity of the thalweg upstream of the fold axis, and also an increase in gradient of the thalweg profile downstream of the fold. These changes in gradient have an effect on the behaviour of turbidity currents within the channel. Flows decelerate as gradient is reduced, which leads to deposition of the coarsest sediments within the flow. Deposition thus occurs upstream of the folds where gradient is decreased and knickpoints are formed downstream, where the gradient is increased and erosion is enhanced by flow acceleration (Fig. 4.10A). Similar process of sand deposition by turbidity currents on shallower upstream flanks and erosion or bypass on steeper downslope flanks is thought to be the mechanism by which upstream-migrating sediment waves are formed (e.g. Ercilla et al., 2002; Wynn and Stow, 2002). Adeogba et al. (2005) calculated that depositional fans developed after a 50-57 % reduction of gradient but 40 % change would be sufficient. In this study the thalweg gradient reduction is 55 % where deposition occurs upstream of folds.

It is proposed that knickpoints begin as small scours eroded by turbidity currents and that grow into larger features by positive feedback, in which steeper gradient enhances erosion and this newly formed erosional scour promotes further erosion. Increase in turbulence in steeper parts of the channel or hydraulic jumps (Komar, 1971) at the base of knickpoint faces may also play a role in increased erosion. Once formed, the knickpoints can smooth out or migrate upstream as zones of erosion and deposition (Fig. 4.10A; T_3 - T_4). It is possible, that after migration of a knickpoint, no evidence of deposits is left (T_4A) or that coarse sediments are preserved preferentially upstream due to the increased erosion rate downstream of fold (T_4B). Increased erosion rate may also lead to preservation of older deposits upstream but not downstream (T_4C) (Fig. 4.10).

The location of knickpoint 1 upstream of a fold suggests that it has migrated upstream. Similar upstream migrations of knickpoints have also occurred on the Alaskan and Barbados accretionary prisms (Mitchell, 2006). Knickpoints 3 and 4 differ from 1 and 2 as they do not have 500 m wide arcuate knickpoint lips and widened thalwegs upstream of them. Their lips are as wide as the thalweg and also much steeper and shorter (Fig. 4.7). This may be the result of slightly different pre-conditions, such as rate of uplift or variability in the susceptibility of

the substrate to erosion, or represent a different stage in knickpoint development. Figure 4.10B illustrates two possibilities for the planform evolution of the knickpoints of this study.

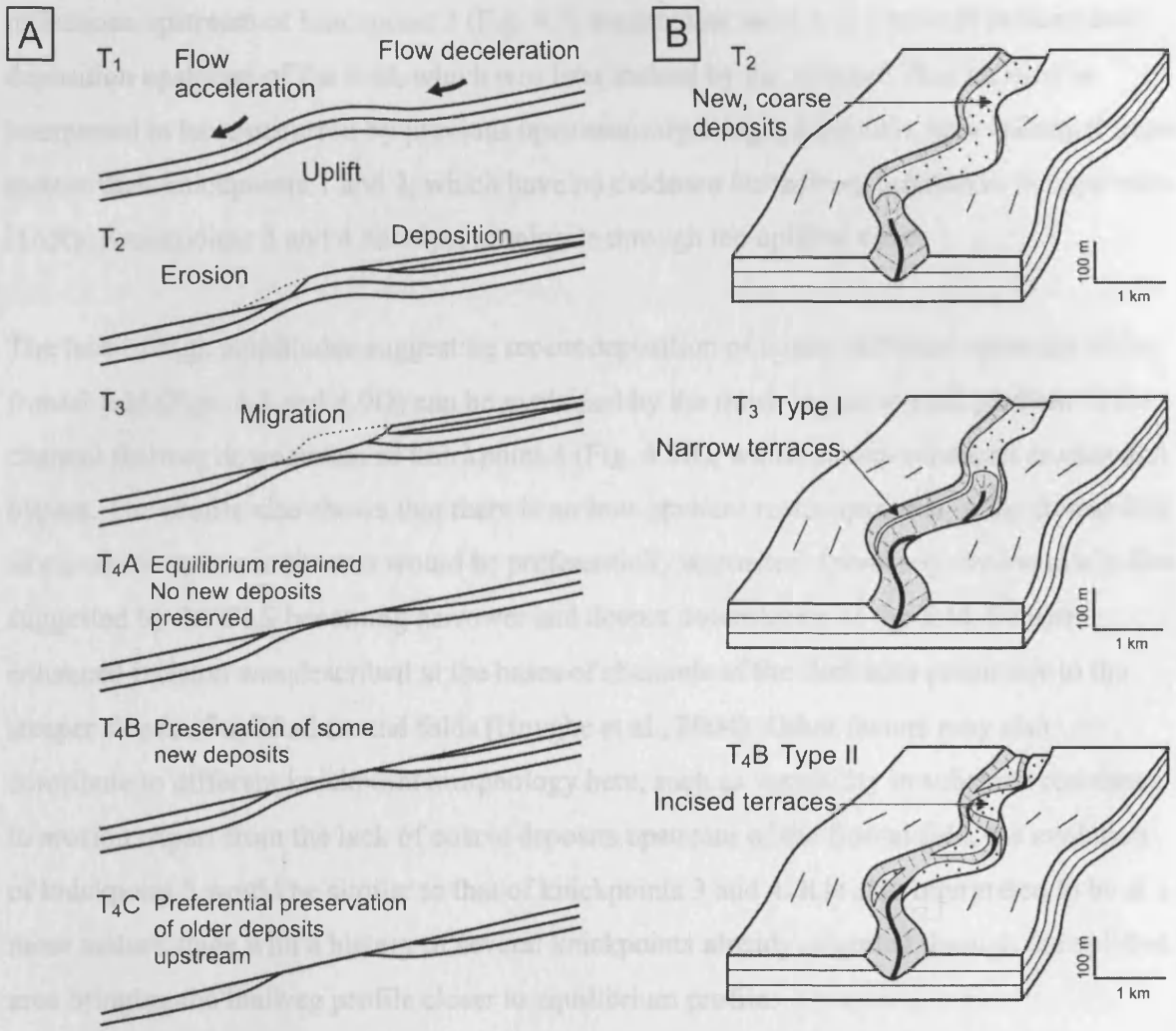

Figure 4.10. Idealised evolution of a channel-confined knickpoint. Not to scale. (A) Erosional and depositional processes along thalweg. At time T_1 the growing fold lifts the channel profile out of equilibrium. The uplift leads to local reduction of thalweg gradient upstream and increase in gradient downstream of the fold. This decelerates flows and causes deposition upstream and accelerates flows causing erosion downstream forming a knickpoint (T_2). The knickpoint can migrate upstream as erosion continues along the steep knickpoint face (T_3). The thalweg will regain its equilibrium profile eventually with no coarse sediments preserved upstream (T_4A), some coarse sediments preserved (T_4B) or preferential preservation of older sediments upstream and erosion downstream (T_4C). (B) 3D cartoons illustrating key development stages and variety of erosion and depositional patterns. Stippled pattern represents coarse sediments deposited upstream of folds due to fold growth. T_2-T_4 corresponds to T_2-T_4 in (A). Type I illustrates how a wide, headward-migrating knickpoint leaves only narrow terraces of coarse deposits behind, typical of knickpoints 1 and 2. Type II illustrates how a narrow thalweg incises into coarse deposits, cutting them into small terraces representative of the evolution of knickpoints 3-4.

Both models assume that the knickpoints migrate upstream (advect) rather than smooth out (diffuse). The assumption is based on the presence of cut terraces, sharp knickpoint lip morphology and the location of some knickpoints upstream of folds. Once formed, the valley-wide arcuate knickpoint can migrate upstream leaving only narrow cut terraces behind (Fig.

4.10B; T_3) as is observed in knickpoints 1 and 2. Alternatively, a thalweg-wide knickpoint can migrate upstream and the channel cuts into previously deposited coarse sediment leaving remnant sandy deposits on terraces above it (Fig. 4.10B; T_4). The zone of high-amplitude reflections upstream of knickpoint 3 (Fig. 4.9) suggest that there was a zone of preferential deposition upstream of the fold, which was later incised by the channel. This incision is interpreted to have occurred by previous upstream-migrating knickpoints, thus making it more mature than knickpoints 1 and 2, which have no evidence for thalweg incision in the upstream HARs. Knickpoints 3 and 4 have yet to migrate through the uplifted zone.

The lack of high amplitudes suggesting recent deposition of coarse sediment upstream of the frontal fold (Figs. 4.8 and 4.9D) can be explained by the much higher overall gradient of the channel thalweg downstream of knickpoint 4 (Fig. 4.4B), which causes enhanced erosion and bypass. The profile also shows that there is no low-gradient reach upstream of the frontal fold along which coarse sediments would be preferentially deposited. Increased erosion rate is also suggested by the CLS becoming narrower and deeper downstream of the fold. Similar enhanced incision was described at the bases of channels of the Barbados prism due to the steeper slopes of uplifted frontal folds (Huyghe et al., 2004). Other factors may also contribute to different knickpoint morphology here, such as variability in substrate resistance to erosion. Apart from the lack of coarse deposits upstream of the frontal fold, the evolution of knickpoint 5 would be similar to that of knickpoints 3 and 4. It is also interpreted to be at a more mature stage with a history of several knickpoints already migrated through the uplifted area bringing the thalweg profile closer to equilibrium profile.

4.8 DISCUSSION

4.8.1 Role of knickpoints in influencing channel architecture

Submarine channel complexes commonly show complex architectures with multiple internal erosion surfaces (Beaubouef et al., 1999; Deptuck et al., 2003; Posamentier and Kolla, 2003). Furthermore, knickpoints are being increasingly recognised in submarine channels (Table 4.1). Consequently, the role of knickpoint migration versus other processes, such as erosion by increasing the density and velocity of gravity flows within channels, is unclear.

The presence of knickpoints on the present day channel thalweg of the western Niger Delta suggests that their development could be a common process, which has likely occurred

throughout the evolution of the channel-levee system. Due to the limitations of seismic resolution, no knickpoints have been identified in the subsurface of the study area. The sinuous ribbon-like channel-fill elements have been cannibalised by younger channels, making mapping of a continuous channel-axis deposit and identification of knickpoints in the subsurface extremely challenging. It is, however, anticipated that the kind of knickpoints described in this paper can occur at any stage of channel evolution. Due to the transient nature of knickpoints, it is difficult to assess whether uplifted folds were eroded by erosive flows or by knickpoint migration, but the latter appears to be the dominant process by which they are eroded in the study area. It is also worth considering, when interpreting outcrops of channel-levee systems with multiple erosion surfaces, that the erosion could have been caused by local deformation of the channel profile, rather than wholesale changes in flow parameters.

The largest deposits upstream of knickpoints described here are tens of metres thick and thus in general only one reflection thick and difficult to identify in the subsurface from seismic reflection data. The sections across the channel both upstream and downstream of knickpoints (Figs. 4.5-4.7) indicate that there are much more continuous parallel high-amplitude reflections (i.e. relatively coarse sediments) upstream than downstream of the knickpoints. The implication of this is that stacking patterns and seismic facies of channel-fill can vary dramatically over short (100s of metres) distances along channel. This could be due to various processes. Sediments deposited uniformly along channel may be preferentially preserved upstream of folds, whereas enhanced erosion on steeper slopes downstream erodes them away. However, the distribution of high-amplitude values along present day thalweg (Fig. 4.9) strongly suggests that there are zones of preferential deposition of coarser sediments upstream of knickpoints 1-3. It is likely that they have also been zones of preferential deposition previously, resulting in more continuous reflections on seismic data upstream of folds. Depocentres forming upstream of diapirs are known in other submarine systems (e.g. Adeogba et al., 2005; Gee and Gawthorpe, 2006). Deposition upstream of anticlinal folds, and formation of knickpoints downstream of them, has also been documented in some fluvial systems, e.g. Wheeler Ridge (Burbank et al., 1996) and Kabul River (Burbank and Anderson, 2001). Additionally, the stream table experiments of Ouchi (1985) and the numerical models of Humphrey and Konrad (2000) and Snow and Slingerland (1990) had similar results. Both preferential deposition and preservation potential are higher upstream of folds, therefore coarser channel-axis deposits are more likely to be found upstream of folds.

Although the model presented here predicts migration of knickpoints and erosion of coarse deposits upstream of folds, they may also be preserved under certain conditions, e.g. by preferential preservation as discussed above or if the channel was abandoned and filled with hemipelagic sediments. Alternatively, avulsion within the channel-belt could also lead to preservation. One possible scenario for this is shown schematically in Figure 4.11. Avulsion may take place if the deposition on the upstream reach continues until it fills the channel to the height of adjacent terraces. The channel may then abandon the old thalweg reach containing the knickpoint and coarse sediment deposits, which would subsequently become sealed by fine-grained sediments from the upper parts of turbidity currents and hemipelagic sedimentation. In the studied system, large abandoned meanderloops occur near the folds (Fig. 4.2), suggesting that avulsion and sinuosity changes were more common in the earlier stages of channel evolution, probably when the channel was less confined and therefore meander bend growth easier. These lateral shifts were most likely influenced by the growth of the underlying structures with channels diverting around emerging folds or changing their sinuosity.

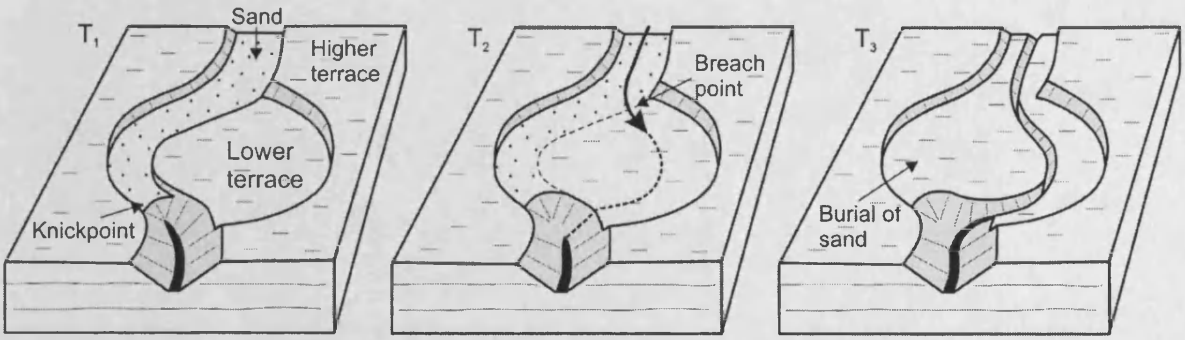

Figure 4.11. Simplified cartoon model showing the preservation of coarse sediment (stippled) upstream of knickpoint by avulsion within the channel-belt. Deposition upstream of a knickpoint fills the channel up to the level of an adjacent terrace (T_2), which is subsequently breached by a younger channel thalweg taking a different path (T_3). The coarser sediments are thus preserved underneath finer-grained parts of turbidity currents and hemipelagites.

4.8.2 The origin of high-amplitude terraces

The deposits on terraces are sometimes used to indicate the thickness or the volume of flows within channels (Babonneau et al., 2004). Small volume flows remain confined within the thalweg, whereas larger flows overflow onto terraces. In the studied system, the highest amplitudes are found only within the thalweg and the terraces closest to the thalweg (Fig. 4.9). The terraces with coarsest sediments lie less than 23 m above the thalweg and could therefore indicate the thickness of the coarse part of turbidity currents. However, regarding

Africa (Prather, 2003). Sediments accumulated on low-gradient reaches upstream of uplifted areas in the studied channel are interpreted to represent deposits from the coarsest part of turbidity currents and therefore could constitute a good reservoir. As individual deposits have volumes of < 0.1 km^3, they would not be large enough to be economic by themselves, but could be an element of a larger reservoir complex. Although upstream-migrating knickpoints may erode these deposits or cut them into small compartments, as illustrated in Figure 4.10B, the observations of this study indicate that there are more continuous HARs upstream of folds. This implies that both preferential deposition and preservation of coarse deposits occur upstream of folds where slope is locally reduced, and that sand distribution is at least partly controlled by structure.

4.9 CONCLUSIONS

1. Knickpoints form on a present day thalweg of a channel-levee system on the western Niger Delta as a result of the uplift of folds orthogonal to the channel. They are divided into three types according to their size, morphology and maturity. Type I knickpoints 1 and 2 are largest and least mature, Type II knickpoints 3 and 4 are intermediate, and the Type III is the smallest and most mature knickpoint type found across the frontal fold.
2. The high degree of confinement of the studied channel-levee system may restrict lateral changes of the channel in response to gradient changes and it therefore tries to readjust to equilibrium by erosional and depositional processes in specific areas. The reduction of thalweg gradient upstream of an anticline leads to deceleration of turbidity currents and deposition of their coarsest load. This interpretation is supported by the presence of several kilometres long zones of high-amplitude reflections representing relatively coarse-grained sediments along the channel upstream of some folds. Where the gradient is steeper on the basinward limb of the fold, the currents accelerate or increase in turbulence, enhancing erosion and causing the formation of knickpoints.
3. The knickpoints migrate upstream eroding the deposits upstream of them or incising them into terraces. High amplitudes on terraces adjacent to channel thalweg thus most likely record a history of deposition of coarse sediments. This is as a result of gradient reduction and subsequent incision and compartmentalisation of these deposits by a headward-migrating knickpoint, rather than thickness or volume changes of turbidity currents within the channel.

4. Knickpoint formation and migration may be an important process by which channels cut through uplifting thrust and fold belts as they strive to obtain their equilibrium profiles. However, as knickpoints are transient features, distinguishing the evidence of knickpoint migration from erosional currents from subsurface seismic data or outcrops is highly challenging.
5. Knickpoints influence the 3D architecture of channel-levee systems where they intersect dynamically changing seabed topography increasing the erosive character of stacked channel deposits and leading to more discontinuous HARs. Stacking patterns can vary dramatically over short distances along channel with more high-amplitude parallel reflections found upstream of folds.
6. The coarse deposits upstream of knickpoints could constitute an important element of reservoir architecture. The deposits are preserved e.g. if the channel system is abandoned or avulsion within the channel-belt occurs. The examples of this study suggest that avulsion and at least partial preservation takes place in this system at present day.

Chapter 5

5 CURRENT-GENERATED GIANT DEPRESSIONS ALONG SUBMARINE CHANNELS ON THE CONTINENTAL MARGIN OF THE ESPIRITO SANTO BASIN, BRAZIL

5.1 ABSTRACT

3D seismic data from the Espirito Santo Basin on the Brazilian continental margin reveal trails of depressions that follow the courses of underlying erosional submarine channels in Neogene strata. The depressions are interpreted to have formed as a result of Froude-supercritical turbidity currents flowing down the steep slopes and interacting with topographical irregularities at the bases of the channels. These irregularities cause instabilities within the currents and changes in the flow regime, bed shear stress and the capacity of currents to carry sediment. This results in the formation of zones dominated by deposition or erosion and bypass, which leads to the formation of sediment waves. As the sediment waves are confined within channels, they appear as asymmetric, flute-shaped depressions in plan view. The depressions become more symmetrical and circular as deposition increases on the shallow, upstream-dipping stoss flanks. Some depressions are filled with mounded onlap fill, which most likely resulted from changes in flow conditions. Examples on the present-day seafloor and from another dataset confirm that sediment waves and circular depressions develop above irregularities on the subsurface, such as knickpoints, failure scarps and the irregular tops of mass transport complexes. This paper gives the first description of trails of depressions that form due to flow dynamics in submarine settings using 3D seismic data. The process is ubiquitous, therefore the features should be common in submarine slope settings globally. The process probably plays an important role in how sediment is dispersed and preserved in submarine slopes and in how submarine landscapes are formed and modified.

5.2 INTRODUCTION

Continental margins have been the subject of considerable research effort since the discovery of meandering submarine channels on the continental margins of North America (Menard, 1955), especially after the advent of seismic reflection technology and now that deepwater channels have become important hydrocarbon reservoirs (e.g. Deptuck et al., 2003; Posamentier and Kolla, 2003). However, regardless of the vast amount of research into these submarine settings, many fundamental questions still remain with regard to depositional and erosional processes responsible for the architecture of continental margins and many features

are left unexplained. This paper focuses on one potentially important feature occurring in deepwater channels, namely roughly circular depressions that occur individually or in trails on steep slopes, in this case on the continental margin of Brazil.

Roughly circular depressions are common geomorphic features on continental margins. They can have several possible origins, such as salt withdrawal basins, gas pockmarks and collapse structures. Circular depressions that occur in trails above buried submarine channels are commonly ascribed to pockmarks due to de-fluidisation of channel-fill sands and hydrocarbon migration from deeper levels (Gay et al., 2003) or expulsion of fluidised channel deposits onto seafloor as a result of overpressure (Davies, 2003). However, turbidity currents can also, in certain conditions, erode the seabed and form trails of depressions. Such scours are referred to as 'cyclic steps' (Fildani et al., 2006). The term was first used by Whipple et al. (1998) to describe periodic upstream-migrating step-like bedforms, which are bounded upstream and downstream by hydraulic jumps (a sudden transition from supercritical to subcritical flow conditions) within the overriding flows (e.g. Fagherazzi and Sun, 2003; Taki and Parker, 2005; Fildani et al., 2006). They form when Froude-supercritical flows erode and deposit sediments on a steep seafloor in a way that leads to the formation of a trail of erosional scours if the flows are net-erosional or upstream-migrating sediment waves if the flows are net-depositional (Fagherazzi and Sun, 2003; Fildani et al., 2006).

This paper provides the first description of depressions, which are the result of flow dynamics and which are imaged by high quality 3D seismic data. Fildani et al. (2006) demonstrated that a trail of kilometre-scale flute-shaped depressions can be formed on the seafloor by Froude-supercritical turbidity currents and suggested that cyclic steps may be the process by which submarine channels initiate. This paper concentrates on the role they may play in modifying channel-fill architectures and the submarine landscape.

The aim of this paper is to describe trails of large depressions (200-600 m across) located above erosional channels and individual depressions located above scarps on the Espirito Santo Basin on the Brazilian continental margin, and propose a model for their formation by the actions of gravity flows. Analogous features on the present-day seafloor, shallow section and an additional dataset from the Niger Delta are studied to support the interpretation. 3D imaging and detailed analysis of reflection geometries of the seismic data enable the determination of the 3D morphology and evolution of the depressions. Based on this analysis

and supported by published models, it is concluded that these depressions are formed by erosional and depositional processes of gravity flows confined within slope channels.

5.3 SUBCRITICAL AND SUPERCRITICAL FLOWS AND THE FORMATION OF UNDULATING TOPOGRAPHY

Turbidity currents are submarine sediment-gravity flows, in which sediment is held in suspension by fluid turbulence (Middleton, 1993). They provide an important mechanism by which sediment is transported down continental slopes into deep sea (Deptuck et al., 2003). Turbidity currents are characterised by the dimensionless densimetric Froude number

$$Fr_d = U/(RCgh)^{1/2},$$

in which U is the depth-averaged flow velocity, R is the submerged specific gravity of the sediment, C is the layer-averaged volume of sediment in concentration, g is the gravitational acceleration and h is the flow depth (e.g. Fildani et al., 2006). Flows are said to be supercritical when $Fr_d > 1$ and subcritical when $Fr_d < 1$. Supercritical flows are swift and thin and more likely to be capable of eroding seafloor because of higher flow velocities (Nemec, 1990; Kubo and Nakajima, 2002; Fagherazzi and Sun, 2003). Subcritical flows are slow and thick and promote sediment deposition. However, flow regime alone does not determine whether erosion or deposition occurs. There is a correlation with slope gradient, velocity of the currents and sedimentation rate (e.g. Nakajima and Satoh, 2001; Ercilla et al., 2002). If none of the other parameters change, then the flow velocity controls the sedimentation rate across an undulating surface (Flood, 1988). Turbidity currents accelerate on steep slopes and decelerate where slope angle decreases. High velocity and shear stress at the base of the flow cause bypass or erosion on steeper slopes (Flood, 1988; Nemec, 1990; Nakajima and Satoh, 2001). At a break in slope, supercritical flow can abruptly transform into subcritical flow and thus form a hydraulic jump (Komar, 1971; Garcia and Parker, 1989; Fildani et al., 2006). This sudden drop in velocity and shear stress leads to enhanced deposition (Garcia and Parker, 1989). Deposition is caused by the loss of the capacity of the turbidity current to carry sediment in suspension when the velocity drops and turbulence weakens (Hiscott, 1994).

Turbidity currents that flow down submarine slopes have a wide range of local densimetric Froude numbers (Nakajima and Satoh, 2001). Irregularities in the topography of the seafloor may initiate instabilities in flows leading to the development of internal waves (Flood, 1988;

Ercilla et al., 2002) and the formation of wavy topography. Sediment waves, for example, are common undulating features on the seafloor, characterised by steeper lee flanks and shallower or upstream-dipping stoss flanks (Ercilla et al., 2002; Wynn et al., 2002a). Steeper slopes and lee flanks of sediment waves are sites of bypass and erosion (McHugh and Ryan, 2000; Nakajima and Satoh, 2001). This is evident from the observations of truncated reflections, erosional scours and flute marks found on several sediment wave lee flanks (McHugh and Ryan, 2000; Migeon et al., 2001). Sediment waves occur mainly as extensive wave fields on the seafloor or on levees of submarine channels (e.g. Wynn et al., 2000b; Wynn et al., 2000a; Nakajima and Satoh, 2001; Ercilla et al., 2002), but can also be confined within channels (Wynn et al., 2000b; Wynn et al., 2002b).

Sediment waves migrate upcurrent due to deposition on stoss flanks and bypass or erosion on lee flanks, but how they are initiated is still a matter of a debate. Two hydraulic models are most commonly proposed for the formation of sediment waves: the antidune model (Kolla et al., 1980; Normark et al., 1980; Wynn et al., 2000b; Wynn et al., 2000a) and the lee wave model (Flood, 1988; Howe, 1996). It has been suggested, however, that these models cannot explain the formation of sediment waves on the seafloor by turbidity currents, because the required hydraulic conditions cannot be met (Nakajima and Satoh, 2001; Kubo and Nakajima, 2002). Lee wave formation needs a steady flow with a $Fr_d < 0.32$ and antidunes are unstable short-lived bedforms that require Froude numbers of 0.844-1.77 for their formation (Nakajima and Satoh, 2001). In fact, it has been observed, that flows have highly variable Froude numbers on undulating surfaces (Kubo and Nakajima, 2002). Several authors have suggested that sediment wave formation is initiated as a result of variations in bottom slopes (Flood, 1988; Nakajima and Satoh, 2001; Ercilla et al., 2002; Kubo and Nakajima, 2002; Wynn and Stow, 2002; Fildani et al., 2006). Migeon et al. (2001) speculated that sediment wave initiation is the result of interaction between turbulent flows and loose seafloor. Fildani et al. (2006) proposed that some sediment waves are formed as transportational cyclic steps from depositional currents, whereas erosional currents produce a trail of depressions. Recent numerical and analogue models and experiments of Fagherazzi and Sun (2003), Kubo and Nakajima (2002), Nakajima and Satoh (2001), Sun and Parker (2005) and Taki and Parker (2005) have increased the understanding of the processes, which lead to the formation of wavy structures by turbidity currents, however, there is still a shortage of natural examples of these phenomena, especially in the submarine realm.

5.4 DATA AND METHODS

The 3D seismic reflection data cover an area of 1600 km^2 in the Espirito Santo Basin on the Brazilian continental margin in a present day water depth of 35 to 1800 m (Fig. 5.1). The line spacing is 12.5 m in both inline and crossline direction and the sample interval is 2 ms (milliseconds). The data are zero-phase migrated and displayed with SEG normal polarity and so that an increase in acoustic impedance is represented by a black-red-black reflection loop. No lithological or well data were available for this research, therefore estimated seismic velocities are used when calculating thicknesses of sediment packages and dips of horizons. A seismic velocity of 1500 ms^{-1} is used for seawater and 1800 ms^{-1} for the studied succession. Present day horizontal is used when converting and recording dips. The dominant frequency of the studied interval is c. 40 Hz. Using the average velocity of 1800 ms^{-1}, the dominant wavelength is c. 45 m and thus vertical resolution or tuning thickness ($\lambda 4^{-1}$) is c. 11 m. The work is based on a careful analysis of reflection geometries from vertical seismic sections and seismic geomorphology of horizons produced by mapping 3D seismic reflections. The nomenclature of Mitchum et al. (1977) is used when describing reflection geometries.

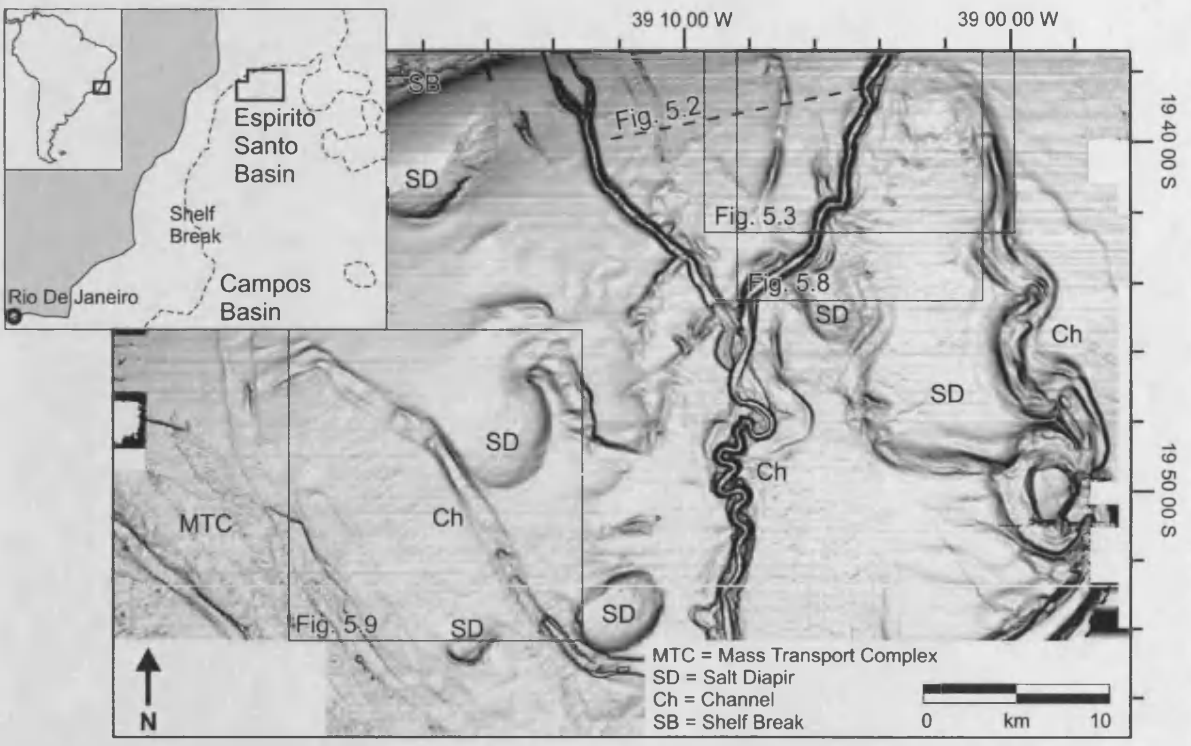

Figure 5.1. Seabed dip magnitude map of the 3D seismic data with location of Espirito Santo Basin on the Brazilian continental margin shown in the inset figures. Darker shading indicates greater dip. The main environments in the data are the shelf break (SB), salt diapirs (D) slope channels (Ch) and slumps/debrisflows (MTC). Location of Figures 5.2, 5.3, 5.8 and 5.9 are shown.

5.5 GEOLOGICAL SETTING

The Espirito Santo Basin is located on the continental margin of Brazil (Fig. 5.1). It is bounded by Campos Basin to the south and the volcanic Abrolhos Plateau to the north. The modern Doce River supplies sediment to the basin from the Mantiqueira and Espinhaço mountain chains. The structural evolution of the basin from late Jurassic to the late Aptian/early Albian includes pre-rift, synrift and transition stages, followed by continental drift stage (Fiduk et al., 2004). Stratigraphically, the basin is divided into five depositional megasequences: pre-rift, rift, transitional, transgressive marine and regressive marine (Fiduk et al., 2004). Aptian-age salt has been deforming into diapirs, rollers, canopies and thrusts (Jackson et al., 1994) from Albian until the Present. Since the Eocene, the Espirito Santo Basin has been a prograding shelf and slope environment (Fiduk et al., 2004).

The dataset is located immediately downstream of the present day shelf break and is dominated by salt diapirs, incised canyons, channels, slumps and debris flows, all visible on a dip map of the seafloor (Fig. 5.1). This paper focuses on a 100 km^2 area in the northeastern part of the dataset, where the seabed and shallow section are dominated by slope channels. As no stratigraphical or lithologic data were available for this work, the sub-division of the strata is based on seismic character (Units 1-4) and the work of Fiduk et al. (2004). The stratigraphy of the study area is illustrated by a representative seismic line (Fig. 5.2). At the bottom of the section, Cretaceous strata are overlain by high-amplitude, syn-compressional growth strata and low-amplitude, continuous reflections of Unit 1, which is of Palaeocene-Eocene age (Fig. 5.2). The Horizon E/O is an unconformity marking the change from low-amplitude to high-amplitude reflection character. The high-amplitude character of Unit 2 is caused by volcaniclastic material derived from the Abrolhos Plateau and other extrusions onshore (Fiduk et al., 2004). The Abrolhos Plateau was emplaced during the early to middle Eocene, thus making the age of the unconformity post middle Eocene or Oligocene in age. The c. 500 m thick Unit 3 has dominantly low-amplitude hummocky reflection configuration. Unit 4 is characterised by high-amplitude reflections and multiple small channels. Its top c. 50 m consists of a low-amplitude package with concordant reflections.

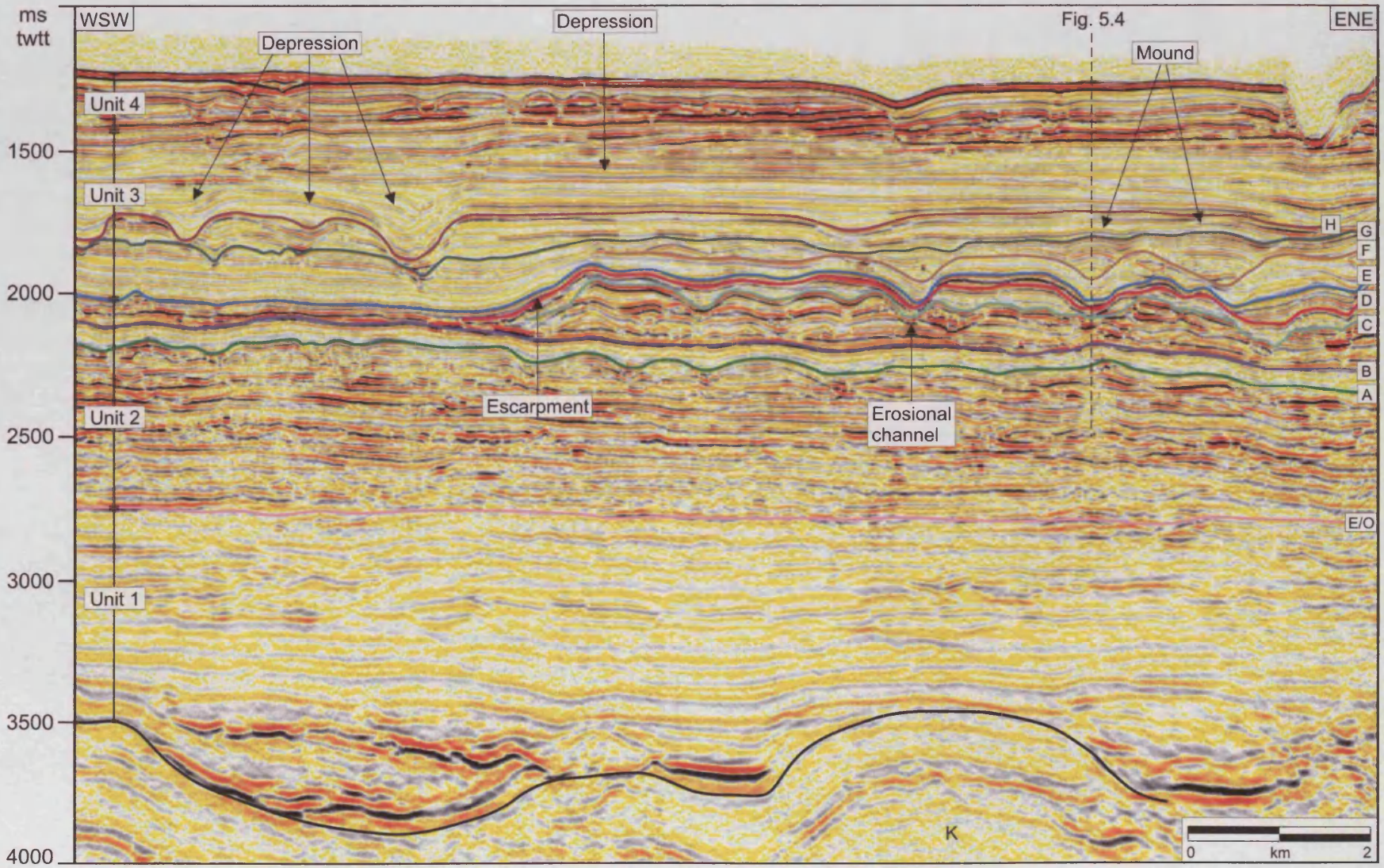

Figure 5.2. A seismic line across the study area showing the stratigraphy from Cretaceous basement (K) to the present day seafloor. The key horizons are interpreted and labelled A-H. E/O = post Middle Eocene-Oligocene unconformity. Location of the line is shown in figure 5.1.

5.6 3D SEISMIC CHARACTERISATION OF DEPRESSIONS

This paper focuses on the interval of the seismic data 0.5-1 seconds two-way-travel time (twtt) below the seabed, which includes the top part of Unit 2 and the bottom part Unit 3 (Fig. 5.2). The key horizons are labelled from bottom to top with letters A-H (Fig. 5.2). The truncation of seismic reflections indicates that there have been several phases of channel incision and infill. Horizon A is characterised by a number of erosional low-sinuosity channels, which are filled with low-amplitude reflection package A-B. The overlying package B-C consists of high-amplitude channelised deposits. The low-amplitude interval C-H is the interval, in which the depressions are found, mainly above the erosional channels of horizons C and G. Horizons C, D, E and G are described in more detail below.

5.6.1 Description of key horizons

Dip magnitude maps of the key horizons show a morphological evolution from a horizon cut by erosional channels to horizons with depressions and finally to a horizon with mounds (Fig. 5.3). The darker grey colour on the dip maps indicates higher dip, with highest measured value of approximately 35°. Horizon C is characterised by several erosional channels, which converge into one trending towards south and another one trending towards southeast (Fig. 5.3A). The channels are up to 85 m deep and 1.1 km wide measured from their margins, the bases of channels are up to 600 m wide. They incise into previous deposits of the package B-C (Fig. 5.2) and have dominantly sharp margins, although some channels with more rounded margins are found on both the eastern and western edges of the horizon (Fig. 5.3A). The western edge of the horizon marks the location where the reflection package B-C is truncated by a c. 120 m high escarpment (Fig. 5.2). Three arcuate scarps face towards the south in the middle of the horizon.

Horizon D is the first continuous reflection above Horizon C (Fig. 5.2). It is dominated by asymmetric depressions, which occur in trails that coincide with the location of the channels on Horizon C (Fig. 5.3B). Some depressions are roughly circular and some are elongate along the channel axis (see also Table 5.1). The colour variation on the dip map indicates that upstream flanks of the depressions are much steeper than downstream flanks. Especially the depressions on the eastern part of the horizon have very shallow downstream flanks and their plan view appearance resemble giant flute marks (Fig. 5.3B). The margins of the channels appear rounded and are occasionally marked by channel-margin faults.

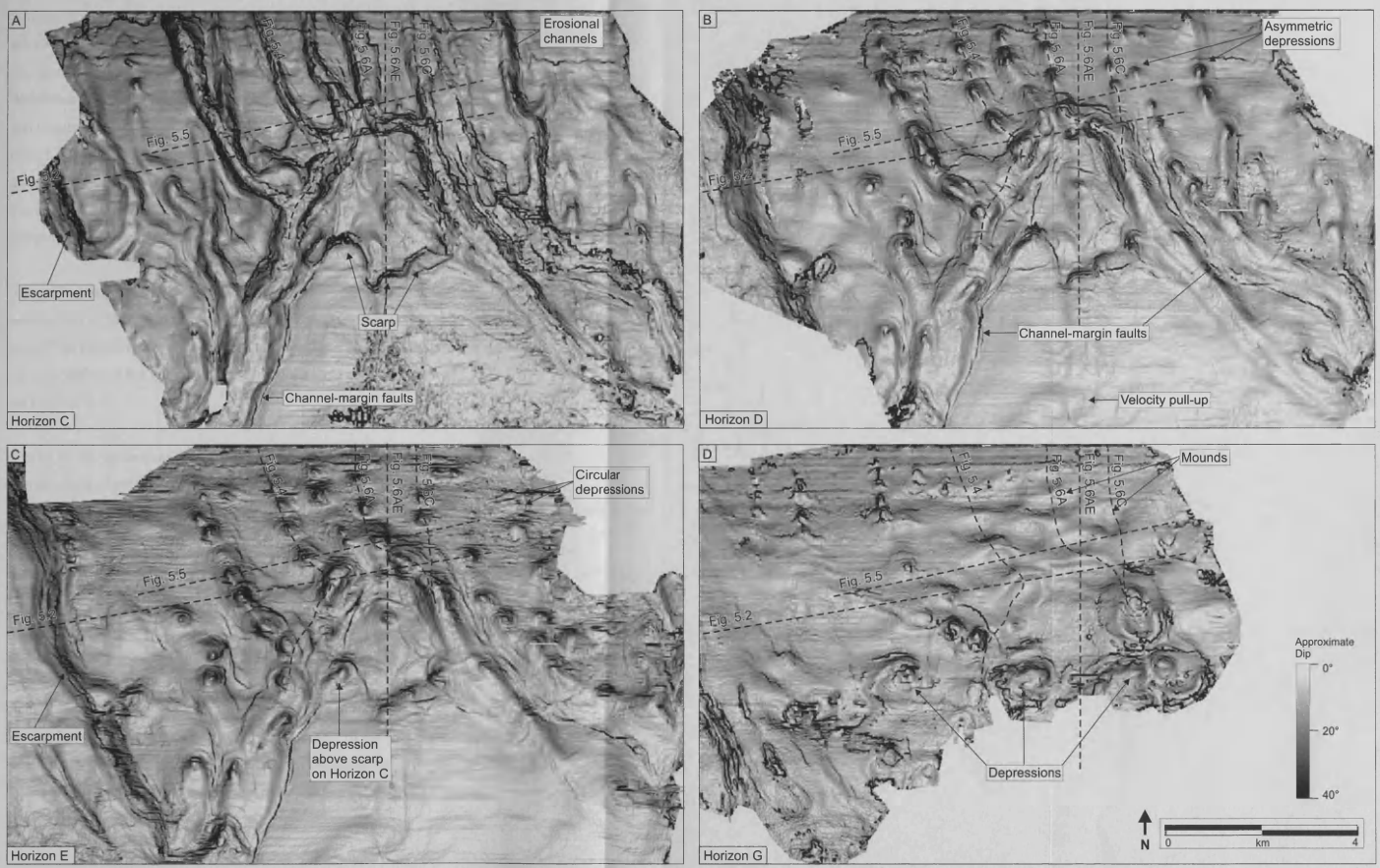

Figure 5.3. Dip magnitude maps of four key horizons. Location of Figures 5.2, 5.4 and 5.5 shown. (A) Erosional channels with sharp margins on the Horizon C. Note also arcuate scarps in the middle of the horizon. (B) Depressions on the Horizon D occur along the path of the erosional channels on C and are asymmetric with steeper upstream flanks and shallower downstream flanks. (C) More symmetrical, roughly circular depressions on the Horizon E. Note the depression that has formed above a scarp on Horizon C. (D) Horizon G has oval shaped mounds, which are located over some depressions on Horizons D and E. Some depressions occur on the southern part of the horizon. Scales are the same for each horizon.

Horizon E is a continuous reflection above Horizon D. It also is dominated by depressions, whose location correlates with the underlying channels on Horizon C (Figs. 5.3A and C). The depressions are nested above the depressions on Horizon D, however, there are 14 fewer depressions on Horizon E than on Horizon D (Table 5.1). The depressions are more circular and symmetrical with more prominent downstream flanks on Horizon E than on Horizon D (Fig. 5.3, Table 5.1). The axis of their deepest points does not align perfectly with the underlying channel on Horizon C, but is shifted up to 50 m to the east. The features on Horizon E have dominantly rounded appearance, the only sharp features are the channel-margin faults (Fig. 5.3C).

The most striking features on Horizon G are the rounded mounds, which occur on the north-eastern part of the horizon (Fig. 5.3D). They are up to 1 km across and slightly elongate along slope. The southern part contains circular depressions up to 1 km in diameter (Fig. 5.3D). The mounds and most but not all of the depressions align perfectly vertically with the depressions on Horizon E.

Not all of the depressions are located above erosional channels. One of the large (c. 1 km across) depressions on Horizon G (Fig. 5.3D) is located above an underlying arcuate scarp on Horizon C (Fig. 5.3A). The scarp itself is c. 60 m high and has a maximum dip of 35°. The depression can be seen also on Horizon E, at which level it is 37 m deep and has flanks that dip 23° downslope and 8° upslope (Fig. 5.3C).

5.6.2 Detailed description of depression and reflection geometry

The seismic character of the key reflections and reflection packages are described below using a representative seismic traverse along one of the erosional channels on Horizon C (Fig. 5.4) and an across-channel traverse following the strike of the slope (along slope) (Fig. 5.5). The along-channel traverse shows a typical development of the channel-fill from a relatively smooth profile (Horizon C) to undulating with depressions (Horizons D-F) to undulating with mounds (Horizon F) (Fig. 5.4). Further examples are presented in Figure 5.6.

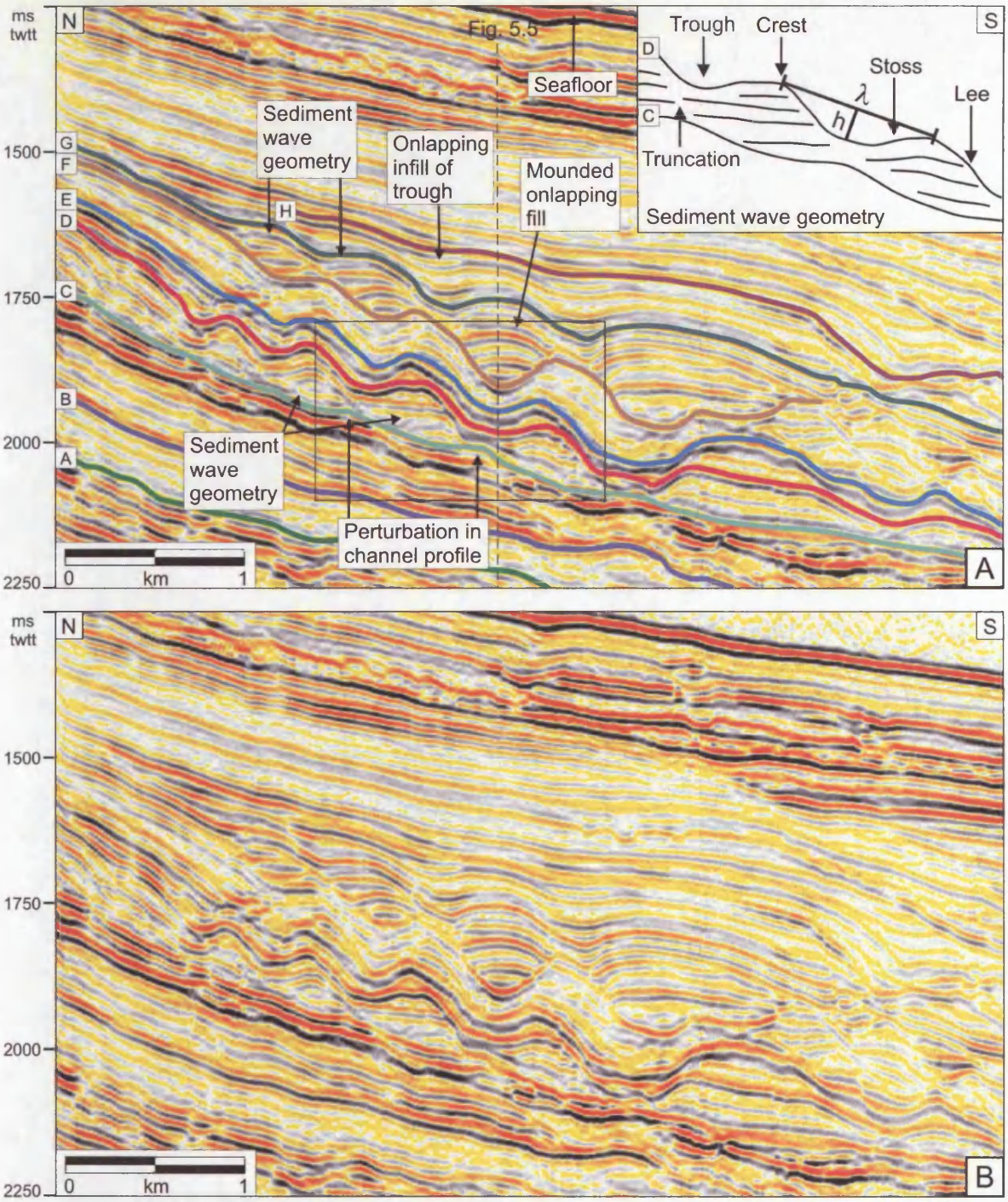

Figure 5.4. (A) Seismic traverse along one of the erosional channels of Horizon C showing the reflection geometry of the key horizons and reflection packages. The inset shows sediment wave terminology, which is used to describe the reflection package C-D. λ is the crest-to-crest distance (also the length of the depressions) and h denotes the depth of the depression forming between the crests. Location of the line shown in Figure 5.3. (B) Same line uninterpreted.

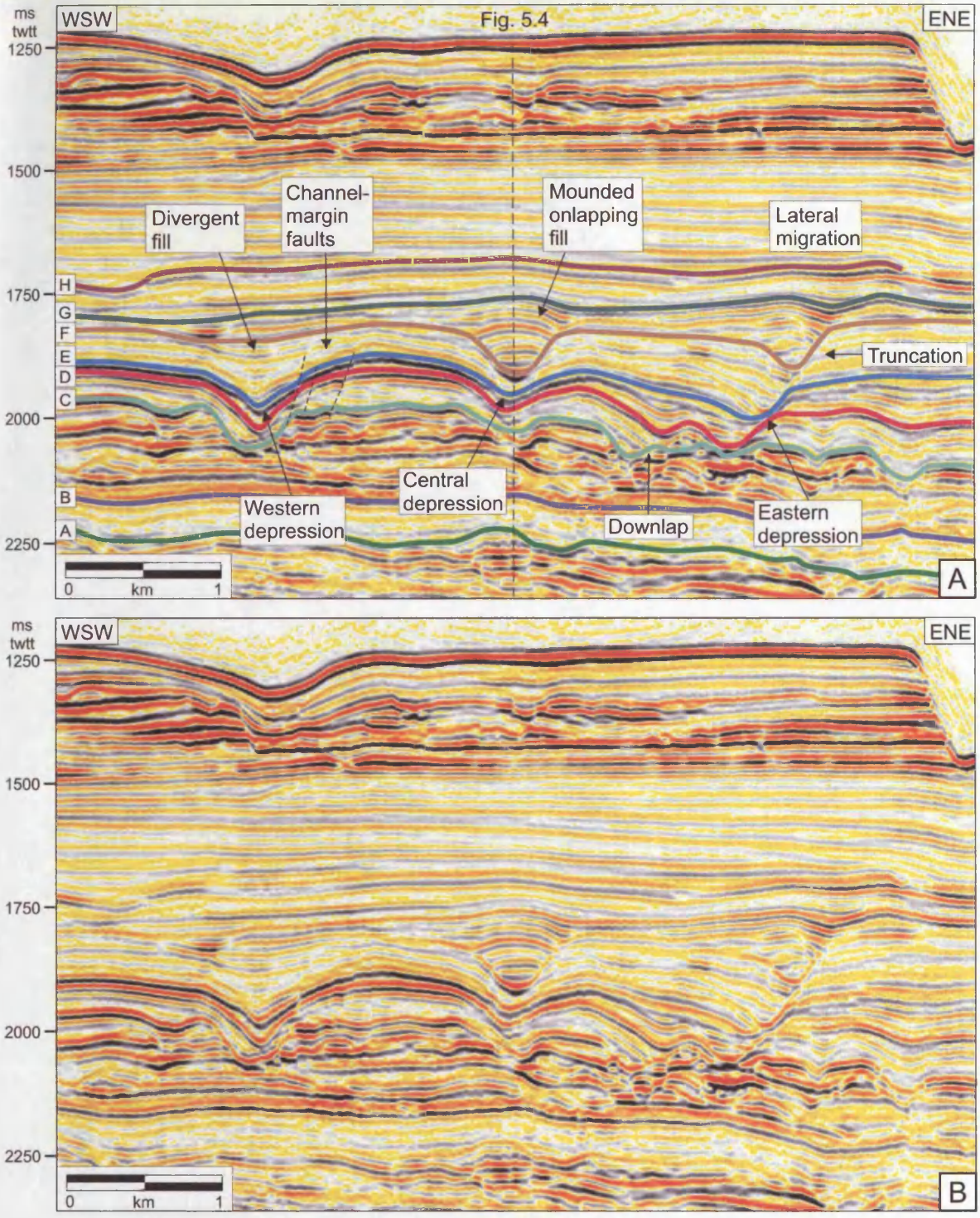

Figure 5.5. (A) Seismic traverse along-slope and across some of the erosional channels showing the reflection geometry in the vicinity of three depressions on Horizon E. The western depression has been mainly filled by divergent fill reflection package E-F. The central and eastern depression have mounded onlap fills between reflections F and G. The eastern channel-depression complex shows also lateral migration towards east. Location of the line is shown in Figure 5.3. (B) Uninterpreted.

The base of one of the erosional channels on Horizon C has a relatively smooth concave profile with some undulations (Fig. 5.4). Its gradient changes from 5-7° at the proximal end to 1.5-3° at the distal part of the profile. The truncation of the reflections of package B-C indicates that the channel is incised into previous deposits (Figs. 5.2 and 5.5). Above the erosional channel on Horizon C, the reflection package C-D contains hummocky/undulating reflections, which form a configuration resembling upstream-migrating sediment waves, and therefore wave terminology is used to describe them (see inset in Fig. 5.4). The reflection package is thickest at the crests and the reflections are truncated on the downslope (lee) flanks (Fig. 5.4). In cross section, the package C-D has an irregular thickness with diverging reflections (Fig. 5.5). Some reflections apparently downlap onto channel floor on Horizon C or are truncated by Horizon D.

The continuous reflection D drapes the wave-like reflections of the package C-D (Fig. 5.4). A typical crest to crest distance (λ) measured at this level is c. 400 m (Table 5.1). This undulating morphology is confined within the channel so that the troughs, which are bounded by the wave crests and the channel margins, form a series of depressions along the channel. Lee flanks of the waves make the upslope flanks of the depressions and stoss flanks the downslope flanks (Figs. 5.3B and 5.4). The depressions are asymmetrical with steep upslope flanks, which dip 4-20° and shallower downslope flanks that dip 1-14° in the upslope direction (Fig. 5.4, Table 5.1). The depressions are typically c. 20 m deep when measured along the channel (h in inset of Fig. 5.4), but range from c. 8 to up to 56 m (Table 5.1). The depressions tend to be shallower in the proximal and distal areas.

Horizon E has a similar appearance on the along-channel section to Horizon D (Fig. 5.4). The angles measured along-channel are similar on upslope flanks (5.5-13°), but the downslope flanks of Horizon E are much steeper, dipping 5-17° to upslope direction (Table 5.1). This confirms the observation made on the dip maps that the depressions are more symmetrical on Horizon E than on Horizon D (Figs. 5.3C and B). The package D-E has a relatively even thickness on the along-channel traverse (Fig. 5.4), but the across-channel section shows divergent and onlapping reflection geometries filling some of the depressions (Fig. 5.5).

The low-amplitude package E-F has a relatively constant thickness along-channel (Fig. 5.4), but shows variation along slope (Fig. 5.5). It is thinner within the central depression crossed by Figure 5.4 and fills the depression to the west of it with a divergent fill (Fig. 5.5). The

reflections apparently downlap and onlap the eastern flank of the easternmost depression, which leads to lateral migration of the depression geometry eastward as the stratigraphy is being built up.

The interval F-G fills in the remaining depressions with onlap or mounded onlap fill (Figs. 5.4 and 5.5). The crests of the mounds align vertically with the bases of depressions. These reflections form roughly symmetrical mounds in cross sections (Fig. 5.5), but on the along-channel section some of them have an asymmetrical geometry, with reflections stepping upslope and resembling upstream-migrating sediment waves (Fig. 5.4). The elongate depressions between the mounds are filled by divergent reflections of package G-H.

Traverses along the other channels show similar reflection morphology to what described above although fewer depressions (Figs. 5.6A-D). A seismic line aligned dewnslope and located between the two channels shown in Figures 5.6A-D show no wavy geometry between horizons C to F except for when it crosses a channel and also above a large scarp (Figs. 5.6E-F).

There is a weak linear relationship with the diameter and the depth of the depressions, especially on the depressions on Horizon E if the diameter is measured along channel (length of depression) (Fig. 5.7A-C). The morphometric measurements of the depressions reveal also the greater circularity of the depressions on Horizon E (average length:width ratio 1.17) than on Horizon D (length:width ratio 1.46) (Fig. 5.7E-F, Table 5.1).

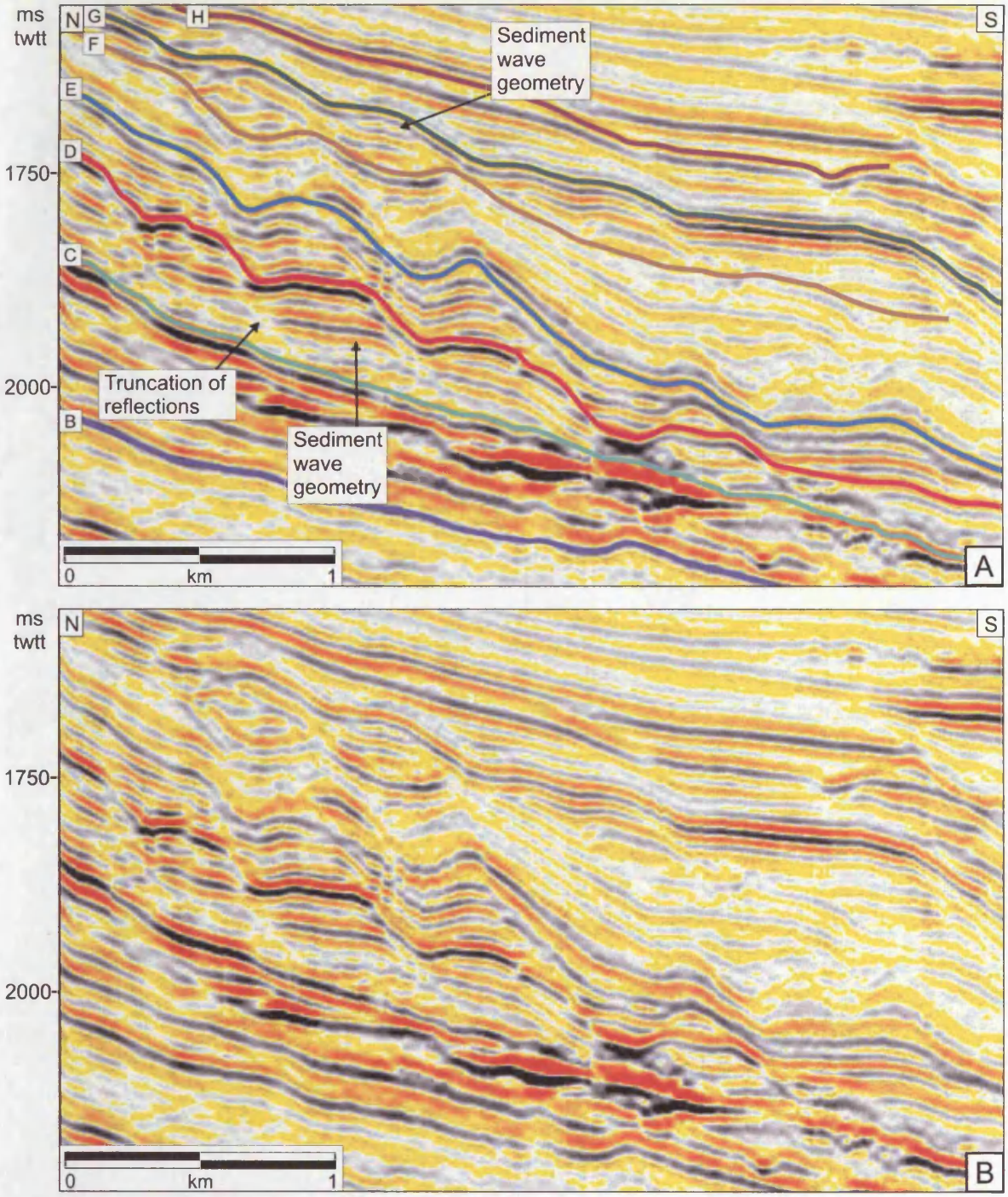

Figure 5.6. (A) Seismic traverse along one of the erosional channels of Horizon C showing the reflection geometry of the key horizons and reflection packages. Note the truncation of reflections on the downslope side within packages C-D and D-E that gives them a sediment wave geometry. (B) (A) uninterpreted. Location of the line shown in Figure 5.3.

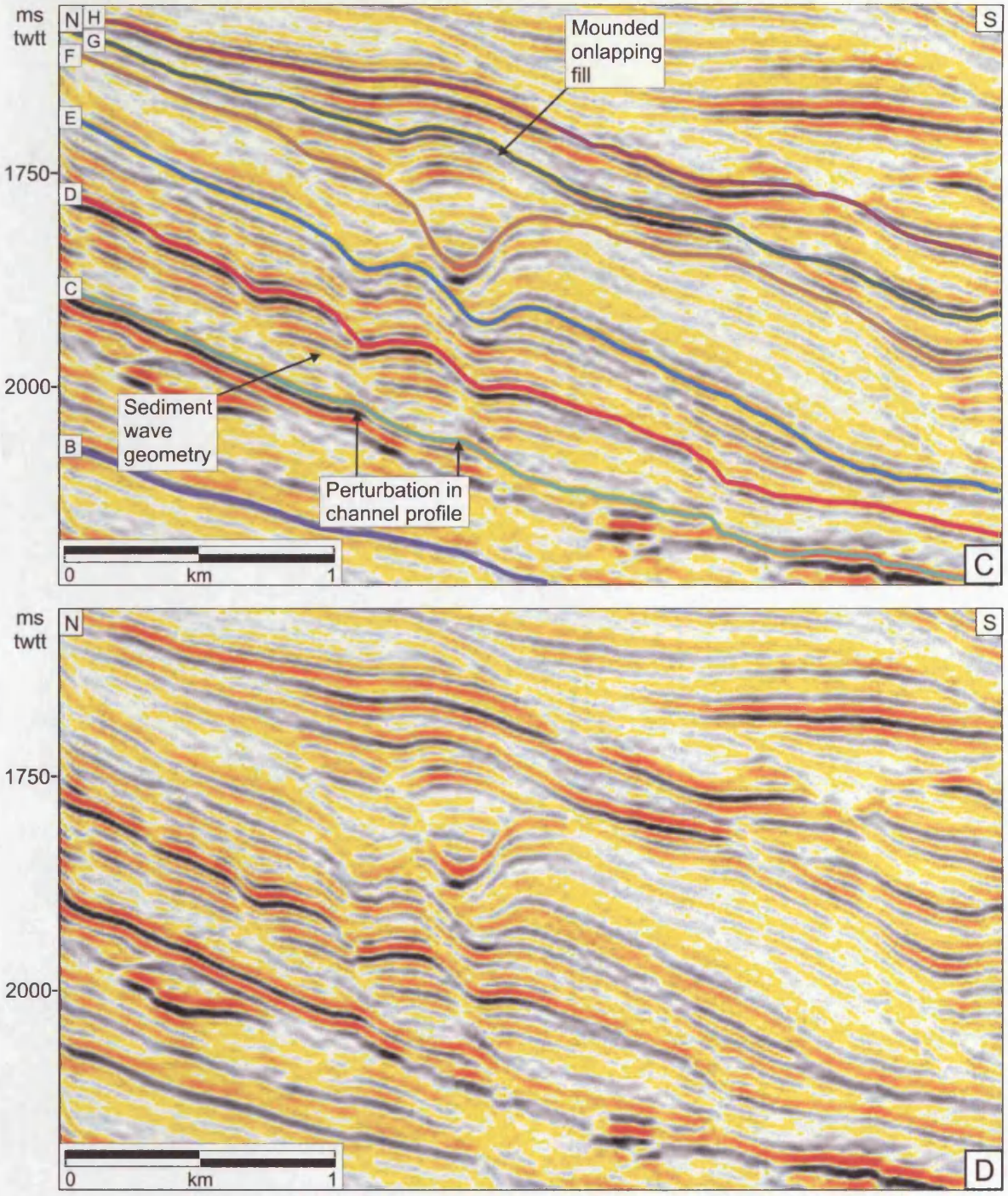

Figure 5.6. (continued). (C) Seismic traverse along one of the erosional channels of Horizon C showing the reflection geometry of the key horizons and reflection packages. Note the truncation of reflections on the downslope side within packages C-D that gives them a sediment wave geometry. Note also that on the horizon C there are 3 depressions, 2 on horizon E but only one on horizon F. (D) (C) uninterpreted. Location of the line shown in Figure 5.3.

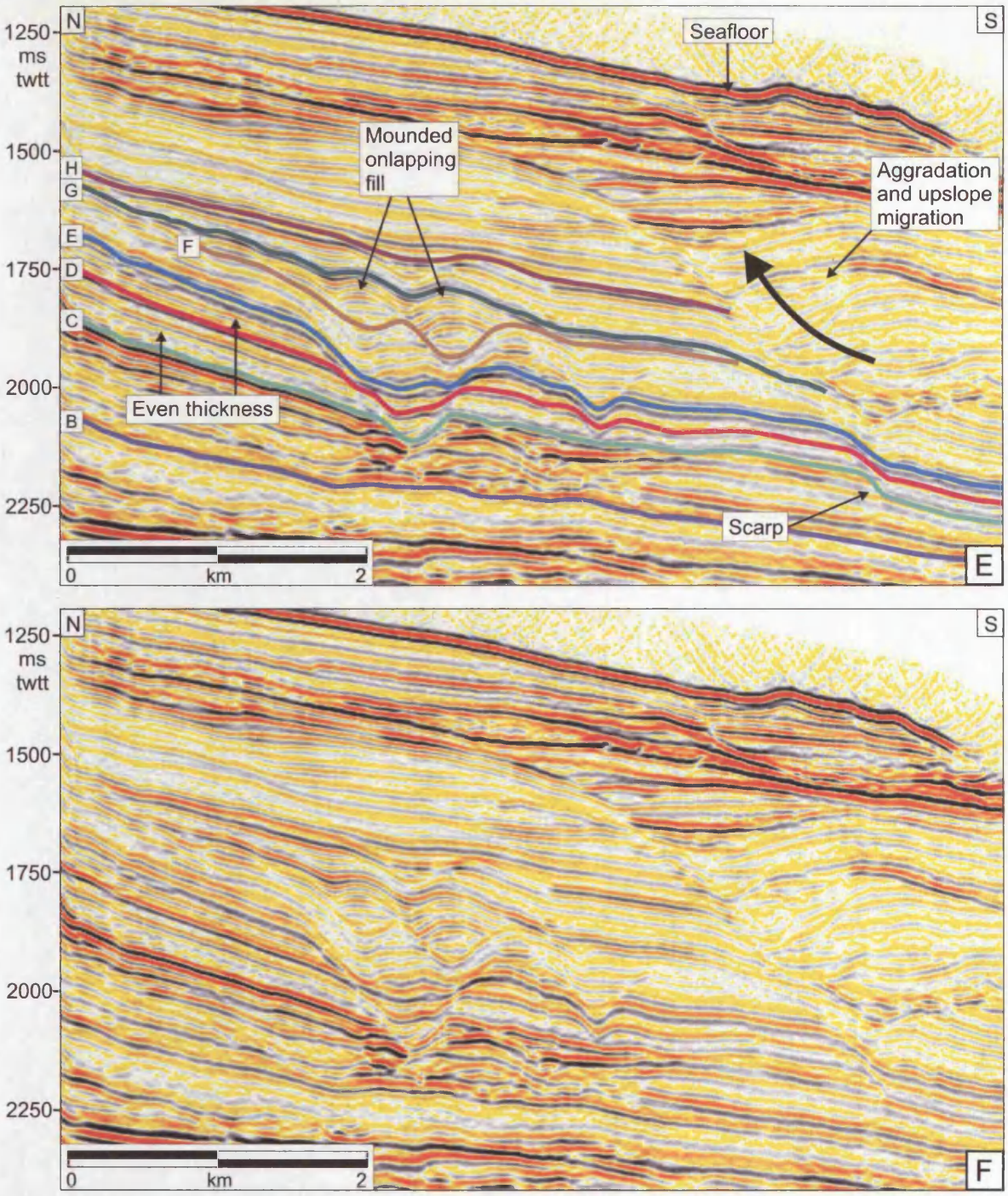

Figure 5.6. (continued). (E) A seismic line aligned downslope and located between two channels on horizon C. See location in Figure 5.3. Note the even thickness of the seismic packages C-D and D-E in comparison to the sediment wave geometry observed in Figures 5.6A-D. The line crosses one of the channels, above which two mounds with mounded onlapping fill have formed. A depression-mound complex has also aggraded and migrated upslope. Its lowest stratigraphic position is located above a scarp. (F) (E) uninterpreted.

Table 5.1. Morphometric measurements of depressions on Horizons D and E and the seafloor.

	Horizon D *(n=55)*	**Horizon E** *(n=41)*	**Seafloor** *(n=12)*
Depression depth (m)			
average	23.63	32.50	19.84
min	7.79	10.60	8.57
max	56.36	64.25	31.00
mode			
median	22.58	32.69	18.85
Upslope angles (degrees)			
average	12.97	13.33	6.81
min	4.19	5.50	4.58
max	21.51	21.77	9.26
mode			
median	12.94	13.00	6.72
Downslope angles (degrees)			
average	-2.27	-4.75	-3.42
min	-14.09	-17.02	-6.88
max	7.62	0.72	0.30
mode			
median	-1.74	-4.28	-3.55
Depression diameter (slope parallel) (m)			
average	293.08	404.17	531.25
min	125.00	137.50	362.50
max	587.50	750.00	850.00
mode	337.50	375.00	462.50
median	287.50	381.25	531.25
Depression diameter (slope normal) (m)			
average	405.13	448.21	397.92
min	162.50	162.50	238.00
max	800.00	1062.50	612.50
mode	337.50	325.00	350.00
median	343.75	406.25	362.50
Depression length:width ratio			
average	1.46	1.17	0.80
min	0.61	0.51	0.40
max	3.06	2.00	1.48
mode	1.45	2.00	
median	1.40	1.10	0.70
Depression area (km^2)			
average	0.11	0.16	0.40
min	0.02	0.03	0.13
max	0.36	0.50	3.14
mode	0.11	0.03	0.16
median	0.08	0.13	0.16

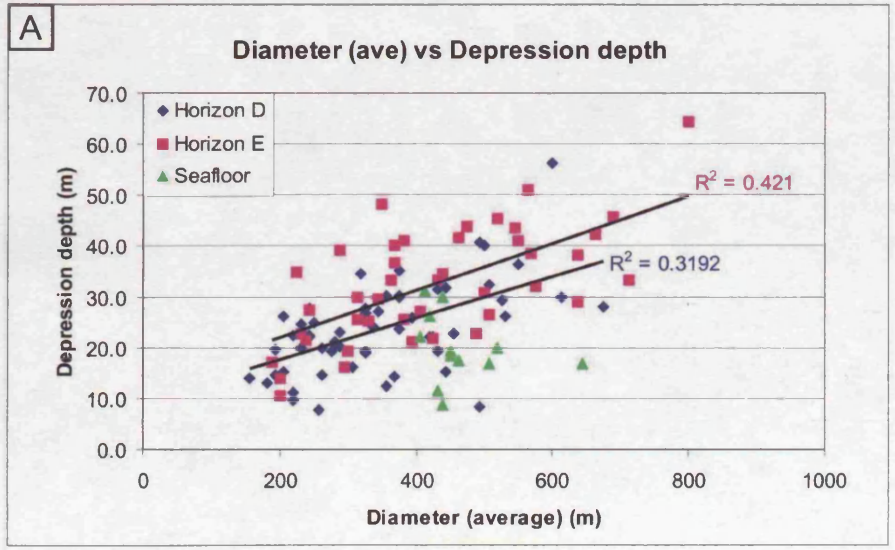

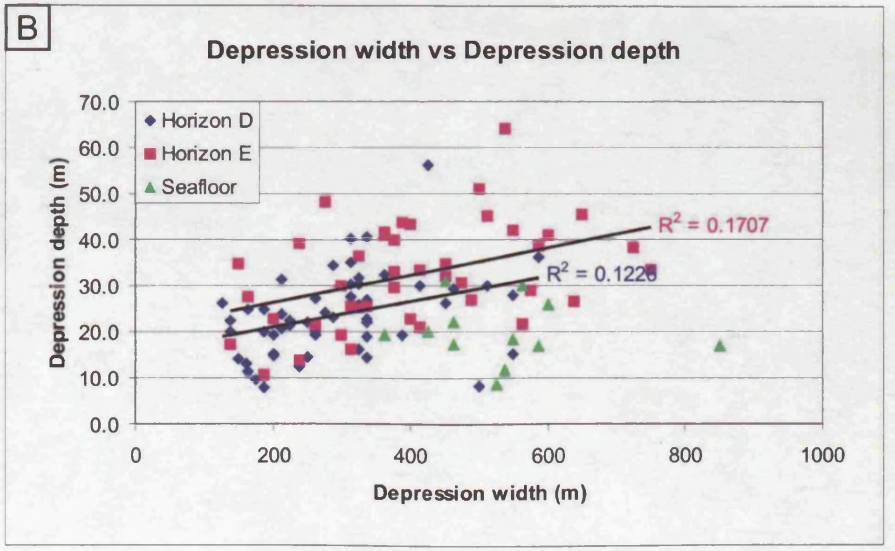

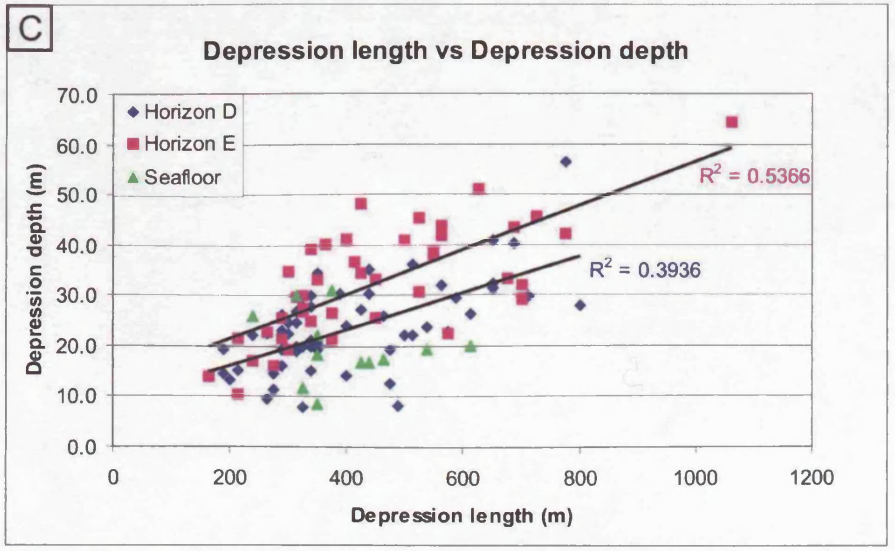

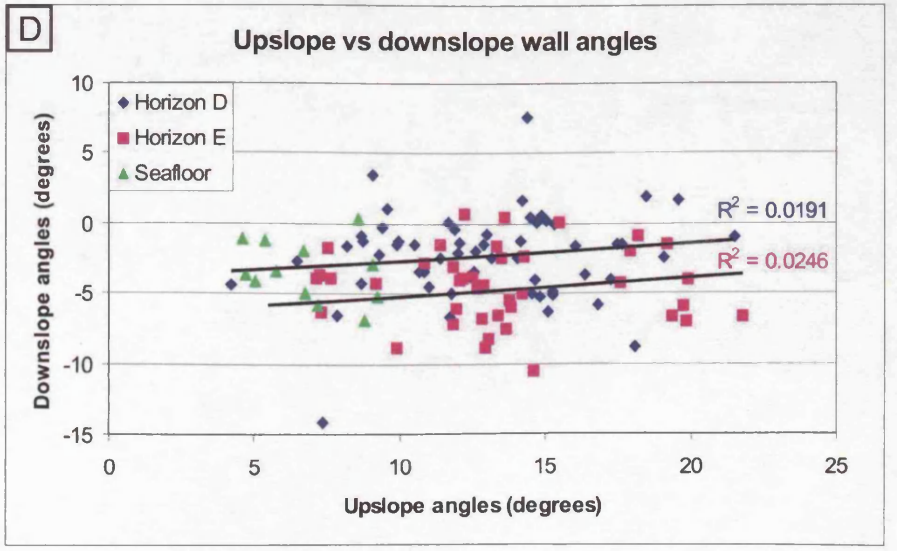

Figure 5.7. (continues)

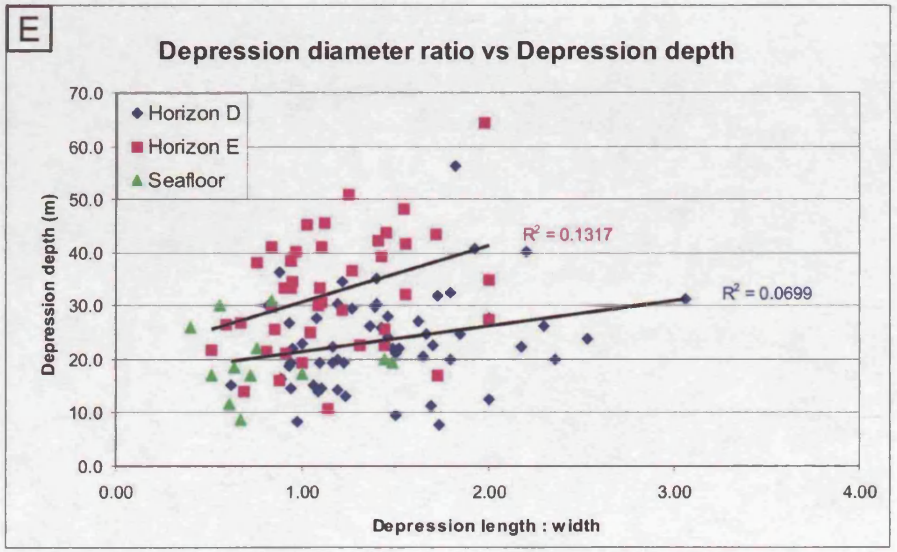

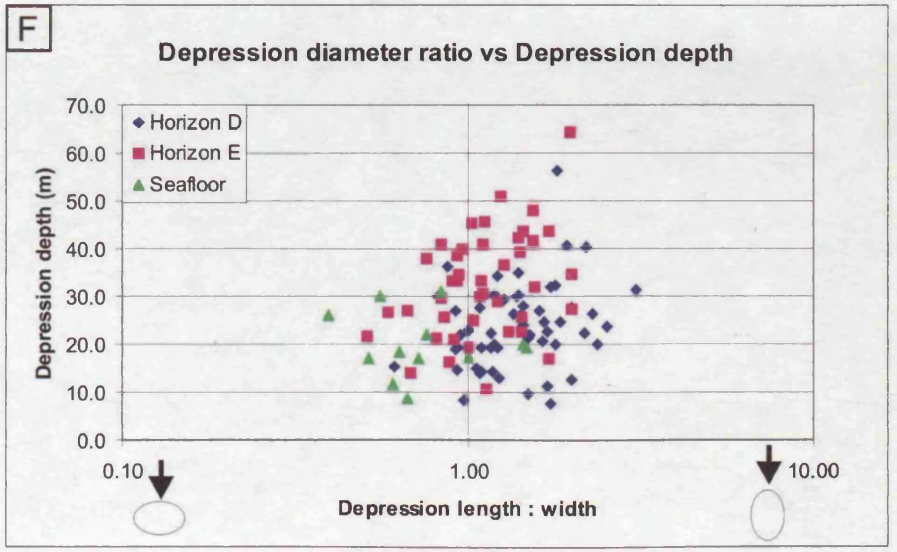

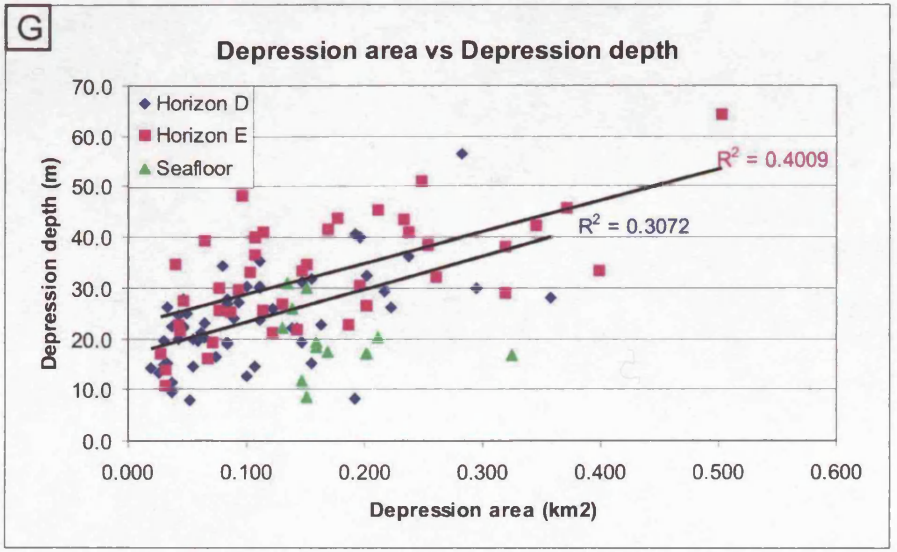

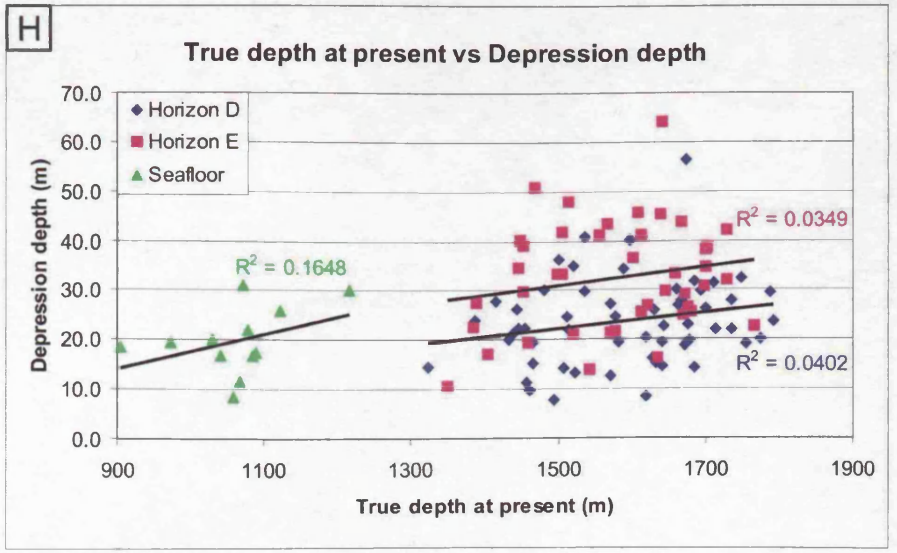

Figure 5.7. (continued)

Figure 5.7 (previous pages). Graphs showing relationships between selected dimensions of the depressions on the buried Horizons D and E and on the seafloor. The results are also tabulated in Table 5.1. (A-C) Graphs showing weak correlation with depression deiameter and depth within the buried depressions but not on the seafloor. (D) A graph showing no correlation between the angles of downslope and upslope walls of the depressions. (E-F) Graphs illustrating the circularity of the depressions. The depressions on Horizon D are longer than they are wide (elongate along channel), whereas the depressions on Horizon E are more circular (with values close to 1) and the depressions on the seafloor are slightly elongate along slope (wider than long). (G) A graph showing a weak linear correlation between the depression area and depth within the buried depressions but not within the seafloor examples. (H) Graph showing no correlation between depression depth and the true depth of the depression (from present day seafloor disregarding compaction).

5.7 DEPRESSIONS ON THE SEAFLOOR

Although the depressions in the Espirito Santo Basin are most abundant within the interval C-H, similar features are found on higher stratigraphic levels of Unit 3 (Fig. 5.2), as well as on the present day seafloor (Figs. 5.1, 5.8 and 5.9). The seafloor examples show clear evidence for flow activity and provide more details of how the formation of depressions and sediment waves may have been initiated. Similar features are also observed in other datasets, suggesting that their formation is a common process.

5.7.1 Depressions and sediment waves on the present day seafloor

A channel with rounded margins and an undulating profile on the seafloor is shown in the north-western corner of Figure 5.8A. The low-amplitude reflection package beneath the seafloor has an even thickness of c. 60 m on both sides of the channel (Figs. 5.8B and D), but along the channel its thickness varies remarkably (Fig. 5.8C). The reflection geometry resembles two upstream-migrating sediment waves with reflections stepping upslope on the stoss flanks and being truncated or thinned downslope on the lee flanks. The lee flanks have absolute dips of 5.35° and 5.69° and the dip of the stoss flanks of the first wave is 1.28°, whereas the second one dips 1.25° in the upslope direction, as measured on the seafloor. This means that a depression bounded by the wave crests and the channel margins is formed (Figs. 5.8A and C). The channel is 150 m wide, the crest to crest distance is 600 m and the depression is 17 m deep and circular in plan view, which makes it similar in scale and morphology to the depressions on Horizon D.

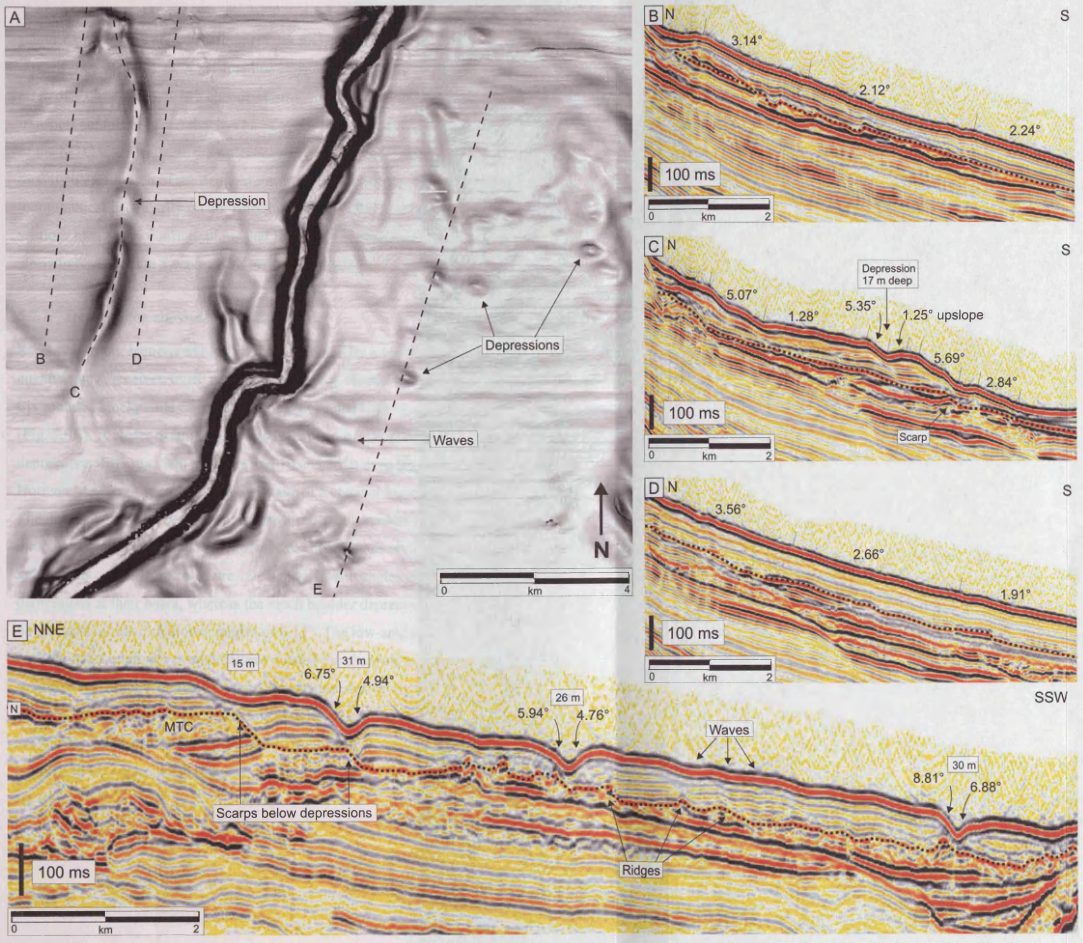

Figure 5.8. Irregular channel fill and depressions on seafloor formed above irregularities. (A) Dip map of the seafloor showing a channel with rounded margins west of an active channel. On eastern side of the active channel there are several, roughly circular depressions, c. 300 m across, on the seafloor. Location shown in Figure 5.1. (B) Seismic section west of the channel with smooth gradient and parallel reflections between Horizon N (dotted line) and seafloor. (C) Seismic traverse along the channel showing two sediment waves forming within the package N-seafloor. (D) Seismic section east of the channel with smooth gradient and parallel reflections between Horizon N and seafloor. (E) Seismic section across small depressions on the seafloor showing how they form above scarps on the underlying mass transport complex (MTC) and migrate upslope. Small sediment waves have formed above smaller irregularities on the Horizon N.

There are also several roughly circular depressions that are c. 300 m across and have a rounded appearance on the seafloor (Fig. 5.8A). The depressions are 9-31 m deep with flanks dipping 7-9° (Table 5.1). A seismic line across some of them shows that buried underneath c. 60 m of sediments, there is a chaotic seismic reflection package interpreted as a mass transport complex (MTC) that has an irregular top surface (Horizon N) (Fig. 5.8E). The relief of the MTC visibly affects the reflection geometry of the N-seafloor package. Significantly, directly beneath each of the depressions on the seafloor there is a scarp or a large topographical irregularity on the Horizon N. Some of the reflections of the package N-seafloor have wavy configurations that follow the underlying irregularities in relief of Horizon N. There are 5 waves with lee flanks dipping c. 2.6° and stoss flanks 0.7°.

5.7.2 Depressions above knickpoints

Knickpoints, i.e. sections of high gradient bounded by lower gradients, along submarine channels have received much recent attention (e.g. Heiniö and Davies, 2006; Mitchell, 2006). Six rounded knickpoints can be seen along a channel with rounded margins on the seafloor (Fig. 5.9A). A closer examination reveals that two of them (KP2 and KP4) are actually depressions that are c. 300 m across and 10 and 36 m deep (Fig. 5.9C). The high-amplitude Horizon M marks the end of an active stage of a channel located c. 60 m below the seafloor. The dip map of the horizon reveals sharp arcuate knickpoints along the channel, located directly beneath the rounded knickpoints and depressions on the seafloor (Fig. 5.9B). The knickpoints on the Horizon M are 18-30 m high with angles of 11-14° and with some small depressions at their bases, whereas the much broader depressions with rounded morphology on the seafloor have shallower angles of 6-11°. The low-amplitude reflection package M-seafloor has a relatively even thickness outside the channel, where it smoothes out irregularities on the Horizon M. Along the channel, however, the thickness of the package varies significantly above the sharp knickpoints on the Horizon M (Fig. 5.9C). The M-seafloor package also thins downstream of knickpoint 3 and thickens again after the channel has passed the adjacent salt diapir (Figs. 5.9A and B).

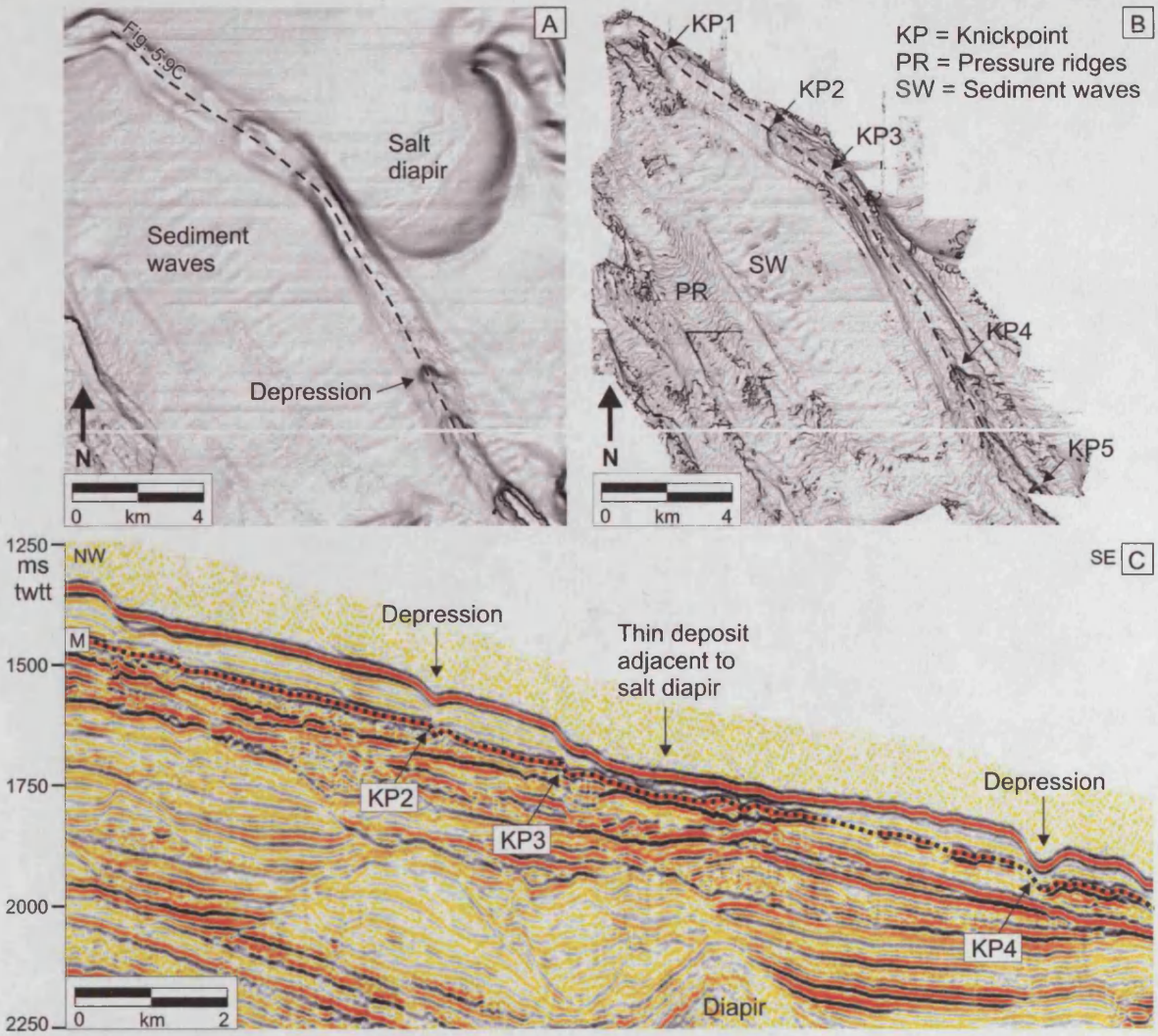

Figure 5.9. Depressions and knickpoints along a recent, inactive channel. (A) Seabed dip map showing a channel with rounded margins. Location shown in Figure 5.1. (B) Dip map of the Horizon M showing sharp arcuate knickpoints (KP1-KP5) along the channel. (C) Along-channel seismic traverse reveals sharp knickpoints with plunge pools at their bases on Horizon M beneath the rounded knickpoints and depressions on the seafloor. The sharp knickpoints on Horizon M are abrupt breaks in slope that create disruptions in flows within the channel. The notches at the bases of the knickpoints on Horizon M are interpreted as plunge pools, commonly found at the bases of knickpoints along submarine channels and canyons (Mitchell, 2006) and not unlike troughs formed at slope-rise transition (Pratson et al., 2000), although much smaller. Formation of a hydraulic jump as a supercritical flow slows down and becomes subcritical, enhances the excavation of a plunge pool beneath a knickpoint, as the currents expend their energy at the base of the slope (Pratson et al., 2000) (Fig. 5.12).

5.7.3 Depressions in other datasets

Depressions similar to those described here and by Fildani et al. (2006), have also been observed in other datasets. In Mitchell's (2006) Figure 4, a trail of depressions can bee seen on the seafloor adjacent to a canyon and some sediment waves on the Gulf of Alaska continental slope, and some depressions are also present near the Astoria Canyon offshore Oregon (Mitchell, 2006, their Fig. 6). Several trails of depressions are also found along a partly buried channel-levee complex on the western Niger Delta. A part of this system is

shown in Figure 5.12. The similarity with the trails of depressions in the Espirito Basin are remarkable, as both have a depression morphology that develops from asymmetric scour-shaped depressions into more rounded and symmetrical ones and are formed along a channel. The depressions on Niger Delta are found in much deeper water (>2500 m), but the slope is still relatively steep (c. 1.2°). The presence of sediment waves along the channel-belt and the adjacent seafloor indicate the presence of downslope currents. The channel-belt is not buried completely, therefore the flows are likely to be at least weakly confined within it. The confinement of flows may be the key to the formation of the depression trails. The process described here may also play a role in the formation of the 'ovoid depressions' on the same dataset described by Heiniö and Davies (2006).

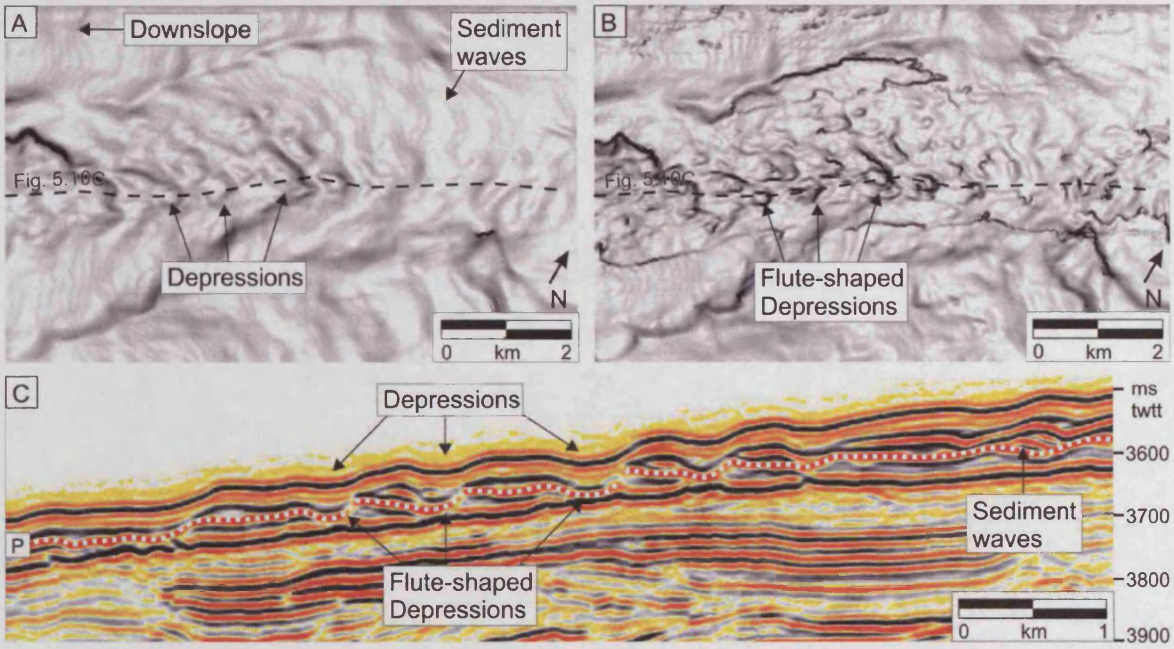

Figure 5.10. Depressions along a deepwater channel on western Niger Delta. (A) Seafloor dip map showing a part of a channel-belt of a buried channel-levee system. Sediment waves occur within the channel-belt and outside of it. Depressions with a diameter of several hundred meters occur along the channel. (B) Dip magnitude map of Horizon P approximately 70 m beneath the seafloor showing asymmetric, horseshoe-shaped depressions along the channel. (C) Seismic traverse along the channel-belt showing depressions on the seafloor and their scour-shaped morphology on Horizon P (dotted). See location of (A) and (B) in Figure 2.4B.

5.8 THE ORIGIN OF LARGE DEPRESSIONS IN THE ESPIRITO SANTO BASIN

5.8.1 Interpretation of general morphology

Although no sedimentological or wireline log data were available for this work, some general interpretations on specific sedimentary environments can be made based on general sedimentary setting, reflection geometry and seismic amplitude (e.g. Deptuck et al., 2003;

Posamentier and Kolla, 2003). Several phases of erosion and deposition were identified from the seismic data, also noted by Fiduk et al. (2004). These phases may reflect changes in the relative sea level or other external controls, which are beyond the scope of this paper. Sharp features are interpreted to have formed by erosional processes and rounded features by depositional and reworking processes. For example, Horizon C is dominated by erosional features, such as channels and scarps, but Horizons D, E and G are dominated by depositional features (Fig. 5.3). The big escarpment is interpreted as an erosional feature, as reflections are truncated against it (Figs. 5.2 and 5.3). It may be a lateral margin of a major slide scar.

The interval A-H is mainly aggradational with recurrent erosional phases. Variable infill patterns suggest variable current conditions throughout the evolution of the basin. Accumulation of hemipelagic drape and the formation of onlap and divergent fill normally indicate low energy, whereas mounded onlap fill indicate deposition by high-energy turbidity currents (Sangree and Widmier, 1977).

Sediment wave morphology observed in seismic lines along channels (Figs. 5.4, 5.6 and 5.8) is interpreted to have formed by sediment gravity current activity. The formation of the depressions is interpreted to be linked to this process. Before describing the preferred model for depression development, alternative interpretations are considered to eliminate the possibility of the depressions in the Espirito Santo Basin having an origin as fluid escape features or slope failures.

5.8.2 Fluid escape origin

Trails of circular depressions above buried submarine channels are most commonly ascribed to pockmarks caused when fluids trapped in buried channel sands escape to the surface (e.g. Gay et al., 2003). Some of them are considered to be giant fluidisation features (Davies, 2003). Due to the similarity in scale and the association with underlying channels, these interpretations are discussed below in more detail.

Pockmarks form as a result of catastrophic gas and/or pore water eruption on the seafloor. They are commonly 10-700 m in diameter and 1-45 m deep (Hovland, 2002). Strings of pockmarks are commonly found above fault zones and channels (Hovland, 2002). One such string follows the sinuous course of an underlying channel in the Lower Congo Basin (Gay et al., 2003). Those depressions are of similar scale (100-800 m in diameter and up to 40 m

deep) as the depressions in Espirito Santo Basin. They are connected by seismic chimneys to an underlying channel-levee interface, which is buried under 200 m of sediment. This is clear evidence that they are pockmarks formed by dewatering of fluids trapped in the channel sands. The data from the Espirito Santo Basin, however, show no evidence for fluid escape and the depressions are therefore not likely to be pockmarks. This argument can be further supported by the following observations:

1. The underlying channels have no channel-axis deposits (high-amplitude reflections). Instead, they are erosional channels incised into steep slopes. Furthermore, a 130-240 m thick sediment cover is needed for enough excess pore pressure to develop for fluids to escape from channel sands (Gay et al., 2003). The Espirito Santo depressions occur only few tens of metres above the channel and therefore there would not be enough excess pore pressure developed even if channel-axis deposits were present.
2. There is no evidence for fluid flow below or above the depressions. No unit pockmarks, faults, seismic chimneys or other seismic disturbance or amplitude anomalies that could indicate fluid escape or presence of gas are found in the data.
3. Locations of depressions not only above channels, but also above irregularities on the subsurface, e.g. scarps, suggest that channels are not crucial for their formation. Although fluid migration can also focus on structural highs, the evidence from near-seafloor examples prove that fluid escape does not occur above seafloor irregularities (see discussion below).
4. The formation of pockmarks is associated with focused vertical fluid flow thus forming vertical "pipes" or "chimneys". The Espirito Santo depressions are not located directly on top of each other, but have migrated slightly towards east by Horizon E (Figs. 5.3C and 5.5). This reflection pattern with both aggradation and lateral migration suggests depositional origin with possibly some reworking by bottom currents.

The circular depressions above a deep-water channel on the Niger Delta are of similar scale (600-900 m in diameter and 30-50 m deep) as Espirito Santo depressions. Davies (2003) interpreted them as a result of soft-sediment deformation, in which fluidised buried channel sands were expelled to the seafloor through a pipe system as a result of differential loading. Although the depressions in the Espirito Santo Basin are superficially similar to the ones on the Niger Delta, the absence of underlying channel deposits, overburden deformation and

evidence of a pipe system makes soft-sediment deformation an unlikely origin for them. The depressions on the Espirito Santo Basin occur on a steep slope (1.5-7°) in a proximal part of the slope, whereas the depressions on both Congo and Niger Delta are located on more distal and much shallower slope (generally <1°). The sediment wave-like geometry of the reflection package C-D could also be mistaken as a result of rotational slope failure, however, this could not explain the reflection geometry, as there is no evidence for a detachment fault.

5.8.3 Model for depression development

The observations on reflection geometries and the formation and evolution of the depressions are summarised in a schematic figure (Fig. 5.11). It breaks the evolution of the features into four stages representing the development at the time when Horizons C, D, E and G were the contemporaneous seabed. At stage 1, erosional currents incise a channel into the seafloor (Fig. 5.11A). Because the slope is steep and the flows are erosional, it can be assumed that the flows are dominantly supercritical (e.g. Nemec, 1990). The along-channel profile is illustrated as a smooth concave curve for simplicity, however, some irregularities were probably present on its surface, such as channel-margin slumps, erosional scours or pockmarks. These topographical irregularities, or an abrupt shallowing of the gradient, are likely to cause instabilities in the flows within the channel at stage 2 (Fig. 5.11B). For example, an irregularity with positive relief acts as an obstacle and would cause the flows to decelerate upstream of it and then accelerate on a locally steepened downstream side of the obstacle (Bursik and Woods, 2000). The deceleration of flows reduces bed shear stress imposed by the flows and causes increase in sedimentation rate. The opposite is true for the steeper slope, where flow acceleration increases bed shear stress and decreases sedimentation rate (Flood, 1988; Nakajima and Satoh, 2001; Fildani et al., 2006). This deceleration and acceleration of flows leads to deposition and erosion/nondeposition respectively across the obstacle. It may also bring a change in flow regime. When the flows are slowed down on shallower slopes and upstream of obstacles, they can become subcritical, as observed in the experiments of Bursik and Woods (2000). The inferred transition from supercritical to subcritical flow may also produce a hydraulic jump at abrupt changes in slope, such as bases of lee slopes. Shear stress is increased at the hydraulic jump, which enhances erosion at the base of the break in slope and causes increased deposition immediately after it (Garcia and Parker, 1989; Pratson et al., 2000; Kubo and Nakajima, 2002) (Fig. 5.12).

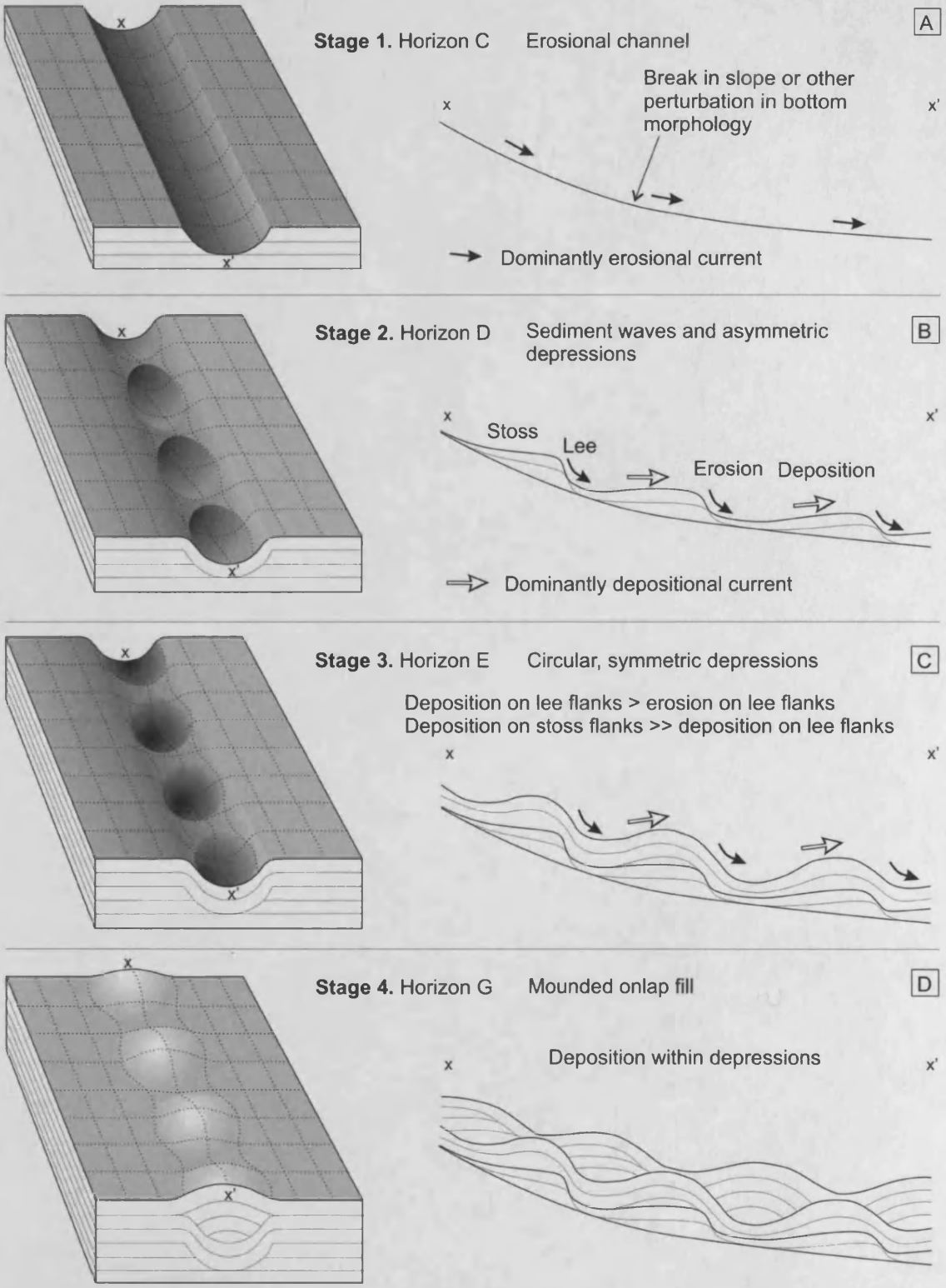

Figure 5.11. A schematic breaking down the evolution of the depressions. Not to scale. (A) At stage 1, an erosional channel is incised into previous deposits on a steep slope. The channel has concave, approximately smooth profile. (B) Stage 2 begins, when a perturbation or gradient change on the channel floor destabilises flows within the channel. Zones of slow, subcritical currents (white arrows) lead to deposition on locally shallower slopes and fast, supercritical currents (black arrows) erode locally steepened slopes leading to the formation of upstream-migrating sediment waves along the channel. The stoss flanks are shallow or upstream-dipping and lee flanks are steep, making the depressions asymmetric. (C) The depression morphology develops into more symmetrical and rounded by increased deposition on stoss flanks. (D) At stage 4 mounded onlapping fill fills the depressions and creates mounds on the seafloor.

The development of zones dominated by either deposition or bypass and erosion along the channel leads to the development of sediment wave-like bedforms in the reflection package C-D (Fig. 5.11B). After forming, the waves build up by preferential deposition on the upstream flanks and erosion on the downstream flanks. At the base of the steep lee flank of the most basinward wave, the newly formed break in slope may trigger the formation of another wave downstream (Kubo and Nakajima, 2002).

Because the sediment waves have steep lee flanks and upstream-dipping stoss flanks and are confined within the channel, the troughs appear like flute-shaped depressions in plan view (Figs. 5.11B and 5.3D). The flute-shaped geometry on Horizon D is not preserved by upstream migration or smoothed out, as may be expected. Instead, the depressions are built into deeper, more symmetrical depressions by depositing more sediments on the crestal areas but less on the troughs (Fig. 5.11C). This evolution from Horizon D to E likely represents changes in flow conditions at stage 3. However, the exact mechanism by which the flute-shaped depressions develop into more circular depressions with steep downslope flanks on Horizon E and F is not possible to be deduced from seismic data alone. The seismic data indicate that at this stage there is no more erosion on the lee flanks and more deposition occurs on the stoss flanks of the sediment waves, which leads to the building of upslope-dipping downslope flanks for the depressions (Fig. 5.4). Alternatively, an increase in hemipelagic sedimentation may cancel out the effect of erosion on lee slopes (Kubo and Nakajima, 2002). The observation that Horizon D has 14 more depressions than Horizon E indicates that some of them have been filled by the package D-E, and suggests that the flows were more depositional. However, some erosion or nondeposition must still have been present to keep the depression morphology from filling in. Pratson et al. (2000) observed that greatest erosion occurs at the base of slope and leads to the formation of an erosional trough and that thickest deposits are found immediately after this trough (Fig. 5.12). Similar phenomenon occurs in plunge pools of the bases of continental slopes (Lee et al., 2002). The inferred transformation from supercritical to subcritical flow condition via a hydraulic jump at the bottom of the steep lee flank could have resulted in enhanced deposition on the stoss flank.

The filling of the depressions begins after Horizon F, where the reflection character changes from low-amplitude hummocky to mounded onlap fill with intermediate amplitude reflections (Fig. 5.4). Some fill patterns aggrade vertically, but others step upslope as a result of preferential deposition after a break in slope at the base of the depression (Figs. 5.4 and 5.6D).

This change in reflection pattern is most likely due to changes in flow conditions at stage 4 (Fig. 5.11D). Mounded onlap fill indicates dominantly high-energy depositional turbidity currents flowing down the channel (Sangree and Widmier, 1977). The troughs that form between the mounds on Horizon G are infilled by onlapping reflections of the package G-H smoothing out the topography (Fig. 5.4). This onlapping geometry indicates that the mounds are depositional features and not caused by e.g. differential compaction.

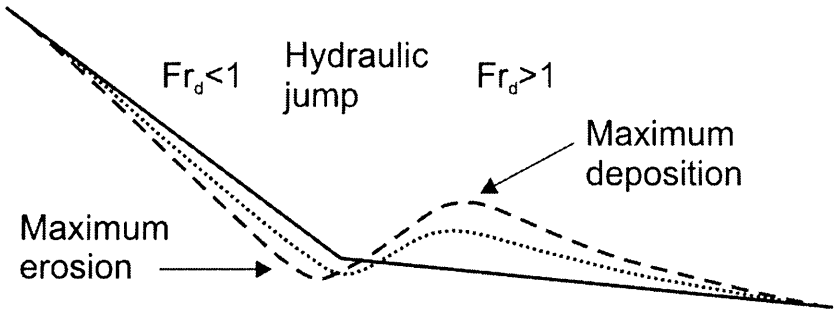

Figure 5.12. Idealised schematic of erosion and deposition patterns in the vicinity of a hydraulic jump. The solid line represents the original slope profile, dotted and dashed lines show how the profile evolves after supercritical ($Fr_d > 1$) flows erode the steep slope with maximum erosion occurring at the base of slope, where the flow undergoes a sudden transformation to subcritical flow ($Fr_d < 1$) via a hydraulic jump. Maximum deposition occurs immediately after the hydraulic jump.

The apparent downlap of some of the reflections of packages C-D and E-F onto the channel walls, seen in the traverse across the channels (Fig. 5.5), leads to lateral migration of the channel and the trail of depressions towards the east as the stratigraphy is built up. This geometry may arise from the erosion of the eastern channel margins and deposition on western margins, however, it could also be due to variation in depositional thickness so that it is below seismic resolution on the eastern side. Many factors may control this lateral migration, for example bottom currents interacting with gravity currents (Rasmussen, 1994; Viana et al., 2003).

The depressions on the seafloor that were presented in Figure 5.8 are clearly not related to any underlying channels, but instead they are related to the variations in the underlying topography. The depressions were formed above the scarps on Horizon N in a similar manner as described above, with erosion or nondeposition on locally steeper slopes and maximum amount of erosion at the base of the scarps, where it is inferred that a swift supercritical flows decelerate to subcritical flows (Fig. 5.12). This deceleration leads to increased deposition immediately downslope form the base of the scarp, producing an upslope-dipping downslope

flank for the depression. Similar, but much larger depression also formed above a scarp on Horizon C (Fig. 5.3).

The subtle sediment waves seen on the seismic traverse (Fig. 5.8E) are also inferred to have initiated on irregularities on the Horizon N, with sediment deposition concentrated on areas with lower gradient and behind small ridges. Bypass or less deposition occurred on steeper areas and downslope from ridges where the gradient was locally steepened. These examples suggest that sedimentation in the study area is controlled by gravity flows interacting with surface topography and depressions have formed by the actions of unstable gravity flows.

The depressions associated with the knickpoints along a channel (Fig. 5.9) show some similarity in geometries to the depressions in the interval A-H and they are of similar scale (Figs. 5.2-5.5 and Table 5.1). They illustrate how current activity can create circular depressions above perturbations along channel profile. Furthermore, they reveal that rounded knickpoints and other geomorphic features on the seafloor may be due to irregular deposition of sediments onto underlying sharp topography, therefore care must be taken when inferring processes from seafloor data alone.

Although the reflection configuration between the Horizon M and seafloor is mainly aggradational and does not show channelised deposits (Fig. 5.9), the areas of non-deposition or erosion along the channel indicate that some current activity must have occurred down the channel. The locations of these areas are most likely controlled by pre-existing structure or irregularities in the channel profile, for example, the package M-seafloor is thinnest next to a salt diapir (Fig. 5.9). This structural high may cause acceleration of the gravity flows flowing down the channel due to a funneling effect or gradient increase, thus causing sediment bypass or erosion on the channel floor adjacent to the diapir. The formation of sediment waves on the adjacent seafloor suggests the presence of down-slope currents.

5.9 DISCUSSION

The examples shown in this paper show asymmetric patterns of erosion and deposition on the upstream and downstream sides of topographical irregularities. Roughly circular depressions form by depositional and erosional processes of sediment-gravity flows, arisen when currents interact with changes in gradient of the seafloor and become unstable. The formation of trails of depressions is more likely to occur along channels, because confined flow is more likely to

respond to irregularities in the bottom topography than unconfined flow. Individual depressions tend to form above scarps and other topographical irregularities on unconfined seafloor. The examples on the modern seafloor of the Espirito Santo Basin (Figs. 5.8 and 5.9) illustrate asymmetric deposition and the formation of sediment waves across topographical irregularities on the seafloor. A perturbation in topography brings about changes in velocity, shear stress and flow regime. A flow may transform from supercritical to subcritical flow condition due to deceleration when a slope shallows. The bottom shear stress imposed by flow will also decrease. This all leads to erosion on steeper local slopes and deposition after a slope break. Differential draping of sediment can also be explained by suspension-flow theory, in which sediment deposition rate varies on slopes with various gradients (Hiscott, 1994). Deceleration of flows, where slopes become shallower or inverse, causes loss of their capacity to carry sediment in suspension and leads to deposition regardless of flow conditions (Hiscott, 1994; Nakajima and Satoh, 2001). Deposition can also be instigated by partial blocking of the current by an obstacle and by deflecting some of the current upslope (Nemec, 1990; Bursik and Woods, 2000).

The formation of sediment waves is an important mechanism, to which the formation of the depressions is related. Sediment waves normally form on slopes steeper than 0.4° (Nakajima and Satoh, 2001) but shallower than 2° (Wynn et al., 2000a). The erosional channels on the Espirito Santo Basin slope have much greater slopes, but the wave-like bedforms only occur on slopes of c. 2-6° (Fig. 5.4). Slopes with higher and lower angles do not exhibit sediment waves or depressions in the study area. The depression on the seafloor that is formed between two sediment waves within a channel (Fig. 5.8C) may represent an early stage of formation of a series of depressions, similar to what was described above for the C-H interval and corresponding to stage 2 of the evolutionary model (Fig. 5.11B). It strongly supports the argument that sediment waves are formed within channels and their troughs form channel-confined depressions. The occurrence of sediment waves only within the channels and not on the adjacent seafloor may be because the flows are different in a confined channel than on unconfined seafloor (Fildani et al., 2006). The formation of sediment waves is thought to be a result of the flows becoming unstable and vertically undulating as they interact with irregular topography on the base of the channel (Fig. 5.8C). Although the wave-like reflections of the package C-D are interpreted as sediment waves (Fig. 5.4), they are different from common sediment waves because (1) they do not form a field but are confined within a channel, (2) they are much larger in amplitude than other channel-confined sediment waves and (3) they

occur on much steeper slopes than most sediment waves. They are, however, similar in scale and morphology to the sediment waves of the numerical models of Kubo and Nakajima (2002) and Fildani et al. (2006). The laboratory experiments and numerical simulations of Kubo and Nakajima (2002) produced wavy structures with 4-5 crests after several thousand turbidity currents with asymmetrical deposition and erosion pattern. Their model results (Kubo and Nakajima, 2002, their Fig. 2) have similar morphology and slope angles as the seismic reflection pattern on the along-channel traverse between Horizons C and D (Fig. 5.4). Their conclusion that wave formation is due to preferential deposition resulting from variation in bottom slope is shared by other workers, e.g. Fagherazzi and Sun (2003), whose numerical model predicts the formation of a series of transportational cyclic steps from a single perturbation at the bottom topography. Similarly, the experiments of Taki and Parker (2005) showed that a Froude-supercritical flow over erodible bed evolves into a series of steps with spatially varying patterns of erosion and deposition.

Similar features to those described in this paper are also found elsewhere, suggesting that the processes responsible for their formation are ubiquitous. The large scour-shaped depressions on Monterey Fan valley, described by Fildani et al. (2006) and interpreted as erosional scours formed by supercritical flows that were overflown from the main channel, are probably the closest in terms of morphology and formation mechanism. They are much larger (3.5-4.6 km wide, 80-200 m deep) and formed on shallower slope than the depressions in the Espirito Santo Basin, but bear similarities with them, especially at the level of Horizon D (Fig. 5.3B). The numerical simulations of Fildani et al. (2006) resulted in the formation of several sediment waves beneath a break in slope when flows were depositional, which is also what is observed in the Espirito Santo Basin. The measurement of Fr_d values by Fildani et al. (2006) confirmed that the flow was undergoing a hydraulic jump above each wave, therefore they could be classified as cyclic steps. Although this paper is based on 3D seismic data alone, reflection geometry and comparison to published models enable the deduction that mainly the supercritical gravity flows travelling down the steep slopes of the Espirito Santo Basin on Brazilian continental margin become unstable when they interact with bottom slope and create wavy bedforms and roughly circular depressions on seafloor.

It is likely that other depressions found on submarine slopes are formed in a similar manner and more depressions will be identified in the future. The process may be similar to the development of sinuosity in channels, which is also thought to initiate when a current

encounter a perturbation in the subsurface. Although most of the depressions described in this paper have a similar scale with a diameter of several hundred metres, the depressions described by Fildani et al (2006) have diameters of kilometres. Therefore the process is thought to be scale-independent.

5.10 CONCLUSIONS

Trails of depressions are found along channels and individual depressions above scarps and other topographical irregularities in the Espirito Santo Basin on the continental margin of Brazil. They are interpreted to be a result of Froude-supercritical flows interacting with perturbations in topography and becoming unstable. This means that when flows travel on locally steeper slopes, they accelerate and become more capable to erode because of higher velocity and shear stress. On locally shallower slopes and upstream of obstacles, the flows decelerate and deposition of suspended sediment is enhanced. A local break in slope may also bring about a change in flow regime from supercritical to subcritical flow via a hydraulic jump, which will enhance erosion at break and deposition immediately after it, thus forming a depression. The depressions are thus likely be comparable to transportational cyclic steps. Cyclic steps have been formed in non-marine environments, laboratory experiments and numerical models, but have never before been described from 3D seismic data in the submarine realm. The 3D data from the Espirito Santo Basin enabled the establishment of the evolution of the 3D morphology of the depression formation in detail.

Chapter 6

6 DISCUSSION

The aim of this chapter is to synthesise the key findings of the previous chapters and to discuss some common themes within them, for example the effect of changes in slope on the sedimentary elements, such as mass transport complexes and channels. The importance of this research is discussed in the context of other analytical techniques including outcrop analysis, flume tank experiments and numerical modelling. The limitations and weaknesses of this work are also discussed, and future research is recommended.

6.1 SUMMARY AND KEY POINTS

The two datasets analysed during this project were introduced in Chapter 2. The dominant sedimentary elements in the Niger Delta dataset are large channel-levee systems, mass transport complexes and local slope failures on the flanks of thrust-related folds. The Espirito Santo Basin dataset, with steep slopes just beneath the shelf break, reveals smaller channels that do not have levees. It also contains a canyon system that has undergone several phases of incision and infill at least from the Oligocene until Present. Deformational structures that cause uplift have deformed the seafloor in both of the study areas. The topography created by these structures, anticlines on the Niger Delta and salt diapirs in the Espirito Santo Basin, affects the location and morphology of the sedimentary elements.

Chapter 3 concentrated on the erosional and depositional features that are formed as the anticlines on the Niger Delta degrade. Four different types of slope failure were identified and their style and runout distances were interpreted to have been controlled by slope morphology, sedimentology and the presence of anisotropies.

Chapter 4 examined the formation and evolution of knickpoints along the present day thalweg of a channel-levee system on the Niger Delta. The knickpoints were interpreted to have formed as a response of turbidity currents within the channel to the uplift of the fold and thrust belt. The knickpoints are characterised by deposits of coarser sediments upstream of them and erosion occurring downstream of these deposits. They tend to migrate upstream and evolve in various ways, leaving either erosional terraces or no evidence for their existence at all in the sedimentary record.

The large-scale depressions that occur in trails above erosional slope channels in the Espirito Santo Basin, and also individually above topographical irregularities were interpreted in Chapter 5 to have formed as a result of Froude-supercritical turbidity currents becoming unstable when encountering topographical irregularities. This creates erosional scours and deposits similar to sediment waves, which, when confined within channels, appear as roughly circular depressions.

6.2 THE EFFECTS OF CHANGES IN SLOPE

6.2.1 Introduction

Changes in slope angle have an influence on all of the sedimentary features discussed in this thesis. Both study areas exhibit deformation of the seafloor, which have introduced variable local slopes. The effects that changes in the slope angles have on the sedimentary elements include (1) the location and morphology of channel deposits and MTCs, (2) the style and type of resedimentation that occurs and their runout distances and (3) the effect on sediment-gravity flows, creating instabilities that produce asymmetric sedimentation and erosion patterns and form knickpoints, sediment waves and depressions. These were discussed in Chapter 2, Chapter 3 and Chapters 4 and 5 respectively. The key points are brought together below.

6.2.2 The role of slope failures and resedimentation in the study areas

It was noted in Chapter 3 that the slope angle variations and slope lengths have an effect on the style of resedimentation. In the Niger Delta study area, evidence for mass wasting is most commonly found on the local slopes created by the anticlines. The folds are eroded mainly by mechanical failures that leave erosional surfaces and scarps on the crests and flanks of the folds and produce slumps, debris flow deposits and turbidites at their bases. This kind of slope degradation does not occur along the flanks of the salt diapirs in the Espirito Santo Basin, although some evidence for failures initiated from the flanks of the diapirs can be seen. The diapirs have a larger effect on directing mass transport flows rather than causing local slope failures, whereas this is the opposite on the Niger Delta. Majority of the slope failures in the Espirito Santo Basin occur on the steep continental slope.

The MTCs that are not associated with the degradation of the anticlines are relatively uncommon in the Niger Delta study area, but few extensive MTCs that are several tens of

metres thick, and some smaller MTCs that plug channels are found within the dataset. All of them originate from outside of the data area, and therefore probably originate from large scale failures that occur closer to shore and possibly correspond to periods of relative sea level fall, as also suggested by Posamentier and Kolla (2003).

Some of the MTCs in the Espirito Santo Basin are also several tens of metres thick (e.g. in Fig. 2.16), but the majority are much smaller. There are a lot more mass transport deposits in the Espirito Santo Basin than in the Niger Delta, and many of them can be linked directly to a head scarp (e.g. Fig. 2.15). The characteristic features they exhibit, such as longitudinal grooves at their bases, blocky top surfaces and pressure ridges (Figs. 2.15 and 5.9B), are more prominent and common than the similar features in the large MTCs on the Niger Delta. The MTCs in the Espirito Santo Basin are more similar to the fold degradation features on the Niger Delta than the larger MTCs. This may be due to the relatively short transport distances. The failed sediment masses are more prone to create grooves at the bases and pressure ridges at the toes of the MTCs, because they are probably quite coherent closer to the source, whereas longer transport distances are likely to disintegrate the sediment masses. Although failures can occur on very shallow slopes of less than 0.5° (Sultan et al., 2004) and there are many factors that contribute to slope stability, a failure is more likely to occur on steeper slopes, as discussed in Chapter 3. The steep slopes and proximity to the shelf break in the Espirito Santo Basin dataset thus help to explain the abundance of small slope failures in that dataset and the rarity of them in the Niger Delta dataset.

6.2.3 The effect of slope gradient on the channels

6.2.3.1 Channels in the study areas

Although located in different settings, the channels in both of the datasets have many similarities, for example, evidence for their evolution involving several phases of incision and infill is seen in the slope channels and canyon systems in the Espirito Santo Basin and the large channel-levee systems of the Niger Delta. The main differences are the style of the channels. The Niger Delta CLSs are confined within erosional fairways and large outer levees, which are lacking in the slope channels of the Espirito Santo Basin, however, some channels are confined within the canyon systems, the appearances of which are very similar to the erosional fairways of the CLSs in the Niger Delta. Individual channel-axis deposits tend to show similar widths (c. 80-100 m) and sinuosities in all of the channels at all depths in both datasets.

6.2.3.2 The importance of channel gradients and the occurrence of knickpoints

Both the slope and the present day channels on the Espirito Santo Basin have concave profiles, whereas the studied channel thalweg on the shallower slope of the Niger Delta has a slightly convex profile due to the uplift associated with the fold and thrust belt. The average gradient of the present day channel thalweg on the Niger Delta is much shallower (0.5-0.6°) than of the channels in the Espirito Santo Basin, where the steepest parts of the channels have gradients of up to 9.4° where the slope is the steepest (up to 15°). The channel profiles in neither datasets are in equilibrium, as manifested by the occurrence of knickpoints along them.

The formation of the knickpoints in the Niger Delta dataset is a result of the sediment-gravity flows within the channels reacting to changes in gradient along the channel, as discussed in Chapter 4. On the seafloor of the Espirito Santo Basin, the knickpoint along the tributary channel (e.g. Fig. 5.1) is a hanging valley formed as a result of a greater rate of incision along the eastern tributary. The knickpoint has migrated upstream along the channel a distance of over 2 km. The formation mechanism of the knickpoints along the shallowly buried channel in the Espirito Santo Basin (Fig. 5.11) is uncertain, but their morphology is similar to the other knickpoints seen in both datasets. There are several possible ways, in which these knickpoints may have formed, but the most likely case is by current activity or a mechanical failure. Turbidity currents and other sediment gravity flows are capable of eroding seafloor and can form knickpoints in certain conditions as discussed in Chapter 4, e.g. if there are variations in bed resistance or erosional power of the currents. Sediment may also fail within a channel forming an arcuate headwall scarp across the channel that is morphologically identical to a current-generated knickpoint.

Although the knickpoints have formed by different mechanisms on both datasets and in different settings, their abundance suggest that knickpoint formation is an important part of channel evolution and one of the ways in which the channels try to reach their equilibrium profiles. It may be the key mechanism by which uplifted reaches are eroded and by which channels are incised into steep slopes. Several experimental results support this argument. Knickpoint formation and upstream-migration have been observed in many flume tank experiments that study the channelisation of turbidity currents and debris flows on submarine fans (e.g. Yu et al., 2006).

6.2.4 The formation of depressions

In this thesis depressions were described from five different settings; (1) along and above erosional channels in the Espirito Santo Basin, (2) along an almost buried channel-belt in the Niger Delta, (3) above knickpoints within steep slope channels, (4) above scarps in the Espirito Santo Basin and (5) above an anticline in the Niger Delta. (1) - (4) were discussed in Chapter 5 and (5) in Chapter 3. The formation mechanism of depressions above an anticline in the Niger Delta was not determined, but it was suggested, that they were formed by partly mechanical failure of sediment caused by the uplift of the fold and a subsequent modification by bottom currents. The other depressions were interpreted to be a result of sediment gravity flow activity. In all cases the trigger for depression formation appears to be a change in slope gradient. This is most obvious in the case of depressions that occur above knickpoints and scarps because there is a substantial break in slope at the base of scarps and knickpoints (Figs. 5.8 and 5.9). The break in slope causes an inferred transition from a swift supercritical flow condition to a slow subcritical flow condition via a hydraulic jump, which promotes erosion at the base of slope and deposition immediately after it creating a plunge pool (e.g. Pratson et al., 2000). Alternatively, plunge pools may be excavated by the impact of high-momentum sediment density flow (Lee et al., 2002). The depressions above the anticline on the Niger Delta may have formed in a similar manner.

The depressions occurring along channels in the Espirito Santo Basin and the Niger Delta are considered to have formed as channel-confined sediment waves that develop into more circular depressions by subsequent currents reacting to the wavy surface. This process is similar to transportational cyclic steps, which also depend on changes in flow regime (e.g.Fildani et al., 2006). These flows are at least weakly confined within the channels, which results in the formation of a series of sediment waves and depressions, whereas the depressions above scarps and knickpoints occur mainly as single depressions.

Origin of the depressions as fluid escape structures was discussed in Chapters 3 and 5 but the evidence suggest that a current origin is a more likely mechanism in forming the depressions. However, since fluid escape and pockmarks occur in similar settings, it cannot be ruled out completely that some fluid escape may have occurred. This could have created bottom irregularity that affected the currents causing them to erode and deposit sediment in specific areas and creating knickpoints, depressions or sediment waves.

6.3 THE IMPORTANCE OF OUTCROPS

6.3.1 The identification of degradation complexes, knickpoints and depressions from outcrops

The interpretation of sedimentary features from 3D seismic data raises the question of how these features can be identified from outcrops and furthermore, can the 3D seismic interpretation give clues about the formation of features seen in outcrops? Degradation complexes that create erosional surfaces and debris flow deposits at the bases of slopes have been interpreted in outcrops of many foreland basins. Progressive unconformities have been identified on the flanks of growing structures and growth strata that are deposited on top of or on the flanks from outcrops (e.g. Burbank and Raynolds, 1988; Deramond et al., 1993; Rafini and Mercier, 2002), some of which are analogous to the degradation of submarine folds discussed in Chapter 3.

The identification of knickpoints and the depressions or channel-confined sediment waves from outcrops may be more challenging. There may be many reasons why they have not been identified from outcrops so far. Although several excellent and well-studied outcrops of deepwater channels exist, for example Brushy Canyon in Texas, (Gardner and Borer, 2000; Gardner et al., 2003), Ross Formation in Ireland (Lien et al., 2003), Grès d'Annot in France (McCaffrey and Kneller, 2001; Bourgeois et al., 2004; Moraes et al., 2004), Kirkgeçit Formation in Eastern Turkey (Cronin et al., 2000) and Tabernas Solitary Channel, Spain (Clark and Pickering, 1996; Haughton, 2000; Pickering et al., 2001), and they show similar architectural elements and evolution to channels seen in 3D seismic data, some architectural elements, for example levees are seldom found in outcrops (Peakall et al., 2000b). Outcrops are inherently two-dimensional and too small to encompass features like sediment waves or depressions within the channel-fill. Another possibility is that there is evidence for them within the outcrops, but they have not been looked for and therefore not found. The low relief and low angles of dip of these deposits may prevent their identification from outcrops.

Unexpected channel-fill geometries have been identified from some outcrops, however, and interpreted to have formed by similar processes to what have been inferred from the 3D seismic data in this thesis. Pickering et al. (2001) identified bedforms they called sandy macroforms from the outcrops of the Late Miocene Solitary Channel in the Tabernas-Sorbas Basin. These entirely channel-confined, backstepping bedforms are 30-40 m long, 2-5 m high

and inclined 12-15° to upslope direction and occur behind ridges within an underlying debris-flow deposit. The changes in gradient of the base of the channel are interpreted to be the seeding points for their deposition. Brown and Branney (2004) noticed similar sigmoidal upstream-dipping regressive lenses of similar scale within the ignimbrite deposits in Tenerife. Similarly, they interpreted their formation as a result of turbulent currents decreasing in velocity and capacity where the gradient is decreased, this leading to deposition and upstream migration of the bedforms. The outcrops show scours, indicating that the currents were locally erosional. Giant flute-like sours with high aspect ratios (5:1) were also identified in the Solitary Channel outcrops (Pickering et al., 2001). These examples indicate that the behaviour of flows within channels is most likely much more complicated than what are interpreted from outcrops, because they normally only represent a very small part of an extensive system. Although the bedforms and erosional features of these outcrops would not be resolved from seismic data, their presence confirms the variable erosion and deposition processes along channel especially where there are topographical irregularities. The backstepping macroforms of the Solitary channel may be analogous to the channel-confined sediment waves within the channels in the Espirito Santo Basin, although they are of smaller scale. Furthermore, they may actually represent only a small part of a larger depositional element that could be seismically resolvable.

Outcrops give the chance for the determination of bed-scale features and heterogeneity 2D, as well as the nature of contacts between different channel-fill elements and other channels within a channel complex or the country rock (Fig. 6.1). Many questions remain, for example, how evidence for erosion by knickpoint migration can be identified from outcrops. Knickpoint migration creates terraces and erosional surfaces along channels, but even if these were found on outcrop, distinguishing them from channel incision without knickpoint migration would not be possible unless the actual preserved knickpoint was found. A knickpoint could be recognized from outcrop by much steeper erosional surface than what the rest of the channel has, however, outcrops are not commonly extensive enough or have the three-dimensionality required for identifying such features. Nevertheless, the discussion in this thesis suggests that knickpoint formation and migration is an important process of how slope channels are incised, and therefore evidence for it should be looked for in outcrops. The same applies to channel-confined sediment waves and other along-channel variations in the channel-fill patterns. These could be identified from outcrop by recording changes in the dip magnitude or direction of channel-fill elements. Upstream-dipping channel-fill elements may

indicate the location of stoss flank of a sediment wave (or a downslope wall of a depression). Similarly, a lee flank migh be recognised by erosional surfaces cutting previously deposited sediments or by higher dip magnitude of channel deposits, possibly exhibiting erosional scours or flute marks that would indicate the locally erosive nature of the currents.

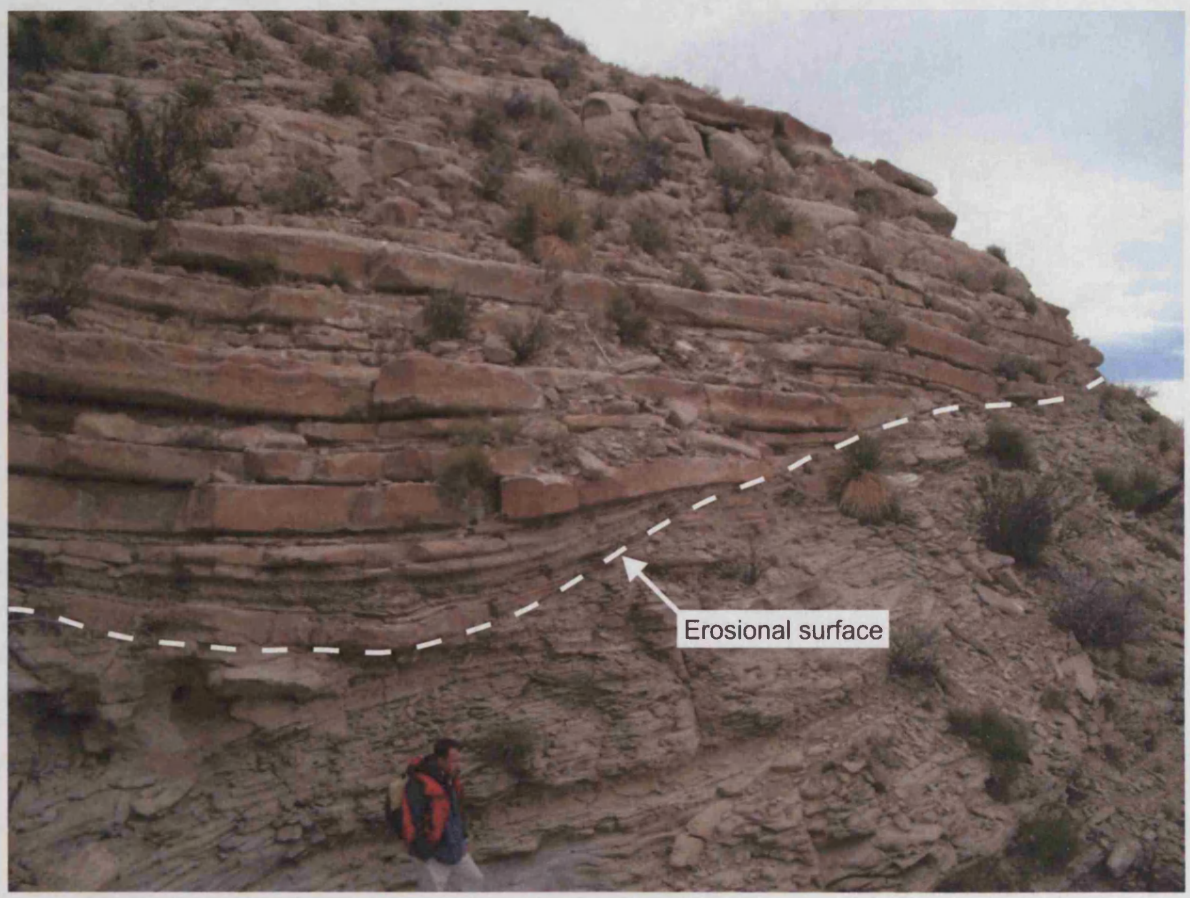

Figure 6.1. An outcrop of a slope channel from the Brushy Canyon, West Texas. The channel cuts into mudstone and is filled with lens-shaped beds of sandstone. What process created the erosional surface?

6.3.2 The resolution of outcrops vs seismic data

Deptuck et al. (2003) illustrated the differences in the scales of observation of channel-fill elements from outcrops and seismic data by comparing several examples. The CLSs on seismic data are normally viewed with at least a 7x vertical exaggeration, and some features, such as vertical aggradation of channels is difficult to distinguish when viewed with no vertical exaggeration or when studying outcrops (Deptuck et al., 2003).

The difference in scale and resolution of seismic data and outcrops can be highlighted easily by discussing lateral accretion packages and forward seismic modelling of outcrops. Abreu et al. (2003) compared conventional resolution (35 Hz) seismic data with high-resolution (65

Hz) seismic data and observed that evidence for lateral migration of a deepwater channel can only be seen in the high-resolution data. Similar observations are made from synthetic seismic data produced from outcrops, e.g. Solitary Channel (Abreu et al., 2003), Big Rock Quarry Face (Coleman et al., 2000), San Clemente (Campion et al., 2000; Campion et al., 2005) and a part of the Grès d'Annot (Bourgeois et al., 2004). The internal geometry of the channels were not resolvable at all in normal 35 Hz seismic data, however, higher frequencies allowed some internal geometry to be resolved.

The interpretation of the seismic data in this thesis showed that channels commonly have several phases of incision and infill and cut into previously deposited channel-fill elements. Some submarine channels exhibit steeply dipping high-amplitude reflections on the inside of channel bends, see also the CLSs of the Niger Delta (Fig. 2.11). These are interpreted to be lateral accretion surfaces analogous to point bars (Peakall et al., 2000a) and to mark the position of inner banks of channel during migration (Abreu et al., 2003). These lateral accretion packages (LAPs) are also seen on seismic data in the Nile delta (Samuel et al., 2003), Angola (Abreu et al., 2003) and Indus (McHargue and Webb, 1986). Their absence in seismic data does not necessarily mean that they are not there, but that they are too small to be resolved (Wonham et al., 2000).

Channel migration and avulsion are separate processes, migration being a gradual shift of the channel by systematic erosion on outer bends and deposition on inner bends and avulsion being a cut-and-fill process (Abreu et al., 2003). Abreu et al. (2003) interpreted both processes from the seismic data, however, it is argued here that although both processes may occur in submarine channels they may not be distinguished form each other from seismic data alone. What looks like channel migration on seismic data may be the result of avulsion, where each channel is incised into the previous one partly cannibalising it. This argument is supported by the work by Campion et al. (2000) and Campion et al. (2005), who interpret the lateral amalgamation of ten slope channels within the outcrops of San Clemente to have formed by autocyclic avulsions, i.e. subsequent cutting and filling of the channels. Their forward seismic modelling of the outcrops reveals that what in the outcrop can be identified as eight discrete channels that cut into each other and are laterally amalgamated, in the seismic data appear as two or three channels (Fig. 6.2).

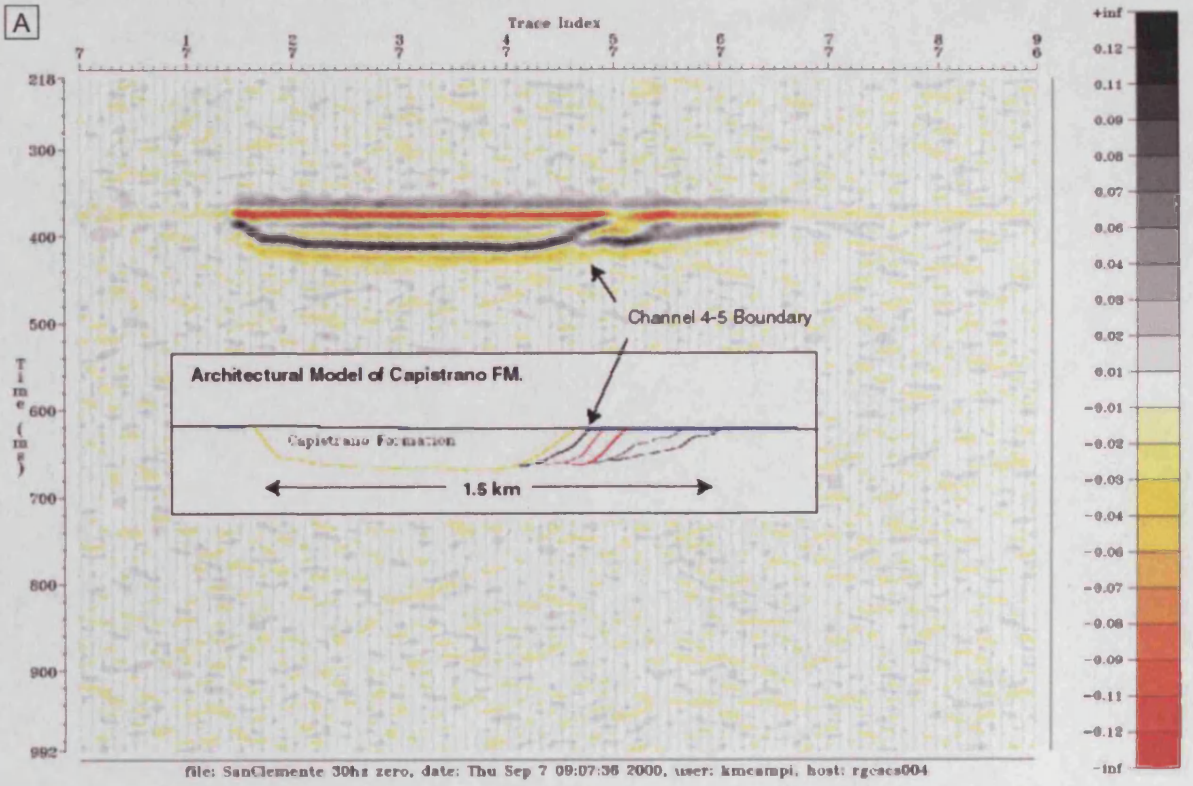

Figure 6.2. (A) Forward seismic model of Capistrano Formation (from Campion et al., 2000, their Fig. 7) illustrating that with a 35 Hz seismic data only the boundaries between channels 2-3 and 4-5 can be resolved. (B) A photograph of the boundaries between channels 4, 5 and 6 of the Capistrano Formation. The interpretation is based on Campion et al. (2000) and Campion et al. (2005). Red dashed line marks the boundary between the channels 4 and 5 and blue dashed line the boundary between the channels 5 and 6. Both erosional surfaces are draped by mud drape. These kinds of heterogeneities cannot be resolved from seismic data.

The channels of the Capistrano and Brushy Canyon Formations are deposited on relatively steep slopes and are analogous to the Espirito Santo Basin channels. There is therefore potential for the existence of knickpoints and sediment waves or depressions within these successions. However, these features are highly challenging, if not impossible, to be recognised from outcrops, as discussed in the previous section. Furthermore, although well exposed, the required scale or three-dimensionality cannot be achieved on most outcrops. Therefore 3D seismic data is crucial for determining such features within deepwater sedimentary successions. New techniques, such as the laser-based mapping technique Lidar (LIght Detection And Ranging) combined with ground-penetrating radar (GPR) can generate 3D models of outcrops and may provide the opportunity to determine seismic-scale features from outcrops in the future (e.g. Bellian et al., 2005).

6.4 THE IMPORTANCE OF EXPERIMENTS AND MODELLING

Experimental and numerical modelling of sediment-gravity flows have increased the understanding of the behaviour and deposits of the flows tremendously. Measurements made from controlled experiments have enabled the determination of the structure and variations within flows and revealed features, such as secondary flow cells within submarine channels (Keevil et al., 2006). A review of several recent experimental and mathematical studies is given in Kneller and Buckee (2000). One of the advantages of flume tank experiments done in laboratory is that changes of particular parameters to the behaviour of flow can be investigated in order to either reproduce a naturally occurring feature or simply to find out how various parameters affect the flow behaviour.

The evolutionary models for knickpoint formation and migration that was given in Chapter 4 and for the formation of channel-confined sediment waves and depressions that was given in Chapter 5 were supported with the knowledge of depositional and erosional behaviour of turbidity currents that was acquired from experimental and numerical modelling. The experimental work and numerical models referenced in those chapters were crucial for making the inference of the processes that produced the features seen in the seismic data more scientifically sound. The analysis of 3D seismic data also provides natural examples of some features that have previously mainly been seen in models, such as the depressions that were found in the Espirito Santo Basin (Chapter 5). Different analytical methods complement each other and combining them in the analysis of data is desirable.

6.5 LIMITATIONS AND WEAKNESSES

The limitations and weaknesses of this work are mainly related to the limitations within the data and the limitations within the methods used to analyse the data. Both 3D seismic datasets analysed for this project were of very high quality and have very few artefacts, which made the interpretation process easier. The main limitations of the seismic data were their physical boundaries and resolution. The extent of some features, for example the MTCs in the Niger Delta could not be investigated properly, because their full extents were not present in the dataset. Also the channel-levee systems within the data represent only a part of the entire system. However, it may have been impossible to analyse a more extensive dataset in the time frame of the project.

The resolution (tuning thickness) of both the 3D seismic datasets was around 10 metres. Even though smaller features could be defined from the interpreted horizons, the work was done above bed-scale and thus many important features and clues about the processes that created them could not be identified. But as discussed in the previous section, 3D seismic data gives the opportunity to visualise the features in three dimensions and at a larger scale than outcrop data, which normally exposes only a partial 2D view, and some features that are identified in 3D seismic data are most likely impossible to be detected from outcrops.

The project would have benefited from additional data, such as well logs or sediment cores to enable the determination of the subsurface lithology and depositional environments more accurately. Unfortunately these data were not available, however, sufficient information was acquired from literature for the purposes of this thesis. The errors in the measurements, for example thicknesses of sedimentary packages and slope angles, that were based on estimations of seismic velocities rather than real data are negligible and do not change the main results significantly.

The manipulation of the 3D seismic data can be done in numerous ways, and to find the best method for the analysis of a desired feature was not always straightforward. The hardware and software that were used produced some limitations for the interpretation, as some analysis of the data could not always be done with the analytical tools available. Also, new techniques had to be tried, because normal methods were not producing desired level of quality or could not be applied to some features. For example, the methods commonly used for the analysis of

submarine channels from 3D seismic data are more suitable for aggradational channels and not for degradational channels that occur on a folded slope.

6.6 FUTURE RESEARCH

Some questions were answered in this thesis, but many more arose. Suggestions for future research were highlighted where applicable. Ultimately, given the variety and the three-dimensional complexity of the degradation complexes, knickpoints and the depressions that form along channels and above topographical irregularities, identifying them from other seismic volumes and different type of data would be essential to fully characterise and predict their formation and importance in the submarine environment.

In this thesis, models were put forward to explain the evolution of several sedimentary features that were interpreted from 3D seismic data. Further research into the mechanisms and prediction of those features could be conducted. Especially flume tank experiments that would aim to reproduce the formation of channel-confined sediment waves, cyclic steps and knickpoints would be beneficial for the understanding of these processes.

Acquiring more data on systems that are active on the present day would be interesting and useful. Where features such as knickpoints are found on the present day seafloor, the evolution of their morphology and rates of migration could be determined more quantitatively if new data were collected at certain time intervals. Sampling of sediment by for example drop cores and measuring current properties across these features would also increase the quantitative analysis.

The work done for this thesis concentrated on particular areas of continental margins. It would be very interesting to study a whole sedimentary system from source to sink in detail. This would involve obtaining and analysing an enormous amount of data that include canyons, channels and frontal splays and show the structure and evolution of the continental margin. Well data and sedimentary cores would be important for this kind of work to establish the detailed sedimentology of the system. This kind of project could be taken to great lengths by incorporating and synthesising various data and methods, such as provenance and climate studies and, experimental work and modelling to determine the detailed evolution of the whole system.

New technologies, such as Lidar, combined with GPR could be used to look for features that are commonly resolved only from 3D seismic data from outcrops. Finding evidence for depressions, knickpoints and sediment waves within channel-fill on outcrops and other data should be attempted.

The growing interest in deepwater continental margins by both the scientific community and the hydrocarbon industry and the increasing amount and quality of data and new technologies to analyse them ensure that there is a plethora of opportunity for future research in this field.

Chapter 7

7 CONCLUSIONS

7.1 ARCHITECTURAL ELEMENTS OF THE STUDY AREAS

- The dominant architectural elements in the Niger Delta dataset are large channel-levee systems, MTCs and smaller failures that originate from the flanks of thrust-related anticlines. In the Espirito Santo Basin dataset, there are salt diapirs, large canyon systems, small channels and slope failures including slumps, slides and debris flows, which are originated from the steep slopes beneath the shelf break.

- Both datasets have a range of erosional and depositional features, the location and style of which are influenced by the uplift of structures that actively deform the seafloor. Regardless of the differences in the settings, many of the architectural elements of these two datasets have similar seismic character and morphology, although they commonly occur at different scales.

- The main differences in the architectural elements in the two datasets are that (1) the large canyon systems are only present in Espirito Santo Basin dataset, (2) the large, confined channel-levee systems are only found in the Niger Delta dataset and (3) more slope failures are found in the Espirito Santo Basin. These failures are smaller than the MTCs on the Niger Delta, although similar small failures occur on the flanks of the anticlines on the Niger Delta.

- The sediment pathways are influenced by pre-existing and actively forming structures. The locations of the channel-levee systems on the Niger Delta are influenced by transfer zones and the uplift rate of the anticlines. The canyons, channels and MTCs in the Espirito Santo Basin are influenced by the location of the salt diapirs and the underlying salt ridges.

7.2 DEGRADATION OF COMPRESSIONAL FOLDS ON THE NIGER DELTA

- Several different styles of submarine fold degradation result from various failure and transport processes. These include (1) small failures on the backlimbs and forelimbs, which produce debris flows and deposits no more than a few tens of metres thick, (2) large slumps with evidence for internal deformation, (3) ovoid depressions, probably

formed as a combination of slumping and bottom current erosion and (4) degradation by deepwater channel erosion and channel margin slumping.

- Channel erosion is volumetrically the most important fold degradation mechanism in this particular dataset, but the most common style is that of multiple, retrogressive, small volume failures, the locations of which are affected by pre-existing planes of weakness, such as crestal faults, if they are present.

- The difference in the geometries of the backlimbs and forelimbs of thrust propagation folds is a fundamental control on the style of failures and the runout distances of failed sediment masses. The abrupt break in slope at the foot of the forelimb reduces the velocity of the failed sediment mass due to the reduced effect of gravity and increased effect of friction. This causes deposition resulting in relatively thick, short and wide deposits, whereas the longer but shallower slope of the backlimb leads to disintegration of failed sediment mass into debris flows or turbidity currents that produce widespread, thin deposits with longer runout distances.

- Both backlimb and forelimb failures are likely to form deposits that are below seismic resolution. They are therefore difficult, if not impossible, to identify adjacent to buried folds where the seismic resolution is low.

- The failure of sediments with higher internal shear strength forms more coherent downslope mass movements on a basal detachment, which show evidence for shortening by internal imbricate thrusting.

- Ovoid depressions that occur above folds that have only a minor relief on the seafloor are considered to have formed by small scale slumping and have subsequently been modified by bottom currents.

- Fold degradation produces laterally discontinuous erosional surfaces and poorly sorted deposits along the folds. The impact on reservoir prediction is that significant amount of sediment is removed from the folds and thick deposits of non-reservoir accumulates

adjacent to folds. Laterally discontinuous erosion surfaces and deposits along the folds can cause very complicated reflection geometries.

7.3 KNICKPOINT MIGRATION IN SUBMARINE CHANNELS

- Knickpoints form on a present day thalweg of a channel-levee system on the western Niger Delta as a result of uplift of folds orthogonal to the CLS. The knickpoints are classified according to their size, morphology and maturity. Type I knickpoints are the largest and the least mature, Type II knickpoints are intermediate, and the Type III comprises the smallest and most mature knickpoints found across the frontal fold, where the local gradient is the steepest.

- The high degree of confinement of the channel-levee system may restrict the channel to respond to the changes in gradients caused by the folding by lateral migration of the thalweg (swing and sweep). Instead, it tries to readjust to equilibrium profile by adjusting the vertical position of the thalweg by erosion and deposition in specific areas.

- The reduction of the thalweg gradient upstream of an anticline leads to deceleration of turbidity currents and deposition of their coarsest sediment load. This interpretation is supported by the presence of several kilometres long zones of high-amplitude reflections, which represent relatively coarse-grained sediments along the channel upstream of some folds. Where the gradient is steeper on the basinward limb of the fold, the currents accelerate and become able to erode the seafloor. These specific areas of erosion and deposition leads to formation of the knickpoints.

- As the knickpoints migrate upstream, they erode the sediment deposits upstream of them completely or incise into them cutting them into terraces. High amplitudes on some of the terraces adjacent to channel thalweg are thus more likely to record a history of deposition of coarse sediments, which were subsequently incised and compartmentalised by a headward-migrating knickpoint, rather than giving clues about the thickness or volume of turbidity currents within the channel.

- The relatively coarse deposits upstream of knickpoints can be preserved for example if the channel system is abandoned or avulsion within the channel-belt occurs. The evidence from this case study suggests that avulsion and at least partial preservation takes place in this system at the present day.

- The 3D architecture of channel-levee systems is influenced by knickpoints where the channels intersect dynamically changing seabed topography. The occurrence of knickpoints increases the erosive character of stacked channel deposits and leads to the development of discontinuous channel-axis deposits. However, evidence for deposits of coarser sediments can be found within the channel reaches upstream of folds. These deposits could constitute an important element of reservoir architecture, but stacking patterns can vary dramatically over short distances along channels.

- Knickpoint formation and migration may be an important process by which channels cut through uplifting thrust and fold belts as they strive to obtain their equilibrium profiles. However, as knickpoints are predominantly transient features, distinguishing the evidence of knickpoint migration from erosional currents from subsurface seismic data or outcrops is highly challenging.

7.4 CURRENT-GENERATED DEPRESSIONS ALONG CHANNELS

- Trails of depressions that follow underlying erosional slope channels are found in the Espirito Santo Basin on the continental margin of Brazil. Individual depressions are also found above scarps, knickpoints and other topographical irregularities. The depressions are typically several hundred metres across and tens of metres deep (typically 600 m and 30 m respectively). The 3D seismic data enabled the establishment of the evolution of the 3D morphology of the depressions in detail.

- The formation of the depressions is interpreted to be the result of the interaction of Froude-supercritical flows with perturbations in topography. This makes the flows unstable and creates zones of preferential deposition and erosion. A local break in slope may also bring about a change in flow regime from supercritical to subcritical flow via a hydraulic jump, which will enhance erosion at the base of the break in slope and deposition immediately after it, thus forming a depression.

- The trails of depressions that follow the underlying channels are interpreted as channel-confined sediment waves, which are likely to be comparable to transportational cyclic steps. Cyclic steps have been described in non-marine environments, laboratory experiments and numerical models, but have never before been described from 3D seismic data in the submarine realm.

- Trails of depressions that have been described before are caused by fluid escape producing trails of pockmarks above channel-axis deposits. Their development relies on the development of overpressure in buried sediment, requiring rather different conditions than what were described here.

- Similar trails of depressions to what was described in the Espirito Santo Basin are observed in other datasets and also produced by modelling and experiments. The phenomenon is thus expected to be ubiquitous and further examples are likely to be found in other basins.

- The formation of depressions by current activity is likely to be far more widespread on deepwater slopes also because supercritical flow conditions are common on steep submarine slopes and there are many mechanisms by which a perturbation can develop on the seafloor. However, particularly steep slopes or confined flows may be required to create the ideal conditions for this process to occur. Nevertheless, continental slopes cover a large area of the Earth and therefore this process is likely to have global significance.

7.5 GENERAL CONCLUSIONS

- Changes in the slope angles have a significant effect on the type, size and location of erosional and depositional elements of the study areas. They affect for example (1) slope stability, making a failure more likely the steeper the slopes are, (2) runout distances and the level of disintegration of failed sediment, (3) gravity and bed shear stress, and therefore the velocity of the sediment-gravity flows and their capability and tendency to erode or deposit sediment and (4) stability of the flows, causing changes in flow conditions and regime, and leading to the formation of knickpoints, sediment waves and depressions.

- The actively forming structures in the two datasets, the thrust and fold belt in the Niger Delta and the salt diapirs in the Espirito Santo Basin, affect sedimentation and erosion in different ways. Some channels are deflected around the anticlines and some mass transport complexes are curved around the salt diapirs. The folds provide the sites and the origin for small slope failures, but similar degradation of the diapir flanks is not observed. The small slope failures in the Espirito Santo Basin originate from the steep continental slope instead.

- Although the channels in the two datasets are different in that in the Espirito Santo Basin they are mainly smaller converging slope channels and channels that are confined within a canyon system, and in the Niger Delta they are large channel-levee systems, they share some common features. Channel deposits of similar width, sinuosity and amalgamation are found within the canyons of the Espirito Santo Basin and the basal parts of the CLSs on the Niger Delta. Sinuosity in the channels of the Niger Delta does not appear to be affected by gradient, mainly due to the confinement of the channels, but in the Espirito Santo Basin there is a clear correlation with sinuosity and slope. Meander bend formation and cutoff have been important processes during the evolution of the Ijebu CLS on the Niger Delta, however, most likely only during periods of time when the channels were less confined.

- The channels on or near the seafloor of both of the datasets have knickpoints along them, although the slope channel profiles are concave in the Espirito Santo Basin and slightly convex on the Niger Delta. Although the formation mechanisms of the knickpoints are different, it is suggested that knickpoint migration is an important mechanism of how channel incision occurs.

- Sediment-gravity currents are responsible for the formation of many features on submarine slopes, such as channels, knickpoints, sediment waves and depressions. They play a major role in the modification of the morphology of the deepwater slopes. The observations made in this thesis have significance in understanding sediment dispersal patterns in submarine realm and how submarine landscapes are created and modified.

- The identification of the sedimentary features discussed in this thesis from outcrops can be very challenging, as outcrops are not commonly large enough to encompass the whole feature or to enable the establishment of its 3D architecture. Some erosional surfaces seen in outcrops of channels may have been formed by upstream-migrating knickpoints and some strata within a channel-fill may be a channel-confined sediment wave, but they may never be identified from outcrops.

- Different analytical methods complement each other. The study of outcrops, flume tank experiments and numerical modelling are important tools to aid the interpretation of 3D seismic data. They have increased the understanding of the processes and behaviour of sediment-gravity flows and reveal many small-scale features that cannot be identified form seismic data. 3D seismic data also provides natural examples of geometries and morphologies in large scale whose formation modelling can try to solve.

- There is a great opportunity and desire for future research in the field of deepwater sedimentary systems. The increasing amount and quality of data and technologies to acquire and analyse them alone enables this. Many features that have only been resolved from 3D seismic data should be looked for in other seismic volumes and other kinds of data. The understanding of the formation mechanisms and conditions of features, like knickpoints and channel-confined sediment waves, depressions and cyclic steps could be greatly advanced by conducting more experiments and analysing more datasets.

References

8 REFERENCES

Abreu, V., Sullivan, M., Pirmez, C. and Mohrig, D., 2003. Lateral accretion packages (LAPs): an important reservoir element in deep water sinuous channels. *Marine and Petroleum Geology* 20(6-8), 631-648.

Adams, E.W. and Schlager, W., 2000. Basic types of submarine slope curvature. *Journal of Sedimentary Research* 70(4), 814-828.

Adeogba, A.A., McHargue, T.R. and Graham, S.A., 2005. Transient fan architecture and depositional controls from near-surface 3-D seismic data, Niger Delta continental slope. *AAPG Bulletin* 89(5), 627-643.

Ambraseys, N.N., 1988. Engineering Seismology. *Earthquake engineering and structural dynamics* 17, 1-105.

Armentrout, J.M., Kanschat, K.A., Meisling, K.E., Tsakma, J.J., Antrim, L. and McConnell, D.R., 2000. Neogene turbidite systems of the Gulf of Guinea continental margin slope, offshore Nigeria. In: Bouma, A.H. and Stone, C.G. (Eds.), *Fine-Grained Turbidite Systems*. AAPG Memoir 72/SEPM Special Publication No. 68, Tulsa, pp. 93-108.

Babonneau, N., Savoye, B., Cremer, M. and Klein, B., 2002. Morphology and architecture of the present canyon and channel system of the Zaire deep-sea fan. *Marine and Petroleum Geology* 19(4), 445-467.

Babonneau, N., Savoye, B., Cremer, M. and Bez, M., 2004. Multiple terraces within the deep incised Zaire Valley (ZaïAngo Project): are they confined levees? In: Lomas, S.A. and Joseph, P. (Eds.), *Confined Turbidite Systems*. Geological Society, London, Special Publications, 222, pp. 91-114.

Bacon, M., Simm, R. and Redshaw, T., 2003. *3-D seismic interpretation*. Cambridge University Press, 212 pp.

Beaubouef, R.T., Rossen, C., Zelt, F.B., Sullivan, M.D., Mohrig, D.C. and Jennette, D.C., 1999. *Deep-water sandstones, Brushy Canyon Formation, West Texas*. Field guide for AAPG Hedberg field research conference. AAPG Continuing Education Course Note Series No. 40.

Bellian, J.A., Kerans, C. and Jennette, D.C., 2005. Digital Outcrop Models: Applications of Terrestrial Scanning Lidar Technology in Stratigraphic Modeling. *Journal of Sedimentary Research* 75(2), 166-176.

Berger, M. and Roberts, A.M., 1999. The Zeta Structure; a footwall degradation complex formed by gravity sliding on the western margin of the Tampen Spur, northern North Sea. In: Fleet, A.J. and Boldy, S.A.R. (Eds.), *Petroleum geology of Northwest Europe; proceedings of the 5th conference held at the Barbican Centre, London, 26-29 October 1997*. The Geological Society of London, London, United Kingdom, pp. 106-116.

Bouma, A.H., 2004. Key controls on the characteristics of turbidite systems. In: Lomas, S.A. and Joseph, P. (Eds.), *Confined turbidite systems*. Geological Society, London, Special Publications, 222, pp. 9-22.

Bourgeois, A., Joseph, P. and Lecomte, J.C., 2004. Three-dimensional full wave seismic modelling versus one-dimensional convolution: the seismic appearance of the Grés d'Annot turbidite system. In: Joseph, P. and Lomas, S.A. (Eds.), *Deep-Water Sedimentation in the Alpine Basin of SE France: New perspective on the Grés d'Annot and related systems*. Geological Society, London, Special Publications, 221, pp. 401-417.

Brown, A.R., 1999. *Interpretation of Three-Dimensional Seismic Data*. AAPG Memoir 42, 5th edition, 510 pp.

Brown, R.J. and Branney, M.J., 2004. Bypassing and diachronous deposition from density currents: Evidence from a giant regressive bed form in the Poris ignimbrite, Tenerife, Canary Islands. *Geology* 32(5), 445-448.

Burbank, D.W. and Raynolds, G.H., 1988. Stratigraphic Keys to the Timing of Thrusting in Terrestrial Foreland Basins: Applications to the Northwestern Himalaya. In: Kleinspehn, K.L. and Paola, C. (Eds.), *New Perspectives in Basin Analysis*. Springer-Verlag, New York, pp. 331-351.

Burbank, D.W., Meigs, A. and Brozovic, N., 1996. Interactions of growing folds and coeval depositional systems. *Basin Research* 8, 199-223.

Burbank, D.W. and Anderson, R.S., 2001. *Tectonic Geomorphology*. Blackwell Science Ltd., 274 pp.

Bursik, M.I. and Woods, A.W., 2000. The effects of topography on sedimentation from particle-laden turbulent density currents. *Journal of Sedimentary Research* 70(1), 53-63.

Campion, K.M., Sprague, A.R., Mohrig, D.C., Lovell, R.W., Drzewiecki, P.A., Sullivan, M.D., Ardill, J.A., Jensen, G.N. and Sickafoose, D.K., 2000. Outcrop expression of confined channel complexes. In: Weimer, P., Slatt, R.M., Coleman, J., Rossen, N.C., Nelson, H., Bouma, A.H. and Styzen, M.J. (Eds.), *Deep-water reservoirs of the world*. GCSSEPM Foundation 20th Annual Research Conference, pp. 127-151.

Campion, K.M., Sprague, A.R. and Sullivan, M.D., 2005. *Architecture and Lithofacies of the Capistrano Formation (Miocene-Pliocene), San Clemente, California*. Fieldtrip Guidebook Prepared for the Pacific Section SEPM Annual Fall Fieldtrip, San Clemente, California. The Pacific Section SEPM, 42 pp.

Canals, M., Lastras, G., Urgeles, R., Casamor, J.L., Mienert, J., Cattaneo, A., De Batist, M., Haflidason, H., Imbo, Y. and Laberg, J.S., 2004. Slope failure dynamics and impacts from seafloor and shallow sub-seafloor geophysical data: case studies from the COSTA project. *Marine Geology* 213(1-4), 9-72.

Cartwright, J., 1989. The kinematics of inversion in the Danish Central Graben. In: Cooper, M.A. and Williams, G.D. (Eds.), *Inversion Tectonics*. Geological Society Special Publications No. 44, pp. 153-175.

Chang, H.K., Kowsmann, R.O., Figueiredo, A.M.F. and Bender, A.A., 1992. Tectonics and stratigraphy of the East Brazil Rift system: an overview. *Tectonophysics* 213(1-2), 97-138.

Clark, J.D. and Pickering, K.T., 1996. Architectural elements and growth patterns of submarine channels; application to hydrocarbon exploration. *AAPG Bulletin* 80(2), 194-221.

Cohen, H.A. and McClay, K., 1996. Sedimentation and shale tectonics of the northwestern Niger Delta front. *Marine and Petroleum Geology* 13(3), 313-328.

Coleman, J.L.J., Sheppard, F.C. and Jones, T.K., 2000. Seismic resolution of submarine channel architecture as indicated by outcrop analogs. In: Bouma, A.H. and Stone, C.G. (Eds.), *Fine-grained turbidite systems*. AAPG Memoir 72/SEPM Special Publication 68, pp. 119-126.

Corredor, F., Shaw, J.H. and Bilotti, F., 2005. Structural styles in the deep-water fold and thrust belts of the Niger Delta. *AAPG Bulletin* 89(6), 753-780.

Cramez, C. and Jackson, M.P.A., 2000. Superposed deformation straddling the continental-oceanic transition in deep-water Angola. *Marine and Petroleum Geology* 17(10), 1095-1109.

Cronin, B.T., Hurst, A., Celik, H. and Turkmen, I., 2000. Superb exposure of a channel, levee and overbank complex in an ancient deep-water slope environment. *Sedimentary Geology* 132(3-4), 205-216.

Damuth, J.E., 1994. Neogene gravity tectonics and depositional processes on the deep Niger Delta continental margin. *Marine and Petroleum Geology* 11(3), 320-346.

Davies, R.J., 2003. Kilometer-scale fluidization structures formed during early burial of a deep-water slope channel on the Niger Delta. *Geology (Boulder)* 31(11), 949-952.

Demyttenaere, R., Tromp, J.P., Ibrahim, A., Allman-Ward, P. and Meckel, T., 2000. Brunei deep water exploration: from sea floor images and shallow seismic analogues to depositional models in a slope turbidite setting. In: Weimer, P., Slatt, R.M., Coleman, J., Rossen, N.C., Nelson, H., Bouma, A.H. and Styzen, M.J. (Eds.), *Deep-Water Reservoirs of the World*. GCSSEPM 20th Annual Research Conference, pp. 304-317.

Deptuck, M.E., Steffens, G.S., Barton, M. and Pirmez, C., 2003. Architecture and evolution of upper fan channel-belts on the Niger Delta slope and in the Arabian Sea. *Marine and Petroleum Geology* 20(6-8), 649-676.

Deramond, J., Souquet, P., Fondecave-Wallez, M.-J. and Specht, M., 1993. Relationships between thrust tectonics and sequence stratigraphy surfaces in foredeeps: model and examples from the Pyrenees (Cretaceous-Eocene, France, Spain). In: Williams, D.G.

and Dobb, A. (Eds.), *Tectonics and Seismic Sequence Stratigraphy*. Geological Society Special Publication No. 71, pp. 193-219.

Doust, H. and Omatsola, E., 1990. Niger Delta. In: Edwards, J.D. and Santogrossi, P.A. (Eds.), *Divergent/passive margin basins*. AAPG Memoir. American Association of Petroleum Geologists, Tulsa, OK, United States, pp. 201-238.

Droz, L., Rigaut, F., Cochonat, P. and Tofani, R., 1996. Morphology and Recent evolution of the Zaire turbidite system (Gulf of Guinea). *Geological Society of America Bulletin* 108(3), 253-269.

Droz, L., Marsset, T., Ondreas, H., Lopez, M., Savoye, B. and Spy, A.F.L., 2003. Architecture of an active mud-rich turbidite system; the Zaire Fan (Congo-Angola margin Southeast Atlantic); results from ZaiAngo 1 and 2 cruises. *AAPG Bulletin* 87(7), 1145-1168.

Edwards, R.A., Whitmarsh, R.B. and Scrutton, R.A., 1997. Synthesis of the crustal structure of the transform continental margin off Ghana, northern Gulf of Guinea. *Geo-Marine Letters* 17, 12-20.

Ercilla, G., Wynn, R.B., Alonso, B. and Baraza, J., 2002. Initiation and evolution of turbidity current sediment waves in the Magdalena turbidite system. *Marine Geology* 192(1-3), 153-169.

Eschard, R., 2001. Geological factors controlling sediment transport from platform to deep basin: a review. *Marine and Petroleum Geology* 18(4), 487-490.

Estrada, F., Ercilla, G. and Alonso, B., 2005. Quantitative study of a Magdalena submarine channel (Caribbean Sea): implications for sedimentary dynamics. *Marine and Petroleum Geology* 22(5), 623-635.

Fagherazzi, S. and Sun, T., 2003. Numerical simulations of transportational cyclic steps. *Computers & Geosciences* 29(9), 1143-1154.

Fiduk, J.C., Brush, E.R., Anderson, L.E., Gibbs, P.B. and Rowan, M.G., 2004. Salt deformation, magmatism, and hydrocarbon prospectivity in the Espirito Santo Basin, offshore Brazil. In: Post, P.J., Olson, D.L., Lyons, K.T., Palmes, S.L., Harison, P.F. and Rosen, N.C. (Eds.), *Salt-sediment interactions and hydrocarbon prospectivity: Concepts, applications, and case studies for the 21st century*. GCSSEPM 24th Annual Research Conference, pp. 370-392.

Fildani, A., Normark, W.R., Kostic, S. and Parker, G., 2006. Channel formation by flow stripping: large-scale scour features along the Monterey East Channel and their relation to sediment waves. *Sedimentology* 53(6), 1265-1287.

Flood, R.D., 1988. A lee wave model for deep-sea mudwave activity. *Deep Sea Research Part A. Oceanographic Research Papers* 35(6), 973-983.

Fonnesu, F., 2003. 3D seismic images of a low-sinuosity slope channel and related depositional lobe (West Africa deep-offshore). *Marine and Petroleum Geology* 20(6-8), 615-629.

Frey Martinez, J., Cartwright, J. and Hall, B., 2005. 3D seismic interpretation of slump complexes: examples from the continental margin of israel. *Basin Research* 71(1), 83-108.

Galloway, W.E., 1998. Siliciclastic slope and base-of-slope depositional systems; component facies, stratigraphic architecture, and classification. *AAPG Bulletin* 82(4), 569-595.

Garcia, M. and Parker, G., 1989. Experiments on hydraulic jumps in turbidity currents near a canyon-fan transition. *Science* 245(4916), 393-396.

Gardner, M.H. and Borer, J.M., 2000. Submarine channel architecture along a slope to basin profile, Brushy Canyon Formation, west Texas. In: Bouma, A.H. and Stone, C.G. (Eds.), *Fine-grained turbidite systems*. AAPG Memoir 72/SEPM Special Publication 68, pp. 195-214.

Gardner, M.H., Borer, J.M., Melick, J.J., Mavilla, N., Dechesne, M. and Wagerle, R.N., 2003. Stratigraphic process-response model for submarine channels and related features from studies of Permian Brushy Canyon outcrops, West Texas. *Marine and Petroleum Geology* 20(6-8), 757-787.

Gardner, T.W., 1983. Experimental study of knickpoint and longitudinal profile evolution in cohesive, homogeneous material. *Geological Society of America Bulletin* 94(5), 664-672.

Gay, A., Lopez, M., Cochonat, P., Sultan, N., Cauquil, E. and Brigaud, F., 2003. Sinuous pockmark belt as indicator of a shallow buried turbiditic channel on the lower slope of the Congo basin, West African margin. In: Van Ransbergen, P., Hillis, R.R., Maltman, A.J. and Morley, C.K. (Eds.), *Subsurface Sediment Mobilization*. Geological Society, London, Special Publications, pp. 173-189.

Gee, M.J.R. and Gawthorpe, R.L., 2006. Submarine channels controlled by salt tectonics: Examples from 3D seismic data offshore Angola. *Marine and Petroleum Geology* 23(4), 443-458.

Grando, G. and McClay, K., 2004. Structural evolution of the Frampton growth fold system, Atwater Valley-Southern Green Canyon area, deep water Gulf of Mexico. *Marine and Petroleum Geology* 21(7), 889-910.

Haack, R.C., Sundararaman, P., Diedjomahor, J.O., Xiao, H., Gant, N.J., May, E.D. and Kelsch, K., 2000. Niger Delta petroleum systems, Nigeria. In: Mello, M.R. and Katz, B.J. (Eds.), *Petroleum Systems of South Atlantic Margins*. AAPG Memoir 73, pp. 213-231.

Hampton, M.A., Lee, H.J. and Locat, J., 1996. Submarine landslides. *Reviews of Geophysics* 34(1), 33-59.

Hardy, S. and Poblet, J., 1995. The velocity description of deformation; Paper 2, Sediment geometries associated with fault-bend and fault-propagation folds. *Marine and Petroleum Geology* 12(2), 165-176.

Hart, B.S., 1999. Definition of subsurface stratigraphy, structure and rock properties from 3-D seismic data. *Earth-Science Reviews* 47(3-4), 189-218.

Haughton, P.D.W., 2000. Evolving turbidite systems on a deforming basin floor, Tabernas, SE Spain. *Sedimentology* 47(3), 497-518.

Heezen, B.C. and Ewing, M., 1955. Orleansville earthquake and turbidity currents. *AAPG Bulletin* 39(12), 2505-2514.

Heiniö, P. and Davies, R.J., 2006. Degradation of compressional fold belts: Deep-water Niger Delta. *AAPG Bulletin* 90(5), 753-770.

Hesthammer, J. and Fossen, H., 1999. Evolution and geometries of gravitational collapse structures with examples from the Statfjord Field, northern North Sea. *Marine and Petroleum Geology* 16(3), 259-281.

Hills, E.S., 1972. Tectonic analysis of folds. In: Hills, E.S. (Ed.), *Elements of Structural Geology*. Chapman and Hall Ltd, London, pp. 261-294.

Hiscott, R.N., 1994. Loss of capacity, not competence, as the fundamental process governing deposition form turbidity currents. *Journal of Sedimentary Research* A64(2), 209-214.

Hooper, R.J., Fitzsimmons, R.J., Grant, N. and Vendeville, B.C., 2002. The role of deformation in controlling depositional patterns in the south-central Niger Delta, West Africa. *Journal of Structural Geology* 24(4), 847-859.

Hovland, M., 2002. The significance of pockmarks to understanding fluid flow processes and geohazards. *Geofluids* 2, 127-136.

Howard, A.D., Dietrich, W.E. and Seidl, M.A., 1994. Modeling fluvial erosion on regional to continental scales. *Journal of Geophysical Research, B, Solid Earth and Planets* 99(7), 13,971-13,986.

Howe, J., 1996. Turbidite and contourite sediment waves in the northern Rockall Trough, North Atlantic Ocean. *Sedimentology* 43(2), 219-234.

Hübscher, C., Spiess, V., Breitzke, M. and Weber, M.E., 1997. The youngest channel-levee system of the Bengal Fan; results from digital sediment echosounder data. *Marine Geology* 141(1-4), 125-145.

Humphrey, N.F. and Konrad, S.K., 2000. River incision or diversion in response to bedrock uplift. *Geology* 28(1), 43-46.

Huyghe, P., Foata, M., Deville, E., Mascle, G. and Caramba Working Group, 2004. Channel profiles through the active thrust front of the southern Barbados prism. *Geology* 32(5), 429-432.

Ingram, G.M., Chisholm, T.J., Grant, C.J., Hedlund, C.A., Stuart-Smith, P. and Teasdale, J., 2004. Deepwater North West Borneo: hydrocarbon accumulation in an active fold and thrust belt. *Marine and Petroleum Geology* 21(7), 879-887.

Jackson, M.P.A., Vendeville, B.C. and Schultz-Ela, D.D., 1994. Structural dynamics of salt systems. *Annual Review Earth Planetary Systems* 22, 93-117.

Kastens, K.A. and Shor, A.N., 1986. Evolution of a channel meander on the Mississippi deep-sea fan. *Marine Geology* 71(1-2), 165-175.

Kearey, P. and Brooks, M., 1991. *An introduction to geophysical exploration*. Blackwell Science, 2nd edition, 254 pp.

Keevil, G.M., Peakall, J., Best, J.L. and Amos, K.J., 2006. Flow structure in sinuous submarine channels: Velocity and turbulence structure of an experimental submarine channel. *Marine Geology* 229(3-4), 241-257.

Khripounoff, A., Vangriesheim, A., Babonneau, N., Crassous, P., Dennielou, B. and Savoye, B., 2003. Direct observation of intense turbidity current activity in the Zaire submarine valley at 4000 m water depth. *Marine Geology* 194(3-4), 151-158.

Kneller, B., 1995. Beyond the turbidite paradigm: physical models for deposition of turbidites and their implications for reservoir prediction. In: Hartley, A.J. and Prosser, D.J. (Eds.), *Characterization of Deep Marine Clastic Systems. Geological Society Special Publication No 94*. pp. 31-49.

Kneller, B. and Buckee, C., 2000. The structure and fluid mechanics of turbidity currents: a review of some recent studies and their geological implications. *Sedimentology* 47(s1), 62-94.

Kneller, B., 2003. The influence of flow parameters on turbidite slope channel architecture. *Marine and Petroleum Geology* 20(6-8), 901-910.

Kneller, B.C. and McCaffrey, W.D., 2003. The Interpretation of Vertical Sequences in Turbidite Beds: The Influence of Longitudinal Flow Structure. *Journal of Sedimentary Research* 73(5), 706-713.

Knox, G.J. and Omatsola, E., M, 1989. Development of the Cenozoic Niger Delta in terms of the 'Escalator Regression' model and impact on hydrocarbon distribution. *Proceedings KNGMG Symposium 'Coastal Lowlands, Geology and Geotechnology'*, 181-202.

Kolla, V., Eittreim, S., Sullivan, L., Kostecki, J.A. and Burckle, L.H., 1980. Current-controlled, abyssal microtopography and sedimentation in Mozambique Basin, southwest Indian Ocean. *Marine Geology* 34(3-4), 171-206.

Kolla, V., Bourges, P., Urruty, J.M. and Safa, P., 2001. Evolution of deep-water Tertiary sinuous channels offshore Angola (West Africa) and implications for reservoir architecture. *AAPG Bulletin* 85(8), 1373-1405.

Komar, P.D., 1969. The channelized flow of turbidity currents with application to Monterey deep-sea fan channel. *Journal of Geophysical Research* 74(18), 4544-4558.

Komar, P.D., 1971. Hydraulic jumps in turbidity currents. *GSA Bulletin* 82(6), 1477-1487.

Krause, D.C., White, W.C., Piper, D.J.W. and Heezen, B.C., 1970. Turbidity currents and cable breaks in the western New Britain trench. *GSA Bulletin* 81(7), 2153-2160.

Kubo, Y. and Nakajima, T., 2002. Laboratory experiments and numerical simulation of sediment-wave formation by turbidity currents. *Marine Geology* 192(1-3), 105-121.

Kukowski, N., Schillhorn, T., Huhn, K., von Rad, U., Husen, S. and Flueh, E.R., 2001. Morphotectonics and mechanics of the central Makran accretionary wedge off Pakistan. *Marine Geology* 173(1-4), 1-19.

Lastras, G., Canals, M., Urgeles, R., Hughes-Clarke, J.E. and Acosta, J., 2004. Shallow slides and pockmark swarms in the Eivissa Channel, western Mediterranean Sea. *Sedimentology* 51, 837-850.

Lee, S.E., Talling, P.J., Ernst, G.G.J. and Hogg, A.J., 2002. Occurrence and origin of submarine plunge pools at the base of the US continental slope. *Marine Geology* 185(3-4), 363-377.

Leeder, M., 1999. *Sedimentology and sedimentary basins. From turbulence to tectonics.* Blackwell Science Ltd, 592 pp.

Lien, T., Walker, R.G. and Martinsen, O.J., 2003. Turbidites in the Upper Carboniferous Ross Formation, western Ireland: reconstruction of a channel and spillover system. *Sedimentology* 50(1), 113-148.

Locat, J., 2001. Instabilities along ocean margins: a geomorphological and geotechnical perspective. *Marine and Petroleum Geology* 18(4), 503-512.

Locat, J. and Lee, H.J., 2002. Submarine landslides: advances and challenges. *Canadian Geotechnical Journal* 39, 193-212.

Lopez, M., 2001. Architecture and depositional pattern of the Quaternary deep-sea fan of the Amazon. *Marine and Petroleum Geology* 18(4), 479-486.

Marr, J.G., Elverhoi, A., Harbitz, C., Imran, J. and Harff, P., 2002. Numerical simulation of mud-rich subaqueous debris flows on the glacially active margins of the Svalbard-Barents Sea. *Marine Geology* 188(3-4), 351-364.

Masson, D.G., Kenyon, N.H., Gardner, J.V. and Field, M.E., 1995. Monterey Fan: channel and overbank morphology. In: Pickering, K.T., Hiscott, R.N., Kenyon, N.H., Ricci Lucchi, F.R. and Smith, R.D.A. (Eds.), *Atlas of deep water environments - Architectural style in turbidite systems*. Chapman & Hall, pp. 74-79.

Mayall, M. and Stewart, I., 2000. The Architecture of Turbidite Slope Channels. *GCSSEPM Foundation 20th Annual Research Conference Deep-Water Reservoirs of the World, December 3-6, 2000, p. 578-86.*

Mayall, M., Jones, E. and Casey, M., 2006. Turbidite channel reservoirs - Key elements in facies prediction and effective development. *Marine and Petroleum Geology* 23(8), 821-841.

McCaffrey, W. and Kneller, B., 2001. Process Controls on the Development of Stratigraphic Trap Potential on the Margins of Confined Turbidite Systems and Aids to Reservoir Evaluation. *AAPG Bulletin* 85(6), 971-988.

McClay, K., Dooley, T., Ferguson, A. and Poblet, J., 2000. Tectonic Evolution of the Sanga Sanga Block, Mahakam Delta, Kalimantan, Indonesia. *AAPG Bulletin* 84(6), 765-786.

McHargue, T.R. and Webb, J.E., 1986. Internal geometry, seismic facies, and petroleum potential of canyons and inner fan channels of the Indus submarine fan. *AAPG Bulletin* 70(2), 161-180.

McHugh, C.M.G. and Ryan, W.B.F., 2000. Sedimentary features associated with channel overbank flow; examples from the Monterey Fan. *Marine Geology* 163(1-4), 199-215.

McLeod, A.E. and Underhill, J.R., 1999. Processes and products of footwall degradation, northern Brent Field, northern North Sea. In: Fleet, A.J. and Boldy, S.A.R. (Eds.), *Petroleum geology of Northwest Europe; proceedings of the 5th conference held at the Barbican Centre, London, 26-29 October 1997.* The Geological Society of London, London, United Kingdom, pp. 91-106.

Mello, U.T. and Pratson, L.F., 1999. Regional slope stability and slope-failure mechanics from the two-dimensional state of stress in an infinite slope. *Marine Geology* 154(1-4), 339-356.

Menard, H.W., 1955. Deep-sea channels, topography, and sedimentation. *AAPG Bulletin* 39(2), 236-255.

Middleton, G.V., 1993. Sediment deposition from turbidity currents. *Annual Review Earth Planetary Systems* 21, 89-114.

Migeon, S., Savoye, B., Zanella, E., Mulder, T., Faugeres, J.C. and Weber, O., 2001. Detailed seismic-reflection and sedimentary study of turbidite sediment waves on the Var Sedimentary Ridge (SE France): significance for sediment transport and deposition and for the mechanisms of sediment-wave construction. *Marine and Petroleum Geology* 18(2), 179-208.

Mitchell, N.C., 2004. Form of submarine erosion from confluences in Atlantic USA continental slope canyons. *American Journal of Science* 304, 590-611.

Mitchell, N.C., 2006. Morphologies of knickpoints in submarine canyons. *Geological Society of America Bulletin* 118(5-6), 589-605.

Mitchum, R.M., Jr., Vail, P.R. and Sangree, J.B., 1977. Seismic stratigraphy and global changes of sea level, part 6: Stratigraphic interpretation of seismic reflection patterns in depositional sequences. In: Payton, C.E. (Ed.), *Seismic stratigraphy - applications to hydrocarbon exploration. AAPG Memoir 26*. Tulsa, Ok, pp. 117-133.

Mohrig, D., Elverhoi, A. and Parker, G., 1999. Experiments on the relative mobility of muddy subaqueous and subaerial debris flows, and their capacity to remobilize antecedent deposits. *Marine Geology* 154(1-4), 117-129.

Mohrig, D. and Marr, J.G., 2003. Constraining the efficiency of turbidity current generation from submarine debris flows and slides using laboratory experiments. *Marine and Petroleum Geology* 20(6-8), 883-899.

Moraes, M.A.S., Blaskovski, P.R. and Joseph, P., 2004. The Grés d'Annot as an analogue for Brazilian Cretaceous sandstone reservoirs: comparing convergent to passive-margin confined turbidites. In: Joseph, P. and Lomas, S.A. (Eds.), *Deep-Water Sedimentation in the Alpine Basin of SE France: New perspective on the Grés d'Annot and related systems*. Geological Society, Geological Society, London, Special Publications, pp. 419-436.

Morgan, R., 2003. Prospectivity in ultradeep water: the case for petroleum generation and migration within the outer parts of the Niger Delta apron. In: Arthur, T.J., MacGregor, D.S. and Cameron, N.R. (Eds.), *Petroleum Geology of Africa: New themes and Developing technologies*. Geological society, London, Special Publications, pp. 151-164.

Morgan, R., 2004. Structural controls on the positioning of submarine channels on the lower slopes of the Niger Delta. In: Davies, R.J., Cartwright, J.A., Stewart, S.A., Lappin, M. and Underhill, J.R. (Eds.), *3D Seismic Technology: Application to the Exploration of Sedimentary Basins*. Geological Society, London, Memoirs, 29, pp. 45-51.

Morisawa, M., 1985. River morphology: channel pattern, *Rivers*. Longman Group Limited, pp. 222.

Mulder, T. and Cochonat, P., 1996. Classification of offshore mass movements. *Journal of Sedimentary Research* 66(1), 43-57.

Mulder, T., Savoye, B. and Syvitski, J.P.M., 1997. Numerical modelling of a mid-sized gravity flow: the 1979 Nice turbidity current (dynamics, processes, sediment budget and seafloor impact). *Sedimentology* 44(2), 305-326.

Mulder, T. and Alexander, J., 2001. The physical character of subaqueous sedimentary density flows and their deposits. *Sedimentology* 48(2), 269-299.

Nakajima, T. and Satoh, M., 2001. The formation of large mudwaves by turbidity currents on the levees of the Toyama deep-sea channel, Japan Sea. *Sedimentology* 48(2), 435-463.

Nemec, W., 1990. Aspects of sediment movement on steep delta slopes. In: Colella, A. and Prior, D.B. (Eds.), *Coarse-grained Deltas*. Special Publication of the International Association of Sedimentologists, 10, Blackwell, Oxford, pp. 29-73.

Nigro, F. and Renda, P., 2004. Growth pattern of underlithified strata during thrust-related folding. *Journal of Structural Geology* 26(10), 1913-1930.

Normark, W.R., Hess, G.R., Stow, D.A.V. and Bowen, A.J., 1980. Sediment waves on the monterey fan levee: A preliminary physical interpretation. *Marine Geology* 37(1-2), 1-18.

Normark, W.R., Posamentier, H.W. and Mutti, E., 1993. Turbidite systems: State of the art and future directions. *Reviews of Geophysics* 31(2), 91-116.

Ojeda, H.A.O., 1982. Structural framework, stratigraphy, and evolution of Brazilian marginal basins. *AAPG Bulletin* 66(6), 732-749.

Ouchi, S., 1985. Response of alluvial rivers to slow active tectonic movement. *Geological Society of America Bulletin* 96(4), 504-515.

Parker, G., Fukushima, Y. and Pantin, H.M., 1986. Self-accelerating turbidity currents. *Journal of Fluid Mechanics* 171, 145-181.

Peakall, J., McCaffrey, W.D., Kneller, B.C., Stelting, C.E., McHargue, T.R. and Schweller, W.J., 2000a. A process model for the evolution of submarine fan channels; implications for sedimentary architecture. In: Bouma, A.H. and Stone, C.G. (Eds.), *Fine-grained turbidite systems.* American Association of Petroleum Geologists. Tulsa, OK, United States. 2000.

Peakall, J., McCaffrey, B. and Kneller, B., 2000b. A process model for the evolution, morphology, and architecture of sinuous submarine channels. *Journal of Sedimentary Research* 70(3), 434-448.

Pickering, K.T., Hodgson, D.M., Platzman, E., Clark, J.D. and Stephens, C., 2001. A New Type of Bedform Produced by Backfilling Processes in a Submarine Channel, Late Miocene, Tabernas-Sorbas Basin, SE Spain. *Journal of Sedimentary Research* 71(5), 692-704.

Pirmez, C., Beaubouef, R.T., Friedmann, S.J. and Mohrig, D., 2000. Equilibrium profile and baselevel in submarine channels: examples from late pleistocene systems and implications for the architecture of deepwater reservoirs. In: Weimer, P., Slatt, R.M., Coleman, J., Rossen, N.C., Nelson, H., Bouma, A.H. and Styzen, M.J. (Eds.), *Deep-Water Reservoirs of the World.* GCSSEPM Foundation 20th Annual Research Conference, pp. 782-805.

Popescu, I., Lericolais, G., Panin, N., Wong, H.K. and Droz, L., 2001. Late Quaternary channel avulsions on the Danube deep-sea fan, Black Sea. *Marine Geology* 179(1-2), 25-37.

Popescu, I., Lericolais, G., Panin, N., Normand, A., Dinu, C. and Le Drezen, E., 2004. The Danube submarine canyon (Black Sea): morphology and sedimentary processes. *Marine Geology* 206(1-4), 249-265.

Posamentier, H.W. and Kolla, V., 2003. Seismic geomorphology and stratigraphy of depositional elements in deep-water settings. *Journal of Sedimentary Research* 73(3), 367-388.

Posamentier, H.W., 2003. Depositional elements associated with a basin floor channel-levee system: case study from the Gulf of Mexico. *Marine and Petroleum Geology* 20(6-8), 677-690.

Prather, B.E., 2003. Controls on reservoir distribution, architecture and stratigraphic trapping in slope settings. *Marine and Petroleum Geology* 20(6-8), 529-545.

Pratson, L.E., Imran, J., Parker, G., Syvitski, J.P.M. and Hutton, E., 2000. Debris flows vs. turbidity currents; a modeling comparison of their dynamics and deposits. In: Bouma, A.H. and Stone, C.G. (Eds.), *Fine-grained turbidite systems.* American Association of Petroleum Geologists. Tulsa, OK, United States. 2000.

Pratson, L.F. and Coakley, B.J., 1996. A model for the headward erosion of submarine canyons induced by downslope-eroding sediment flows. *Geological Society of America Bulletin* 108(2), 225-234.

Prior, D.B. and Coleman, J.M., 1982. Active slides and flows in underconsolidated marine sediments on the slopes of the Mississippi delta. In: Saxov, S. and Nieuwenhuis, J.K. (Eds.), *Marine slides and other mass movements*. Plenum Press, New York, pp. 21-49.

Prior, D.B., Bornhold, B.D. and Johns, M.W., 1984. Depositional characteristics of a submarine debris flow. *Journal of Geology* 92(6), 707-727.

Rafini, S. and Mercier, E., 2002. Forward modelling of foreland basins progressive unconformities. *Sedimentary Geology* 146(1-2), 75-89.

Rasmussen, E.S., 1994. The relationship between submarine canyon fill and sea-level change: an example from Middle Miocene offshore Gabon, West Africa. *Sedimentary Geology* 90, 61-75.

Reading, H.G. and Richards, M., 1994. Turbidite systems in deep-water basin margins classified by grain size and feeder system. *AAPG Bulletin* 78(5), 792-822.

Richards, M., Bowman, M. and Reading, H., 1998. Submarine-fan systems; I, Characterization and stratigraphic prediction. *Marine and Petroleum Geology* 15(7), 689-717.

Saller, A.H., Noah, J.T., Ruzuar, A.P. and Schneider, R., 2004. Linked lowstand delta to basin-floor fan deposition, offshore Indonesia: An analog for deep-water reservoir systems. *AAPG Bulletin* 88(1), 21-46.

Samuel, A., Kneller, B., Raslan, S., Sharp, A. and Parsons, C., 2003. Prolific deep-marine slope channels of the Nile Delta, Egypt. *AAPG Bulletin* 87(4), 541-560.

Sangree, J.B. and Widmier, J.M., 1977. Seismic stratigraphy and global changes of sea level, part 9: Seismic interpretation of clastic depositional facies, *Seismic stratigraphy - applications to hydrocarbon exploration. AAPG Memoir 26.* pp. 165-184.

Schnellmann, M., Anselmetti, F.S., Giardini, D. and McKenzie, J.A., 2005. Mass movement-induced fold-and-thrust belt structures in unconsolidated sediments in Lake Lucrene (Switzerland). *Sedimentology* 52(2), 271-289.

Sheriff, R.E. and Geldart, L.P., 1995. *Exploration seismology.* Cambridge University Press, Cambridge, 2nd edition, 592 pp.

Smallwood, J.R., 2004. Tertiary inversion in the Faroe-Shetland Channel and the development of major erosional scarps. In: Davies, R.J., Cartwright, J.A., Stewart, S.A., Lappin, M. and Underhill, J.R. (Eds.), *3D Seismic Technology: Application to the Exploration of Sedimentary Basins.* Geological Society, London, Memoirs, 29, pp. 187-198.

Smith, R., 2004. Silled sub-basins to connected tortuous corridors; sediment distribution systems on topographically complex sub-aqueous slopes. In: Lomas, S.A. and Joseph, P. (Eds.), *Confined turbidite systems.* Geological Society, London, Special Publications, 222, pp. 23-43.

Snow, R.S. and Slingerland, R.L., 1990. Stream profile adjustment to crustal warping; nonlinear results from a simple model. *Journal of Geology* 98(5), 699-708.

Soh, W. and Tokuyama, H., 2002. Rejuvenation of submarine canyon associated with ridge subduction, Tenryu Canyon, off Tokai, central Japan. *Marine Geology* 187(1-2), 203-220.

Steidtmann, J.R. and Schmitt, J.G., 1988. Provenance and Dispersal of Tectonic Sediments in Thin-Skinned, Thrusted Terrains. In: Kleinspehn, K.L. and Paola, C. (Eds.), *New Perspectives in Basin Analysis.* Springer-Verlag, New York, pp. 353-366.

Stewart, S.A., 1999. Seismic interpretation of circular geological structures. *Petroleum Geoscience* 5, 273-285.

Stewart, S.A. and Reeds, A., 2003. Geomorphology of kilometer-scale extensional fault scarps; factors that impact seismic interpretation. *AAPG Bulletin* 87(2), 251-272.

Storti, F. and Poblet, J., 1997. Growth stratal architectures associated to decollement folds and fault-propagation folds; inferences on fold kinematics. In: Cloetingh, S., Fernandez, M., Munoz, J.A., Sassi, W. and Horvath, F. (Eds.), *Structural controls on sedimentary basin formation.* Tectonophysics. Elsevier, Amsterdam, Netherlands, pp. 353-373.

Stow, D.A., 1986. Deep Clastic Seas. In: Reading, H.G. (Ed.), *Sedimentary Environments and Facies.* Blackwell Scientific Publications, Oxford, pp. 399-444.

Stow, D.A.V. and Mayall, M., 2000. Deep-water sedimentary systems; new models for the 21st century. In: Stow, D.A.V. and Mayall, M. (Eds.), *Deep-water sedimentary systems; new models for the 21st century.* Pergamon. Oxford, International. 2000.

Sultan, N., Cochonat, P., Cayocca, F., Bourillet, J.F. and Colliat, J.L., 2004. Analysis of submarine slumping in the Gabon continental slope. *AAPG Bulletin* 88(6), 781-799.

Sun, T. and Parker, G., 2005. Transportational cyclic steps created by flow over an erodible bed. Part 2. Theory and numerical simulation. *Journal of Hydraulic Research* 43(5), 502-514.

Taki, K. and Parker, G., 2005. Transportational cyclic steps created by flow over an erodible bed. Part 1. Experiments. *Journal of Hydraulic Research* 43(5), 488-501.

Torres, J., Droz, L., Savoye, B., Terentieva, E., Cochonat, P., Kenyon, N.H. and Canals, M., 1997. Deep-sea avulsion and morphosedimentary evolution of the Rhone fan valley and neofan during the late Quaternary (north-western Mediterranean Sea). *Sedimentology* 44(3), 457-477.

Underhill, J.R., Sawyer, M.J., Hodgson, P., Shallcross, M.D. and Gawthorpe, R.L., 1997. Implications of fault scarp degradation for Brent Group prospectivity, Ninian Field, northern North Sea. *AAPG Bulletin* 81(6), 999-1022.

Vail, P.R. and Mitchum Jr., R.M., 1977. Seismic stratigraphy and global changes of sea level, part 1: Overview. In: Payton, C.E. (Ed.), *Seismic stratigraphy - applications to hydrocarbon exploration. AAPG Memoir 26.* Tulsa, Ok, pp. 51-62.

Varnes, D.J., 1978. Slope movement types and processes. In: Schuster, R.L. and Krizek, R.J. (Eds.), *Landslides; analysis and control.* Special Report - Transportation Research Board, National Research Council. Transportation Research Board, National Research Council, Washington, DC, United States, pp. 11-33.

Viana, A., Figueiredo, A.G., Faugeres, J.C., Lima, A.F., Gonthier, E., Brehme, I. and Zaragosi, S., 2003. The Sao Tome deep-sea turbidite system (southern Brazil Basin); Cenozoic seismic stratigraphy and sedimentary processes. *AAPG Bulletin* 87(5), 873-894.

von Rad, U. and Tahir, M., 1997. Late Quaternary sedimentation on the outer Indus shelf and slope (Pakistan); evidence from high-resolution seismic data and coring. *Marine Geology* 138(3-4), 193-236.

Whipple, K.X., Parker, G., Paola, C. and Mohrig, D.C., 1998. Channel dynamics, sediment transport and the slope of alluvial fans: experimental study. *Journal of Geology* 106, 677-693.

Winker, C.D. and Booth, J.R., 2000. Sediment Dynamics of the Salt-Dominated Continental Slope, Gulf of Mexico: Integration of Observations from the Seafloor, Near-Surface, and Deep Subsurface. *GCSSEPM Foundation 20th Annual Research Conference Deep-Water Reservoirs of the World, December 3-6, 2000*, 1059-1086.

Wonham, J.P., Jayr, S., Mougamba, R. and Chuilon, P., 2000. 3D sedimentary evolution of a canyon fill (Lower Miocene-age) from the Mandorove Formation, offshore Gabon. *Marine and Petroleum Geology* 17(2), 175-197.

Wynn, R.B., Weaver, P.P.E., Ercilla, G., Stow, D.A.V. and Masson, D.G., 2000a. Sedimentary processes in the Selvage sediment-wave field, NE Atlantic: new insights into the formation of sediment waves by turbidity currents. *Sedimentology* 47(6), 1181-1197.

Wynn, R.B., Masson, D.G., Stow, D.A.V. and Weaver, P.P.E., 2000b. Turbidity current sediment waves on the submarine slopes of the western Canary Islands. *Marine Geology* 163(1-4), 185-198.

Wynn, R.B., Kenyon, N.H., Masson, D.G., Stow, D.A.V. and Weaver, P.P.E., 2002a. Characterization and recognition of deep-water channel-lobe transition zones. *AAPG Bulletin* 86(8), 1441-1462.

Wynn, R.B., Piper, D.J.W. and Gee, M.J.R., 2002b. Generation and migration of coarse-grained sediment waves in turbidity current channels and channel-lobe transition zones. *Marine Geology* 192(1-3), 59-78.

Wynn, R.B. and Stow, D.A.V., 2002. Classification and characterisation of deep-water sediment waves. *Marine Geology* 192(1-3), 7-22.

Yu, B., Cantelli, A., Marr, J., Pirmez, C., O'Byrne, C. and Parker, G., 2006. Experiments on Self-Channelized Subaqueous Fans Emplaced by Turbidity Currents and Dilute Mudflows. *Journal of Sedimentary Research* 76(6), 889-902.

Appendix 1
Glossary

GLOSSARY

H	Height, elevation difference.
2D	Two-dimensional.
3D	Three-dimensional.
Acoustic impedance	Defined by density and seismic velocity ($Z = \rho v$). Changes in acoustic impedance are recorded in seismic data.
Amplitude extraction	Extractions of seismic attribute amplitude from horizons, slices or volumes, which is useful for studying subtle stratigraphic features.
Attribute	A derivate of a seismic measurement, such as time, amplitude, frequency and azimuth.
Avulsion	Lateral shift of the position of a channel by cut-and-fill process.
Azimuth map	Shows the direction in which the horizon is locally dipping.
Backlimb	Shallower limb of a thrust-propagation fold that dips the same direction as the thrust fault.
Bottom current	Currents caused by thermohaline circulation able to erode, transport and deposit sediment on the seafloor.
BSR	Bottom simulating reflection.
Canyon	Deep, often v-shaped valley incised into continental slope, often fed by a river.
Canyon system	A series of stacked canyons that have same source.
Channel	Physical confine of flows, normally with negative topography.
Channel-axis deposit	Deposits on the floor of the channel near its axis.
Channel-belt	The container bordered by basal erosional fairway and outer levees, in which channel-fill deposits and inner levees are deposited.
Channel-fill	Channel-fill elements comprise HARs, passive fill, channel-axis deposits and debris flow and other mass transport deposits that fill channels.
Channel-levee complex	A series of stacked channel-levee systems that are fed by the same canyon.
Channel-levee system	A single channel-belt that is bordered by outer levees.

CLC Channel-levee complex.

CLS Channel-levee system.

Continental margin Area around the continental and oceanic crust boundary including shelf, slope and rise..

Debris flow Viscous sediment-gravity flows that show plastic flow behaviour.

Deepwater water depth of 0.5-1.5 km.

Degradation complex Any type of sediment failure, transport and deposition.

Dipmap, dip magnitude map Shows the local dip of the horizon surface.

Equilibrium profile A profile that sustains little aggradation or degradation along the channel with prevailing sediment discharge.

Erosional fairway Canyon-like incision of a deepwater channel into underlying substrate that can be hundreds of metres deep.

f Frequency.

Forelimb The steep limb of a thrust-propagation fold that is adjacent to the thrust fault.

Frequency Number of peaks passing one point per second.

Frontal fold/thrust The most basinward thrust or fold within a thrust and fold belt.

HAR High-amplitude reflection.

Headwall scarp The scarp that is left in the proximal part of slope failure as sediment is removed.

Hemipelagic sediment Terrigenous sediment transported mainly by wind and surface currents.

Horizon A map produced by interpreting (picking) particular seismic reflection.

Horizontal resolution Defines the area from which a reflection is received called Fresnel zone. Theoretically the Fresnel zone could be reduced to a radius of a quarter of a wavelength.

Hydraulic jump An abrupt transformation from supercritical to subcritical flow condition.

Inner levees Bench-like terraces within the channel-belt with depositional origin.

Isoproportional slicing Technique in which artificial surfaces are created by combining different proportions of two reference horizons.

Knickpoint Steep gradient section between lower gradient sections along a course of a river or channel.

KP Knickpoint.

KPL Knickpoint lip.

L Length, runout distance.

Lee The often shallow or upstream-dipping flank of a sediment wave that faces downcurrent.

Mass transport complex General term that includes slumps, slides and debris flows. Recognised on seismic data by contorted, chaotic low-amplitude reflections.

Migration Channel migration is a gradual shift of the channel by systematic erosion on outer bends and deposition on inner bends.

MTC Mass transport complex.

Outer levees The large, often wedge-shaped in cross section element that border channel-belts and is formed by overbank deposition.

Passive fill Parallel, subhorizontal reflections within channel or channel-belt that show now evidence for channelisation.

Peak Positive amplitude, increase in Z (SEG normal polarity).

Pelagic sediment Sediment composed of planktonic organisms and related organic matter.

Phase/zero phase Describes the motion of periodic waves. Zero phase means that the wavelet is symmetrical, with the central lobe coinciding with the interface.

Pockmark Depressioins formed as a result of catastrophic gas and/or porewater eruption on the seafloor.

Resedimentation All processes driven by gravitational forces that move sediment downslope.

Runout distance The horizontal distance from crest of the scarp to the tip of the deposit. The mobility of submarine landslides is illustrated by the ratio of elevation difference and the runout distance.

Sediment wave	Undulating sedimentary structures found on the seafloor and on levees, characterised by steeper lee flanks and shallower or upstream-dipping stoss flanks.
Sediment-gravity flow	A flow in which the driving force is gravity acting on the sediment particles.
SEG	Society for Exploration Geologists.
SEG normal polarity	Increase in the acoustic impedance downwards is positive amplitude (peak) and decrease negative amplitude (trough).
SEG reverse polarity	Increase in the acoustic impedance downwards is negative amplitude (trough) and decrease positive amplitude (peak).
Seismic amplitude	Amplitude value of a horizon or a volume of seismic data.
Seismic attribute	See 'attribute'.
Seismic velocity	The velocity (v), with which seismic waves travel through rocks.
Seismic wave	Wave of elastic energy that propagate outwards from a seismic source.
Shelf break	The often abrupt change from shallowly-dipping continental shelf to steeper slope environment.
Slice/slicing of data	Seismic data can be sliced along vertical or horizontal lines or along arbitrary traverses and interpreted horizons.
Slide	Shear strain with movement along one or several planar surfaces.
Slope	Continental slope is the steep (commonly 1-10°) slope below shelf break. Slope is also used to describe inclined surfaces.
Slope failure	Any resedimentation process including submarine landslides, slumps, slides, where sediment deposits fail on a slope.
Slump	Rotational, commonly spoon-shaped slide that typically shows extensional faults and scars at the head and compressional structures at the toe area.
Stoss	The often steep flank of a sediment wave that faces upcurrent.
Subcritical flow	Turbidity currents are subcritical, when densimetric Froude number (Fr_d) is less than 1. Subcritical flows are slow and thick.
Supercritical flow	Turbidity currents are supercritical, when densimetric Froude number (Fr_d) is larger than 1. Supercritical flows are swift and thin.

Sweep	Progressive downstream translation of meander bends.
Swing	Increase in amplitude of channel thalweg or a meander bend involving lateral translation.
Terrace	See 'inner levee'. Terraces can also be formed by erosional processes.
Thalweg	Deepest part of the channel.
Traverse	Arbitrary cross-section of seismic data.
Trough	Negative amplitude, decrease in Z (SEG normal polarity).
Tuning	Constructional interference that occurs when layer thickness is one quarter of a wavelength. The amplitude can be boosted as the bed thins.
Turbidity current	Relatively dilute sediment-suspension-driven sediment-gravity flows that occur in subaqueous environment. Commonly used term even when type of flow cannot be determined.
TWT, twtt	Two-way travel time of a seismic wave, measured in s or ms.
Ultra-deepwater	water depth more than 1.5 km.
v	Acoustic/seismic velocity.
Vertical resolution	Defines the potential for the seismic data to distinguish individual layers. Measured in terms of wavelength.
Voxel	The 3D unit of seismic data consisting x, y and z dimensions with individual amplitude values.
Wavelet	Record of changes in acoustic impedances including peaks and troughs that represent increase and decrease in acoustic impedance.
Z	Acoustic impedance.
λ	Wavelength, the distance of two peaks, crest-to-crest distance.
ρ	Density.

ADDITIONAL IMAGES OF THE NIGER DELTA DATASET

The following pages show seismic lines (inlines and crosslines) across the Niger Delta dataset taken in 6.25 km intervals. The inlines (ILN) show how the structural style of the thrusts and folds changes along the thrust and fold belt. The crosslines (CLN) show the seismic character of cross sections of the 3 channel-levee systems (Epe, Ijebu and Iwo CLSs) at different parts of the data. The locations of the lines are shown on the dipmap of the seafloor. The line numbers are indicated at the bottom left corner of each line.

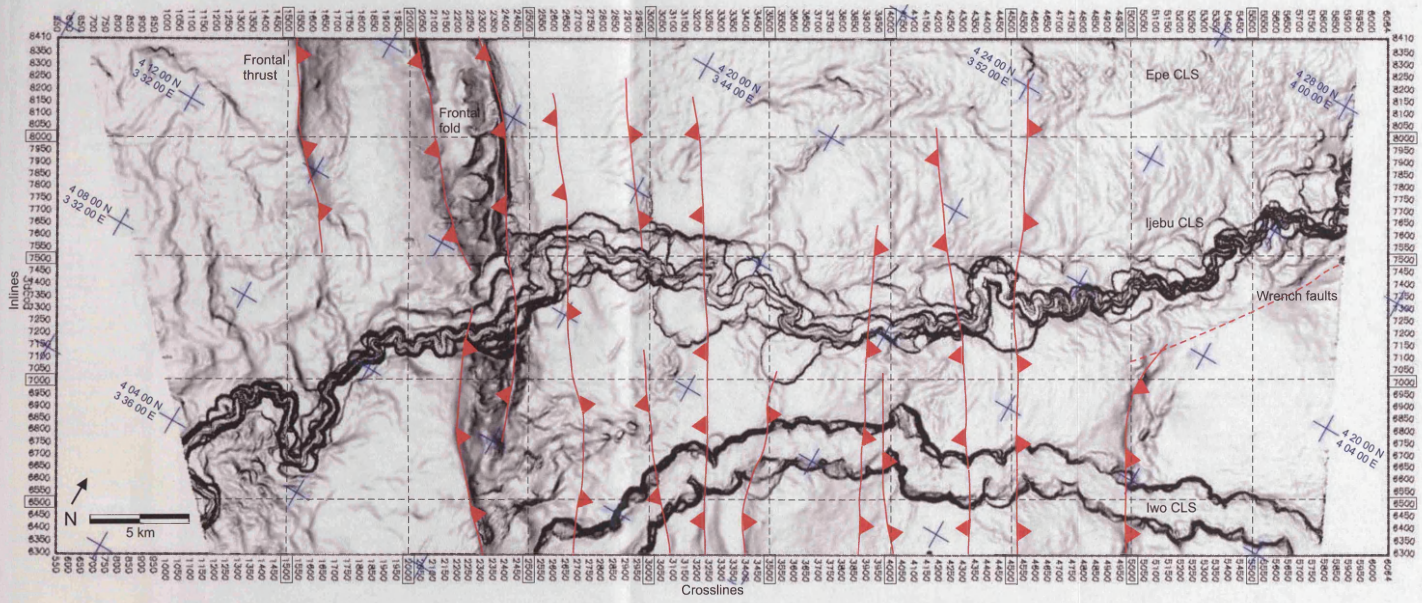

Dipmap of the seafloor of the Niger Delta dataset.

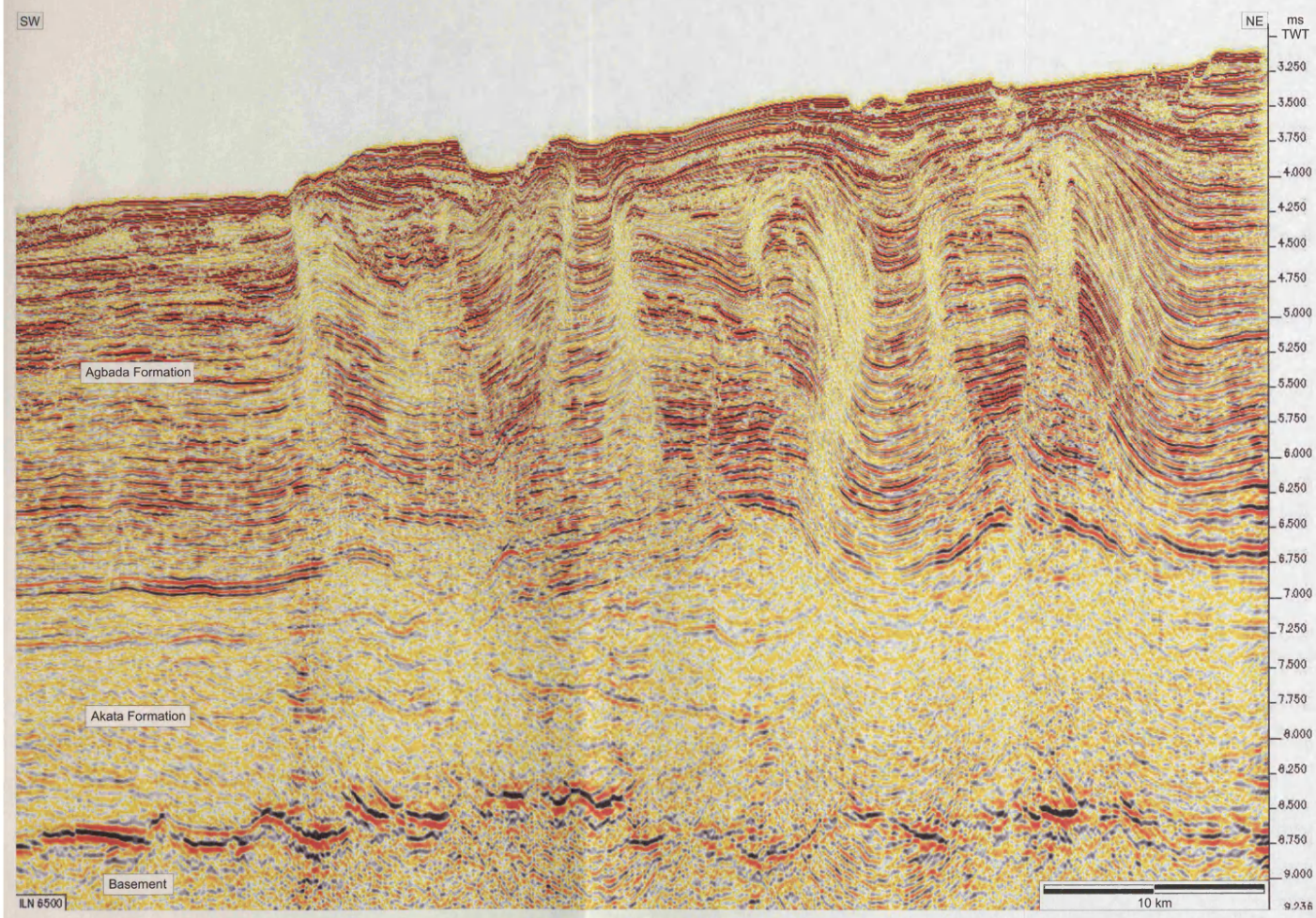
SW
NE
ms
TWT
3.250
3.500
3.750
4.000
4.250
4.500
4.750
5.000
5.250
5.500
5.750
6.000
6.250
6.500
6.750
7.000
7.250
7.500
7.750
8.000
8.250
8.500
8.750
9.000
9.236
Agbada Formation
Akata Formation
Basement
ILN 6500
10 km

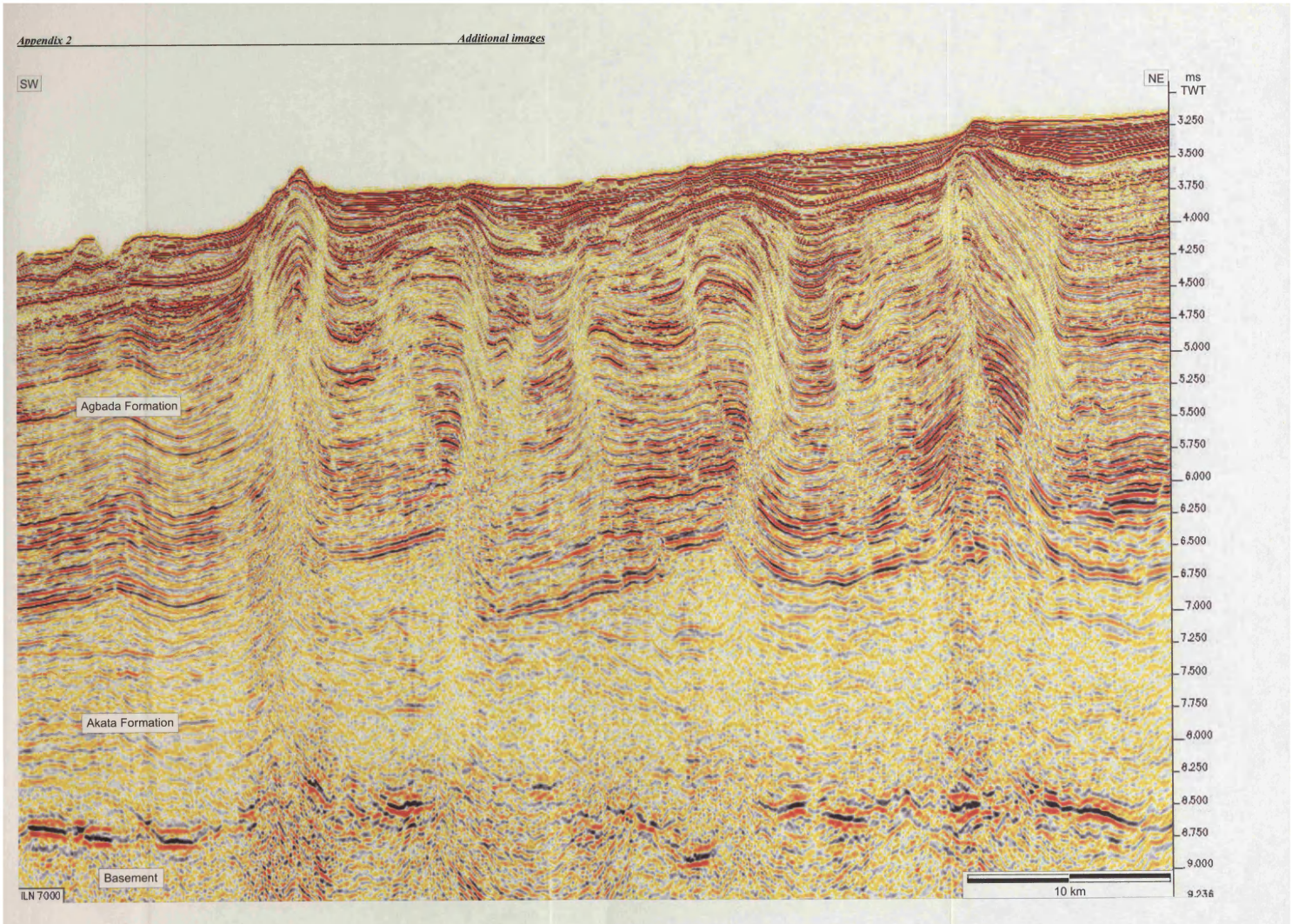
SW
NE
ms
TWT
3.250
3.500
3.750
4.000
4.250
4.500
4.750
5.000
5.250
5.500
5.750
6.000
6.250
6.500
6.750
7.000
7.250
7.500
7.750
8.000
8.250
8.500
8.750
9.000
Agbada Formation
Akata Formation
Basement
ILN 7000
10 km

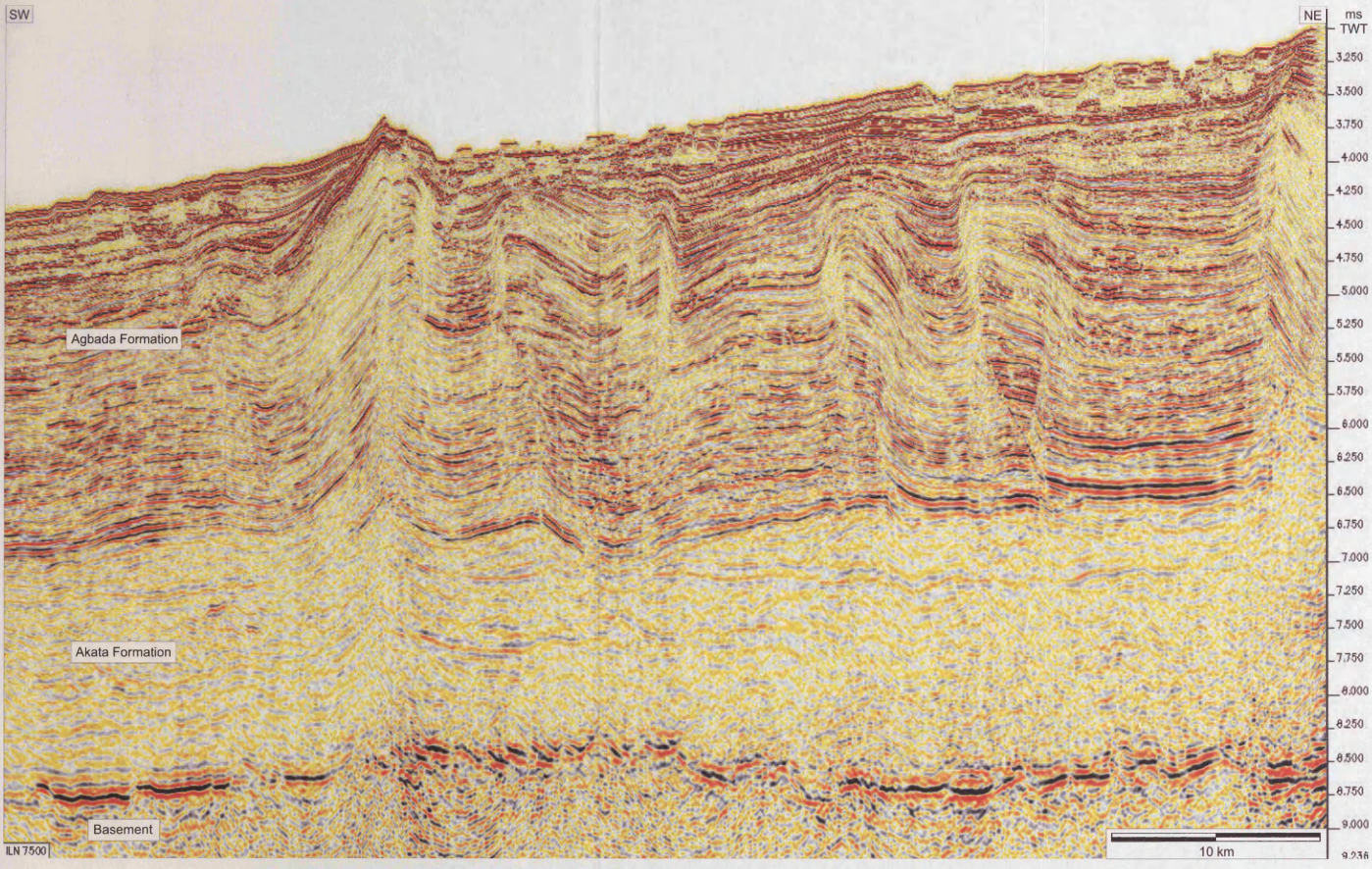
SW
NE
ms
TWT
3.250
3.500
3.750
4.000
4.250
4.500
4.750
5.000
5.250
5.500
5.750
6.000
6.250
6.500
6.750
7.000
7.250
7.500
7.750
8.000
8.250
8.500
8.750
9.000
9.236
Agbada Formation
Akata Formation
Basement
ILN 7500
10 km

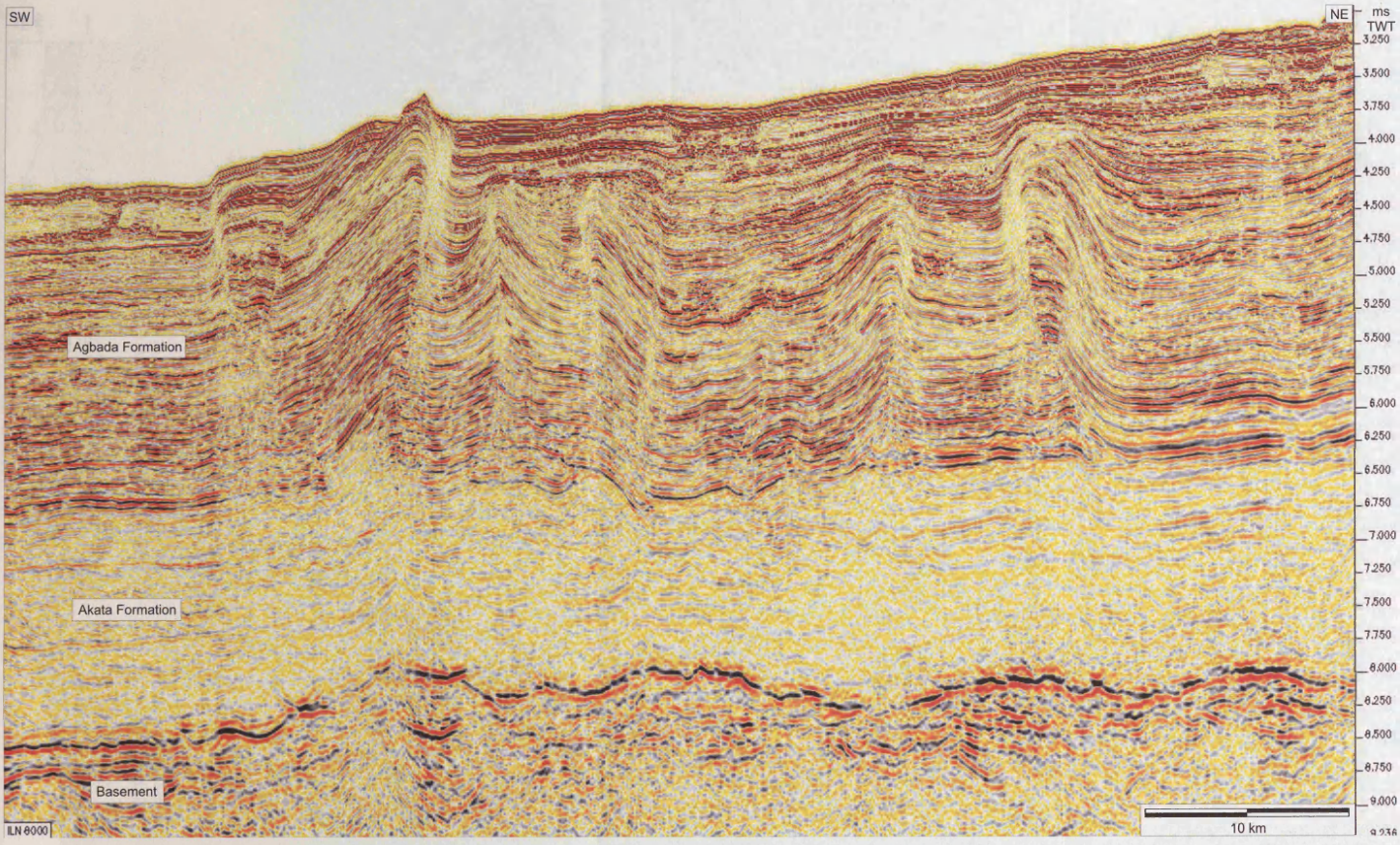
SW
NE
ms
TWT
3.250
3.500
3.750
4.000
4.250
4.500
4.750
5.000
5.250
5.500
5.750
6.000
6.250
6.500
6.750
7.000
7.250
7.500
7.750
8.000
8.250
8.500
8.750
9.000
Agbada Formation
Akata Formation
Basement
ILN 8000
10 km

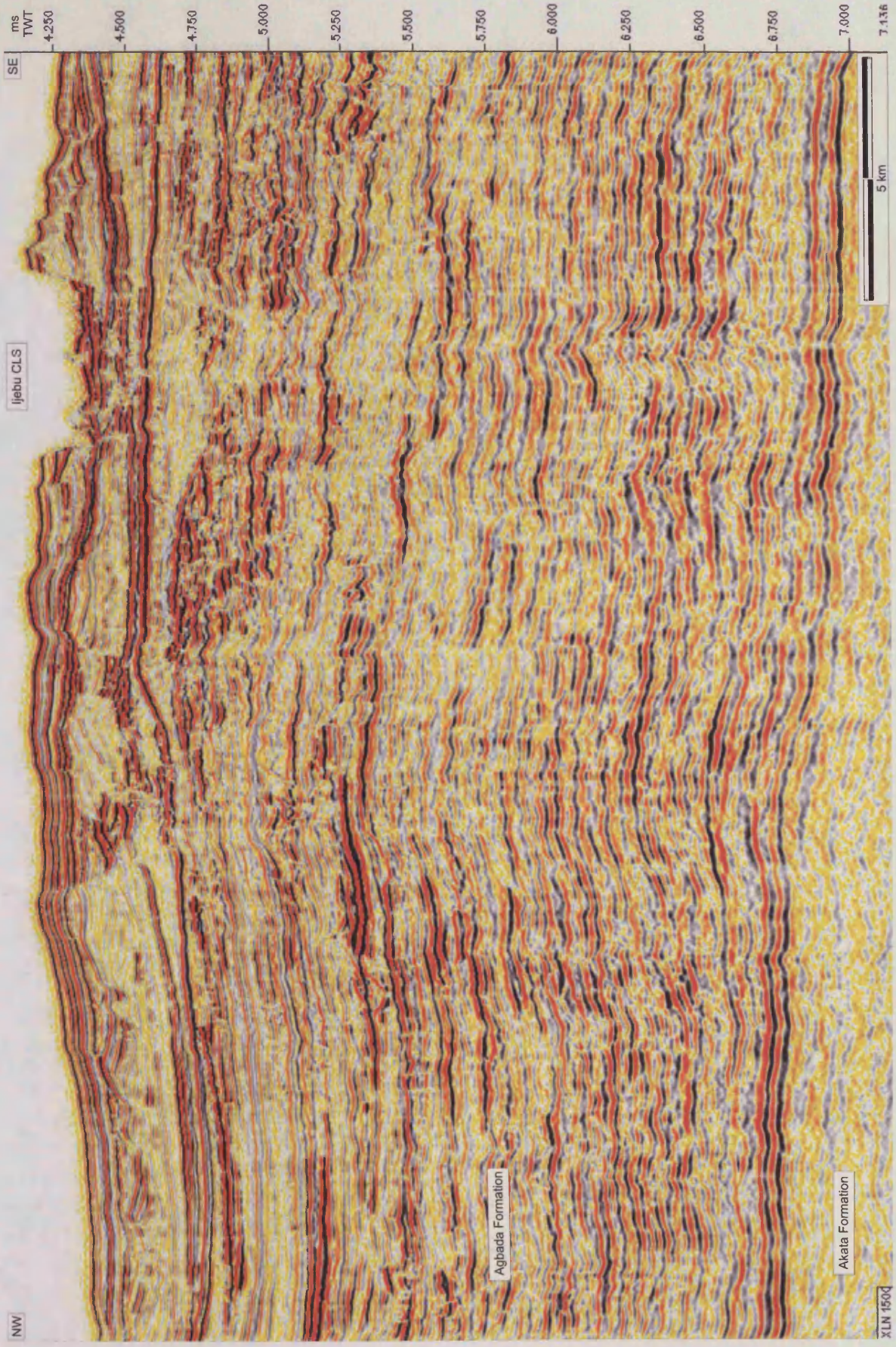
ms
TWT
4.250
4.500
4.750
5.000
5.250
5.500
5.750
6.000
6.250
6.500
6.750
7.000
7.136
SE
Ijebu CLS
NW
5 km
Agbada Formation
Akata Formation
XLN 1500

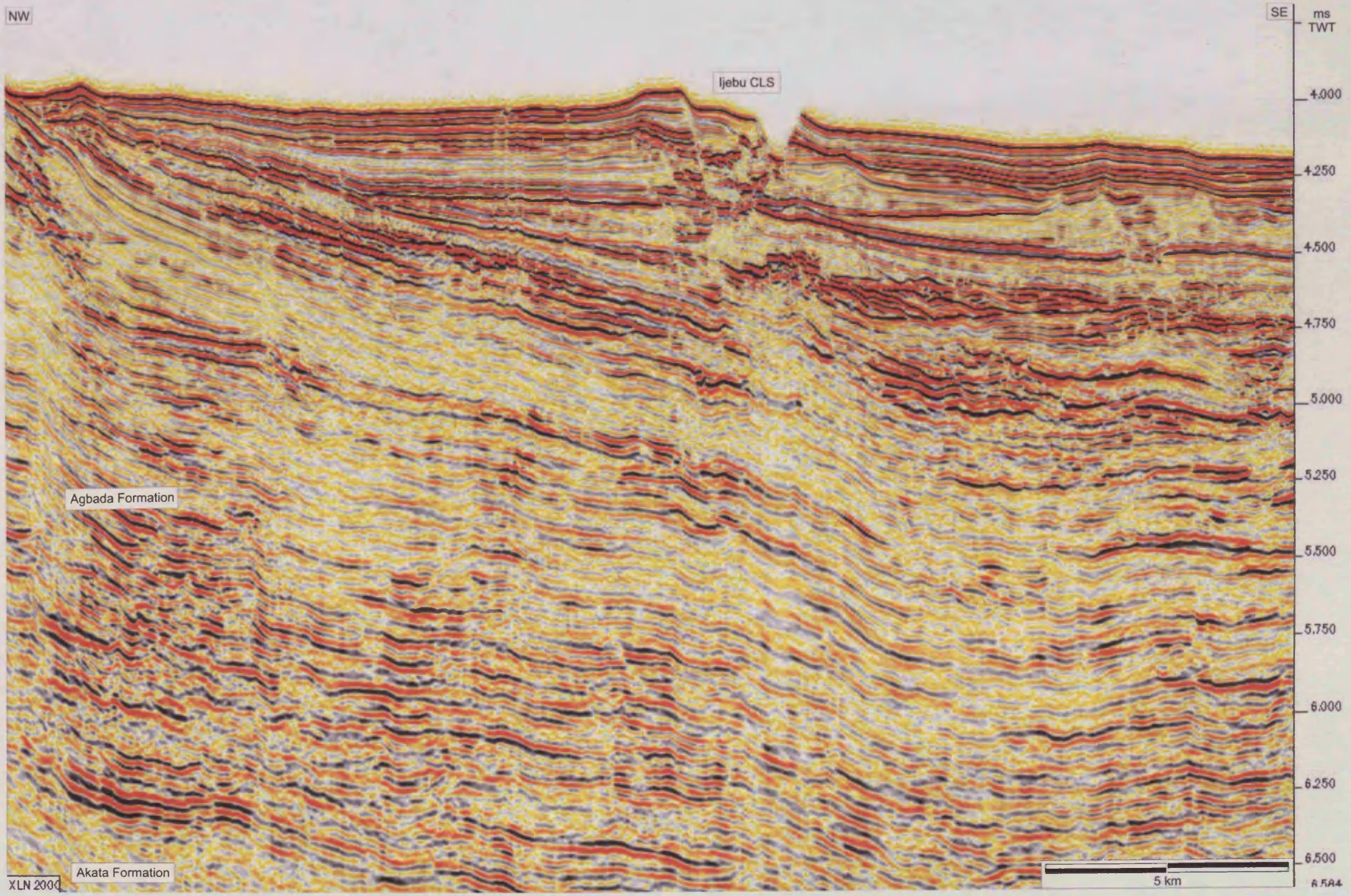
NW
SE
ms
TWT
Ijebu CLS
4.000
4.250
4.500
4.750
5.000
5.250
5.500
5.750
6.000
6.250
6.500
6.584
Agbada Formation
Akata Formation
XLN 2000
5 km

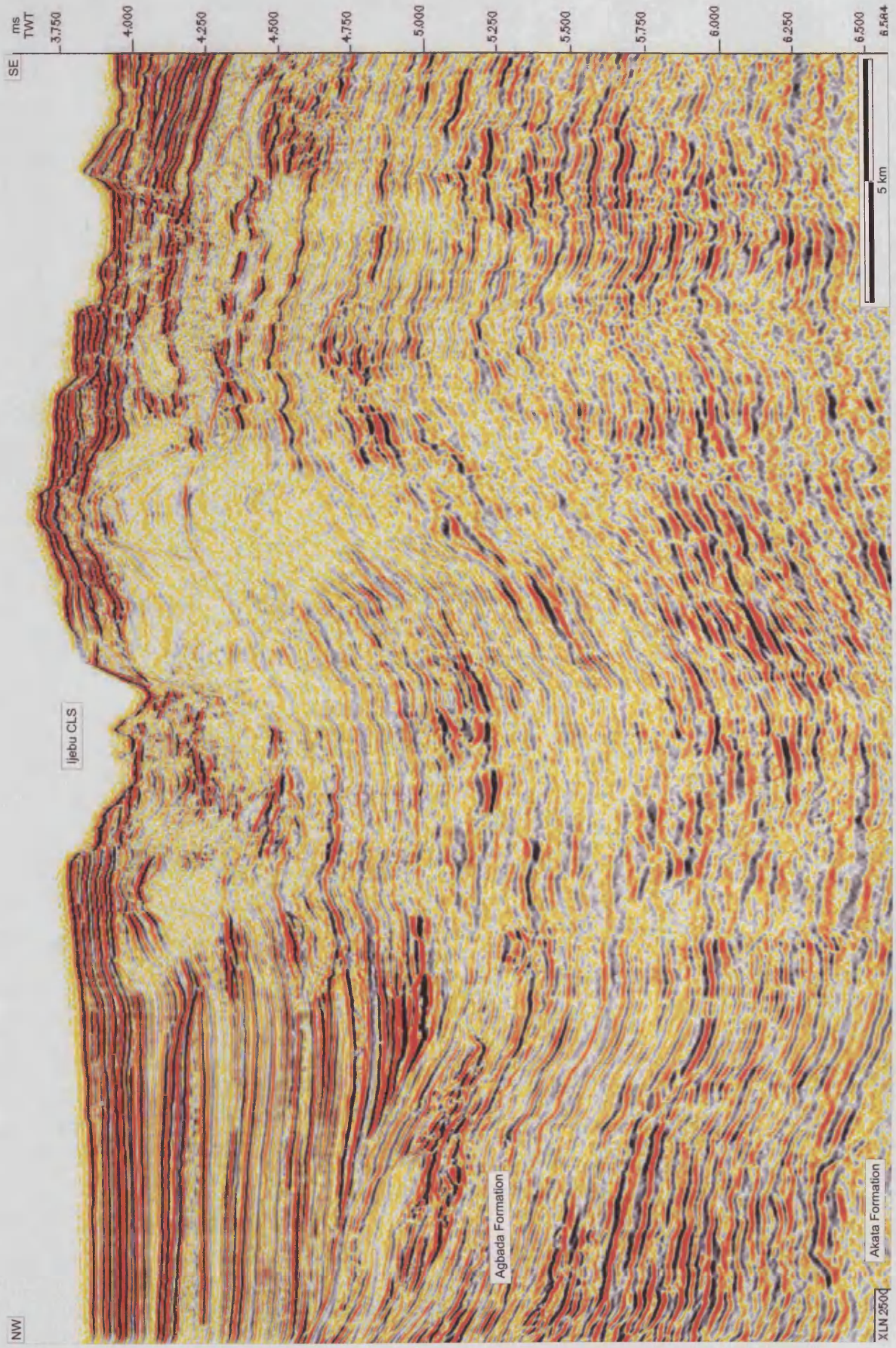
ms
TWT
3.750
4.000
4.250
4.500
4.750
5.000
5.250
5.500
5.750
6.000
6.250
6.500
8.564
SE
NW
Ijebu CLS
Agbada Formation
Akata Formation
XLN 2500
5 km

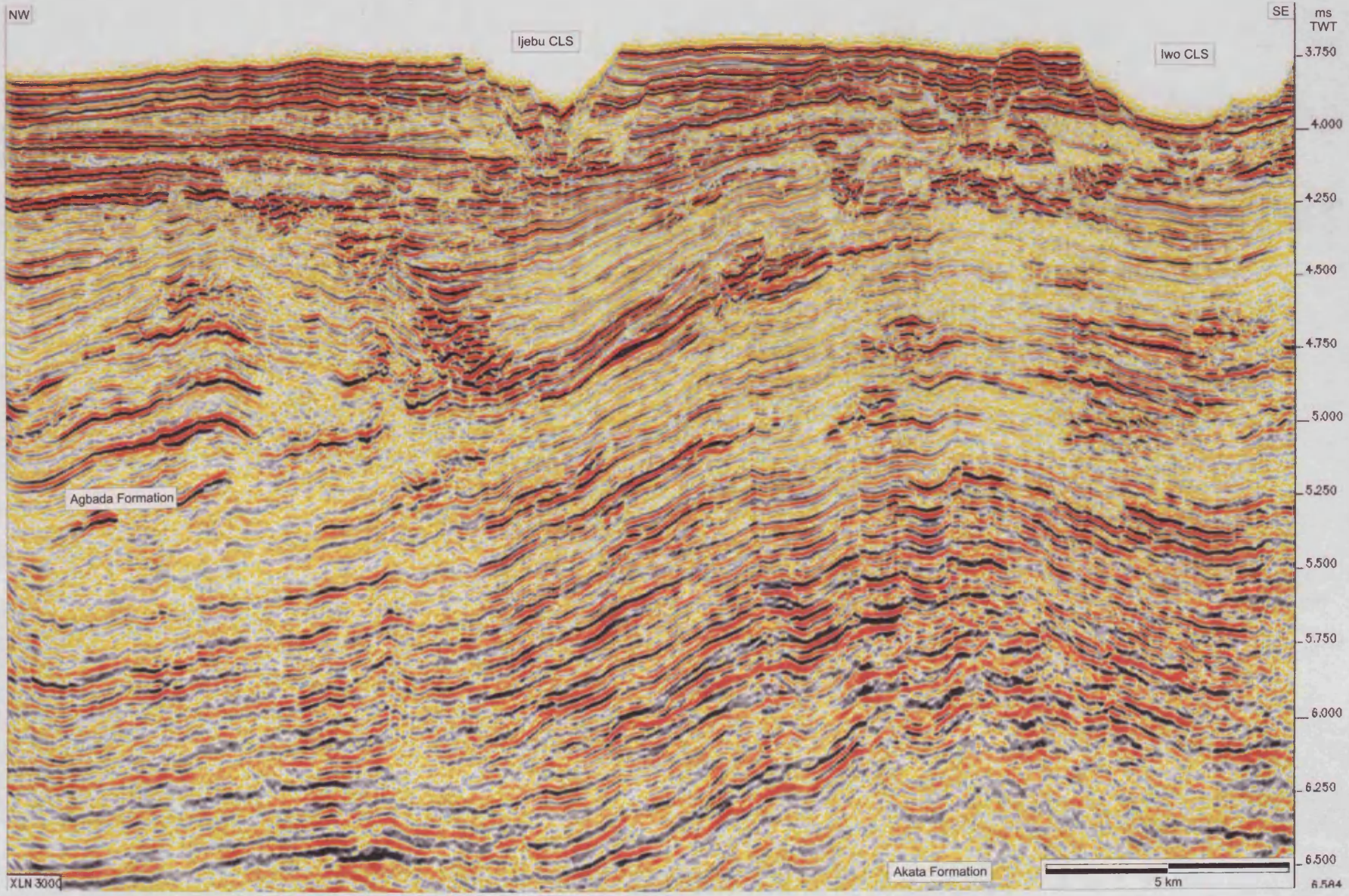
NW
SE
Ijebu CLS
Iwo CLS
ms
TWT
3.750
4.000
4.250
4.500
4.750
5.000
5.250
5.500
5.750
6.000
6.250
6.500
6.584
Agbada Formation
Akata Formation
XLN 3000
5 km

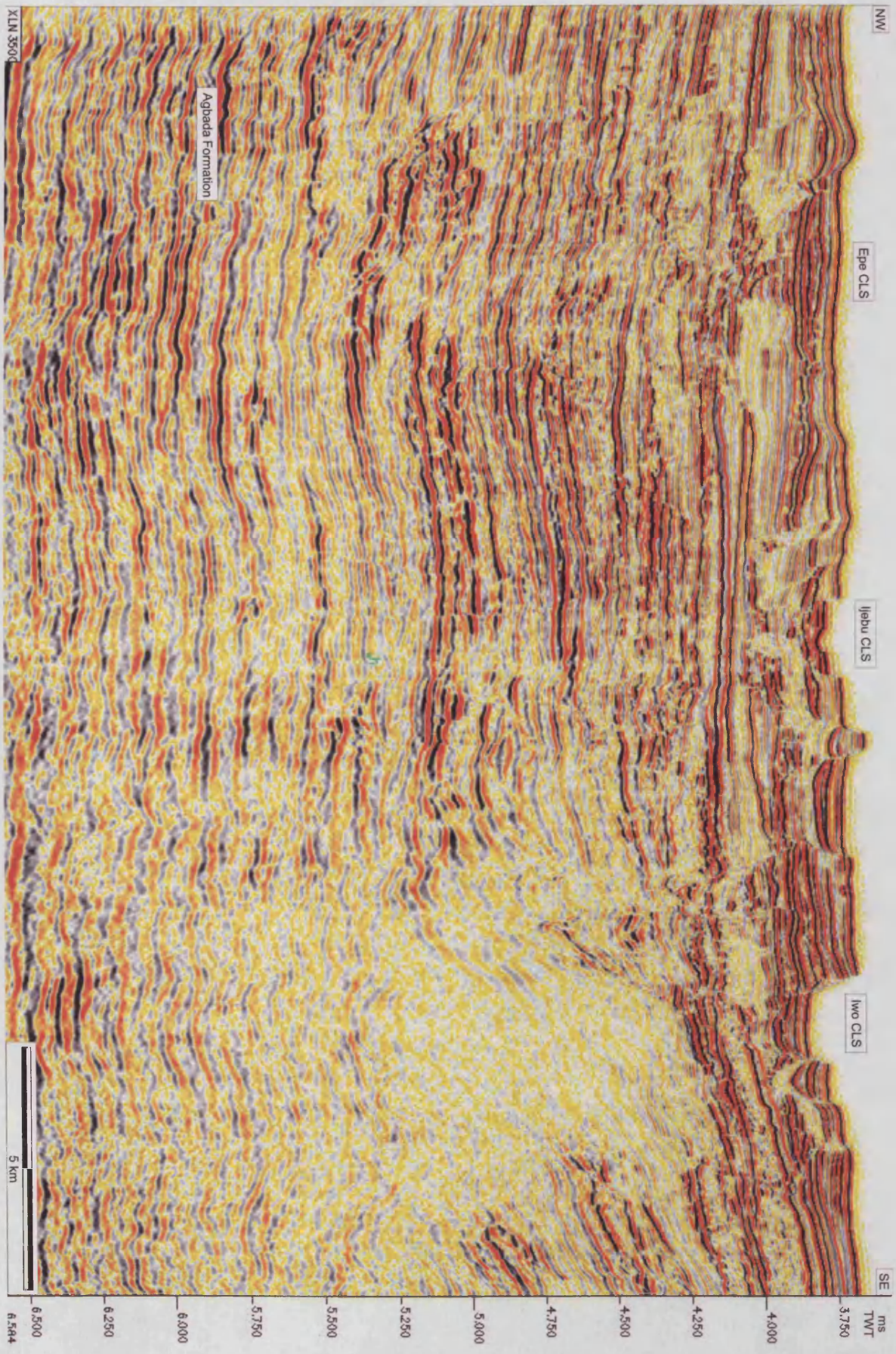

Appendix 2 *Additional images*


ms
TWT
3.750
4.000
4.250
4.500
4.750
5.000
5.250
5.500
5.750
6.000
6.250
6.500
6.544
SE
Iwo CLS
Ijebu CLS
Epe CLS
NW
Agbada Formation
5 km
XLN 4000

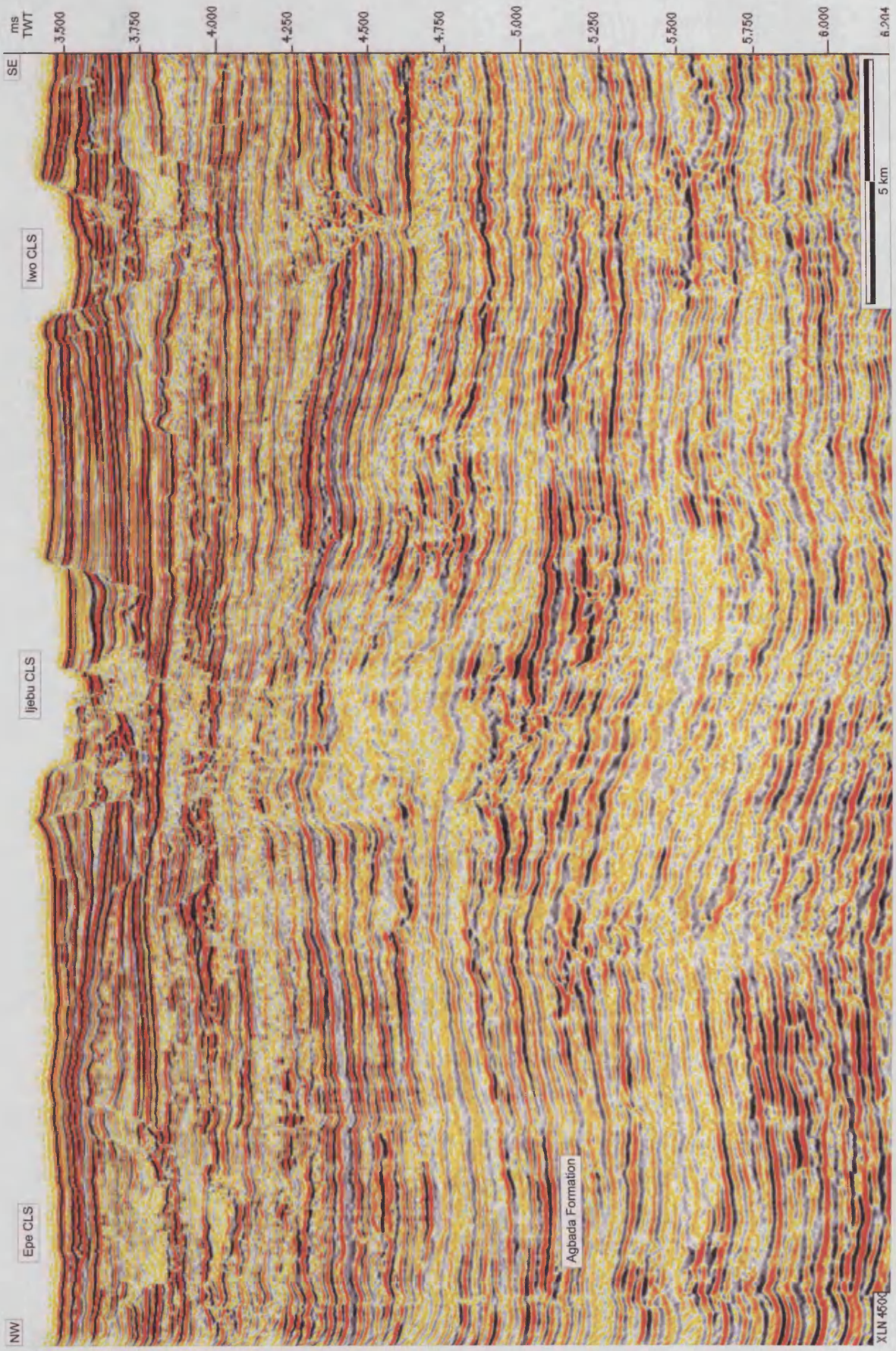
ms
TWT
3,500
3,750
4,000
4,250
4,500
4,750
5,000
5,250
5,500
5,750
6,000
6,204
SE
NW
Iwo CLS
Ijebu CLS
Epe CLS
Agbada Formation
5 km
XLN 4500

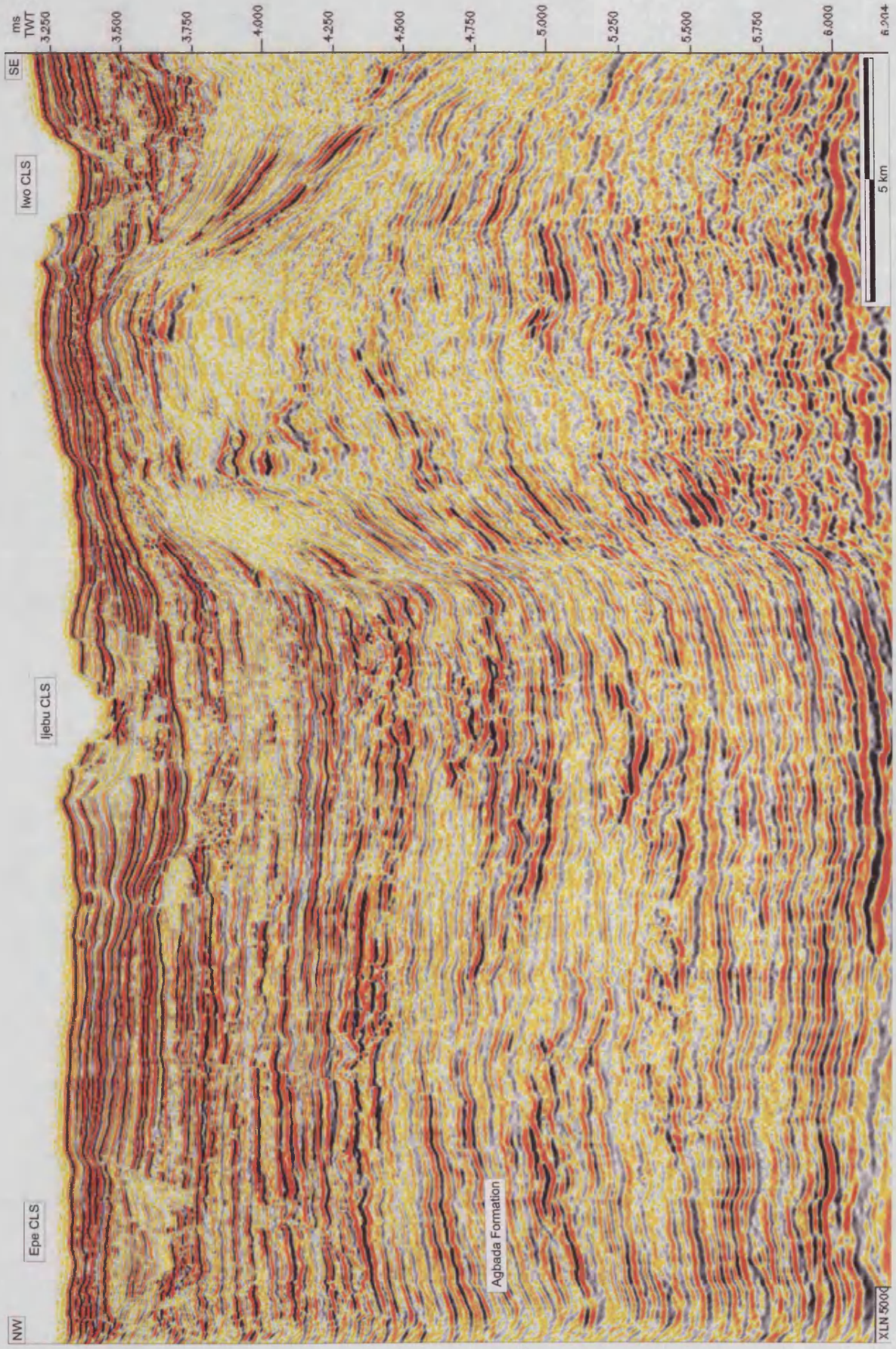
ms
TWT
3,250
3,500
3,750
4,000
4,250
4,500
4,750
5,000
5,250
5,500
5,750
6,000
SE
Iwo CLS
Ijebu CLS
Epe CLS
NW
Agbada Formation
5 km
XLN 5000

CARDIFF UNIVERSITY
PRIFYSGOL CAERDYDD

BINDING SERVICES
Tel +44 (0)29 2087 4949
Fax.+44 (0)29 2037 1921
E-Mail Bindery@Cardiff.ac.uk

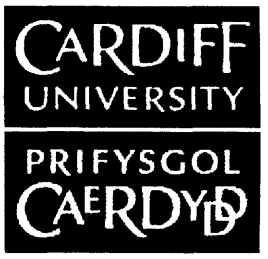

3D SEISMIC ANALYSIS OF SEDIMENTARY PROCESSES ON DEEPWATER CONTINENTAL MARGINS

PÄIVI TUULI HEINIÖ

Cardiff University

July 2007

DECLARATION

This work has not previously been accepted in substance for any degree and is not concurrently submitted in candidature for any degree.

Signed ..Päivi Heinö..... (candidate)
Date ...31/07/07.....

STATEMENT 1

This thesis is being submitted in partial fulfilment of the requirements for the degree of PhD.

Signed ..Päivi Heinö..... (candidate)
Date ...31/07/07.....

STATEMENT 2

This thesis is the result of my own independent work/investigation, except where otherwise stated. Other sources are acknowledged by explicit references.

Signed ..Päivi Heinö..... (candidate)
Date ...31/07/07.....

STATEMENT 3

I hereby give consent for my thesis, if accepted, to be available for photocopying and for inter-library loan, and for the title and summary to be made available to outside organisations.

Signed ..Päivi Heinö..... (candidate)
Date ...31/07/07.....

STATEMENT 4

I hereby give consent for my thesis, if accepted, to be available for photocopying and for inter-library loans after expiry of a bar on access approved by the Graduate Development Committee.

Signed ..Päivi Heinö..... (candidate)
Date ...31/07/07.....

SUMMARY

Two 3D seismic reflection datasets from the West African and Brazilian continental margins were analysed to determine their architectural elements and to further the understanding of the sedimentary processes that control their morphology. The results suggest a strong influence of local slope variations on the sedimentary processes and depositional and erosional products within these complex deepwater settings.

The Niger Delta dataset is characterised by large channel-levee systems and thrust-related folds. The folds degrade by channel erosion and slope failure, which creates laterally discontinuous erosional surfaces on the crests and flanks of the anticlines and chaotic deposits at their bases. The type of slope failure depends on the length and morphology of the local slope, sediment properties and the presence of anisotropies, such as faults.

The location and morphology of the channel-levee systems on the Niger Delta are affected by topographical effects associated with thrust-related folding. Fold-induced local changes in gradient cause turbidity currents to deposit sediment upstream of the folds and erode the seafloor downstream of them. This results in the formation of knickpoints along the present-day thalweg of a channel-levee system. A model for the formation and evolution of the knickpoints predicts that they migrate upstream and leave internal erosion surfaces and terraces with coarse sediments in the sedimentary record. They may be an important process by which channels cut through uplifting fold belts.

The Espirito Santo Basin dataset is characterised by salt diapirs, slope failures, channels and canyons. Interaction of turbidity currents with variations in topography has led to the formation of large depressions, which occur above abrupt breaks in slope and in trails that follow underlying erosional channels. They are inferred to form by Froude-supercritical currents that become unstable as they encounter topographical irregularities, such as scarps and knickpoints. This leads to the formation of erosional scours and deposits similar to sediment waves, which, when confined within channels, appear as roughly circular depressions.

AUTHOR'S NOTE

Chapters 3, 4 and 5 of the thesis have been published or submitted for publication in different international scientific journals. The status of these publications at the time of the submission of the thesis is as follows:

- Chapter 3 has been published as:

Heiniö, P. and Davies, R.J. 2006. Degradation of compressional fold belts: Deep-water Niger Delta. *AAPG Bulletin* 90(5), 753-770. Doi: 10.1306/11210505090

- Chapter 4 has been published as:

Heiniö, P. and Davies, R.J. 2007. Knickpoint migration in submarine channels in response to fold growth, western Niger Delta. *Marine and Petroleum Geology.* Doi: 10.1016/j.marpetgeo.2006.09.002

- Chapter 5 has been accepted for publication as:

Heiniö, P. and Davies, R.J. Current-generated giant depressions along submarine channels on the continental margin of the Espirito Santo Basin, Brazil. *GSA Bulletin.*

ACKNOWLEDGEMENTS

A much greater number of people than can be mentioned here deserve my thanks for making this PhD project possible, better and more enjoyable. Firstly, I'd like to thank my supervisor Richard Davies for giving me the opportunity to undertake this research. His enthusiasm and constant encouragement helped me in so many aspects of the project. I am grateful for CGGVeritas and Richard Morgan for providing data and Cardiff University, The Finnish Cultural Foundation and Helsingin Sanomat Centennial Foundation for funding. Steve Corfield and Martin Gee are thanked for recommending me for this PhD.

I'd like to thank the reviewers of my papers: Art Saller, Bill Brumbaugh, Jeff Peakall, Mark Deptuck and Russell Wynn and also Neil Mitchell, Dorthe Hansen, Joe Cartwright, and Simon Higgins for improving the quality of the papers. I am grateful for all the feedback and discussions I had with numerous people in Cardiff and at conferences, including Joe, Dorthe, Mads Huuse and David James. I thank David Mohrig and Kyle Straub for introducing turbidity currents and flume tank experiments to me. Gwen Pettigrew, Andrew Wiltshire, Derek John and Neil Ferguson are thanked for sorting out so many computer-related issues. Thanks are also due to Jeff Peakall and Paul Wright who examined this thesis.

Many people have made my life in Cardiff fun and enjoyable and are kindly thanked for this. Catherine Baudon and Simon Higgins deserve special thanks for being such tolerant and lovely officemates and making the office a nice place with good music, inspirational discussions and lots of coffee. I've been really lucky to have such fantastic bunch of people to share my life with in Cardiff. The numerous pints of beer and glasses of wine consumed at pubs, parks and house parties, and the trips to the beach, countryside and Africa in such good company kept me more or less sane during my time here and gave me fond memories. So thank you Cat, Bryan, Wendy, Lizzie, Sarah, Julia, Dave, Alan, Ruth, Mostyn, Cathal, Dan, Anna, Helena, Christian, Rich, Simon, Jess, Rob, Suzy, Marcus, Martin, Katrien, Shanshan, Cat, Mairi, Chloe, Simon S., Aggie and everybody else. I also want to thank friends outside Cardiff for keeping in touch and helping me remember another kind of life out there.

Finally I'd like to thank all my family, especially my parents Ulla and Ari, sisters Laura and Jonna, brother-in-law Paavo, little nephews Okko and Aki and my grandparents, who all have been a great source of motivation, inspiration and support.

TABLE OF CONTENTS

LIST OF FIGURES

Chapter 1. Introduction

Chapter 2. Geological setting and architectural elements of the study areas

Chapter 3. Degradation of compressional fold belts: deepwater Niger Delta

Chapter 4. Knickpoint migration in submarine channels in response to fold growth, western Niger Delta

Chapter 5. Current-generated giant depressions along submarine channels on the continental margin of the Espirito Santo Basin, Brazil

Chapter 6. Discussion

LIST OF TABLES

Chapter 3. Degradation of compressional fold belts: deepwater Niger Delta

Chapter 4. Knickpoint migration in submarine channels in response to fold growth, western Niger Delta

Chapter 5. Current-generated giant depressions along submarine channels on the continental margin of the Espirito Santo Basin, Brazil

Chapter 1

1 INTRODUCTION

This chapter provides the background and the rationale for this thesis. The aims, objectives and scope of this project are given and the thesis layout is explained. This chapter also introduces the 3D seismic method and sedimentary processes in the deepwater setting.

1.1 AIMS AND RATIONALE

This PhD project seeks to understand a range of deepwater sedimentary processes and their products in a novel way through the use of 3D seismic data from the African and Brazilian continental margins. The aim is to improve the understanding of the fundamental processes that control the morphology and the architecture of depositional and erosional features in deepwater settings.

Deepwater and ultra-deepwater (>1.5 km) areas of continental margins are of major scientific interest, because they are one of the least understood sedimentary environments. The analysis of the common architectural elements, and the understanding of the processes controlling these environments, are less advanced compared to subaerial and shallow marine systems, due to previous lack of data coverage and the difficulty of obtaining direct observations. Research of continental margins has also wider implications, because their overall architecture, morphology and the spatial and temporal distribution of sediment deposits provide a record of past changes in relative sea level, climatic and oceanic conditions and tectonic events.

The study of deep-sea sediments started in the early 20th century (see Stow, 1986), and the first channels formed by turbidity currents were discovered in the late 1940s and early 1950s on the continental margins of North America (Menard, 1955). The interest in the deep marine environment has been increasing since. Between the 1960's and 1980's, deepwater depositional systems were studied using outcrops, bathymetric swath and side-scan sonar data and 2D seismic lines (Posamentier and Kolla, 2003). Recently, the interpretation of submarine systems from 3D seismic data has become more common, because these datasets have been made available by the hydrocarbon industry, which is interested in these settings (e.g. Mayall and Stewart, 2000; Abreu et al., 2003; Fonnesu, 2003; Morgan, 2003; Mayall et al., 2006). 3D seismic surveys have proven deepwater fans to have much more complex architecture and internal structures than what was interpreted from 2D surveys (Eschard, 2001). They have

enabled the establishment of the true 3D morphology of depositional elements (Mayall and Stewart, 2000; Abreu et al., 2003; Deptuck et al., 2003; Fonnesu, 2003; Posamentier, 2003; Posamentier and Kolla, 2003; Mayall et al., 2006) and excellent imaging of hydrocarbon reservoir architecture (Mayall and Stewart, 2000; Fonnesu, 2003; Samuel et al., 2003; Mayall et al., 2006). The study of deepwater sedimentary systems and especially turbidite channels has indeed been driven by hydrocarbon industry, and the quantity and quality of 3D seismic datasets have increased while the cost has decreased (Posamentier and Kolla, 2003; Mayall et al., 2006). Despite this increase in data and methods, the deep marine realm is still one of the least well understood depositional environments (Wonham et al., 2000; Eschard, 2001).

This PhD project aims to further the understanding of deepwater sedimentary processes and products from 3D seismic reflection data. The analysis of deposits and erosional features and the inference of what processes led to their development and control their distribution have wider significance for sedimentary basin analysis, including basin modelling, hydrocarbon exploration, fluid dynamics and turbidity current studies.

1.2 OBJECTIVES

This thesis will:

- Depict the architectural elements of confined deepwater channel-levee systems and debris flows on the western Niger Delta.
- Develop a better understanding of some of the processes involved in the formation of sinuous channels and associated features, such as levees.
- Analyse the distribution of depositional and erosional elements relative to structures that create seafloor topography.
- Analyse evidence for sediment remobilisation and recycling in the deepwater setting, especially the degradation of submarine folds.
- Develop a better understanding of the erosional and depositional patterns and processes along continental margins and establish models for their formation.
- Demonstrate how 3D seismic data can be used to understand a range of deepwater sedimentary processes.

1.3 METHODS – 3D SEISMIC INTERPRETATION

The interpretation of the 3D seismic reflection data was done by Unix-run Sun workstations using Schlumberger's Geoframe IESX and GeoViz software. This section gives a brief introduction to 3D seismic data, interpretation and visualisation, and the nature of seismic reflections.

1.3.1 Introduction to 3D seismic method

The 3D seismic method was initiated in the 1960s, but it was not until the 1990s for it to be commonly used by industry and academia (Hart, 1999). 3D seismic data have also increased the understanding of subsurface geology and the controls of local processes and proved many interpretations based on 2D seismic to be wrong (Hart, 1999). Although 2D seismic data commonly have higher resolution than 3D data, 3D seismic data are better for determining the 3D geometry of many features, such as sediment deposits, because of denser seismic grid and 3D, rather than 2D migration process (Hart, 1999; Stewart, 1999; Bacon et al., 2003). The method has significantly enhanced drilling success and thus has been of enormous importance to the petroleum industry.

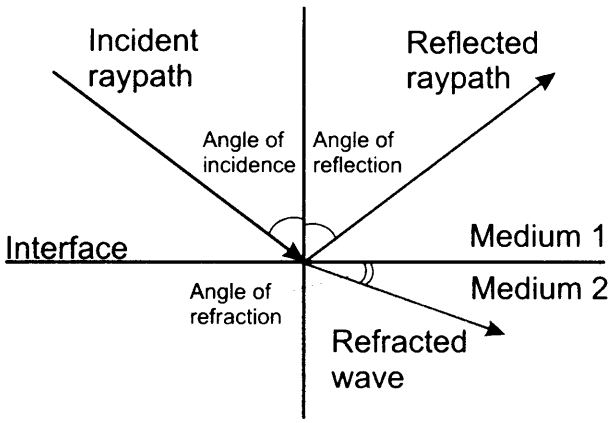

Figure 1.1. The behaviour of a wavefront as it meets an interface of two media with contrasting acoustic impedances. The angle of the incident wave is the same to the reflected wave in an isotropic media. The angle of refraction depends on the seismic velocity of the medium. Modified from Kearey and Brooks (1991).

Marine 3D seismic data are acquired by generating an acoustic pulse near the sea surface, normally by airgun arrays (Hart, 1999; Bacon et al., 2003). Some of the energy is reflected from subsurface interfaces, where there are changes in acoustic velocity and density (Fig. 1.1). This reflected energy is detected by hydrophones. The time a seismic wave takes to travel from the source to the receiver is measured in seconds or milliseconds two-way time (TWT), also sometimes referred to as two-way travel time or twtt. The data have to be

processed and migrated to place all the reflection points in the right location, get rid of unwanted features and increase the quality of the data. A fuller account of seismic acquisition and processing is given in Sheriff and Geldart (1995).

1.3.2 Nature and nomenclature of seismic waves and reflections

Seismic waves are waves of elastic energy that propagate outwards from a seismic source (Kearey and Brooks, 1991). Marine seismic data acquisition is mainly concerned with the detection of compressional P-waves (Kearey and Brooks, 1991; Hart, 1999). The most important parameters of seismic waves are their velocity and frequency. The velocity (v) with which seismic waves travel through rocks vary depending on composition, texture, porosity, fluid content, elastic modulus and the density of the rocks (Kearey and Brooks, 1991). Seismic velocity increases with depth as rocks become more compacted (Brown, 1999). Frequency (f) is defined by the number of peaks passing one point per second (Brown, 1999). It decreases with depth because higher frequencies are attenuated as the waves propagate through rock.

Seismic reflections record changes in the acoustic impedance of the subsurface. Acoustic Impedance (Z) is defined by density (ρ) and seismic velocity (v) of the rocks ($Z=\rho v$) (Kearey and Brooks, 1991; Brown, 1999). As a seismic wave meets an interface of two layers with contrasting acoustic impedance, some of the energy is reflected upwards and some is refracted downwards (Fig. 1.1) (Kearey and Brooks, 1991; Brown, 1999). The changes in acoustic impedance across the interface are recorded as wavelets (Fig. 1.2). The size of a wavelet measured normal to the propagation direction of the wave is given as amplitude. The distance between two peaks is wavelength (λ) (Fig. 1.2), and is proportional to velocity and frequency of the wave ($\lambda=v/f$) (Brown, 1999). The greater the difference between acoustic impedances of two layers, the greater proportion of energy is transmitted through the interface (Kearey and Brooks, 1991). Furthermore, if a geologically significant interface does not have a difference in acoustic impedance, it will not be visible on seismic data (Bacon et al., 2003).

An increase in the acoustic impedance downwards is referred to as a positive amplitude or 'peak' and a decrease is referred to as a negative amplitude or a 'trough'. This is called the 'SEG (Society of Exploration Geologists) normal polarity' (Sheriff and Geldart, 1995). Some

data are displayed as 'SEG reverse polarity', which shows negative values for increases in acoustic impedance. Peaks and troughs are normally displayed in different colours (Fig. 1.2).

The motion of periodic waves is described by phase. Seismic surveys can be of maximum, minimum or zero phase. Most surveys are zero phase, which means that the wavelet is symmetrical, with the majority of the energy being concentrated in the central lobe which also coincides with the interface (Brown, 1999) (Fig. 1.2).

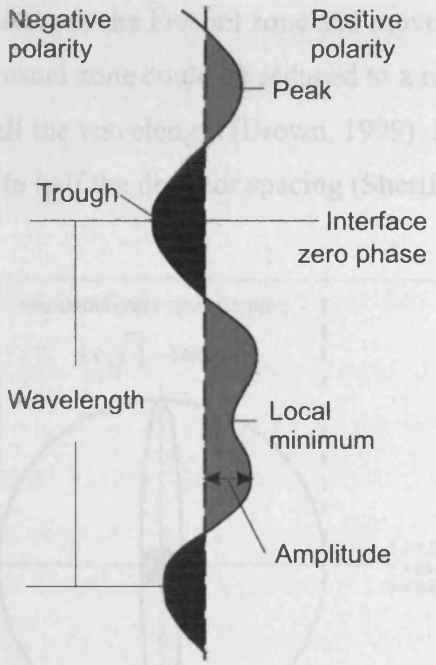

Figure 1.2. Nomenclature of a seismic wavelet of SEG normal polarity zero phase data, in which positive amplitudes (peaks) are displayed in red and negative amplitudes (troughs) in black. Amplitude is the size of the wavelet, and wavelength measures the distance from crest to crest.

1.3.3 Resolution

Vertical resolution defines the potential for the seismic data to distinguish individual layers. It is measured in terms of wavelength. As frequency decreases with depth, vertical resolution deteriorates. A typical wavelength in the shallow part of the seismic data (top 1-2 seconds TWT below seafloor) is approximately 40 m (for a velocity of 2000 ms^{-1} and frequency of 50 Hz) and approximately 250 m in deep section (velocity of 5000 ms^{-1} and frequency of 20 Hz) (Brown, 1999). Maximum resolution of a wavelet in terms of a quarter of a wavelength would thus be approximately 10 m and 63 m respectively. When layer thickness is one quarter of the wavelength, constructive interference called tuning occurs (Sheriff and Geldart, 1995; Brown, 1999). This means that amplitude can be boosted as the bed thins. As beds become thinner,

they get attenuated until invisible. However, even beds with a thickness of $\lambda/30$ can be detected, but their thicknesses cannot be determined (Sheriff and Geldart, 1995).

Horizontal resolution is more complex to quantify. Seismic waves travel in three dimensions from their source and thus the seismic reflection comes from an area rather than a point. This area defining the horizontal resolution is called the Fresnel zone and it is a function of velocity and frequency of the wave and the TWT to the reflector (Fig. 1.3) (Sheriff and Geldart, 1995; Brown, 1999). The migration process improves horizontal resolution by concentrating the energy spread over the Fresnel zone and moves reflections to their right position. Theoretically, the Fresnel zone could be reduced to a radius of quarter wavelength, but in reality this is only to half the wavelength (Brown, 1999). For a flat-lying reflector the horizontal resolution is equal to half the detector spacing (Sheriff and Geldart, 1995).

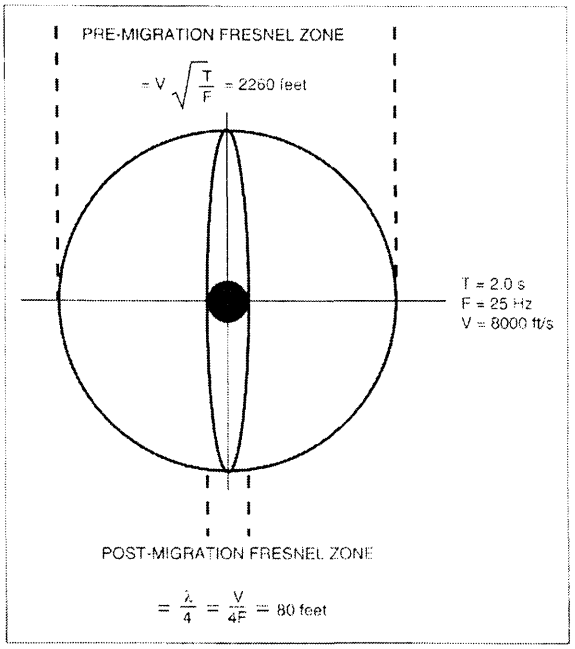

Figure 1.3. The Fresnel zone defines the area from which a reflection is received. The large circle represents the Fresnel zone before migration, the oval is the Fresnel zone after 2D migration. Ideally, Fresnel zone could be reduced to the radius of 1/4 of the wavelength, represented by the black dot in the middle. From Brown (1999).

The issue of resolution is illustrated by Abreu et al. (2003), who compared conventional resolution (35 Hz) seismic data with high-resolution (65 Hz) seismic data, and observed that evidence for lateral migration of a deepwater channel can only be seen in the high-resolution data.

1.3.4 Artefacts and pitfalls

Seismic energy can, and commonly is, reflected more than once from strong reflectors (Brown, 1999). This positions reflections in a false location and causes 'multiples', however, they can normally be removed by seismic processing (Kearey and Brooks, 1991).

Velocity anomalies are caused by lateral variations in lithology or fluid content. For example, a high-velocity channel-fill can cause the underlying reflections to be pulled up causing apparent but non-existing anticlinal fold (velocity pull-up) (Brown, 1999). Velocity push-down can occur below low velocity zones and gas accumulations. The seismic interpreter needs to be aware of this phenomenon, as well as other issues, such as the problem of interpreting onlapping and toplapping reflections. Truncated reflections may seem to continue as the reflections that truncate them (Brown, 1999).

1.3.5 3D seismic interpretation and visualisation approach

The purpose of 3D seismic visualisation is to produce images of numerical data to aid in the interpretation and communication of the interpretation of the data (Hart, 1999). The objectives are to define subsurface stratigraphy, structure and the physical properties of rocks.
3D seismic data can be thought of as consisting of bins with x, y and z dimensions which represent a single seismic trace. These units of volume are called voxels and they have an individual amplitude value (Fig. 1.4). X and y dimensions are measured in metres and z in milliseconds (Bacon et al., 2003).

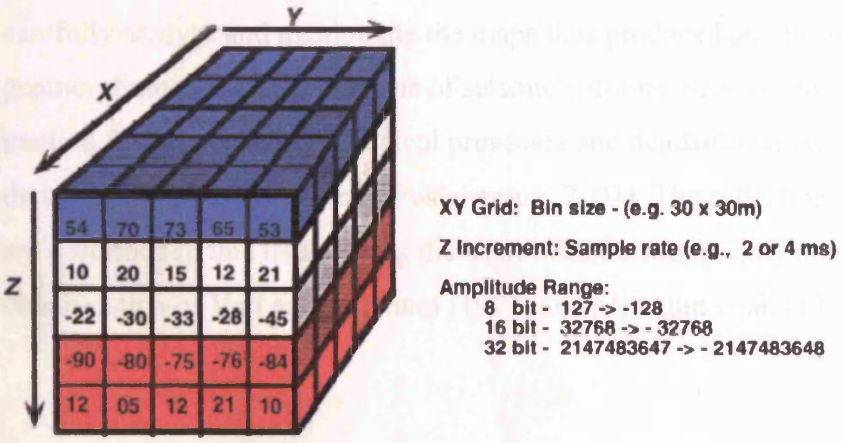

Figure 1.4. Diagram representing 3D seismic data volume from Hart (1999). Each voxel is characterised by x, y and z coordinates and an amplitude value. The x and y values represent the bin size and the z value is the sampling interval, determined by acquisition parameters. The colours given to the negative and positive amplitude values are determined by the interpreter.

3D seismic data can be manipulated in many ways. Only the approach and methods used in this project are outlined here. The line of section to be viewed can be chosen as inlines (vertical section in the direction of data acquisition), crosslines or arbitrary lines (traverse) through the data. Horizontal sections, or timeslices (xy in Fig. 1.4), can also be viewed. They show the stratigraphy intersection on a plane of constant two-way time. Slicing of the data can also be made along arbitrary planes and interpreted horizons. Volumes of data and interpreted horizons can also be viewed in 3D space.

3D seismic interpretation involves horizon picking, which produces a structure map, or a horizon that can be converted to true depth if velocity data is available. An attribute is a derivate of a seismic measurement, such as time, amplitude, frequency and azimuth. Attribute maps provide structural and stratigraphic information that is not so obvious on other means of interpretation (Brown, 1999). The most commonly used attributes in this thesis are dip magnitude and seismic amplitude. Dip magnitude measures the local dip of the horizon surface. It compares time values of voxels with their neighbours and forms a plane between these values to illustrate the attribute dip. Dip maps can reveal very subtle features (even sub-sampling resolution), such as faults and flexures. Seismic amplitude shows the amplitude value at a horizon or two-way time. Amplitude extractions can also be made within an assigned window of time or with reference to interpreted horizons within the data. They are useful when studying subtle stratigraphic features that have anomalous amplitude values, such as channels.

The technique used to carry out this research is to map seismic reflections of interest and carefully analyse and manipulate the maps thus produced and to combine seismic geomorphology with the analysis of seismic sections. Seismic geomorphology is a fairly new method for determining geological processes and depositional systems from plan view images derived from 3D seismic data (Posamentier, 2003). The reflection patterns and characteristics are described in this thesis using the basic seismic stratigraphy nomenclature and classification of Vail and Mitchum (1977) and Mitchum et al. (1977) where applicable.

1.4 SEDIMENTARY PROCESSES IN CONTINENTAL MARGINS

1.4.1 Deepwater sedimentary processes

1.4.1.1 The nature of passive continental margins and their sedimentary processes

Continental margins cover large areas of the Earth and include shelf, slope, rise and abyssal plain (Fig. 1.5). Shelves dip typically at gradients of approximately 0.5°, and the slope and rise commonly have gradients around 1-10° (Stow, 1986). Continental margins can have very variable geometries, affected by many factors, such as regional tectonics, climate, relative sea levels and different depositional environments. For example, mud-dominated margins generally have lower slope angles (Reading and Richards, 1994; Adams and Schlager, 2000). Slope systems are classified into 12 classes based on grain size and sediment feeder system and the nature and controls of each type are discussed thoroughly in Reading and Richards (1994).

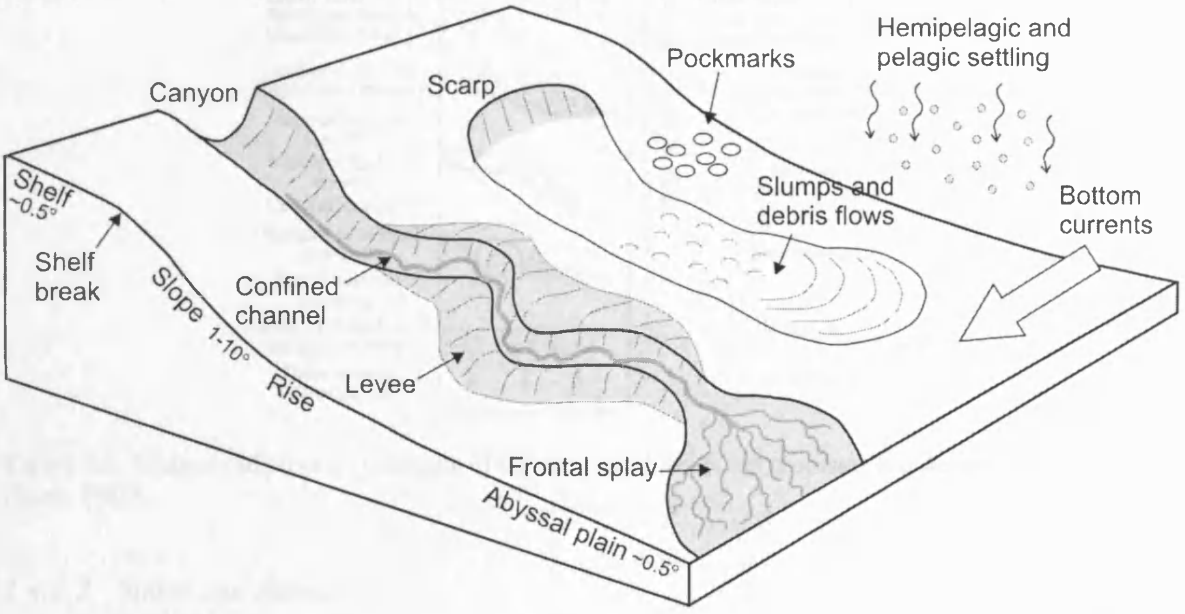

Figure 1.5. A schematic of a passive continental margin and the main sedimentary processes and architectural elements that occur along it and are of interest to this research. Not to scale.

Continental margins are important sites of clastic sediment transport from continents into deep water. Clastic material can be transported over hundreds of kilometres even where the gradient is very low (Eschard, 2001). Downslope processes that deliver sediment into deep water are varied and complex (Stow and Mayall, 2000), and many classification schemes exist (e.g. Mulder and Cochonat, 1996; Locat, 2001). Stow (1986) classifies deepwater processes according to the mechanical behaviour of flow, transport mechanism and sediment

support system. They form a continuum of behaviour from elastic to plastic to viscous fluid and settling (Fig. 1.6). All processes driven by gravitational forces that move sediment to deep water are called 'resedimentation processes'. These, together with normal bottom currents and pelagic and hemipelagic settling, are the main processes capable of transporting and depositing sediment in the deep sea (Stow, 1986). The processes important in this thesis are described briefly below.

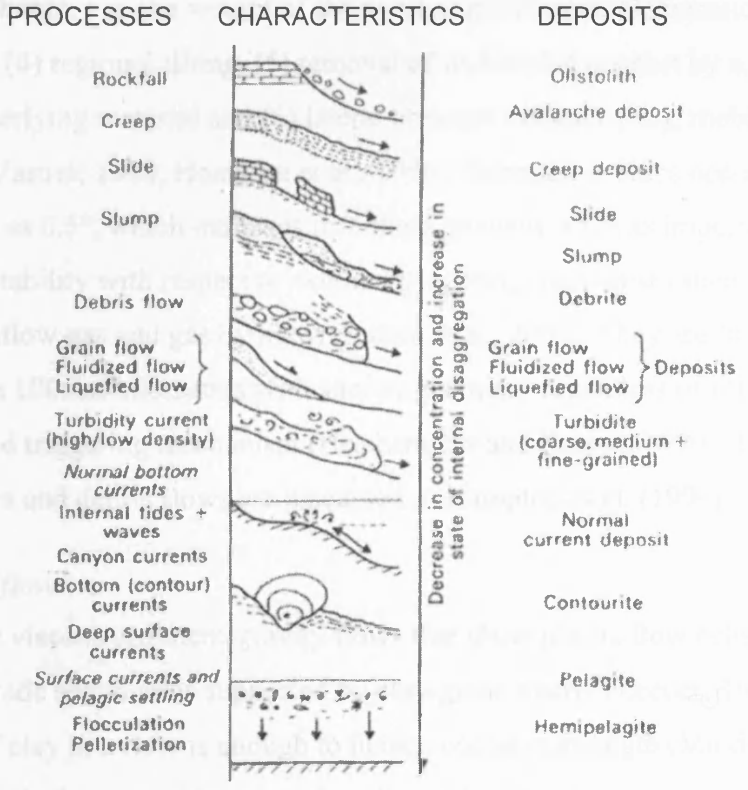

Figure 1.6. Summary of process continuum of the main resedimentation processes and deposits in the deep sea (Stow, 1986).

1.4.1.2 Slides and slumps

Slides and slumps are defined as semi-consolidated, internally coherent sediment masses that are displaced along a basal shear plane (Stow, 1986). A slide can be described as a shear strain with movement along one or several planar surfaces, whereas a slump is a rotational, commonly spoon-shaped slide (Varnes, 1978). A typical slump deposit has (1) a head with extensional faults, scars and sediment deficiency, (2) a relatively undisturbed body and (3) a toe area characterised by compressional structures such as thrusting and overriding of beds (Varnes, 1978; Stow, 1986). They can disintegrate into debris flows and turbidity currents. The transition from a slide to a debris flow to a turbidity current has been observed in nature,

for example in the Nice airport event in 1979 (Mulder et al., 1997) and in Grand Banks in 1929 (Heezen and Ewing, 1955).

Submarine sediment failure, such as slumping and sliding can be initiated if shear stress exceeds the shear strength of sediment. Shear strength is a function of the cohesion between the grains and the intergranular friction (Stow, 1986). Shear stress can be increased by several means, for example by (1) removal of lateral support by e.g. erosion by channels or previous failures, (2) surcharge, e.g. the weight of the overlying sediment, (3) transitory earth stresses, i.e. earthquakes, (4) regional tilting, (5) removal of underlying support by e.g. losing strength or failure of underlying material and (6) lateral pressure caused by e.g. mobilisation of residual stress (Varnes, 1978; Hampton et al., 1996). Submarine slides occur on slopes with gradients as low as 0.5°, which indicates that slope gradient is not as important a factor in marine slope instability with respect to external triggering mechanism such as fluid flow, earthquakes, shallow gas and gas hydrates (Sultan et al., 2004). They are found at scales of less than 1 cm to 100s of kilometres with similar geometry regardless of lithology, degree of consolidation and triggering mechanism (Hesthammer and Fossen, 1999). The dynamics of submarine failure and debris flows are discussed in Hampton et al. (1996).

1.4.1.3 Debris flows

Debris flows are viscous sediment-gravity flows that show plastic flow behaviour (Stow, 1986). Mixed-grade sediment is supported by clay-grade matrix (Leeder, 1999). A 5 % concentration of clay in a flow is enough to induce cohesive strength (Mulder and Cochonat, 1996). Many debris flows contain so much sediment that the water component is interstitial (Mohrig and Marr, 2003). Unlike turbidity currents, debris flows conserve their density when travelling down slopes (Pratson et al., 2000). The high density and clay content prevent settling of sediment from flows and cause poorly-sorted 'en masse' deposition (Kneller and McCaffrey, 2003). Debris flow deposits commonly exhibit pressure ridges at the toe of the deposit. Longitudinal grooves at the base of the deposits and blocky top surfaces indicate the presence of cohesive blocks transported within the debris flow (Prior et al., 1984).

1.4.1.4 Turbidity currents

Turbidity currents are relatively dilute sediment suspension-driven sediment-gravity flows that occur in subaqueous environment (e.g. Kneller, 1995; Kolla et al., 2001). They transport clastic material over hundreds of kilometres from continents to deep ocean over very low slope gradients (Eschard, 2001; Deptuck et al., 2003; Mohrig and Marr, 2003). Sediment is

kept in suspension by the upward component of fluid turbulence (Stow, 1986; Middleton, 1993; Leeder, 1999; Mohrig and Marr, 2003), however, substantial amounts of sediment can also be transported as bedload (Normark et al., 1993). Turbulence is largely the result of friction at the boundaries of the flow with seafloor and ambient water (Stow, 1986).

Turbidity currents are density stratified (Peakall et al., 2000b), and most consist of a dense laminar bottom flow and a turbulent upper plume, so strictly speaking they are gravity flows (Mulder et al., 1997). The term 'turbidity current' has become a general term applied to many sediment gravity flows, even if they cannot be determined to be turbidity currents, and terms like density current or gravity current should probably be used instead (Kneller and Buckee, 2000). Further classification of subaqueous density flows is given in Mulder and Alexander (2001).

Turbidity currents develop a typical anatomy consisting of a head, neck, body and tail (Fig. 1.7) (Stow, 1986; Kneller and Buckee, 2000). They change their density constantly through erosion, deposition and entrainment (Pratson et al., 2000). Most of the erosion and entrainment of ambient fluid occurs at the head. Billows are formed at the upper boundary behind the head where ambient fluid is mixed with the current (Middleton, 1993; Kneller and Buckee, 2000). The body moves faster than the head, and consequently the height of the head increases (Kneller and Buckee, 2000).

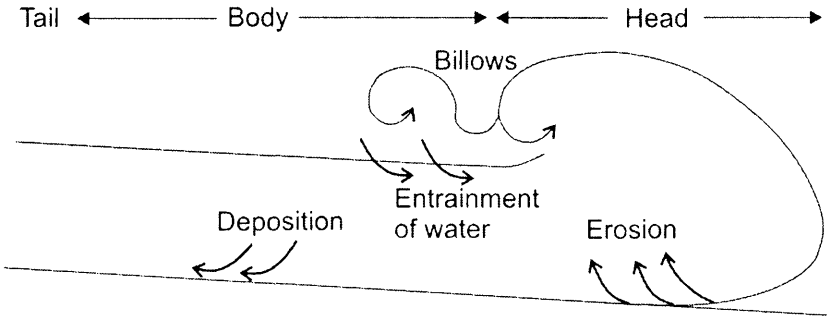

Figure 1.7. The simplified anatomy of a turbidity current. Most erosion occurs at the head and deposition along the body. A mixing vortex of sediment and ambient water occurs at the back of the head causing billows.

Deposition from turbidity currents occurs progressively by settling from a steady or waxing flow (Kneller and McCaffrey, 2003). Turbidity current deposits, i.e. turbidites, can be a few millimetres to 10 m thick and commonly exhibit components of the Bouma sequence or Lowe sequence (e.g. Kneller, 1995). Differences in deposits due to complex flow structures are described in Kneller and McCaffrey (2003) and Kneller (1995).

Deposition and erosion by turbidity currents is controlled by density and velocity of the current (Parker et al., 1986). Currents accelerate as slope gradient increases because of greater effect of gravity on steeper slopes (Parker et al., 1986; Leeder, 1999). As they accelerate, more energy is available for erosion (Parker et al., 1986). Similarly, the currents are likely to deposit as they decelerate (Leeder, 1999). A swift turbidity current can have enough power to erode and incorporate sediment into the flow even without a gradient increase. This increases its density and weight, and as a result the current can accelerate and erode more sediment (Parker et al., 1986). This is called self-acceleration or ignition. Accelerations during transport and deposition affect the character and distribution of turbidite sandstones (Kneller, 1995).

Changes in bottom topography influence erosion and deposition by turbidity currents. Obstacles and changes in slope affect velocity and thus deposition from turbidity currents (Kneller, 1995). The effects of topography depend on the velocity of the current, obstacle height, current density and density stratification (Kneller and Buckee, 2000). Partial blocking of currents causes them to undergo a rapid decrease in both competence and capacity to carry sediment in suspension, and sedimentation is likely to occur as a result (Hiscott, 1994; Kneller and Buckee, 2000).

Turbidity currents are thought to be mainly short-lived surge type flows that last about up to a few tens of hours and do not have a permanent sediment supply (i.e. are often sourced by sediment failures), but where a canyon is connected to a river, quasi-steady flows lasting from hours to months can form (Mulder and Alexander, 2001). Most direct observations of turbidity currents come from cable break data (e.g. Heezen and Ewing, 1955; Krause et al., 1970; Mulder et al., 1997), with suggested velocities of approximately 20-60 km h^{-1}. Direct measurements have been done at least once, however. Khripounoff et al. (2003) measured velocities and turbulence and collected sediment samples before and during a turbidity current on Zaire submarine valley at water depths of 4000 m and also on a levee 13 km away from the channel axis. Although some of their equipment were damaged or broken, they measured a velocity change from a normal 2.8 cm s^{-1} to over 121 cm s^{-1} 150 m above channel. Normal velocity at the base of the channel was 3.4 cm s^{-1}, but the meter broke when the turbidity current hit it. Sediment traps trapped coarse sand and plant debris 40 m above the channel. The current was approximately 400 m thick, but the thickness of the overflow current on the levee was less than 40 m. The duration of the turbidity current was 10 days.

Due to the difficulty in observing and measuring natural turbidity currents and submarine debris flows, most knowledge is gained from interpreting erosional and depositional features from outcrops and subsurface data (Kneller, 2003), and also from laboratory experiments (e.g. Kneller, 1995; Mulder and Cochonat, 1996; Mohrig et al., 1999; Bursik and Woods, 2000; Peakall et al., 2000b; Marr et al., 2002; Mohrig and Marr, 2003) and numerical modelling (e.g. Pratson et al., 2000). These studies give valuable quantitative information of fluid dynamics, characters and the effect of changes in their controlling parameters, such as density, discharge, velocity and structure.

Turbidity currents can be characterised by many dimensioless parameters, most commonly Reynolds, Richardson and Froude numbers (e.g. Kneller and Buckee, 2000). Reynolds number reflects the ratio of inertial to viscous forces acting on a fluid flow. It is the criterion for turbulence in Newtonian fluids and needs to be over 2000 for a fully turbulent flow (Kneller and Buckee, 2000). Turbulence depends on the concentration, velocity and thickness of the flow. Richardson number describes the ability of the current to entrain. Froude number reflects the ratio of inertial to gravitational forces acting on a fluid flow (Kneller and Buckee, 2000). The densimetric Froude number, which is probably most used for describing turbidity currents, is defined by

$$Fr_d = U/(RCgh)^{1/2},$$

in which U is the depth-averaged flow velocity, R is the submerged specific gravity of the sediment, C is the layer-averaged volume of sediment in concentration, g is the gravitational acceleration and h is the flow depth (e.g. Fildani et al., 2006). When $Fr_d > 1$, flows are supercritical and when $Fr_d < 1$, they are subcritical. Supercritical flows are swift, thin and more likely to be capable of eroding seafloor because of higher flow velocities (Nemec, 1990; Kubo and Nakajima, 2002; Fagherazzi and Sun, 2003). Subcritical flows are slow and thick and promote sediment deposition. However, flow regime alone does not determine whether erosion or deposition occurs, but other factors, such as slope gradient and velocity of the currents affect sedimentation rate, too (e.g. Nakajima and Satoh, 2001; Ercilla et al., 2002).

Turbidity currents can be formed from slides, slumps, debris flows (Mulder and Cochonat, 1996; Mohrig and Marr, 2003), but have also been interpreted to be generated by e.g. storms (Parker et al., 1986) and hyperpycnal plumes from river effluent, commonly associated with

flooding events (Leeder, 1999; Kneller and Buckee, 2000; Mulder and Alexander, 2001). However, Khripounoff et al. (2003) observed that although flooding provided the material to the turbidity current, there was no other connection between them, i.e. the timing of flooding did not coincide with the onset of the turbidity current. The dynamic evolution of offshore slope processes and various origins of turbidity currents are discussed in Mulder and Cochonat (1996) and Mulder and Alexander (2001).

1.4.1.5 Bottom currents

Bottom currents are caused by thermohaline circulation and are not gravity-controlled or driven by sediment suspension (Stow, 1986). They are able to erode, transport and deposit sediment on the seafloor and create furrows and construct large elongate sediment drifts and contourites (Stow, 1986).

1.4.1.6 Pelagic and hemipelagic settling

Pelagic sediments are composed of planktonic organisms and related organic matter, whereas hemipelagic sediments are terrigenous elements transported mainly by winds and surface currents (Stow, 1986). Pelagic and hemipelagic sedimentation form commonly drapes because they are settled down through the water column.

1.4.1.7 Other processes

Several other processes that affect the architecture of deepwater environments occur in continental margins. These include structural deformation, for example faulting, folding and mud and salt diapirism, which all are able to create topography and slope instabilities. Diagenesis and compaction can cause overpressure and fluid flow. This can result, for example, in pockmark formation and the development of mud volcanoes, which are common components of continental margins.

1.4.1.8 Controls on continental margin sedimentation

Several factors contribute to the style of sediment transport on continental margins. The main controls are sediment supply, tectonics and sea level fluctuations, but there are also numerous secondary controls (Stow, 1986). These are for example basin size and configuration, slope length and gradient, seafloor rugosity, amount and type of resedimentation, deposition rate, local tectonics, bottom currents and relative sea level variations (Posamentier and Kolla, 2003). The nature of the hinterland affects the source material, and shelf width and the presence of canyons incising the margin affect the ease of sediment bypass into deep water. Slope instability and faulting may lead to resedimentation downslope and processes like salt

CARDIFF UNIVERSITY

tectonics and sub-basin formation may trap sediments and divert flows (Normark et al., 1993; Reading and Richards, 1994; Richards et al., 1998; Eschard, 2001). The nature of sediment supply can also be an important factor in determining the nature of the deposit. Decreasing grain size causes a decrease in the slope gradient and the tendency of channel-levee systems to develop, whereas slumping and meandering increase (Stow and Mayall, 2000).

There is still some controversy in reaching a consensus on models of deepwater processes and deposits. To understand ancient systems, it is important to map the architecture and stacking patterns of the present day examples (Stow and Mayall, 2000). However, modern submarine fans, such as Amazon, Nile and Mississippi, only exhibit processes occurring during relative sea level highstand with low sediment supply rates, which may cause some limitations in applying models derived from recent systems to ancient deepwater basins (Eschard, 2001).

1.5 THE SCOPE AND LAYOUT OF THE THESIS

This thesis contains seven chapters, of which Chapters 2-5 are the main result chapters. Chapters 3-5 are written for publication in scientific journals, which has affected their style and caused some repetition. At the time of submission of this thesis, Chapter 3 has been published, Chapter 4 is in press and Chapter 5 is in review. The specific topics of the chapters were chosen with the intent to produce new, topical and exciting science. Therefore the general architectural elements are not discussed in detail here, but more emphasis is given on rather narrower topics instead.

The work is based on 3D seismic reflection data. No specific lithological or well log data were available from the areas of the 3D seismic surveys, but general information could be gleaned from limited published sources. The main limitations for the work were the data available and limitations within, such as resolution, interpretational uncertainties and errors.

Chapter 2 gives the geological background of the Niger Delta and the Espirito Santo Basin and introduces the two datasets that this research is based on. The chapter focuses on the common deepwater depositional and erosional elements that are found in these datasets. Together with Chapter 1, it provides the context for the Chapters 3-5. Chapter 3 concentrates on the resedimentation phenomena and the degradation of structural highs, namely the toe-of-slope thrust and fold belt folds on the Niger Delta. Chapter 4 focuses on the present day thalweg of a submarine channel-levee system on the Niger Delta, and the formation and

evolution of knickpoints as a result of uplift associated with the thrust and fold belt. Chapter 5 examines peculiar, large depressions that form individually or in trails along underlying erosional channels in the Espirito Santo Basin and that are interpreted to have been formed by erosion and deposition by unstable gravity flows. The key results of the Chapters 2-5 are drawn together in Chapter 6, and selected topics, such as the effects of slope variation to the sedimentary processes are discussed further. The results and shortcomings of this research are discussed in the context of other analytical methods. The conclusions of this PhD project are drawn in Chapter 7.

Chapter 2

2 GEOLOGICAL SETTING AND ARCHITECTURAL ELEMENTS OF THE STUDY AREAS

2.1 INTRODUCTION

This chapter provides the background information on architectural elements that are common on continental margins, concentrating on depositional and erosional features, especially on channels and mass transport complexes. It gives an overview of the geological settings of the Niger Delta and Espirito Santo Basin on both sides of the Atlantic Ocean and describes the different sedimentary elements that characterise the shallow parts of the studied datasets. The datasets differ from each other, as the data from Espirito Santo Basin are located just beneath the shelf break at water depths of 0.5-2 km and the area is dominated by salt diapirs, whereas the data from the Niger Delta have a more distal location at water depths of 2.2-3.4 km, dominated by toe-of-slope thrust and fold belt.

2.1.1 Architectural elements in deepwater settings

Depositional elements are the basic components that are mappable in all scales from field to subsurface studies (Posamentier and Kolla, 2003). Morphological elements in deepwater environments include for example canyons, channels, levees, lobes, mounds, drifts, slumps, debris flows and mass transport complexes (Stow, 1986; Stow and Mayall, 2000; Posamentier and Kolla, 2003; Mayall et al., 2006) (Fig. 2.1). These occur mainly in specific areas within continental margins, for example, shelf edge areas are commonly dominated by large-scale erosional features, such as failures and canyons, slopes are sites for the development of channels and the distal basin is dominated by hemipelagites (Normark et al., 1993).

Much of the previous work on deepwater architectural elements has concentrated on the submarine channels and channel-levee complexes, the architectural complexities of which are described and classified by many authors (e.g. Clark and Pickering, 1996; Galloway, 1998; Deptuck et al., 2003; Posamentier and Kolla, 2003). The terminology is still somewhat confusing, because the study of deep marine sedimentary processes and products is still relatively young. In this thesis, the terminology and classification of Deptuck et al. (2003) is used where applicable. They define a channel-levee system (CLS) as "a single channel-belt, bordered by outer levees" and a channel-levee complex (CLC) as "a series of stacked channel-levee systems that are fed by the same canyon".

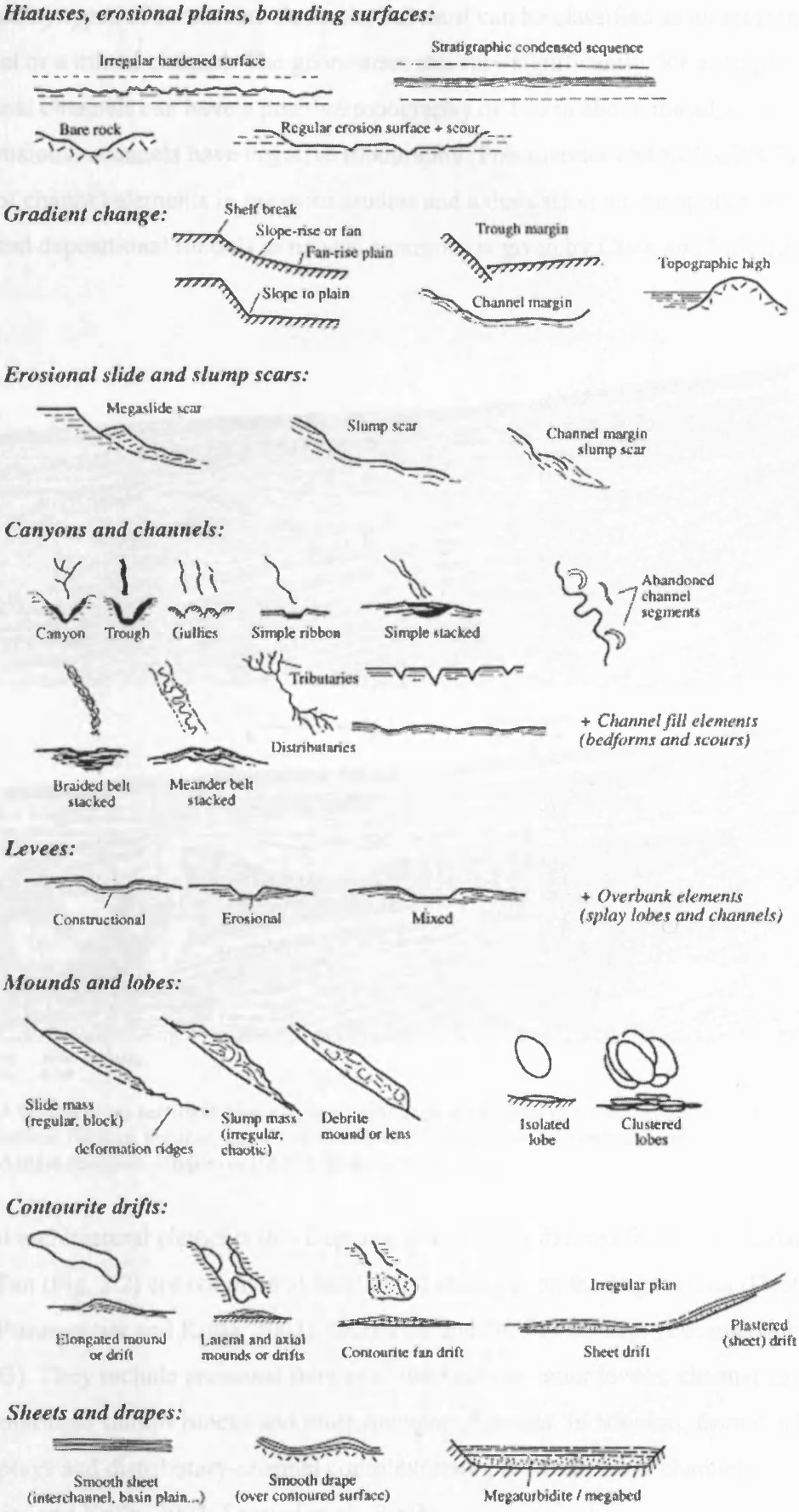

Figure 2.1. The principal architectural elements in deepwater sedimentary systems (Stow and Mayall, 2000).

There are many types of submarine channels, but most can be classified as an erosional, depositional or a mixed channel. The geometries can vary significantly, for example, aggradational channels can have a positive topography of 100 m above the adjacent seafloor, whereas erosional channels have negative topography (Posamentier and Kolla, 2003). A gooc summary of channel elements in previous studies and a discussion on the application of erosional and depositional models to natural examples is given by Clark and Pickering (1996).

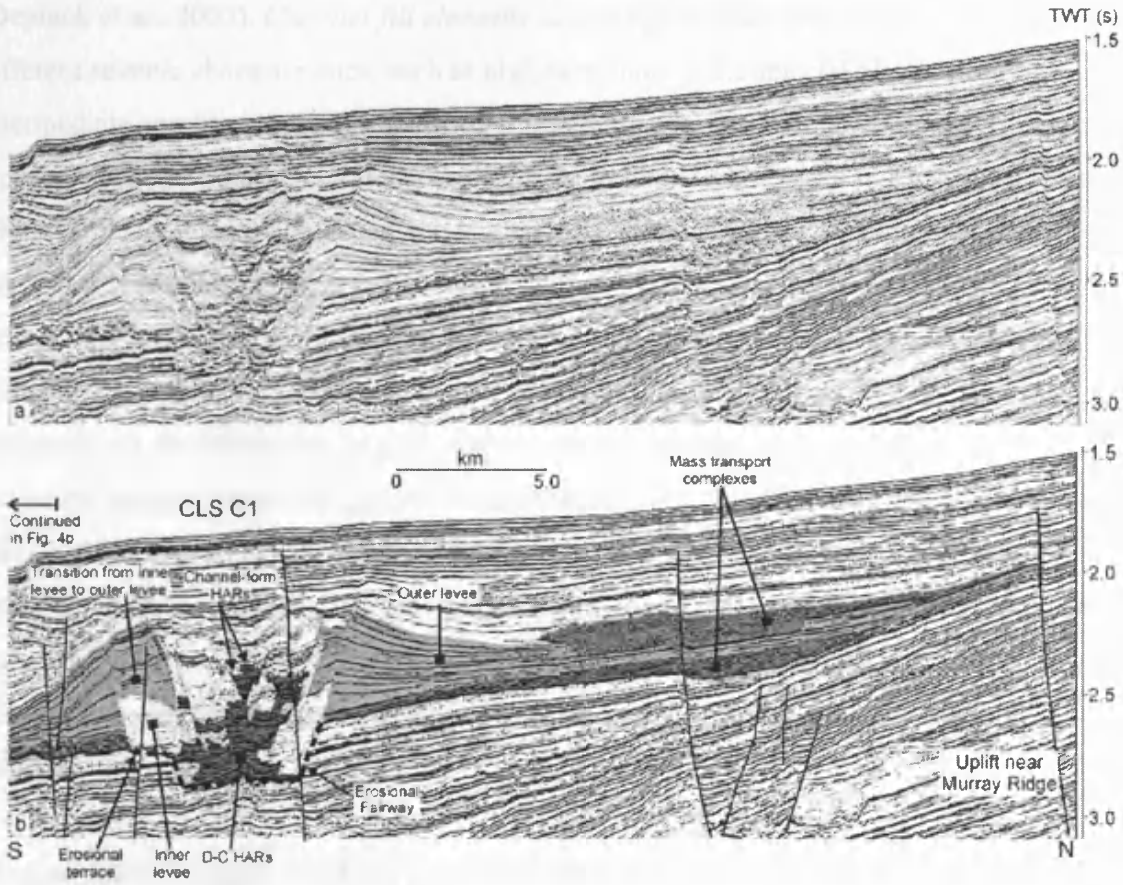

Figure 2.2. A typical cross-sectional geometry and architectural elements of a channel-levee system (CLS) including erosional fairway, terraces, inner and outer levees, channel-axis deposits (channel-form HARs and D-C HARs) and mass transport complexes (MTC) (Deptuck et al, 2003).

The typical architectural elements that Deptuck et al. (2003) defined from seismic data from the Indus Fan (Fig. 2.2) are common at least in the channels on the Niger Delta (Deptuck et al., 2003; Posamentier and Kolla, 2003), Indonesia and Gulf of Mexico (Posamentier and Kolla, 2003). They include erosional fairways, outer levees, inner levees, channel-axis deposits, rotational slumps blocks and mass transport deposits. In addition, frontal splays, crevasse splays and distributary-channel complexes are present in some channels (Posamentier and Kolla, 2003; Samuel et al., 2003).

Following the classification of Deptuck et al. (2003), a channel-levee system (CLS) is characterised by a channel-belt, where channel-axis deposits and inner levees, together with mass transport deposits and slump blocks, are the dominant architectural elements. The channel-belt is bordered by a basal erosional fairway and outer levees of varying thickness (Deptuck et al., 2003).

Erosional fairways are canyon-like incisions that can be up to hundreds of metres deep (Deptuck et al., 2003). *Channel-fill elements* can comprise of several types of deposits with different seismic characteristics, such as high-amplitude reflections (HARs), parallel intermediate amplitude reflections and low-amplitude chaotic reflections. HARs within channel-belts are usually interpreted to be coarse-grained sediments (e.g. Kastens and Shor, 1986; Deptuck et al., 2003; Posamentier and Kolla, 2003). The term channel-axis deposit is used here to distinguish the deposits on the floor of the channel near its axis, disregarding the further division of them into three distinct seismic types according to their width, acoustic character and vertical stacking by Deptuck et al. (2003). Channel-axis deposits are often partly eroded, but the preserved parts commonly show evidence that helps to reveal channel evolution, such as channel migration, which is further described and discussed by Abreu et al. (2003). Parallel, horizontal reflections within the channel-fill that show no evidence for channelisation are referred to as 'passive fill' after Posamentier and Kolla (2003) *or inner levees*, if they form bench-like terraces within the channel-belt (Deptuck et al., 2003). Chaotic low-amplitude seismic facies is often interpreted as debris flow and other mass transport deposits.

Mass transport complex (MTC) is a general term that includes slumps, slides and debris flows. Mass transport deposits are recognised on seismic data by contorted, chaotic low-amplitude reflections. They commonly occur between channel-levee systems (Lopez, 2001; Popescu et al., 2001; Deptuck et al., 2003) and can be up to 150 m thick and tens of kilometres wide (Posamentier and Kolla, 2003). Debris flows have various morphologies, such as sheets, lobes and channels (Posamentier and Kolla, 2003) and form commonly mounds with steep margins (3-4°), but also some of them thin gradually. Individual debris flow deposits can be 80 m thick and reach as far into the basin as turbidites (Posamentier and Kolla, 2003). Erosional scours and long linear grooves at the base of debris flows and irregular top surfaces suggest the presence of large cohesive blocks of sediment within the flow (Prior et al., 1984; Posamentier and Kolla, 2003).

Outer levees are the result of channel overbank deposition and form wedge-shaped cross-sectional geometries (Deptuck et al., 2003). They can be hundreds of metres high and thin away over distances of approximately 10 km. Outer levees are typically an order of magnitude wider than their channels (Posamentier and Kolla, 2003), and commonly interbedded with pelagic sediments and may therefore record changes in global climate (Clark and Pickering, 1996). In highly erosional systems, levees can be completely absent (Posamentier and Kolla, 2003). Levee height decreases down-CLS due to flow stripping and overspill (Peakall et al., 2000b; Posamentier and Kolla, 2003).

Some levees are characterised by sediment waves. They can have a height of 1-70 m, a wavelength of 0.1-6 km and the wave crests can be 60 km long (Wynn et al., 2000b). Sediment waves are orientated roughly perpendicular to the transport direction and they migrate upslope (Wynn et al., 2000b). They occur normally on slopes with a slope <2° (Wynn et al., 2000a).

Frontal splays are the lobe-shaped depositional elements at the termini of channel-levee systems (Posamentier and Kolla, 2003). Frontal splays commonly occur at a significant break in slope where channels are reduced in width, depth and sinuosity (Posamentier and Kolla, 2003). The transition from confined to unconfined flow and the location of the frontal splays is also a function of the sand-to-mud ratio and of slope curvature (Posamentier and Kolla, 2003). Frontal splays and lobes are further discussed by Droz et al. (2003) and Posamentier and Kolla (2003).

Much work is still required to characterise and quantify the architectural elements of deepwater systems. Lateral and vertical connectivity of submarine channel-fill elements and transitional features are still not well characterised (Stow and Mayall, 2000). Understanding stacking patterns is important for the hydrocarbon industry for determining reservoir distribution (Mayall et al., 2006). However, each channel is different, because there are so many parameters that control their formation and final geometries, e.g. sediment type and supply rate, tectonic setting and activity, climate and sea level variations (Bouma, 2004).

2.2 NIGER DELTA

2.2.1 Geological setting

The Niger Delta is a large, up to 12 km thick delta on the Gulf of Guinea on the West African passive continental margin (Fig. 2.3). The delta has formed in the southern culmination of the Benue Trough, a failed arm of a triple junction that formed during the opening of the Atlantic in the Late Cretaceous (Doust and Omatsola, 1990). The Niger and Benue rivers have delivered sediment to the delta at least since the Eocene (Morgan, 2003). The present day annual sediment discharge of the Niger River upstream of the point where the distributary system fans out is 19 million m^3 (Doust and Omatsola, 1990).

The delta is divided into three main stratigraphic formations: Akata, Agbada and Benin (e.g. Knox and Omatsola, 1989; Doust and Omatsola, 1990; Damuth, 1994; Cohen and McClay, 1996; Morgan, 2004). The Late Cretaceous-Palaeocene Akata Formation overlies the continental and oceanic crust and is 2-7 km thick (Corredor et al., 2005). It consists of a succession of overpressured shales, clays and silts (Doust and Omatsola, 1990; Damuth, 1994; Morgan, 2003). Overlying the Akata Formation, the mixed clastic Agbada Formation, consisting of sands, silts and clays (Doust and Omatsola, 1990; Damuth, 1994), can reach a thickness of 5 km (Corredor et al., 2005). The topmost, largely fluvial Benin Formation is the thinnest (up to 2.5 km) and laterally the least extensive formation (Cohen and McClay, 1996) (Fig. 2.3B). The Akata Formation is the distal equivalent of the Agbada Formation, which is the marine equivalent to the nonmarine Benin Formation. The stratigraphic division is made based on differences in seismic character and velocity (Morgan, 2003) (Fig. 2.4). Overall, the delta is dominated by mudstone (>80 %) interbedded with channel-laid sands and has a high sedimentation rate (Davies, 2003).

The Niger Delta can be divided into three broad structural domains: (1) an extensional domain characterised by growth faults, (2) a translational domain with shale diapirs and (3) a compressional domain dominated by imbricated toe-of-slope thrusts (Fig. 2.3B). This division is due to gravity tectonics, caused by rapid progradation of the delta (Knox and Omatsola, 1989; Doust and Omatsola, 1990; Damuth, 1994; Cohen and McClay, 1996; Hooper et al., 2002; Morgan, 2003). Corredor et al. (2005) divide the delta into 5 structural zones: extensional mud diapir, inner fold and thrust belt (with imbricate, basinward-verging thrusts), transitional detachment fold zone, and outer fold and thrust belt (with thrusts verging both

land- and basinward), and give further description of different structural styles of the fault-related folds.

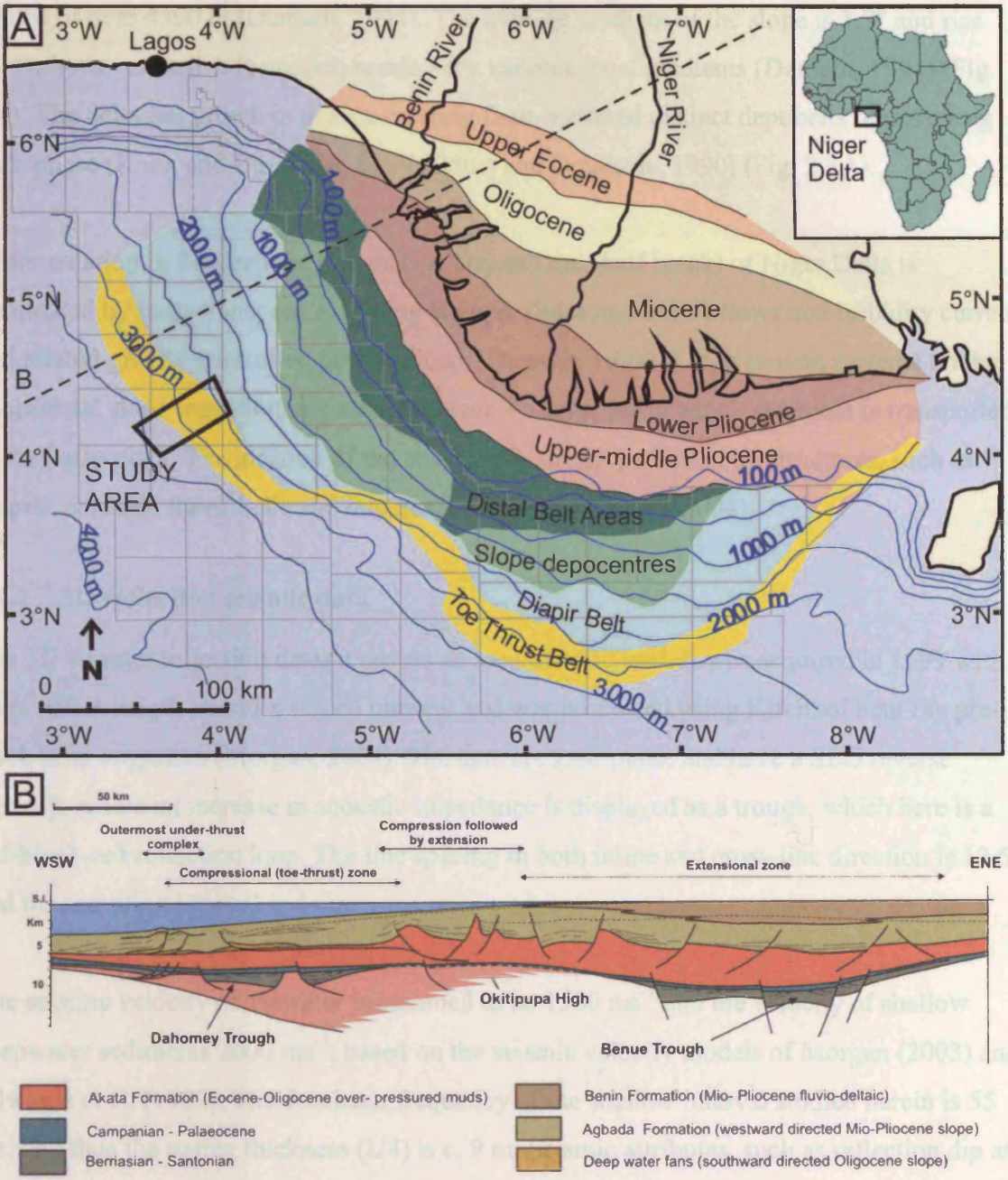

Figure 2.3. Location of the 3D seismic data on the Niger Delta, western Africa. (A) A map of the Niger Delta and its main onshore depobelts and offshore tectonic areas (after Knox and Omatsola, 1989; Doust and Omatsola, 1990; Armentrout et al., 2000). The grey grid marks the location of deepwater hydrocarbon industry licence blocks. (B) A simplified line drawing showing a cross section of the delta with extensional faults at the proximal end, translational zone with mud diapirs and distal compressional zone with toe-thrust and fold belt (Morgan, 2004).

Hydrocarbon exploration and production in the Niger Delta area is prolific, with increasing interest in the deep and ultradeepwater (1500-4000 m) parts of the delta (e.g. Morgan, 2003). The shelf break occurs at the water depth of 150-210 m, and the abyssal plain is reached at depths of over 4500 m (Damuth, 1994). The average gradient of the slope is 1.7° and rise 0.16°, however, active tectonism create very variable local gradients (Damuth, 1994) (Fig. 2.4). The delta has grown in phases creating fault-bordered distinct depobelts representing each phase (Knox and Omatsola, 1989; Doust and Omatsola, 1990) (Fig. 2.3A).

Sedimentation in the deepwater parts (i.e. beneath the shelf break) of Niger Delta is dominated by mass transport, including slumps, slides and debris flows and turbidity currents and related gravity-controlled density flows (Damuth, 1994). Large canyon systems on the continental slope transition into channel-levee systems, along which sediment is transported to the basin plain. The location of the channels is strongly affected by structures, such as diapirs, fold and thrust belts and transfer fault zones (Morgan, 2004).

2.2.2 3D reflection seismic data

The 3D seismic reflection dataset covers an area of 1630 km^2. It was acquired in 1999 with a 6 km offset length and 12 s record interval and was processed using Kirchhof bent ray pre-stack time migration (Morgan, 2004). The data are zero-phase and have a SEG reverse polarity, where an increase in acoustic impedance is displayed as a trough, which here is a red-black-red reflection loop. The line spacing in both inline and cross-line direction is 12.5 m and the sampling interval is 4 ms.

The seismic velocity of seawater is assumed to be 1500 ms^{-1} and the velocity of shallow deepwater sediments 2000 ms^{-1}, based on the seismic velocity models of Morgan (2003) and Edwards et al. (1997). The dominant frequency of the shallow interval studied herein is 55 Hz, and thus the tuning thickness ($\lambda/4$) is c. 9 m. Seismic attributes, such as reflection dip and amplitude were used to reveal depositional and deformational features. Lithological interpretations follow earlier work done by Deptuck et al. (2003) and Posamentier and Kolla (2003), and is based on the recognition of seismic reflection character, amplitude and geometry.

2.2.3 Overview of the architectural elements

The data are located on the western lobe of the Niger Delta, c. 150 km away from the shoreline (Fig. 2.3A). This area is dominated by thrust-cored anticlines and large channel-levee systems, which are also the main features visible on the seafloor (Figs. 2.4 and 2.5). Other common features include slope failures, mass-transport complexes and sediment waves (Fig. 2.5). The failure scars and depositional lobes that characterise the anticline limbs are described and analysed in Chapter 3 and sediment waves are discussed further in Chapter 5. This chapter concentrates on the other features, especially the channel-levee systems and the architectural elements associated with them. A description of each architectural element and a brief discussion of its significance and formation are given below.

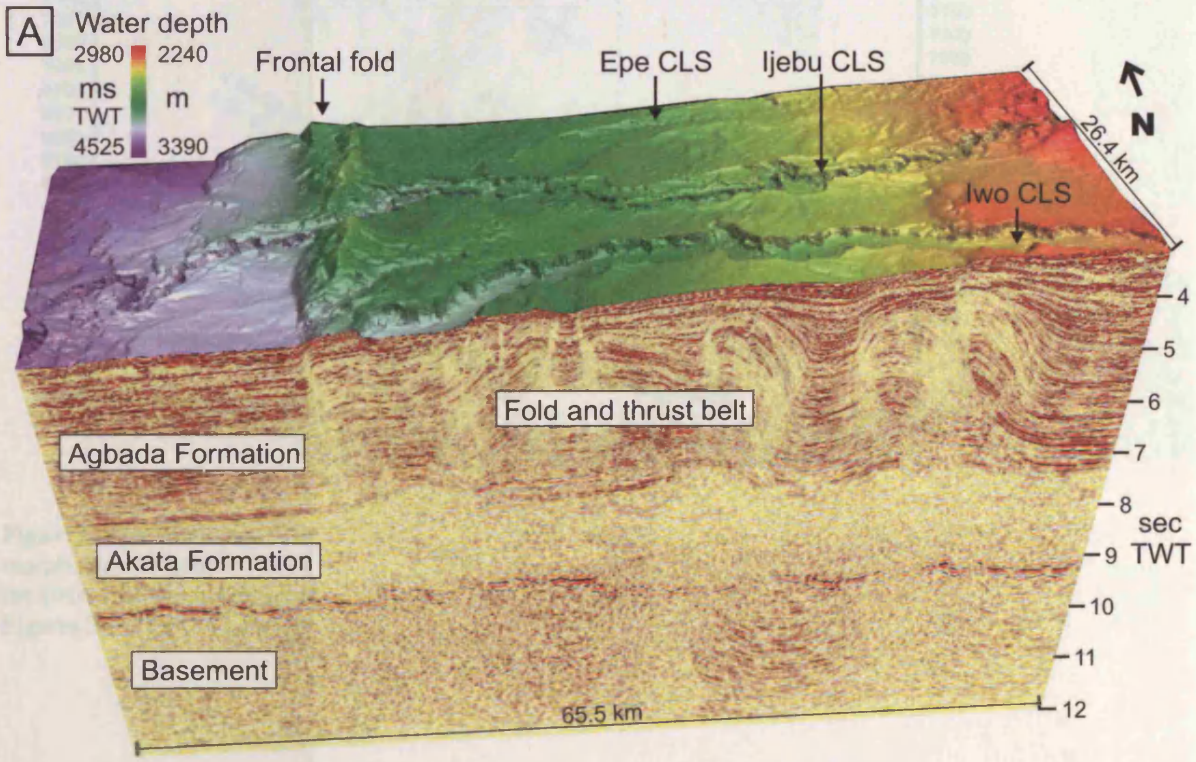

Figure 2.4. (A) A 3D view of the seismic data showing the extent of the data and the main structural and stratigraphic features that characterize it. Thrust-related folds have topography on the seafloor, on which the three main channel-levee systems (CLS) are the dominant features. Continues on next page.

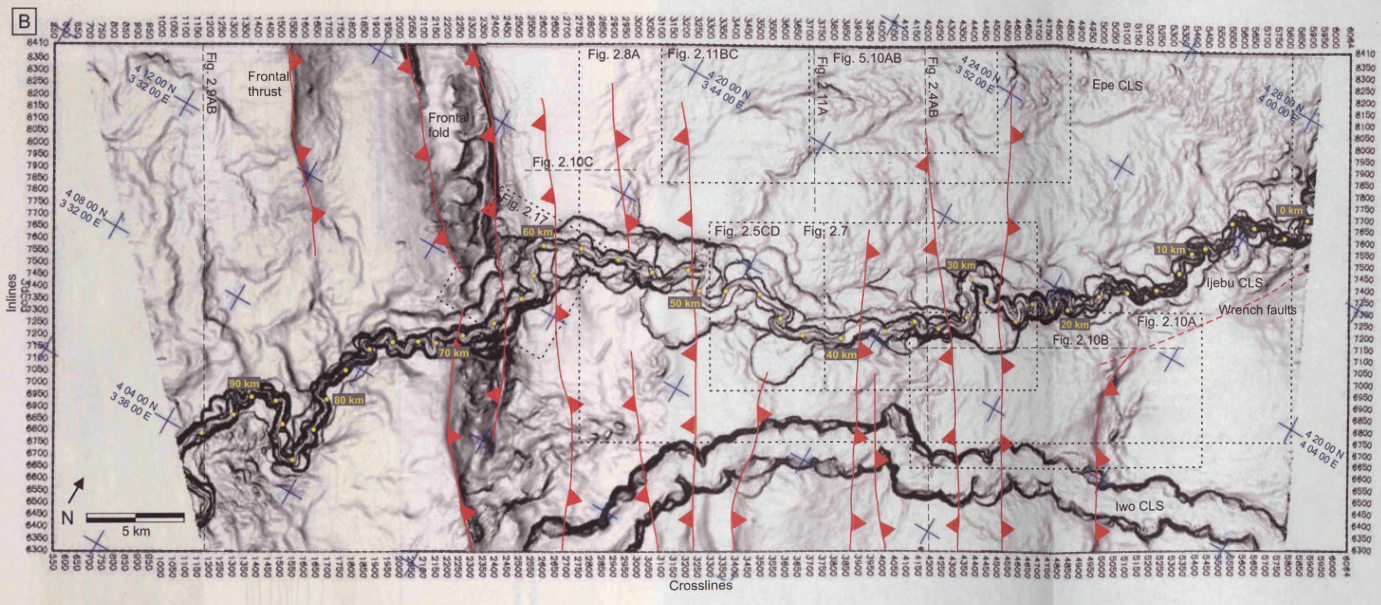

Figure 2.4 (continued) (B) A dip map of the seafloor of the Niger Delta dataset showing the main morphological features. The locations of the main thrusts are traced in red. The yellow dots and numbers along the Ijebu CLS are the datapoints from which the measurements of Figures 2.6 and 4.4 were taken. Locations of Figures 2.5-2.11, 2.17 and 5.10 are shown.

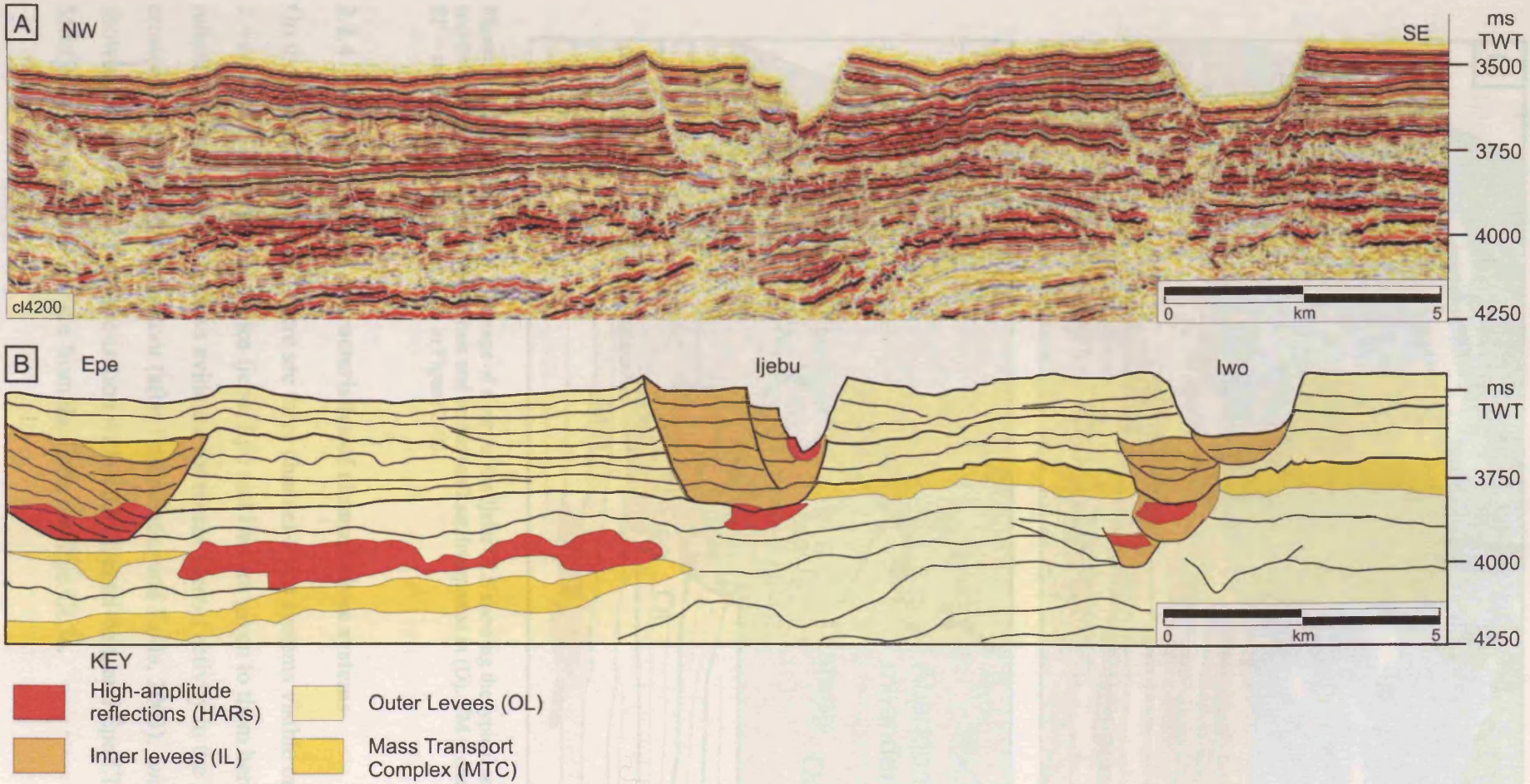

Figure 2.5. (A) A representative seismic line across the data showing three channel-levee systems in the shallow section. For more seismic lines, see Appendix 2. (B) A line drawing with the interpretation of the main seismic facies and architectural elements important for this project. See location in Figure 2.4B. (C) and (D) on next page.

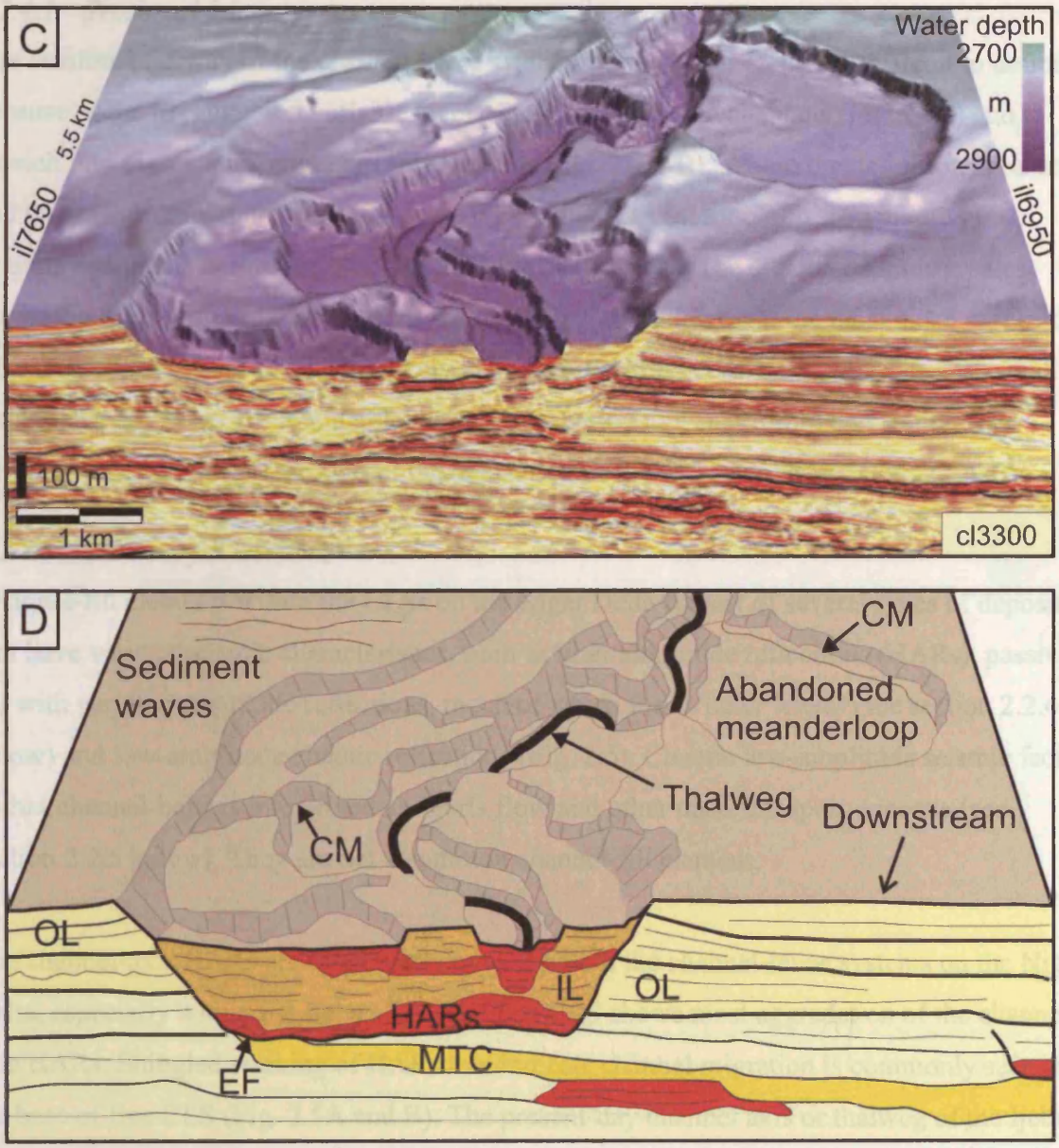

Figure 2.5. (Continued) (C) A 3D image of a part of the Ijebu CLS showing the typical seismic facies and architectural elements in seismic section and on the seafloor, interpreted in (D). CM = channel-margin collapse. EF = erosional fairway. See location in Figure 2.4B.

2.2.4 Morphology and characteristics of channel-levee systems

On the Niger Delta dataset, there are three channel-levee systems visible on the seafloor (Figs. 2.4 and 2.5). The informal names Ijebu, Epe and Iwo are given to them here for the ease of reference. The Ijebu CLS shows evidence for recent current activity in the form of presence of erosional channels on the seafloor (after Posamentier and Kolla, 2003), Iwo CLS is inactive, showing no evidence of channelisation within the channel-belt, and Epe CLS is almost buried. Most of the examples below are from the Ijebu and Epe CLSs.

2.2.4.1 *Erosional fairway*

The erosional fairway of the channel-levee systems on the Niger Delta are difficult to define, because of the irregular and variable level of incision along the channels (Fig. 2.6F) and erosion into pre-existing channel-levee systems (Fig. 2.5A-B). Where the definition is easier and the measurements are more accurate, they indicate an incision of c. 150 m into pre-existing sediments before the base of extensive outer levees. The erosion depth is greatest across the folds with greatest uplift of the seafloor and shallowest at the most distal part of the CLS (Fig. 2.6F). These results are likely to be slightly exaggerated, however, because small wedge-shaped levees are found at lower levels occasionally, suggesting that some levee-building occurred before the start of the deposition of the extensive levees (Fig. 2.5A-B).

2.2.4.2 *Channel-fill elements*

Channel-fill elements within the CLSs on the Niger Delta consist of several types of deposits that have various seismic characteristics, such as high-amplitude reflections (HARs), passive fill with variable amplitude reflections, much of which forms inner levees (see section 2.2.4.3 below) and low-amplitude chaotic reflections (Fig. 2.5). Chaotic low-amplitude seismic facies within channel-belts is interpreted as debris flow and other mass transport deposits (see section 2.2.5 below). They are not a common channel-fill element.

The channel-axis HARs are often partly eroded within the channel-levee systems on the Niger Delta, especially within the Ijebu CLS. The Epe CLS shows most aggradation of the channel-axis HARs. Shingled stacking of HARs that indicate channel migration is commonly seen at the base of Epe CLS (Fig. 2.5A and B). The present-day channel axis or thalweg of the Ijebu CLS is c. 80 m wide (Figs. 2.5D and 2.6C). Figure 2.7 reveals that this is a common width for channel-axes deposits throughout the evolution of the channel-levee system. It also illustrates the process of meander bend cutoff. The present day thalweg is further described and discussed in Chapter 4.

2.2.4.3 *Inner levees*

The Ijebu CLS has several levels of terraces, the elevation of which is highly variable with respect to the thalweg (Fig. 2.5C and D). The seismic character of the inner levees varies from low to high-amplitude continuous to chaotic reflections and they can be very different to outer levees (Fig. 2.5). This suggests a different composition and origin for inner and outer levees (Deptuck et al., 2003). Inner levees are commonly bordered by erosive surfaces inclined less than 25° (Deptuck et al., 2003), however, on the Niger Delta these surfaces can be up to 35°.

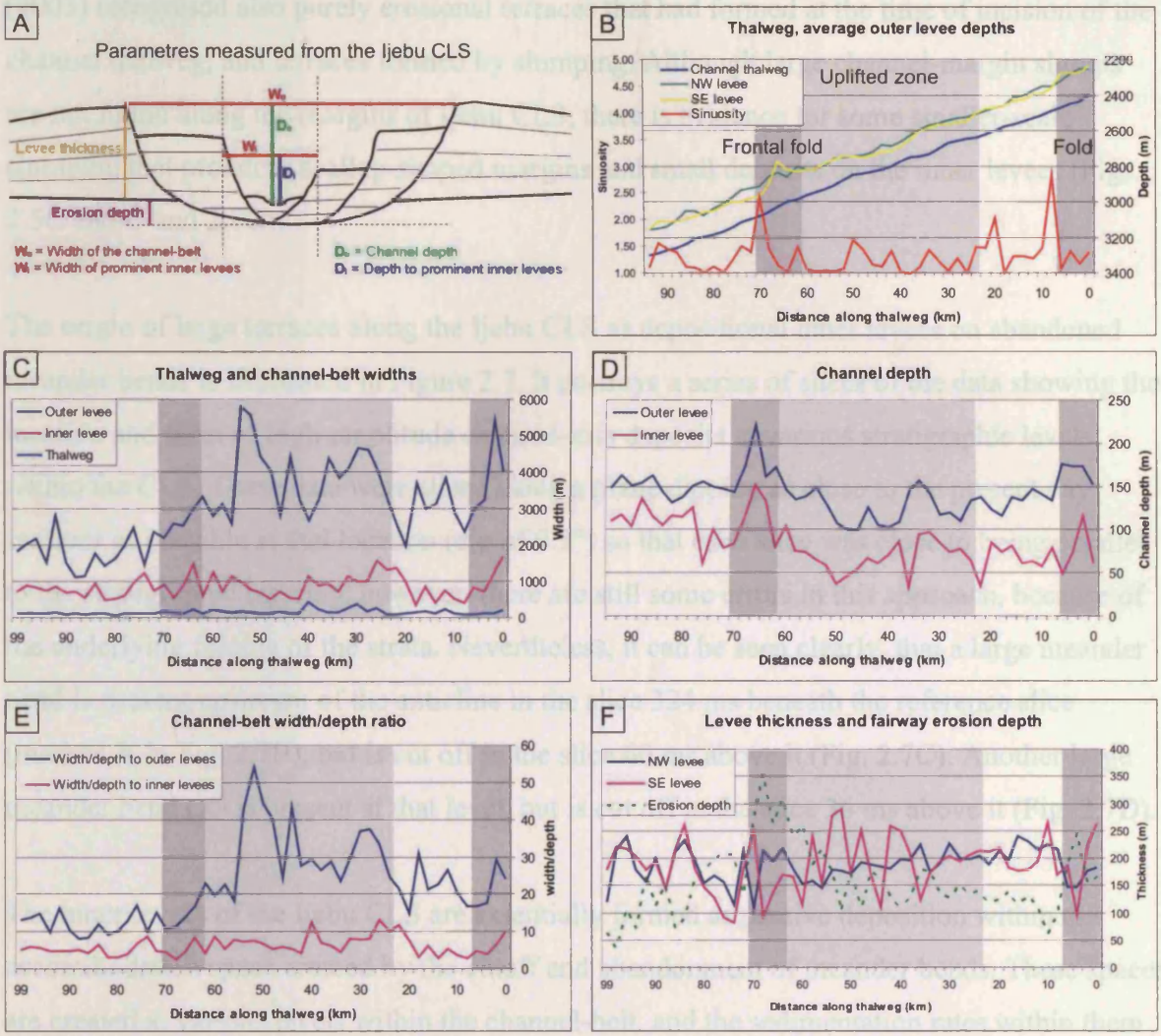

Figure 2.6. Quantification of morphological features of the Ijebu channel-levee system. The measurements of the parameters shown in (A) are recorded along the present day Ijebu thalweg every 2 km. (B) A graph showing the water depth along the course of the Ijebu thalweg and the crest of the outer levees, plotted together with sinuosity values from the thalweg. (C) Width of the channel-belt, prominent inner levees and thalweg. The width of the channel-belt decrease dramatically inboard of the frontal fold. (D) The depth of channel shows increase half way down the system. (E) Channel width/depth ratio. (F) Measurements of the levee thicknesses and the depth of erosion of the fairway. Quality of the measurements is lower where thrusts are present. Depth to the most prominent inner levees does not change. Datapoints located in Figure 2.4B.

Similar terraces to what are observed on the Niger Delta are recognised in the channels of many fans, such as the Indus (McHargue and Webb, 1986; von Rad and Tahir, 1997; Deptuck et al., 2003), Zaire (Droz et al., 1996; Babonneau et al., 2002; Droz et al., 2003; Babonneau et al., 2004), Bengal (Hübscher et al., 1997), Sao Tomé (Viana et al., 2003) and Rhône (Torres et al., 1997) fans. They have been interpreted as levee margin growth faults (Clark and Pickering, 1996), slumped levees and channel margins, depositional terraces and confined inner levees. Recent interpretation of 3D seismic data has proved their origin as inner levees deposited on the space created by channel erosion (Babonneau et al., 2004). Deptuck et al.

(2003) recognised also purely erosional terraces that had formed at the time of incision of the channel thalweg, and terraces formed by slumping. Although large channel-margin slumps are not found along the margins of Ijebu CLS, there is evidence for some smaller-scale slumping that produces scallop-shaped margins and small deposits on the inner levees (Figs. 2.5C and D and 2.7G).

The origin of large terraces along the Ijebu CLS as depositional inner levees on abandoned meander bends is illustrated in Figure 2.7. It portrays a series of slices of the data showing the location and form of high-amplitude channel-axis deposits at various stratigraphic levels within the CLS. These data were sliced along a plane dipping as close to the present day seafloor as possible at that location (dip of 0.3°) so that each slice was close to being parallel to the stratigraphic layering, however, there are still some errors in this approach, because of the underlying folding of the strata. Nevertheless, it can be seen clearly, that a large meander bend is present upstream of the anticline in the slice 324 ms beneath the reference slice (marked Y in Fig. 2.7B), but is cut off in the slice 60 ms above it (Fig. 2.7C). Another large meander bend (X) is present at that level, but is cut off in the slice 36 ms above it (Fig. 2.7D).

The inner levees of the Ijebu CLS are essentially formed as passive deposition within the accommodation space created by the cutoff and abandonment of meander bends. These spaces are created at various levels within the channel-belt, and the sedimentation rates within them are variable. Therefore the thickness of an inner levee does not necessarily reflect its age, and the terraces cannot be correlated based on their height above the channel thalweg alone.

2.2.4.4 Outer levees

The large outer levees that border Ijebu channel-belt are wedge-shaped, exhibit both high and low-amplitude reflections and are approximately 5 km wide (Fig. 2.5A and B). The levees on both sides are typically c. 200 m thick (Fig. 2.6F). However, as pointed out above, small wedge-shaped deposits are found locally at lower stratigraphic levels, and therefore the levees could be much thicker.

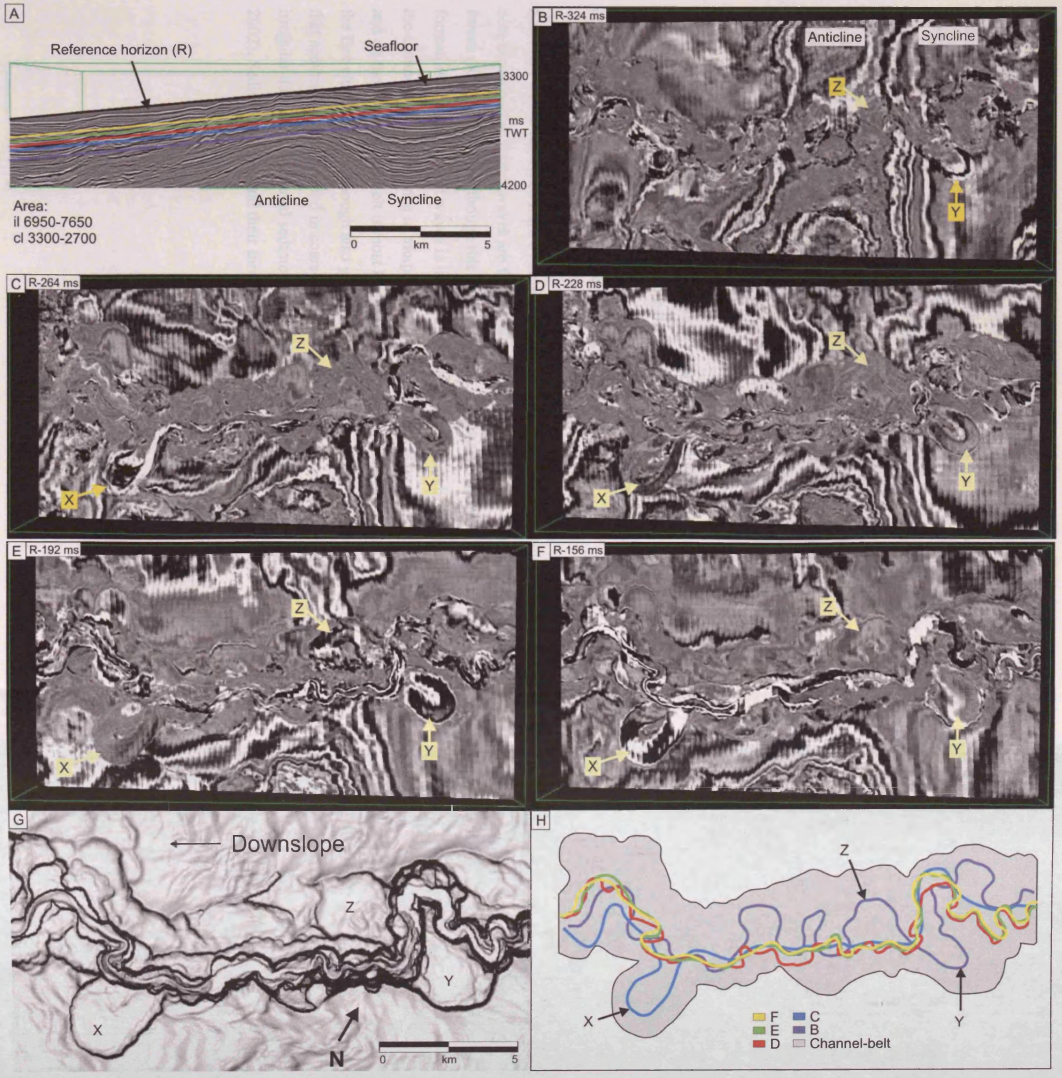

Figure 2.7. (continues to next page) Formation of terraces by channel thalweg migration and meander bend cutoff. (A) A cross section of the seismic volume, which is sliced along an arbitrary plane (R). This reference slice inclined to dip 0.3° to match the approximate seafloor dip. (B-F) Slices of the seismic data showing the variation in the location of the channel-axis deposits, shown in bright colours (high amplitudes) and the evolution of meander bend cutoffs into large terraces (X, Y and Z) within the channel-belt. (G) Seafloor dip map of the same are showing the large terraces (X, Y and Z). (H) A line drawing, in which the most prominent channel-axis deposits from each slice and the limits of the present day channel-belt are superimposed. See locations in Figure 2.4B.

2.2.4.5 Sediment waves

Sediment waves are a prominent feature on the levees of the Ijebu CLS (Fig. 2.8). The linear and arcuate crests of the waves are typically several kilometres long and orientated oblique to the channel-belt. A typical crest to crest distance is approximately 1 km and the waves are up to 20 m high (Fig. 2.8B). An azimuth map that shows the direction of dip of the local seafloor slopes reveals that most stoss flanks dip upslope (Fig. 2.8A). A seismic section across some of the waves on the levees shows evidence for the growth and upstream migration of the waves by preferential deposition on the stoss flanks (Fig. 2.8B). Some of the reflections have a high seismic amplitude signal on the stoss flanks, suggesting the presence of relatively coarse sediment (Fig. 2.8B; see also Fig. 2.9).

Sediment waves are also found on the seafloor overlying the buried channel-belt of the Epe CLS (Fig. 2.8C). These waves have more irregular morphology and are more closely spaced than the waves on the levees. They have developed above a passive channel-fill and do not occur below the level of 130 ms below the present seafloor.

Sediment waves on levees form by flow-stripping from turbidity currents within channels and best-developed sediment waves are found outboard of the outer bends due to centrifugal forces (Komar, 1969). Although this phenomenon is not observed on the Niger Delta, the formation of the sediment waves is likely to be related to the turbidity currents flowing down the channels. The difference in morphology of sediment waves on the intra-channel seafloor and on the Epe channel-belt is most likely due to the weak confinement of the flows within the Epe channel-belt, although also grain-size can affect the sediment wave morphology so that sediment waves formed in coarse-grained sediments are commonly smaller and more irregular than in fine-grained sediment and associated with erosional scours (Wynn and Stow, 2002). Sediment waves and their formation are further discussed in Chapter 5.

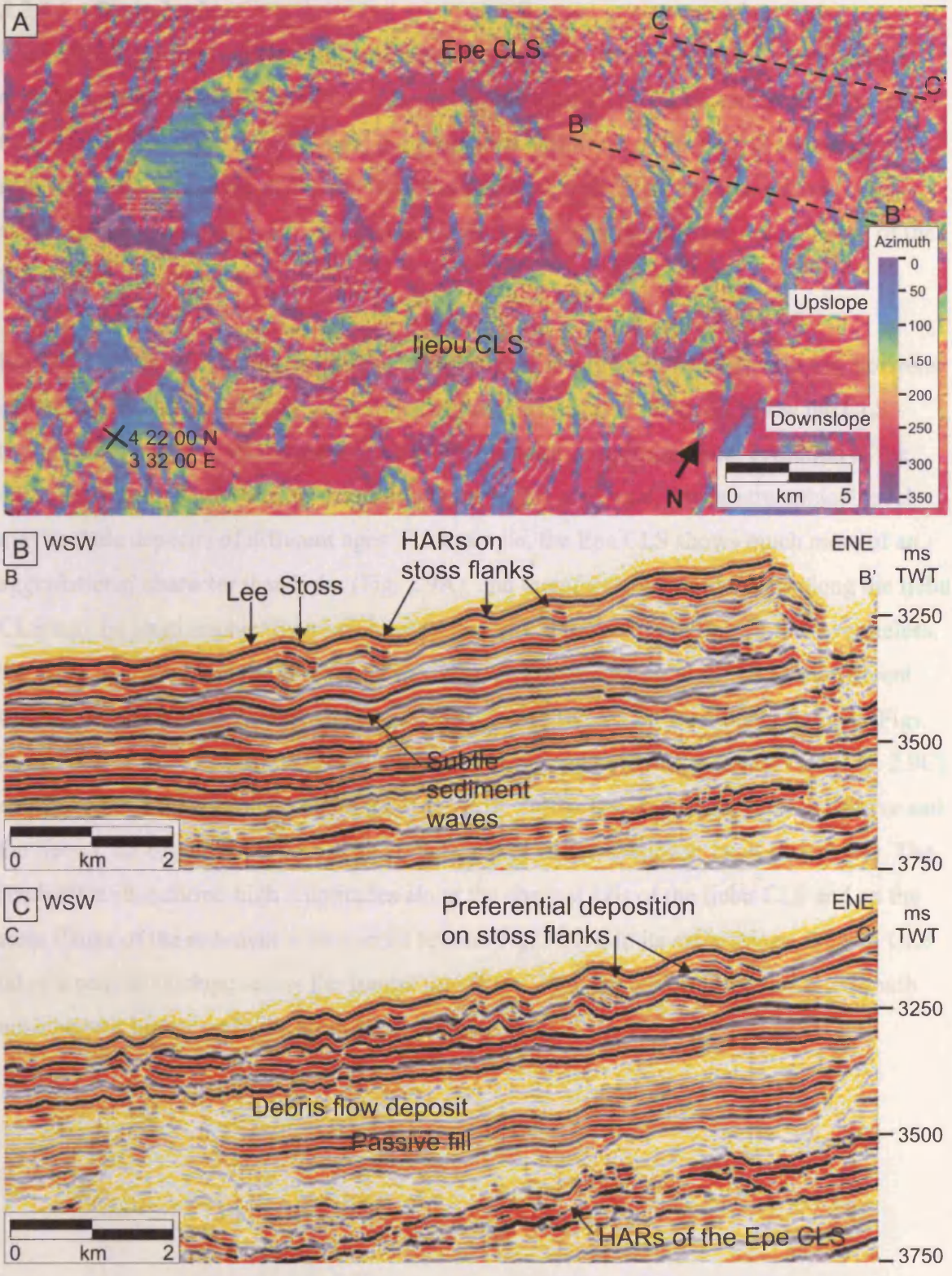

Figure 2.8. Sediment waves on the levees of Ijebu and on the channel-belt of Epe. (A) A dip azimuth map showing the direction, into which the local seafloor slopes are dipping. The sediment waves on both sides of Ijebu CLS have upslope-dipping stoss flanks. The wave crests are up to 4 km long and have a wavelength of c. 1 km. The sediment waves on Epe CLS are slightly smaller and less regular. See location in Figure 2.4B. (B) Sediment waves on a levee, crests approximately parallel to slope. Waves are subtle c. 250 ms below the seafloor but become larger up-section with much more deposition on the upslope (stoss) flanks. (C) Sediment waves along the Epe channel-belt occur on the top c. 100 ms and are very irregular. The traverse shows an along-section channel-fill of the Epe CLS.

2.2.4.6 Frontal splays

The extensive frontal splays of the channel-levee systems on the Niger Delta are located outside the data area (Morgan, 2004). However, the location of the frontal splay of the Epe CLS used to lie within the data area, but prograded basinward as the CLS grew longer. The splay is visible as a layer of chaotic HARs at the base of the Epe CLS on a seismic cross-section (Fig. 2.9A) and as a high-amplitude fan-shaped area that spreads out outboard of the frontal fold in plan view (Fig. 2.9C).

Figure 2.9 shows maximum amplitude extractions of seismic volumes between two horizons created by combining various proportions of the seabed and the horizon below the CLS (horizon BC in Fig. 2.9B) in order to establish the seismic stratigraphical evolution of the CLSs. However, since some of the channels are highly erosional, one stratigraphical level may include deposits of different ages. For example, the Epe CLS shows much more of an aggradational character than Ijebu (Fig. 2.9A), and therefore younger deposits along the Ijebu CLS may lie stratigraphically much lower than older deposits of the Epe CLS. Nevertheless, the gross evolution and the location of the channel-axis deposits and the CLSs at different levels can be established. At lower levels, the Epe and Iwo CLSs are most prominent (Figs. 2.9C-D). The Epe CLS transitions into a frontal splay outboard of the frontal fold (Fig. 2.9C), and sinuous CLS is developed onto the splay (Fig. 2.9E). The Epe CLS becomes passive and the Ijebu CLS becomes the CLS with strongest imprint at a shallower level (Fig. 2.9G). The shallowest slice shows high amplitudes along the channel axis of the Ijebu CLS and on the stoss flanks of the sediment waves on its levees (Fig. 2.9H). In its early stages, the Iwo CLS takes a path downslope across the frontal fold (Figs. 2.9C-E), but becomes deflected south upslope of it higher up in the stratigraphy (Fig. 2.9H).

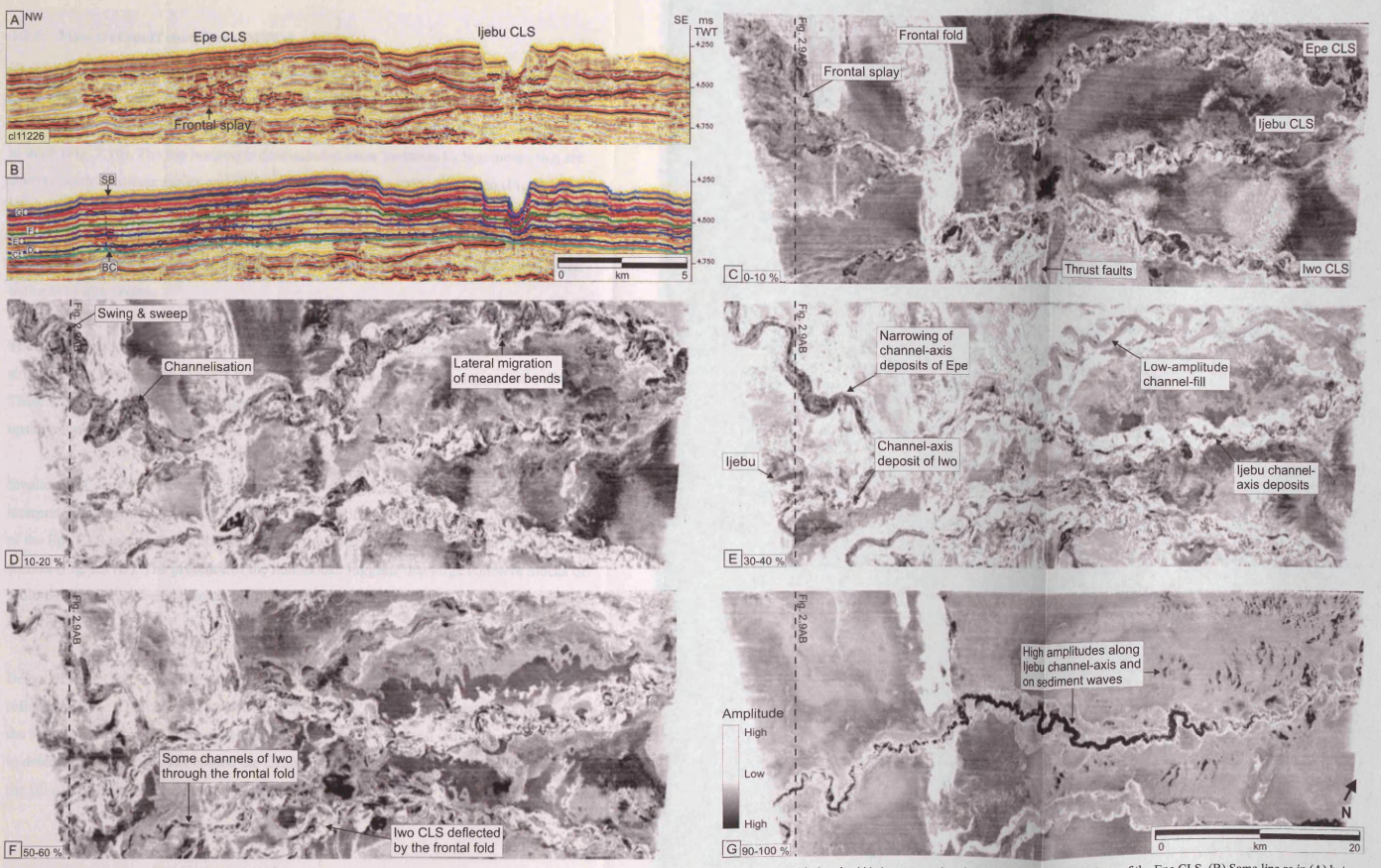

Figure 2.9. A series of maximum amplitude extractions between isoproportional slices showing the seismic facies of the CLSs at different stratigraphic levels. (A) A cross section showing a frontal splay at the base of the Epe CLS. (B) Same line as in (A) but with the isoproportional slices between the green horizon (BC) and the seabed (SB) superimposed on it. The percentage of seafloor used is shown on (C-G). (C) Maximum amplitude extraction between BC and the lowest slice. It shows the depositional frontal splay outboard of the frontal fold. (D) Channels of the Epe CLS showing both swing and sweep become confined on the splay. The path of the Iwo CLS is roughly straight outboard and across the frontal fold, better seen in (E) with a single channel clearly visible. Sinuous channel-axis deposits are seen also along the Epe and Ijebu CLSs at this level. (F) The imprint of the Ijebu CLS becomes stronger at this level. The path of Iwo CLS is deflected south before the frontal thrust. Epe CLS is passive. (G) High amplitudes are seen along Ijebu thalweg and low terraces, and also on upslope flanks of sediment waves on the levees in the extraction between seafloor and the topmost slice.

2.2.5 Mass transport complexes (MTCs)

There are several MTC deposits on the Niger Delta, mainly in the shallow part of the data (top 1-2 s TWT below seafloor). One particularly extensive MTC that extends almost across the whole data area is located beneath the 3 channel-levee systems (Fig. 2.5) and is typically c. 60 m thick (Fig. 2.10). The top horizon is dominated at some locations by hummocks that are several hundred metres across and slightly elongate in a downslope direction (Fig. 2.10A). The onlap of reflections onto the hummocks (Fig. 2.10B) indicates that they were present at the time of the deposition of the MTC, and are thus interpreted as coherent blocks that were transported within the mass flow. Some preferential deposition on the upslope sides of the hummocks also occurs.

The MTC has a low-amplitude chaotic seismic reflection character, however, some internal structures can be observed in some locations, for example steeply dipping internal reflections. These are interpreted as imbricate thrusts formed within the MTC, typically found on the upslope limb of an anticline (Fig. 2.10C).

Smaller MTCs are also frequent within the data. Some are confined within channels and interpreted as debris flow deposits (Fig. 2.11). A debris flow deposit on top of the passive fill of the Epe CLS is completely confined within the Epe channel-belt and has a hummocky top surface (Fig. 2.11B). The presence of the hummocks suggests that large cohesive blocks of sediment may have been transported within the debris flow (Prior et al., 1984; Posamentier and Kolla, 2003).

Below the Epe CLS, a distinct u-shaped channel scour is filled with low-amplitude chaotic reflections (Fig. 2.11A). This channel-fill element has a constant thickness of c. 110 m along the sinuous course of the channel, which can be traced over several tens of km. It is difficult to determine the process that eroded the channel, but based on the reflection characteristics, the fill can be identified as a debris flow deposit.

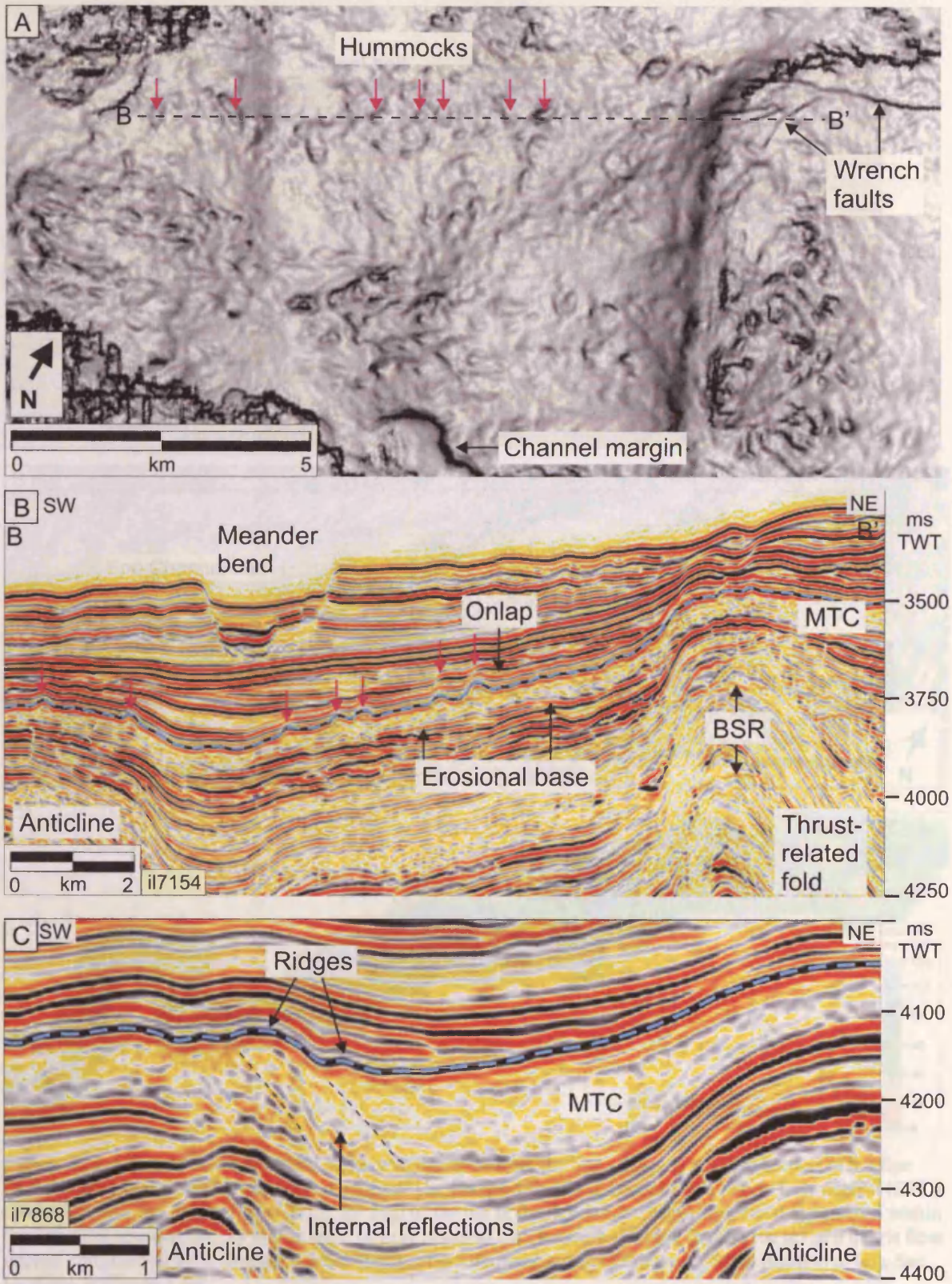

Figure 2.10. Seismic characteristics of an extensive mass transport complex (MTC) on the Niger Delta. (A) A dip map displaying a part of the top surface of the MTC and showing hummocks that are slightly elongate in the downslope direction. (B) A cross-section showing the typical low-amplitude chaotic seismic character of the MTC. The MTC is approximately 60 m thick and has an erosional base and hummocks on its top surface (blue dashed line). These hummocks are onlapped by subsequent reflections with preferential deposition on the upslope sides. (C) An example of internal structures within the MTC (dashed lines) that are interpreted as imbricate thrusts. See locations in Figure 2.4B.

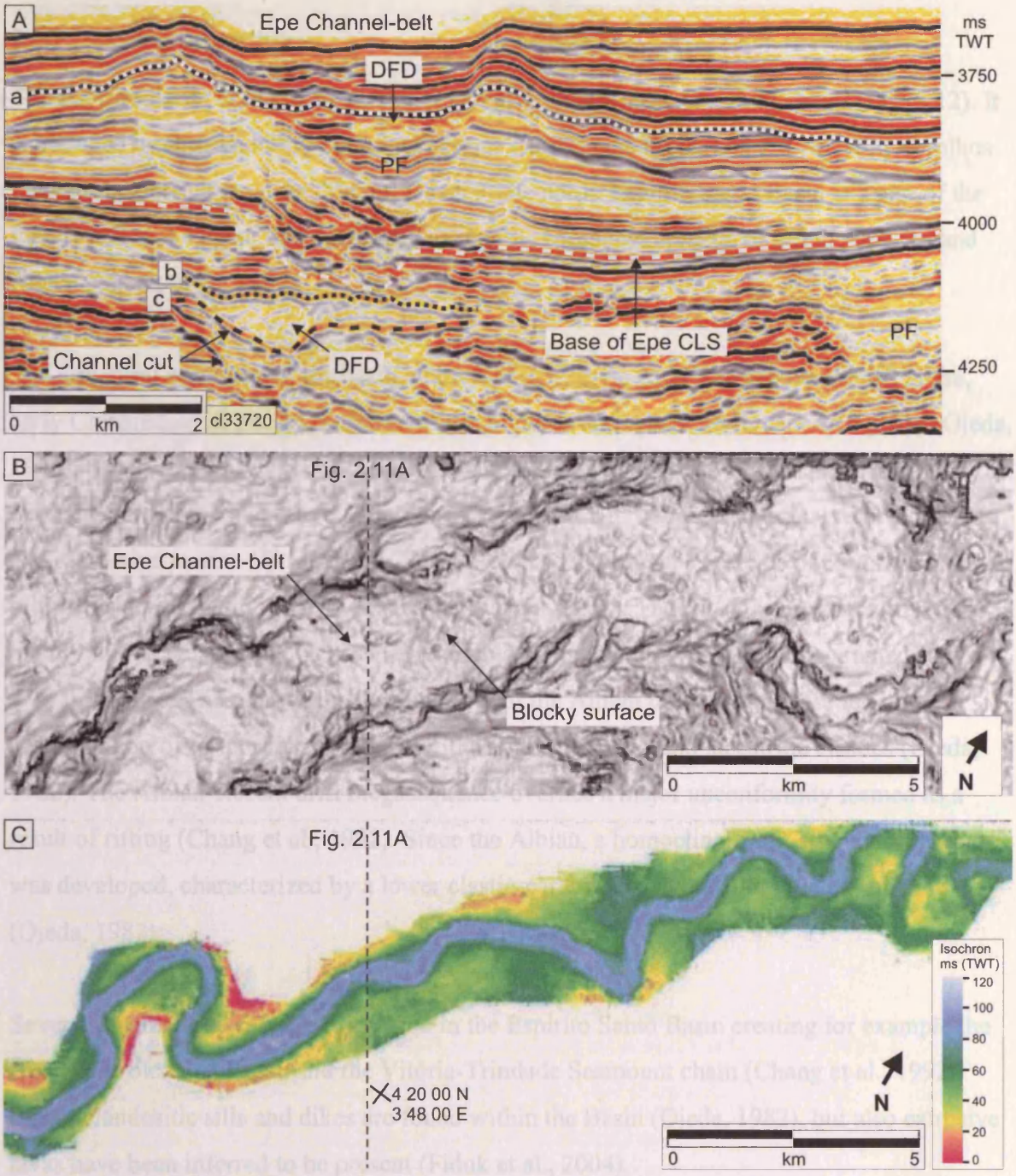

Figure 2.11. Channel-confined debris flows within and beneath the Epe CLS. (A) A cross-section of the Epe CLS showing lateral shift towards the southeast. The passive fill (PF) is overlain by a debris flow deposit (DFD) confined within the channel-belt. (B) A dip map of the top of the debris flow deposit (horizon a) confined within the Epe CLS showing blocky appearance. (C) An isochron map between the base (b) and top (c) of a debris flow deposit confined within a channel beneath the Epe CLS showing constant thickness. Same location as (B). See locations in Figure 2.4B.

2.3 ESPIRITO SANTO BASIN

2.3.1 Geological setting

The Espirito Santo Basin is located on the passive continental margin of Brazil (Fig. 2.12). It is bounded by the structurally similar Campos Basin to the south, and the volcanic Abrolhos Plateau separates it from the Mucuri Basin to the north. Espirito Santo Basin is a part of the East Brazil Rift system that developed during the Mesozoic breakup of South America and Africa (Chang et al., 1992).

The structural evolution of the basin includes late Jurassic-early Cretaceous pre-rift phase, early Cretaceous rift phase, Aptian transitional phase and Albian to Recent drift phase (Ojeda, 1982). Stratigraphically, the basin is divided into five depositional megasequences that correspond to the structural evolution phases: pre-rift, rift, transitional, transgressive marine and regressive marine (Fiduk et al., 2004). The pre-rift sequence consists of continental sediments deposited in intracratonic basins (Ojeda, 1982). The rift-phase sediments are mainly fluvial, deltaic and lacustrine sediments, dominated by fine to coarse-grained sands, silts and shales. The relative tectonic stability of the Albian transitional phase led to the accumulation of evaporitic succession with some carbonates and lacustrine clastics (Ojeda, 1982). The Albian-Recent drift megasequence overlies a major unconformity formed as a result of rifting (Chang et al., 1992). Since the Albian, a homoclinal shelf-slope morphology was developed, characterized by a lower clastic-carbonate unit and an upper clastic unit (Ojeda, 1982).

Several magmatic events have occurred in the Espirito Santo Basin creating for example the Abrolhos volcanic plateau and the Vitória-Trindade Seamount chain (Chang et al., 1992). Basaltic/andesitic sills and dikes are found within the Basin (Ojeda, 1982), but also extrusive lavas have been inferred to be present (Fiduk et al., 2004).

The basin has been deformed by salt tectonics, growth faulting and inversion along its margin since the Albian (Ojeda, 1982). Aptian-age salt has been deformed into pillow structures, diapirs, rollers, canopies and thrusts (Ojeda, 1982; Jackson et al., 1994). This deformation is ongoing and mainly driven by gravity gliding (Fiduk et al., 2004). Since the Eocene, the Espirito Santo Basin has been a prograding shelf and slope environment (Fiduk et al., 2004). Several canyons have incised into the basin slope and modified the geometry and depositional

evolution of the basin during its development. Today, the Doce River supplies sediment to the basin from the Mantiqueira and Espinhaço mountain chains.

2.3.2 3D seismic reflection data

The 3D seismic reflection data of the Espirito Santo Basin cover an area of 1600 km^2, where the present day water depth is between 35 and 1800 m (Fig. 2.12). The data was collected using 12.5x25 m bin spacing (Fiduk et al., 2004). The sample interval is 2 ms and the record interval is 4 s TWT. The data are zero-phase migrated and displayed with SEG normal polarity so that an increase in acoustic impedance is a black-red-black reflection loop. Lithological or well data were not availablefor this work. Seismic velocities of 1500 ms^{-1} for seawater and 1800 ms^{-1} for the shallow succession were suggested by the data provider (Schultz, CGGVeritas, personal communication) and are used when calculating thicknesses of sediment packages and dips of horizons. The prevailing frequency of the studied, shallow interval is c. 40 Hz. Using the average velocity of 1800 ms^{-1}, the dominant wavelength is c. 45 m and thus vertical resolution in the context of tuning thickness ($\lambda 4^{-1}$) is c. 11 m.

2.3.3 Overview of the data

The dataset is located immediately downstream of the present day shelf break and is dominated by salt diapirs, incised canyons, channels, slumps and debris flows (Fig. 2.12). The shelf break occurs at present day water depth of 100 m. The proximal slope angles are up to 15° and shallow to 1-2° more distally. The salt diapirs deform the seafloor and modify local slopes.

The sub-division of the strata is based on seismic character and the work of Fiduk et al. (2004). A representative seismic traverse across the slope shows the typical seismic facies observed within the dataset, and the division of the stratigraphy into 4 units according to seismic character (Fig. 2.12B).

The Unit 1 is a Palaeocene-Eocene-age, low-amplitude, continuous reflection package that overlies the Cretaceous deposits. The Horizon E/O marking the change from low-amplitude to high-amplitude reflection character between Units 1 and 2 is inferred to be the post middle Eocene or Oligocene unconformity (Fiduk et al., 2004). The high-amplitude character of the reflections of Unit 2 is caused by volcaniclastic material derived from the Abrolhos Plateau

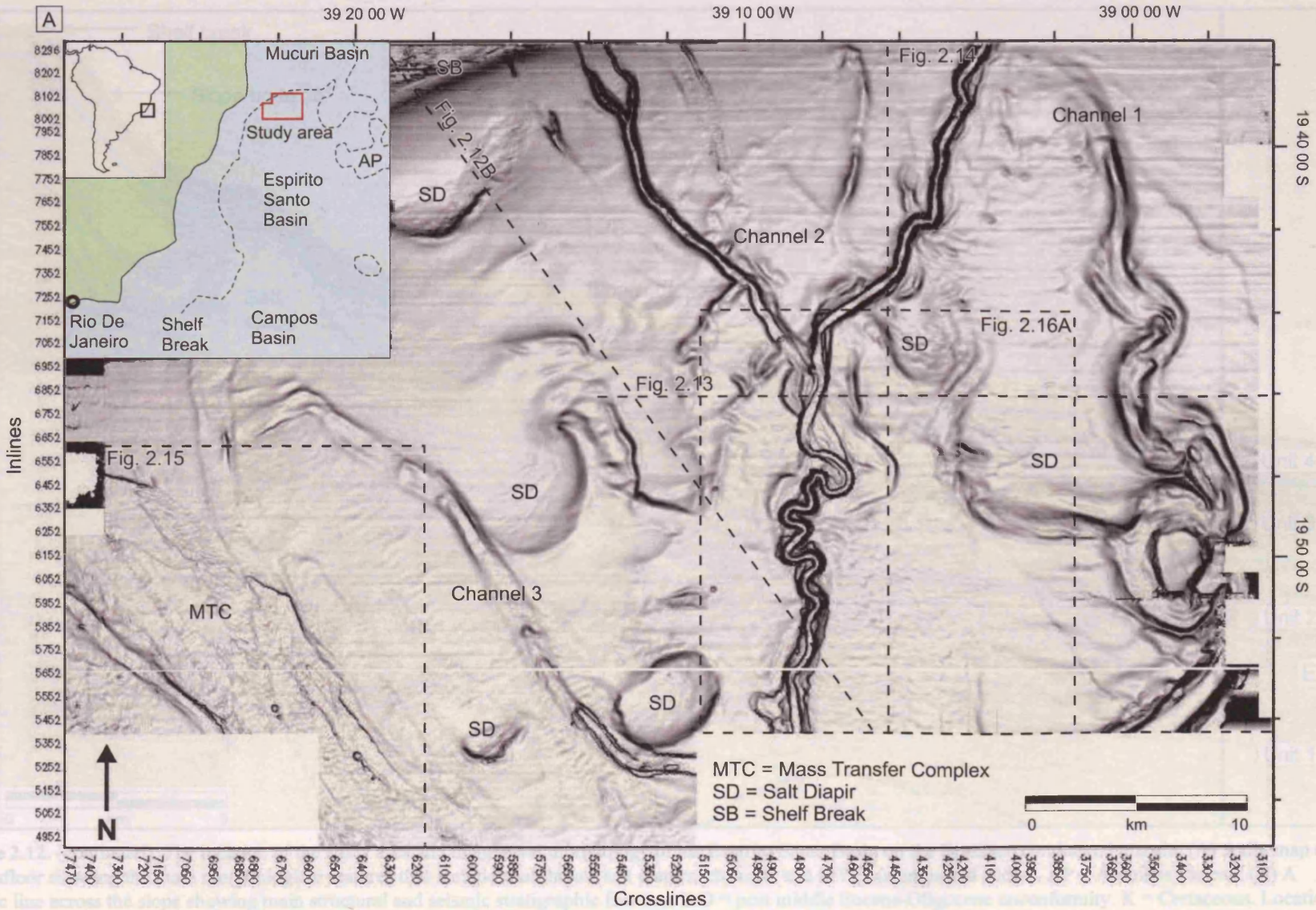

Figure 2.12. (continues to next page).

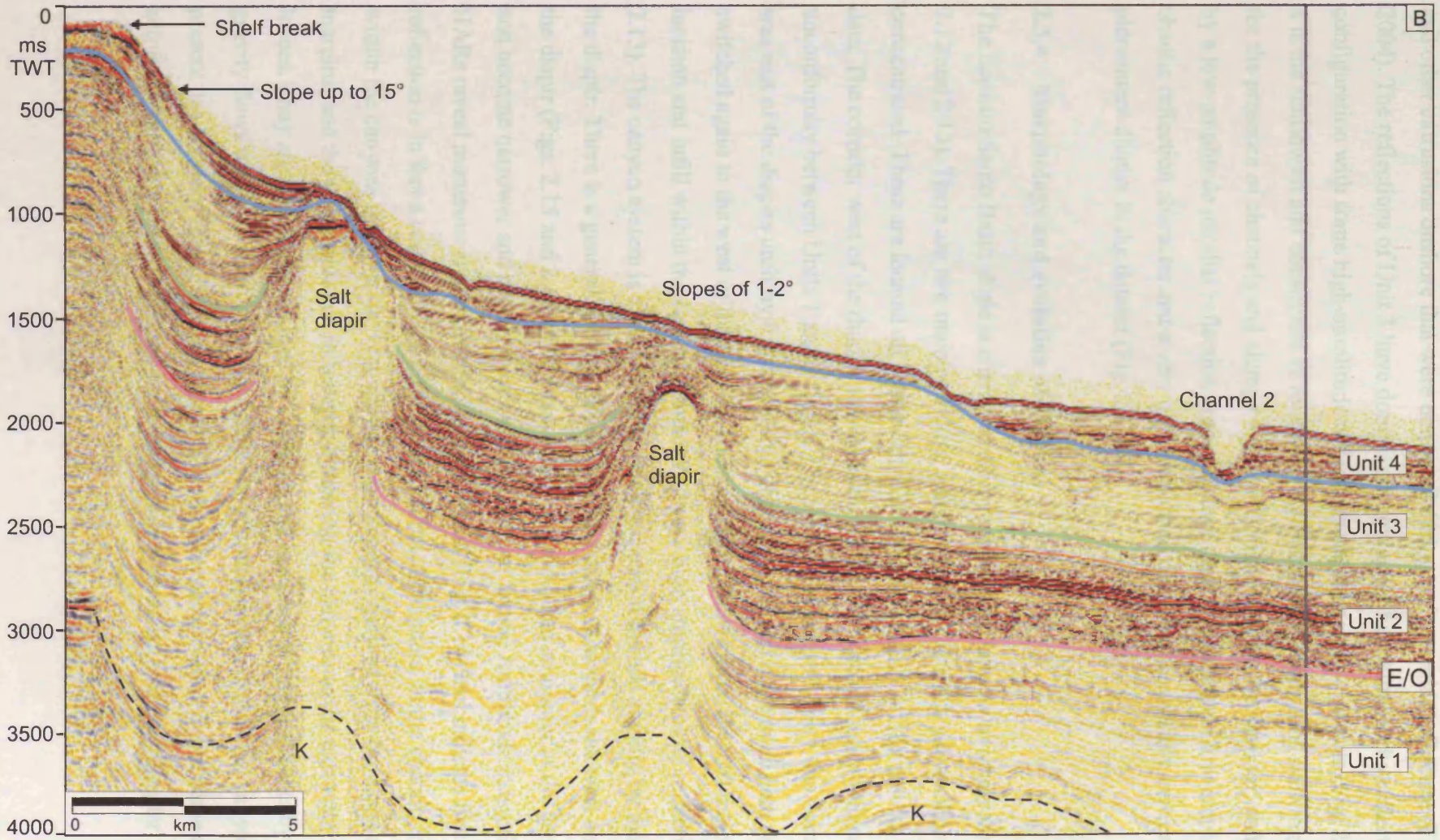

Figure 2.12. (continued). The location of the study area and the general morphology of the Espirito Santo Basin on the Brazilian continental margin. (A) A dip map of the seafloor showing the main morphological features that include shelf break, salt diapirs, channels and MTCs (slumps and slides). AP = Abrolhos Plateau. (B) A seismic line across the slope showing main structural and seismic stratigraphic features. E/O = post middle Eocene-Oligocene unconformity. K = Cretaceous. Location of the Cretaceous-Cenozoic boundary is uncertain.

and other extrusions onshore that were emplaced during early to middle Eocene (Fiduk et al., 2004). The reflections of Unit 3 have dominantly low-amplitude hummocky reflection configuration with some high-amplitude reflections and numerous channels (Fig. 2.12B). Unit 4 is the shallowest and constitutes of relatively high-amplitude reflections showing evidence for the presence of channels and slumps within c. 300 ms beneath the seafloor, and is capped by a low-amplitude parallel reflection drape package. Salt diapirs have a low-amplitude chaotic reflection character and a very high amplitude cap. They are mainly vertical piercement diapirs in the dataset (Fig. 2.12B).

2.3.4 Morphology and evolution of canyons

The Espirito Santo Basin slope is characterised by numerous channels and canyons (Figs. 2.12 and 2.13). There are two main corridors, along which the canyons and channels are concentrated. These are located on both sides of the two salt diapirs on the eastern part of the data. The corridor west of the diapirs was dominant prior to the post Eocene-Oligocene unconformity between Units 1 and 2 (Fig. 2.13). Above the unconformity, the dominant path was east of the diapirs until by the time of the deposition of Unit 4 the main path was switched again to the west of the diapirs. The succession shows more than 10 major phases of incision and infill within the canyon system with very high amplitude basal reflections (Fig. 2.13). The canyon system is almost 1 km in thickness and deformed slightly by the uplift of the diapir. There is a general trend of migration of the canyons towards the west and towards the diapir (Figs. 2.13 and 2.14). The basal HARs are wider and straighter at the deeper level, and become narrower and more sinuous at the shallower levels. Amplitude extractions of the HARs reveal numerous channels within one reflection (Fig. 2.14) and indicate that each reflection is in fact a composite of several, amalgamated channels. Some chaotic reflections within the canyons are most likely mass-transport deposits derived from the slope and canyon margins, and the low-amplitude reflections bordering the canyons to the east resemble inner levees. They are most likely formed by overspill and modification of sediments by sediment-gravity flows within the canyons (Fig. 2.13). The rounded appearance of the canyon on the present day seafloor (Fig. 2.12) suggests that no erosion occurs along it, but some current activity is probably present to form the rounded scours on its surface (see Chapter 5).

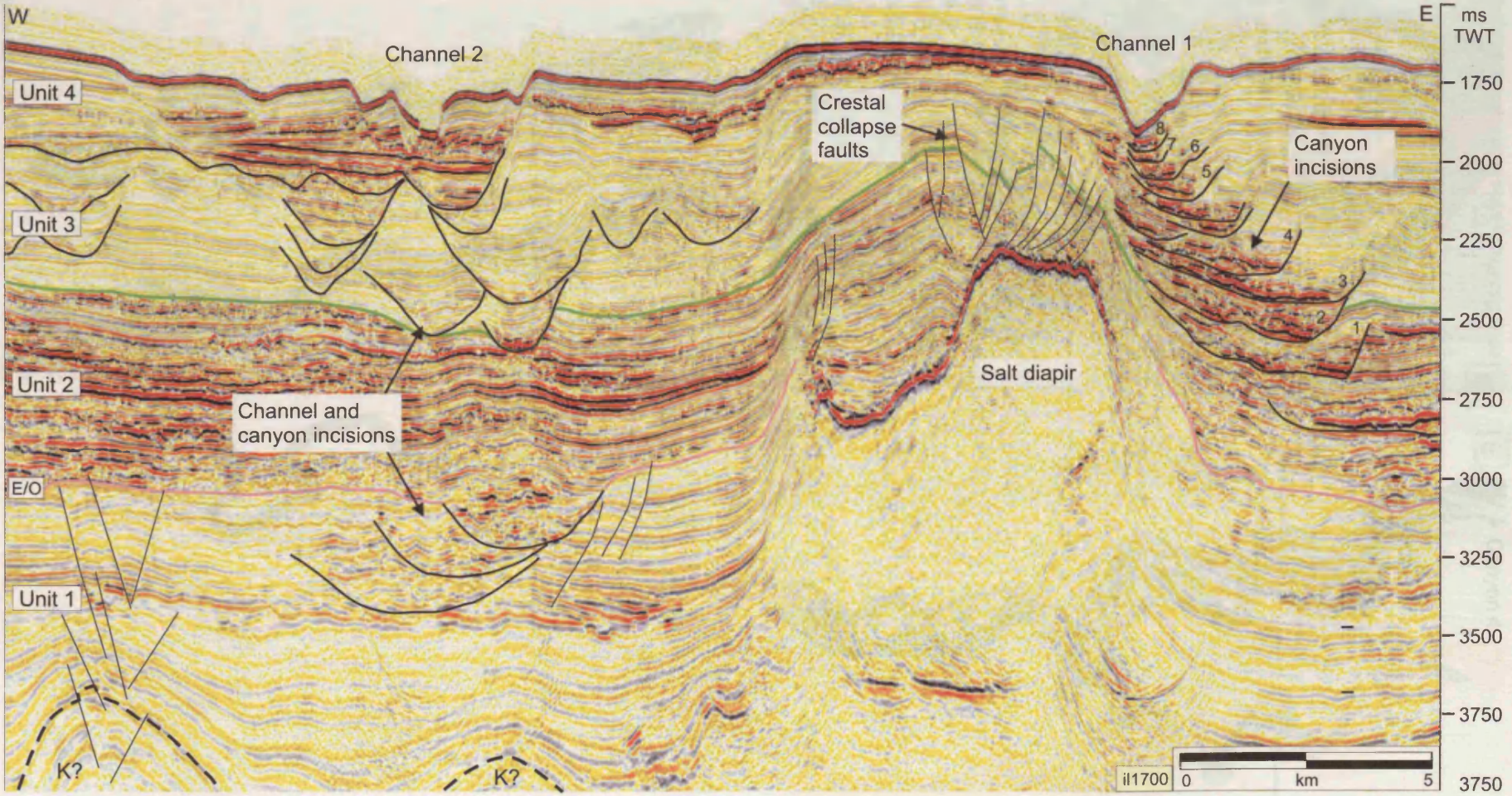

Figure 2.13. A seismic traverse showing the cross-sectional seismic character of the channels and canyons on the Espirito Santo Basin. The canyon system has several phases of incision and infill and has migrated westward. The present day channel 2 shows lateral shift of channel-axis HARs and formation of inner levees. Location of the line in Fig. 2.12A.

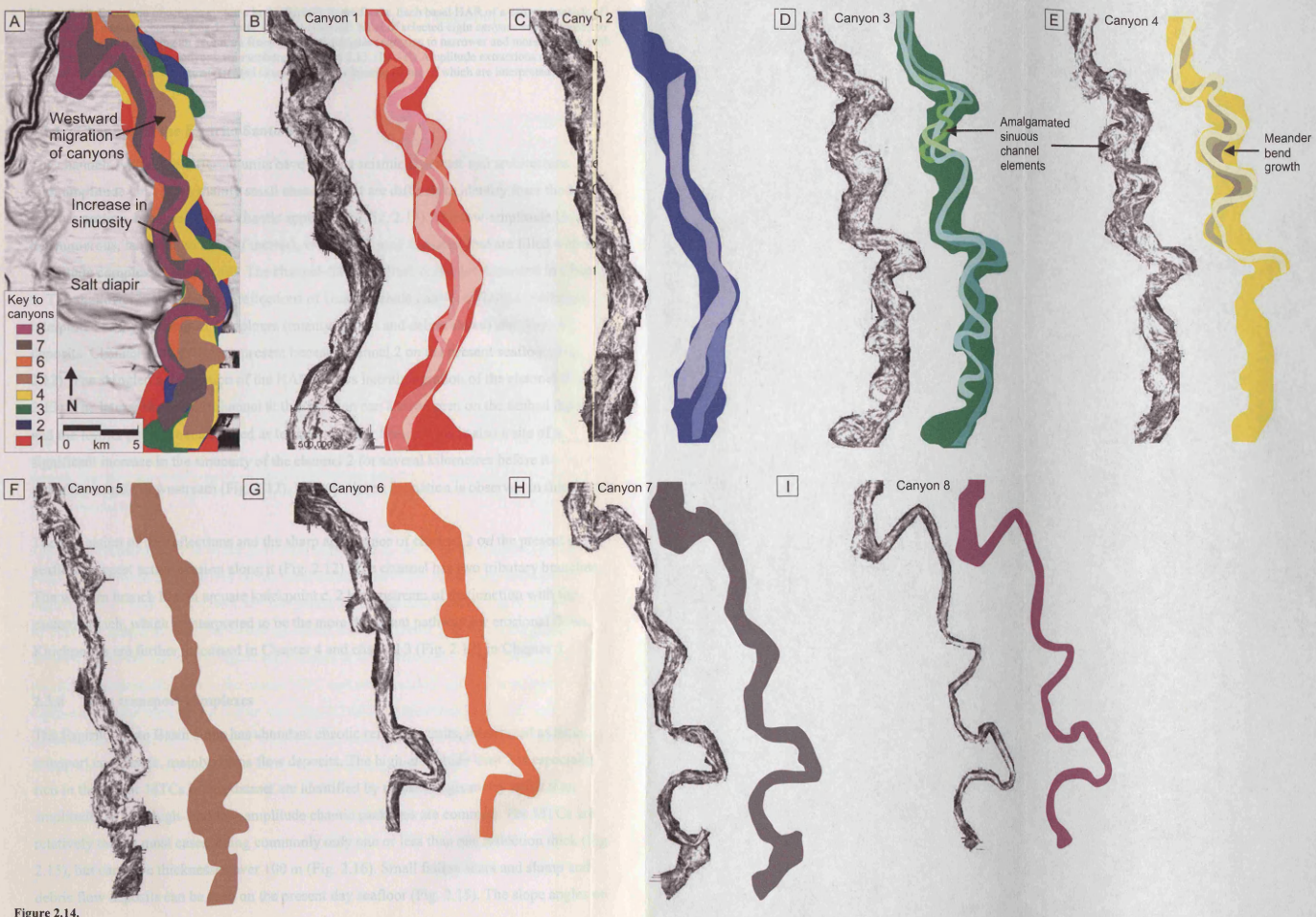
A
Westward migration of canyons
Increase in sinuosity
Salt diapir
Key to canyons
8
7
6
5
4
3
2
1
N
0 km 5
B
Canyon 1
C
Canyon 2
D
Canyon 3
Amalgamated sinuous channel elements
E
Canyon 4
Meander bend growth
F
Canyon 5
G
Canyon 6
H
Canyon 7
I
Canyon 8

Figure 2.14.

Figure 2.14. Evolution of canyon systems in the Espirito Santo Basin. Each basal HAR of a canyon consists of amalgamated sinuous channel-axis deposits. (A) The erosional bases of selected eight canyons superimposed to the seabed dip map showing an evolution from wider and straighter canyons to narrower and more sinuous, with some lateral migration. The canyons are numbered in Figure 2.13. (B) – (I) Amplitude extractions of the basal HAR of the canyons showing amalgamated sinuous channel elements, some of which are interpreted.

2.3.5 Channels in the Espirito Santo Basin

The channels within the different units have various seismic character and architecture. The high-amplitude Unit 2 has mainly small channels that are difficult to identify from the MTCs in cross section, because of their chaotic appearance (Fig. 2.13). The low-amplitude Unit 3 has numerous, large (up to 100s of metres), v- and u-shaped incisions that are filled with low-amplitude complex or chaotic fill. The channel-fill of this unit is further discussed in Chapter 5. The shallower high-amplitude reflections of Unit 4 include chaotic reflection packages, interpreted as mass transport complexes (mainly slumps and debris flows) and channel deposits. Channel-axis HARs are present beneath channel 2 on the present seafloor (Fig. 2.12). The shingled organisation of the HARs shows lateral migration of the channel (Fig. 2.13). The lateral shift of the channel at this location can also be seen on the seabed dip map, and the former paths are manifested as terraces or inner levees. This is also a site of a significant increase in the sinuosity of the channel 2 for several kilometres before it straightens again downstream (Fig. 2.12). No outer levee formation is observed in this dataset.

The truncation of the reflections and the sharp appearance of channel 2 on the present day seafloor suggest active erosion along it (Fig. 2.12). The channel has two tributary branches. The western branch has an arcuate knickpoint c. 2 km upstream of the junction with the eastern branch, which is interpreted to be the more dominant pathway for erosional flows. Knickpoints are further discussed in Chapter 4 and channel 3 (Fig. 2.12) in Chapter 5.

2.3.6 Mass transport complexes

The Espirito Santo Basin slope has abundant chaotic reflection units, interpreted as mass transport complexes, mainly debris flow deposits. The high-amplitude Unit 2 is especially rich in them. The MTCs in this dataset are identified by reflection geometry rather than amplitude, as both high- and low-amplitude chaotic packages are common. The MTCs are relatively thin in most cases, being commonly only one or less than one reflection thick (Fig. 2.15), but can have thicknesses over 100 m (Fig. 2.16). Small failure scars and slump and debris flow deposits can be seen on the present day seafloor (Fig. 2.15). The slope angles on

this part of the seafloor shallow from approximately 2.5° to 1.7°, suggesting the slope angle is not an important factor for failures to occur in the study area.

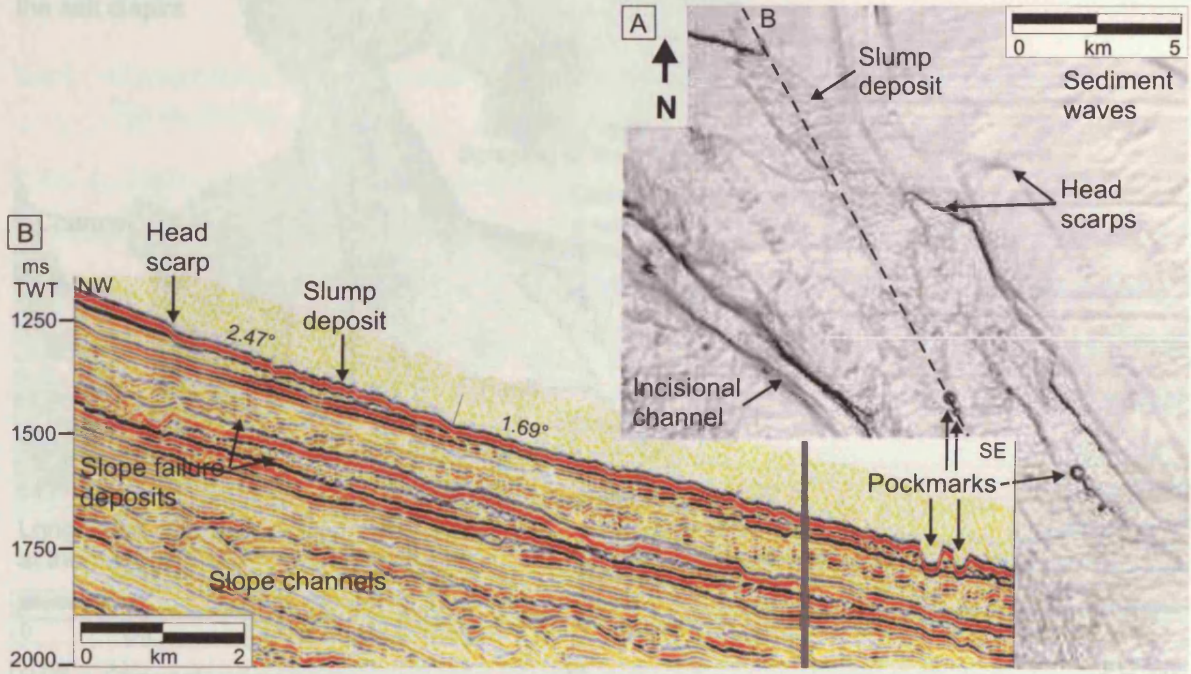

Figure 2.15. Slope failure features near the seafloor on the slope of Espirito Santo Basin. (A) Sea floor dip map showing steep head scarps and irregular surface of MTCs (slump deposits). See location in Figure 2.14A. (B) A seismic traverse showing the cross-sectional expression of a slope failure with a head scarp and a thin deposit with an irregular top surface.

The transport paths of some of the MTCs are controlled by the slope structure. The transport path can be indicated by grooves on the basal surface that curve around and between the salt diapirs (Fig. 2.16A). The grooves are interpreted to have formed by scouring of the seafloor by coherent blocks of sediment within the debris flow. A seismic line across the deposit shows the grooves and also irregular top surfaces of the debris flows (Fig. 2.16B). The parallel reflections adjacent to the lowest MTC unit are truncated, and that truncation may represent a lateral margin of a failure scar (Fig. 2.16B). All the subsequent high- and moderate-amplitude reflections and the MTCs are confined within this corridor, and the strata is undisturbed to the east of it, as if in the 'lee' of the large salt diapir.

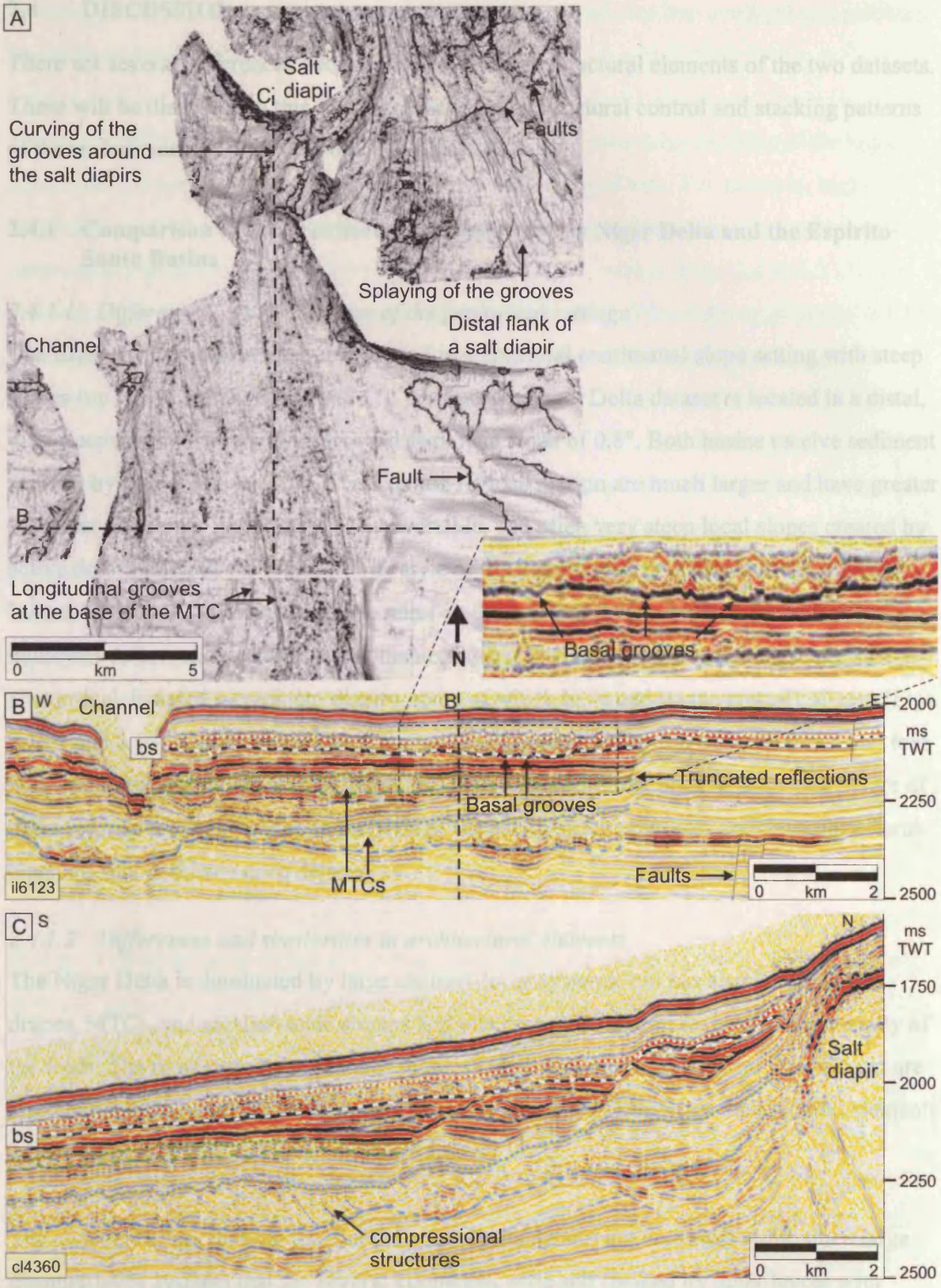

Figure 2.16. Mass transport complexes on the slope of the Espirito Santo Basin. (A) A dip map of a basal surface of a MTC (marked bs in B and C) showing longitudinal grooves that curve around the salt diapirs. See location in Figure 2.14A. (B) Seismic line across the MTC showing the grooves at its base in cross-section. Several MTCs are confined within this corridor. (C) A seismic line showing the cross section along the MTCs. The lowest one shows some internal compressional structures.

2.4 DISCUSSION

There are several differences and similarities in the architectural elements of the two datasets. These will be discussed in this section, as well as the structural control and stacking patterns of these elements and the sinuosity of the channels.

2.4.1 Comparison of the architectural elements of the Niger Delta and the Espirito Santo Basins

2.4.1.1 Differences and similarities of the geological settings

The Espirito Santo Basin dataset is located in a proximal continental slope setting with steep slopes (up to 15° but shallowing to 1°), whereas the Niger Delta dataset is located in a distal, ultra-deepwater delta environment with shallower slope of 0.8°. Both basins receive sediment sourced by rivers, however, the rivers on the African margin are much larger and have greater sediment discharge. Both datasets have variable, and often very steep local slopes created by active deformation of the seafloor. The style of the deformation is different in the different basins, but both styles create positive relief on the seafloor. In the Espirito Santo Basin, the dominant deformation process is salt diapirism, and the majority of the diapirs in the dataset are vertical, isolated piercement diapirs, some of which have undergone crestal collapse (Figs. 2.12B and 2.14). On the Niger Delta, the seafloor is deformed by toe-of-slope thrust and fold belt, which creates ridges normal to the sediment transport direction (Fig. 2.5). The nature of these settings has significance to the style of the sedimentary processes and the architectural elements that dominate each dataset.

2.4.1.2 Differences and similarities in architectural elements

The Niger Delta is dominated by large channel-levee systems, but has also hemipelagic drapes, MTCs, and smaller-scale slumps and other resedimentation features in the vicinity of the folds. The most prominent features in the shallow section of the Espirito Santo Basin are also channels, however, slope failures and MTCs are equally important architectural elements in this dataset, as well as are hemipelagic drapes.

The channels at the shallow level of the Niger Delta dataset are confined within three large channel-levee systems that are several kilometres wide and flanked by outer levees with sediment waves (Figs. 2.4 and 2.5). The channel-fill elements are complex, and include channel-axis HARs, chaotic and passive fill facies, and a number of inner levees. In the Espirito Santo Basin, many small gullies and tributary channels dominate, due to the

proximity of the shelf break and the steep slope. The channels are less confined and no outer levees have developed.

There are some similarities between the channel 2 on the present day seafloor of the Espirito Santo Basin (Figs. 2.12 and 2.13) and the CLSs on the Niger Delta. For example, high-amplitude channel-axis deposits show lateral migration of the channel locally, and inner levee terraces have been formed above previous incisions of the channel (Figs. 2.4 and 2.13). The thalweg of the channel 2 is c. 100 m wide, whereas the width of the thalweg of the Ijebu CLS on the Niger Delta is c. 80 m. Both datasets show evidence of several phases of channel incision and infill.

Although the smaller channels in the Espirito Santo Basin are not confined within levees as on the Niger Delta, some confinement also occurs, and channelised deposits form stacks hundreds of metres thick (Fig. 2.13). The best example of these very long-term sediment transport pathways, active from at least the Oligocene to the Present, is the canyon system on the eastern part of the dataset that has over 10 major phases of incision and erosion. The high-amplitude basal reflections are several kilometres wide and consist of amalgamated ribbons of channel-axis deposits. Mass transport deposits also fill parts of these canyons. This architectural element is found only within the steep slopes of the Espirito Santo Basin, although the basal HARs within the CLSs of the Niger Delta are similar in scale and seismic character.

The mass transport complexes have similar, low-amplitude chaotic seismic character in both datasets, however, also high-amplitude MTCs are identified in the Espirito Santo Basin. The MTCs on the Niger Delta are tens of metres thick and not very common. They occur as extensive sheets or are channelised, most likely plugging existing channel scours within the CLSs (Figs. 2.10 and 2.11). In the Espirito Santo Basin, the MTCs are in general much thinner, although some deposits of several tens of metres thickness are also found. The areal extent of the MTCs in the Espirito Santo Basin is much smaller than on the Niger Delta, but the frequency of their occurrence is much higher (Figs. 2.13, 2.15 and 2.16). They can be defined more easily with more features clearly visible, such as erosional grooves on their basal surfaces. In many cases, the whole feature including slump scar and the related deposit can be identified (Fig. 2.15). Small slope failures like this occur also in the Niger Delta dataset, but they are restricted to the fold limbs (see Chapter 3). The MTCs in both datasets

exhibit some internal structures, interpreted as imbricate thrusts and pressure ridges, and have erosional bases and blocky top surfaces. Therefore it can be suggested, that the processes that formed them are similar, regardless of the differences in settings and scales. The more proximal location and steep slopes of the Espirito Santo Basin make slope failure more likely, and the features better defined due to shorter transport distances.

2.4.2 Structural control on sedimentary systems

Both pre-existing and actively deforming structures have an influence on sediment dispersal patterns and style. The data described in this chapter reveal several examples, where sedimentation is controlled by structure. On the Niger Delta, the Ijebu and Epe CLSs appear to breach through the middle of the frontal fold and the Iwo CLS is deflected southward away from it (Fig. 2.5). The location of the CLSs is not coincidental, however. A transfer zone that coincides with the major Chain Fracture Zone has affected the positioning of the CLSs in the dataset (Morgan, 2004). Furthermore, the location, where the fold is breached by the channels, is the location where the underlying thrust faults change vergence (see Fig. 4.2), and was therefore likely a weak or a low point in the early growth history of the fold, and thus a preferred path for the channels to be positioned. The isoproportional slicing through the CLSs revealed that the deflection of the Iwo CLS by the fold occurred at a late stage of its evolution (Fig. 2.9), and this is interpreted to be as a response of higher uplift rate of the northern part of the fold. The location of the frontal splay was also most likely controlled by structure, based on the observation that in the early stages of the Epe CLS evolution, it was located immediately outboard of the frontal fold, where there was likely a significant break in slope.

Some of the sediment pathways in the Espirito Santo Basin are also clearly influenced by structure. The salt diapirs themselves are located on anticlinal ridges that are orientated in the downslope direction. The channels and the canyon system have been concentrated within the structural lows between these ridges at least since the Eocene (Fig. 2.14). Sediment-gravity flows preferably travel down the path where the slope is steepest. This is well illustrated by the scours at the base of a MTC that curve around the salt diapirs (Fig. 2.15A).

Although minibasin development and ponding of sediment within them is not prominent in either of the datasets, the highest accumulation of sediments is concentrated in the accommodation space created by the structures on both datasets. The synclines between the anticlines on the Niger Delta can have very thick accumulations of sediment (Fig. 2.5 and

Chapter 3), and the development of salt-cored ridges in the Espirito Santo Basin most likely also resulted in the formation of synclines due to salt withdrawal between them, which concentrated the sediment-gravity flows within these structural lows.

2.4.3 Sinuosity of the submarine channels in the study areas

The mechanisms by which sinuosity is established in submarine channels are still being discussed in the literature (Eschard, 2001). The observations of channel sinuosity from the two datasets are discussed below in the context of (1) slope gradients, (2) types of sinuosity and (3) sinuosity evolution. The observations from the Espirito Santo Basin are mainly qualitative, but quantitative observations were made in the Niger Delta dataset.

2.4.3.1 The effect of slope gradients on sinuosity

Deepwater channel migration and sinuosity evolution are complex and sometimes related to sea floor topography. Generally, straight and low sinuosity channels suggest an originally steep slope gradient, whereas higher sinuosity channels form on lower gradients (Fonnesu, 2003; Posamentier and Kolla, 2003).

The effect of slope gradients on sinuosity can be best observed in the Espirito Santo Basin, where the slope gradients change dramatically within the data area. The channels exhibit low sinuosities, where the slope gradients are several degrees, but when the gradient shallows to 1-2°, several prominent meander loops develop along the Channel 2 (Fig. 2.12).

On the Niger Delta, the slope gradient does not appear to affect the present day thalweg sinuosity. The measurements of the sinuosity of the thalweg show no real correlation with slope angles (Fig. 2.6). Two peaks of high sinuosity occur just outboard of folds that have moderate or high topography on the present day seafloor, however, this is more likely to be a coincidence rather than a real relationship, because the rest of the data does not exhibit predicted relationships. The slope gradient may have had some effect on the sinuosity of the channels in the Niger Delta in the earlier stages of their development. The terraces formed on abandoned meander bends are most abundant and largest within the uplifted part of the Ijebu channel-belt, suggesting that the lower gradients caused by the uplift affected the development of high sinuosity at earlier stages of the CLS, when the channels were less confined (e.g. Fig. 2.7).

2.4.3.2 Types of sinuosity

Sinuosity is not just a function of gradient, but it is due to a combination of factors including erosion from turbidity currents, lateral shifting and stacking of channels due to channel filling and incision (Mayall and Stewart, 2000; Mayall et al., 2006). There are several different types of sinuosity, and they have impact on sand distribution within channels (Mayall et al., 2006). Mayall et al. (2006) recognise four categories of sinuosity: (1) initial erosional base, (2) lateral shifting, (3) lateral accretion and (4) sinuosity caused by seafloor topography, e.g. faults and folds.

The erosional fairways of the channel-levee systems on the Niger Delta exhibit low sinuosity, however, the channel-axis deposits within them have high sinuosities (Fig. 2.9). Similar observations can be made from the canyon systems in the Espirito Santo Basin (Fig. 2.14). The sinuosity of the canyons increase as they become younger, however, the channels within the canyons are sinuous throughout the evolution of the canyon system. The sinuosity of these channels and the channels within the CLSs of the Niger Delta seem to be mainly increased by lateral migration and shifting of the channels. Meander bend cutoff decreases sinuosity and produces accommodation space for terraces and inner levees (Fig. 2.7). Meander bend cutoffs are not as common in submarine channels as in their subaerial counterparts (Peakall et al., 2000b; Posamentier and Kolla, 2003). They may have been more common within the Ijebu CLS during times when the channels were less confined, however, evidence of meander bend cutoff can also be observed on the present day seafloor (Fig. 2.17).

The seafloor topography affects the sinuosity of the channels to some extent in both of the datasets. The morphology of the Ijebu CLS changes above the thrust and fold belt (Fig. 2.6). That region has more and larger terraces that were formed by abandonment of large meander bends (Fig. 2.7). Their formation may have been due to the increase in sinuosity on lower gradients that were created by the uplift of the fold belt, or the channel location may have been affected by the emerging folds on the seafloor. This kind of correlation between the seafloor topography and the quantitative measurements of the present day thalweg cannot be made, neither do the present day meander bends correlate to any underlying folds or faults. Some meander bends on a near-seafloor channel of the Espirito Santo Basin appear to be controlled by the location of the salt diapirs, however (Fig. 2.12).

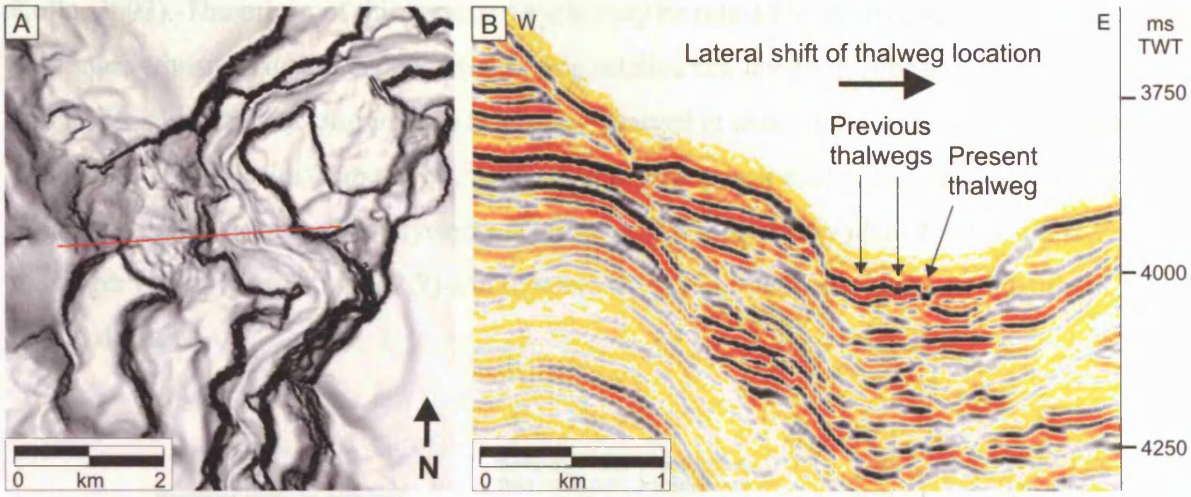

Figure 2.17. Meander bend cutoff at the present day thalweg of the Ijebu CLS, Niger Delta. (A) A dipmap of the seafloor showing the straightening of the present day thalweg in two steps moving eastward. See location in Figure 2.4B. (B) A seismic traverse across the thalweg showing the present course of the thalweg being deeper than the abandoned ones.

2.4.3.3 Sinuosity evolution

The evolution from straight to sinuous is common in submarine channels that have an aggradational history (Kastens and Shor, 1986; Clark and Pickering, 1996; Peakall et al., 2000a; Wonham et al., 2000; Kolla et al., 2001; Deptuck et al., 2003). Peakall et al. (2000a) proposed a three-stage model for the evolution of high-sinuosity aggradational submarine channels. In this model, lateral accumulation and bend growth occurs, until an equilibrium phase is reached. The channel then has a stable planform geometry aggrading nearly vertically until abandonment. As Peakall et al. (2000a) anticipated, this process model may not apply to all submarine channels, as it was derived from aggradational channels, and this kind of evolution is indeed not observed in the channels of the Niger Delta or Espirito Santo basins, except for perhaps in the large scale evolution of the canyon system in the Espirito Santo Basin (Fig. 2.14). It evolves from straight and wide to narrow and sinuous, however, this may be more analogous to the typical evolution of channel-levee systems from wide, erosional fairways to narrow, confined channels, which is also observed in the Niger Delta CLSs, and which Deptuck et al. (2003) interpreted to reflect the changes in gravity flow character, such as velocity and magnitude (Posamentier and Kolla, 2003).

2.4.4 Stacking patterns and facies prediction

Deep-water successions have commonly predictable stacking patterns with mass-transport deposits at the base, overlain by frontal splay deposits and leveed-channel deposits, and finally draped by condensed-section deposits (hemipelagites and pelagites) (Posamentier and

Kolla, 2003). The origin of this repeated cycle may be related to relative sea-level changes with mass-transport deposits deposited during relative sea-level fall (Posamentier and Kolla, 2003). This kind of stacking pattern has been observed at least in the Amazon (Posamentier and Kolla, 2003), Zaire (Droz et al., 2003), Danube (Popescu et al., 2001) and Sao Tomé (Viana et al., 2003) deepwater systems. This pattern is also clearly identifiable on Epe CLS of the Niger Delta (Figs. 2.5 and 2.9) and to some extent, but not completely, by the other CLSs in that dataset.

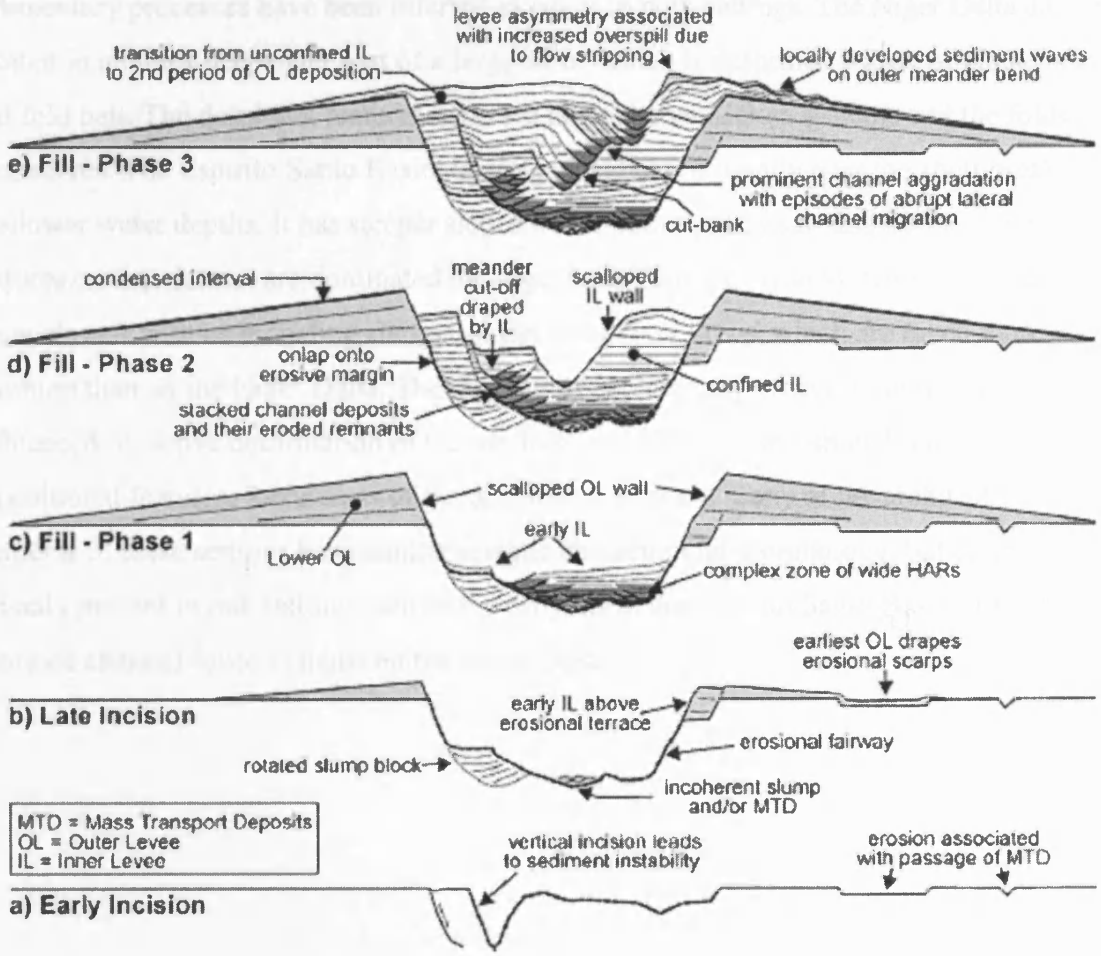

Figure 2.18. Evolutionary stages of Benin-major channel-levee system showing several phases of incision and infill (Deptuck et al., 2003).

The key characteristic of the Ijebu CLS is that it has undergone several phases of incision and infill that have produced a complex stacking pattern within the channel-belt. Erosion, infill and abandonment is a typical evolution path of submarine channels and occurs repeatedly (e.g. Hübscher et al., 1997; Posamentier and Kolla, 2003). The evolution of a submarine channel-levee system with both erosional and depositional components and that is comparable

to the CLSs on the Niger Delta, is described by Deptuck et al. (2003) (Fig. 2.18). The evolution of the CLS starts with the incision of a channel fairway, continues with levee building and infilling of the channel-belt with channel-axis deposits and inner levees until abandonment by a mass transport deposit plugging the remaining depositional relief.

2.5 CONCLUSIONS

The two 3D seismic datasets from opposite margins of the Atlantic Ocean are located in differing structural, stratigraphic and slope-morphological settings, however, similar sedimentary processes have been inferred to occur in both settings. The Niger Delta dataset is located in an ultra-deepwater part of a large delta, which is deformed by toe-of-slope thrust and fold belt. The dominant features there are large channel-levee systems and the folds themselves. The Espirito Santo Basin dataset is located proximally near the shelf break at shallower water depths. It has steeper slopes and is deformed by salt diapirs. Sedimentary features on that dataset are dominated by large, long-lasting canyon systems and small slope channels and failures including slumps, slides and debris flows, which are much more common than on the Niger Delta. The downslope sedimentary processes in both datasets are influenced by active deformation of the seafloor, and both datasets show both erosional and depositional features. Regardless of the differences in scale, many of the architectural elements of these settings have similar seismic character and morphology, but certain features are only present in one setting, such as the canyons in the Espirito Santo Basin or the large, confined channel-levee systems on the Niger Delta.

Chapter 3

3 DEGRADATION OF COMPRESSIONAL FOLD BELTS: DEEPWATER NIGER DELTA

3.1 ABSTRACT

3D seismic interpretation of the toe-of-slope region of the western Niger Delta reveals a range of erosional and depositional features that are the result of the degradation of thrust-propagation folds and include (1) backlimb and forelimb failures that cause debris flows and deposits no more than a few tens of metres thick, (2) large slumps with evidence for internal deformation, (3) more enigmatic ovoid depressions, probably formed as a result of slumping and bottom current erosion and (4) degradation by deepwater channel erosion and channel margin slumping. Thrust-propagation folds in the study area have up to 200 m of relief on the seafloor and are at various stages of degradation and burial. The dominant style of degradation of these folds occurs as retrogradational, small volume failures that form thin deposits at or below seismic resolution. Slope morphology, sedimentology and the presence of anisotropies affect the type of failure that occurs. The backlimb is long and shallow (6°), and the failed sediment masses have longer runout distances than on the forelimb, which has a steeper slope (15°), which abruptly shallows causing the flow velocity to drop. A generic model for fold degradation in this submarine setting is synthesised, and it is predicted that a significant proportion of the sediment deposited in adjacent minibasins has been recycled from the fold crests and is a non-reservoir. Stratigraphic variability means that along-strike and across-fault correlation of deposits and erosional surfaces is difficult at shallow level and highly problematic in buried, potentially prospective, degraded folds.

3.2 INTRODUCTION

Compressional fold belts that typify foreland basins, accretionary wedges and the toe-of-slopes of deltas are a fundamental component of many sedimentary basins. These basins undergo significant modification during fold growth as folds create local relief, and slopes with increased gradients become prone to failure. Fold and thrust belts in deepwater continental passive margins are the focus of recent hydrocarbon exploration, e.g. in Nigeria (Morgan, 2003), Angola (Cramez and Jackson, 2000), Gulf of Mexico (Grando and McClay, 2004), northwestern Borneo (Demyttenaere et al., 2000; McClay et al., 2000; Ingram et al., 2004) and East Kalimantan (Saller et al., 2004). Compressional anticlines are targets for exploration boreholes, and therefore the seismic-based recognition of unconformities formed

by fold degradation and remobilised sediment deposits adjacent to the fold limbs is important. Furthermore, submarine landslides and other types of slope failure are potential hazards for offshore installations.

In submarine slope settings, there is a continuum of gravity-driven resedimentation processes, ranging from rock falls to slumps and slides to viscous debris flows and dilute turbidity currents to pelagic settling (Stow, 1986). Several authors have described and classified these processes (Varnes, 1978; Stow, 1986; Mulder and Alexander, 2001; Lastras et al., 2004). The shear strength of the slope sediment is a function of the cohesion between the grains and the intergranular friction (Stow, 1986), with failure occurring once the shear stress exceeds it. Sediment properties, such as chemical composition, cohesion, and angle of internal friction and the presence of free gas or gas hydrates also affect slope stability (Nigro and Renda, 2004).

Submarine slope failures have common features that are independent of scale. Arcuate headwall scarps commonly form at the upslope reach of a failure and often grade or transform abruptly into a listric shear surface (Varnes, 1978; Prior and Coleman, 1982; Lastras et al., 2004). These shear surfaces often have a lower dip than the seafloor and therefore intersect it (Mello and Pratson, 1999). A scar is left behind if the failed sediment mass is mobilised post-failure and moved downslope. The failed mass, if coherent, commonly exhibits evidence for extensional deformation near the scarp and compressional deformation, such as pressure ridges, near the toe of the deposit. In some cases, blocks of sediment become detached from the main mass of failed sediment and glide further down the slope, forming outrunner blocks (e.g. Lastras et al., 2004). Failed sediment masses are identified from seismic data on the basis of their low-amplitude chaotic reflection pattern (Lastras et al., 2004; Frey Martinez et al., 2005).

Three-dimensional seismic data acquired by the hydrocarbon industry over the compressional domain of the deepwater West Niger Delta allow for the first detailed analysis of the seafloor and subsurface expression of degradation complexes associated with submarine folds. The term "degradation complex" has been used to describe the collapse of footwalls of extensional fault scarps in the North Sea, United Kingdom (Underhill et al., 1997; Berger and Roberts, 1999; McLeod and Underhill, 1999). Given the difficulty in objectively defining the actual

process or processes from seismic data, this term is adopted here, as it encapsulates all modes of sediment failure, transport and deposition in these settings.

The aims of this chapter are to (1) define and describe a range of features that form during fold degradation, (2) illustrate their three-dimensional complexity and the variety of resedimentation styles, (3) demonstrate the role of pre-existing structure and slope morphology in degradation complex development, (4) speculate on the transport mechanism on the basis of specific, objective observations, such as seismic geometry and a general knowledge of sediment properties and (5) synthesize a general model for the evolution of fold degradation phenomena in this geological setting. Subsequently, the chapter provides information essential for understanding the stratigraphic results of to-be-drilled exploration, development and production boreholes that target deepwater compressional folds.

3.3 PREVIOUS STUDIES OF FOLD DEGRADATION

Submarine failures have been widely studied on continental slopes (Prior and Coleman, 1982; Hampton et al., 1996; Locat and Lee, 2002; Canals et al., 2004; Lastras et al., 2004; Sultan et al., 2004; Frey Martinez et al., 2005). Degradation of growing folds, however, has been studied mostly in subaerial depositional settings, where the sedimentary processes can be observed and the key variables measured (Burbank and Raynolds, 1988; Steidtmann and Schmitt, 1988). Folds in subaerial settings are commonly lithified and predominantly degraded by stream erosion and are thus not comparable to submarine settings. Submarine fold degradation has been recognised by previous workers, who have proposed a number of geometric and numerical models to quantify the evolution of compressional structures and the associated syntectonic growth strata that develop on their flanks (Hardy and Poblet, 1995; Storti and Poblet, 1997; Rafini and Mercier, 2002). Many of these models, however, concentrate on fold kinematics and simplify sedimentation and erosion processes and the depositional products. Outcrop analysis of slope degradation and resedimentation caused by fold growth generally allow for a detailed understanding of these depositional products (Nigro and Renda, 2004), but is generally limited by the two-dimensional nature and limited scale of the exposures. Evidence for slumping and other mass wasting of submarine growth folds have been identified e.g. in North Sea (Cartwright, 1989) and northwestern Borneo (Ingram et al., 2004). Nevertheless, to our knowledge, the three-dimensional morphology and stratal geometries created by the degradation of compressional folds in submarine settings at scales from tens of metres to kilometres, have not been described elsewhere.

3.4 GEOLOGICAL SETTING

The Niger Delta is a 12 km thick, regressive Cenozoic delta on the West African passive margin. It is a prolific hydrocarbon exploration and production area, generating increasing interest in the deepwater and the ultradeepwater domains of the delta slope in the past 5-10 years. The Akata, Agbada and Benin Formations (e.g. Doust and Omatsola, 1990; Damuth, 1994; Morgan, 2004) overlie stretched continental and oceanic crust. This article focuses on the ultradeepwater compressional domain of the western Niger Delta (Fig. 3.1A), where the Agbada Formation comprises deepwater channel-levee systems, mass transport complexes and hemipelagic sediments (Deptuck et al., 2003). The delta is divided into three structural domains: (1) an extensional domain dominated by growth faults, (2) a translational domain characterised by mud diapirism and (3) a compressional domain dominated by toe-of-slope thrusts (Fig. 3.1B). This structural configuration is caused by gravitationally-driven delta tectonics, where the Agbada Formation is collapsing on a detachment within the Akata Formation (e.g. Damuth, 1994; Cohen and McClay, 1996; Morgan, 2004).

3.5 DATA AND METHODS

The 3D seismic dataset covers an area of 1630 km^2. It is zero-phase migrated and displayed so that an increase in acoustic impedance is a red-black-red reflection loop. The line spacing is 12.5 m in both inline and crossline direction. For the conversion of two-way-travel time (TWT) to depth, a velocity of 1480 ms^{-1} is used for seawater and 2000 ms^{-1} for sediment. The frequency of the studied shallow section is 55 Hz, and thus the tuning thickness (and thus the maximum vertical resolution) is c. 9 m. It is important to note that the frequency changes with depth, thus buried and older structures would have different geometry. The succession is subdivided using seismic reflections that define units that have distinct internal seismic facies. Seismic attributes, including reflection dip and amplitude, were used to reveal depositional and deformational features.

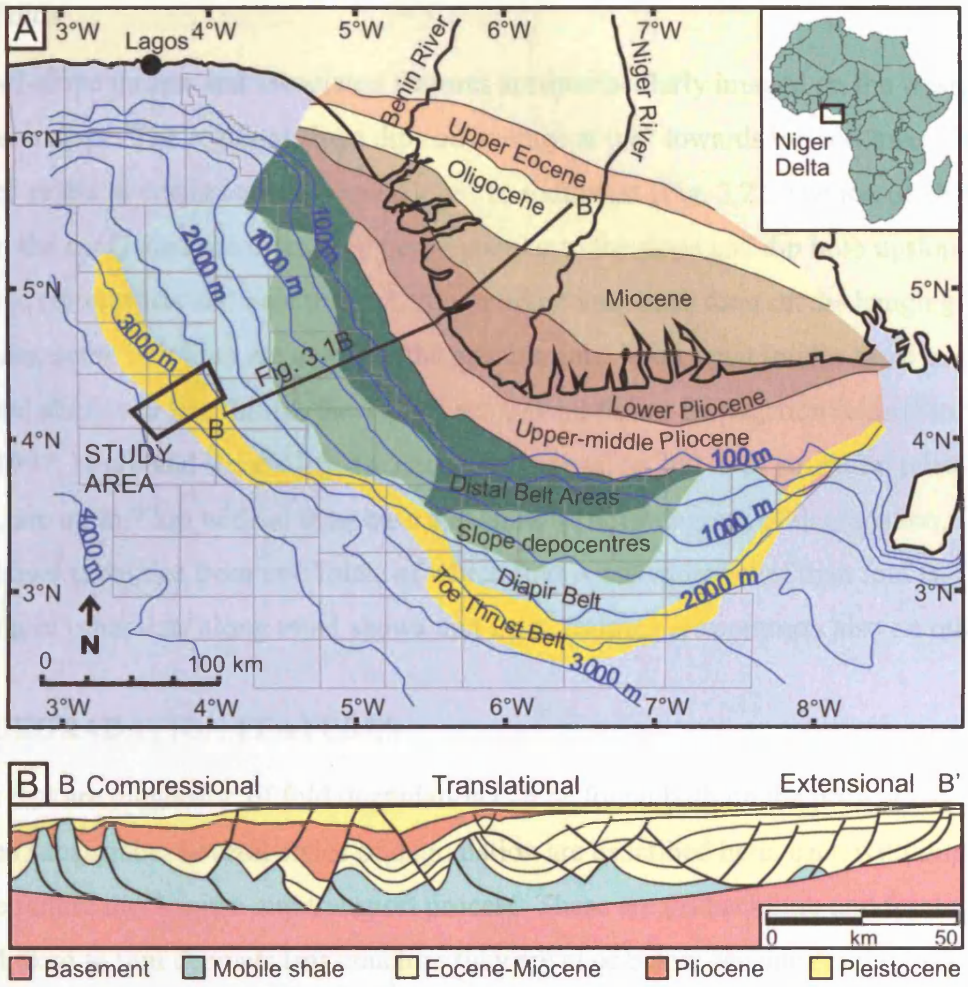

Figure 3.1. (A) Location of the study area in the compressional toe-of-slope thrust belt of western Niger Delta. Depobelts from Armentrout et al. (2000) and Hooper et al. (2002). (B) Simplified schematic cross-section from delta-top to deepwater, after Haack et al. (2000). Vertical exaggeration = 2.

3.6 SEISMIC FACIES AND ARCHITECTURAL ELEMENTS

Typical architectural elements and seismic facies of submarine slopes have been described elsewhere (Deptuck et al., 2003; Posamentier and Kolla, 2003). The lithological interpretation of the seismic facies in this article follows this earlier work and is based on the recognition of seismic reflection character and geometry, as well as unpublished well calibrations within the deepwater domain. The main seismic facies and architectural elements relevant to this study are: (1) low- to high-amplitude, continuous reflections, which can have subparallel, hummocky or divergent geometry and are interpreted as levee deposits and hemipelagic drape and (2) low-amplitude chaotic reflection packages, which are typical of mass transport complexes. High-amplitude channel-fill elements are also very common. A high-amplitude reflection that cross-cuts stratal reflections is noted in the dataset. This bottom simulating reflection (BSR) is considered to be caused by the base of gas hydrate.

3.6.1 Folds

The toe-of-slope thrusts and associated features are spectacularly imaged on the western Niger Delta slope. The regional slope dips on average at 0.8° towards the southwest, therefore "upslope" refers to northeast and "downslope" to southwest (Fig. 3.2). The toe-of-slope thrusts in the study area are orientated perpendicular to the slope and dip both upslope and downslope (forethrusts and backthrusts). Asymmetric anticlines form on the hangingwalls of these faults, some of which are active at the present time. With steep forelimbs adjacent to the thrusts and shallower backlimbs, these folds are typical thrust-propagation folds (Storti and Poblet, 1997; Nigro and Renda, 2004). The folds have up to 200 m of structural relief on the seafloor, are up to 7 km wide at their base and show various degrees of degradation. This article shows examples from two folds, of which fold A has more relief than fold B. Inspection of other data along trend shows that these features are common also on other folds.

3.7 DEGRADATION FEATURES

Features that are diagnostic of fold degradation can be found both on the present day seafloor and in the subsurface. Several styles of degradation are described here, each with implications for slope failure mechanism and transport process. These are (a) backlimb and forelimb failures linked to thin deposits (inasmuch as they are at or below seismic resolution and up to 50 m thick), (b) slumps that show clear evidence for internal deformation and relatively short transport distances, (c) failures associated with ovoid depressions, the interpretation of which remains enigmatic and (d) degradation by deepwater channel erosion and associated channel margin collapse. The creation of erosional truncation surfaces is common to all styles.

3.7.1 Truncation surfaces in folds

Growing folds commonly have truncation surfaces on their crests and limbs (Cartwright, 1989; Hardy and Poblet, 1995; Storti and Poblet, 1997; Rafini and Mercier, 2002). These submarine erosional surfaces can be extensive and indicate that a substantial amount of material has been removed. Degradation of folds A and B (Fig. 3.2) results in the formation of distinct erosional surfaces (Fig. 3.3C). In these examples, the reflections are truncated down to 100 m (Fig. 3.3C). These erosional surfaces are only 300-2000 m wide along strike, and therefore laterally discontinuous. This is caused by their formation mechanism as single small events or a laterally restricted process, e.g. channel erosion instead of a uniform erosional

process across the whole structure. Nevertheless, these erosional surfaces indicate that a large amount of sediment has been removed from the structural highs.

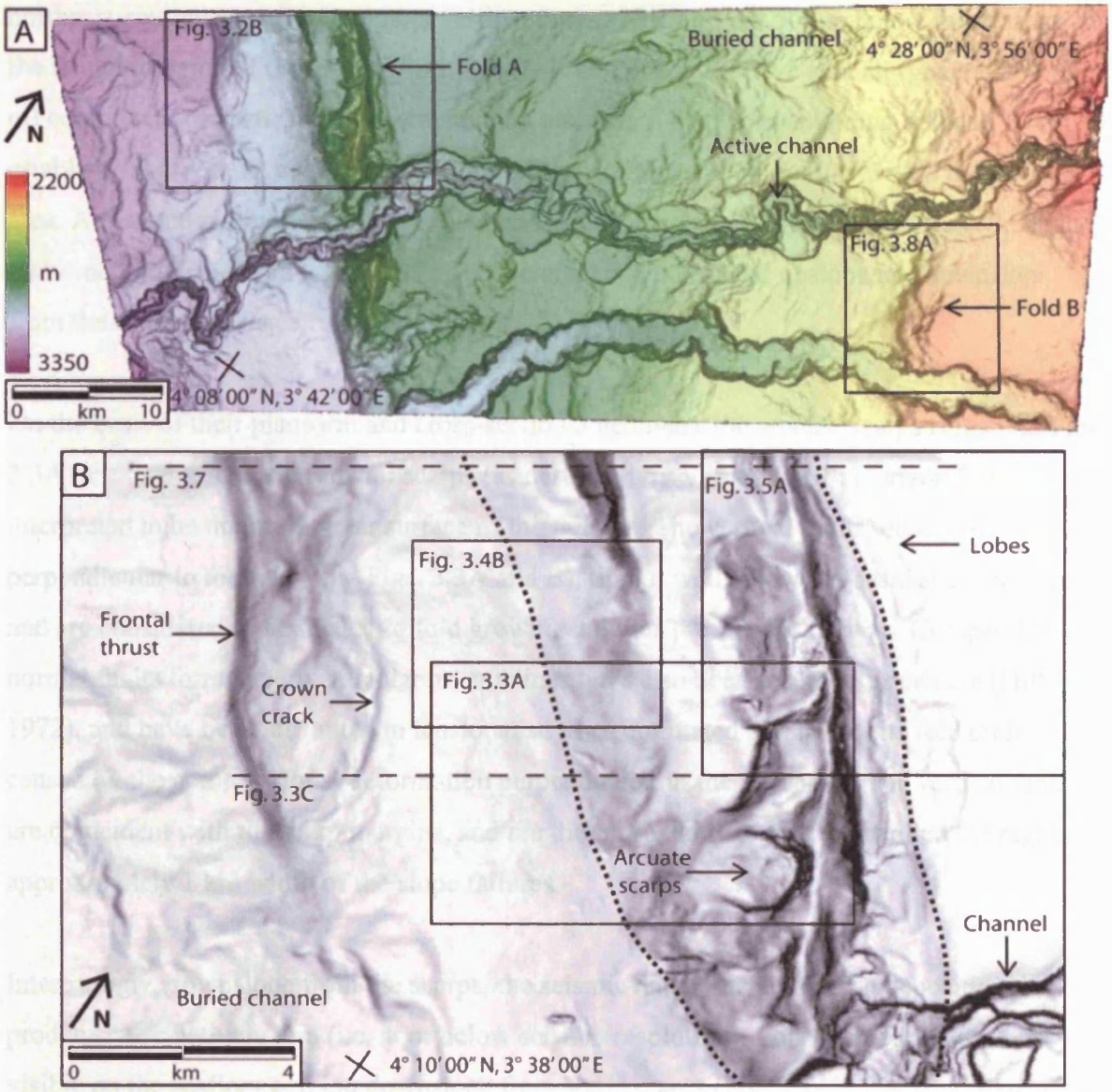

Figure 3.2. Seabed dip magnitude maps showing locations of Figures and folds A and B. (A) Seabed map showing turbidite channels and thrust-propagation folds. The slope dips towards the southwest. (B) Seabed dip magnitude map of the area in which the study is concentrated. Darker colours mean greater dip. Fold A is outlined by a dotted line. Note the arcuate scarps on the southwestern side and lobe-shaped features on the northeastern side.

3.7.2 Backlimb failures linked to thin deposits

The backlimb of fold A is dipping c. 6° towards the abyssal plain. It is dominated by arcuate scarps with thin deposits found downdip of them. The scarps and characteristic deposits are described below.

Arcuate scarps occur on the backlimb of the fold A (Figs. 3.2-3.5). A typical scarp is c. 700-1700 m wide, 10-19° steep and cuts through approximately 100 m of stratigraphy (Figs. 3.3 and 3.4). A cross section parallel to the fold axis dissects the scarps (Fig. 3.3B) revealing northeast-southwest striking, almost vertical faults, which tip out 500 m below the seafloor at the lateral margins of the scarps (Figs. 3.3A and B). The faults have a small (generally < 10 m) component of vertical displacement, with any lateral displacement being difficult to establish. These faults occur only on the backlimb of this and other folds within the study area. A distinctive high-amplitude reflection 50-200 m below the seabed (S in Figs. 3.3B and C) borders truncated reflection packages laterally (Fig. 3.3B) and upslope and downslope from the scarp (packages A and B in Fig. 3.3C).

On the basis of their planform and cross-sectional geometry the arcuate scarps (Figs. 3.2B and 3.3A) are interpreted as headwall scarps (as described by Varnes 1978). Horizon S is interpreted to be the basal shear surface of the failures. The vertical faults, observed perpendicular to the fold axis (Figs. 3.3A and B), tip out well below the basal shear surface and are considered to be related to fold growth, and thus predate the failures. Comparable normal faults formed perpendicular to anticlines have also been recorded elsewhere (Hills, 1972), and have been attributed to tensional stresses orientated parallel to the fold crest caused by the compressional deformation perpendicular to the fold crest. The vertical faults are coincident with the scarp margins, and are therefore likely to have controlled the regular approximately 1 km width of the slope failures.

Interestingly, downslope from the scarps, the seismic data indicate that the depositional products are relatively thin (i.e. at or below seismic resolution). Lobe-shaped features are visible on the seafloor c. 6 km downslope from some scarps (Fig. 3.3A). They correlate with a slight thickening and lowering of amplitude of a reflection near the seafloor (Fig. 3.3D). They are interpreted as thin (<10 m) deposits of sediment that failed on the fold and were then transported as a debris flow. The limited thickness with respect to seismic resolution of these deposits makes it difficult to correlate lobes with scarps, and many thin deposits are probably unresolved by the seismic data. Although the above interpretation is preferred, the absence of obvious depositional products could also be caused by erosion or very long transport distances (>20 km), so that the failed sediments now lie outside the area covered by the dataset.

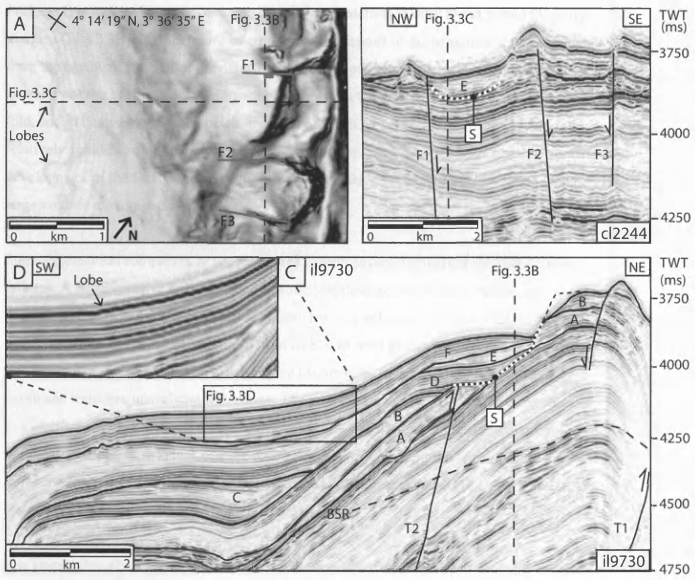

Figure 3.3. Degradation of a backlimb. (A) Dip magnitude map of seabed showing arcuate scarps on the backlimb and lobe-shaped features downslope from them. Darker colours mean greater dip (0-20°). F1-F3 = faults. (B) A section across the scarps showing subvertical faults at the margins of scarps, also marked in (A). Horizon S, marked with white dashed line, is the basal shear surface of failure. (C) A dip-orientated seismic line across a scarp. The wedge-shaped chaotic package E is the deposit of a degraded headwall scarp (also visible in B), the original geometry of which is interpreted in a black dashed line. The packages A and B are truncated by the basal shear surface S and subsequently onlapped by packages D and F. The reflection geometry at the intersection of A and S is repeated in many places in the stratigraphy, e.g. in package C. BSR = bottom simulating reflection, T1 and T2 = thrusts. (D) Thin deposit of failed sediment is represented as a slight thickening and lowering of amplitude at seabed. It correlates with a lobe-shaped feature visible on seabed (A). See location in Fig. 3.2B.

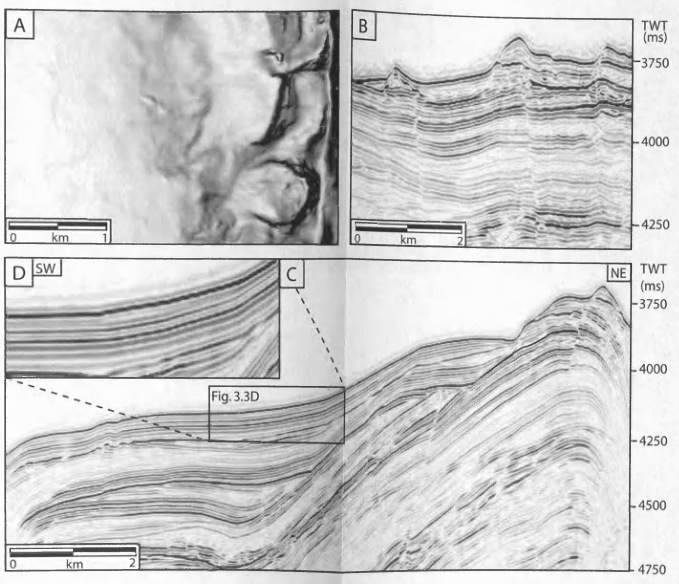

Figure 3.3. Uninterpreted.

Other examples of thin failure deposits on the backlimb consist of low-amplitude, chaotic wedge-shaped seismic reflection packages. For instance, seismic package E (Figs. 3.3B and C), which has a maximum thickness of 30 m and volume of 6 x 10^7 m^3, is located at the foot of the headwall scarp. The basal shear surface of previous failures (horizon S) is onlapped by packages D and F, which are interpreted as levee and hemipelagic deposits respectively.

Package E is located between packages D and F and laterally is only found within the scarp margins (Fig. 3.3B). It is therefore interpreted as the deposit of failed sediment that originated from the headwall scarp after the deposition of D and prior to the deposition of F. The original geometry of the headwall scarp is interpreted based on the geometry of other scarps on the fold, and indicated as a dashed black line in Figure 3.3C. Failures from the head scarp are relatively small in volume relative to the volume of the final scar, which suggests a protracted development of the final scar due to multiple retrogressive failure events, instead of a single large volume movement.

Some degradation complexes in the study area exhibit several typical characteristics of slope failures. A representative dip-orientated seismic line through one of them reveals an approximately 55 m thick low-amplitude discontinuous reflection package 80 m below the seabed (Fig. 3.4). It is located downdip from an 850 m wide arcuate headwall scarp with a maximum dip of about 19°. The basal surface (dashed line in Fig. 3.4A) of the deposit is listric and truncates underlying reflections. The package thins downdip, where it corresponds to a high-amplitude reflection with a 'corrugated' cross-sectional geometry. In planform, these corrugations form ridges that are clearly visible on a dip magnitude map of the top reflection (dotted line in Fig. 3.4B). The ridges exhibit a maximum height of 11 m and have a crest-crest wavelength of approximately 100 m.

The feature described above is interpreted as the deposit of a mass failure, probably a debris flow, mudflow or slump, with the ridges being pressure ridges comparable to those described by Prior and Coleman (1982) and Nemec (1990). Ridges occur in some but not all examples of thin backlimb failure deposits in the study area.

The types of failure on backlimbs described in this section result in a distinctive reflection configuration, which comprises of reflection packages that are truncated upslope at an almost horizontal angle (A and B in Fig. 3.3C). Subsequent reflections are draped on this truncation. This pattern is repeated throughout the stratigraphy of the backlimb, e.g. in package C (Fig. 3.3C), which is truncated both upslope and downslope. These geometries are not laterally continuous and are thus significantly different from the typical models of growth stratal geometries.

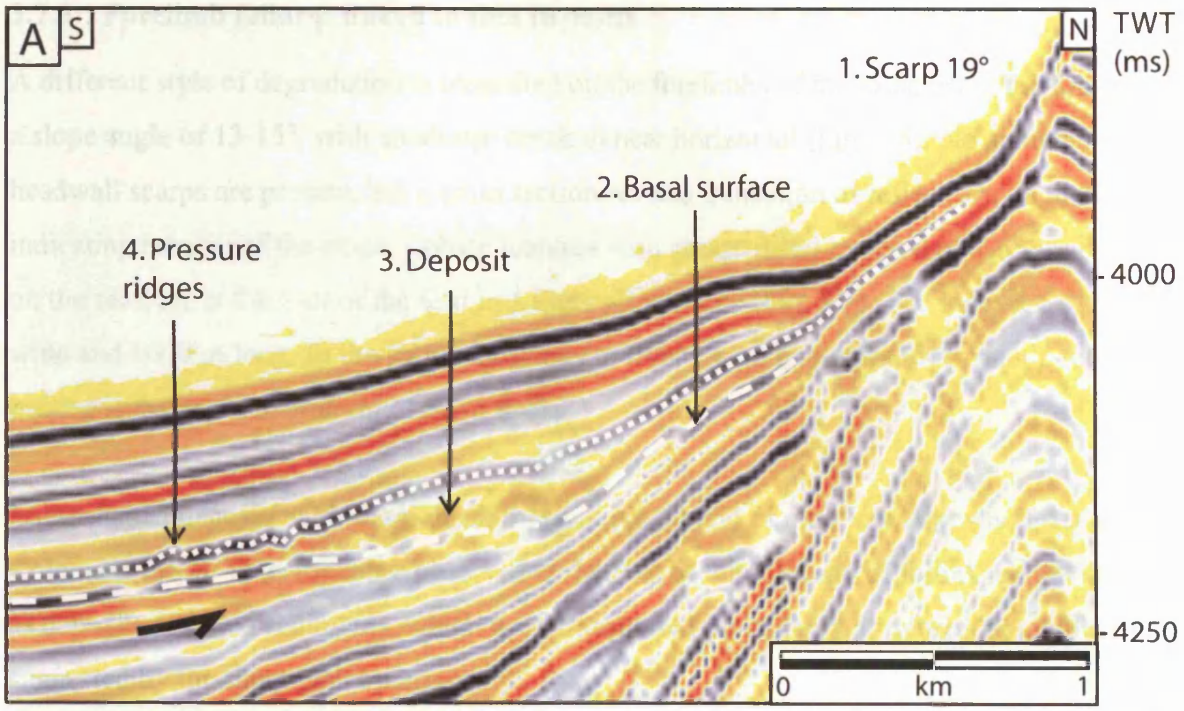

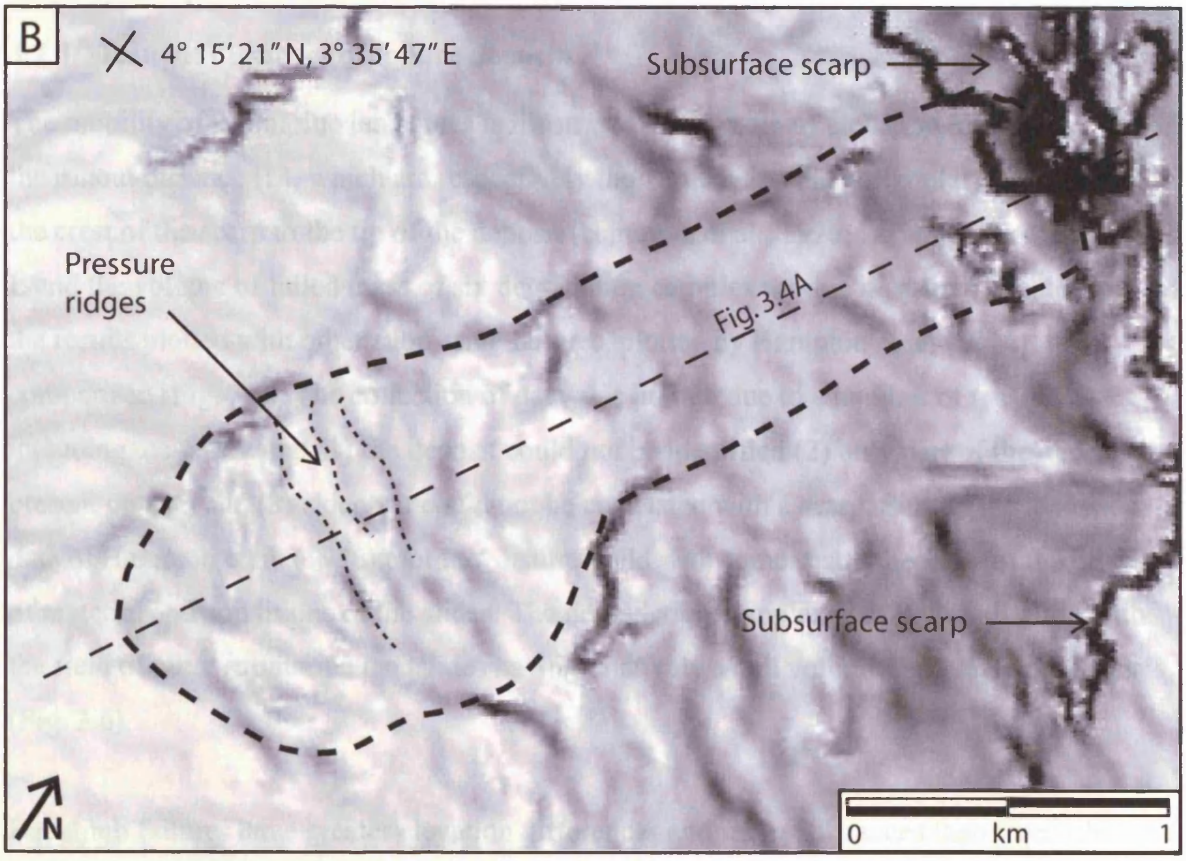

Figure 3.4. (A) A representative seismic line along the middle of a degradation complex showing all typical features: (1) arcuate headwall scarp, (2) listric basal surface truncating reflections beneath it (dashed line), (3) chaotic, low-amplitude deposit buried under 80 m of levee and hemipelagic sediments (between dashed and dotted line) and (4) pressure ridges, visible as corrugations in the top horizon (dotted line). TWT = two-way travel time. (B) A dip magnitude map of the top horizon of the deposit showing pressure ridges at the toe of the deposit. The deposit is outlined with a dashed line. See location in Fig. 3.2B.

3.7.3 Forelimb failures linked to thin deposits

A different style of degradation is identified on the forelimbs of the folds. Here the fold A has a slope angle of 13-15°, with an abrupt break to near horizontal (Fig. 3.5). No arcuate headwall scarps are present, but a cross section reveals truncation of reflections on the fold indicating erosion of the slope. Lobate features with abrupt distal margins of 2-6° are present on the seafloor at the foot of the fold in a footwall syncline (Fig. 3.5). The lobes are c. 2000 m wide and 1000 m long. In the subsurface, they correlate with low-amplitude chaotic reflection packages that are a maximum of 30 m thick.

Lobe-shaped deposits with sharp distal margins are typical of mudflow deposits (Prior and Coleman, 1982). Thus the lobes observed at the foot of the forelimb of fold A are interpreted as deposits of failed sediments, which were transported most likely as debris- or mudflows, as suggested by the sharp distal margins.

3.7.4 Runout distances of failure deposits

The mobility of submarine landslides is illustrated by the ratio of elevation difference (H) and the runout distance (L), which are respectively the vertical and the horizontal distances from the crest of the scarp to the tip of the deposit (Hampton et al., 1996; Locat and Lee, 2002). H, L and the volume of failed mass of six degradation complexes were measured (Table 3.1) and the results plotted with other submarine failures, plotted by Hampton et al. (1996), for comparison (Fig. 3.6). The collection of data was limited due to a number of reasons including the following: (1) the deposit could not be identified (2) only part of the deposit was present on data and (3) a deposit could not be correlated with a scarp. Submarine landslide data of Hampton et al. (1996) plot in a distinct field with some scatter because of the diversity of material and conditions of the slides. The degradation complexes of this study fit in with the field of other submarine landslides having relatively small volumes and high H/L ratios (Fig. 3.6).

Backlimb failures have greater elevation differences and runout distances than forelimb failures (Table 3.1). The H/L ratio is also higher for backlimb failures (0.1) than forelimb failures (0.07), and they plot higher on the graph (Fig. 3.6). It has been suggested that H/L ratio can be used to distinguish the transport mechanism from translational slides (< 0.15) and rotational slumps (> 0.33) (Mulder and Alexander, 2001). The data (Table 3.1, Fig. 3.6)

suggests that the degradation complexes measured for this work are translational slides. However, if the failed sediment mass have transformed into plastic flows (e.g. debris flows), that classification would be inappropriate.

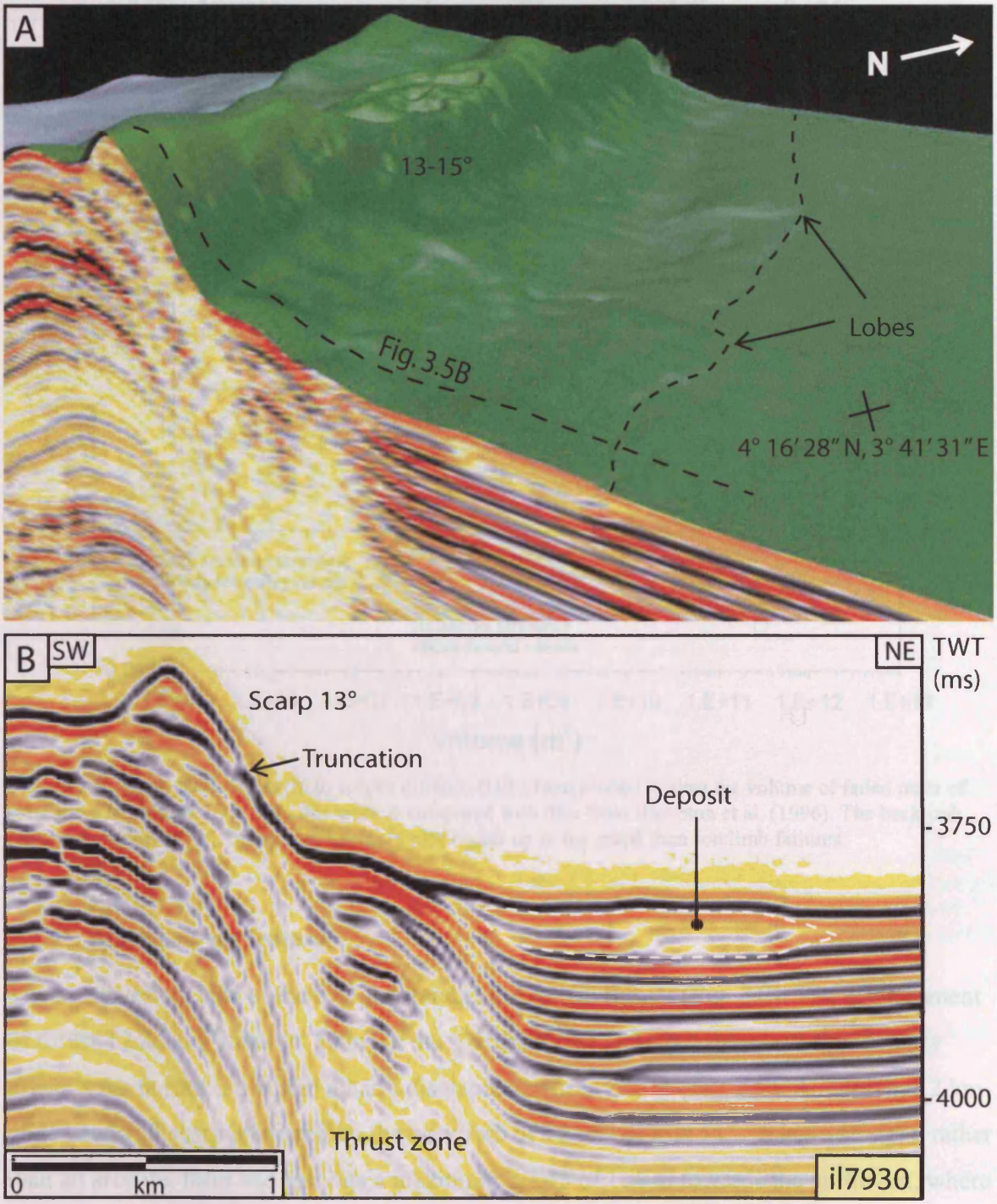

Figure 3.5. Degradation of a forelimb. (A) Oblique view of the seabed on the forelimb side showing the 170 m high fold, which is dipping 13-15°. The lobes at the foot of the fold are wide and short (2 by 1 km). (B) A representative seismic line across the forelimb. The reflections are truncated at the scarp. The low-amplitude package at the foot of the fold (outlined by dashed line) is the deposit of failed sediment. In the subsurface the reflections are disturbed due to steep angle of strata and fracturing by thrust. TWT = two-way travel time.

Table 3.1. Height, runout distance and volume of some degradation complexes of this study.

	H (m)	L (m)	Volume (m^3)	H/L ratio
backlimb 1	227	1950	$6.00*10^7$	0.1163
backlimb 2	365	3125	$6.16*10^7$	0.1166
backlimb 3	508	6300	$2.82*10^7$	0.0806
Average	***366***	***3792***	***$4.99*10^7$***	***0.1045***
forelimb 1	172	2275	$4.01*10^7$	0.0756
forelimb 2	178	2425	$6.23*10^7$	0.0735
forelimb 3	227	3600	$1.95*10^7$	0.0631
Average	***192***	***2767***	***$4.06*10^7$***	***0.0707***

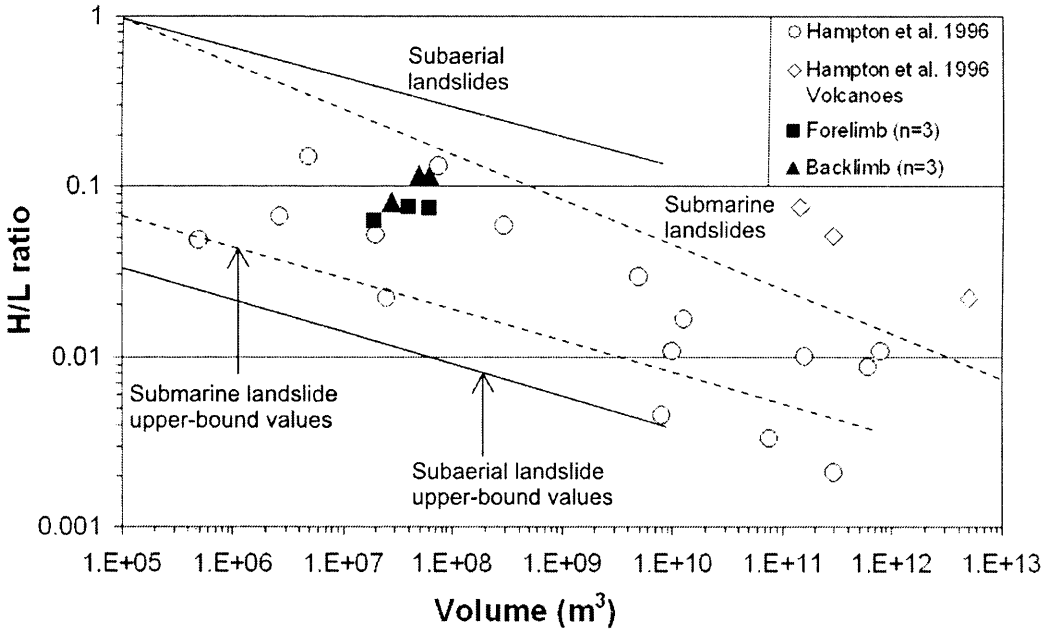

Figure 3.6. Graph showing height to runout distance (H/L) ratio plotted against the volume of failed mass of submarine landslides. Data from this work is compared with data from Hampton et al. (1996). The backlimb failures have higher H/L ratios, and therefore plot higher up in the graph than forelimb failures.

3.7.5 Buried slump feature

The northwestern part of the fold A is comprised of two thrusts (Fig. 3.7). The displacement of thrust T2 is very small (c. 10 m) in the southeast (Fig. 3.3), but increases significantly towards the northwest, where it has a displacement of c. 200 m (Fig. 3.7). A more than 2 km wide headwall scarp is located on the backlimb of T2 and dips at 11°. It has a straight, rather than an arcuate, form and exhibits a maximum height of 165 m towards the northwest, where it meets the outer extent of the data coverage.

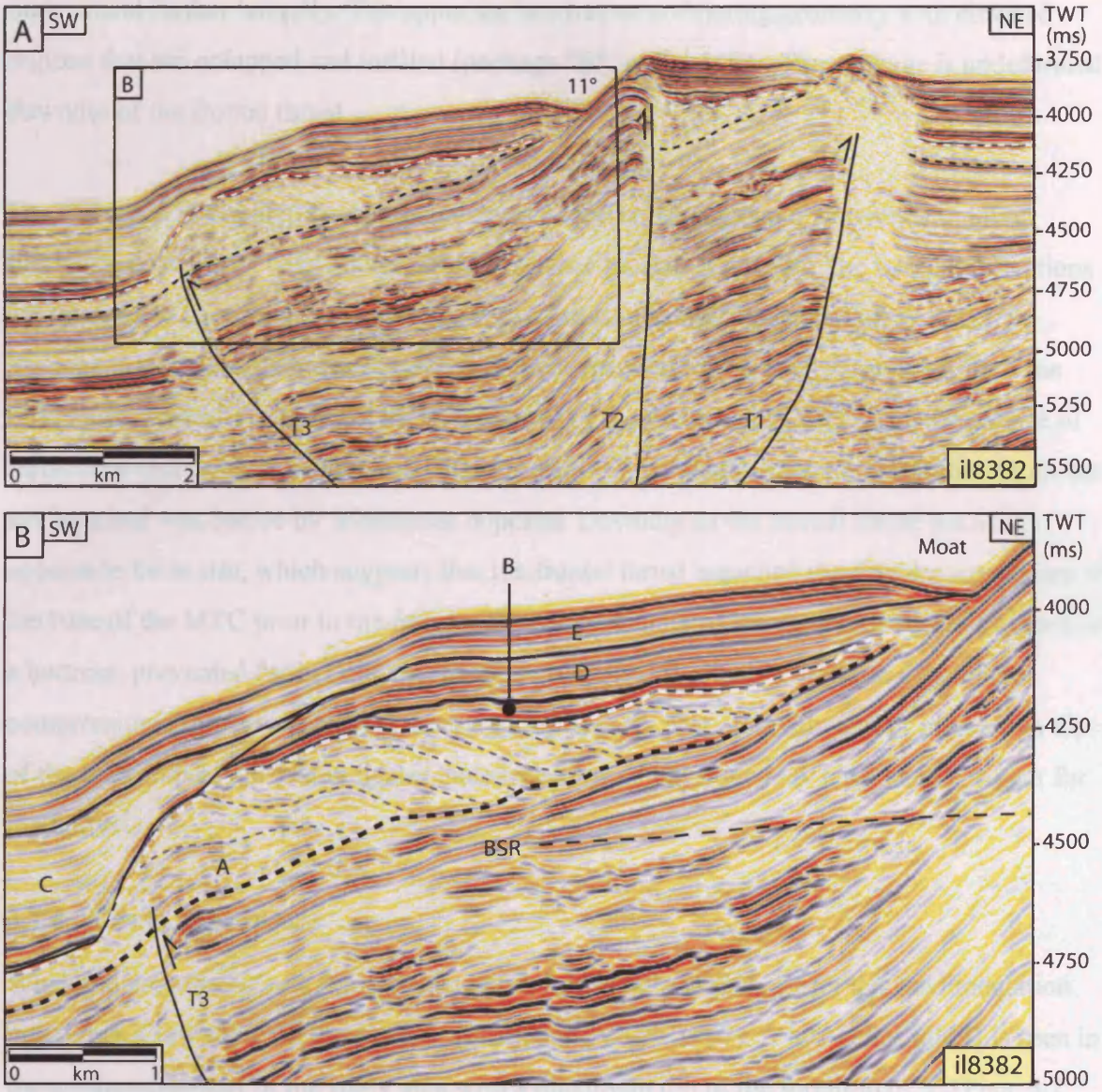

Figure 3.7. Degradation by slumping. (A) A representative seismic line across the fold A composed of two backthrusts T1 and T2 and a frontal thrust T3. The base of the MTC is marked with black dashed line, the top with a white dashed line. The slump is located between T3 and T2 and buried underneath levee and hemipelagic deposits. (B) Slumped unit A showing internal reflections interpreted as thrusts that formed as the movement along basal surface ceased. Subsequent reflections infill and smooth out the geometry (B-E). The moat adjacent to the scarp is thought to have formed by bottom current activity. TWT = two-way travel time.

Seismic package A has a distinctive, low-amplitude chaotic reflection character and it can be traced over most of the seismic volume (Fig. 3.7). Its spatial extent and seismic facies is consistent with it originally being a much more extensive mass transport complex that was deposited on this part of the delta slope. It is generally 60-70 m thick and buried under c. 260-380 m of sediment. Downdip of the scarp, however, its thickness increases to a maximum of 220 m between the frontal thrust and T2 (Fig. 3.7). Here the package shows internal upslope-dipping reflections, which have a regular spacing of c. 60 m and form an imbricate duplex geometry. The feature is at least 1 km wide, but because it is located at the edge of the data, it

may extend further laterally. The upper surface has an undulating geometry with elevated regions that are onlapped and infilled (package "B" in Fig. 3.7B). The package is undeformed downdip of the frontal thrust.

The feature is interpreted as a mass transport complex deposit that underwent slumping following deposition, with the detachment surface located at its base. The internal reflections are interpreted as imbricate thrusts that formed as downslope movement of the sediment package on the detachment surface ceased. This is supported by the c. 60 m spacing of the reflections, which is equivalent to the thickness of the undeformed MTC. The occurrence of reflections that onlap the undulating upper surface of the slump suggests that it formed on the seafloor and was buried by subsequent deposits. Downdip of the frontal thrust the MTC appears to be *in situ*, which suggests that the frontal thrust breached the detachment surface at the base of the MTC prior to the failure. This discontinuity of the detachment surface acted as a buttress, prevented further downslope movement, and resulted in the formation of the compressional thrust structures at the toe of the deposit. The relatively abrupt increase in dip of the backlimb of the fold indicates that steepening of the slope may have been a trigger for the failure.

3.7.6 Ovoid depressions

When the growth rate of a thrust-propagation fold is only slightly faster than sedimentation rate, it has a low relief on the seafloor (Storti and Poblet, 1997). A low-relief fold B is seen in the northeastern part of the study area with a maximum dip of the forelimb of 5° (Figs. 3.2 and 3.8). Its degradation character is different to that of the fold A. Localised low-amplitude zones of disruption radiate upwards in the core of the fold (Figs. 3.8B and C). These are interpreted as radial faults that formed due to extension caused by the fold growth and are common in other submarine growth folds (e.g. Ingram et al., 2004). Wrench faults at the lateral margin of the thrust reach the seafloor indicating recent movement on the thrust (Fig. 3.8A).

Several 300-700 m long oval depressions are found on the seafloor above the fold B with small seafloor expression (Fig. 3.8). The depressions occur above the crest or on the backlimb (upslope) of the fold. They have rounded appearance and are elongate parallel to the fold axis. Some depressions have walls truncating stratigraphy to about 100 m at a maximum angle of 16° (X in Fig. 3.8C). Similar reflection truncations are found in the subsurface (Z in Fig.

3.8C). Other seabed depressions are much shallower and located above listric zones of reflection truncations in the subsurface (Y in Fig. 3.8C). The shaded reflection package in Figure 3.8C consists of continuous parallel reflections to the east of fold B and divergent reflections showing offlap to the west. Between depressions X and Y the package forms a small upslope-dipping wedge (M) that consists of chaotic reflections.

The ovoid depressions may have formed by several processes. They may be (1) rotational failures on a listric decollement, (2) a result of bottom current activity, (3) possibly a combination of both processes, or (4) pockmarks associated with escaping gas. The depth, down to which reflections are cut by the depressions, is in all cases 100 m, therefore it can be assumed that this is a critical depth for a failure. A weak layer may exist at that depth e.g. because of dewatering and overpressure generation. The low-amplitude wedge M is interpreted as a deposit of mass failure. Depression Y is thus the seafloor expression of a buried headwall scarp at depth. Alternatively, the depressions may have been formed by current activity. This is supported by the roundedness of the depressions and evidence of current activity in the form of sediment waves on the seafloor (Fig. 3.8A). In addition, depression X does not have any detectable deposit downdip from the scarp, which may suggest it formed as a result of current scouring. Bottom currents are known to erode steep scarps on their path e.g. in Judd Deeps in the Faeroe-Shetland Channel (Smallwood, 2004). Currents may accelerate locally and scour more effectively when they encounter an obstacle in their path or the slope flattens (Nemec, 1990). Fold B would be such an obstacle.

Pockmarks on the seafloor above toe-thrust anticlines in northwest Borneo have been attributed to upward migration of thermogenic gas (Demyttenaere et al., 2000). During fold growth the outer arc of the fold experienced tensional stresses that are manifested by fold-crest faults that have an upward radiating geometry in cross section. These faults could provide migration paths for gas (Ingram et al., 2004) and cause pockmarks on the seafloor. However, in this case, the geometries of depressions X and Y are more consistent for the ovoid depressions to be the result of a combination of mechanical failure and bottom current activity.

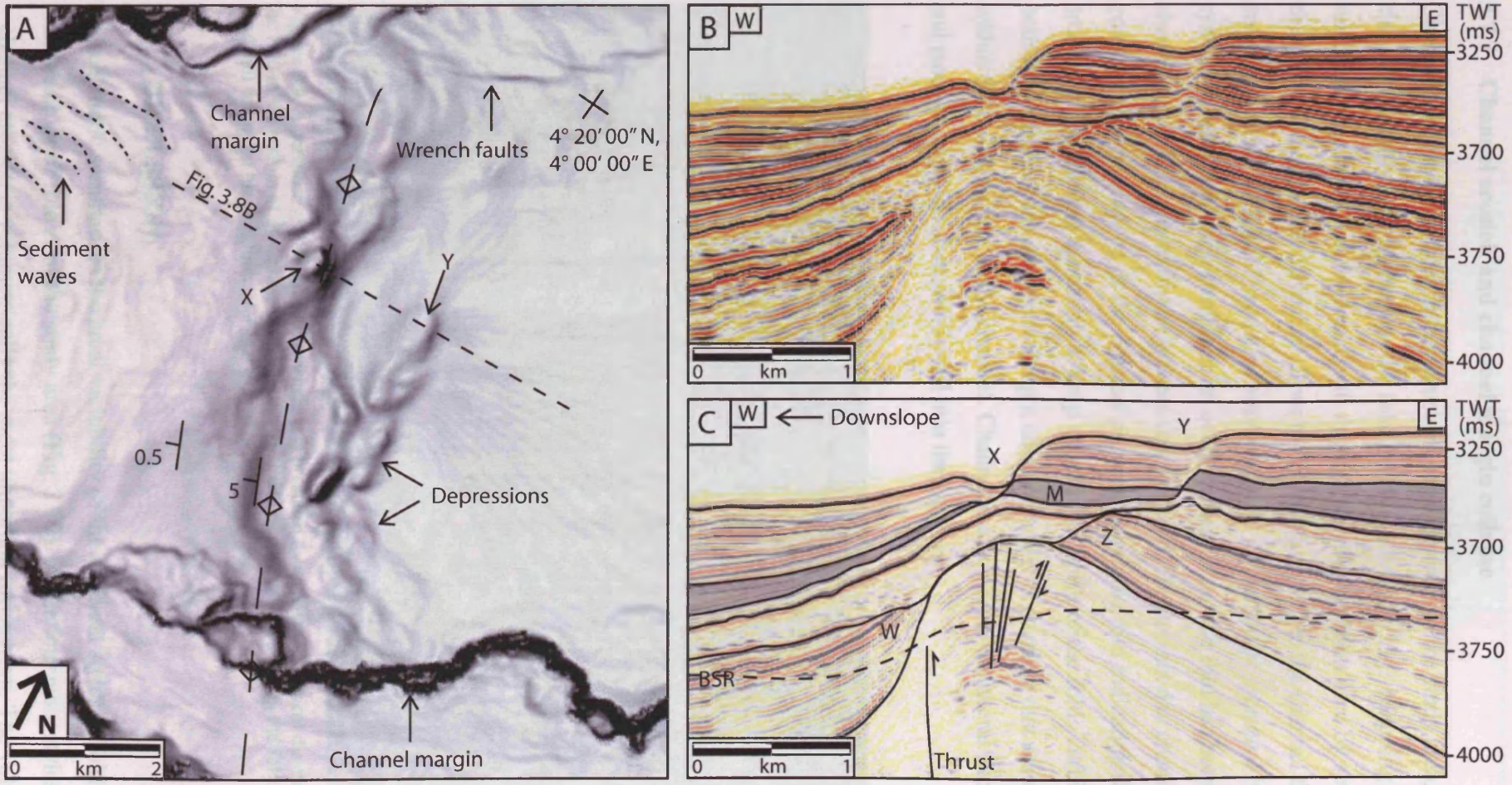

Figure 3.8. Degradation of fold B with only minor seafloor expression. (A) Seabed dip magnitude map showing oval depressions that occur on and upslope of a fold crest. Note the sediment waves near the active channel and wrench faulting caused by thrusting. (B) Representative seismic line with interpretation (C) across two oval-shaped depressions (X and Y). Reflections are truncated down to 100 m at X. The depression Y is located above a listric zone of reflection truncation at subsurface. Similar geometry can be found deeper in the section (Z). The package M (shaded grey) is interpreted to have failed with a buried headwall scarp below Y and deposit of failed sediment between X and Y. BSR = bottom simulating reflection. Note also radial faults in the core of the fold. TWT = two-way travel time.

3.7.7 Channel erosion and channel margin collapse

Channel-levee systems breach the thrust-propagation folds in the study area, with an active channel currently cutting through the fold A (Figs. 3.2A and 3.9). Mapping of channels in the subsurface indicates that the same path through the fold has been used by several buried channels. The elevation difference from the crest of the fold to the channel thalweg is 420 m and the volume of the fold eroded is approximately 1.3 km^3. The erosional base of the channel system is, however, buried and thus an even greater part of the fold has been eroded by channels than is apparent on the present day seafloor. The present day channel thalweg gradient does not change as the channel passes through the fold indicating that the rate of erosion of the channel is enough to keep up with the uplift of the fold. Turbidity currents can both erode and deposit sediment along a channel, and it is possible that erosion occurs mainly within the uplifting part of the channel. Channel erosion removes lateral support for sediment and parts of the fold subsequently fail into the channel.

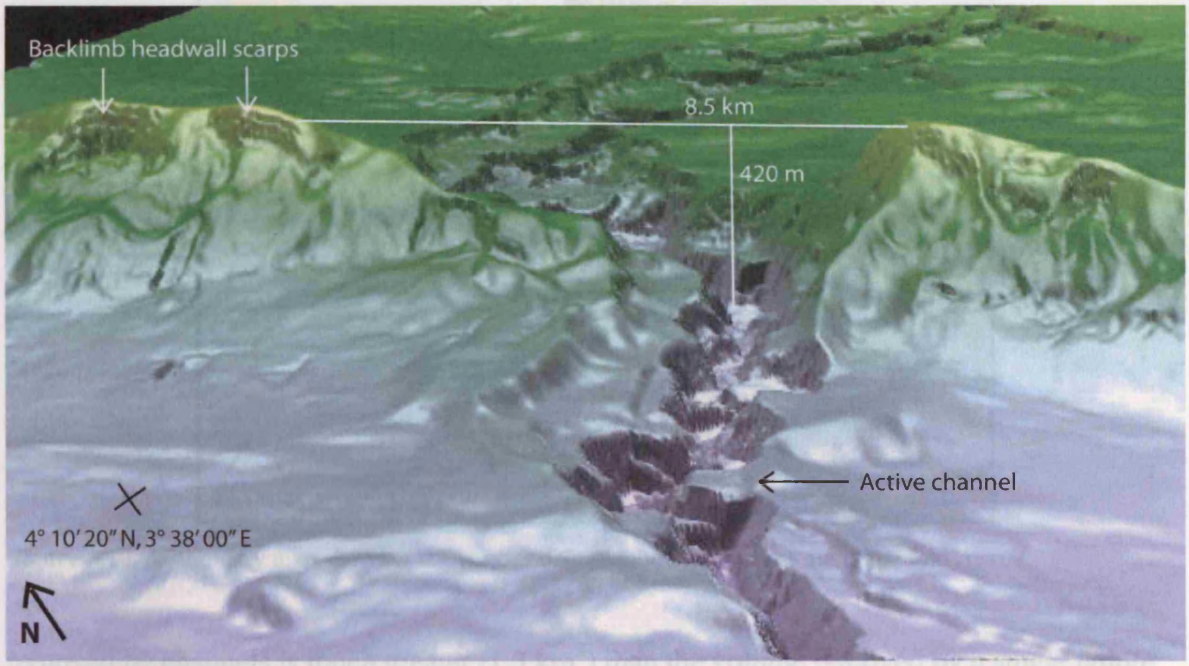

Figure 3.9. A perspective view of fold A where it is breached by a channel. Vertical distance from the crest of the fold to the bottom of the active channel is 420 m. Field of view is 15 km along the fold. Note the arcuate headwall scarps on the backlimb. Vertical exaggeration is c. 2.5.

3.8 DISCUSSION

A schematic summarises the areal variability of the different styles of fold degradation near the seafloor of fold A of the study area (Fig. 3.10). Of the four main styles of degradation, channel erosion is volumetrically the most important mechanism. The volume of sediment

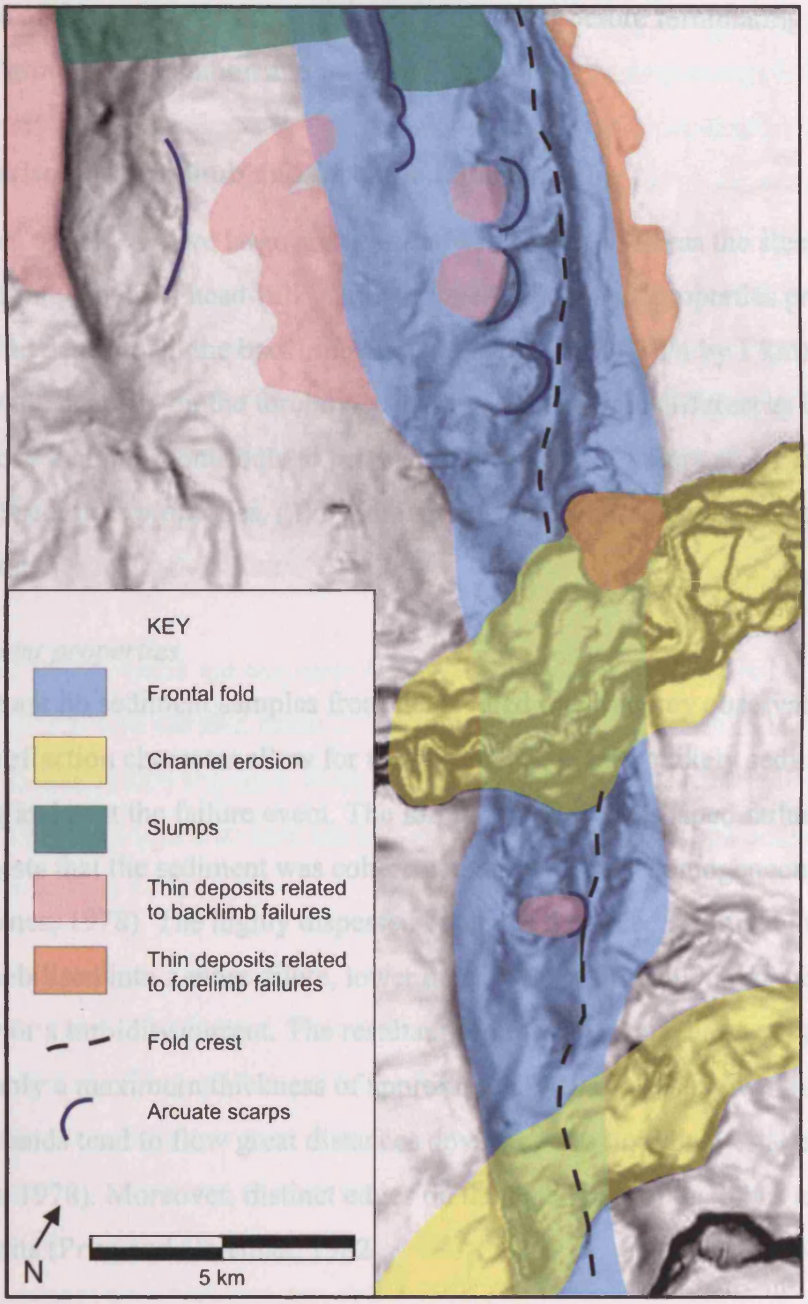

Figure 3.10. A summary map showing the various degradation mechanisms along the fold A.

removed by channels is much greater (1.3 km^3) than the volume removed by a single failure (up to 0.062 km^3, Table 3.1). Channel erosion can be considered as a continuous process and thus differs from the other degradation mechanisms, which are considered as individual, repetitive failure events. The backlimb and forelimb failures associated with thin, almost seismically indiscernible sedimentary deposits downdip are by far the most common types of degradation in the study area and have been identified within other 3D seismic datasets in this part of the Niger Delta, and therefore are the focus in this discussion. The main controls on

the architecture of these types of failure are considered first before formulating a generic model for fold growth, degradation and burial.

3.8.1 Comparison of backlimb and forelimb failures

Backlimb slopes of fold A have large arcuate headwall scarps, whereas the steeper forelimb does not exhibit any obvious headwall scarps despite the sediment properties probably being very similar. The deposits on the backlimb are long and narrow (3 km by 1 km) compared to the short and wide deposits on the forelimb (1 km by 2 km). Some differences in the pre-failure conditions that may contribute to producing the different failure styles and depositional features are (1) sediment properties, (2) the presence and orientation of anisotropies and (3) slope morphology.

3.8.1.1 Sediment properties

Although there are no sediment samples from the studied interval, key observations of deposit geometry and reflection character allow for the consideration of the likely sediment properties prior to, during and post the failure event. The formation of scoop-shaped failures on the backlimb suggests that the sediment was coherent and most likely homogeneous at the time of the failure (Varnes, 1978). The highly dispersed nature of the failed sediment mass suggests that it was remobilised into a more dilute, lower density flow, probably in the form of a debris flow, mudflow or a turbidity current. The resultant sediment package has a very low aspect ratio and probably a maximum thickness of approximately 10 m. It is known that soft clays and loose fine sands tend to flow great distances downslope as liquid material even on gentle slopes (Varnes, 1978). Moreover, distinct edges on the distal part of the lobes are typical of mudflow deposits (Prior and Coleman, 1982).

The presence of slumps with internal slip planes indicates that movement could also occur as more coherent and viscous sediment bodies. The slump described in this paper (Fig. 3.8) occurred due to the remobilisation of a mass transport complex deposit. This more coherent style of sediment transport could be a coincidental relationship, but may also suggest that the mass transport complexes had different sediment properties prior to failure than levee and hemipelagic sediments and this affected the type of failure that occurred.

3.8.1.2 Anisotropies

The presence and orientation of stratigraphic and structural anisotropies can influence mass wasting processes (e.g. Stewart and Reeds, 2003). Planes of weakness reduce the shear strength of sediment and enable failure to occur with lower imposed shear stresses. The main anisotropies in the study area are bedding planes and the sub-vertical faults associated with fold growth (Fig. 3.3). The dip of the strata is greater in the forelimb than on the backlimb, which may result in more slab-like failures along bedding planes on the steeper forelimbs. However, close inspection of the forelimb failures shows that there is no evidence for bedding-parallel detachment surfaces. Instead, the strata are clearly truncated (Fig. 3.5). This means that the failure plane is steeper than the dip of the strata of the forelimbs, and thus unlikely to be controlled by bedding-parallel slip.

The sub-vertical faults, which are perpendicular to the fold axes, are present on the backlimbs but do not continue across the fold crests to the forelimbs. The faults coincide with the lateral margins of the failure scarps and most likely control the width of the scarps. Forelimbs lack these planes of weakness and also lack arcuate failure scarps, indicating a possible relationship between the two.

3.8.1.3 Slope morphology

The backlimb and forelimb of fold A have different slope morphologies. The forelimb is steep (15°) and short, and the slope gradient reduces abruptly, whereas the backlimb is shallower (6°), longer and has no abrupt changes in dip. Slope morphology may determine the type of slope degradation that occurs, because it determines the failure plane geometry and affects the runout distance. The orientation of slip plane is controlled by the distribution of principal stresses on the slope (Mello and Pratson, 1999). The orientation of stress field rotates within a slope, because the upper part is under an extensional stress regime, whereas the lower part is in a compressional stress regime simply due to gravitational force. This means that the direction of the slip planes will rotate producing listric surfaces in shallow slopes and more planar and slope-parallel as the slope steepens. Mello and Pratson (1999) predict that sediments fail when the slope inclination is $\geq 2/3$ of the friction angle. In marine sediments this should be approximately 13° (Mello and Pratson, 1999), however, other factors (e.g. high pore pressures) will contribute to the failure of shallower slopes. The arcuate headwall scarps on the backlimb and the forelimb slope with truncated reflections have an angle of 13-15°. This fits in well with the prediction of the angle of failure initiation.

Submarine slides occur on slopes with gradients as low as 0.5°, and slope gradient is thus not always considered an important factor in marine slope instability (Sultan et al., 2004). However, the gravitational shear stress and the weight of the overlying sediment increase if a slope steepens. Therefore, steeper slopes are predicted to be more prone to failures. Also increased transport velocities can be attained on steeper slopes. An abrupt break in slope causes increased basal friction, deceleration and deposition of the failed sediment mass, resulting in relatively thick deposits (Nemec, 1990). On a longer, more uniform slope, the failed sediment mass has more time and space to dilute by the entrainment of ambient water and hence disintegrate. This increase sediment transport distance and dispersal, leading to the formation of thin, widespread deposits, because both basal and internal friction are reduced. The observations of the degradation complexes in the study area match perfectly with these predictions.

3.8.2 Model for fold degradation

Several mechanisms for fold degradation were described above. Here a general synoptic model that accounts for the dominant style of degradation observed in the study area is synthesised (Fig. 3.11).

An asymmetric fold forms on the hangingwall of an underlying thrust (Fig. 3.11A). During folding, normal faults may form perpendicular to the fold axis on the backlimb of the fold. Initial slope failure occurs once the stresses become large enough for compressional failure on the lower part of the slope (Mello and Pratson, 1999) (Fig. 3.11B). This may be triggered by several factors, e.g. slope steepening or earthquakes. The headwall scarps on the backlimb are arcuate in plan view, which is typical of homogeneous materials with a relatively shallow slope dip (Varnes, 1978). The width of the scarps is most likely controlled by the pre-existing normal faults that act as planes of weakness. On the forelimb there are no arcuate scarps because the slope is steeper, which causes the slip plane to have an orientation parallel to the slope surface (Mello and Pratson, 1999). The sediment mass that fails disintegrates after failure during transport. It is transported down the slope as a debris/mudflow or a turbidity current as more ambient water is entrained by it and dilutes it. The transport distance is great enough that the failure scar is completely evacuated. The deposits are widespread thin lobes on the long shallow backlimb (<10 x 3000 m), whereas on the forelimb that has an abrupt break in slope, the sediment is deposited at the foot of the fold in thicker and shorter deposits (30 m x 1000 m).

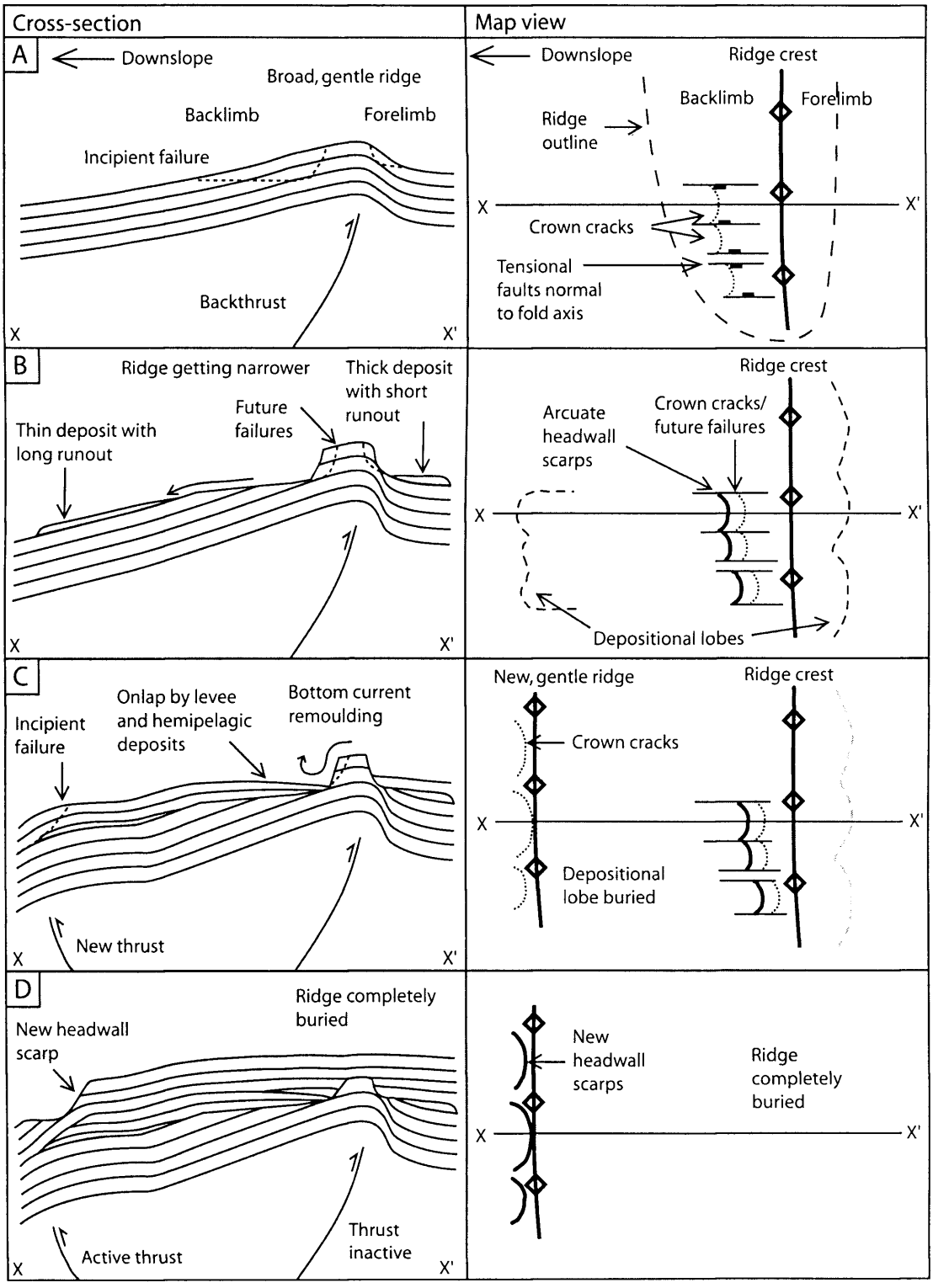

Figure 3.11. A simplified cartoon showing the formation of stratal geometry observed repeatedly on the folds in cross-section and plan view. Not to scale. (A) A thrust-propagation fold at pre-failure stage forming a broad and gentle fold on the seafloor. Tensional faults normal to the fold axis are formed on the backlimb. Incipient failures are listric in shape. (B) Fold at an early stage of degradation. Part of the fold fails and produces thin deposits with a long runout distances on the gentle backlimb and a short runout distances on the forelimb with an abrupt break in slope. The deposits form lobe-shaped features in plan view. Crown cracks form upslope of previous headwall scarps. (C) Fold at a later stage of failure. The fold is getting narrower due to repeated retrogradation of the headwall scarps. Levee and hemipelagic deposits onlap the fold and the failure scars. Bottom currents may modify the stratal geometries. A new frontal thrust starts to develop and causes a new fold to be uplifted. (D) The fold has been completely degraded and buried. New fold has continued to be uplifted and is now the centre of degradation.

Upslope of the scarps, new crown cracks develop as a result of the removal of lateral support and mark the location of subsequent failures (Fig. 3.11B). The scarp retrogrades upslope as a result of multiple small volume failures. Subsequently, levee and hemipelagic deposits onlap the empty failure scar (Fig. 3.11C) and bottom currents modify the stratal geometries. When a new thrust forms basinward of the previous thrust, less displacement occurs on the older thrust. A new fold starts to form on the seafloor and failure occurs above it (Figs. 3.11C and D). The old fold is eventually degraded and buried completely as erosion and sedimentation rates outpace the rate of uplift.

3.8.3 Initiation mechanisms

It is well established that shear stress can be increased or shear strength decreased by (1) earthquake shaking, (2) imposing a tilt, (3) high sedimentation rate and the weight of overlying sediment, (4) removal of underlying or lateral support (for example, erosion by channels or previous failures), (5) presence of gas or destabilisation of gas hydrates and (6) lateral pressure caused by e.g. mobilisation of residual stress (e.g. Varnes et al. 1978, Hampton et al., 1996). The most common trigger mechanisms for slope failure are earthquake shaking (Canals et al., 2004) and gas seepage (Lastras et al., 2004; Sultan et al., 2004).

Dewatering and pore fluid migration caused by folding and burial may contribute to the destabilisation of sediments on slopes. Elevated pore fluid pressures can create permeable extensional fracture networks (Ingram et al., 2004). These and the extensional faults on fold crests caused by folding can act as pathways for pore fluid and hydrocarbon migration. No pore pressure or sediment strength information from the study area was available for this work, and it is therefore difficult to be unequivocal about trigger mechanisms. The BSR (Fig. 3.3) indicates the presence of gas hydrates in the study area, however, there is no evidence for dissociation or seepage in the seismic data, suggesting that gas seepage is an unlikely trigger of the failures. The area is tectonically quiescent, with only a few earthquakes with greater than magnitude 4 recorded in historical times (c. 200 years) (Ambraseys, 1988). However, larger earthquakes may be less frequent and thus not recorded. Moreover, thrust propagation may have produced small earthquakes, which are capable of triggering sediment failures. All the failures in this study occur on slopes with increased inclination (6-15°) and no similar failures are found where the slope is 0.8°. This suggests that slope inclination is an important factor contributing to failure generation here. In addition, the sedimentation rate is high on the Niger Delta, and overpressure is likely to be generated due to disequilibrium compaction.

This could explain the similar heights of many headwall scarps, suggesting that effective stress is reduced sufficiently at c. 100 m burial depth. High sedimentation rates also lead to thick piles of unlithified sediment, which fail more easily than thin piles or lithified rock (Schnellmann et al., 2005).

Other failures are triggered by removal of lateral support. Channel erosion removes lateral support and as a result parts of the fold failed into the channel. The same principle can be applied to the retrogradational failure process as each failure will result in the removal of lateral support.

3.9 IMPLICATIONS FOR HYDROCARBON EXPLORATION

This study highlights the formation of erosional surfaces on fold crests and limbs and the deposition of degradation products on the margins of the folds. It is likely that both of these phenomena will be penetrated by exploration, development and production wells in the future, and therefore the recognition of unconformities and deposits of failed and remobilised sediments is important for predicting stratigraphy prior to drilling. The failed sediment deposits are not likely to be of good reservoir quality as this part of Niger Delta is extremely mud-prone. Even in sandier systems, debris-flow deposits are commonly too poorly sorted to be a good hydrocarbon reservoir. Furthermore, although not considered here, uplift and erosion of folds may have implications for seal integrity (Ingram et al., 2004), and accurate estimation of the amount of unroofing is therefore important. Although the degradation complexes described in this paper are relatively small, unloading the fold crest by larger failures could lead to depressurising of gas hydrates. Gas and fluid derived from the gas hydrates or from escaping free gas trapped beneath the gas hydrates could contribute to the destabilisation of sediments and the degradation of the fold.

Based on the seismic interpretation of the study area, it is evident that different styles of degradation occur along the same structure, separated by only a few hundreds of metres. This results in significant along-strike variability in the erosional and depositional features and means that unconformities and individual seismic reflections can only be traced locally (Fig. 3.10). In addition, it was shown that the dominant degradation products are thin debris flows or turbidites, many of which are probably not seismically resolvable even close to the seabed. Their function in filling minibasins that developed between the folds is easily underestimated, particularly where seismic resolution is reduced. The complexity associated with fold growth

and degradation will therefore be further amplified in buried examples making the correct correlation of reflections across and along fold structures difficult and accurate stratigraphic predictions highly challenging.

Deepwater compressional fold and thrust belts are important hydrocarbon exploration targets throughout the world. Hangingwall anticlines host major hydrocarbon accumulations offshore East Kalimantan (Saller et al., 2004) and northwestern Borneo (Demyttenaere et al., 2000; Ingram et al., 2004). In addition, other deepwater compressional structures, such as shale and salt diapirs and ridges that dominate other major hydrocarbon provinces, e.g. Gulf of Mexico (Winker and Booth, 2000; Grando and McClay, 2004) and Angola (Corredor et al., 2005) may have similar degradational patterns that influence reservoir geology. Slumps have been observed near anticlines in deepwater Borneo (Ingram et al., 2004) and on basin inversion anticlines in the North Sea (Cartwright, 1989). Inspection of other three-dimensional datasets along trend on the Niger Delta shows that the styles of degradation described here are common on fold-related highs. It is also likely that these styles of degradation complexes are not unique but will typify other compressional settings.

3.10 CONCLUSIONS

This paper describes several different styles of submarine fold degradation complexes that are the result of various failure and transport processes and produce laterally discontinuous erosional surfaces and deposits that have impact on reservoir prediction. A significant amount of sediment is removed from folds and thick deposits of non-reservoir accumulated in minibasins adjacent to folds. In this particular dataset, channel erosion is volumetrically the most important degradation mechanism. The dominant style in this part of the western Niger Delta, however, is that of multiple, retrogressive, small volume failures that can have a common locus, if pre-existing planes of weakness are present. The difference in the geometries of the backlimbs and forelimbs of thrust propagation folds is a fundamental control on the style of degradation and the runout distance of such failures. The abrupt break in slope on forelimbs reduces the velocity of the failed sediment mass and causes deposition resulting in relatively thick, short and wide deposits, whereas the longer but shallower slope of the backlimb leads into disintegration of failed sediment mass into debris flows or turbidity currents that produce widespread, thin deposits with longer runout distances. Both backlimb and forelimb failures are likely to form deposits that are below seismic resolution. They are therefore difficult, if not impossible, to identify adjacent to buried folds where the seismic

resolution is reduced. These deposits are likely to be muddy and even in sandier systems poorly sorted and therefore not good reservoir.

Other degradation styles have also been observed in the study area. Sediments with higher internal shear strength form more coherent downslope mass movements on a basal detachment and shortening by internal imbricate thrusting. More enigmatic ovoid depressions are considered to represent small scale slumping that are modified by bottom currents. This style shows that folds that have only a minor relief on the seafloor degrade differently to folds with greater relief, i.e. through a combination of brittle failure and bottom current erosion. Given the variety and three-dimensional complexity of these degradation complexes, comparison with other seismic volumes would be essential to fully characterise degradation in compressional submarine settings.

Chapter 4

4 KNICKPOINT MIGRATION IN SUBMARINE CHANNELS IN RESPONSE TO FOLD GROWTH, WESTERN NIGER DELTA

4.1 ABSTRACT

Several knickpoints have been identified along the present day thalweg of a sinuous submarine channel on the slope of the western Niger Delta using 3D seismic data. The knickpoints form as a result of gradient changes caused by the uplift of a thrust and fold belt orthogonal to the channel. The channel gradient is lower locally upstream of folds causing turbidity currents within the channel to decelerate and deposit the coarsest sediment load. The basinward dipping fold limb causes local steepening of the gradient, which leads to increased flow velocity and turbulence within the turbidity currents. This enhances erosion at the base of the channel and leads to the formation of a knickpoint. If preserved, e.g. as a result of channel avulsion or abandonment, the deposits upstream of the knickpoints could constitute an important hydrocarbon reservoir element. They can, however, also be partially eroded by headward-migrating knickpoints, as the channel strives to regain its equilibrium profile, leaving remnant sand pockets preserved on channel margins. Although knickpoints are difficult to recognise from subsurface seismic or outcrop data, it is anticipated that they can form at any stage of the evolution of a channel-levee system and may be particularly important in controlling 3D channel architecture where channels intersect dynamically changing seabed topography.

4.2 INTRODUCTION

Deepwater channels have been a focus of significant research effort since their discovery in the 1940s on the continental margins of North America (Menard, 1955) and more recently since they have been recognised as important hydrocarbon reservoirs. Channel-fill elements, together with terminal and intraslope fans and crevasse splays, are exploration targets in buried turbidite systems. Many of the reservoirs in recent discoveries off West Africa consist of sinuous shoe-string, ribbon- and pod-shaped sand bodies deposited within canyons and valleys (Prather, 2003). Outcrop analysis, seismic data, borehole and hydrocarbon production data all show that many deepwater channels have complex internal fills, with multiple phases of erosion, bypass and fill (e.g. Deptuck et al., 2003; Posamentier and Kolla, 2003). This complexity could be the result of external factors, such as changes in sediment supply from

the shelf, climate and relative sea level (e.g. Posamentier and Kolla, 2003). It could also be due to the dynamic nature of slopes, which are complicated by active, growing structures such as faults, folds, salt or mud diapirs and withdrawal basins.

Deepwater channels act as conduits for sediment to be transported by gravity flows, such as turbidity currents and debris flows, into the deep sea (Deptuck et al., 2003). Gravity flows travelling down slopes react in various ways to changes in topography. This depends on several factors, such as rate of seafloor deformation and the type, grain size and density of the flows (Pirmez et al., 2000; Kneller, 2003). Some channels are diverted around structures on the seafloor (Kukowski et al., 2001; Smith, 2004) or dammed by growing structures leading to abandonment (Demyttenaere et al., 2000; Huyghe et al., 2004). In other cases, however, compressional structures orthogonal to channels have apparently little effect on the channel location, but along with some changes in planform morphology they mainly cause changes in channel profile, e.g. steepening of gradient across the thrust front of the Barbados accretionary prism (Huyghe et al., 2004). This is also characteristic of the channel of this paper.

Channels constantly adjust their profiles towards equilibrium, i.e. a profile that sustains little aggradation or degradation along the channel with prevailing sediment discharge conditions (Pirmez et al., 2000). This is achieved mainly by erosional and depositional processes of turbidity currents, including changes in channel sinuosity and development of distributary channels and aggradational sheets (Pirmez et al., 2000; Kneller, 2003; Adeogba et al., 2005). Despite complex seafloor topography, many submarine channels form concave-up equilibrium profiles (Pirmez et al., 2000).

Submarine channels may also adjust their profiles towards equilibrium via the formation of knickpoints, a process that is well known in fluvial settings. The role of this process in determining the internal architecture of deepwater channel complexes in regions of evolving topography has received much less attention until very recently (Pirmez et al., 2000; Mitchell, 2006). This paper presents an analysis of knickpoints on the ultra-deepwater Niger Delta using 3D seismic data. The knickpoints formed along a present day channel thalweg due to fold growth. Detailed analysis of knickpoints shows how a confined submarine channel evolves as it traverses across an uplifting thrust and fold belt and suggests that knickpoint migration plays a significant role in controlling the architecture of channel-levee complexes.

4.2.1 Knickpoints

A knickpoint is defined in fluvial systems as a steep gradient section between lower gradient sections along a river course (Howard et al., 1994) and thus represents a disruption in equilibrium profile. Knickpoints and rapids form in fluvial systems as a result of changes in base level (i.e. sea level), sediment flux, bedrock resistance and tectonic deformation across the river course (e.g. Howard et al., 1994). Stream power increases along the steep gradient causing enhancement of sediment or bedrock erosion. The increased erosion increases sediment flux downstream (Burbank and Anderson, 2001 p. 162) leading to enhanced deposition.

Knickpoints will, in certain conditions, migrate upstream retaining the morphology (parallel retreat) leaving cut terraces behind, but they can also be smoothed out with or without upstream-migration by gradual decrease of the knickpoint lip gradient (slope replacement) (Gardner, 1983; Howard et al., 1994). The type of knickpoint evolution depends on the relationship between bottom shear stress (τ_o) and critical shear stress needed to initiate motion (τ_c), bed-load transport discontinuities and spatial variability of bed resistance (Gardner, 1983). Knickpoint retreat is most likely to occur if there is a resistant caprock where $\tau_c > \tau_o$ overlying a non-resistant layer, but retreat can also occur in homogeneous rock if the knickpoint has a height to flow depth ratio greater than 1 and the flow is sufficient to transport material away from the base (Burbank and Anderson, 2001). Knickpoint replacement occurs in uniformly resistant material where $\tau_c > \tau_o$ within the knickpoint reach, such as cohesive silts, clay and alluvial channels. Knickpoints can be formed due to differential erosion due to variation in resistance to erosion along channel (Burbank and Anderson, 2001). In the numerical models of Howard et al. (1994), knickpoints migrate when erosion rate is proportional to stream power but become rounded and smoothed out when erosion rate is proportional to bed shear stress.

Knickpoints have been identified along several submarine channels and canyons and can have various origins (Table 4.1). Although formed in a different environment, submarine knickpoints have many similar characteristics to their fluvial counterparts. Submarine channels are cut mainly by turbidity current scouring (Pratson and Coakley, 1996). According to Pirmez et al. (2000), turbidity currents can erode several tens of metres of seafloor in a few thousand years. Incision at the base of a flow increases when velocity increases (Mulder and

Cochonat, 1996) and velocity increases when slope steepens, therefore the incision rate increases when slope steepens (Pirmez et al., 2000; Kneller, 2003). Velocity reduction, flow spreading and deposition occur in topographically unconfined areas, areas of lower gradient and downslope from abrupt reductions in gradient (Nemec, 1990; Demyttenaere et al., 2000; Pirmez et al., 2000; Prather, 2003; Smith, 2004). The adjustment to the equilibrium profile across many knickpoints occurs by erosion and deposition as summarised in the model of Pirmez et al. (2000), in which erosion occurs along the channel upstream of the knickpoint and deposition of sediments occurs downstream, where the channel profile is lower than the equilibrium profile, until the equilibrium profile is restored.

Table 4.1. Submarine knickpoints in the literature

Origin of knickpoint	**System**	**Reference**
Avulsion	The Amazon	(Pirmez et al., 2000)
	The Rhone	(Pirmez et al., 2000)
	The Zaire	(Babonneau et al., 2002)
	The Magdalena	(Estrada et al., 2005)
Tributary confluences i.e. hanging valleys	The East Breaks (the Gulf of Mexico)	(Pirmez et al., 2000)
Normal faulting	The East Breaks (the Gulf of Mexico)	(Pirmez et al., 2000)
	The Niger Delta	(Pirmez et al., 2000; Adeogba et al., 2005)
Transition from one sub-basin to another	The East Breaks (the Gulf of Mexico)	(Pirmez et al., 2000)
	The Niger Delta	(Pirmez et al., 2000; Prather, 2003; Smith, 2004; Adeogba et al., 2005)
Diapirism	The Niger Delta	(Adeogba et al., 2005)
Variability in substrate properties	The Central Atlantic USA Margin	(Mitchell, 2004)
Folding in convergent plate margins	The Barbados Ridge Complex, the Caribbean	(Huyghe et al., 2004; Mitchell, 2006)
	The Makran accretionary wedge, Pakistan	(Kukowski et al., 2001)
	The Tenryu Canyon, Tokai Prism, Japan	(Soh and Tokuyama, 2002)
	Astoria Canyon, USA	(Mitchell, 2006)
	Alaskan slope, USA	(Mitchell, 2006)
? Canyon - channel transition	The Danube Canyon, Black Sea	(Popescu et al., 2004)
? Landslide headwalls	New Jersey continental Slope, USA	(Mitchell, 2006)
? Slope retreat	San Antonio Canyon, Chile	(Mitchell, 2006)
? Break of slope	Angola	(Gee and Gawthorpe, 2006)
Not specified	Monterey Channel, Western USA	(Masson et al., 1995)

Knickpoint evolution and morphology is influenced by various factors. Mitchell (2006) used numerical modelling of advection (migration) and diffusion (smoothing out) to replicate the morphology of knickpoints in the Barbados Canyon. The model reveals that advection sharpens knickpoint lips and diffusion rounds them, but when a boundary condition of nondeposition or erosion is applied at the base of the knickpoint, the diffusion only model can produce knickpoint morphology similar to the advection model.

The term knickpoint is used somewhat loosely here to describe a reach with a higher gradient than the adjacent reaches. Knickpoint terminology is adapted from Gardner (1983), where the knickpoint lip is the break in slope where the channel becomes oversteepened and the knickpoint face is the steep reach between the lip and the base of the knickpoint.

4.3 GEOLOGICAL SETTING AND DATABASE

The Niger Delta on the West African continental margin (Fig. 4.1) is a prolific hydrocarbon province. The delta is undergoing gravitational downslope collapse and this results in three structural domains: (1) an extensional domain dominated by growth faults, (2) a translational domain characterised by mud diapirism and (3) a compressional domain dominated by toe-of-slope thrusts (Damuth, 1994; Cohen and McClay, 1996; Morgan, 2004). This case study focuses on the ultra-deep-water compressional domain of the western Niger Delta, where the regional slope dips on average at 0.8° towards the southwest (Fig. 4.1). The toe-of-slope thrusts are orientated perpendicular to the slope and dip both upslope and downslope (forethrusts and backthrusts) (Fig. 4.2). Anticlines on the hangingwalls of these faults have up to 200 m of positive relief on the seafloor and are up to 7 km wide (Heiniö and Davies, 2006). This paper considers the response of the thalweg of an active channel-levee system (CLS) to growing folds orthogonal to its path.

The 3D seismic data cover an area of 1630 km^2 of the western Niger Delta (Fig. 4.1). It is zero-phase migrated and displayed so that an increase in acoustic impedance is a red-black-red reflection loop (see Brown, 1999 p. 35-47). The line spacing is 12.5 m in both the inline and crossline direction. For the conversion of two-way-travel time (TWT) to depth a velocity of 1480 ms^{-1} is used for seawater and 2000 ms^{-1} is used for sediment. The dominant frequency of the studied shallow section is 55 Hz and thus the tuning thickness ($\lambda/4$) is c. 9 m. The succession is subdivided using seismic reflections that define units with distinct internal seismic facies. Seismic attributes, including reflection dip and amplitude were used to reveal

depositional and deformational features. There are very few publicly available boreholes in this part of the Niger Delta. Lithological interpretation of the seismic facies in this paper follows earlier work done by Posamentier and Kolla (2003) and Deptuck et al. (2003), and is based on the recognition of seismic reflection character, amplitude and geometry, as well as the knowledge of unpublished well calibrations within the deepwater domain.

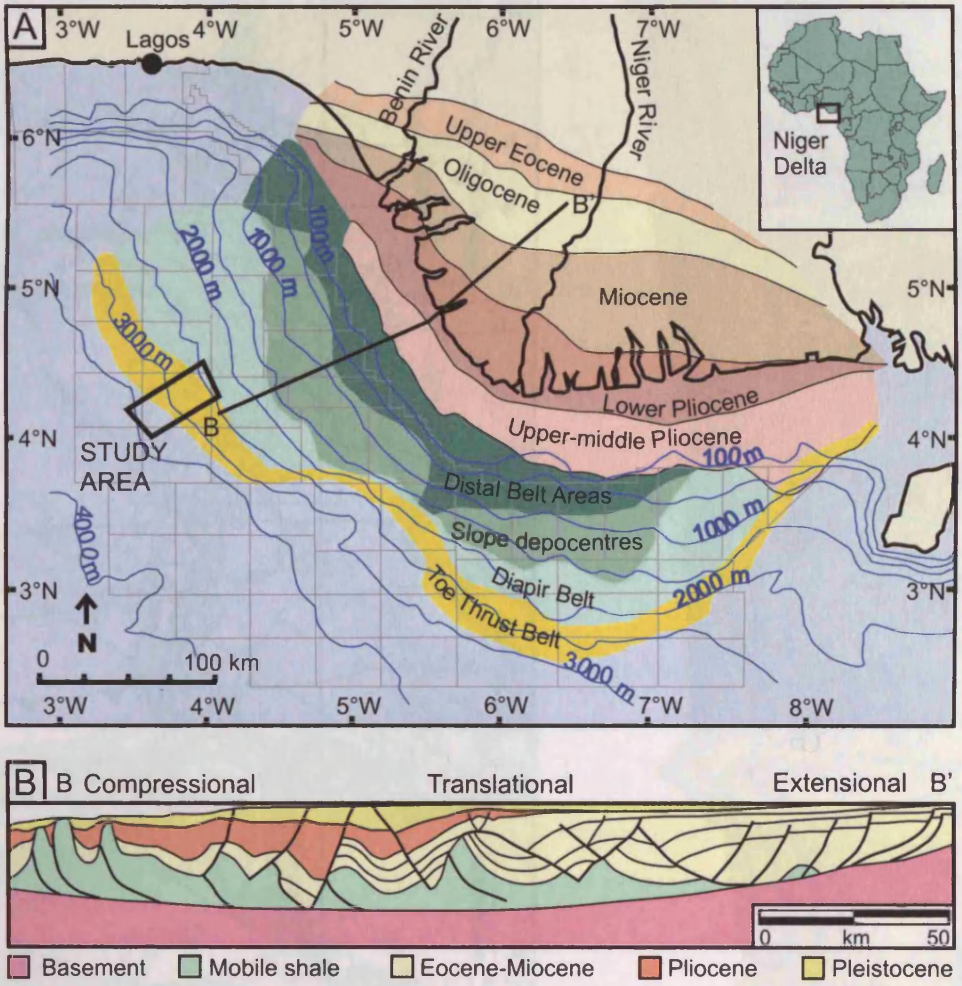

Figure 4.1. (A) Location of the study area at the outer thrust belt of western Niger Delta. Depobelts from Armentrout et al. (2000) and Hooper et al. (2002). Boxes outline offshore licence blocks. (B) Schematic cross section through the delta. Modified after Haack et al. (2000). Vertical exaggeration = 2.

4.4 CHANNEL-LEVEE SYSTEM (CLS)

4.4.1 Architectural elements

Two active channel-levee systems and a partially buried one are clearly visible on the seafloor of the study area (Fig. 4.2A). The CLS analysed here has a 1.5-6 km wide channel-belt, in which inner levees and channel-axis deposits are the dominant architectural elements (Fig. 4.3). The channel-belt is underlain by a basal erosional fairway and bordered by wedge-

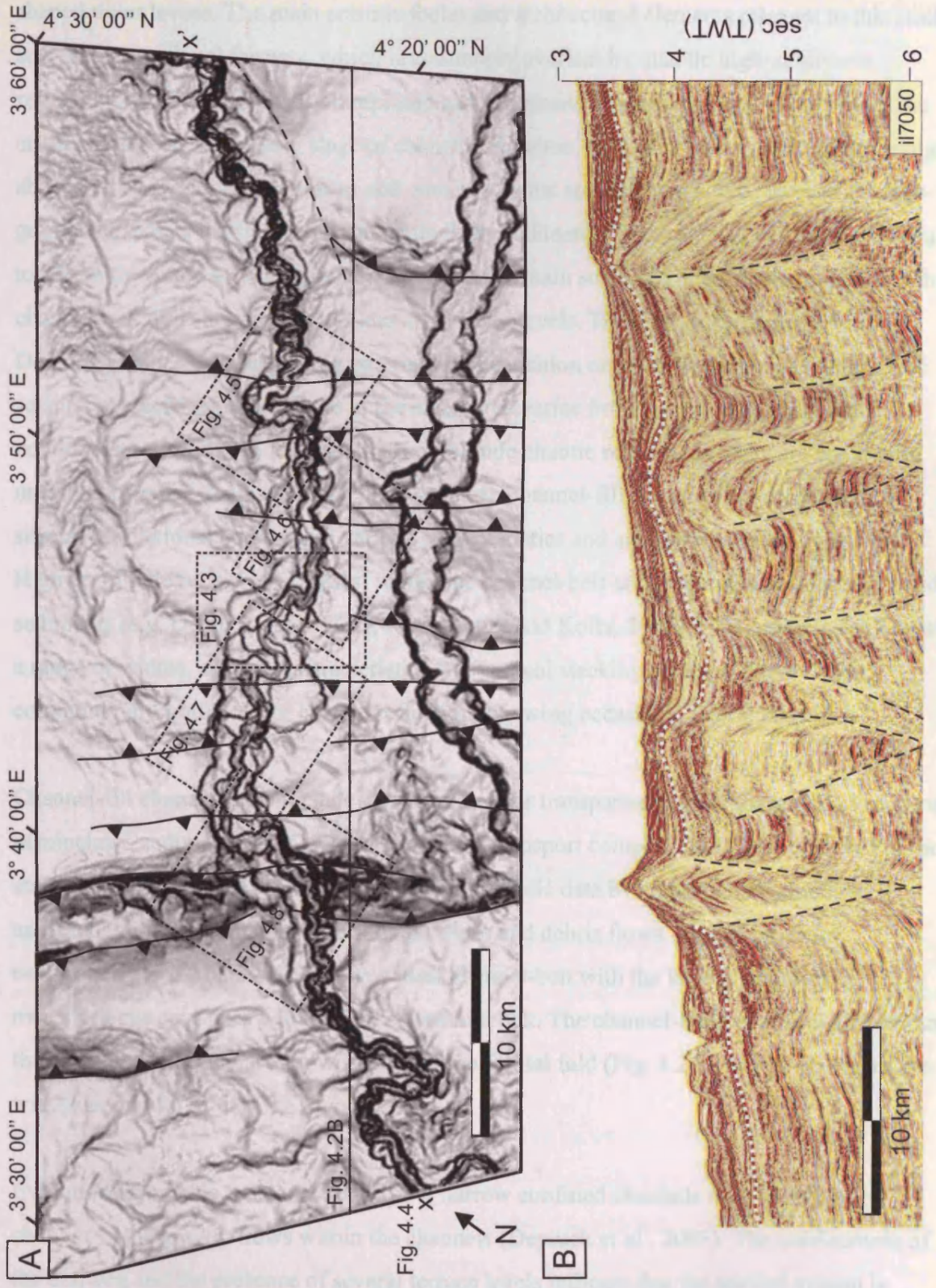

Figure 4.2. (A) Seabed dip magnitude map of the study area with the main thrusts in the subsurface traced and locations of Figures 4.5-4.8 indicated (dashed boxes). X-x' = location of end points of profiles shown in Fig. 4.4 along the studied channel. Darker shading means higher angle of dip. Maximum dip is c. 35° at some channel margins. Flow direction is from right to left. Location of area shown on Fig. 4.1A. (B) Downslope-orientated seismic line with main thrust faults traced. Dotted line marks the top of a mass transport complex, which is commonly incised by the studied CLS. Sec TWT = seconds two-way-travel time.

shaped outer levees. The main seismic facies and architectural elements relevant to this study are: (1) An erosional fairway, which is commonly overlain by chaotic high-amplitude reflections (HARs), which are interpreted as the deposits of semi-confined flows within the erosional fairway at an early stage of channel formation. (2) Outer levees, which form wedge-shaped cross-sectional geometries and consist of what are interpreted to be overspilled fine-grained turbidites interbedded with hemipelagic sediments. In the studied system they are up to 250 m thick and several kilometres wide and contain some sediment waves. (3) Within the channel-belt there are arcuate terraces at multiple levels. These are called inner levees by Deptuck et al. (2003) suggesting an origin by deposition on abandoned meander loops. The seismic character of inner levees in the study area varies from low- to high-amplitude continuous reflections to low- and high-amplitude chaotic reflections. They are commonly modified by small-scale slumping (Fig. 4.3). (4) Channel-fill elements are comprised of several depositional bodies with various characteristics and are commonly partly eroded. High-amplitude reflections (HARs) within the channel-belt are interpreted as coarse-grained sediments (e.g. Deptuck et al., 2003; Posamentier and Kolla, 2003). Channel-axis HARs show a range of widths, acoustic characteristics and vertical stacking patterns, but are most commonly discontinuous or chaotic reflections showing occasional lateral migration.

Channel-fill elements also include low-amplitude or transparent facies interpreted as mud-rich hemipelagic sediments. (5) One extensive mass transport complex (MTC) is identified in the study area (Fig. 4.3). MTCs are recognised on seismic data by contorted, chaotic low-amplitude reflections and include slumps, slides and debris flows. They contribute occasionally to the channel-fill. The widest channel-belt with the largest abandoned meanderloops coincides with the thrust and fold belt. The channel-belt becomes narrower and the channel depth increases downstream of the frontal fold (Fig. 4.2A), which decreases the width/depth ratio of the CLS significantly.

Evolution from wide erosional fairways to narrow confined channels may be caused by changes in the gravity flows within the channels (Deptuck et al., 2003). The confinement of the thalweg and the presence of several terrace levels indicate that the studied system is dominated by erosional flows but has a complex history involving several phases of incision and aggradation. Present day deposition occurs dominantly on inner levees and occasionally by overspilling on outer levees, as suggested by the wedge-shaped morphology and the presence of sediment waves on some parts of the outer levees (Fig. 4.3).

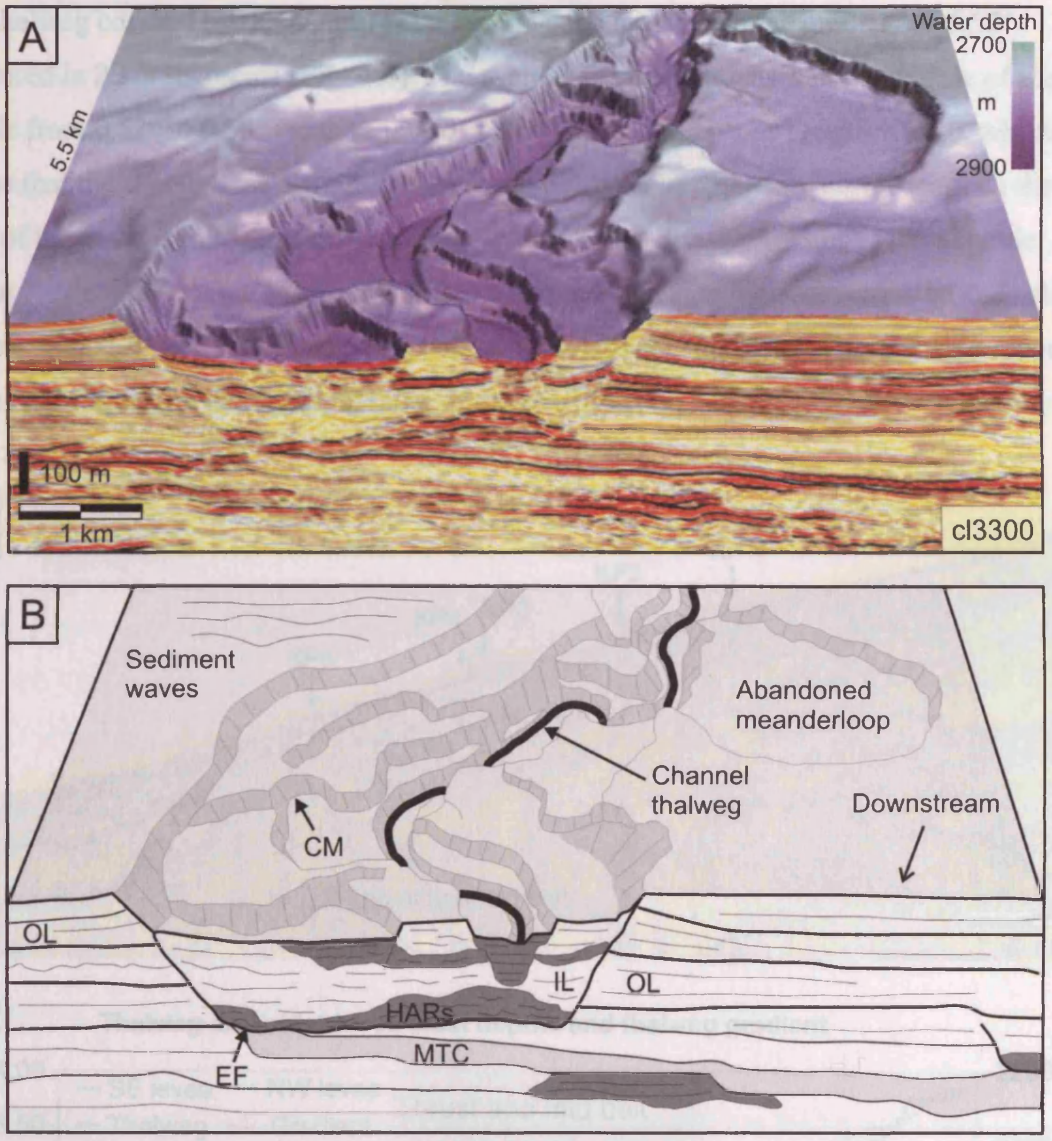

Figure 4.3. Seismic facies and architectural elements of the channel-levee system (CLS). (A) Seismic line with seabed structure map. Vertical exaggeration = 2.5. Location shown in Fig. 4.2A. (B) Line drawing of (A). EF = erosional fairway of the channel-belt, overlain by chaotic high-amplitude reflections (HARs). OL = outer levees, which confine the channel-belt. IL = inner levees. CM = collapsed margin. MTC = mass transport complex.

4.4.2 Present day channel thalweg

The present day channel thalweg is located 100-220 m below the outer levee crests. The channel walls can have slopes up to 36°. Channel wall morphology is most likely to be determined by the activity of turbidity currents within the channel. Centrifugal forces cause increased flow stripping onto levees and erosion at the base of outer bends. This results in higher and steeper walls on the outer bends and gentler walls on inner bends (Babonneau et al., 2004). In plan view the channel thalweg is c. 80 m wide. Measured in 2 km segments, the average sinuosity of the thalweg is 1.3, ranging from 1.0 to 2.8 and the mean radius of curvature measured from best-fit circles at each bend (Morisawa, 1985) is c. 350 m.

The thalweg covered by the dataset is 95 km long and has an average gradient of 0.55° measured in 2 km segments (Fig. 4.4). The average gradient increases in the middle of the profile from 0.52° to 0.59° (with ranges of 0.08-1.14° and 0.32-0.89° respectively), which means that the channel has a slightly convex-up profile. The convexity correlates with the zone of thrusts and folds across the channel and indicates that the thalweg is not at grade (sensu Prather, 2003), but has been uplifted above grade due to thrust propagation and fold growth. The right and left levee crest profiles are relatively similar to each other and record some of the uplift by convex-up flexure of the profiles (Fig. 4.4B).

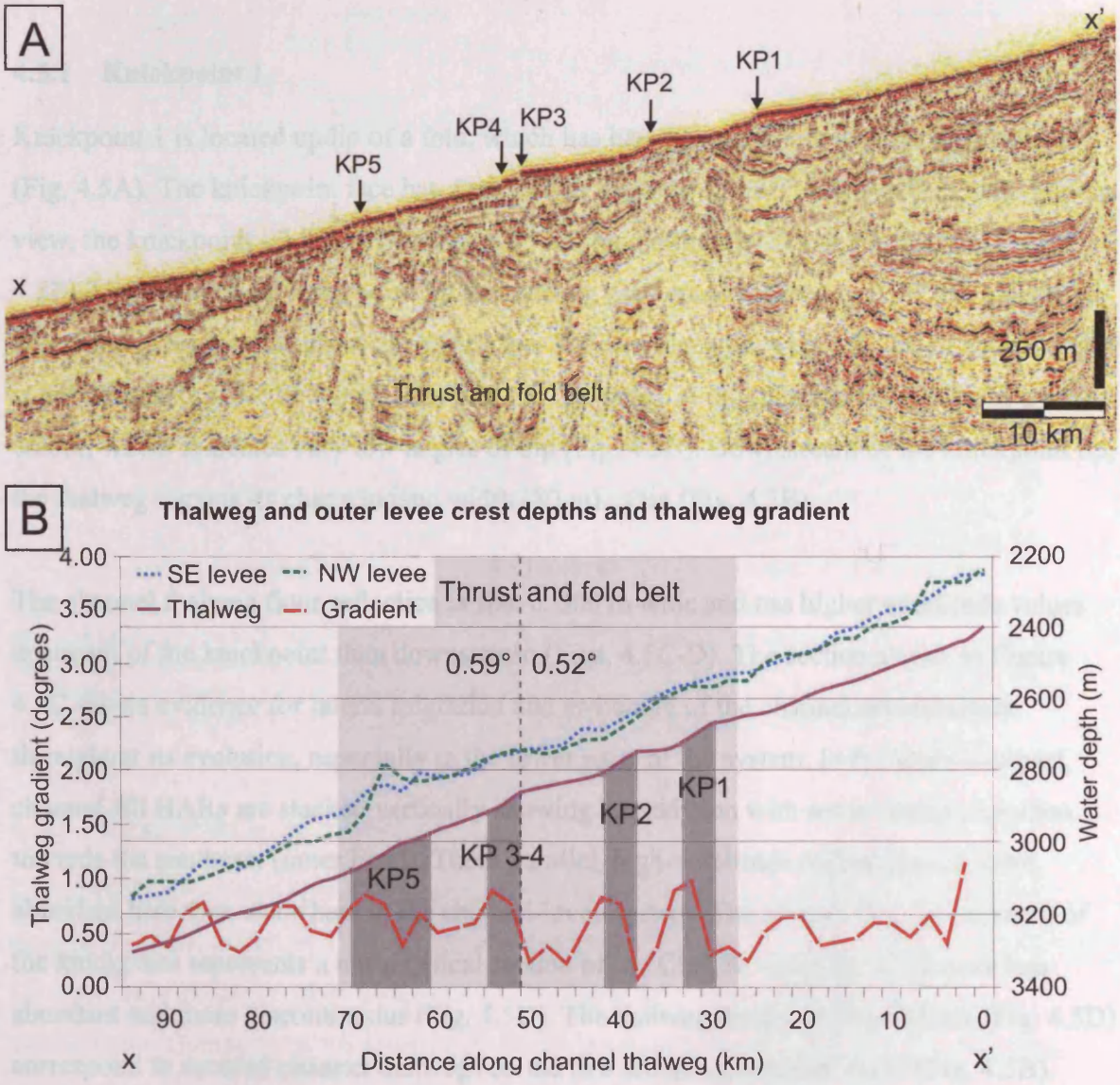

Figure 4.4. Present day channel thalweg profile. The knickpoints described in this paper are marked as KP1-KP5. (A) Seismic line along the sinuous channel thalweg. Location of x-x' shown on Fig. 4.2A. The thrusts and folds are not clearly imaged due to the sinuous course of the seismic line. (B) Graph showing the thalweg profile and gradient and levee profiles measured in 2 km increments. Note the increase of the gradient values in the middle of the uplifted thrust and fold belt (shaded). Datapoints shown in Figure 2.4B.

4.5 KNICKPOINTS 1-5

The present day channel has several knickpoints along its thalweg. The largest knickpoints occur above the thrust and fold belt, and are clearly identified from the thalweg profile because of their high gradients (Fig. 4.4). In addition, some knickpoints are characterised by very low gradient reaches upstream of them. Three types of knickpoints are distinguished according to their size, morphology and maturity. Five representative examples (KP 1-5) are described below. Knickpoints 1 and 2 represent the largest and the least mature Type I, knickpoints 3 and 4 the intermediate Type II and knickpoint 5 the most mature and smallest knickpoint Type III.

4.5.1 Knickpoint 1

Knickpoint 1 is located updip of a fold, which has bathymetric effect on adjacent seafloor (Fig. 4.5A). The knickpoint face has a maximum gradient of 4.86° and is 200 m long. In plan view, the knickpoint lip forms two arcs c. 850 m long obliquely across the channel (Fig. 4.5B). Upstream of the knickpoint lip the thalweg gradient is reduced to 0.30° for a distance of c. 5 km. This reach is characterised by a c. 500 m wide zone, where the 80 m wide thalweg is not defined (i.e. the thalweg becomes c. 500 m wide). A dip map represents this as a white colour, which indicates very low angles of dip (Fig. 4.5B). Downstream of the knickpoint lip, the thalweg regains its characteristic width (80 m) again (Fig. 4.5B).

The channel thalweg floor reflection is flat, c. 500 m wide and has higher amplitude values upstream of the knickpoint than downstream (Figs. 4.5C-D). The section shown in Figure 4.5C shows evidence for lateral migration and switching of the channel several times throughout its evolution, especially in the lower parts of the system. In the shallower part, channel-fill HARs are stacked vertically showing aggradation with some lateral migration towards the southeast (inner bend). These parallel, high-amplitude reflections are more abundant here than elsewhere in the channel-levee system. The seismic line downstream of the knickpoint represents a more typical section of the CLS, in which the HARs are less abundant and more discontinuous (Fig. 4.5D). The thalweg scours on the seafloor (Fig. 4.5D) correspond to scoured channel thalwegs on the two arcuate knickpoint faces (Fig. 4.5B).

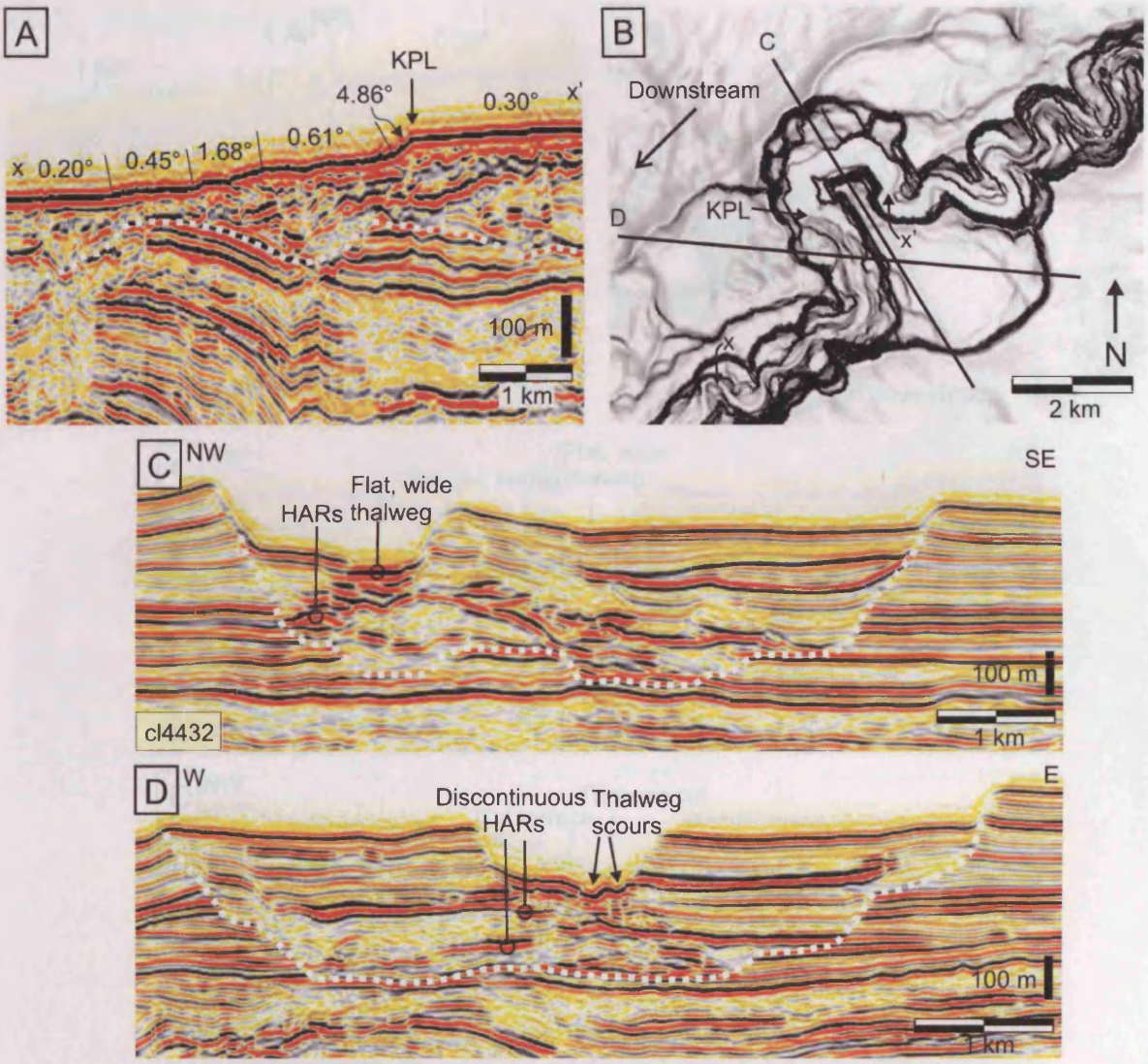

Figure 4.5. Morphology of knickpoint 1. (A) Thalweg profile across knickpoint 1. KPL = knickpoint lip in this and subsequent Figures. (B) Seabed dip map showing planform morphology of knickpoint 1. Note how knickpoint lip comprises two arcs. X-x' marks the location of (A) along thalweg. Location shown in Fig. 4.2A. (C) Seismic line across the channel-levee system upstream of knickpoint 1. (D) Seismic line across the CLS downstream of knickpoint 1. Dotted line on all cross sections marks the base of the CLS.

4.5.2 Knickpoint 2

Knickpoint 2 is located above the forelimb of a thrust-propagation fold and has a similar morphology to knickpoint 1 (Fig. 4.6). The maximum gradient of the knickpoint face is 4.74° for a distance of 300 m, after which the gradient gradually decreases to 0.42° going downstream. Upstream of the knickpoint lip the gradient is 0.20° for c. 2.5 km. This low-gradient reach also correlates to widening of the thalweg from 80 m to 500 m (Fig. 4.6B). The knickpoint lip is arc-shaped in plan view and c. 570 m long. Downstream the thalweg is 80 m wide again.

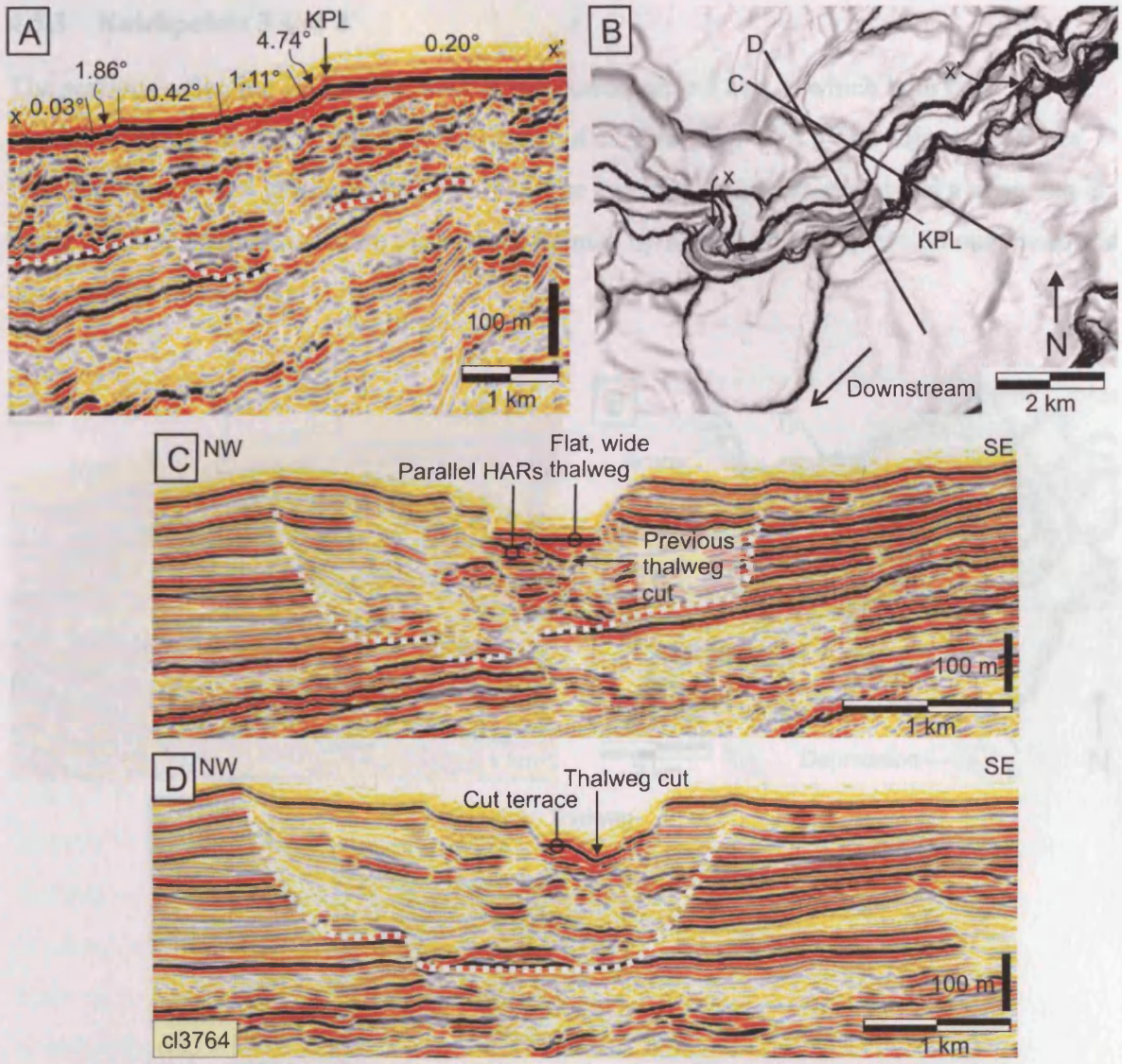

Figure 4.6. Morphology of knickpoint 2. (A) Thalweg profile across knickpoint 2. (B) Seabed dip map showing planform morphology of knickpoint 2. Location shown in Fig. 4.2A. (C) Seismic line across the channel-levee system upstream of knickpoint 2. Note the previous thalweg cut below the present day 400 m wide thalweg reflection. (D) Seismic line across channel downstream of knickpoint 2 showing v-shaped morphology. The terrace on the north-western side is interpreted as a remnant deposit cut by the thalweg. Dotted line on all cross sections marks the base of the CLS.

The cross section upstream of knickpoint 2 shows continuous parallel HARs in the channel-fill (Fig. 4.6C). The present day thalweg is 400 m wide in the section. It is flat and has very high amplitude. Directly beneath it, a reflection dips towards the southeast before flattening to a c. 80 m wide horizontal reflection. 1.2 km downstream, the channel-levee system has a different architecture with fewer HARs. The channel is v-shaped and the thalweg is 80 m wide (Fig. 4.6D).

4.5.3 Knickpoints 3 and 4

The seafloor reflection is discontinuous across knickpoints 3 and 4, which both have maximum angles of c. 25° and a vertical relief of c. 25 m (Fig. 4.7A). The adjacent reaches have low to very low gradients (0.30-0.03°). The knickpoints are located above a zone that is being uplifted, as manifested on the seabed dip map by a scarp and a depression outside of the channel-belt (Fig. 4.7B).

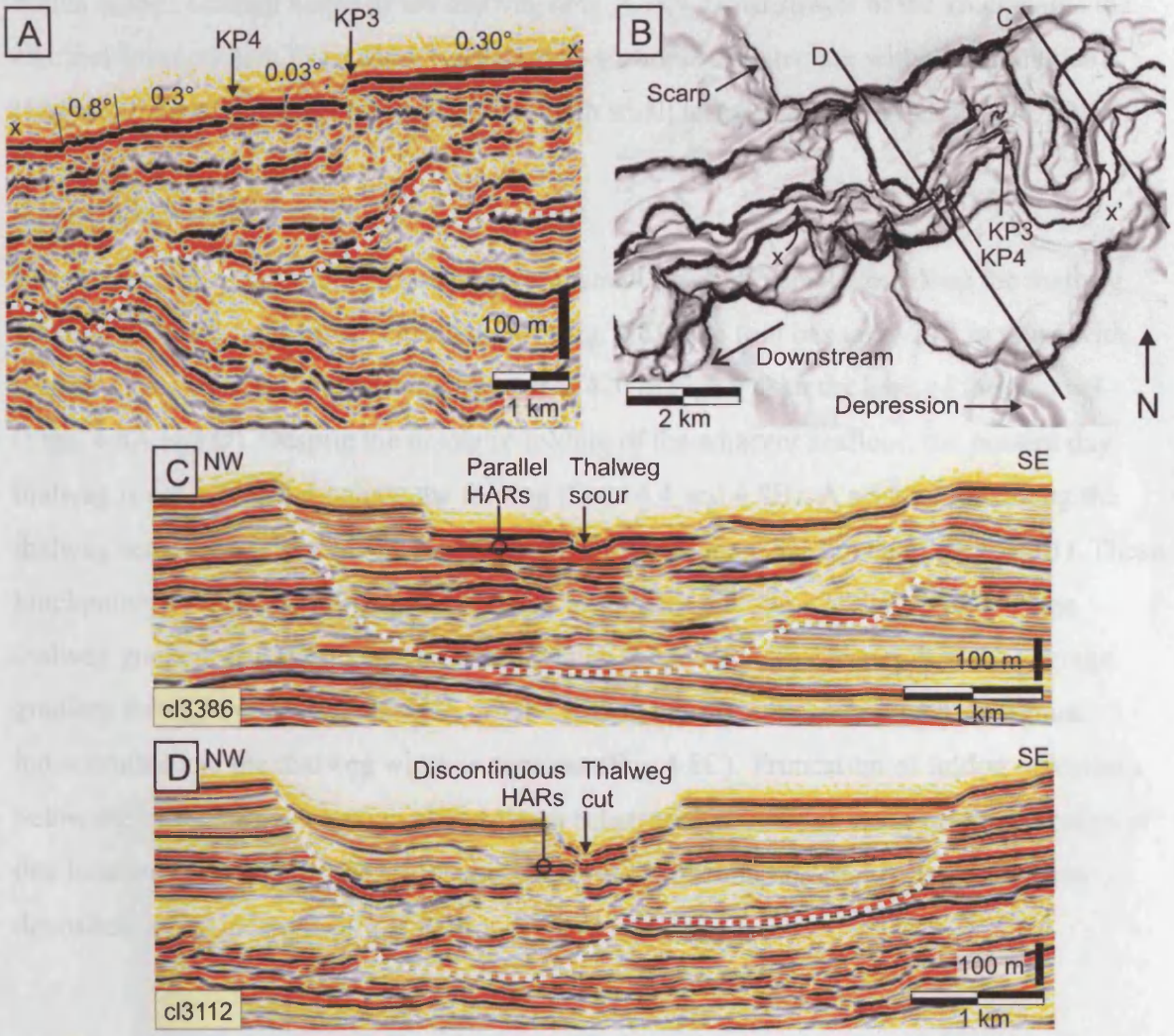

Figure 4.7. Morphology of knickpoints 3 and 4 (KP3 and KP4). (A) Thalweg profile across knickpoints 3 and 4 showing discontinuous seabed reflection with stepped appearance across the knickpoints. (B) Seabed dip map showing the planform morphology of knickpoints 3 and 4. The knickpoint lips are as wide as the thalweg, which can be traced upstream of them in contrast to knickpoints 1 and 2. The scarp and the depression are formed above the uplifting anticline. Location shown in Fig. 4.2A. (C) Seismic line across the CLS upstream of knickpoint 3. Thalweg scour is c. 20 m below the high-amplitude terraces. Note dominant parallel continuous HARs in the channel-fill. (D) Seismic line across channel downstream of knickpoint 4. Note the lack of parallel HARs. Dotted line on all cross sections marks the base of the CLS.

Knickpoints 3 and 4 can be identified on the seabed dip map as abrupt deeper incisions of the thalweg, which appear as darker outlines of the thalweg (Fig. 4.7B). The knickpoint lips are thus as wide as the thalweg. The gradient is low upstream of the knickpoint lips, but unlike in knickpoints 1 and 2, the 80 m wide thalweg can be traced throughout the uplifted zone. This can also be seen in the cross section of the channel upstream of knickpoint 3 (Fig. 4.7C). The most recent part of the system is dominated by continuous parallel HARs that are incised by the thalweg to a depth of c. 20 m. The scour is 280 m wide but its flat base is 80 m wide, which is the common width of the thalweg (Fig. 4.7C). Downstream of the knickpoints the channel-levee system has a more typical cross-sectional architecture with discontinuous HARs and deeply incised, narrow thalweg with small terraces adjacent to it (Fig. 4.7D).

4.5.4 Knickpoint 5

The last example comprises a zone of several small knickpoints located along the thalweg where it passes through a large frontal fold (Fig. 4.8). The fold has up to 200 m relief with respect to the adjacent seafloor and its crest is 420 m higher than the base of the channel (Figs. 4.8A and D). Despite the dramatic folding of the adjacent seafloor, the present day thalweg is not affected much by the folding (Figs. 4.4 and 4.8B). A seismic line along the thalweg across the fold shows a series of small knickpoints 0.5-1 km apart (Fig. 4.8B). These knickpoints have 6-10 m high and 50-100 m long faces with dips of 4-7°. The average thalweg gradient is 0.68° along this reach, which is considerably steeper than the average gradient throughout the data (0.55°). On the seabed dip map the knickpoints are almost indiscernible and the thalweg width is constant (Fig. 4.8C). Truncation of folded reflections below the channel-levee system shows that a substantial amount of strata has been eroded at this location (Fig. 4.8B). The CLS is only c. 100 m thick and no outer levees have been deposited at this location (Fig. 4.8D).

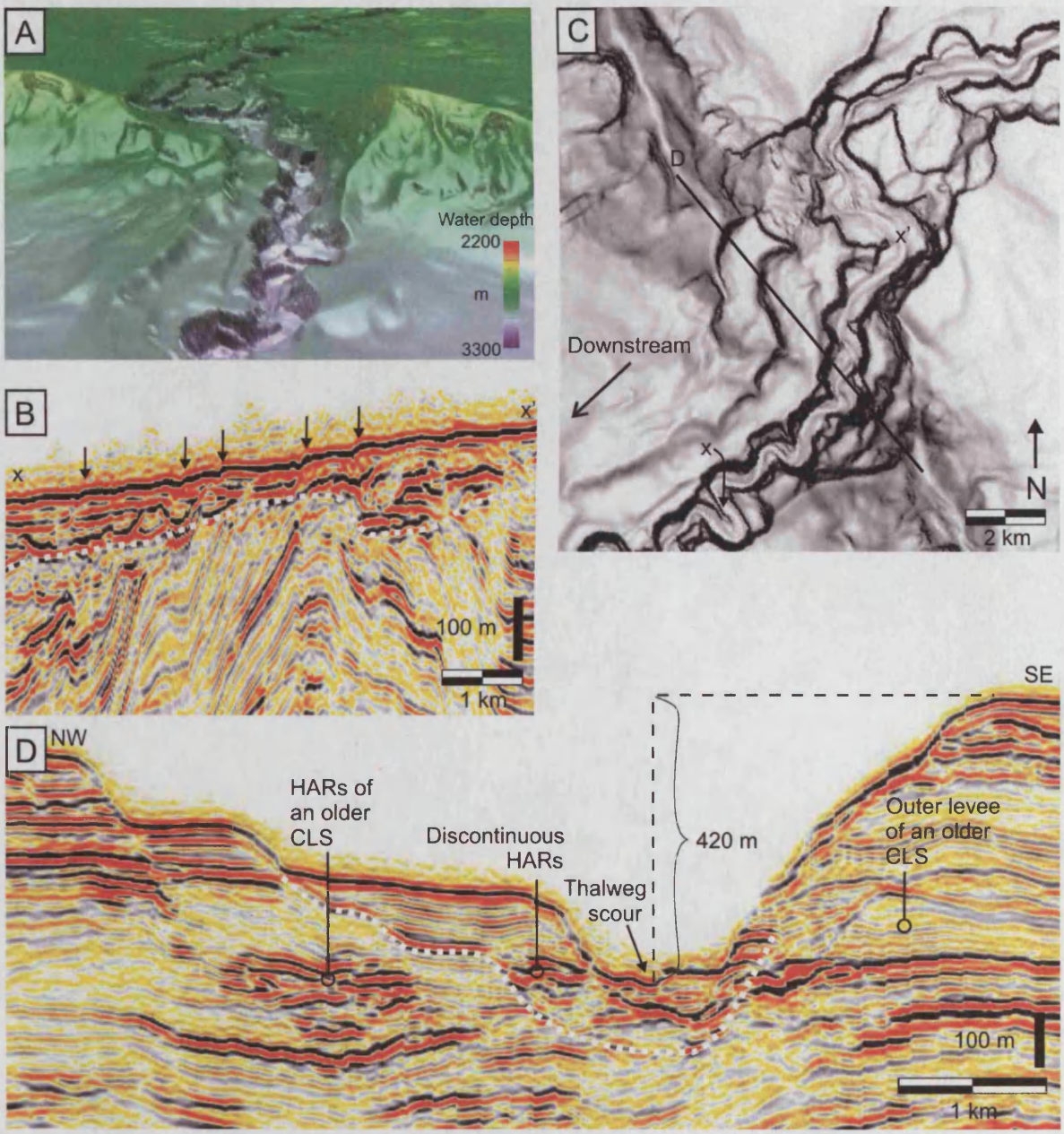

Figure 4.8. Morphology of the channel across the frontal fold (knickpoint 5). (A) 3D perspective view of seabed showing the channel as it breaches through the frontal fold. (B) Seismic section along the sinuous thalweg showing its profile and truncation of underlying folded reflections. Small knickpoints, 6-10 m high and 4-7° steep, are marked with arrows. Location of x-x' shown in (C). (C) Seabed dip magnitude map with present day thalweg imaged as a white line and locations of (B) and (D) indicated. Location shown in Fig. 4.2A. (D) Seismic line across the CLS at frontal fold. Parts of older channel systems are preserved on both sides of the present day channel. Dotted line on all cross sections marks the base of the CLS.

4.5.5 Reflection amplitude

The amplitude patterns of the seabed reflection in the vicinity of knickpoints are shown in Figure 4.9. The inter-channel seabed and most terraces are dominated by low-amplitude values shown in purple. The terraces closest to the thalweg commonly exhibit intermediate amplitude values shown in green. These terraces are no more than 30 m above the thalweg.

The highest values are shown in red and yellow and are found mainly in several kilometres long elongate zones within the channel upstream of knickpoints 1 and 2, where the thalweg is widened 6-fold and has a low gradient (Figs. 4.9A and B), and on the terraces upstream of knickpoint 3 (Fig. 4.9C). The high-amplitude (red and yellow) terraces upstream of knickpoint 3 are found in a c. 500 m wide and c. 5 km long zone, very similar to knickpoints 1 and 2 (Fig. 4.9C). The terraces are separated by the c. 80 m wide thalweg, which is entrenched 6-20 m below them. Small terraces with only intermediate amplitudes are observed adjacent to the thalweg across the frontal fold, no high-amplitude values are observed upstream of the fold (Fig. 4.9D).

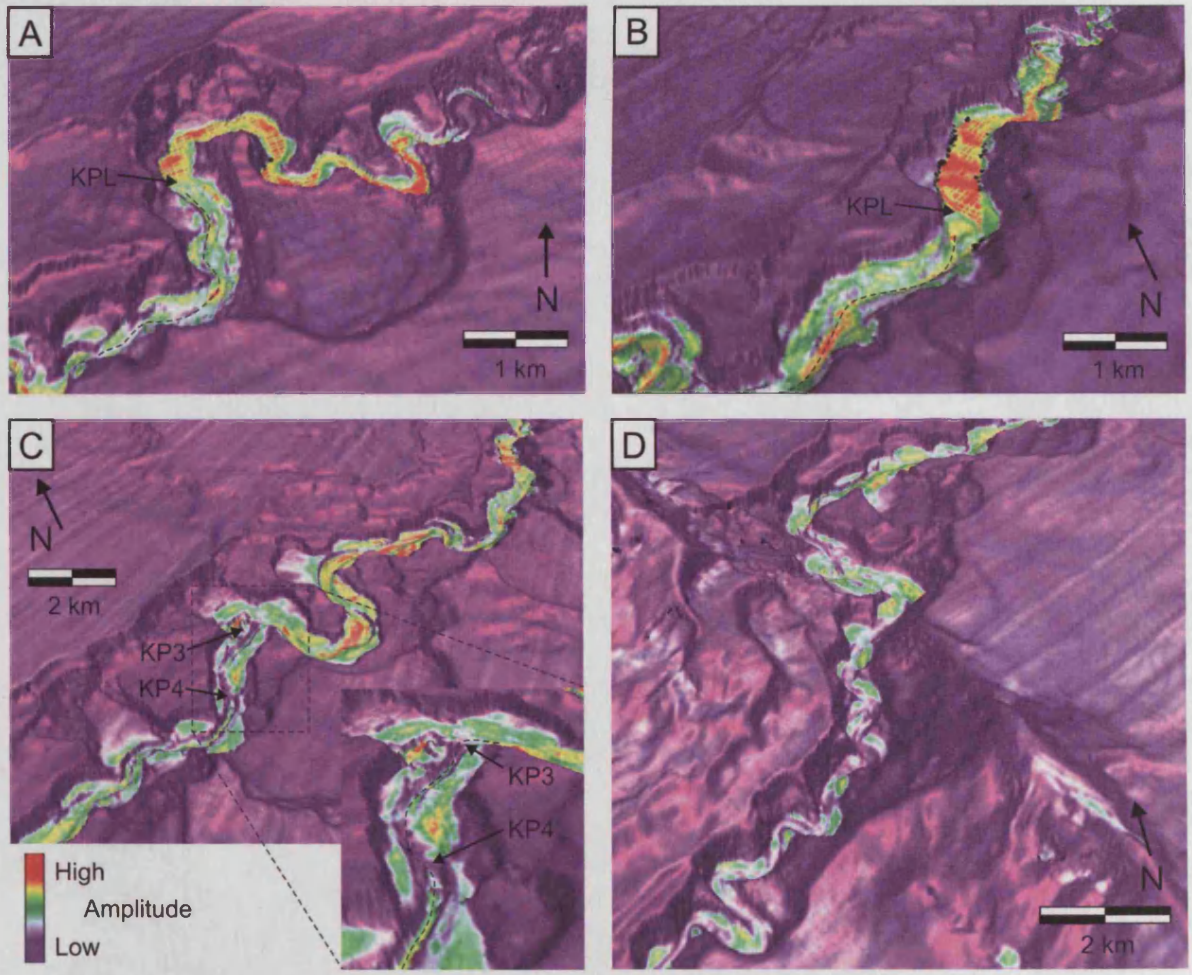

Figure 4.9. Perspective views of knickpoints with acoustic amplitude values of the seabed reflection shown. (A) Knickpoint 1 with high amplitudes shown in red and yellow concentrated on wide low-angle zone upstream of the arcuate knickpoint lip (KPL). (B) Knickpoint 2 with high amplitudes upstream of knickpoint lip. (C) High amplitude values on terraces several kilometres upstream of knickpoint 3. (D) Terraces and channel floor across the frontal fold and upstream of it show moderate amplitude values (green).

4.6 INTERPRETATION OF SEISMIC DATA

The amplitude value of a reflection can give clues about grain size, with high amplitudes commonly corresponding to coarse-grained sediments (Deptuck et al., 2003; Posamentier and Kolla, 2003). Therefore the high amplitudes of some terraces and along the thalweg upstream of knickpoints 1-3 are interpreted as deposits of the coarsest load of turbidity currents. Although no information on real grain size is available, these deposits are referred to as "coarse deposits" below. The low-amplitude values on higher terraces and the inter-channel seabed are interpreted to correspond to fine-grained sediments derived from the turbidity current plume and hemipelagic sedimentation.

The high-amplitude reflections are interpreted to have a recent depositional origin based on the reflection geometry and thalweg morphology. The dipping reflection beneath the present day thalweg reflection upstream of knickpoint 2 (Fig. 4.6C) is interpreted as a previous channel cut that has been subsequently filled by coarse deposits manifested by flat HARs. The v-shaped geometry of the channel cross section downstream of knickpoint 2 (Fig. 4.6D) suggests less deposition and more dominant bypass or erosion by turbidity currents at this location and the channel is interpreted to be empty of coarse deposits. A high-amplitude terrace located on the northwest side of the thalweg in Figure 4.6 is interpreted as a cut terrace, i.e. an erosional remnant of high-amplitude channel-fill left behind after knickpoint migration. Truncation of folded reflections beneath the CLS and the low thickness of the CLS deposits across the frontal fold (Fig. 4.8) suggest that it has been a zone of erosion and bypass for a long time. However, it is difficult to assess the relative timing of phases of fold growth, channel erosion and fill. It is likely that both fold amplification and erosion have occurred episodically and that several knickpoints have already migrated through the entire frontal fold bringing the channel profile closer to equilibrium. Thus knickpoint 5 represents a more mature stage of knickpoint migration.

4.7 MODEL FOR KNICKPOINT FORMATION AND MIGRATION

The knickpoints in the studied channel-levee system are interpreted to have formed in response to gradient changes along the thalweg, brought about by the growth of the folds (Fig. 4.10). Although knickpoints could form as a response to changes in gravity flows, the location of knickpoints above the thrust and fold belt suggests structural control for their formation. Gradient changes can cause changes in sinuosity in some submarine channels (Pirmez et al.,

2000; Adeogba et al., 2005), however, the high degree of confinement of the studied thalweg within its levees (100-220 m deep) prevents major avulsion or sinuosity changes. Instead, flows passing through the channel respond to the uplift by depositing and eroding in specific areas. The uplift of an anticline across the channel causes local reduction of gradient and concavity of the thalweg upstream of the fold axis, and also an increase in gradient of the thalweg profile downstream of the fold. These changes in gradient have an effect on the behaviour of turbidity currents within the channel. Flows decelerate as gradient is reduced, which leads to deposition of the coarsest sediments within the flow. Deposition thus occurs upstream of the folds where gradient is decreased and knickpoints are formed downstream, where the gradient is increased and erosion is enhanced by flow acceleration (Fig. 4.10A). Similar process of sand deposition by turbidity currents on shallower upstream flanks and erosion or bypass on steeper downslope flanks is thought to be the mechanism by which upstream-migrating sediment waves are formed (e.g. Ercilla et al., 2002; Wynn and Stow, 2002). Adeogba et al. (2005) calculated that depositional fans developed after a 50-57 % reduction of gradient but 40 % change would be sufficient. In this study the thalweg gradient reduction is 55 % where deposition occurs upstream of folds.

It is proposed that knickpoints begin as small scours eroded by turbidity currents and that grow into larger features by positive feedback, in which steeper gradient enhances erosion and this newly formed erosional scour promotes further erosion. Increase in turbulence in steeper parts of the channel or hydraulic jumps (Komar, 1971) at the base of knickpoint faces may also play a role in increased erosion. Once formed, the knickpoints can smooth out or migrate upstream as zones of erosion and deposition (Fig. 4.10A; T_3 - T_4). It is possible, that after migration of a knickpoint, no evidence of deposits is left (T_4A) or that coarse sediments are preserved preferentially upstream due to the increased erosion rate downstream of fold (T_4B). Increased erosion rate may also lead to preservation of older deposits upstream but not downstream (T_4C) (Fig. 4.10).

The location of knickpoint 1 upstream of a fold suggests that it has migrated upstream. Similar upstream migrations of knickpoints have also occurred on the Alaskan and Barbados accretionary prisms (Mitchell, 2006). Knickpoints 3 and 4 differ from 1 and 2 as they do not have 500 m wide arcuate knickpoint lips and widened thalwegs upstream of them. Their lips are as wide as the thalweg and also much steeper and shorter (Fig. 4.7). This may be the result of slightly different pre-conditions, such as rate of uplift or variability in the susceptibility of

the substrate to erosion, or represent a different stage in knickpoint development. Figure 4.10B illustrates two possibilities for the planform evolution of the knickpoints of this study.

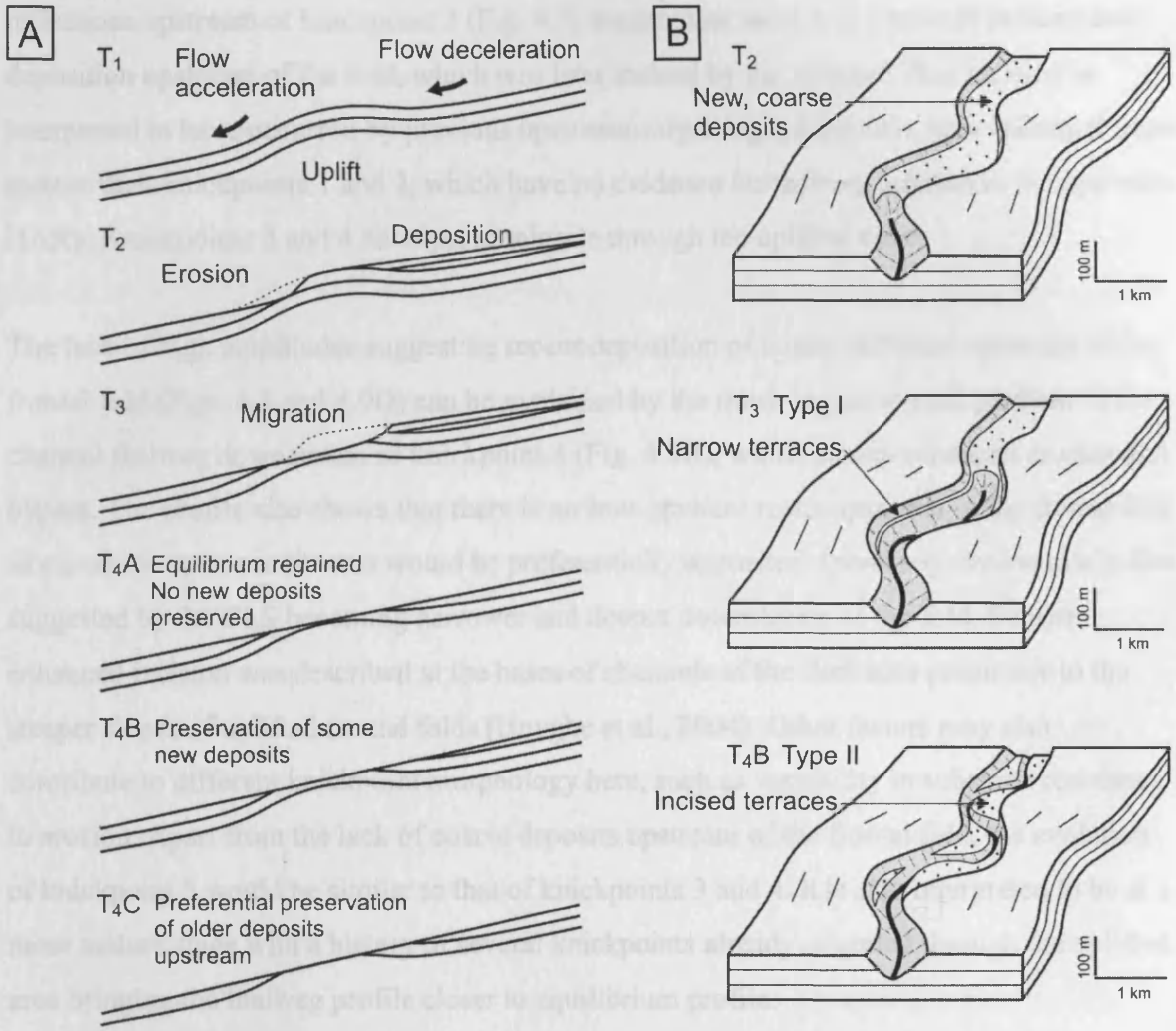

Figure 4.10. Idealised evolution of a channel-confined knickpoint. Not to scale. (A) Erosional and depositional processes along thalweg. At time T_1 the growing fold lifts the channel profile out of equilibrium. The uplift leads to local reduction of thalweg gradient upstream and increase in gradient downstream of the fold. This decelerates flows and causes deposition upstream and accelerates flows causing erosion downstream forming a knickpoint (T_2). The knickpoint can migrate upstream as erosion continues along the steep knickpoint face (T_3). The thalweg will regain its equilibrium profile eventually with no coarse sediments preserved upstream (T_4A), some coarse sediments preserved (T_4B) or preferential preservation of older sediments upstream and erosion downstream (T_4C). (B) 3D cartoons illustrating key development stages and variety of erosion and depositional patterns. Stippled pattern represents coarse sediments deposited upstream of folds due to fold growth. T_2-T_4 corresponds to T_2-T_4 in (A). Type I illustrates how a wide, headward-migrating knickpoint leaves only narrow terraces of coarse deposits behind, typical of knickpoints 1 and 2. Type II illustrates how a narrow thalweg incises into coarse deposits, cutting them into small terraces representative of the evolution of knickpoints 3-4.

Both models assume that the knickpoints migrate upstream (advect) rather than smooth out (diffuse). The assumption is based on the presence of cut terraces, sharp knickpoint lip morphology and the location of some knickpoints upstream of folds. Once formed, the valley-wide arcuate knickpoint can migrate upstream leaving only narrow cut terraces behind (Fig.

4.10B; T_3) as is observed in knickpoints 1 and 2. Alternatively, a thalweg-wide knickpoint can migrate upstream and the channel cuts into previously deposited coarse sediment leaving remnant sandy deposits on terraces above it (Fig. 4.10B; T_4). The zone of high-amplitude reflections upstream of knickpoint 3 (Fig. 4.9) suggest that there was a zone of preferential deposition upstream of the fold, which was later incised by the channel. This incision is interpreted to have occurred by previous upstream-migrating knickpoints, thus making it more mature than knickpoints 1 and 2, which have no evidence for thalweg incision in the upstream HARs. Knickpoints 3 and 4 have yet to migrate through the uplifted zone.

The lack of high amplitudes suggesting recent deposition of coarse sediment upstream of the frontal fold (Figs. 4.8 and 4.9D) can be explained by the much higher overall gradient of the channel thalweg downstream of knickpoint 4 (Fig. 4.4B), which causes enhanced erosion and bypass. The profile also shows that there is no low-gradient reach upstream of the frontal fold along which coarse sediments would be preferentially deposited. Increased erosion rate is also suggested by the CLS becoming narrower and deeper downstream of the fold. Similar enhanced incision was described at the bases of channels of the Barbados prism due to the steeper slopes of uplifted frontal folds (Huyghe et al., 2004). Other factors may also contribute to different knickpoint morphology here, such as variability in substrate resistance to erosion. Apart from the lack of coarse deposits upstream of the frontal fold, the evolution of knickpoint 5 would be similar to that of knickpoints 3 and 4. It is also interpreted to be at a more mature stage with a history of several knickpoints already migrated through the uplifted area bringing the thalweg profile closer to equilibrium profile.

4.8 DISCUSSION

4.8.1 Role of knickpoints in influencing channel architecture

Submarine channel complexes commonly show complex architectures with multiple internal erosion surfaces (Beaubouef et al., 1999; Deptuck et al., 2003; Posamentier and Kolla, 2003). Furthermore, knickpoints are being increasingly recognised in submarine channels (Table 4.1). Consequently, the role of knickpoint migration versus other processes, such as erosion by increasing the density and velocity of gravity flows within channels, is unclear.

The presence of knickpoints on the present day channel thalweg of the western Niger Delta suggests that their development could be a common process, which has likely occurred

throughout the evolution of the channel-levee system. Due to the limitations of seismic resolution, no knickpoints have been identified in the subsurface of the study area. The sinuous ribbon-like channel-fill elements have been cannibalised by younger channels, making mapping of a continuous channel-axis deposit and identification of knickpoints in the subsurface extremely challenging. It is, however, anticipated that the kind of knickpoints described in this paper can occur at any stage of channel evolution. Due to the transient nature of knickpoints, it is difficult to assess whether uplifted folds were eroded by erosive flows or by knickpoint migration, but the latter appears to be the dominant process by which they are eroded in the study area. It is also worth considering, when interpreting outcrops of channel-levee systems with multiple erosion surfaces, that the erosion could have been caused by local deformation of the channel profile, rather than wholesale changes in flow parameters.

The largest deposits upstream of knickpoints described here are tens of metres thick and thus in general only one reflection thick and difficult to identify in the subsurface from seismic reflection data. The sections across the channel both upstream and downstream of knickpoints (Figs. 4.5-4.7) indicate that there are much more continuous parallel high-amplitude reflections (i.e. relatively coarse sediments) upstream than downstream of the knickpoints. The implication of this is that stacking patterns and seismic facies of channel-fill can vary dramatically over short (100s of metres) distances along channel. This could be due to various processes. Sediments deposited uniformly along channel may be preferentially preserved upstream of folds, whereas enhanced erosion on steeper slopes downstream erodes them away. However, the distribution of high-amplitude values along present day thalweg (Fig. 4.9) strongly suggests that there are zones of preferential deposition of coarser sediments upstream of knickpoints 1-3. It is likely that they have also been zones of preferential deposition previously, resulting in more continuous reflections on seismic data upstream of folds. Depocentres forming upstream of diapirs are known in other submarine systems (e.g. Adeogba et al., 2005; Gee and Gawthorpe, 2006). Deposition upstream of anticlinal folds, and formation of knickpoints downstream of them, has also been documented in some fluvial systems, e.g. Wheeler Ridge (Burbank et al., 1996) and Kabul River (Burbank and Anderson, 2001). Additionally, the stream table experiments of Ouchi (1985) and the numerical models of Humphrey and Konrad (2000) and Snow and Slingerland (1990) had similar results. Both preferential deposition and preservation potential are higher upstream of folds, therefore coarser channel-axis deposits are more likely to be found upstream of folds.

Although the model presented here predicts migration of knickpoints and erosion of coarse deposits upstream of folds, they may also be preserved under certain conditions, e.g. by preferential preservation as discussed above or if the channel was abandoned and filled with hemipelagic sediments. Alternatively, avulsion within the channel-belt could also lead to preservation. One possible scenario for this is shown schematically in Figure 4.11. Avulsion may take place if the deposition on the upstream reach continues until it fills the channel to the height of adjacent terraces. The channel may then abandon the old thalweg reach containing the knickpoint and coarse sediment deposits, which would subsequently become sealed by fine-grained sediments from the upper parts of turbidity currents and hemipelagic sedimentation. In the studied system, large abandoned meanderloops occur near the folds (Fig. 4.2), suggesting that avulsion and sinuosity changes were more common in the earlier stages of channel evolution, probably when the channel was less confined and therefore meander bend growth easier. These lateral shifts were most likely influenced by the growth of the underlying structures with channels diverting around emerging folds or changing their sinuosity.

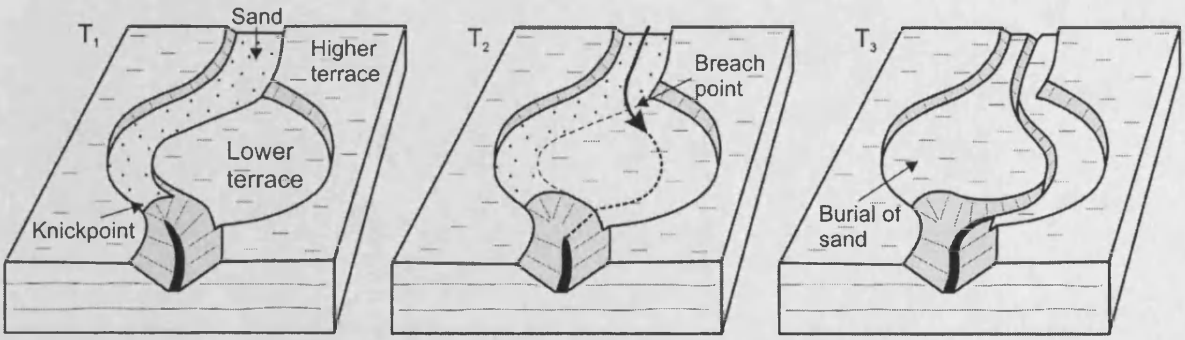

Figure 4.11. Simplified cartoon model showing the preservation of coarse sediment (stippled) upstream of knickpoint by avulsion within the channel-belt. Deposition upstream of a knickpoint fills the channel up to the level of an adjacent terrace (T_2), which is subsequently breached by a younger channel thalweg taking a different path (T_3). The coarser sediments are thus preserved underneath finer-grained parts of turbidity currents and hemipelagites.

4.8.2 The origin of high-amplitude terraces

The deposits on terraces are sometimes used to indicate the thickness or the volume of flows within channels (Babonneau et al., 2004). Small volume flows remain confined within the thalweg, whereas larger flows overflow onto terraces. In the studied system, the highest amplitudes are found only within the thalweg and the terraces closest to the thalweg (Fig. 4.9). The terraces with coarsest sediments lie less than 23 m above the thalweg and could therefore indicate the thickness of the coarse part of turbidity currents. However, regarding

Africa (Prather, 2003). Sediments accumulated on low-gradient reaches upstream of uplifted areas in the studied channel are interpreted to represent deposits from the coarsest part of turbidity currents and therefore could constitute a good reservoir. As individual deposits have volumes of < 0.1 km^3, they would not be large enough to be economic by themselves, but could be an element of a larger reservoir complex. Although upstream-migrating knickpoints may erode these deposits or cut them into small compartments, as illustrated in Figure 4.10B, the observations of this study indicate that there are more continuous HARs upstream of folds. This implies that both preferential deposition and preservation of coarse deposits occur upstream of folds where slope is locally reduced, and that sand distribution is at least partly controlled by structure.

4.9 CONCLUSIONS

1. Knickpoints form on a present day thalweg of a channel-levee system on the western Niger Delta as a result of the uplift of folds orthogonal to the channel. They are divided into three types according to their size, morphology and maturity. Type I knickpoints 1 and 2 are largest and least mature, Type II knickpoints 3 and 4 are intermediate, and the Type III is the smallest and most mature knickpoint type found across the frontal fold.
2. The high degree of confinement of the studied channel-levee system may restrict lateral changes of the channel in response to gradient changes and it therefore tries to readjust to equilibrium by erosional and depositional processes in specific areas. The reduction of thalweg gradient upstream of an anticline leads to deceleration of turbidity currents and deposition of their coarsest load. This interpretation is supported by the presence of several kilometres long zones of high-amplitude reflections representing relatively coarse-grained sediments along the channel upstream of some folds. Where the gradient is steeper on the basinward limb of the fold, the currents accelerate or increase in turbulence, enhancing erosion and causing the formation of knickpoints.
3. The knickpoints migrate upstream eroding the deposits upstream of them or incising them into terraces. High amplitudes on terraces adjacent to channel thalweg thus most likely record a history of deposition of coarse sediments. This is as a result of gradient reduction and subsequent incision and compartmentalisation of these deposits by a headward-migrating knickpoint, rather than thickness or volume changes of turbidity currents within the channel.

4. Knickpoint formation and migration may be an important process by which channels cut through uplifting thrust and fold belts as they strive to obtain their equilibrium profiles. However, as knickpoints are transient features, distinguishing the evidence of knickpoint migration from erosional currents from subsurface seismic data or outcrops is highly challenging.
5. Knickpoints influence the 3D architecture of channel-levee systems where they intersect dynamically changing seabed topography increasing the erosive character of stacked channel deposits and leading to more discontinuous HARs. Stacking patterns can vary dramatically over short distances along channel with more high-amplitude parallel reflections found upstream of folds.
6. The coarse deposits upstream of knickpoints could constitute an important element of reservoir architecture. The deposits are preserved e.g. if the channel system is abandoned or avulsion within the channel-belt occurs. The examples of this study suggest that avulsion and at least partial preservation takes place in this system at present day.

Chapter 5

5 CURRENT-GENERATED GIANT DEPRESSIONS ALONG SUBMARINE CHANNELS ON THE CONTINENTAL MARGIN OF THE ESPIRITO SANTO BASIN, BRAZIL

5.1 ABSTRACT

3D seismic data from the Espirito Santo Basin on the Brazilian continental margin reveal trails of depressions that follow the courses of underlying erosional submarine channels in Neogene strata. The depressions are interpreted to have formed as a result of Froude-supercritical turbidity currents flowing down the steep slopes and interacting with topographical irregularities at the bases of the channels. These irregularities cause instabilities within the currents and changes in the flow regime, bed shear stress and the capacity of currents to carry sediment. This results in the formation of zones dominated by deposition or erosion and bypass, which leads to the formation of sediment waves. As the sediment waves are confined within channels, they appear as asymmetric, flute-shaped depressions in plan view. The depressions become more symmetrical and circular as deposition increases on the shallow, upstream-dipping stoss flanks. Some depressions are filled with mounded onlap fill, which most likely resulted from changes in flow conditions. Examples on the present-day seafloor and from another dataset confirm that sediment waves and circular depressions develop above irregularities on the subsurface, such as knickpoints, failure scarps and the irregular tops of mass transport complexes. This paper gives the first description of trails of depressions that form due to flow dynamics in submarine settings using 3D seismic data. The process is ubiquitous, therefore the features should be common in submarine slope settings globally. The process probably plays an important role in how sediment is dispersed and preserved in submarine slopes and in how submarine landscapes are formed and modified.

5.2 INTRODUCTION

Continental margins have been the subject of considerable research effort since the discovery of meandering submarine channels on the continental margins of North America (Menard, 1955), especially after the advent of seismic reflection technology and now that deepwater channels have become important hydrocarbon reservoirs (e.g. Deptuck et al., 2003; Posamentier and Kolla, 2003). However, regardless of the vast amount of research into these submarine settings, many fundamental questions still remain with regard to depositional and erosional processes responsible for the architecture of continental margins and many features

are left unexplained. This paper focuses on one potentially important feature occurring in deepwater channels, namely roughly circular depressions that occur individually or in trails on steep slopes, in this case on the continental margin of Brazil.

Roughly circular depressions are common geomorphic features on continental margins. They can have several possible origins, such as salt withdrawal basins, gas pockmarks and collapse structures. Circular depressions that occur in trails above buried submarine channels are commonly ascribed to pockmarks due to de-fluidisation of channel-fill sands and hydrocarbon migration from deeper levels (Gay et al., 2003) or expulsion of fluidised channel deposits onto seafloor as a result of overpressure (Davies, 2003). However, turbidity currents can also, in certain conditions, erode the seabed and form trails of depressions. Such scours are referred to as 'cyclic steps' (Fildani et al., 2006). The term was first used by Whipple et al. (1998) to describe periodic upstream-migrating step-like bedforms, which are bounded upstream and downstream by hydraulic jumps (a sudden transition from supercritical to subcritical flow conditions) within the overriding flows (e.g. Fagherazzi and Sun, 2003; Taki and Parker, 2005; Fildani et al., 2006). They form when Froude-supercritical flows erode and deposit sediments on a steep seafloor in a way that leads to the formation of a trail of erosional scours if the flows are net-erosional or upstream-migrating sediment waves if the flows are net-depositional (Fagherazzi and Sun, 2003; Fildani et al., 2006).

This paper provides the first description of depressions, which are the result of flow dynamics and which are imaged by high quality 3D seismic data. Fildani et al. (2006) demonstrated that a trail of kilometre-scale flute-shaped depressions can be formed on the seafloor by Froude-supercritical turbidity currents and suggested that cyclic steps may be the process by which submarine channels initiate. This paper concentrates on the role they may play in modifying channel-fill architectures and the submarine landscape.

The aim of this paper is to describe trails of large depressions (200-600 m across) located above erosional channels and individual depressions located above scarps on the Espirito Santo Basin on the Brazilian continental margin, and propose a model for their formation by the actions of gravity flows. Analogous features on the present-day seafloor, shallow section and an additional dataset from the Niger Delta are studied to support the interpretation. 3D imaging and detailed analysis of reflection geometries of the seismic data enable the determination of the 3D morphology and evolution of the depressions. Based on this analysis

and supported by published models, it is concluded that these depressions are formed by erosional and depositional processes of gravity flows confined within slope channels.

5.3 SUBCRITICAL AND SUPERCRITICAL FLOWS AND THE FORMATION OF UNDULATING TOPOGRAPHY

Turbidity currents are submarine sediment-gravity flows, in which sediment is held in suspension by fluid turbulence (Middleton, 1993). They provide an important mechanism by which sediment is transported down continental slopes into deep sea (Deptuck et al., 2003). Turbidity currents are characterised by the dimensionless densimetric Froude number

$$Fr_d = U/(RCgh)^{1/2},$$

in which U is the depth-averaged flow velocity, R is the submerged specific gravity of the sediment, C is the layer-averaged volume of sediment in concentration, g is the gravitational acceleration and h is the flow depth (e.g. Fildani et al., 2006). Flows are said to be supercritical when $Fr_d > 1$ and subcritical when $Fr_d < 1$. Supercritical flows are swift and thin and more likely to be capable of eroding seafloor because of higher flow velocities (Nemec, 1990; Kubo and Nakajima, 2002; Fagherazzi and Sun, 2003). Subcritical flows are slow and thick and promote sediment deposition. However, flow regime alone does not determine whether erosion or deposition occurs. There is a correlation with slope gradient, velocity of the currents and sedimentation rate (e.g. Nakajima and Satoh, 2001; Ercilla et al., 2002). If none of the other parameters change, then the flow velocity controls the sedimentation rate across an undulating surface (Flood, 1988). Turbidity currents accelerate on steep slopes and decelerate where slope angle decreases. High velocity and shear stress at the base of the flow cause bypass or erosion on steeper slopes (Flood, 1988; Nemec, 1990; Nakajima and Satoh, 2001). At a break in slope, supercritical flow can abruptly transform into subcritical flow and thus form a hydraulic jump (Komar, 1971; Garcia and Parker, 1989; Fildani et al., 2006). This sudden drop in velocity and shear stress leads to enhanced deposition (Garcia and Parker, 1989). Deposition is caused by the loss of the capacity of the turbidity current to carry sediment in suspension when the velocity drops and turbulence weakens (Hiscott, 1994).

Turbidity currents that flow down submarine slopes have a wide range of local densimetric Froude numbers (Nakajima and Satoh, 2001). Irregularities in the topography of the seafloor may initiate instabilities in flows leading to the development of internal waves (Flood, 1988;

Ercilla et al., 2002) and the formation of wavy topography. Sediment waves, for example, are common undulating features on the seafloor, characterised by steeper lee flanks and shallower or upstream-dipping stoss flanks (Ercilla et al., 2002; Wynn et al., 2002a). Steeper slopes and lee flanks of sediment waves are sites of bypass and erosion (McHugh and Ryan, 2000; Nakajima and Satoh, 2001). This is evident from the observations of truncated reflections, erosional scours and flute marks found on several sediment wave lee flanks (McHugh and Ryan, 2000; Migeon et al., 2001). Sediment waves occur mainly as extensive wave fields on the seafloor or on levees of submarine channels (e.g. Wynn et al., 2000b; Wynn et al., 2000a; Nakajima and Satoh, 2001; Ercilla et al., 2002), but can also be confined within channels (Wynn et al., 2000b; Wynn et al., 2002b).

Sediment waves migrate upcurrent due to deposition on stoss flanks and bypass or erosion on lee flanks, but how they are initiated is still a matter of a debate. Two hydraulic models are most commonly proposed for the formation of sediment waves: the antidune model (Kolla et al., 1980; Normark et al., 1980; Wynn et al., 2000b; Wynn et al., 2000a) and the lee wave model (Flood, 1988; Howe, 1996). It has been suggested, however, that these models cannot explain the formation of sediment waves on the seafloor by turbidity currents, because the required hydraulic conditions cannot be met (Nakajima and Satoh, 2001; Kubo and Nakajima, 2002). Lee wave formation needs a steady flow with a $Fr_d < 0.32$ and antidunes are unstable short-lived bedforms that require Froude numbers of 0.844-1.77 for their formation (Nakajima and Satoh, 2001). In fact, it has been observed, that flows have highly variable Froude numbers on undulating surfaces (Kubo and Nakajima, 2002). Several authors have suggested that sediment wave formation is initiated as a result of variations in bottom slopes (Flood, 1988; Nakajima and Satoh, 2001; Ercilla et al., 2002; Kubo and Nakajima, 2002; Wynn and Stow, 2002; Fildani et al., 2006). Migeon et al. (2001) speculated that sediment wave initiation is the result of interaction between turbulent flows and loose seafloor. Fildani et al. (2006) proposed that some sediment waves are formed as transportational cyclic steps from depositional currents, whereas erosional currents produce a trail of depressions. Recent numerical and analogue models and experiments of Fagherazzi and Sun (2003), Kubo and Nakajima (2002), Nakajima and Satoh (2001), Sun and Parker (2005) and Taki and Parker (2005) have increased the understanding of the processes, which lead to the formation of wavy structures by turbidity currents, however, there is still a shortage of natural examples of these phenomena, especially in the submarine realm.

5.4 DATA AND METHODS

The 3D seismic reflection data cover an area of 1600 km^2 in the Espirito Santo Basin on the Brazilian continental margin in a present day water depth of 35 to 1800 m (Fig. 5.1). The line spacing is 12.5 m in both inline and crossline direction and the sample interval is 2 ms (milliseconds). The data are zero-phase migrated and displayed with SEG normal polarity and so that an increase in acoustic impedance is represented by a black-red-black reflection loop. No lithological or well data were available for this research, therefore estimated seismic velocities are used when calculating thicknesses of sediment packages and dips of horizons. A seismic velocity of 1500 ms^{-1} is used for seawater and 1800 ms^{-1} for the studied succession. Present day horizontal is used when converting and recording dips. The dominant frequency of the studied interval is c. 40 Hz. Using the average velocity of 1800 ms^{-1}, the dominant wavelength is c. 45 m and thus vertical resolution or tuning thickness ($\lambda 4^{-1}$) is c. 11 m. The work is based on a careful analysis of reflection geometries from vertical seismic sections and seismic geomorphology of horizons produced by mapping 3D seismic reflections. The nomenclature of Mitchum et al. (1977) is used when describing reflection geometries.

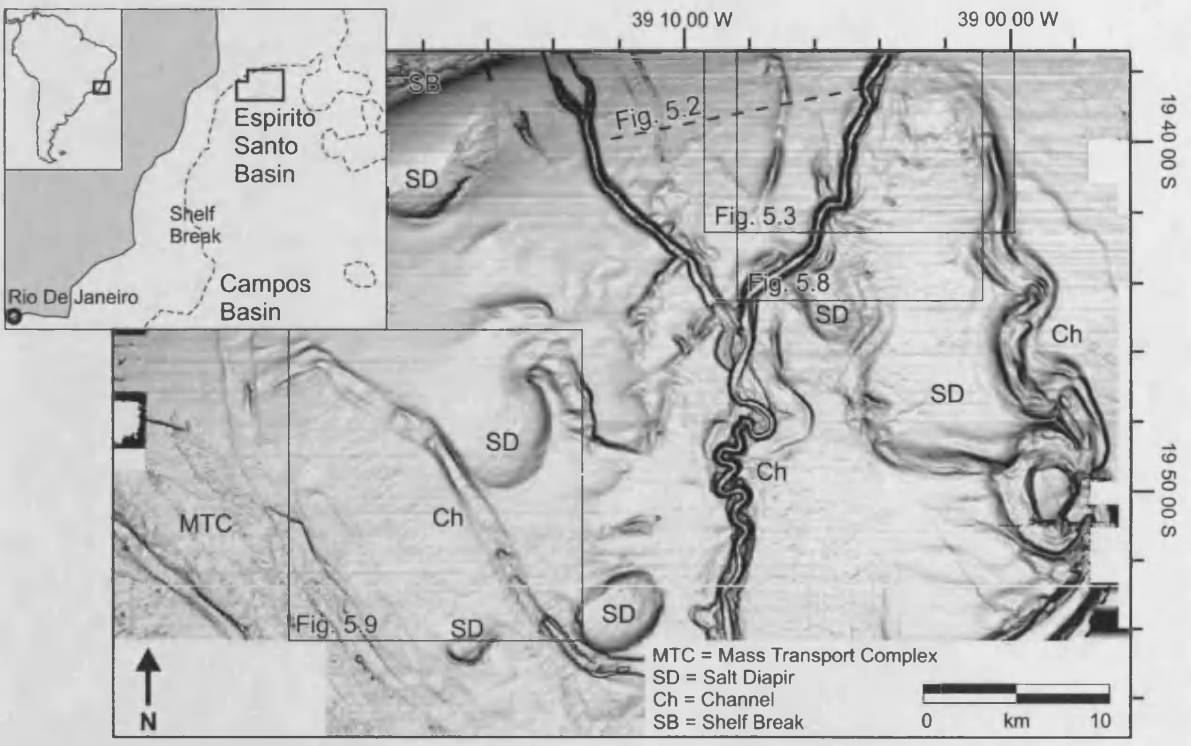

Figure 5.1. Seabed dip magnitude map of the 3D seismic data with location of Espirito Santo Basin on the Brazilian continental margin shown in the inset figures. Darker shading indicates greater dip. The main environments in the data are the shelf break (SB), salt diapirs (D) slope channels (Ch) and slumps/debrisflows (MTC). Location of Figures 5.2, 5.3, 5.8 and 5.9 are shown.

5.5 GEOLOGICAL SETTING

The Espirito Santo Basin is located on the continental margin of Brazil (Fig. 5.1). It is bounded by Campos Basin to the south and the volcanic Abrolhos Plateau to the north. The modern Doce River supplies sediment to the basin from the Mantiqueira and Espinhaço mountain chains. The structural evolution of the basin from late Jurassic to the late Aptian/early Albian includes pre-rift, synrift and transition stages, followed by continental drift stage (Fiduk et al., 2004). Stratigraphically, the basin is divided into five depositional megasequences: pre-rift, rift, transitional, transgressive marine and regressive marine (Fiduk et al., 2004). Aptian-age salt has been deforming into diapirs, rollers, canopies and thrusts (Jackson et al., 1994) from Albian until the Present. Since the Eocene, the Espirito Santo Basin has been a prograding shelf and slope environment (Fiduk et al., 2004).

The dataset is located immediately downstream of the present day shelf break and is dominated by salt diapirs, incised canyons, channels, slumps and debris flows, all visible on a dip map of the seafloor (Fig. 5.1). This paper focuses on a 100 km^2 area in the northeastern part of the dataset, where the seabed and shallow section are dominated by slope channels. As no stratigraphical or lithologic data were available for this work, the sub-division of the strata is based on seismic character (Units 1-4) and the work of Fiduk et al. (2004). The stratigraphy of the study area is illustrated by a representative seismic line (Fig. 5.2). At the bottom of the section, Cretaceous strata are overlain by high-amplitude, syn-compressional growth strata and low-amplitude, continuous reflections of Unit 1, which is of Palaeocene-Eocene age (Fig. 5.2). The Horizon E/O is an unconformity marking the change from low-amplitude to high-amplitude reflection character. The high-amplitude character of Unit 2 is caused by volcaniclastic material derived from the Abrolhos Plateau and other extrusions onshore (Fiduk et al., 2004). The Abrolhos Plateau was emplaced during the early to middle Eocene, thus making the age of the unconformity post middle Eocene or Oligocene in age. The c. 500 m thick Unit 3 has dominantly low-amplitude hummocky reflection configuration. Unit 4 is characterised by high-amplitude reflections and multiple small channels. Its top c. 50 m consists of a low-amplitude package with concordant reflections.

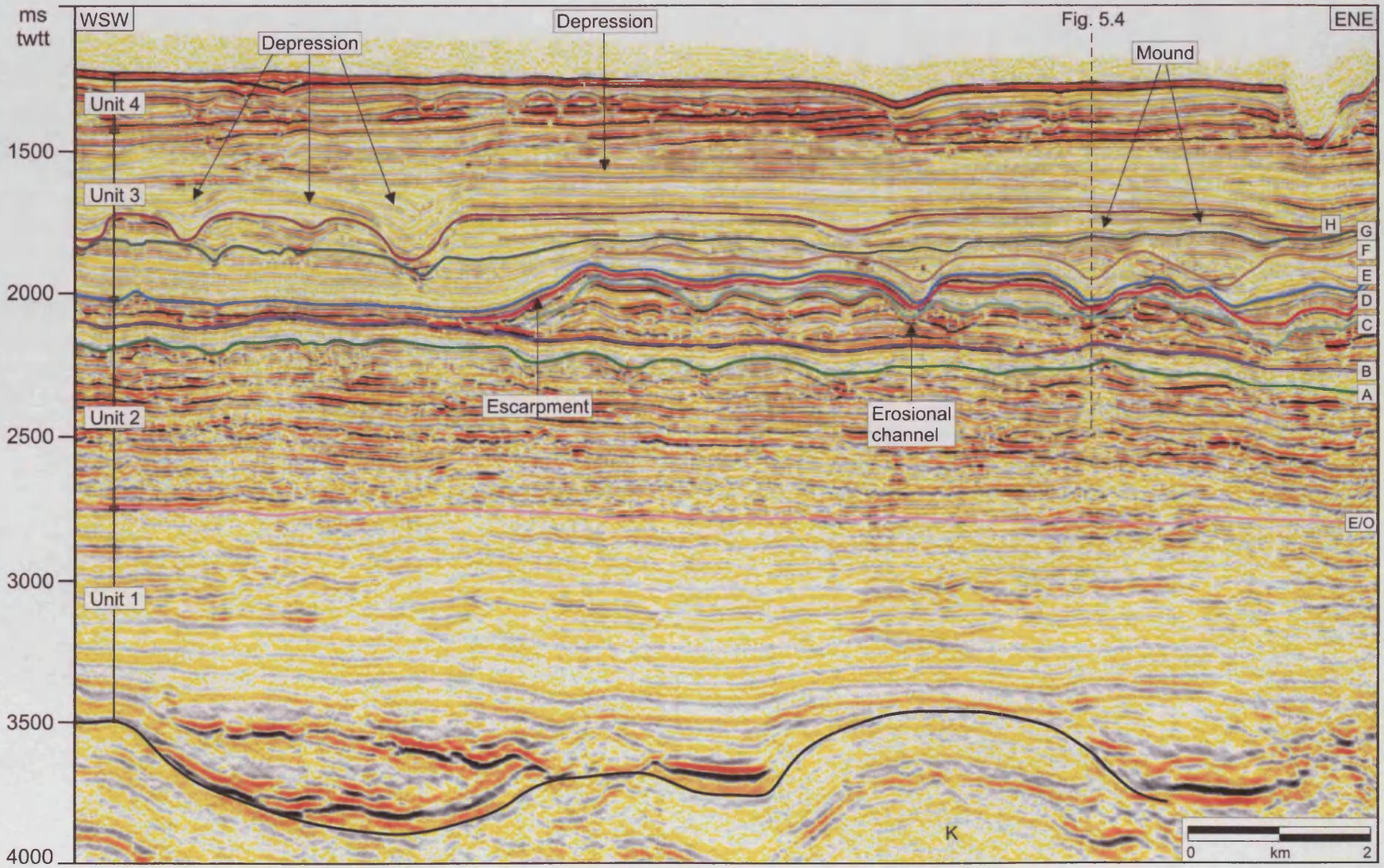

Figure 5.2. A seismic line across the study area showing the stratigraphy from Cretaceous basement (K) to the present day seafloor. The key horizons are interpreted and labelled A-H. E/O = post Middle Eocene-Oligocene unconformity. Location of the line is shown in figure 5.1.

5.6 3D SEISMIC CHARACTERISATION OF DEPRESSIONS

This paper focuses on the interval of the seismic data 0.5-1 seconds two-way-travel time (twtt) below the seabed, which includes the top part of Unit 2 and the bottom part Unit 3 (Fig. 5.2). The key horizons are labelled from bottom to top with letters A-H (Fig. 5.2). The truncation of seismic reflections indicates that there have been several phases of channel incision and infill. Horizon A is characterised by a number of erosional low-sinuosity channels, which are filled with low-amplitude reflection package A-B. The overlying package B-C consists of high-amplitude channelised deposits. The low-amplitude interval C-H is the interval, in which the depressions are found, mainly above the erosional channels of horizons C and G. Horizons C, D, E and G are described in more detail below.

5.6.1 Description of key horizons

Dip magnitude maps of the key horizons show a morphological evolution from a horizon cut by erosional channels to horizons with depressions and finally to a horizon with mounds (Fig. 5.3). The darker grey colour on the dip maps indicates higher dip, with highest measured value of approximately 35°. Horizon C is characterised by several erosional channels, which converge into one trending towards south and another one trending towards southeast (Fig. 5.3A). The channels are up to 85 m deep and 1.1 km wide measured from their margins, the bases of channels are up to 600 m wide. They incise into previous deposits of the package B-C (Fig. 5.2) and have dominantly sharp margins, although some channels with more rounded margins are found on both the eastern and western edges of the horizon (Fig. 5.3A). The western edge of the horizon marks the location where the reflection package B-C is truncated by a c. 120 m high escarpment (Fig. 5.2). Three arcuate scarps face towards the south in the middle of the horizon.

Horizon D is the first continuous reflection above Horizon C (Fig. 5.2). It is dominated by asymmetric depressions, which occur in trails that coincide with the location of the channels on Horizon C (Fig. 5.3B). Some depressions are roughly circular and some are elongate along the channel axis (see also Table 5.1). The colour variation on the dip map indicates that upstream flanks of the depressions are much steeper than downstream flanks. Especially the depressions on the eastern part of the horizon have very shallow downstream flanks and their plan view appearance resemble giant flute marks (Fig. 5.3B). The margins of the channels appear rounded and are occasionally marked by channel-margin faults.

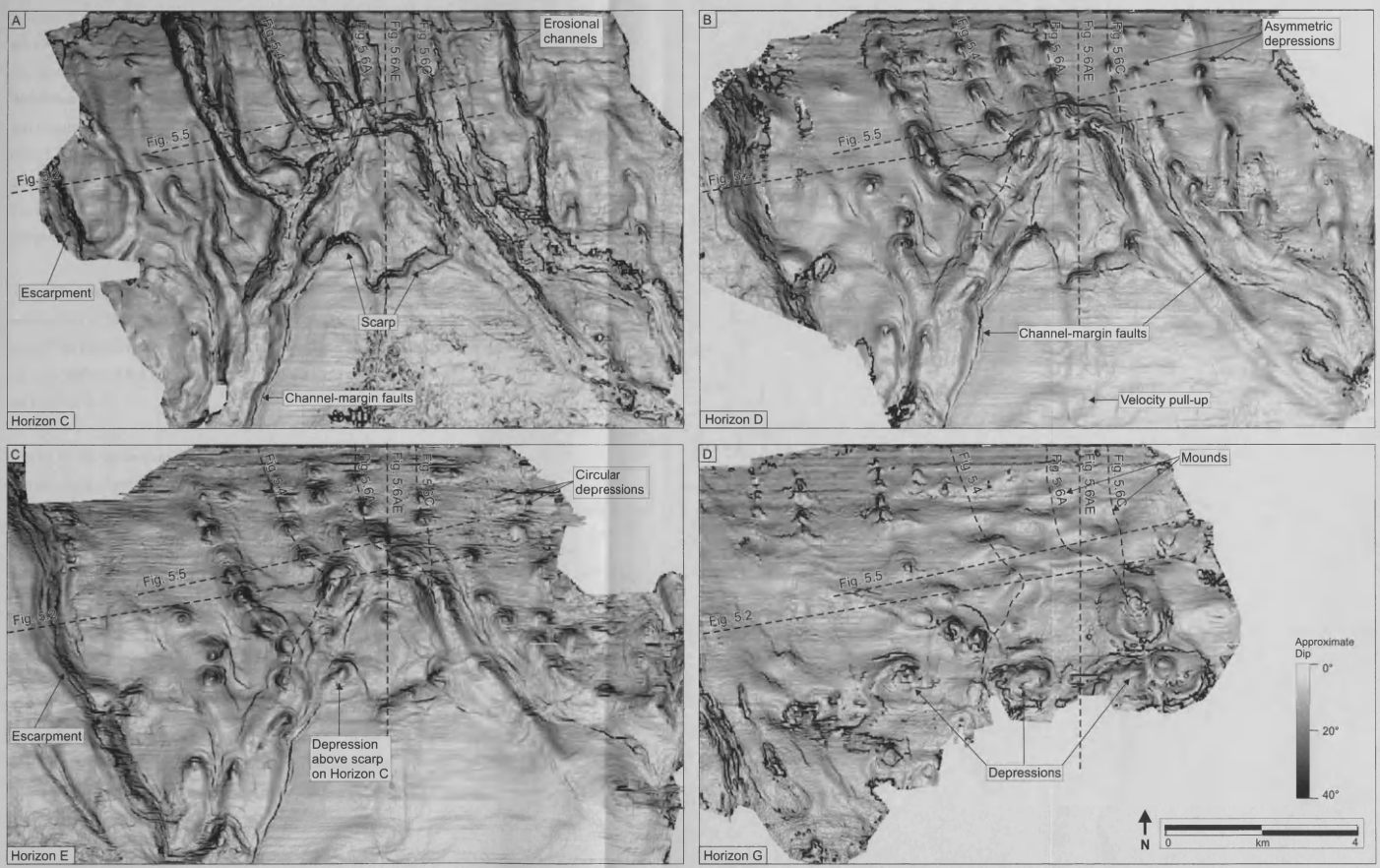

Figure 5.3. Dip magnitude maps of four key horizons. Location of Figures 5.2, 5.4 and 5.5 shown. (A) Erosional channels with sharp margins on the Horizon C. Note also arcuate scarps in the middle of the horizon. (B) Depressions on the Horizon D occur along the path of the erosional channels on C and are asymmetric with steeper upstream flanks and shallower downstream flanks. (C) More symmetrical, roughly circular depressions on the Horizon E. Note the depression that has formed above a scarp on Horizon C. (D) Horizon G has oval shaped mounds, which are located over some depressions on Horizons D and E. Some depressions occur on the southern part of the horizon. Scales are the same for each horizon.

Horizon E is a continuous reflection above Horizon D. It also is dominated by depressions, whose location correlates with the underlying channels on Horizon C (Figs. 5.3A and C). The depressions are nested above the depressions on Horizon D, however, there are 14 fewer depressions on Horizon E than on Horizon D (Table 5.1). The depressions are more circular and symmetrical with more prominent downstream flanks on Horizon E than on Horizon D (Fig. 5.3, Table 5.1). The axis of their deepest points does not align perfectly with the underlying channel on Horizon C, but is shifted up to 50 m to the east. The features on Horizon E have dominantly rounded appearance, the only sharp features are the channel-margin faults (Fig. 5.3C).

The most striking features on Horizon G are the rounded mounds, which occur on the north-eastern part of the horizon (Fig. 5.3D). They are up to 1 km across and slightly elongate along slope. The southern part contains circular depressions up to 1 km in diameter (Fig. 5.3D). The mounds and most but not all of the depressions align perfectly vertically with the depressions on Horizon E.

Not all of the depressions are located above erosional channels. One of the large (c. 1 km across) depressions on Horizon G (Fig. 5.3D) is located above an underlying arcuate scarp on Horizon C (Fig. 5.3A). The scarp itself is c. 60 m high and has a maximum dip of 35°. The depression can be seen also on Horizon E, at which level it is 37 m deep and has flanks that dip 23° downslope and 8° upslope (Fig. 5.3C).

5.6.2 Detailed description of depression and reflection geometry

The seismic character of the key reflections and reflection packages are described below using a representative seismic traverse along one of the erosional channels on Horizon C (Fig. 5.4) and an across-channel traverse following the strike of the slope (along slope) (Fig. 5.5). The along-channel traverse shows a typical development of the channel-fill from a relatively smooth profile (Horizon C) to undulating with depressions (Horizons D-F) to undulating with mounds (Horizon F) (Fig. 5.4). Further examples are presented in Figure 5.6.

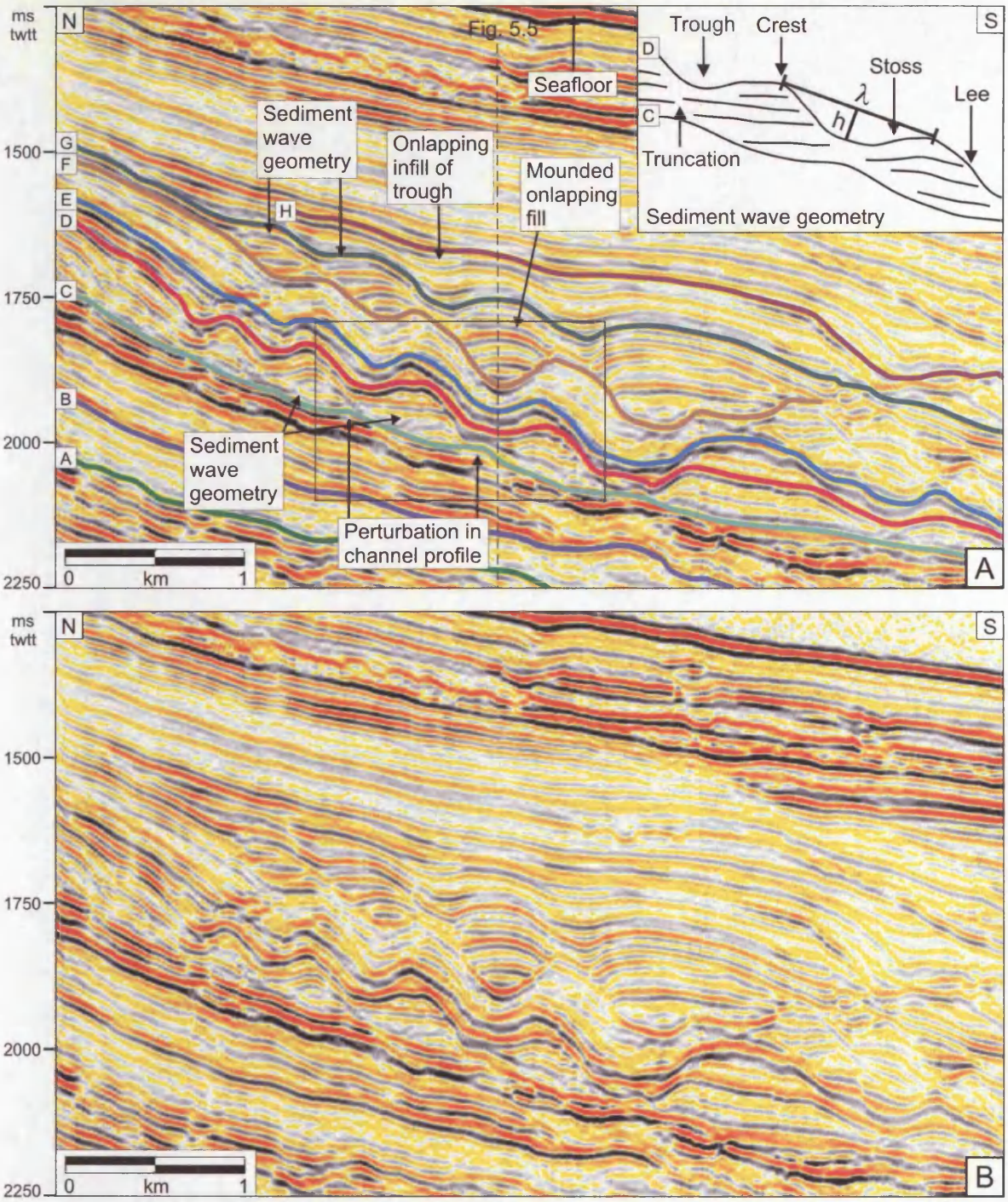

Figure 5.4. (A) Seismic traverse along one of the erosional channels of Horizon C showing the reflection geometry of the key horizons and reflection packages. The inset shows sediment wave terminology, which is used to describe the reflection package C-D. λ is the crest-to-crest distance (also the length of the depressions) and h denotes the depth of the depression forming between the crests. Location of the line shown in Figure 5.3. (B) Same line uninterpreted.

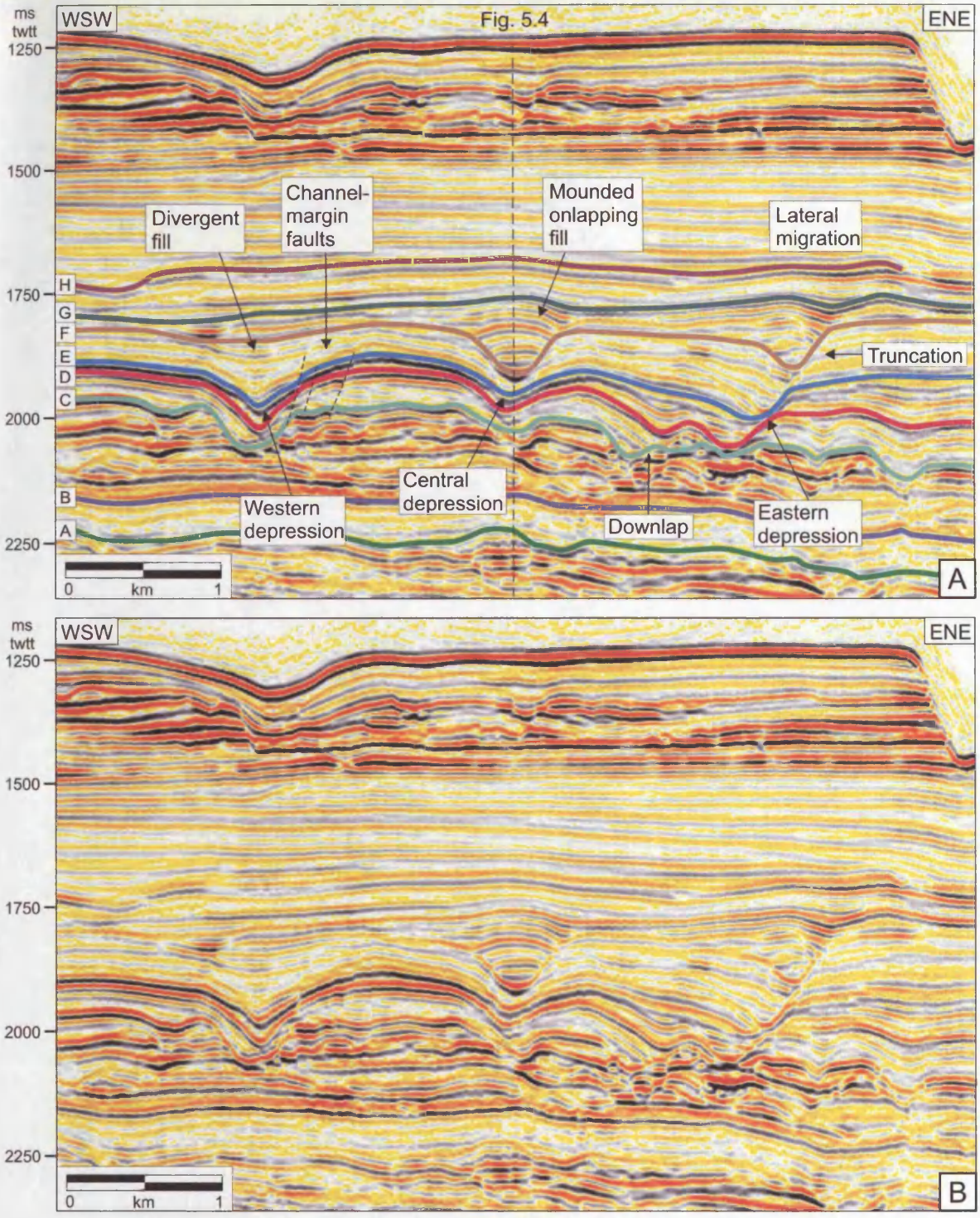

Figure 5.5. (A) Seismic traverse along-slope and across some of the erosional channels showing the reflection geometry in the vicinity of three depressions on Horizon E. The western depression has been mainly filled by divergent fill reflection package E-F. The central and eastern depression have mounded onlap fills between reflections F and G. The eastern channel-depression complex shows also lateral migration towards east. Location of the line is shown in Figure 5.3. (B) Uninterpreted.

The base of one of the erosional channels on Horizon C has a relatively smooth concave profile with some undulations (Fig. 5.4). Its gradient changes from 5-7° at the proximal end to 1.5-3° at the distal part of the profile. The truncation of the reflections of package B-C indicates that the channel is incised into previous deposits (Figs. 5.2 and 5.5). Above the erosional channel on Horizon C, the reflection package C-D contains hummocky/undulating reflections, which form a configuration resembling upstream-migrating sediment waves, and therefore wave terminology is used to describe them (see inset in Fig. 5.4). The reflection package is thickest at the crests and the reflections are truncated on the downslope (lee) flanks (Fig. 5.4). In cross section, the package C-D has an irregular thickness with diverging reflections (Fig. 5.5). Some reflections apparently downlap onto channel floor on Horizon C or are truncated by Horizon D.

The continuous reflection D drapes the wave-like reflections of the package C-D (Fig. 5.4). A typical crest to crest distance (λ) measured at this level is c. 400 m (Table 5.1). This undulating morphology is confined within the channel so that the troughs, which are bounded by the wave crests and the channel margins, form a series of depressions along the channel. Lee flanks of the waves make the upslope flanks of the depressions and stoss flanks the downslope flanks (Figs. 5.3B and 5.4). The depressions are asymmetrical with steep upslope flanks, which dip 4-20° and shallower downslope flanks that dip 1-14° in the upslope direction (Fig. 5.4, Table 5.1). The depressions are typically c. 20 m deep when measured along the channel (h in inset of Fig. 5.4), but range from c. 8 to up to 56 m (Table 5.1). The depressions tend to be shallower in the proximal and distal areas.

Horizon E has a similar appearance on the along-channel section to Horizon D (Fig. 5.4). The angles measured along-channel are similar on upslope flanks (5.5-13°), but the downslope flanks of Horizon E are much steeper, dipping 5-17° to upslope direction (Table 5.1). This confirms the observation made on the dip maps that the depressions are more symmetrical on Horizon E than on Horizon D (Figs. 5.3C and B). The package D-E has a relatively even thickness on the along-channel traverse (Fig. 5.4), but the across-channel section shows divergent and onlapping reflection geometries filling some of the depressions (Fig. 5.5).

The low-amplitude package E-F has a relatively constant thickness along-channel (Fig. 5.4), but shows variation along slope (Fig. 5.5). It is thinner within the central depression crossed by Figure 5.4 and fills the depression to the west of it with a divergent fill (Fig. 5.5). The

reflections apparently downlap and onlap the eastern flank of the easternmost depression, which leads to lateral migration of the depression geometry eastward as the stratigraphy is being built up.

The interval F-G fills in the remaining depressions with onlap or mounded onlap fill (Figs. 5.4 and 5.5). The crests of the mounds align vertically with the bases of depressions. These reflections form roughly symmetrical mounds in cross sections (Fig. 5.5), but on the along-channel section some of them have an asymmetrical geometry, with reflections stepping upslope and resembling upstream-migrating sediment waves (Fig. 5.4). The elongate depressions between the mounds are filled by divergent reflections of package G-H.

Traverses along the other channels show similar reflection morphology to what described above although fewer depressions (Figs. 5.6A-D). A seismic line aligned dewnslope and located between the two channels shown in Figures 5.6A-D show no wavy geometry between horizons C to F except for when it crosses a channel and also above a large scarp (Figs. 5.6E-F).

There is a weak linear relationship with the diameter and the depth of the depressions, especially on the depressions on Horizon E if the diameter is measured along channel (length of depression) (Fig. 5.7A-C). The morphometric measurements of the depressions reveal also the greater circularity of the depressions on Horizon E (average length:width ratio 1.17) than on Horizon D (length:width ratio 1.46) (Fig. 5.7E-F, Table 5.1).

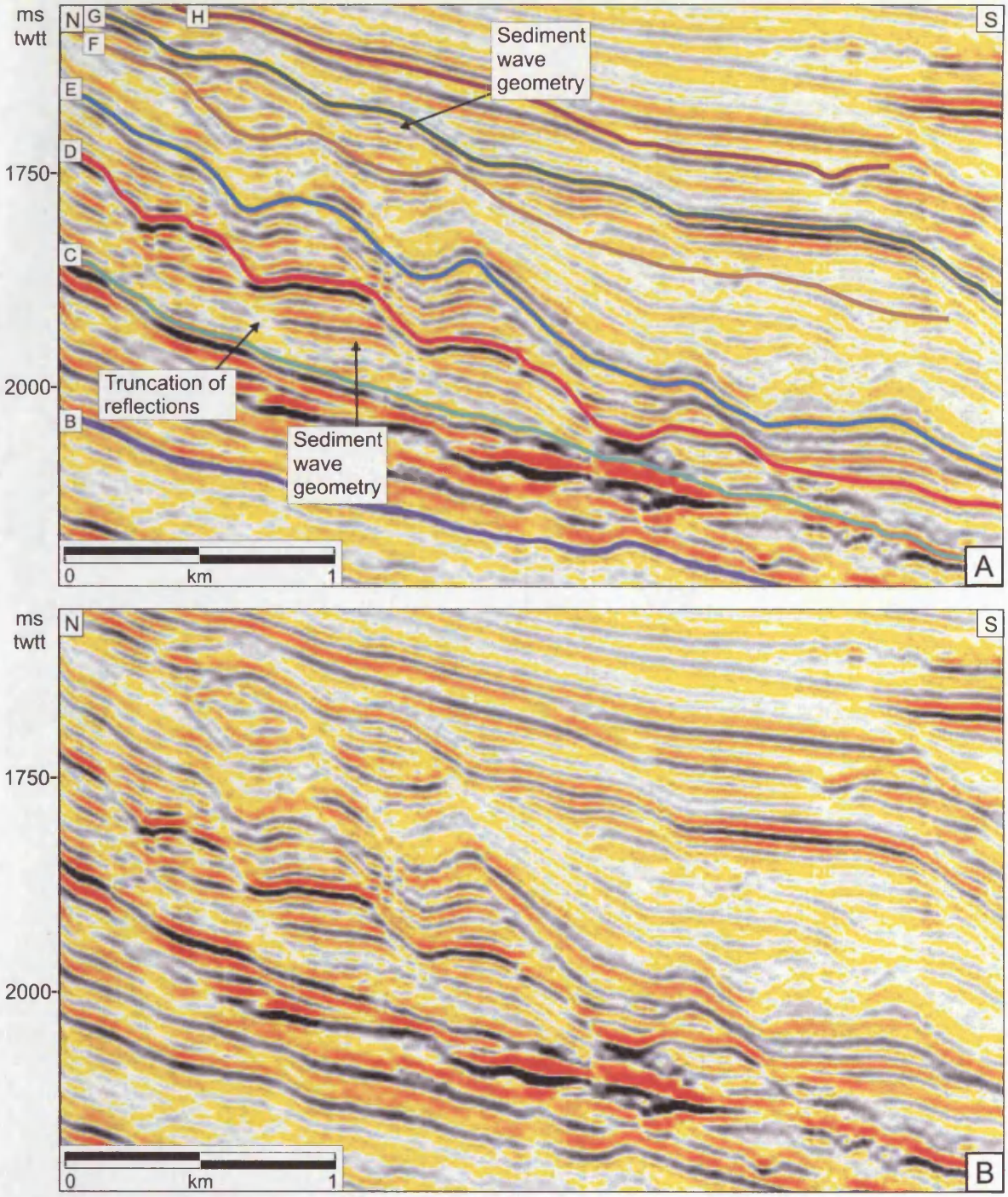

Figure 5.6. (A) Seismic traverse along one of the erosional channels of Horizon C showing the reflection geometry of the key horizons and reflection packages. Note the truncation of reflections on the downslope side within packages C-D and D-E that gives them a sediment wave geometry. (B) (A) uninterpreted. Location of the line shown in Figure 5.3.

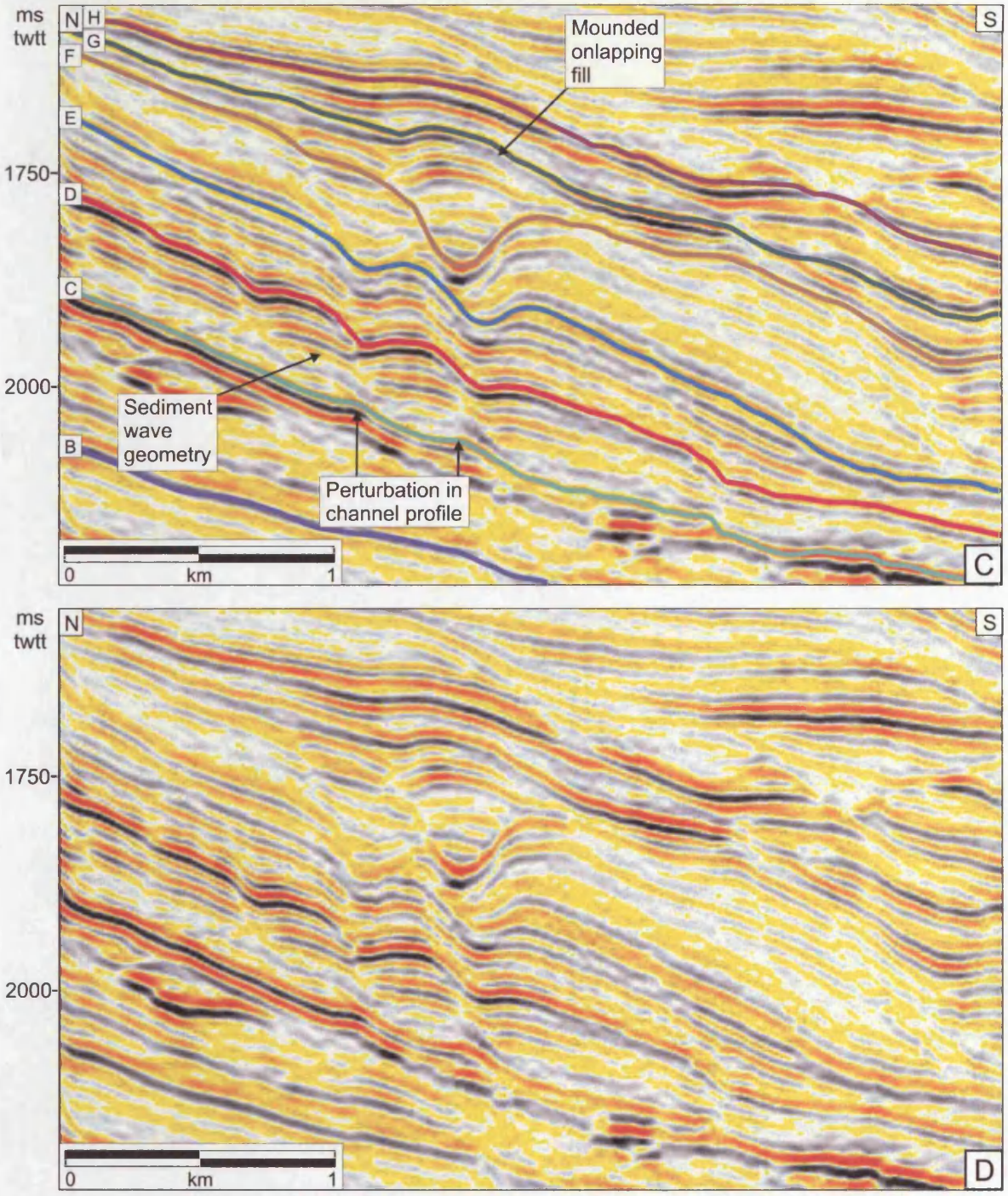

Figure 5.6. (continued). (C) Seismic traverse along one of the erosional channels of Horizon C showing the reflection geometry of the key horizons and reflection packages. Note the truncation of reflections on the downslope side within packages C-D that gives them a sediment wave geometry. Note also that on the horizon C there are 3 depressions, 2 on horizon E but only one on horizon F. (D) (C) uninterpreted. Location of the line shown in Figure 5.3.

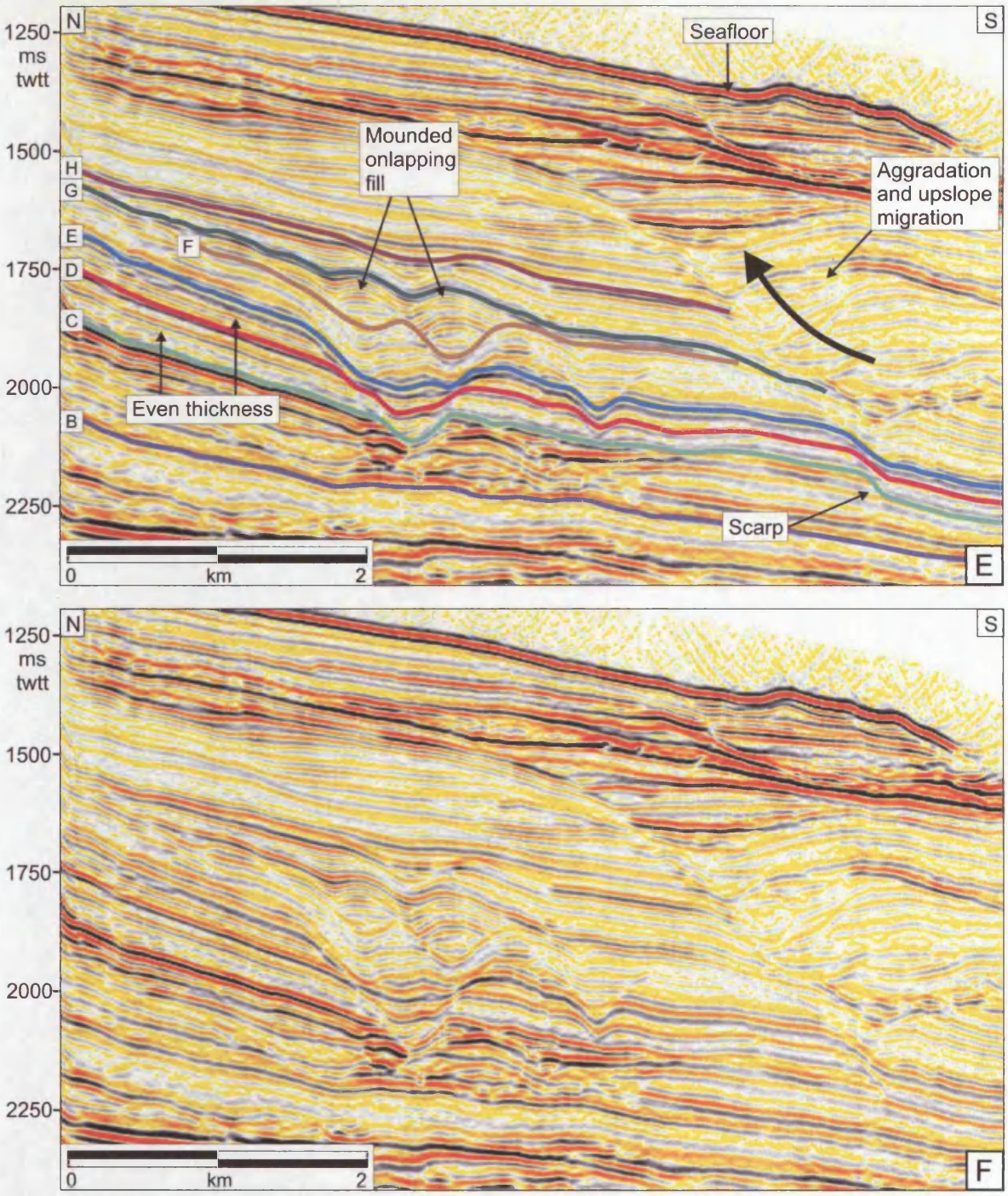

Figure 5.6. (continued). (E) A seismic line aligned downslope and located between two channels on horizon C. See location in Figure 5.3. Note the even thickness of the seismic packages C-D and D-E in comparison to the sediment wave geometry observed in Figures 5.6A-D. The line crosses one of the channels, above which two mounds with mounded onlapping fill have formed. A depression-mound complex has also aggraded and migrated upslope. Its lowest stratigraphic position is located above a scarp. (F) (E) uninterpreted.

Table 5.1. Morphometric measurements of depressions on Horizons D and E and the seafloor.

	Horizon D *(n=55)*	**Horizon E** *(n=41)*	**Seafloor** *(n=12)*
Depression depth (m)			
average	23.63	32.50	19.84
min	7.79	10.60	8.57
max	56.36	64.25	31.00
mode			
median	22.58	32.69	18.85
Upslope angles (degrees)			
average	12.97	13.33	6.81
min	4.19	5.50	4.58
max	21.51	21.77	9.26
mode			
median	12.94	13.00	6.72
Downslope angles (degrees)			
average	-2.27	-4.75	-3.42
min	-14.09	-17.02	-6.88
max	7.62	0.72	0.30
mode			
median	-1.74	-4.28	-3.55
Depression diameter (slope parallel) (m)			
average	293.08	404.17	531.25
min	125.00	137.50	362.50
max	587.50	750.00	850.00
mode	337.50	375.00	462.50
median	287.50	381.25	531.25
Depression diameter (slope normal) (m)			
average	405.13	448.21	397.92
min	162.50	162.50	238.00
max	800.00	1062.50	612.50
mode	337.50	325.00	350.00
median	343.75	406.25	362.50
Depression length:width ratio			
average	1.46	1.17	0.80
min	0.61	0.51	0.40
max	3.06	2.00	1.48
mode	1.45	2.00	
median	1.40	1.10	0.70
Depression area (km^2)			
average	0.11	0.16	0.40
min	0.02	0.03	0.13
max	0.36	0.50	3.14
mode	0.11	0.03	0.16
median	0.08	0.13	0.16

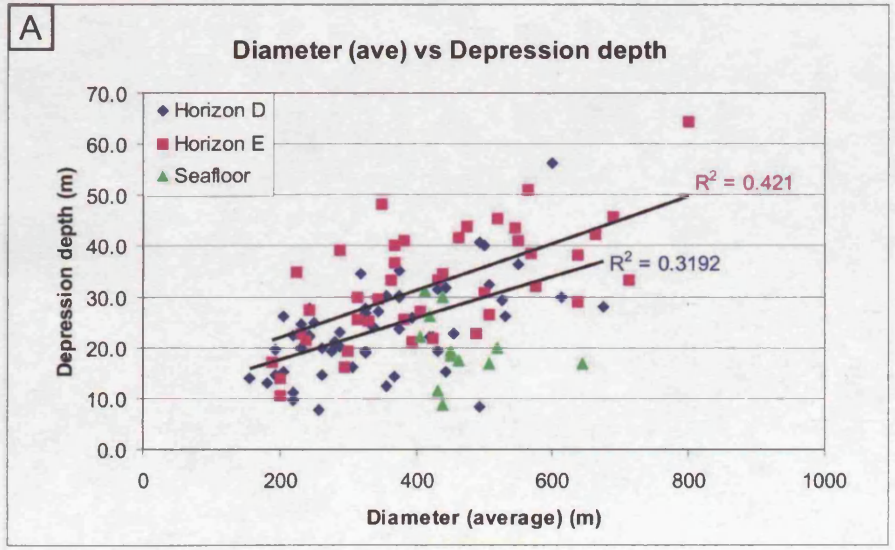

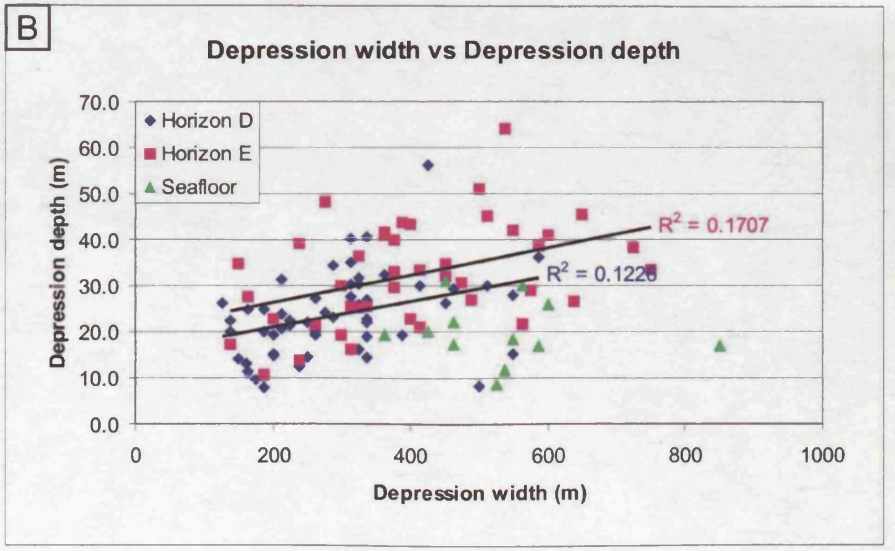

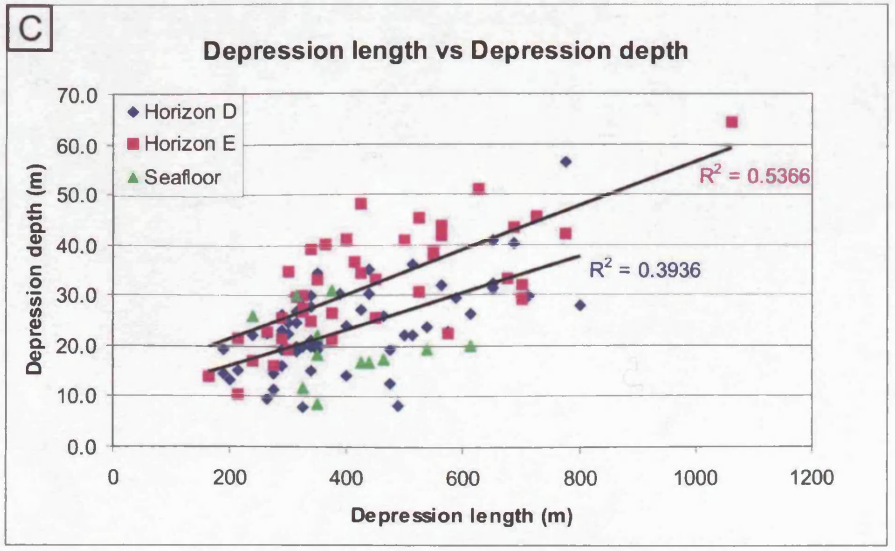

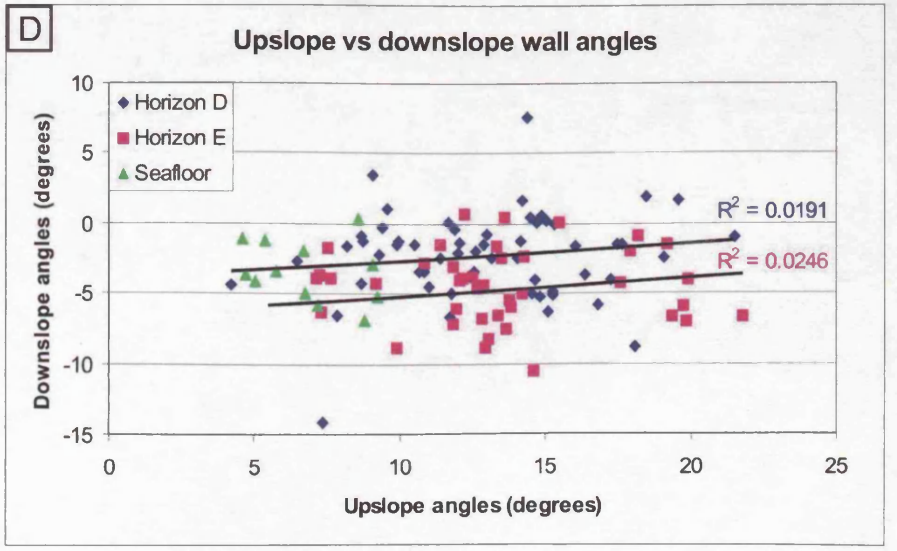

Figure 5.7. (continues)

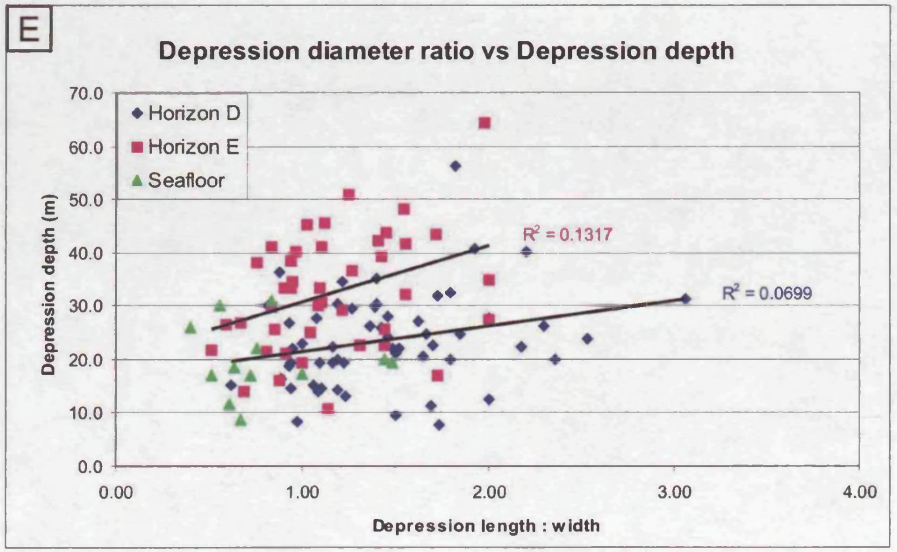

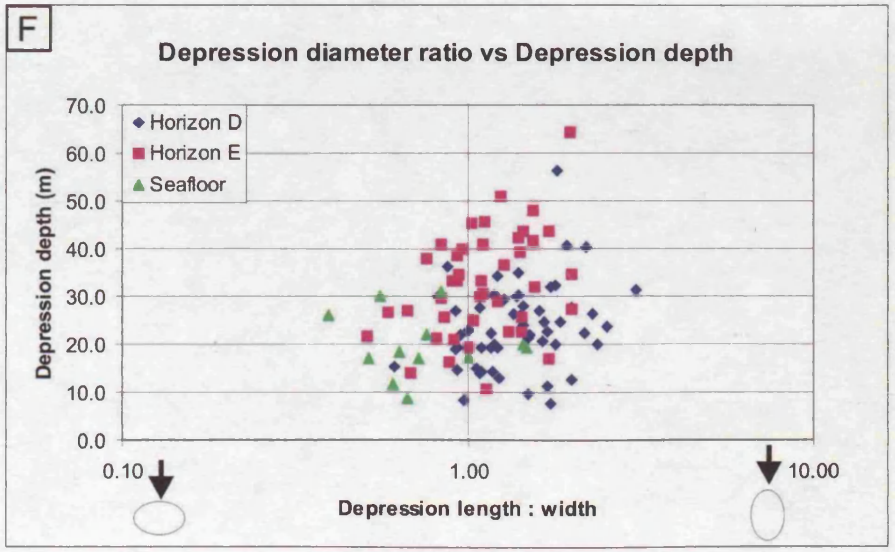

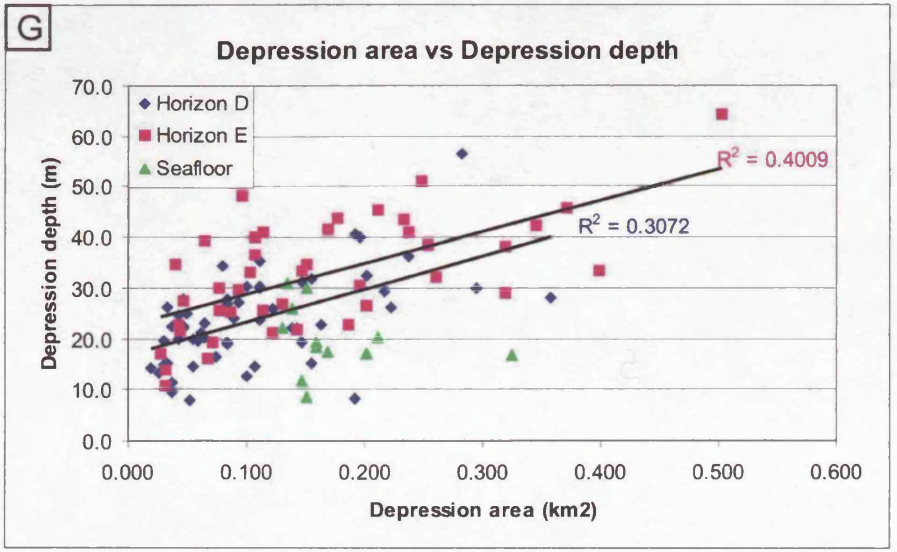

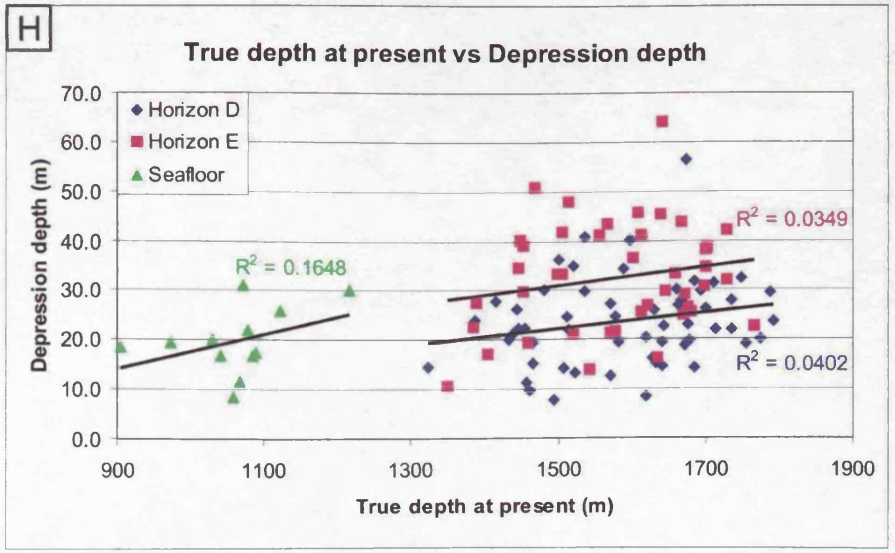

Figure 5.7. (continued)

Figure 5.7 (previous pages). Graphs showing relationships between selected dimensions of the depressions on the buried Horizons D and E and on the seafloor. The results are also tabulated in Table 5.1. (A-C) Graphs showing weak correlation with depression deiameter and depth within the buried depressions but not on the seafloor. (D) A graph showing no correlation between the angles of downslope and upslope walls of the depressions. (E-F) Graphs illustrating the circularity of the depressions. The depressions on Horizon D are longer than they are wide (elongate along channel), whereas the depressions on Horizon E are more circular (with values close to 1) and the depressions on the seafloor are slightly elongate along slope (wider than long). (G) A graph showing a weak linear correlation between the depression area and depth within the buried depressions but not within the seafloor examples. (H) Graph showing no correlation between depression depth and the true depth of the depression (from present day seafloor disregarding compaction).

5.7 DEPRESSIONS ON THE SEAFLOOR

Although the depressions in the Espirito Santo Basin are most abundant within the interval C-H, similar features are found on higher stratigraphic levels of Unit 3 (Fig. 5.2), as well as on the present day seafloor (Figs. 5.1, 5.8 and 5.9). The seafloor examples show clear evidence for flow activity and provide more details of how the formation of depressions and sediment waves may have been initiated. Similar features are also observed in other datasets, suggesting that their formation is a common process.

5.7.1 Depressions and sediment waves on the present day seafloor

A channel with rounded margins and an undulating profile on the seafloor is shown in the north-western corner of Figure 5.8A. The low-amplitude reflection package beneath the seafloor has an even thickness of c. 60 m on both sides of the channel (Figs. 5.8B and D), but along the channel its thickness varies remarkably (Fig. 5.8C). The reflection geometry resembles two upstream-migrating sediment waves with reflections stepping upslope on the stoss flanks and being truncated or thinned downslope on the lee flanks. The lee flanks have absolute dips of 5.35° and 5.69° and the dip of the stoss flanks of the first wave is 1.28°, whereas the second one dips 1.25° in the upslope direction, as measured on the seafloor. This means that a depression bounded by the wave crests and the channel margins is formed (Figs. 5.8A and C). The channel is 150 m wide, the crest to crest distance is 600 m and the depression is 17 m deep and circular in plan view, which makes it similar in scale and morphology to the depressions on Horizon D.

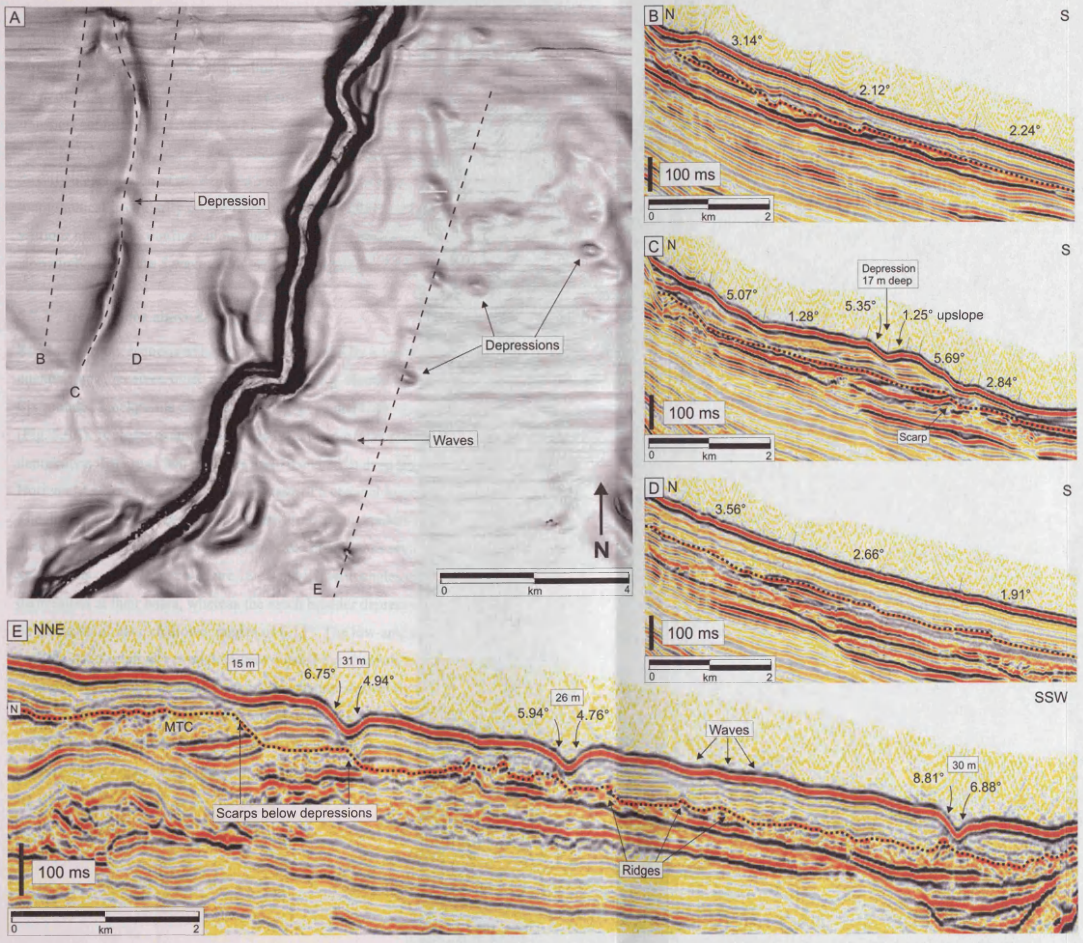

Figure 5.8. Irregular channel fill and depressions on seafloor formed above irregularities. (A) Dip map of the seafloor showing a channel with rounded margins west of an active channel. On eastern side of the active channel there are several, roughly circular depressions, c. 300 m across, on the seafloor. Location shown in Figure 5.1. (B) Seismic section west of the channel with smooth gradient and parallel reflections between Horizon N (dotted line) and seafloor. (C) Seismic traverse along the channel showing two sediment waves forming within the package N-seafloor. (D) Seismic section east of the channel with smooth gradient and parallel reflections between Horizon N and seafloor. (E) Seismic section across small depressions on the seafloor showing how they form above scarps on the underlying mass transport complex (MTC) and migrate upslope. Small sediment waves have formed above smaller irregularities on the Horizon N.

There are also several roughly circular depressions that are c. 300 m across and have a rounded appearance on the seafloor (Fig. 5.8A). The depressions are 9-31 m deep with flanks dipping 7-9° (Table 5.1). A seismic line across some of them shows that buried underneath c. 60 m of sediments, there is a chaotic seismic reflection package interpreted as a mass transport complex (MTC) that has an irregular top surface (Horizon N) (Fig. 5.8E). The relief of the MTC visibly affects the reflection geometry of the N-seafloor package. Significantly, directly beneath each of the depressions on the seafloor there is a scarp or a large topographical irregularity on the Horizon N. Some of the reflections of the package N-seafloor have wavy configurations that follow the underlying irregularities in relief of Horizon N. There are 5 waves with lee flanks dipping c. 2.6° and stoss flanks 0.7°.

5.7.2 Depressions above knickpoints

Knickpoints, i.e. sections of high gradient bounded by lower gradients, along submarine channels have received much recent attention (e.g. Heiniö and Davies, 2006; Mitchell, 2006). Six rounded knickpoints can be seen along a channel with rounded margins on the seafloor (Fig. 5.9A). A closer examination reveals that two of them (KP2 and KP4) are actually depressions that are c. 300 m across and 10 and 36 m deep (Fig. 5.9C). The high-amplitude Horizon M marks the end of an active stage of a channel located c. 60 m below the seafloor. The dip map of the horizon reveals sharp arcuate knickpoints along the channel, located directly beneath the rounded knickpoints and depressions on the seafloor (Fig. 5.9B). The knickpoints on the Horizon M are 18-30 m high with angles of 11-14° and with some small depressions at their bases, whereas the much broader depressions with rounded morphology on the seafloor have shallower angles of 6-11°. The low-amplitude reflection package M-seafloor has a relatively even thickness outside the channel, where it smoothes out irregularities on the Horizon M. Along the channel, however, the thickness of the package varies significantly above the sharp knickpoints on the Horizon M (Fig. 5.9C). The M-seafloor package also thins downstream of knickpoint 3 and thickens again after the channel has passed the adjacent salt diapir (Figs. 5.9A and B).

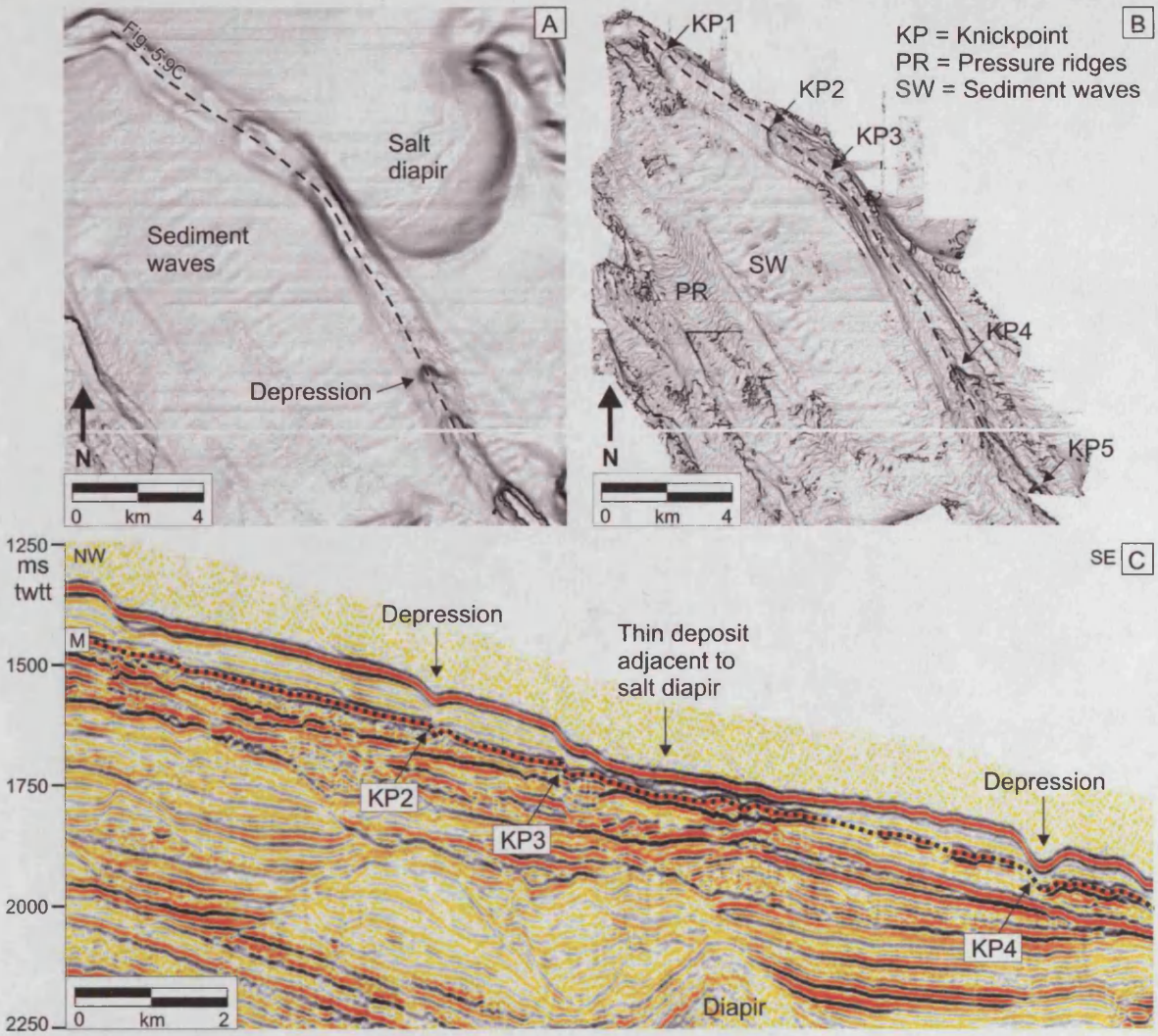

Figure 5.9. Depressions and knickpoints along a recent, inactive channel. (A) Seabed dip map showing a channel with rounded margins. Location shown in Figure 5.1. (B) Dip map of the Horizon M showing sharp arcuate knickpoints (KP1-KP5) along the channel. (C) Along-channel seismic traverse reveals sharp knickpoints with plunge pools at their bases on Horizon M beneath the rounded knickpoints and depressions on the seafloor. The sharp knickpoints on Horizon M are abrupt breaks in slope that create disruptions in flows within the channel. The notches at the bases of the knickpoints on Horizon M are interpreted as plunge pools, commonly found at the bases of knickpoints along submarine channels and canyons (Mitchell, 2006) and not unlike troughs formed at slope-rise transition (Pratson et al., 2000), although much smaller. Formation of a hydraulic jump as a supercritical flow slows down and becomes subcritical, enhances the excavation of a plunge pool beneath a knickpoint, as the currents expend their energy at the base of the slope (Pratson et al., 2000) (Fig. 5.12).

5.7.3 Depressions in other datasets

Depressions similar to those described here and by Fildani et al. (2006), have also been observed in other datasets. In Mitchell's (2006) Figure 4, a trail of depressions can bee seen on the seafloor adjacent to a canyon and some sediment waves on the Gulf of Alaska continental slope, and some depressions are also present near the Astoria Canyon offshore Oregon (Mitchell, 2006, their Fig. 6). Several trails of depressions are also found along a partly buried channel-levee complex on the western Niger Delta. A part of this system is

shown in Figure 5.12. The similarity with the trails of depressions in the Espirito Basin are remarkable, as both have a depression morphology that develops from asymmetric scour-shaped depressions into more rounded and symmetrical ones and are formed along a channel. The depressions on Niger Delta are found in much deeper water (>2500 m), but the slope is still relatively steep (c. 1.2°). The presence of sediment waves along the channel-belt and the adjacent seafloor indicate the presence of downslope currents. The channel-belt is not buried completely, therefore the flows are likely to be at least weakly confined within it. The confinement of flows may be the key to the formation of the depression trails. The process described here may also play a role in the formation of the 'ovoid depressions' on the same dataset described by Heiniö and Davies (2006).

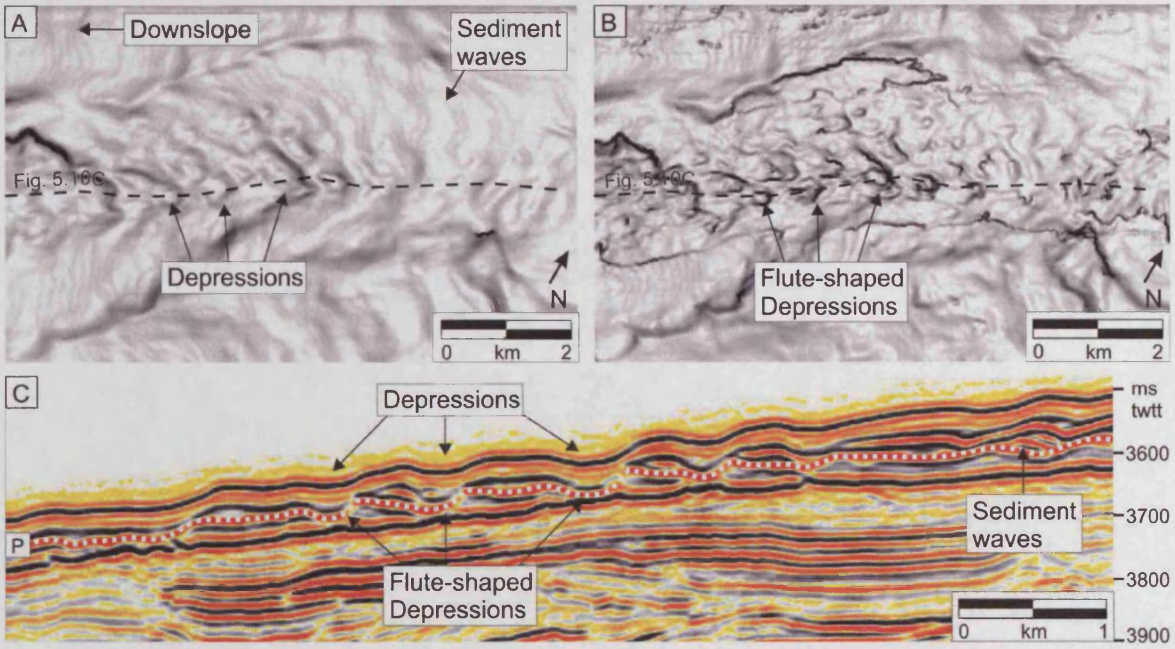

Figure 5.10. Depressions along a deepwater channel on western Niger Delta. (A) Seafloor dip map showing a part of a channel-belt of a buried channel-levee system. Sediment waves occur within the channel-belt and outside of it. Depressions with a diameter of several hundred meters occur along the channel. (B) Dip magnitude map of Horizon P approximately 70 m beneath the seafloor showing asymmetric, horseshoe-shaped depressions along the channel. (C) Seismic traverse along the channel-belt showing depressions on the seafloor and their scour-shaped morphology on Horizon P (dotted). See location of (A) and (B) in Figure 2.4B.

5.8 THE ORIGIN OF LARGE DEPRESSIONS IN THE ESPIRITO SANTO BASIN

5.8.1 Interpretation of general morphology

Although no sedimentological or wireline log data were available for this work, some general interpretations on specific sedimentary environments can be made based on general sedimentary setting, reflection geometry and seismic amplitude (e.g. Deptuck et al., 2003;

Posamentier and Kolla, 2003). Several phases of erosion and deposition were identified from the seismic data, also noted by Fiduk et al. (2004). These phases may reflect changes in the relative sea level or other external controls, which are beyond the scope of this paper. Sharp features are interpreted to have formed by erosional processes and rounded features by depositional and reworking processes. For example, Horizon C is dominated by erosional features, such as channels and scarps, but Horizons D, E and G are dominated by depositional features (Fig. 5.3). The big escarpment is interpreted as an erosional feature, as reflections are truncated against it (Figs. 5.2 and 5.3). It may be a lateral margin of a major slide scar.

The interval A-H is mainly aggradational with recurrent erosional phases. Variable infill patterns suggest variable current conditions throughout the evolution of the basin. Accumulation of hemipelagic drape and the formation of onlap and divergent fill normally indicate low energy, whereas mounded onlap fill indicate deposition by high-energy turbidity currents (Sangree and Widmier, 1977).

Sediment wave morphology observed in seismic lines along channels (Figs. 5.4, 5.6 and 5.8) is interpreted to have formed by sediment gravity current activity. The formation of the depressions is interpreted to be linked to this process. Before describing the preferred model for depression development, alternative interpretations are considered to eliminate the possibility of the depressions in the Espirito Santo Basin having an origin as fluid escape features or slope failures.

5.8.2 Fluid escape origin

Trails of circular depressions above buried submarine channels are most commonly ascribed to pockmarks caused when fluids trapped in buried channel sands escape to the surface (e.g. Gay et al., 2003). Some of them are considered to be giant fluidisation features (Davies, 2003). Due to the similarity in scale and the association with underlying channels, these interpretations are discussed below in more detail.

Pockmarks form as a result of catastrophic gas and/or pore water eruption on the seafloor. They are commonly 10-700 m in diameter and 1-45 m deep (Hovland, 2002). Strings of pockmarks are commonly found above fault zones and channels (Hovland, 2002). One such string follows the sinuous course of an underlying channel in the Lower Congo Basin (Gay et al., 2003). Those depressions are of similar scale (100-800 m in diameter and up to 40 m

deep) as the depressions in Espirito Santo Basin. They are connected by seismic chimneys to an underlying channel-levee interface, which is buried under 200 m of sediment. This is clear evidence that they are pockmarks formed by dewatering of fluids trapped in the channel sands. The data from the Espirito Santo Basin, however, show no evidence for fluid escape and the depressions are therefore not likely to be pockmarks. This argument can be further supported by the following observations:

1. The underlying channels have no channel-axis deposits (high-amplitude reflections). Instead, they are erosional channels incised into steep slopes. Furthermore, a 130-240 m thick sediment cover is needed for enough excess pore pressure to develop for fluids to escape from channel sands (Gay et al., 2003). The Espirito Santo depressions occur only few tens of metres above the channel and therefore there would not be enough excess pore pressure developed even if channel-axis deposits were present.
2. There is no evidence for fluid flow below or above the depressions. No unit pockmarks, faults, seismic chimneys or other seismic disturbance or amplitude anomalies that could indicate fluid escape or presence of gas are found in the data.
3. Locations of depressions not only above channels, but also above irregularities on the subsurface, e.g. scarps, suggest that channels are not crucial for their formation. Although fluid migration can also focus on structural highs, the evidence from near-seafloor examples prove that fluid escape does not occur above seafloor irregularities (see discussion below).
4. The formation of pockmarks is associated with focused vertical fluid flow thus forming vertical "pipes" or "chimneys". The Espirito Santo depressions are not located directly on top of each other, but have migrated slightly towards east by Horizon E (Figs. 5.3C and 5.5). This reflection pattern with both aggradation and lateral migration suggests depositional origin with possibly some reworking by bottom currents.

The circular depressions above a deep-water channel on the Niger Delta are of similar scale (600-900 m in diameter and 30-50 m deep) as Espirito Santo depressions. Davies (2003) interpreted them as a result of soft-sediment deformation, in which fluidised buried channel sands were expelled to the seafloor through a pipe system as a result of differential loading. Although the depressions in the Espirito Santo Basin are superficially similar to the ones on the Niger Delta, the absence of underlying channel deposits, overburden deformation and

evidence of a pipe system makes soft-sediment deformation an unlikely origin for them. The depressions on the Espirito Santo Basin occur on a steep slope (1.5-7°) in a proximal part of the slope, whereas the depressions on both Congo and Niger Delta are located on more distal and much shallower slope (generally <1°). The sediment wave-like geometry of the reflection package C-D could also be mistaken as a result of rotational slope failure, however, this could not explain the reflection geometry, as there is no evidence for a detachment fault.

5.8.3 Model for depression development

The observations on reflection geometries and the formation and evolution of the depressions are summarised in a schematic figure (Fig. 5.11). It breaks the evolution of the features into four stages representing the development at the time when Horizons C, D, E and G were the contemporaneous seabed. At stage 1, erosional currents incise a channel into the seafloor (Fig. 5.11A). Because the slope is steep and the flows are erosional, it can be assumed that the flows are dominantly supercritical (e.g. Nemec, 1990). The along-channel profile is illustrated as a smooth concave curve for simplicity, however, some irregularities were probably present on its surface, such as channel-margin slumps, erosional scours or pockmarks. These topographical irregularities, or an abrupt shallowing of the gradient, are likely to cause instabilities in the flows within the channel at stage 2 (Fig. 5.11B). For example, an irregularity with positive relief acts as an obstacle and would cause the flows to decelerate upstream of it and then accelerate on a locally steepened downstream side of the obstacle (Bursik and Woods, 2000). The deceleration of flows reduces bed shear stress imposed by the flows and causes increase in sedimentation rate. The opposite is true for the steeper slope, where flow acceleration increases bed shear stress and decreases sedimentation rate (Flood, 1988; Nakajima and Satoh, 2001; Fildani et al., 2006). This deceleration and acceleration of flows leads to deposition and erosion/nondeposition respectively across the obstacle. It may also bring a change in flow regime. When the flows are slowed down on shallower slopes and upstream of obstacles, they can become subcritical, as observed in the experiments of Bursik and Woods (2000). The inferred transition from supercritical to subcritical flow may also produce a hydraulic jump at abrupt changes in slope, such as bases of lee slopes. Shear stress is increased at the hydraulic jump, which enhances erosion at the base of the break in slope and causes increased deposition immediately after it (Garcia and Parker, 1989; Pratson et al., 2000; Kubo and Nakajima, 2002) (Fig. 5.12).

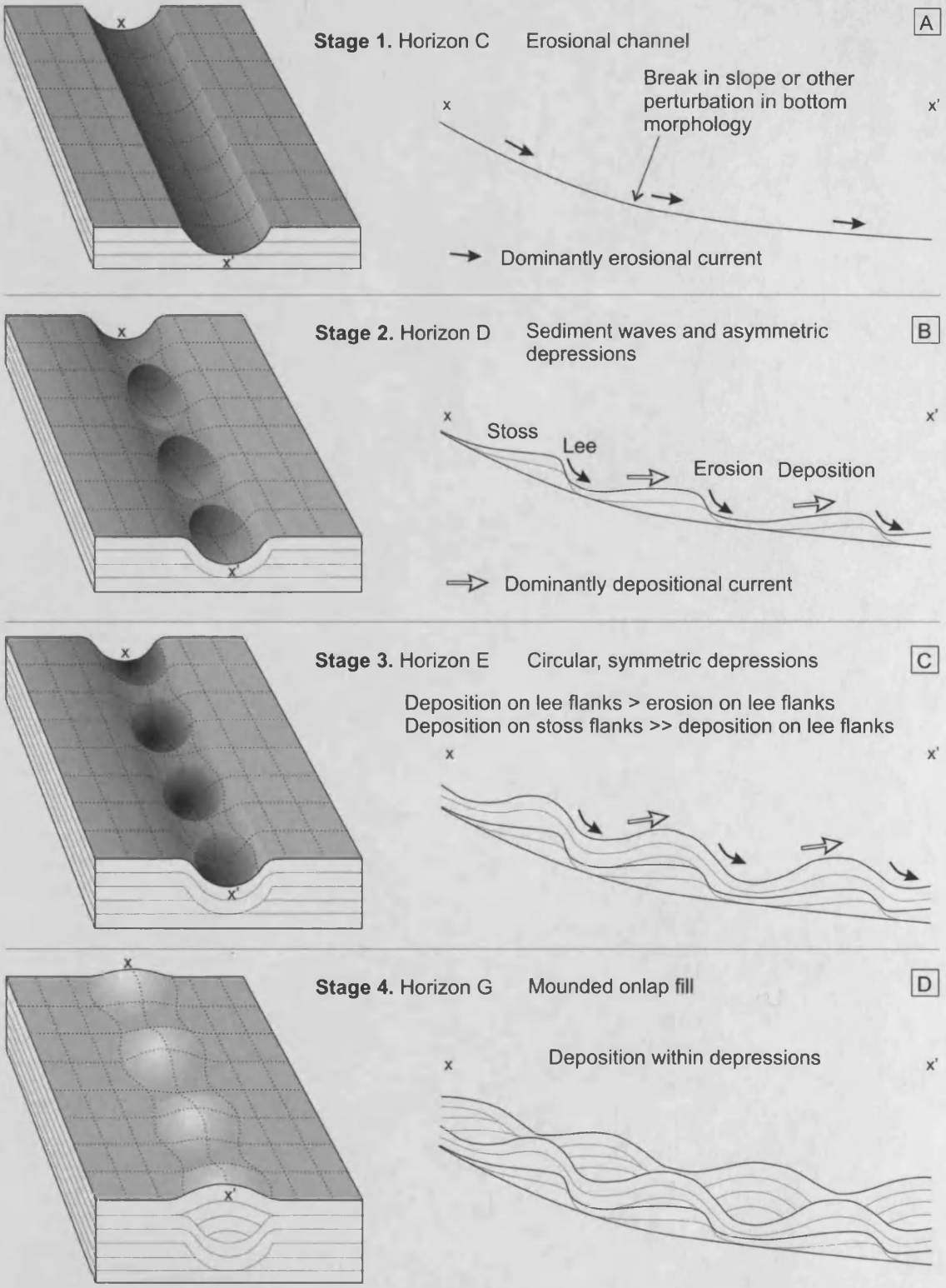

Figure 5.11. A schematic breaking down the evolution of the depressions. Not to scale. (A) At stage 1, an erosional channel is incised into previous deposits on a steep slope. The channel has concave, approximately smooth profile. (B) Stage 2 begins, when a perturbation or gradient change on the channel floor destabilises flows within the channel. Zones of slow, subcritical currents (white arrows) lead to deposition on locally shallower slopes and fast, supercritical currents (black arrows) erode locally steepened slopes leading to the formation of upstream-migrating sediment waves along the channel. The stoss flanks are shallow or upstream-dipping and lee flanks are steep, making the depressions asymmetric. (C) The depression morphology develops into more symmetrical and rounded by increased deposition on stoss flanks. (D) At stage 4 mounded onlapping fill fills the depressions and creates mounds on the seafloor.

The development of zones dominated by either deposition or bypass and erosion along the channel leads to the development of sediment wave-like bedforms in the reflection package C-D (Fig. 5.11B). After forming, the waves build up by preferential deposition on the upstream flanks and erosion on the downstream flanks. At the base of the steep lee flank of the most basinward wave, the newly formed break in slope may trigger the formation of another wave downstream (Kubo and Nakajima, 2002).

Because the sediment waves have steep lee flanks and upstream-dipping stoss flanks and are confined within the channel, the troughs appear like flute-shaped depressions in plan view (Figs. 5.11B and 5.3D). The flute-shaped geometry on Horizon D is not preserved by upstream migration or smoothed out, as may be expected. Instead, the depressions are built into deeper, more symmetrical depressions by depositing more sediments on the crestal areas but less on the troughs (Fig. 5.11C). This evolution from Horizon D to E likely represents changes in flow conditions at stage 3. However, the exact mechanism by which the flute-shaped depressions develop into more circular depressions with steep downslope flanks on Horizon E and F is not possible to be deduced from seismic data alone. The seismic data indicate that at this stage there is no more erosion on the lee flanks and more deposition occurs on the stoss flanks of the sediment waves, which leads to the building of upslope-dipping downslope flanks for the depressions (Fig. 5.4). Alternatively, an increase in hemipelagic sedimentation may cancel out the effect of erosion on lee slopes (Kubo and Nakajima, 2002). The observation that Horizon D has 14 more depressions than Horizon E indicates that some of them have been filled by the package D-E, and suggests that the flows were more depositional. However, some erosion or nondeposition must still have been present to keep the depression morphology from filling in. Pratson et al. (2000) observed that greatest erosion occurs at the base of slope and leads to the formation of an erosional trough and that thickest deposits are found immediately after this trough (Fig. 5.12). Similar phenomenon occurs in plunge pools of the bases of continental slopes (Lee et al., 2002). The inferred transformation from supercritical to subcritical flow condition via a hydraulic jump at the bottom of the steep lee flank could have resulted in enhanced deposition on the stoss flank.

The filling of the depressions begins after Horizon F, where the reflection character changes from low-amplitude hummocky to mounded onlap fill with intermediate amplitude reflections (Fig. 5.4). Some fill patterns aggrade vertically, but others step upslope as a result of preferential deposition after a break in slope at the base of the depression (Figs. 5.4 and 5.6D).

This change in reflection pattern is most likely due to changes in flow conditions at stage 4 (Fig. 5.11D). Mounded onlap fill indicates dominantly high-energy depositional turbidity currents flowing down the channel (Sangree and Widmier, 1977). The troughs that form between the mounds on Horizon G are infilled by onlapping reflections of the package G-H smoothing out the topography (Fig. 5.4). This onlapping geometry indicates that the mounds are depositional features and not caused by e.g. differential compaction.

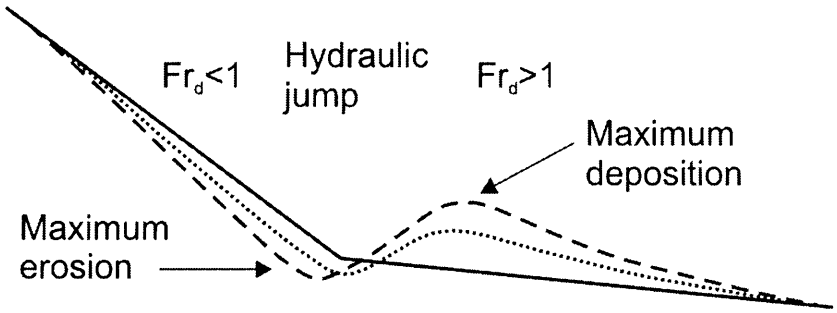

Figure 5.12. Idealised schematic of erosion and deposition patterns in the vicinity of a hydraulic jump. The solid line represents the original slope profile, dotted and dashed lines show how the profile evolves after supercritical ($Fr_d > 1$) flows erode the steep slope with maximum erosion occurring at the base of slope, where the flow undergoes a sudden transformation to subcritical flow ($Fr_d < 1$) via a hydraulic jump. Maximum deposition occurs immediately after the hydraulic jump.

The apparent downlap of some of the reflections of packages C-D and E-F onto the channel walls, seen in the traverse across the channels (Fig. 5.5), leads to lateral migration of the channel and the trail of depressions towards the east as the stratigraphy is built up. This geometry may arise from the erosion of the eastern channel margins and deposition on western margins, however, it could also be due to variation in depositional thickness so that it is below seismic resolution on the eastern side. Many factors may control this lateral migration, for example bottom currents interacting with gravity currents (Rasmussen, 1994; Viana et al., 2003).

The depressions on the seafloor that were presented in Figure 5.8 are clearly not related to any underlying channels, but instead they are related to the variations in the underlying topography. The depressions were formed above the scarps on Horizon N in a similar manner as described above, with erosion or nondeposition on locally steeper slopes and maximum amount of erosion at the base of the scarps, where it is inferred that a swift supercritical flows decelerate to subcritical flows (Fig. 5.12). This deceleration leads to increased deposition immediately downslope form the base of the scarp, producing an upslope-dipping downslope

flank for the depression. Similar, but much larger depression also formed above a scarp on Horizon C (Fig. 5.3).

The subtle sediment waves seen on the seismic traverse (Fig. 5.8E) are also inferred to have initiated on irregularities on the Horizon N, with sediment deposition concentrated on areas with lower gradient and behind small ridges. Bypass or less deposition occurred on steeper areas and downslope from ridges where the gradient was locally steepened. These examples suggest that sedimentation in the study area is controlled by gravity flows interacting with surface topography and depressions have formed by the actions of unstable gravity flows.

The depressions associated with the knickpoints along a channel (Fig. 5.9) show some similarity in geometries to the depressions in the interval A-H and they are of similar scale (Figs. 5.2-5.5 and Table 5.1). They illustrate how current activity can create circular depressions above perturbations along channel profile. Furthermore, they reveal that rounded knickpoints and other geomorphic features on the seafloor may be due to irregular deposition of sediments onto underlying sharp topography, therefore care must be taken when inferring processes from seafloor data alone.

Although the reflection configuration between the Horizon M and seafloor is mainly aggradational and does not show channelised deposits (Fig. 5.9), the areas of non-deposition or erosion along the channel indicate that some current activity must have occurred down the channel. The locations of these areas are most likely controlled by pre-existing structure or irregularities in the channel profile, for example, the package M-seafloor is thinnest next to a salt diapir (Fig. 5.9). This structural high may cause acceleration of the gravity flows flowing down the channel due to a funneling effect or gradient increase, thus causing sediment bypass or erosion on the channel floor adjacent to the diapir. The formation of sediment waves on the adjacent seafloor suggests the presence of down-slope currents.

5.9 DISCUSSION

The examples shown in this paper show asymmetric patterns of erosion and deposition on the upstream and downstream sides of topographical irregularities. Roughly circular depressions form by depositional and erosional processes of sediment-gravity flows, arisen when currents interact with changes in gradient of the seafloor and become unstable. The formation of trails of depressions is more likely to occur along channels, because confined flow is more likely to

respond to irregularities in the bottom topography than unconfined flow. Individual depressions tend to form above scarps and other topographical irregularities on unconfined seafloor. The examples on the modern seafloor of the Espirito Santo Basin (Figs. 5.8 and 5.9) illustrate asymmetric deposition and the formation of sediment waves across topographical irregularities on the seafloor. A perturbation in topography brings about changes in velocity, shear stress and flow regime. A flow may transform from supercritical to subcritical flow condition due to deceleration when a slope shallows. The bottom shear stress imposed by flow will also decrease. This all leads to erosion on steeper local slopes and deposition after a slope break. Differential draping of sediment can also be explained by suspension-flow theory, in which sediment deposition rate varies on slopes with various gradients (Hiscott, 1994). Deceleration of flows, where slopes become shallower or inverse, causes loss of their capacity to carry sediment in suspension and leads to deposition regardless of flow conditions (Hiscott, 1994; Nakajima and Satoh, 2001). Deposition can also be instigated by partial blocking of the current by an obstacle and by deflecting some of the current upslope (Nemec, 1990; Bursik and Woods, 2000).

The formation of sediment waves is an important mechanism, to which the formation of the depressions is related. Sediment waves normally form on slopes steeper than 0.4° (Nakajima and Satoh, 2001) but shallower than 2° (Wynn et al., 2000a). The erosional channels on the Espirito Santo Basin slope have much greater slopes, but the wave-like bedforms only occur on slopes of c. 2-6° (Fig. 5.4). Slopes with higher and lower angles do not exhibit sediment waves or depressions in the study area. The depression on the seafloor that is formed between two sediment waves within a channel (Fig. 5.8C) may represent an early stage of formation of a series of depressions, similar to what was described above for the C-H interval and corresponding to stage 2 of the evolutionary model (Fig. 5.11B). It strongly supports the argument that sediment waves are formed within channels and their troughs form channel-confined depressions. The occurrence of sediment waves only within the channels and not on the adjacent seafloor may be because the flows are different in a confined channel than on unconfined seafloor (Fildani et al., 2006). The formation of sediment waves is thought to be a result of the flows becoming unstable and vertically undulating as they interact with irregular topography on the base of the channel (Fig. 5.8C). Although the wave-like reflections of the package C-D are interpreted as sediment waves (Fig. 5.4), they are different from common sediment waves because (1) they do not form a field but are confined within a channel, (2) they are much larger in amplitude than other channel-confined sediment waves and (3) they

occur on much steeper slopes than most sediment waves. They are, however, similar in scale and morphology to the sediment waves of the numerical models of Kubo and Nakajima (2002) and Fildani et al. (2006). The laboratory experiments and numerical simulations of Kubo and Nakajima (2002) produced wavy structures with 4-5 crests after several thousand turbidity currents with asymmetrical deposition and erosion pattern. Their model results (Kubo and Nakajima, 2002, their Fig. 2) have similar morphology and slope angles as the seismic reflection pattern on the along-channel traverse between Horizons C and D (Fig. 5.4). Their conclusion that wave formation is due to preferential deposition resulting from variation in bottom slope is shared by other workers, e.g. Fagherazzi and Sun (2003), whose numerical model predicts the formation of a series of transportational cyclic steps from a single perturbation at the bottom topography. Similarly, the experiments of Taki and Parker (2005) showed that a Froude-supercritical flow over erodible bed evolves into a series of steps with spatially varying patterns of erosion and deposition.

Similar features to those described in this paper are also found elsewhere, suggesting that the processes responsible for their formation are ubiquitous. The large scour-shaped depressions on Monterey Fan valley, described by Fildani et al. (2006) and interpreted as erosional scours formed by supercritical flows that were overflown from the main channel, are probably the closest in terms of morphology and formation mechanism. They are much larger (3.5-4.6 km wide, 80-200 m deep) and formed on shallower slope than the depressions in the Espirito Santo Basin, but bear similarities with them, especially at the level of Horizon D (Fig. 5.3B). The numerical simulations of Fildani et al. (2006) resulted in the formation of several sediment waves beneath a break in slope when flows were depositional, which is also what is observed in the Espirito Santo Basin. The measurement of Fr_d values by Fildani et al. (2006) confirmed that the flow was undergoing a hydraulic jump above each wave, therefore they could be classified as cyclic steps. Although this paper is based on 3D seismic data alone, reflection geometry and comparison to published models enable the deduction that mainly the supercritical gravity flows travelling down the steep slopes of the Espirito Santo Basin on Brazilian continental margin become unstable when they interact with bottom slope and create wavy bedforms and roughly circular depressions on seafloor.

It is likely that other depressions found on submarine slopes are formed in a similar manner and more depressions will be identified in the future. The process may be similar to the development of sinuosity in channels, which is also thought to initiate when a current

encounter a perturbation in the subsurface. Although most of the depressions described in this paper have a similar scale with a diameter of several hundred metres, the depressions described by Fildani et al (2006) have diameters of kilometres. Therefore the process is thought to be scale-independent.

5.10 CONCLUSIONS

Trails of depressions are found along channels and individual depressions above scarps and other topographical irregularities in the Espirito Santo Basin on the continental margin of Brazil. They are interpreted to be a result of Froude-supercritical flows interacting with perturbations in topography and becoming unstable. This means that when flows travel on locally steeper slopes, they accelerate and become more capable to erode because of higher velocity and shear stress. On locally shallower slopes and upstream of obstacles, the flows decelerate and deposition of suspended sediment is enhanced. A local break in slope may also bring about a change in flow regime from supercritical to subcritical flow via a hydraulic jump, which will enhance erosion at break and deposition immediately after it, thus forming a depression. The depressions are thus likely be comparable to transportational cyclic steps. Cyclic steps have been formed in non-marine environments, laboratory experiments and numerical models, but have never before been described from 3D seismic data in the submarine realm. The 3D data from the Espirito Santo Basin enabled the establishment of the evolution of the 3D morphology of the depression formation in detail.

Chapter 6

6 DISCUSSION

The aim of this chapter is to synthesise the key findings of the previous chapters and to discuss some common themes within them, for example the effect of changes in slope on the sedimentary elements, such as mass transport complexes and channels. The importance of this research is discussed in the context of other analytical techniques including outcrop analysis, flume tank experiments and numerical modelling. The limitations and weaknesses of this work are also discussed, and future research is recommended.

6.1 SUMMARY AND KEY POINTS

The two datasets analysed during this project were introduced in Chapter 2. The dominant sedimentary elements in the Niger Delta dataset are large channel-levee systems, mass transport complexes and local slope failures on the flanks of thrust-related folds. The Espirito Santo Basin dataset, with steep slopes just beneath the shelf break, reveals smaller channels that do not have levees. It also contains a canyon system that has undergone several phases of incision and infill at least from the Oligocene until Present. Deformational structures that cause uplift have deformed the seafloor in both of the study areas. The topography created by these structures, anticlines on the Niger Delta and salt diapirs in the Espirito Santo Basin, affects the location and morphology of the sedimentary elements.

Chapter 3 concentrated on the erosional and depositional features that are formed as the anticlines on the Niger Delta degrade. Four different types of slope failure were identified and their style and runout distances were interpreted to have been controlled by slope morphology, sedimentology and the presence of anisotropies.

Chapter 4 examined the formation and evolution of knickpoints along the present day thalweg of a channel-levee system on the Niger Delta. The knickpoints were interpreted to have formed as a response of turbidity currents within the channel to the uplift of the fold and thrust belt. The knickpoints are characterised by deposits of coarser sediments upstream of them and erosion occurring downstream of these deposits. They tend to migrate upstream and evolve in various ways, leaving either erosional terraces or no evidence for their existence at all in the sedimentary record.

The large-scale depressions that occur in trails above erosional slope channels in the Espirito Santo Basin, and also individually above topographical irregularities were interpreted in Chapter 5 to have formed as a result of Froude-supercritical turbidity currents becoming unstable when encountering topographical irregularities. This creates erosional scours and deposits similar to sediment waves, which, when confined within channels, appear as roughly circular depressions.

6.2 THE EFFECTS OF CHANGES IN SLOPE

6.2.1 Introduction

Changes in slope angle have an influence on all of the sedimentary features discussed in this thesis. Both study areas exhibit deformation of the seafloor, which have introduced variable local slopes. The effects that changes in the slope angles have on the sedimentary elements include (1) the location and morphology of channel deposits and MTCs, (2) the style and type of resedimentation that occurs and their runout distances and (3) the effect on sediment-gravity flows, creating instabilities that produce asymmetric sedimentation and erosion patterns and form knickpoints, sediment waves and depressions. These were discussed in Chapter 2, Chapter 3 and Chapters 4 and 5 respectively. The key points are brought together below.

6.2.2 The role of slope failures and resedimentation in the study areas

It was noted in Chapter 3 that the slope angle variations and slope lengths have an effect on the style of resedimentation. In the Niger Delta study area, evidence for mass wasting is most commonly found on the local slopes created by the anticlines. The folds are eroded mainly by mechanical failures that leave erosional surfaces and scarps on the crests and flanks of the folds and produce slumps, debris flow deposits and turbidites at their bases. This kind of slope degradation does not occur along the flanks of the salt diapirs in the Espirito Santo Basin, although some evidence for failures initiated from the flanks of the diapirs can be seen. The diapirs have a larger effect on directing mass transport flows rather than causing local slope failures, whereas this is the opposite on the Niger Delta. Majority of the slope failures in the Espirito Santo Basin occur on the steep continental slope.

The MTCs that are not associated with the degradation of the anticlines are relatively uncommon in the Niger Delta study area, but few extensive MTCs that are several tens of

metres thick, and some smaller MTCs that plug channels are found within the dataset. All of them originate from outside of the data area, and therefore probably originate from large scale failures that occur closer to shore and possibly correspond to periods of relative sea level fall, as also suggested by Posamentier and Kolla (2003).

Some of the MTCs in the Espirito Santo Basin are also several tens of metres thick (e.g. in Fig. 2.16), but the majority are much smaller. There are a lot more mass transport deposits in the Espirito Santo Basin than in the Niger Delta, and many of them can be linked directly to a head scarp (e.g. Fig. 2.15). The characteristic features they exhibit, such as longitudinal grooves at their bases, blocky top surfaces and pressure ridges (Figs. 2.15 and 5.9B), are more prominent and common than the similar features in the large MTCs on the Niger Delta. The MTCs in the Espirito Santo Basin are more similar to the fold degradation features on the Niger Delta than the larger MTCs. This may be due to the relatively short transport distances. The failed sediment masses are more prone to create grooves at the bases and pressure ridges at the toes of the MTCs, because they are probably quite coherent closer to the source, whereas longer transport distances are likely to disintegrate the sediment masses. Although failures can occur on very shallow slopes of less than 0.5° (Sultan et al., 2004) and there are many factors that contribute to slope stability, a failure is more likely to occur on steeper slopes, as discussed in Chapter 3. The steep slopes and proximity to the shelf break in the Espirito Santo Basin dataset thus help to explain the abundance of small slope failures in that dataset and the rarity of them in the Niger Delta dataset.

6.2.3 The effect of slope gradient on the channels

6.2.3.1 Channels in the study areas

Although located in different settings, the channels in both of the datasets have many similarities, for example, evidence for their evolution involving several phases of incision and infill is seen in the slope channels and canyon systems in the Espirito Santo Basin and the large channel-levee systems of the Niger Delta. The main differences are the style of the channels. The Niger Delta CLSs are confined within erosional fairways and large outer levees, which are lacking in the slope channels of the Espirito Santo Basin, however, some channels are confined within the canyon systems, the appearances of which are very similar to the erosional fairways of the CLSs in the Niger Delta. Individual channel-axis deposits tend to show similar widths (c. 80-100 m) and sinuosities in all of the channels at all depths in both datasets.

6.2.3.2 The importance of channel gradients and the occurrence of knickpoints

Both the slope and the present day channels on the Espirito Santo Basin have concave profiles, whereas the studied channel thalweg on the shallower slope of the Niger Delta has a slightly convex profile due to the uplift associated with the fold and thrust belt. The average gradient of the present day channel thalweg on the Niger Delta is much shallower (0.5-0.6°) than of the channels in the Espirito Santo Basin, where the steepest parts of the channels have gradients of up to 9.4° where the slope is the steepest (up to 15°). The channel profiles in neither datasets are in equilibrium, as manifested by the occurrence of knickpoints along them.

The formation of the knickpoints in the Niger Delta dataset is a result of the sediment-gravity flows within the channels reacting to changes in gradient along the channel, as discussed in Chapter 4. On the seafloor of the Espirito Santo Basin, the knickpoint along the tributary channel (e.g. Fig. 5.1) is a hanging valley formed as a result of a greater rate of incision along the eastern tributary. The knickpoint has migrated upstream along the channel a distance of over 2 km. The formation mechanism of the knickpoints along the shallowly buried channel in the Espirito Santo Basin (Fig. 5.11) is uncertain, but their morphology is similar to the other knickpoints seen in both datasets. There are several possible ways, in which these knickpoints may have formed, but the most likely case is by current activity or a mechanical failure. Turbidity currents and other sediment gravity flows are capable of eroding seafloor and can form knickpoints in certain conditions as discussed in Chapter 4, e.g. if there are variations in bed resistance or erosional power of the currents. Sediment may also fail within a channel forming an arcuate headwall scarp across the channel that is morphologically identical to a current-generated knickpoint.

Although the knickpoints have formed by different mechanisms on both datasets and in different settings, their abundance suggest that knickpoint formation is an important part of channel evolution and one of the ways in which the channels try to reach their equilibrium profiles. It may be the key mechanism by which uplifted reaches are eroded and by which channels are incised into steep slopes. Several experimental results support this argument. Knickpoint formation and upstream-migration have been observed in many flume tank experiments that study the channelisation of turbidity currents and debris flows on submarine fans (e.g. Yu et al., 2006).

6.2.4 The formation of depressions

In this thesis depressions were described from five different settings; (1) along and above erosional channels in the Espirito Santo Basin, (2) along an almost buried channel-belt in the Niger Delta, (3) above knickpoints within steep slope channels, (4) above scarps in the Espirito Santo Basin and (5) above an anticline in the Niger Delta. (1) - (4) were discussed in Chapter 5 and (5) in Chapter 3. The formation mechanism of depressions above an anticline in the Niger Delta was not determined, but it was suggested, that they were formed by partly mechanical failure of sediment caused by the uplift of the fold and a subsequent modification by bottom currents. The other depressions were interpreted to be a result of sediment gravity flow activity. In all cases the trigger for depression formation appears to be a change in slope gradient. This is most obvious in the case of depressions that occur above knickpoints and scarps because there is a substantial break in slope at the base of scarps and knickpoints (Figs. 5.8 and 5.9). The break in slope causes an inferred transition from a swift supercritical flow condition to a slow subcritical flow condition via a hydraulic jump, which promotes erosion at the base of slope and deposition immediately after it creating a plunge pool (e.g. Pratson et al., 2000). Alternatively, plunge pools may be excavated by the impact of high-momentum sediment density flow (Lee et al., 2002). The depressions above the anticline on the Niger Delta may have formed in a similar manner.

The depressions occurring along channels in the Espirito Santo Basin and the Niger Delta are considered to have formed as channel-confined sediment waves that develop into more circular depressions by subsequent currents reacting to the wavy surface. This process is similar to transportational cyclic steps, which also depend on changes in flow regime (e.g.Fildani et al., 2006). These flows are at least weakly confined within the channels, which results in the formation of a series of sediment waves and depressions, whereas the depressions above scarps and knickpoints occur mainly as single depressions.

Origin of the depressions as fluid escape structures was discussed in Chapters 3 and 5 but the evidence suggest that a current origin is a more likely mechanism in forming the depressions. However, since fluid escape and pockmarks occur in similar settings, it cannot be ruled out completely that some fluid escape may have occurred. This could have created bottom irregularity that affected the currents causing them to erode and deposit sediment in specific areas and creating knickpoints, depressions or sediment waves.

6.3 THE IMPORTANCE OF OUTCROPS

6.3.1 The identification of degradation complexes, knickpoints and depressions from outcrops

The interpretation of sedimentary features from 3D seismic data raises the question of how these features can be identified from outcrops and furthermore, can the 3D seismic interpretation give clues about the formation of features seen in outcrops? Degradation complexes that create erosional surfaces and debris flow deposits at the bases of slopes have been interpreted in outcrops of many foreland basins. Progressive unconformities have been identified on the flanks of growing structures and growth strata that are deposited on top of or on the flanks from outcrops (e.g. Burbank and Raynolds, 1988; Deramond et al., 1993; Rafini and Mercier, 2002), some of which are analogous to the degradation of submarine folds discussed in Chapter 3.

The identification of knickpoints and the depressions or channel-confined sediment waves from outcrops may be more challenging. There may be many reasons why they have not been identified from outcrops so far. Although several excellent and well-studied outcrops of deepwater channels exist, for example Brushy Canyon in Texas, (Gardner and Borer, 2000; Gardner et al., 2003), Ross Formation in Ireland (Lien et al., 2003), Grès d'Annot in France (McCaffrey and Kneller, 2001; Bourgeois et al., 2004; Moraes et al., 2004), Kirkgeçit Formation in Eastern Turkey (Cronin et al., 2000) and Tabernas Solitary Channel, Spain (Clark and Pickering, 1996; Haughton, 2000; Pickering et al., 2001), and they show similar architectural elements and evolution to channels seen in 3D seismic data, some architectural elements, for example levees are seldom found in outcrops (Peakall et al., 2000b). Outcrops are inherently two-dimensional and too small to encompass features like sediment waves or depressions within the channel-fill. Another possibility is that there is evidence for them within the outcrops, but they have not been looked for and therefore not found. The low relief and low angles of dip of these deposits may prevent their identification from outcrops.

Unexpected channel-fill geometries have been identified from some outcrops, however, and interpreted to have formed by similar processes to what have been inferred from the 3D seismic data in this thesis. Pickering et al. (2001) identified bedforms they called sandy macroforms from the outcrops of the Late Miocene Solitary Channel in the Tabernas-Sorbas Basin. These entirely channel-confined, backstepping bedforms are 30-40 m long, 2-5 m high

and inclined 12-15° to upslope direction and occur behind ridges within an underlying debris-flow deposit. The changes in gradient of the base of the channel are interpreted to be the seeding points for their deposition. Brown and Branney (2004) noticed similar sigmoidal upstream-dipping regressive lenses of similar scale within the ignimbrite deposits in Tenerife. Similarly, they interpreted their formation as a result of turbulent currents decreasing in velocity and capacity where the gradient is decreased, this leading to deposition and upstream migration of the bedforms. The outcrops show scours, indicating that the currents were locally erosional. Giant flute-like sours with high aspect ratios (5:1) were also identified in the Solitary Channel outcrops (Pickering et al., 2001). These examples indicate that the behaviour of flows within channels is most likely much more complicated than what are interpreted from outcrops, because they normally only represent a very small part of an extensive system. Although the bedforms and erosional features of these outcrops would not be resolved from seismic data, their presence confirms the variable erosion and deposition processes along channel especially where there are topographical irregularities. The backstepping macroforms of the Solitary channel may be analogous to the channel-confined sediment waves within the channels in the Espirito Santo Basin, although they are of smaller scale. Furthermore, they may actually represent only a small part of a larger depositional element that could be seismically resolvable.

Outcrops give the chance for the determination of bed-scale features and heterogeneity 2D, as well as the nature of contacts between different channel-fill elements and other channels within a channel complex or the country rock (Fig. 6.1). Many questions remain, for example, how evidence for erosion by knickpoint migration can be identified from outcrops. Knickpoint migration creates terraces and erosional surfaces along channels, but even if these were found on outcrop, distinguishing them from channel incision without knickpoint migration would not be possible unless the actual preserved knickpoint was found. A knickpoint could be recognized from outcrop by much steeper erosional surface than what the rest of the channel has, however, outcrops are not commonly extensive enough or have the three-dimensionality required for identifying such features. Nevertheless, the discussion in this thesis suggests that knickpoint formation and migration is an important process of how slope channels are incised, and therefore evidence for it should be looked for in outcrops. The same applies to channel-confined sediment waves and other along-channel variations in the channel-fill patterns. These could be identified from outcrop by recording changes in the dip magnitude or direction of channel-fill elements. Upstream-dipping channel-fill elements may

indicate the location of stoss flank of a sediment wave (or a downslope wall of a depression). Similarly, a lee flank migh be recognised by erosional surfaces cutting previously deposited sediments or by higher dip magnitude of channel deposits, possibly exhibiting erosional scours or flute marks that would indicate the locally erosive nature of the currents.

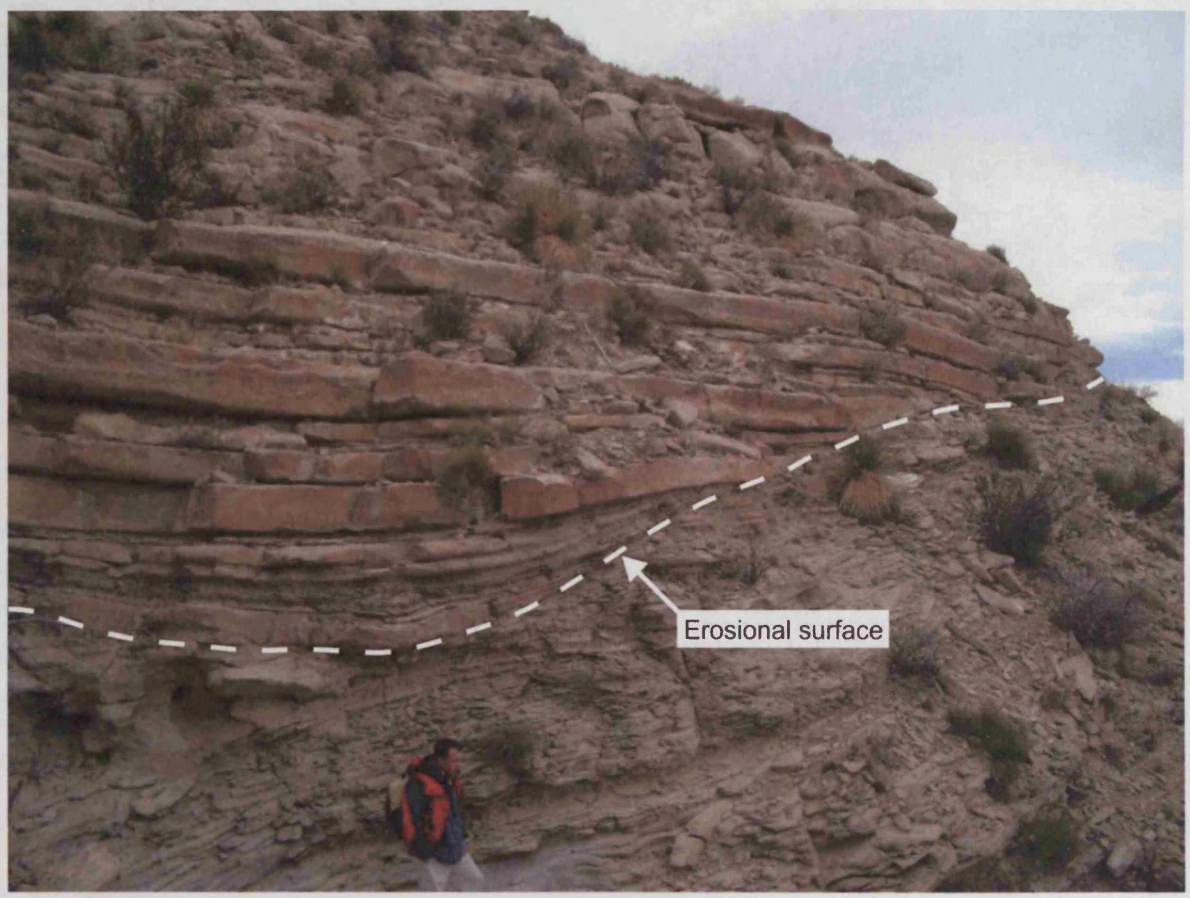

Figure 6.1. An outcrop of a slope channel from the Brushy Canyon, West Texas. The channel cuts into mudstone and is filled with lens-shaped beds of sandstone. What process created the erosional surface?

6.3.2 The resolution of outcrops vs seismic data

Deptuck et al. (2003) illustrated the differences in the scales of observation of channel-fill elements from outcrops and seismic data by comparing several examples. The CLSs on seismic data are normally viewed with at least a 7x vertical exaggeration, and some features, such as vertical aggradation of channels is difficult to distinguish when viewed with no vertical exaggeration or when studying outcrops (Deptuck et al., 2003).

The difference in scale and resolution of seismic data and outcrops can be highlighted easily by discussing lateral accretion packages and forward seismic modelling of outcrops. Abreu et al. (2003) compared conventional resolution (35 Hz) seismic data with high-resolution (65

Hz) seismic data and observed that evidence for lateral migration of a deepwater channel can only be seen in the high-resolution data. Similar observations are made from synthetic seismic data produced from outcrops, e.g. Solitary Channel (Abreu et al., 2003), Big Rock Quarry Face (Coleman et al., 2000), San Clemente (Campion et al., 2000; Campion et al., 2005) and a part of the Grès d'Annot (Bourgeois et al., 2004). The internal geometry of the channels were not resolvable at all in normal 35 Hz seismic data, however, higher frequencies allowed some internal geometry to be resolved.

The interpretation of the seismic data in this thesis showed that channels commonly have several phases of incision and infill and cut into previously deposited channel-fill elements. Some submarine channels exhibit steeply dipping high-amplitude reflections on the inside of channel bends, see also the CLSs of the Niger Delta (Fig. 2.11). These are interpreted to be lateral accretion surfaces analogous to point bars (Peakall et al., 2000a) and to mark the position of inner banks of channel during migration (Abreu et al., 2003). These lateral accretion packages (LAPs) are also seen on seismic data in the Nile delta (Samuel et al., 2003), Angola (Abreu et al., 2003) and Indus (McHargue and Webb, 1986). Their absence in seismic data does not necessarily mean that they are not there, but that they are too small to be resolved (Wonham et al., 2000).

Channel migration and avulsion are separate processes, migration being a gradual shift of the channel by systematic erosion on outer bends and deposition on inner bends and avulsion being a cut-and-fill process (Abreu et al., 2003). Abreu et al. (2003) interpreted both processes from the seismic data, however, it is argued here that although both processes may occur in submarine channels they may not be distinguished form each other from seismic data alone. What looks like channel migration on seismic data may be the result of avulsion, where each channel is incised into the previous one partly cannibalising it. This argument is supported by the work by Campion et al. (2000) and Campion et al. (2005), who interpret the lateral amalgamation of ten slope channels within the outcrops of San Clemente to have formed by autocyclic avulsions, i.e. subsequent cutting and filling of the channels. Their forward seismic modelling of the outcrops reveals that what in the outcrop can be identified as eight discrete channels that cut into each other and are laterally amalgamated, in the seismic data appear as two or three channels (Fig. 6.2).

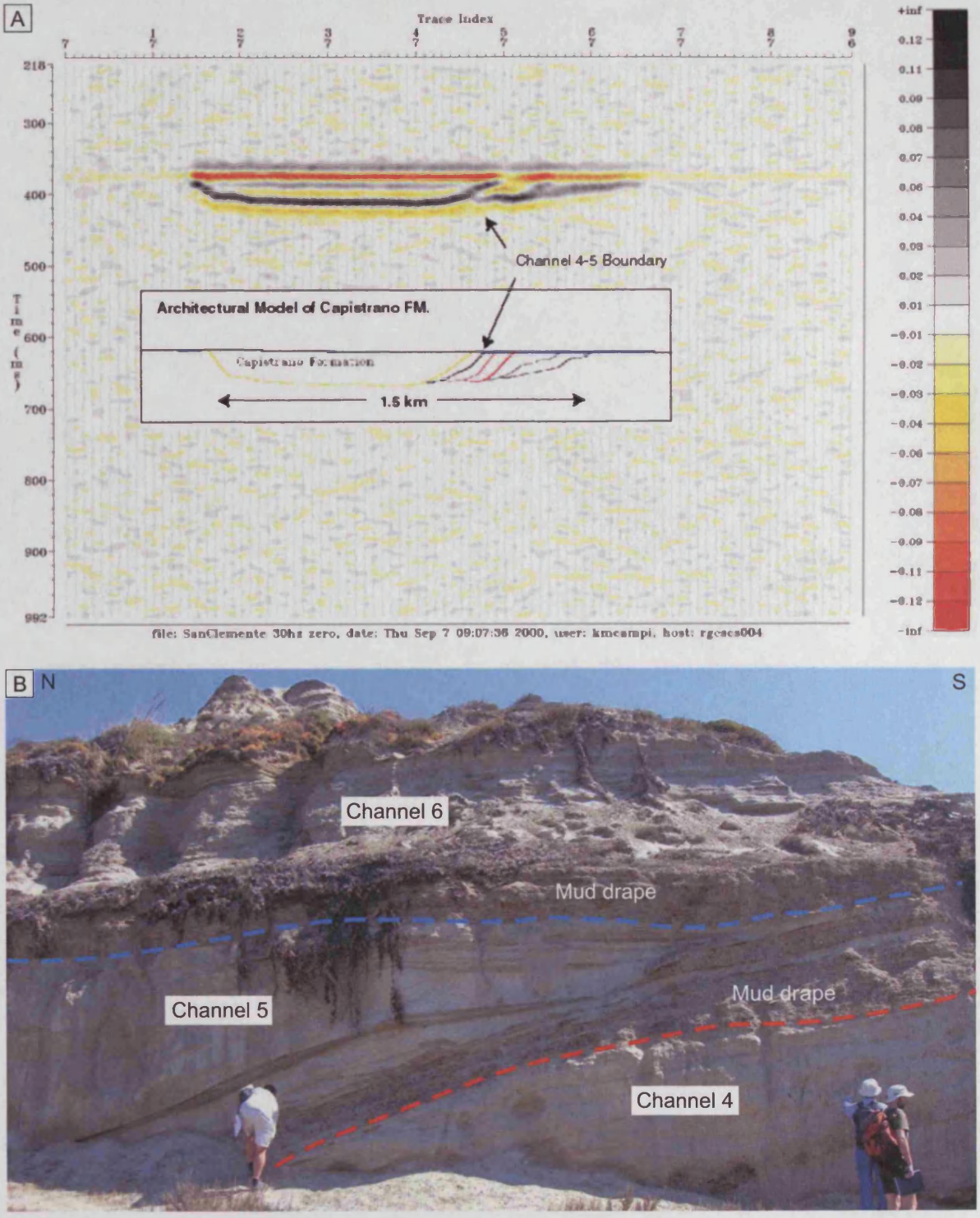

Figure 6.2. (A) Forward seismic model of Capistrano Formation (from Campion et al., 2000, their Fig. 7) illustrating that with a 35 Hz seismic data only the boundaries between channels 2-3 and 4-5 can be resolved. (B) A photograph of the boundaries between channels 4, 5 and 6 of the Capistrano Formation. The interpretation is based on Campion et al. (2000) and Campion et al. (2005). Red dashed line marks the boundary between the channels 4 and 5 and blue dashed line the boundary between the channels 5 and 6. Both erosional surfaces are draped by mud drape. These kinds of heterogeneities cannot be resolved from seismic data.

The channels of the Capistrano and Brushy Canyon Formations are deposited on relatively steep slopes and are analogous to the Espirito Santo Basin channels. There is therefore potential for the existence of knickpoints and sediment waves or depressions within these successions. However, these features are highly challenging, if not impossible, to be recognised from outcrops, as discussed in the previous section. Furthermore, although well exposed, the required scale or three-dimensionality cannot be achieved on most outcrops. Therefore 3D seismic data is crucial for determining such features within deepwater sedimentary successions. New techniques, such as the laser-based mapping technique Lidar (LIght Detection And Ranging) combined with ground-penetrating radar (GPR) can generate 3D models of outcrops and may provide the opportunity to determine seismic-scale features from outcrops in the future (e.g. Bellian et al., 2005).

6.4 THE IMPORTANCE OF EXPERIMENTS AND MODELLING

Experimental and numerical modelling of sediment-gravity flows have increased the understanding of the behaviour and deposits of the flows tremendously. Measurements made from controlled experiments have enabled the determination of the structure and variations within flows and revealed features, such as secondary flow cells within submarine channels (Keevil et al., 2006). A review of several recent experimental and mathematical studies is given in Kneller and Buckee (2000). One of the advantages of flume tank experiments done in laboratory is that changes of particular parameters to the behaviour of flow can be investigated in order to either reproduce a naturally occurring feature or simply to find out how various parameters affect the flow behaviour.

The evolutionary models for knickpoint formation and migration that was given in Chapter 4 and for the formation of channel-confined sediment waves and depressions that was given in Chapter 5 were supported with the knowledge of depositional and erosional behaviour of turbidity currents that was acquired from experimental and numerical modelling. The experimental work and numerical models referenced in those chapters were crucial for making the inference of the processes that produced the features seen in the seismic data more scientifically sound. The analysis of 3D seismic data also provides natural examples of some features that have previously mainly been seen in models, such as the depressions that were found in the Espirito Santo Basin (Chapter 5). Different analytical methods complement each other and combining them in the analysis of data is desirable.

6.5 LIMITATIONS AND WEAKNESSES

The limitations and weaknesses of this work are mainly related to the limitations within the data and the limitations within the methods used to analyse the data. Both 3D seismic datasets analysed for this project were of very high quality and have very few artefacts, which made the interpretation process easier. The main limitations of the seismic data were their physical boundaries and resolution. The extent of some features, for example the MTCs in the Niger Delta could not be investigated properly, because their full extents were not present in the dataset. Also the channel-levee systems within the data represent only a part of the entire system. However, it may have been impossible to analyse a more extensive dataset in the time frame of the project.

The resolution (tuning thickness) of both the 3D seismic datasets was around 10 metres. Even though smaller features could be defined from the interpreted horizons, the work was done above bed-scale and thus many important features and clues about the processes that created them could not be identified. But as discussed in the previous section, 3D seismic data gives the opportunity to visualise the features in three dimensions and at a larger scale than outcrop data, which normally exposes only a partial 2D view, and some features that are identified in 3D seismic data are most likely impossible to be detected from outcrops.

The project would have benefited from additional data, such as well logs or sediment cores to enable the determination of the subsurface lithology and depositional environments more accurately. Unfortunately these data were not available, however, sufficient information was acquired from literature for the purposes of this thesis. The errors in the measurements, for example thicknesses of sedimentary packages and slope angles, that were based on estimations of seismic velocities rather than real data are negligible and do not change the main results significantly.

The manipulation of the 3D seismic data can be done in numerous ways, and to find the best method for the analysis of a desired feature was not always straightforward. The hardware and software that were used produced some limitations for the interpretation, as some analysis of the data could not always be done with the analytical tools available. Also, new techniques had to be tried, because normal methods were not producing desired level of quality or could not be applied to some features. For example, the methods commonly used for the analysis of

submarine channels from 3D seismic data are more suitable for aggradational channels and not for degradational channels that occur on a folded slope.

6.6 FUTURE RESEARCH

Some questions were answered in this thesis, but many more arose. Suggestions for future research were highlighted where applicable. Ultimately, given the variety and the three-dimensional complexity of the degradation complexes, knickpoints and the depressions that form along channels and above topographical irregularities, identifying them from other seismic volumes and different type of data would be essential to fully characterise and predict their formation and importance in the submarine environment.

In this thesis, models were put forward to explain the evolution of several sedimentary features that were interpreted from 3D seismic data. Further research into the mechanisms and prediction of those features could be conducted. Especially flume tank experiments that would aim to reproduce the formation of channel-confined sediment waves, cyclic steps and knickpoints would be beneficial for the understanding of these processes.

Acquiring more data on systems that are active on the present day would be interesting and useful. Where features such as knickpoints are found on the present day seafloor, the evolution of their morphology and rates of migration could be determined more quantitatively if new data were collected at certain time intervals. Sampling of sediment by for example drop cores and measuring current properties across these features would also increase the quantitative analysis.

The work done for this thesis concentrated on particular areas of continental margins. It would be very interesting to study a whole sedimentary system from source to sink in detail. This would involve obtaining and analysing an enormous amount of data that include canyons, channels and frontal splays and show the structure and evolution of the continental margin. Well data and sedimentary cores would be important for this kind of work to establish the detailed sedimentology of the system. This kind of project could be taken to great lengths by incorporating and synthesising various data and methods, such as provenance and climate studies and, experimental work and modelling to determine the detailed evolution of the whole system.

New technologies, such as Lidar, combined with GPR could be used to look for features that are commonly resolved only from 3D seismic data from outcrops. Finding evidence for depressions, knickpoints and sediment waves within channel-fill on outcrops and other data should be attempted.

The growing interest in deepwater continental margins by both the scientific community and the hydrocarbon industry and the increasing amount and quality of data and new technologies to analyse them ensure that there is a plethora of opportunity for future research in this field.

Chapter 7

7 CONCLUSIONS

7.1 ARCHITECTURAL ELEMENTS OF THE STUDY AREAS

- The dominant architectural elements in the Niger Delta dataset are large channel-levee systems, MTCs and smaller failures that originate from the flanks of thrust-related anticlines. In the Espirito Santo Basin dataset, there are salt diapirs, large canyon systems, small channels and slope failures including slumps, slides and debris flows, which are originated from the steep slopes beneath the shelf break.

- Both datasets have a range of erosional and depositional features, the location and style of which are influenced by the uplift of structures that actively deform the seafloor. Regardless of the differences in the settings, many of the architectural elements of these two datasets have similar seismic character and morphology, although they commonly occur at different scales.

- The main differences in the architectural elements in the two datasets are that (1) the large canyon systems are only present in Espirito Santo Basin dataset, (2) the large, confined channel-levee systems are only found in the Niger Delta dataset and (3) more slope failures are found in the Espirito Santo Basin. These failures are smaller than the MTCs on the Niger Delta, although similar small failures occur on the flanks of the anticlines on the Niger Delta.

- The sediment pathways are influenced by pre-existing and actively forming structures. The locations of the channel-levee systems on the Niger Delta are influenced by transfer zones and the uplift rate of the anticlines. The canyons, channels and MTCs in the Espirito Santo Basin are influenced by the location of the salt diapirs and the underlying salt ridges.

7.2 DEGRADATION OF COMPRESSIONAL FOLDS ON THE NIGER DELTA

- Several different styles of submarine fold degradation result from various failure and transport processes. These include (1) small failures on the backlimbs and forelimbs, which produce debris flows and deposits no more than a few tens of metres thick, (2) large slumps with evidence for internal deformation, (3) ovoid depressions, probably

formed as a combination of slumping and bottom current erosion and (4) degradation by deepwater channel erosion and channel margin slumping.

- Channel erosion is volumetrically the most important fold degradation mechanism in this particular dataset, but the most common style is that of multiple, retrogressive, small volume failures, the locations of which are affected by pre-existing planes of weakness, such as crestal faults, if they are present.

- The difference in the geometries of the backlimbs and forelimbs of thrust propagation folds is a fundamental control on the style of failures and the runout distances of failed sediment masses. The abrupt break in slope at the foot of the forelimb reduces the velocity of the failed sediment mass due to the reduced effect of gravity and increased effect of friction. This causes deposition resulting in relatively thick, short and wide deposits, whereas the longer but shallower slope of the backlimb leads to disintegration of failed sediment mass into debris flows or turbidity currents that produce widespread, thin deposits with longer runout distances.

- Both backlimb and forelimb failures are likely to form deposits that are below seismic resolution. They are therefore difficult, if not impossible, to identify adjacent to buried folds where the seismic resolution is low.

- The failure of sediments with higher internal shear strength forms more coherent downslope mass movements on a basal detachment, which show evidence for shortening by internal imbricate thrusting.

- Ovoid depressions that occur above folds that have only a minor relief on the seafloor are considered to have formed by small scale slumping and have subsequently been modified by bottom currents.

- Fold degradation produces laterally discontinuous erosional surfaces and poorly sorted deposits along the folds. The impact on reservoir prediction is that significant amount of sediment is removed from the folds and thick deposits of non-reservoir accumulates

adjacent to folds. Laterally discontinuous erosion surfaces and deposits along the folds can cause very complicated reflection geometries.

7.3 KNICKPOINT MIGRATION IN SUBMARINE CHANNELS

- Knickpoints form on a present day thalweg of a channel-levee system on the western Niger Delta as a result of uplift of folds orthogonal to the CLS. The knickpoints are classified according to their size, morphology and maturity. Type I knickpoints are the largest and the least mature, Type II knickpoints are intermediate, and the Type III comprises the smallest and most mature knickpoints found across the frontal fold, where the local gradient is the steepest.

- The high degree of confinement of the channel-levee system may restrict the channel to respond to the changes in gradients caused by the folding by lateral migration of the thalweg (swing and sweep). Instead, it tries to readjust to equilibrium profile by adjusting the vertical position of the thalweg by erosion and deposition in specific areas.

- The reduction of the thalweg gradient upstream of an anticline leads to deceleration of turbidity currents and deposition of their coarsest sediment load. This interpretation is supported by the presence of several kilometres long zones of high-amplitude reflections, which represent relatively coarse-grained sediments along the channel upstream of some folds. Where the gradient is steeper on the basinward limb of the fold, the currents accelerate and become able to erode the seafloor. These specific areas of erosion and deposition leads to formation of the knickpoints.

- As the knickpoints migrate upstream, they erode the sediment deposits upstream of them completely or incise into them cutting them into terraces. High amplitudes on some of the terraces adjacent to channel thalweg are thus more likely to record a history of deposition of coarse sediments, which were subsequently incised and compartmentalised by a headward-migrating knickpoint, rather than giving clues about the thickness or volume of turbidity currents within the channel.

- The relatively coarse deposits upstream of knickpoints can be preserved for example if the channel system is abandoned or avulsion within the channel-belt occurs. The evidence from this case study suggests that avulsion and at least partial preservation takes place in this system at the present day.

- The 3D architecture of channel-levee systems is influenced by knickpoints where the channels intersect dynamically changing seabed topography. The occurrence of knickpoints increases the erosive character of stacked channel deposits and leads to the development of discontinuous channel-axis deposits. However, evidence for deposits of coarser sediments can be found within the channel reaches upstream of folds. These deposits could constitute an important element of reservoir architecture, but stacking patterns can vary dramatically over short distances along channels.

- Knickpoint formation and migration may be an important process by which channels cut through uplifting thrust and fold belts as they strive to obtain their equilibrium profiles. However, as knickpoints are predominantly transient features, distinguishing the evidence of knickpoint migration from erosional currents from subsurface seismic data or outcrops is highly challenging.

7.4 CURRENT-GENERATED DEPRESSIONS ALONG CHANNELS

- Trails of depressions that follow underlying erosional slope channels are found in the Espirito Santo Basin on the continental margin of Brazil. Individual depressions are also found above scarps, knickpoints and other topographical irregularities. The depressions are typically several hundred metres across and tens of metres deep (typically 600 m and 30 m respectively). The 3D seismic data enabled the establishment of the evolution of the 3D morphology of the depressions in detail.

- The formation of the depressions is interpreted to be the result of the interaction of Froude-supercritical flows with perturbations in topography. This makes the flows unstable and creates zones of preferential deposition and erosion. A local break in slope may also bring about a change in flow regime from supercritical to subcritical flow via a hydraulic jump, which will enhance erosion at the base of the break in slope and deposition immediately after it, thus forming a depression.

- The trails of depressions that follow the underlying channels are interpreted as channel-confined sediment waves, which are likely to be comparable to transportational cyclic steps. Cyclic steps have been described in non-marine environments, laboratory experiments and numerical models, but have never before been described from 3D seismic data in the submarine realm.

- Trails of depressions that have been described before are caused by fluid escape producing trails of pockmarks above channel-axis deposits. Their development relies on the development of overpressure in buried sediment, requiring rather different conditions than what were described here.

- Similar trails of depressions to what was described in the Espirito Santo Basin are observed in other datasets and also produced by modelling and experiments. The phenomenon is thus expected to be ubiquitous and further examples are likely to be found in other basins.

- The formation of depressions by current activity is likely to be far more widespread on deepwater slopes also because supercritical flow conditions are common on steep submarine slopes and there are many mechanisms by which a perturbation can develop on the seafloor. However, particularly steep slopes or confined flows may be required to create the ideal conditions for this process to occur. Nevertheless, continental slopes cover a large area of the Earth and therefore this process is likely to have global significance.

7.5 GENERAL CONCLUSIONS

- Changes in the slope angles have a significant effect on the type, size and location of erosional and depositional elements of the study areas. They affect for example (1) slope stability, making a failure more likely the steeper the slopes are, (2) runout distances and the level of disintegration of failed sediment, (3) gravity and bed shear stress, and therefore the velocity of the sediment-gravity flows and their capability and tendency to erode or deposit sediment and (4) stability of the flows, causing changes in flow conditions and regime, and leading to the formation of knickpoints, sediment waves and depressions.

- The actively forming structures in the two datasets, the thrust and fold belt in the Niger Delta and the salt diapirs in the Espirito Santo Basin, affect sedimentation and erosion in different ways. Some channels are deflected around the anticlines and some mass transport complexes are curved around the salt diapirs. The folds provide the sites and the origin for small slope failures, but similar degradation of the diapir flanks is not observed. The small slope failures in the Espirito Santo Basin originate from the steep continental slope instead.

- Although the channels in the two datasets are different in that in the Espirito Santo Basin they are mainly smaller converging slope channels and channels that are confined within a canyon system, and in the Niger Delta they are large channel-levee systems, they share some common features. Channel deposits of similar width, sinuosity and amalgamation are found within the canyons of the Espirito Santo Basin and the basal parts of the CLSs on the Niger Delta. Sinuosity in the channels of the Niger Delta does not appear to be affected by gradient, mainly due to the confinement of the channels, but in the Espirito Santo Basin there is a clear correlation with sinuosity and slope. Meander bend formation and cutoff have been important processes during the evolution of the Ijebu CLS on the Niger Delta, however, most likely only during periods of time when the channels were less confined.

- The channels on or near the seafloor of both of the datasets have knickpoints along them, although the slope channel profiles are concave in the Espirito Santo Basin and slightly convex on the Niger Delta. Although the formation mechanisms of the knickpoints are different, it is suggested that knickpoint migration is an important mechanism of how channel incision occurs.

- Sediment-gravity currents are responsible for the formation of many features on submarine slopes, such as channels, knickpoints, sediment waves and depressions. They play a major role in the modification of the morphology of the deepwater slopes. The observations made in this thesis have significance in understanding sediment dispersal patterns in submarine realm and how submarine landscapes are created and modified.

- The identification of the sedimentary features discussed in this thesis from outcrops can be very challenging, as outcrops are not commonly large enough to encompass the whole feature or to enable the establishment of its 3D architecture. Some erosional surfaces seen in outcrops of channels may have been formed by upstream-migrating knickpoints and some strata within a channel-fill may be a channel-confined sediment wave, but they may never be identified from outcrops.

- Different analytical methods complement each other. The study of outcrops, flume tank experiments and numerical modelling are important tools to aid the interpretation of 3D seismic data. They have increased the understanding of the processes and behaviour of sediment-gravity flows and reveal many small-scale features that cannot be identified form seismic data. 3D seismic data also provides natural examples of geometries and morphologies in large scale whose formation modelling can try to solve.

- There is a great opportunity and desire for future research in the field of deepwater sedimentary systems. The increasing amount and quality of data and technologies to acquire and analyse them alone enables this. Many features that have only been resolved from 3D seismic data should be looked for in other seismic volumes and other kinds of data. The understanding of the formation mechanisms and conditions of features, like knickpoints and channel-confined sediment waves, depressions and cyclic steps could be greatly advanced by conducting more experiments and analysing more datasets.

References

8 REFERENCES

Abreu, V., Sullivan, M., Pirmez, C. and Mohrig, D., 2003. Lateral accretion packages (LAPs): an important reservoir element in deep water sinuous channels. *Marine and Petroleum Geology* 20(6-8), 631-648.

Adams, E.W. and Schlager, W., 2000. Basic types of submarine slope curvature. *Journal of Sedimentary Research* 70(4), 814-828.

Adeogba, A.A., McHargue, T.R. and Graham, S.A., 2005. Transient fan architecture and depositional controls from near-surface 3-D seismic data, Niger Delta continental slope. *AAPG Bulletin* 89(5), 627-643.

Ambraseys, N.N., 1988. Engineering Seismology. *Earthquake engineering and structural dynamics* 17, 1-105.

Armentrout, J.M., Kanschat, K.A., Meisling, K.E., Tsakma, J.J., Antrim, L. and McConnell, D.R., 2000. Neogene turbidite systems of the Gulf of Guinea continental margin slope, offshore Nigeria. In: Bouma, A.H. and Stone, C.G. (Eds.), *Fine-Grained Turbidite Systems*. AAPG Memoir 72/SEPM Special Publication No. 68, Tulsa, pp. 93-108.

Babonneau, N., Savoye, B., Cremer, M. and Klein, B., 2002. Morphology and architecture of the present canyon and channel system of the Zaire deep-sea fan. *Marine and Petroleum Geology* 19(4), 445-467.

Babonneau, N., Savoye, B., Cremer, M. and Bez, M., 2004. Multiple terraces within the deep incised Zaire Valley (ZaïAngo Project): are they confined levees? In: Lomas, S.A. and Joseph, P. (Eds.), *Confined Turbidite Systems*. Geological Society, London, Special Publications, 222, pp. 91-114.

Bacon, M., Simm, R. and Redshaw, T., 2003. *3-D seismic interpretation*. Cambridge University Press, 212 pp.

Beaubouef, R.T., Rossen, C., Zelt, F.B., Sullivan, M.D., Mohrig, D.C. and Jennette, D.C., 1999. *Deep-water sandstones, Brushy Canyon Formation, West Texas*. Field guide for AAPG Hedberg field research conference. AAPG Continuing Education Course Note Series No. 40.

Bellian, J.A., Kerans, C. and Jennette, D.C., 2005. Digital Outcrop Models: Applications of Terrestrial Scanning Lidar Technology in Stratigraphic Modeling. *Journal of Sedimentary Research* 75(2), 166-176.

Berger, M. and Roberts, A.M., 1999. The Zeta Structure; a footwall degradation complex formed by gravity sliding on the western margin of the Tampen Spur, northern North Sea. In: Fleet, A.J. and Boldy, S.A.R. (Eds.), *Petroleum geology of Northwest Europe; proceedings of the 5th conference held at the Barbican Centre, London, 26-29 October 1997*. The Geological Society of London, London, United Kingdom, pp. 106-116.

Bouma, A.H., 2004. Key controls on the characteristics of turbidite systems. In: Lomas, S.A. and Joseph, P. (Eds.), *Confined turbidite systems*. Geological Society, London, Special Publications, 222, pp. 9-22.

Bourgeois, A., Joseph, P. and Lecomte, J.C., 2004. Three-dimensional full wave seismic modelling versus one-dimensional convolution: the seismic appearance of the Grés d'Annot turbidite system. In: Joseph, P. and Lomas, S.A. (Eds.), *Deep-Water Sedimentation in the Alpine Basin of SE France: New perspective on the Grés d'Annot and related systems*. Geological Society, London, Special Publications, 221, pp. 401-417.

Brown, A.R., 1999. *Interpretation of Three-Dimensional Seismic Data*. AAPG Memoir 42, 5th edition, 510 pp.

Brown, R.J. and Branney, M.J., 2004. Bypassing and diachronous deposition from density currents: Evidence from a giant regressive bed form in the Poris ignimbrite, Tenerife, Canary Islands. *Geology* 32(5), 445-448.

Burbank, D.W. and Raynolds, G.H., 1988. Stratigraphic Keys to the Timing of Thrusting in Terrestrial Foreland Basins: Applications to the Northwestern Himalaya. In: Kleinspehn, K.L. and Paola, C. (Eds.), *New Perspectives in Basin Analysis*. Springer-Verlag, New York, pp. 331-351.

Burbank, D.W., Meigs, A. and Brozovic, N., 1996. Interactions of growing folds and coeval depositional systems. *Basin Research* 8, 199-223.

Burbank, D.W. and Anderson, R.S., 2001. *Tectonic Geomorphology*. Blackwell Science Ltd., 274 pp.

Bursik, M.I. and Woods, A.W., 2000. The effects of topography on sedimentation from particle-laden turbulent density currents. *Journal of Sedimentary Research* 70(1), 53-63.

Campion, K.M., Sprague, A.R., Mohrig, D.C., Lovell, R.W., Drzewiecki, P.A., Sullivan, M.D., Ardill, J.A., Jensen, G.N. and Sickafoose, D.K., 2000. Outcrop expression of confined channel complexes. In: Weimer, P., Slatt, R.M., Coleman, J., Rossen, N.C., Nelson, H., Bouma, A.H. and Styzen, M.J. (Eds.), *Deep-water reservoirs of the world*. GCSSEPM Foundation 20th Annual Research Conference, pp. 127-151.

Campion, K.M., Sprague, A.R. and Sullivan, M.D., 2005. *Architecture and Lithofacies of the Capistrano Formation (Miocene-Pliocene), San Clemente, California*. Fieldtrip Guidebook Prepared for the Pacific Section SEPM Annual Fall Fieldtrip, San Clemente, California. The Pacific Section SEPM, 42 pp.

Canals, M., Lastras, G., Urgeles, R., Casamor, J.L., Mienert, J., Cattaneo, A., De Batist, M., Haflidason, H., Imbo, Y. and Laberg, J.S., 2004. Slope failure dynamics and impacts from seafloor and shallow sub-seafloor geophysical data: case studies from the COSTA project. *Marine Geology* 213(1-4), 9-72.

Cartwright, J., 1989. The kinematics of inversion in the Danish Central Graben. In: Cooper, M.A. and Williams, G.D. (Eds.), *Inversion Tectonics*. Geological Society Special Publications No. 44, pp. 153-175.

Chang, H.K., Kowsmann, R.O., Figueiredo, A.M.F. and Bender, A.A., 1992. Tectonics and stratigraphy of the East Brazil Rift system: an overview. *Tectonophysics* 213(1-2), 97-138.

Clark, J.D. and Pickering, K.T., 1996. Architectural elements and growth patterns of submarine channels; application to hydrocarbon exploration. *AAPG Bulletin* 80(2), 194-221.

Cohen, H.A. and McClay, K., 1996. Sedimentation and shale tectonics of the northwestern Niger Delta front. *Marine and Petroleum Geology* 13(3), 313-328.

Coleman, J.L.J., Sheppard, F.C. and Jones, T.K., 2000. Seismic resolution of submarine channel architecture as indicated by outcrop analogs. In: Bouma, A.H. and Stone, C.G. (Eds.), *Fine-grained turbidite systems*. AAPG Memoir 72/SEPM Special Publication 68, pp. 119-126.

Corredor, F., Shaw, J.H. and Bilotti, F., 2005. Structural styles in the deep-water fold and thrust belts of the Niger Delta. *AAPG Bulletin* 89(6), 753-780.

Cramez, C. and Jackson, M.P.A., 2000. Superposed deformation straddling the continental-oceanic transition in deep-water Angola. *Marine and Petroleum Geology* 17(10), 1095-1109.

Cronin, B.T., Hurst, A., Celik, H. and Turkmen, I., 2000. Superb exposure of a channel, levee and overbank complex in an ancient deep-water slope environment. *Sedimentary Geology* 132(3-4), 205-216.

Damuth, J.E., 1994. Neogene gravity tectonics and depositional processes on the deep Niger Delta continental margin. *Marine and Petroleum Geology* 11(3), 320-346.

Davies, R.J., 2003. Kilometer-scale fluidization structures formed during early burial of a deep-water slope channel on the Niger Delta. *Geology (Boulder)* 31(11), 949-952.

Demyttenaere, R., Tromp, J.P., Ibrahim, A., Allman-Ward, P. and Meckel, T., 2000. Brunei deep water exploration: from sea floor images and shallow seismic analogues to depositional models in a slope turbidite setting. In: Weimer, P., Slatt, R.M., Coleman, J., Rossen, N.C., Nelson, H., Bouma, A.H. and Styzen, M.J. (Eds.), *Deep-Water Reservoirs of the World*. GCSSEPM 20th Annual Research Conference, pp. 304-317.

Deptuck, M.E., Steffens, G.S., Barton, M. and Pirmez, C., 2003. Architecture and evolution of upper fan channel-belts on the Niger Delta slope and in the Arabian Sea. *Marine and Petroleum Geology* 20(6-8), 649-676.

Deramond, J., Souquet, P., Fondecave-Wallez, M.-J. and Specht, M., 1993. Relationships between thrust tectonics and sequence stratigraphy surfaces in foredeeps: model and examples from the Pyrenees (Cretaceous-Eocene, France, Spain). In: Williams, D.G.

and Dobb, A. (Eds.), *Tectonics and Seismic Sequence Stratigraphy*. Geological Society Special Publication No. 71, pp. 193-219.

Doust, H. and Omatsola, E., 1990. Niger Delta. In: Edwards, J.D. and Santogrossi, P.A. (Eds.), *Divergent/passive margin basins*. AAPG Memoir. American Association of Petroleum Geologists, Tulsa, OK, United States, pp. 201-238.

Droz, L., Rigaut, F., Cochonat, P. and Tofani, R., 1996. Morphology and Recent evolution of the Zaire turbidite system (Gulf of Guinea). *Geological Society of America Bulletin* 108(3), 253-269.

Droz, L., Marsset, T., Ondreas, H., Lopez, M., Savoye, B. and Spy, A.F.L., 2003. Architecture of an active mud-rich turbidite system; the Zaire Fan (Congo-Angola margin Southeast Atlantic); results from ZaiAngo 1 and 2 cruises. *AAPG Bulletin* 87(7), 1145-1168.

Edwards, R.A., Whitmarsh, R.B. and Scrutton, R.A., 1997. Synthesis of the crustal structure of the transform continental margin off Ghana, northern Gulf of Guinea. *Geo-Marine Letters* 17, 12-20.

Ercilla, G., Wynn, R.B., Alonso, B. and Baraza, J., 2002. Initiation and evolution of turbidity current sediment waves in the Magdalena turbidite system. *Marine Geology* 192(1-3), 153-169.

Eschard, R., 2001. Geological factors controlling sediment transport from platform to deep basin: a review. *Marine and Petroleum Geology* 18(4), 487-490.

Estrada, F., Ercilla, G. and Alonso, B., 2005. Quantitative study of a Magdalena submarine channel (Caribbean Sea): implications for sedimentary dynamics. *Marine and Petroleum Geology* 22(5), 623-635.

Fagherazzi, S. and Sun, T., 2003. Numerical simulations of transportational cyclic steps. *Computers & Geosciences* 29(9), 1143-1154.

Fiduk, J.C., Brush, E.R., Anderson, L.E., Gibbs, P.B. and Rowan, M.G., 2004. Salt deformation, magmatism, and hydrocarbon prospectivity in the Espirito Santo Basin, offshore Brazil. In: Post, P.J., Olson, D.L., Lyons, K.T., Palmes, S.L., Harison, P.F. and Rosen, N.C. (Eds.), *Salt-sediment interactions and hydrocarbon prospectivity: Concepts, applications, and case studies for the 21st century*. GCSSEPM 24th Annual Research Conference, pp. 370-392.

Fildani, A., Normark, W.R., Kostic, S. and Parker, G., 2006. Channel formation by flow stripping: large-scale scour features along the Monterey East Channel and their relation to sediment waves. *Sedimentology* 53(6), 1265-1287.

Flood, R.D., 1988. A lee wave model for deep-sea mudwave activity. *Deep Sea Research Part A. Oceanographic Research Papers* 35(6), 973-983.

Fonnesu, F., 2003. 3D seismic images of a low-sinuosity slope channel and related depositional lobe (West Africa deep-offshore). *Marine and Petroleum Geology* 20(6-8), 615-629.

Frey Martinez, J., Cartwright, J. and Hall, B., 2005. 3D seismic interpretation of slump complexes: examples from the continental margin of israel. *Basin Research* 71(1), 83-108.

Galloway, W.E., 1998. Siliciclastic slope and base-of-slope depositional systems; component facies, stratigraphic architecture, and classification. *AAPG Bulletin* 82(4), 569-595.

Garcia, M. and Parker, G., 1989. Experiments on hydraulic jumps in turbidity currents near a canyon-fan transition. *Science* 245(4916), 393-396.

Gardner, M.H. and Borer, J.M., 2000. Submarine channel architecture along a slope to basin profile, Brushy Canyon Formation, west Texas. In: Bouma, A.H. and Stone, C.G. (Eds.), *Fine-grained turbidite systems*. AAPG Memoir 72/SEPM Special Publication 68, pp. 195-214.

Gardner, M.H., Borer, J.M., Melick, J.J., Mavilla, N., Dechesne, M. and Wagerle, R.N., 2003. Stratigraphic process-response model for submarine channels and related features from studies of Permian Brushy Canyon outcrops, West Texas. *Marine and Petroleum Geology* 20(6-8), 757-787.

Gardner, T.W., 1983. Experimental study of knickpoint and longitudinal profile evolution in cohesive, homogeneous material. *Geological Society of America Bulletin* 94(5), 664-672.

Gay, A., Lopez, M., Cochonat, P., Sultan, N., Cauquil, E. and Brigaud, F., 2003. Sinuous pockmark belt as indicator of a shallow buried turbiditic channel on the lower slope of the Congo basin, West African margin. In: Van Ransbergen, P., Hillis, R.R., Maltman, A.J. and Morley, C.K. (Eds.), *Subsurface Sediment Mobilization*. Geological Society, London, Special Publications, pp. 173-189.

Gee, M.J.R. and Gawthorpe, R.L., 2006. Submarine channels controlled by salt tectonics: Examples from 3D seismic data offshore Angola. *Marine and Petroleum Geology* 23(4), 443-458.

Grando, G. and McClay, K., 2004. Structural evolution of the Frampton growth fold system, Atwater Valley-Southern Green Canyon area, deep water Gulf of Mexico. *Marine and Petroleum Geology* 21(7), 889-910.

Haack, R.C., Sundararaman, P., Diedjomahor, J.O., Xiao, H., Gant, N.J., May, E.D. and Kelsch, K., 2000. Niger Delta petroleum systems, Nigeria. In: Mello, M.R. and Katz, B.J. (Eds.), *Petroleum Systems of South Atlantic Margins*. AAPG Memoir 73, pp. 213-231.

Hampton, M.A., Lee, H.J. and Locat, J., 1996. Submarine landslides. *Reviews of Geophysics* 34(1), 33-59.

Hardy, S. and Poblet, J., 1995. The velocity description of deformation; Paper 2, Sediment geometries associated with fault-bend and fault-propagation folds. *Marine and Petroleum Geology* 12(2), 165-176.

Hart, B.S., 1999. Definition of subsurface stratigraphy, structure and rock properties from 3-D seismic data. *Earth-Science Reviews* 47(3-4), 189-218.

Haughton, P.D.W., 2000. Evolving turbidite systems on a deforming basin floor, Tabernas, SE Spain. *Sedimentology* 47(3), 497-518.

Heezen, B.C. and Ewing, M., 1955. Orleansville earthquake and turbidity currents. *AAPG Bulletin* 39(12), 2505-2514.

Heiniö, P. and Davies, R.J., 2006. Degradation of compressional fold belts: Deep-water Niger Delta. *AAPG Bulletin* 90(5), 753-770.

Hesthammer, J. and Fossen, H., 1999. Evolution and geometries of gravitational collapse structures with examples from the Statfjord Field, northern North Sea. *Marine and Petroleum Geology* 16(3), 259-281.

Hills, E.S., 1972. Tectonic analysis of folds. In: Hills, E.S. (Ed.), *Elements of Structural Geology*. Chapman and Hall Ltd, London, pp. 261-294.

Hiscott, R.N., 1994. Loss of capacity, not competence, as the fundamental process governing deposition form turbidity currents. *Journal of Sedimentary Research* A64(2), 209-214.

Hooper, R.J., Fitzsimmons, R.J., Grant, N. and Vendeville, B.C., 2002. The role of deformation in controlling depositional patterns in the south-central Niger Delta, West Africa. *Journal of Structural Geology* 24(4), 847-859.

Hovland, M., 2002. The significance of pockmarks to understanding fluid flow processes and geohazards. *Geofluids* 2, 127-136.

Howard, A.D., Dietrich, W.E. and Seidl, M.A., 1994. Modeling fluvial erosion on regional to continental scales. *Journal of Geophysical Research, B, Solid Earth and Planets* 99(7), 13,971-13,986.

Howe, J., 1996. Turbidite and contourite sediment waves in the northern Rockall Trough, North Atlantic Ocean. *Sedimentology* 43(2), 219-234.

Hübscher, C., Spiess, V., Breitzke, M. and Weber, M.E., 1997. The youngest channel-levee system of the Bengal Fan; results from digital sediment echosounder data. *Marine Geology* 141(1-4), 125-145.

Humphrey, N.F. and Konrad, S.K., 2000. River incision or diversion in response to bedrock uplift. *Geology* 28(1), 43-46.

Huyghe, P., Foata, M., Deville, E., Mascle, G. and Caramba Working Group, 2004. Channel profiles through the active thrust front of the southern Barbados prism. *Geology* 32(5), 429-432.

Ingram, G.M., Chisholm, T.J., Grant, C.J., Hedlund, C.A., Stuart-Smith, P. and Teasdale, J., 2004. Deepwater North West Borneo: hydrocarbon accumulation in an active fold and thrust belt. *Marine and Petroleum Geology* 21(7), 879-887.

Jackson, M.P.A., Vendeville, B.C. and Schultz-Ela, D.D., 1994. Structural dynamics of salt systems. *Annual Review Earth Planetary Systems* 22, 93-117.

Kastens, K.A. and Shor, A.N., 1986. Evolution of a channel meander on the Mississippi deep-sea fan. *Marine Geology* 71(1-2), 165-175.

Kearey, P. and Brooks, M., 1991. *An introduction to geophysical exploration.* Blackwell Science, 2nd edition, 254 pp.

Keevil, G.M., Peakall, J., Best, J.L. and Amos, K.J., 2006. Flow structure in sinuous submarine channels: Velocity and turbulence structure of an experimental submarine channel. *Marine Geology* 229(3-4), 241-257.

Khripounoff, A., Vangriesheim, A., Babonneau, N., Crassous, P., Dennielou, B. and Savoye, B., 2003. Direct observation of intense turbidity current activity in the Zaire submarine valley at 4000 m water depth. *Marine Geology* 194(3-4), 151-158.

Kneller, B., 1995. Beyond the turbidite paradigm: physical models for deposition of turbidites and their implications for reservoir prediction. In: Hartley, A.J. and Prosser, D.J. (Eds.), *Characterization of Deep Marine Clastic Systems. Geological Society Special Publication No 94.* pp. 31-49.

Kneller, B. and Buckee, C., 2000. The structure and fluid mechanics of turbidity currents: a review of some recent studies and their geological implications. *Sedimentology* 47(s1), 62-94.

Kneller, B., 2003. The influence of flow parameters on turbidite slope channel architecture. *Marine and Petroleum Geology* 20(6-8), 901-910.

Kneller, B.C. and McCaffrey, W.D., 2003. The Interpretation of Vertical Sequences in Turbidite Beds: The Influence of Longitudinal Flow Structure. *Journal of Sedimentary Research* 73(5), 706-713.

Knox, G.J. and Omatsola, E., M, 1989. Development of the Cenozoic Niger Delta in terms of the 'Escalator Regression' model and impact on hydrocarbon distribution. *Proceedings KNGMG Symposium 'Coastal Lowlands, Geology and Geotechnology'*, 181-202.

Kolla, V., Eittreim, S., Sullivan, L., Kostecki, J.A. and Burckle, L.H., 1980. Current-controlled, abyssal microtopography and sedimentation in Mozambique Basin, southwest Indian Ocean. *Marine Geology* 34(3-4), 171-206.

Kolla, V., Bourges, P., Urruty, J.M. and Safa, P., 2001. Evolution of deep-water Tertiary sinuous channels offshore Angola (West Africa) and implications for reservoir architecture. *AAPG Bulletin* 85(8), 1373-1405.

Komar, P.D., 1969. The channelized flow of turbidity currents with application to Monterey deep-sea fan channel. *Journal of Geophysical Research* 74(18), 4544-4558.

Komar, P.D., 1971. Hydraulic jumps in turbidity currents. *GSA Bulletin* 82(6), 1477-1487.

Krause, D.C., White, W.C., Piper, D.J.W. and Heezen, B.C., 1970. Turbidity currents and cable breaks in the western New Britain trench. *GSA Bulletin* 81(7), 2153-2160.

Kubo, Y. and Nakajima, T., 2002. Laboratory experiments and numerical simulation of sediment-wave formation by turbidity currents. *Marine Geology* 192(1-3), 105-121.

Kukowski, N., Schillhorn, T., Huhn, K., von Rad, U., Husen, S. and Flueh, E.R., 2001. Morphotectonics and mechanics of the central Makran accretionary wedge off Pakistan. *Marine Geology* 173(1-4), 1-19.

Lastras, G., Canals, M., Urgeles, R., Hughes-Clarke, J.E. and Acosta, J., 2004. Shallow slides and pockmark swarms in the Eivissa Channel, western Mediterranean Sea. *Sedimentology* 51, 837-850.

Lee, S.E., Talling, P.J., Ernst, G.G.J. and Hogg, A.J., 2002. Occurrence and origin of submarine plunge pools at the base of the US continental slope. *Marine Geology* 185(3-4), 363-377.

Leeder, M., 1999. *Sedimentology and sedimentary basins. From turbulence to tectonics.* Blackwell Science Ltd, 592 pp.

Lien, T., Walker, R.G. and Martinsen, O.J., 2003. Turbidites in the Upper Carboniferous Ross Formation, western Ireland: reconstruction of a channel and spillover system. *Sedimentology* 50(1), 113-148.

Locat, J., 2001. Instabilities along ocean margins: a geomorphological and geotechnical perspective. *Marine and Petroleum Geology* 18(4), 503-512.

Locat, J. and Lee, H.J., 2002. Submarine landslides: advances and challenges. *Canadian Geotechnical Journal* 39, 193-212.

Lopez, M., 2001. Architecture and depositional pattern of the Quaternary deep-sea fan of the Amazon. *Marine and Petroleum Geology* 18(4), 479-486.

Marr, J.G., Elverhoi, A., Harbitz, C., Imran, J. and Harff, P., 2002. Numerical simulation of mud-rich subaqueous debris flows on the glacially active margins of the Svalbard-Barents Sea. *Marine Geology* 188(3-4), 351-364.

Masson, D.G., Kenyon, N.H., Gardner, J.V. and Field, M.E., 1995. Monterey Fan: channel and overbank morphology. In: Pickering, K.T., Hiscott, R.N., Kenyon, N.H., Ricci Lucchi, F.R. and Smith, R.D.A. (Eds.), *Atlas of deep water environments - Architectural style in turbidite systems*. Chapman & Hall, pp. 74-79.

Mayall, M. and Stewart, I., 2000. The Architecture of Turbidite Slope Channels. *GCSSEPM Foundation 20th Annual Research Conference Deep-Water Reservoirs of the World, December 3-6, 2000, p. 578-86.*

Mayall, M., Jones, E. and Casey, M., 2006. Turbidite channel reservoirs - Key elements in facies prediction and effective development. *Marine and Petroleum Geology* 23(8), 821-841.

McCaffrey, W. and Kneller, B., 2001. Process Controls on the Development of Stratigraphic Trap Potential on the Margins of Confined Turbidite Systems and Aids to Reservoir Evaluation. *AAPG Bulletin* 85(6), 971-988.

McClay, K., Dooley, T., Ferguson, A. and Poblet, J., 2000. Tectonic Evolution of the Sanga Sanga Block, Mahakam Delta, Kalimantan, Indonesia. *AAPG Bulletin* 84(6), 765-786.

McHargue, T.R. and Webb, J.E., 1986. Internal geometry, seismic facies, and petroleum potential of canyons and inner fan channels of the Indus submarine fan. *AAPG Bulletin* 70(2), 161-180.

McHugh, C.M.G. and Ryan, W.B.F., 2000. Sedimentary features associated with channel overbank flow; examples from the Monterey Fan. *Marine Geology* 163(1-4), 199-215.

McLeod, A.E. and Underhill, J.R., 1999. Processes and products of footwall degradation, northern Brent Field, northern North Sea. In: Fleet, A.J. and Boldy, S.A.R. (Eds.), *Petroleum geology of Northwest Europe; proceedings of the 5th conference held at the Barbican Centre, London, 26-29 October 1997.* The Geological Society of London, London, United Kingdom, pp. 91-106.

Mello, U.T. and Pratson, L.F., 1999. Regional slope stability and slope-failure mechanics from the two-dimensional state of stress in an infinite slope. *Marine Geology* 154(1-4), 339-356.

Menard, H.W., 1955. Deep-sea channels, topography, and sedimentation. *AAPG Bulletin* 39(2), 236-255.

Middleton, G.V., 1993. Sediment deposition from turbidity currents. *Annual Review Earth Planetary Systems* 21, 89-114.

Migeon, S., Savoye, B., Zanella, E., Mulder, T., Faugeres, J.C. and Weber, O., 2001. Detailed seismic-reflection and sedimentary study of turbidite sediment waves on the Var Sedimentary Ridge (SE France): significance for sediment transport and deposition and for the mechanisms of sediment-wave construction. *Marine and Petroleum Geology* 18(2), 179-208.

Mitchell, N.C., 2004. Form of submarine erosion from confluences in Atlantic USA continental slope canyons. *American Journal of Science* 304, 590-611.

Mitchell, N.C., 2006. Morphologies of knickpoints in submarine canyons. *Geological Society of America Bulletin* 118(5-6), 589-605.

Mitchum, R.M., Jr., Vail, P.R. and Sangree, J.B., 1977. Seismic stratigraphy and global changes of sea level, part 6: Stratigraphic interpretation of seismic reflection patterns in depositional sequences. In: Payton, C.E. (Ed.), *Seismic stratigraphy - applications to hydrocarbon exploration. AAPG Memoir 26*. Tulsa, Ok, pp. 117-133.

Mohrig, D., Elverhoi, A. and Parker, G., 1999. Experiments on the relative mobility of muddy subaqueous and subaerial debris flows, and their capacity to remobilize antecedent deposits. *Marine Geology* 154(1-4), 117-129.

Mohrig, D. and Marr, J.G., 2003. Constraining the efficiency of turbidity current generation from submarine debris flows and slides using laboratory experiments. *Marine and Petroleum Geology* 20(6-8), 883-899.

Moraes, M.A.S., Blaskovski, P.R. and Joseph, P., 2004. The Grés d'Annot as an analogue for Brazilian Cretaceous sandstone reservoirs: comparing convergent to passive-margin confined turbidites. In: Joseph, P. and Lomas, S.A. (Eds.), *Deep-Water Sedimentation in the Alpine Basin of SE France: New perspective on the Grés d'Annot and related systems*. Geological Society, Geological Society, London, Special Publications, pp. 419-436.

Morgan, R., 2003. Prospectivity in ultradeep water: the case for petroleum generation and migration within the outer parts of the Niger Delta apron. In: Arthur, T.J., MacGregor, D.S. and Cameron, N.R. (Eds.), *Petroleum Geology of Africa: New themes and Developing technologies*. Geological society, London, Special Publications, pp. 151-164.

Morgan, R., 2004. Structural controls on the positioning of submarine channels on the lower slopes of the Niger Delta. In: Davies, R.J., Cartwright, J.A., Stewart, S.A., Lappin, M. and Underhill, J.R. (Eds.), *3D Seismic Technology: Application to the Exploration of Sedimentary Basins*. Geological Society, London, Memoirs, 29, pp. 45-51.

Morisawa, M., 1985. River morphology: channel pattern, *Rivers*. Longman Group Limited, pp. 222.

Mulder, T. and Cochonat, P., 1996. Classification of offshore mass movements. *Journal of Sedimentary Research* 66(1), 43-57.

Mulder, T., Savoye, B. and Syvitski, J.P.M., 1997. Numerical modelling of a mid-sized gravity flow: the 1979 Nice turbidity current (dynamics, processes, sediment budget and seafloor impact). *Sedimentology* 44(2), 305-326.

Mulder, T. and Alexander, J., 2001. The physical character of subaqueous sedimentary density flows and their deposits. *Sedimentology* 48(2), 269-299.

Nakajima, T. and Satoh, M., 2001. The formation of large mudwaves by turbidity currents on the levees of the Toyama deep-sea channel, Japan Sea. *Sedimentology* 48(2), 435-463.

Nemec, W., 1990. Aspects of sediment movement on steep delta slopes. In: Colella, A. and Prior, D.B. (Eds.), *Coarse-grained Deltas*. Special Publication of the International Association of Sedimentologists, 10, Blackwell, Oxford, pp. 29-73.

Nigro, F. and Renda, P., 2004. Growth pattern of underlithified strata during thrust-related folding. *Journal of Structural Geology* 26(10), 1913-1930.

Normark, W.R., Hess, G.R., Stow, D.A.V. and Bowen, A.J., 1980. Sediment waves on the monterey fan levee: A preliminary physical interpretation. *Marine Geology* 37(1-2), 1-18.

Normark, W.R., Posamentier, H.W. and Mutti, E., 1993. Turbidite systems: State of the art and future directions. *Reviews of Geophysics* 31(2), 91-116.

Ojeda, H.A.O., 1982. Structural framework, stratigraphy, and evolution of Brazilian marginal basins. *AAPG Bulletin* 66(6), 732-749.

Ouchi, S., 1985. Response of alluvial rivers to slow active tectonic movement. *Geological Society of America Bulletin* 96(4), 504-515.

Parker, G., Fukushima, Y. and Pantin, H.M., 1986. Self-accelerating turbidity currents. *Journal of Fluid Mechanics* 171, 145-181.

Peakall, J., McCaffrey, W.D., Kneller, B.C., Stelting, C.E., McHargue, T.R. and Schweller, W.J., 2000a. A process model for the evolution of submarine fan channels; implications for sedimentary architecture. In: Bouma, A.H. and Stone, C.G. (Eds.), *Fine-grained turbidite systems.* American Association of Petroleum Geologists. Tulsa, OK, United States. 2000.

Peakall, J., McCaffrey, B. and Kneller, B., 2000b. A process model for the evolution, morphology, and architecture of sinuous submarine channels. *Journal of Sedimentary Research* 70(3), 434-448.

Pickering, K.T., Hodgson, D.M., Platzman, E., Clark, J.D. and Stephens, C., 2001. A New Type of Bedform Produced by Backfilling Processes in a Submarine Channel, Late Miocene, Tabernas-Sorbas Basin, SE Spain. *Journal of Sedimentary Research* 71(5), 692-704.

Pirmez, C., Beaubouef, R.T., Friedmann, S.J. and Mohrig, D., 2000. Equilibrium profile and baselevel in submarine channels: examples from late pleistocene systems and implications for the architecture of deepwater reservoirs. In: Weimer, P., Slatt, R.M., Coleman, J., Rossen, N.C., Nelson, H., Bouma, A.H. and Styzen, M.J. (Eds.), *Deep-Water Reservoirs of the World.* GCSSEPM Foundation 20th Annual Research Conference, pp. 782-805.

Popescu, I., Lericolais, G., Panin, N., Wong, H.K. and Droz, L., 2001. Late Quaternary channel avulsions on the Danube deep-sea fan, Black Sea. *Marine Geology* 179(1-2), 25-37.

Popescu, I., Lericolais, G., Panin, N., Normand, A., Dinu, C. and Le Drezen, E., 2004. The Danube submarine canyon (Black Sea): morphology and sedimentary processes. *Marine Geology* 206(1-4), 249-265.

Posamentier, H.W. and Kolla, V., 2003. Seismic geomorphology and stratigraphy of depositional elements in deep-water settings. *Journal of Sedimentary Research* 73(3), 367-388.

Posamentier, H.W., 2003. Depositional elements associated with a basin floor channel-levee system: case study from the Gulf of Mexico. *Marine and Petroleum Geology* 20(6-8), 677-690.

Prather, B.E., 2003. Controls on reservoir distribution, architecture and stratigraphic trapping in slope settings. *Marine and Petroleum Geology* 20(6-8), 529-545.

Pratson, L.E., Imran, J., Parker, G., Syvitski, J.P.M. and Hutton, E., 2000. Debris flows vs. turbidity currents; a modeling comparison of their dynamics and deposits. In: Bouma, A.H. and Stone, C.G. (Eds.), *Fine-grained turbidite systems.* American Association of Petroleum Geologists. Tulsa, OK, United States. 2000.

Pratson, L.F. and Coakley, B.J., 1996. A model for the headward erosion of submarine canyons induced by downslope-eroding sediment flows. *Geological Society of America Bulletin* 108(2), 225-234.

Prior, D.B. and Coleman, J.M., 1982. Active slides and flows in underconsolidated marine sediments on the slopes of the Mississippi delta. In: Saxov, S. and Nieuwenhuis, J.K. (Eds.), *Marine slides and other mass movements*. Plenum Press, New York, pp. 21-49.

Prior, D.B., Bornhold, B.D. and Johns, M.W., 1984. Depositional characteristics of a submarine debris flow. *Journal of Geology* 92(6), 707-727.

Rafini, S. and Mercier, E., 2002. Forward modelling of foreland basins progressive unconformities. *Sedimentary Geology* 146(1-2), 75-89.

Rasmussen, E.S., 1994. The relationship between submarine canyon fill and sea-level change: an example from Middle Miocene offshore Gabon, West Africa. *Sedimentary Geology* 90, 61-75.

Reading, H.G. and Richards, M., 1994. Turbidite systems in deep-water basin margins classified by grain size and feeder system. *AAPG Bulletin* 78(5), 792-822.

Richards, M., Bowman, M. and Reading, H., 1998. Submarine-fan systems; I, Characterization and stratigraphic prediction. *Marine and Petroleum Geology* 15(7), 689-717.

Saller, A.H., Noah, J.T., Ruzuar, A.P. and Schneider, R., 2004. Linked lowstand delta to basin-floor fan deposition, offshore Indonesia: An analog for deep-water reservoir systems. *AAPG Bulletin* 88(1), 21-46.

Samuel, A., Kneller, B., Raslan, S., Sharp, A. and Parsons, C., 2003. Prolific deep-marine slope channels of the Nile Delta, Egypt. *AAPG Bulletin* 87(4), 541-560.

Sangree, J.B. and Widmier, J.M., 1977. Seismic stratigraphy and global changes of sea level, part 9: Seismic interpretation of clastic depositional facies, *Seismic stratigraphy - applications to hydrocarbon exploration. AAPG Memoir 26.* pp. 165-184.

Schnellmann, M., Anselmetti, F.S., Giardini, D. and McKenzie, J.A., 2005. Mass movement-induced fold-and-thrust belt structures in unconsolidated sediments in Lake Lucrene (Switzerland). *Sedimentology* 52(2), 271-289.

Sheriff, R.E. and Geldart, L.P., 1995. *Exploration seismology.* Cambridge University Press, Cambridge, 2nd edition, 592 pp.

Smallwood, J.R., 2004. Tertiary inversion in the Faroe-Shetland Channel and the development of major erosional scarps. In: Davies, R.J., Cartwright, J.A., Stewart, S.A., Lappin, M. and Underhill, J.R. (Eds.), *3D Seismic Technology: Application to the Exploration of Sedimentary Basins.* Geological Society, London, Memoirs, 29, pp. 187-198.

Smith, R., 2004. Silled sub-basins to connected tortuous corridors; sediment distribution systems on topographically complex sub-aqueous slopes. In: Lomas, S.A. and Joseph, P. (Eds.), *Confined turbidite systems.* Geological Society, London, Special Publications, 222, pp. 23-43.

Snow, R.S. and Slingerland, R.L., 1990. Stream profile adjustment to crustal warping; nonlinear results from a simple model. *Journal of Geology* 98(5), 699-708.

Soh, W. and Tokuyama, H., 2002. Rejuvenation of submarine canyon associated with ridge subduction, Tenryu Canyon, off Tokai, central Japan. *Marine Geology* 187(1-2), 203-220.

Steidtmann, J.R. and Schmitt, J.G., 1988. Provenance and Dispersal of Tectonic Sediments in Thin-Skinned, Thrusted Terrains. In: Kleinspehn, K.L. and Paola, C. (Eds.), *New Perspectives in Basin Analysis.* Springer-Verlag, New York, pp. 353-366.

Stewart, S.A., 1999. Seismic interpretation of circular geological structures. *Petroleum Geoscience* 5, 273-285.

Stewart, S.A. and Reeds, A., 2003. Geomorphology of kilometer-scale extensional fault scarps; factors that impact seismic interpretation. *AAPG Bulletin* 87(2), 251-272.

Storti, F. and Poblet, J., 1997. Growth stratal architectures associated to decollement folds and fault-propagation folds; inferences on fold kinematics. In: Cloetingh, S., Fernandez, M., Munoz, J.A., Sassi, W. and Horvath, F. (Eds.), *Structural controls on sedimentary basin formation.* Tectonophysics. Elsevier, Amsterdam, Netherlands, pp. 353-373.

Stow, D.A., 1986. Deep Clastic Seas. In: Reading, H.G. (Ed.), *Sedimentary Environments and Facies.* Blackwell Scientific Publications, Oxford, pp. 399-444.

Stow, D.A.V. and Mayall, M., 2000. Deep-water sedimentary systems; new models for the 21st century. In: Stow, D.A.V. and Mayall, M. (Eds.), *Deep-water sedimentary systems; new models for the 21st century.* Pergamon. Oxford, International. 2000.

Sultan, N., Cochonat, P., Cayocca, F., Bourillet, J.F. and Colliat, J.L., 2004. Analysis of submarine slumping in the Gabon continental slope. *AAPG Bulletin* 88(6), 781-799.

Sun, T. and Parker, G., 2005. Transportational cyclic steps created by flow over an erodible bed. Part 2. Theory and numerical simulation. *Journal of Hydraulic Research* 43(5), 502-514.

Taki, K. and Parker, G., 2005. Transportational cyclic steps created by flow over an erodible bed. Part 1. Experiments. *Journal of Hydraulic Research* 43(5), 488-501.

Torres, J., Droz, L., Savoye, B., Terentieva, E., Cochonat, P., Kenyon, N.H. and Canals, M., 1997. Deep-sea avulsion and morphosedimentary evolution of the Rhone fan valley and neofan during the late Quaternary (north-western Mediterranean Sea). *Sedimentology* 44(3), 457-477.

Underhill, J.R., Sawyer, M.J., Hodgson, P., Shallcross, M.D. and Gawthorpe, R.L., 1997. Implications of fault scarp degradation for Brent Group prospectivity, Ninian Field, northern North Sea. *AAPG Bulletin* 81(6), 999-1022.

Vail, P.R. and Mitchum Jr., R.M., 1977. Seismic stratigraphy and global changes of sea level, part 1: Overview. In: Payton, C.E. (Ed.), *Seismic stratigraphy - applications to hydrocarbon exploration. AAPG Memoir 26.* Tulsa, Ok, pp. 51-62.

Varnes, D.J., 1978. Slope movement types and processes. In: Schuster, R.L. and Krizek, R.J. (Eds.), *Landslides; analysis and control.* Special Report - Transportation Research Board, National Research Council. Transportation Research Board, National Research Council, Washington, DC, United States, pp. 11-33.

Viana, A., Figueiredo, A.G., Faugeres, J.C., Lima, A.F., Gonthier, E., Brehme, I. and Zaragosi, S., 2003. The Sao Tome deep-sea turbidite system (southern Brazil Basin); Cenozoic seismic stratigraphy and sedimentary processes. *AAPG Bulletin* 87(5), 873-894.

von Rad, U. and Tahir, M., 1997. Late Quaternary sedimentation on the outer Indus shelf and slope (Pakistan); evidence from high-resolution seismic data and coring. *Marine Geology* 138(3-4), 193-236.

Whipple, K.X., Parker, G., Paola, C. and Mohrig, D.C., 1998. Channel dynamics, sediment transport and the slope of alluvial fans: experimental study. *Journal of Geology* 106, 677-693.

Winker, C.D. and Booth, J.R., 2000. Sediment Dynamics of the Salt-Dominated Continental Slope, Gulf of Mexico: Integration of Observations from the Seafloor, Near-Surface, and Deep Subsurface. *GCSSEPM Foundation 20th Annual Research Conference Deep-Water Reservoirs of the World, December 3-6, 2000*, 1059-1086.

Wonham, J.P., Jayr, S., Mougamba, R. and Chuilon, P., 2000. 3D sedimentary evolution of a canyon fill (Lower Miocene-age) from the Mandorove Formation, offshore Gabon. *Marine and Petroleum Geology* 17(2), 175-197.

Wynn, R.B., Weaver, P.P.E., Ercilla, G., Stow, D.A.V. and Masson, D.G., 2000a. Sedimentary processes in the Selvage sediment-wave field, NE Atlantic: new insights into the formation of sediment waves by turbidity currents. *Sedimentology* 47(6), 1181-1197.

Wynn, R.B., Masson, D.G., Stow, D.A.V. and Weaver, P.P.E., 2000b. Turbidity current sediment waves on the submarine slopes of the western Canary Islands. *Marine Geology* 163(1-4), 185-198.

Wynn, R.B., Kenyon, N.H., Masson, D.G., Stow, D.A.V. and Weaver, P.P.E., 2002a. Characterization and recognition of deep-water channel-lobe transition zones. *AAPG Bulletin* 86(8), 1441-1462.

Wynn, R.B., Piper, D.J.W. and Gee, M.J.R., 2002b. Generation and migration of coarse-grained sediment waves in turbidity current channels and channel-lobe transition zones. *Marine Geology* 192(1-3), 59-78.

Wynn, R.B. and Stow, D.A.V., 2002. Classification and characterisation of deep-water sediment waves. *Marine Geology* 192(1-3), 7-22.

Yu, B., Cantelli, A., Marr, J., Pirmez, C., O'Byrne, C. and Parker, G., 2006. Experiments on Self-Channelized Subaqueous Fans Emplaced by Turbidity Currents and Dilute Mudflows. *Journal of Sedimentary Research* 76(6), 889-902.

Appendix 1
Glossary

GLOSSARY

H	Height, elevation difference.
2D	Two-dimensional.
3D	Three-dimensional.
Acoustic impedance	Defined by density and seismic velocity ($Z = \rho v$). Changes in acoustic impedance are recorded in seismic data.
Amplitude extraction	Extractions of seismic attribute amplitude from horizons, slices or volumes, which is useful for studying subtle stratigraphic features.
Attribute	A derivate of a seismic measurement, such as time, amplitude, frequency and azimuth.
Avulsion	Lateral shift of the position of a channel by cut-and-fill process.
Azimuth map	Shows the direction in which the horizon is locally dipping.
Backlimb	Shallower limb of a thrust-propagation fold that dips the same direction as the thrust fault.
Bottom current	Currents caused by thermohaline circulation able to erode, transport and deposit sediment on the seafloor.
BSR	Bottom simulating reflection.
Canyon	Deep, often v-shaped valley incised into continental slope, often fed by a river.
Canyon system	A series of stacked canyons that have same source.
Channel	Physical confine of flows, normally with negative topography.
Channel-axis deposit	Deposits on the floor of the channel near its axis.
Channel-belt	The container bordered by basal erosional fairway and outer levees, in which channel-fill deposits and inner levees are deposited.
Channel-fill	Channel-fill elements comprise HARs, passive fill, channel-axis deposits and debris flow and other mass transport deposits that fill channels.
Channel-levee complex	A series of stacked channel-levee systems that are fed by the same canyon.
Channel-levee system	A single channel-belt that is bordered by outer levees.

CLC Channel-levee complex.

CLS Channel-levee system.

Continental margin Area around the continental and oceanic crust boundary including shelf, slope and rise..

Debris flow Viscous sediment-gravity flows that show plastic flow behaviour.

Deepwater water depth of 0.5-1.5 km.

Degradation complex Any type of sediment failure, transport and deposition.

Dipmap, dip magnitude map Shows the local dip of the horizon surface.

Equilibrium profile A profile that sustains little aggradation or degradation along the channel with prevailing sediment discharge.

Erosional fairway Canyon-like incision of a deepwater channel into underlying substrate that can be hundreds of metres deep.

f Frequency.

Forelimb The steep limb of a thrust-propagation fold that is adjacent to the thrust fault.

Frequency Number of peaks passing one point per second.

Frontal fold/thrust The most basinward thrust or fold within a thrust and fold belt.

HAR High-amplitude reflection.

Headwall scarp The scarp that is left in the proximal part of slope failure as sediment is removed.

Hemipelagic sediment Terrigenous sediment transported mainly by wind and surface currents.

Horizon A map produced by interpreting (picking) particular seismic reflection.

Horizontal resolution Defines the area from which a reflection is received called Fresnel zone. Theoretically the Fresnel zone could be reduced to a radius of a quarter of a wavelength.

Hydraulic jump An abrupt transformation from supercritical to subcritical flow condition.

Inner levees Bench-like terraces within the channel-belt with depositional origin.

Isoproportional slicing Technique in which artificial surfaces are created by combining different proportions of two reference horizons.

Knickpoint Steep gradient section between lower gradient sections along a course of a river or channel.

KP Knickpoint.

KPL Knickpoint lip.

L Length, runout distance.

Lee The often shallow or upstream-dipping flank of a sediment wave that faces downcurrent.

Mass transport complex General term that includes slumps, slides and debris flows. Recognised on seismic data by contorted, chaotic low-amplitude reflections.

Migration Channel migration is a gradual shift of the channel by systematic erosion on outer bends and deposition on inner bends.

MTC Mass transport complex.

Outer levees The large, often wedge-shaped in cross section element that border channel-belts and is formed by overbank deposition.

Passive fill Parallel, subhorizontal reflections within channel or channel-belt that show now evidence for channelisation.

Peak Positive amplitude, increase in Z (SEG normal polarity).

Pelagic sediment Sediment composed of planktonic organisms and related organic matter.

Phase/zero phase Describes the motion of periodic waves. Zero phase means that the wavelet is symmetrical, with the central lobe coinciding with the interface.

Pockmark Depressioins formed as a result of catastrophic gas and/or porewater eruption on the seafloor.

Resedimentation All processes driven by gravitational forces that move sediment downslope.

Runout distance The horizontal distance from crest of the scarp to the tip of the deposit. The mobility of submarine landslides is illustrated by the ratio of elevation difference and the runout distance.

Sediment wave	Undulating sedimentary structures found on the seafloor and on levees, characterised by steeper lee flanks and shallower or upstream-dipping stoss flanks.
Sediment-gravity flow	A flow in which the driving force is gravity acting on the sediment particles.
SEG	Society for Exploration Geologists.
SEG normal polarity	Increase in the acoustic impedance downwards is positive amplitude (peak) and decrease negative amplitude (trough).
SEG reverse polarity	Increase in the acoustic impedance downwards is negative amplitude (trough) and decrease positive amplitude (peak).
Seismic amplitude	Amplitude value of a horizon or a volume of seismic data.
Seismic attribute	See 'attribute'.
Seismic velocity	The velocity (v), with which seismic waves travel through rocks.
Seismic wave	Wave of elastic energy that propagate outwards from a seismic source.
Shelf break	The often abrupt change from shallowly-dipping continental shelf to steeper slope environment.
Slice/slicing of data	Seismic data can be sliced along vertical or horizontal lines or along arbitrary traverses and interpreted horizons.
Slide	Shear strain with movement along one or several planar surfaces.
Slope	Continental slope is the steep (commonly 1-10°) slope below shelf break. Slope is also used to describe inclined surfaces.
Slope failure	Any resedimentation process including submarine landslides, slumps, slides, where sediment deposits fail on a slope.
Slump	Rotational, commonly spoon-shaped slide that typically shows extensional faults and scars at the head and compressional structures at the toe area.
Stoss	The often steep flank of a sediment wave that faces upcurrent.
Subcritical flow	Turbidity currents are subcritical, when densimetric Froude number (Fr_d) is less than 1. Subcritical flows are slow and thick.
Supercritical flow	Turbidity currents are supercritical, when densimetric Froude number (Fr_d) is larger than 1. Supercritical flows are swift and thin.

Sweep	Progressive downstream translation of meander bends.
Swing	Increase in amplitude of channel thalweg or a meander bend involving lateral translation.
Terrace	See 'inner levee'. Terraces can also be formed by erosional processes.
Thalweg	Deepest part of the channel.
Traverse	Arbitrary cross-section of seismic data.
Trough	Negative amplitude, decrease in Z (SEG normal polarity).
Tuning	Constructional interference that occurs when layer thickness is one quarter of a wavelength. The amplitude can be boosted as the bed thins.
Turbidity current	Relatively dilute sediment-suspension-driven sediment-gravity flows that occur in subaqueous environment. Commonly used term even when type of flow cannot be determined.
TWT, twtt	Two-way travel time of a seismic wave, measured in s or ms.
Ultra-deepwater	water depth more than 1.5 km.
v	Acoustic/seismic velocity.
Vertical resolution	Defines the potential for the seismic data to distinguish individual layers. Measured in terms of wavelength.
Voxel	The 3D unit of seismic data consisting x, y and z dimensions with individual amplitude values.
Wavelet	Record of changes in acoustic impedances including peaks and troughs that represent increase and decrease in acoustic impedance.
Z	Acoustic impedance.
λ	Wavelength, the distance of two peaks, crest-to-crest distance.
ρ	Density.

ADDITIONAL IMAGES OF THE NIGER DELTA DATASET

The following pages show seismic lines (inlines and crosslines) across the Niger Delta dataset taken in 6.25 km intervals. The inlines (ILN) show how the structural style of the thrusts and folds changes along the thrust and fold belt. The crosslines (CLN) show the seismic character of cross sections of the 3 channel-levee systems (Epe, Ijebu and Iwo CLSs) at different parts of the data. The locations of the lines are shown on the dipmap of the seafloor. The line numbers are indicated at the bottom left corner of each line.

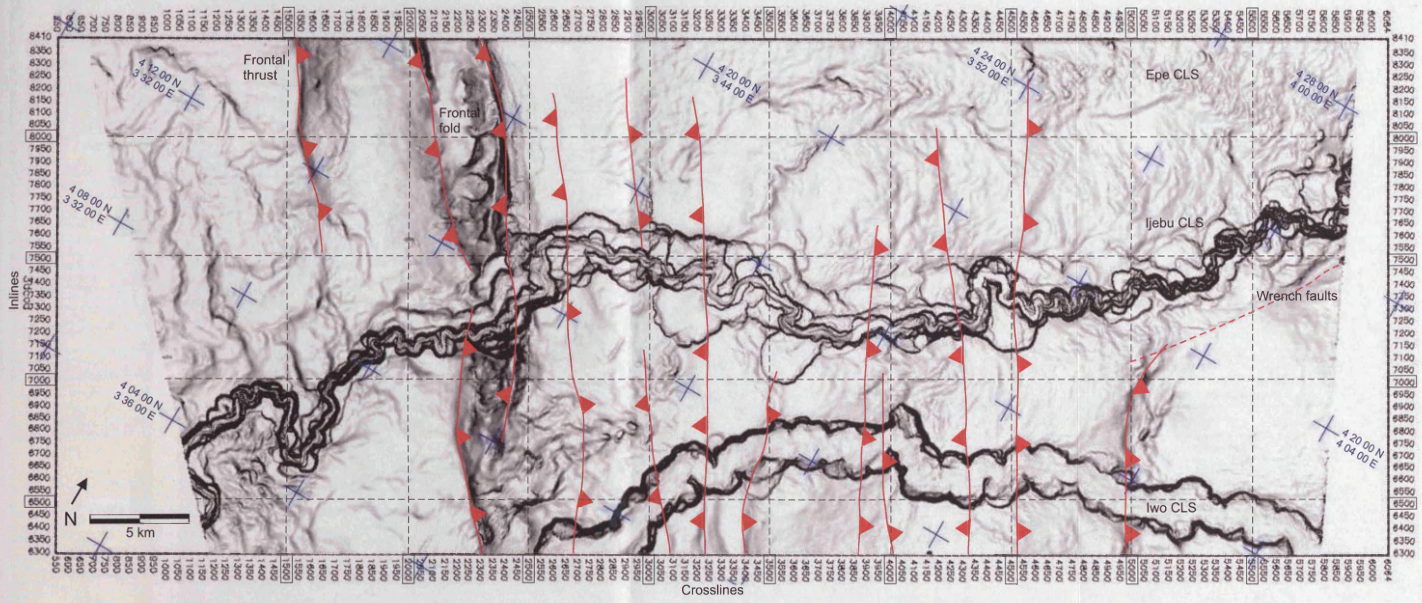

Dipmap of the seafloor of the Niger Delta dataset.

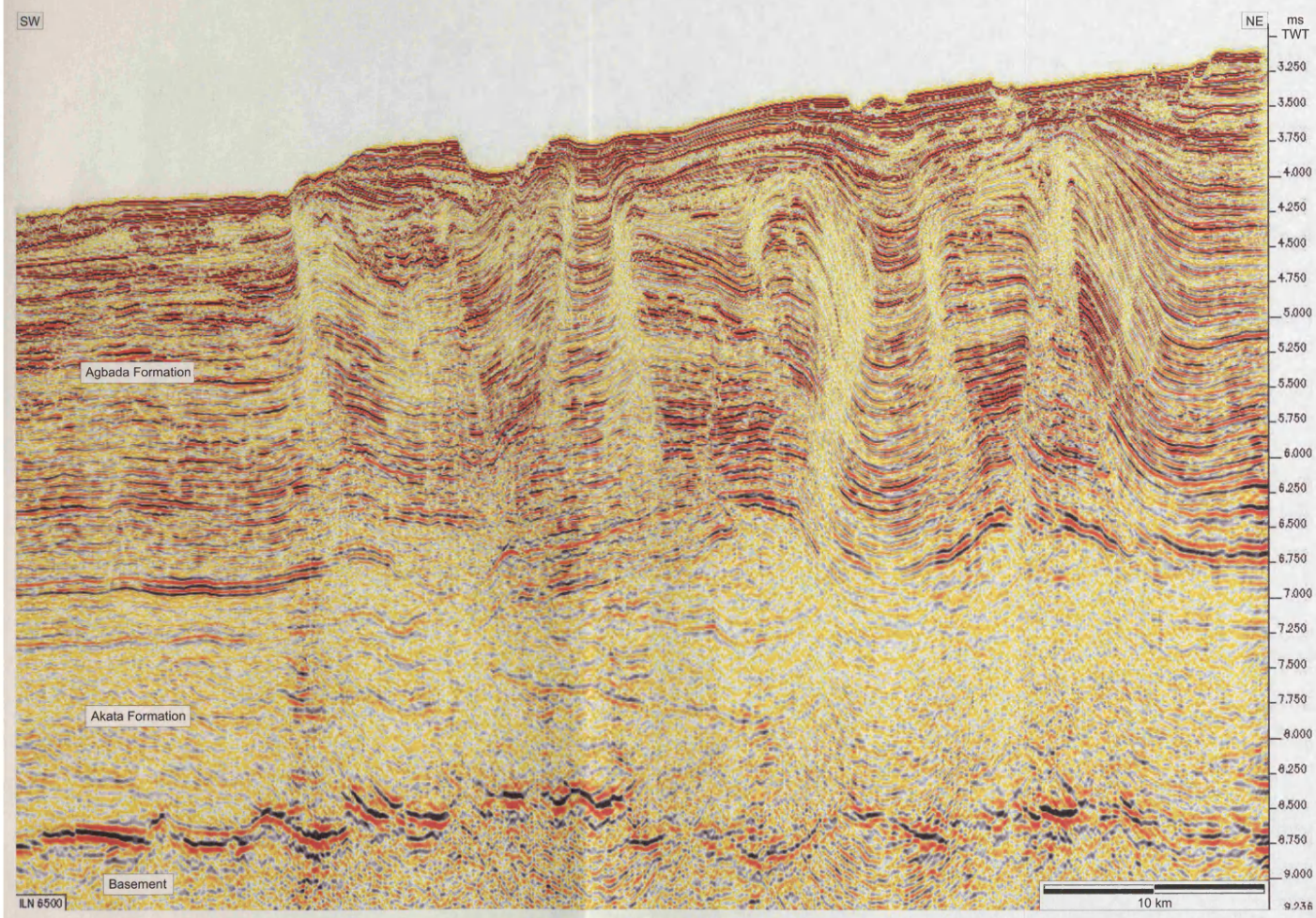
SW
NE
ms
TWT
3.250
3.500
3.750
4.000
4.250
4.500
4.750
5.000
5.250
5.500
5.750
6.000
6.250
6.500
6.750
7.000
7.250
7.500
7.750
8.000
8.250
8.500
8.750
9.000
9.236
Agbada Formation
Akata Formation
Basement
ILN 6500
10 km

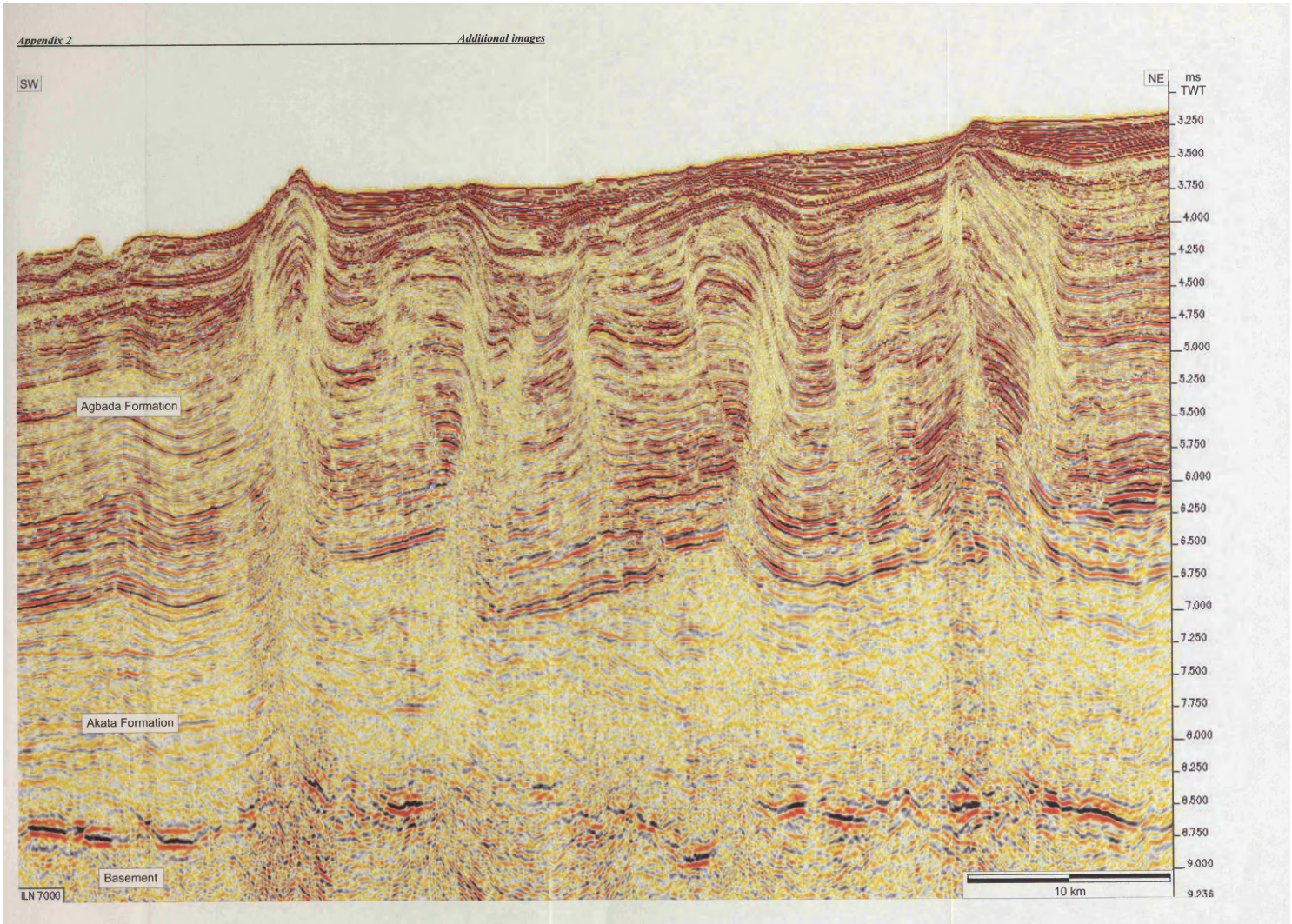
SW
NE
ms
TWT
3.250
3.500
3.750
4.000
4.250
4.500
4.750
5.000
5.250
5.500
5.750
6.000
6.250
6.500
6.750
7.000
7.250
7.500
7.750
8.000
8.250
8.500
8.750
9.000
Agbada Formation
Akata Formation
Basement
ILN 7000
10 km

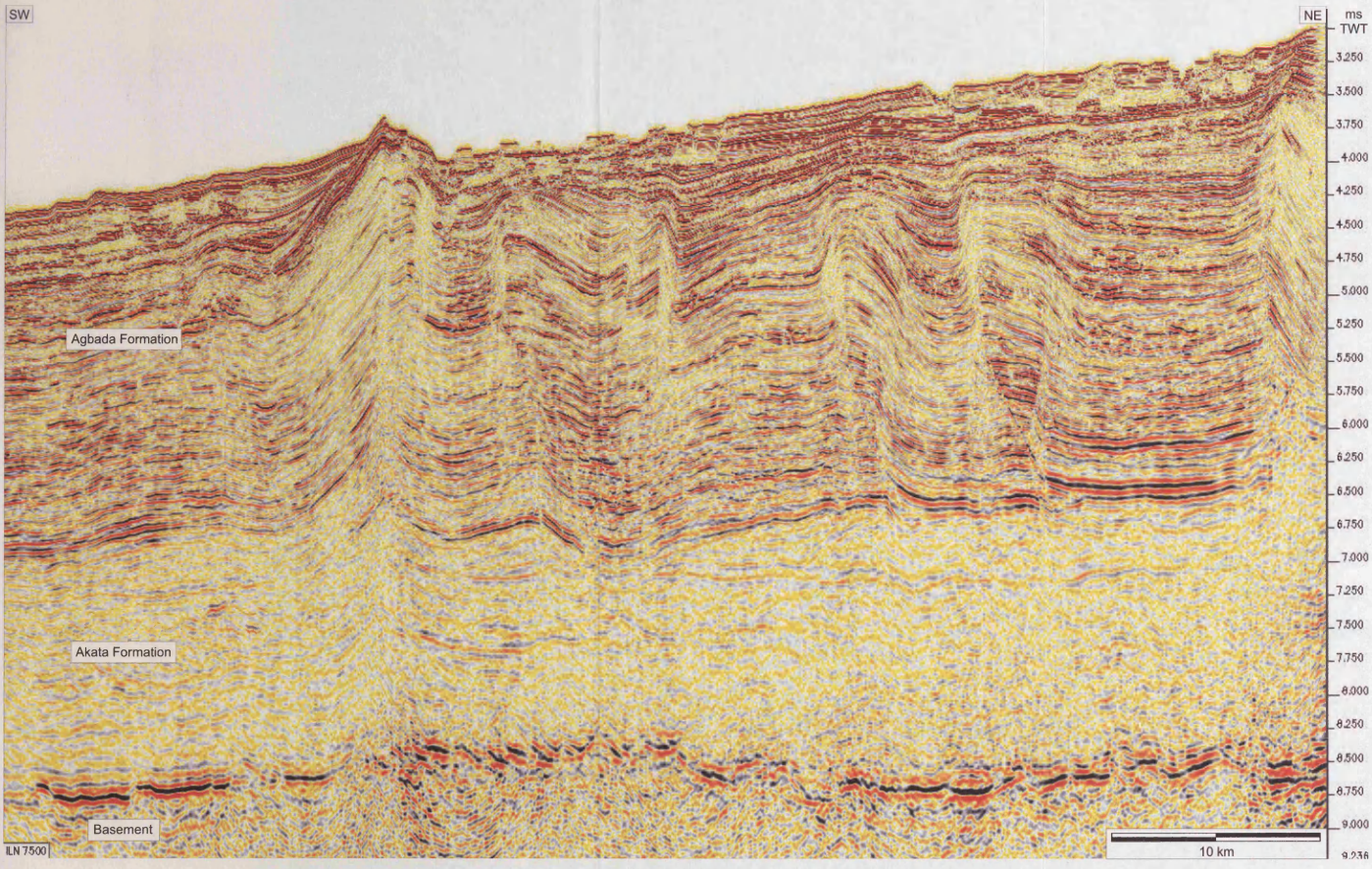
SW
NE
ms
TWT
3.250
3.500
3.750
4.000
4.250
4.500
4.750
5.000
5.250
5.500
5.750
6.000
6.250
6.500
6.750
7.000
7.250
7.500
7.750
8.000
8.250
8.500
8.750
9.000
9.236
Agbada Formation
Akata Formation
Basement
ILN 7500
10 km

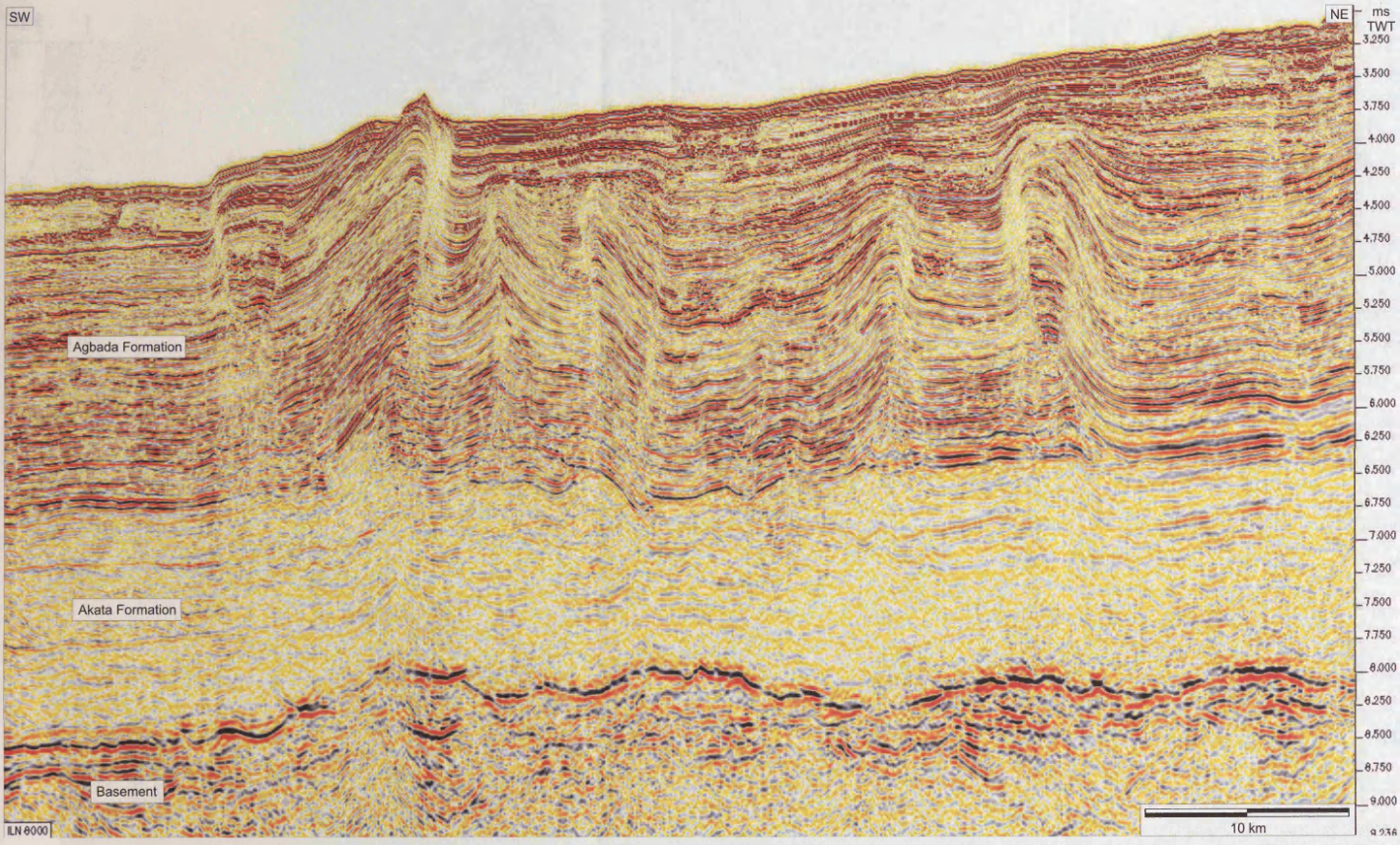
SW
NE
ms
TWT
3.250
3.500
3.750
4.000
4.250
4.500
4.750
5.000
5.250
5.500
5.750
6.000
6.250
6.500
6.750
7.000
7.250
7.500
7.750
8.000
8.250
8.500
8.750
9.000
Agbada Formation
Akata Formation
Basement
ILN 8000
10 km

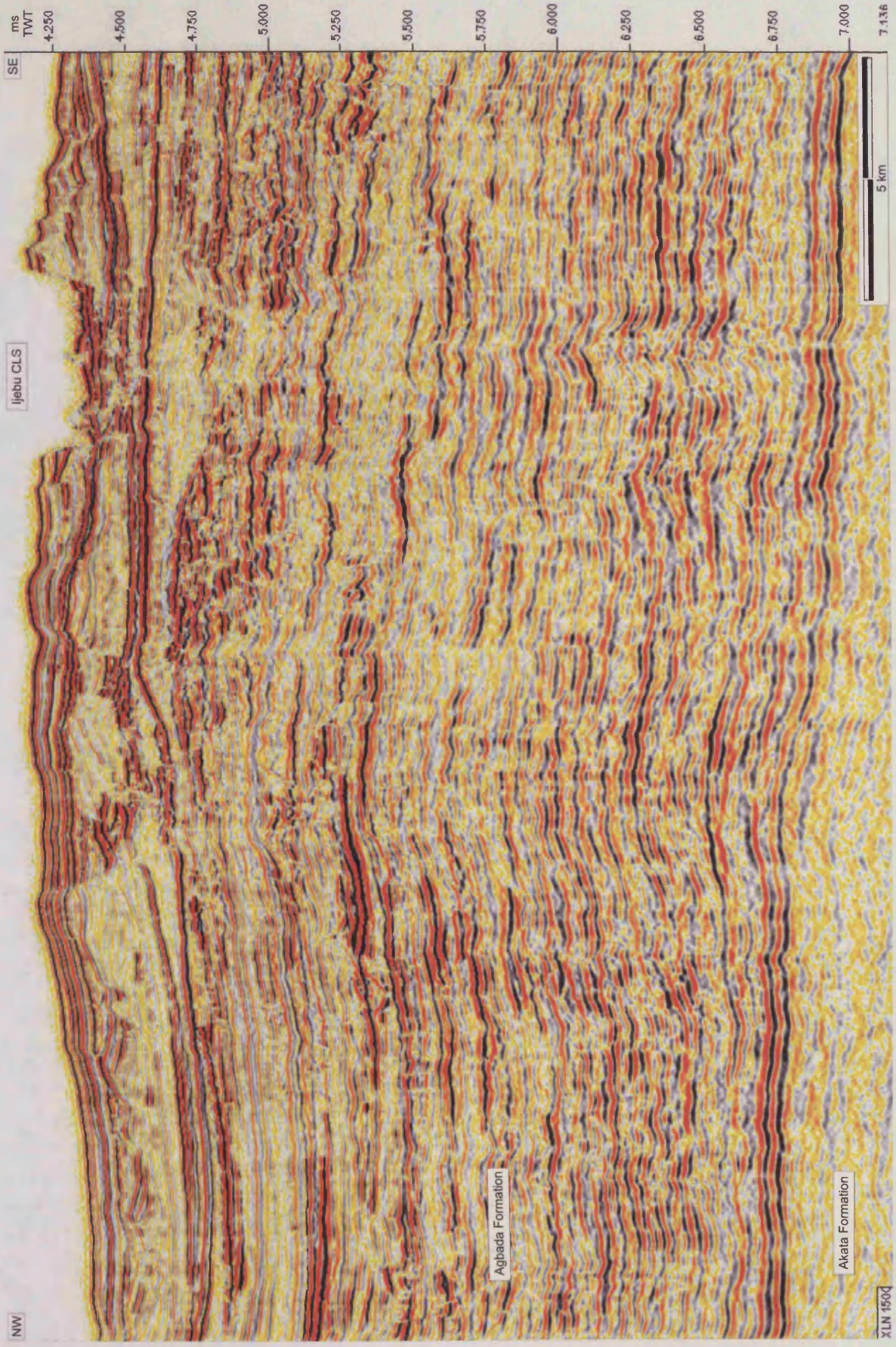
ms
TWT
4.250
4.500
4.750
5.000
5.250
5.500
5.750
6.000
6.250
6.500
6.750
7.000
7.136
SE
Ijebu CLS
NW
5 km
Agbada Formation
Akata Formation
XLN 1500

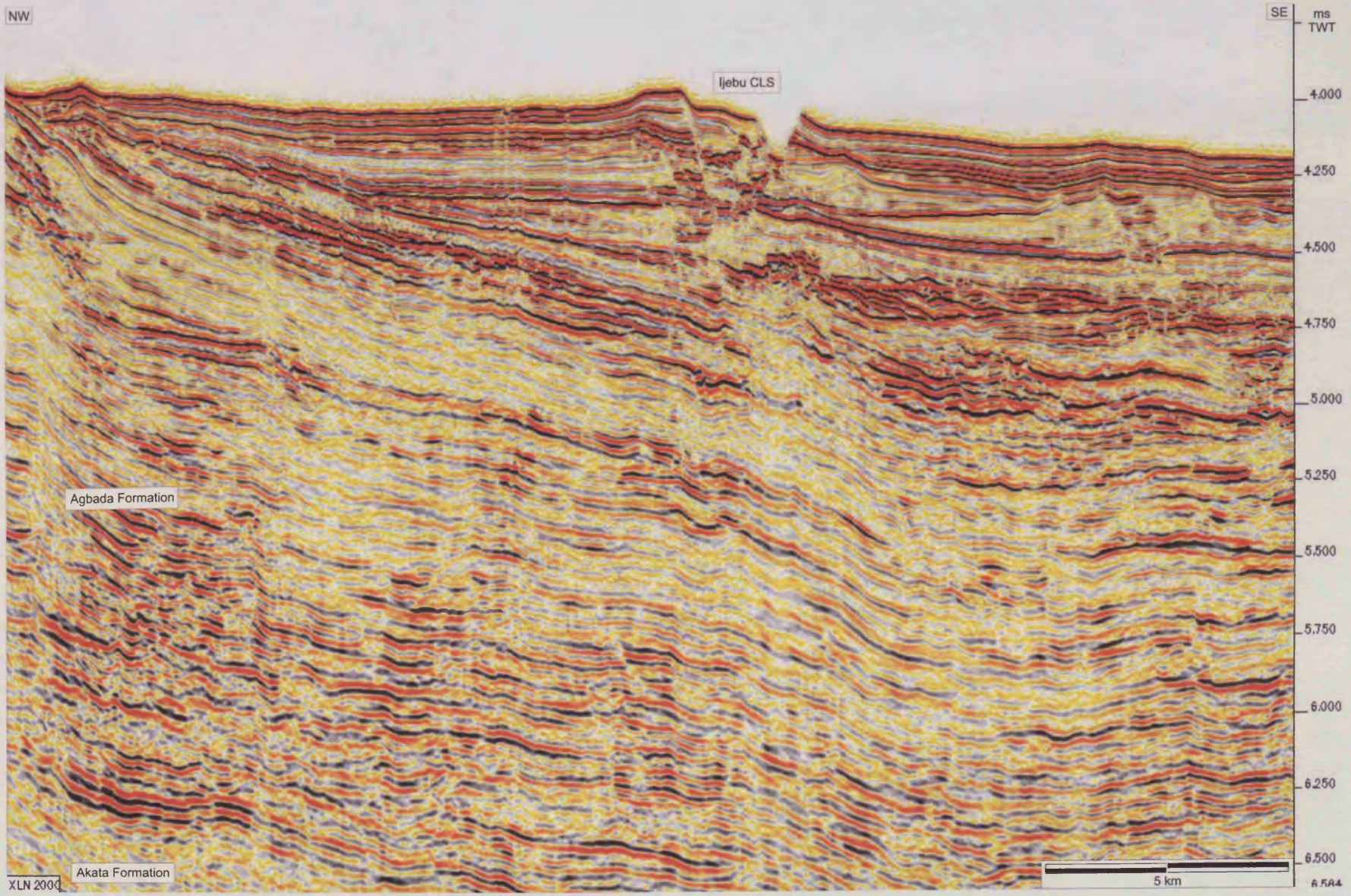
NW
SE
ms
TWT
Ijebu CLS
4.000
4.250
4.500
4.750
5.000
5.250
5.500
5.750
6.000
6.250
6.500
6.584
Agbada Formation
Akata Formation
XLN 2000
5 km

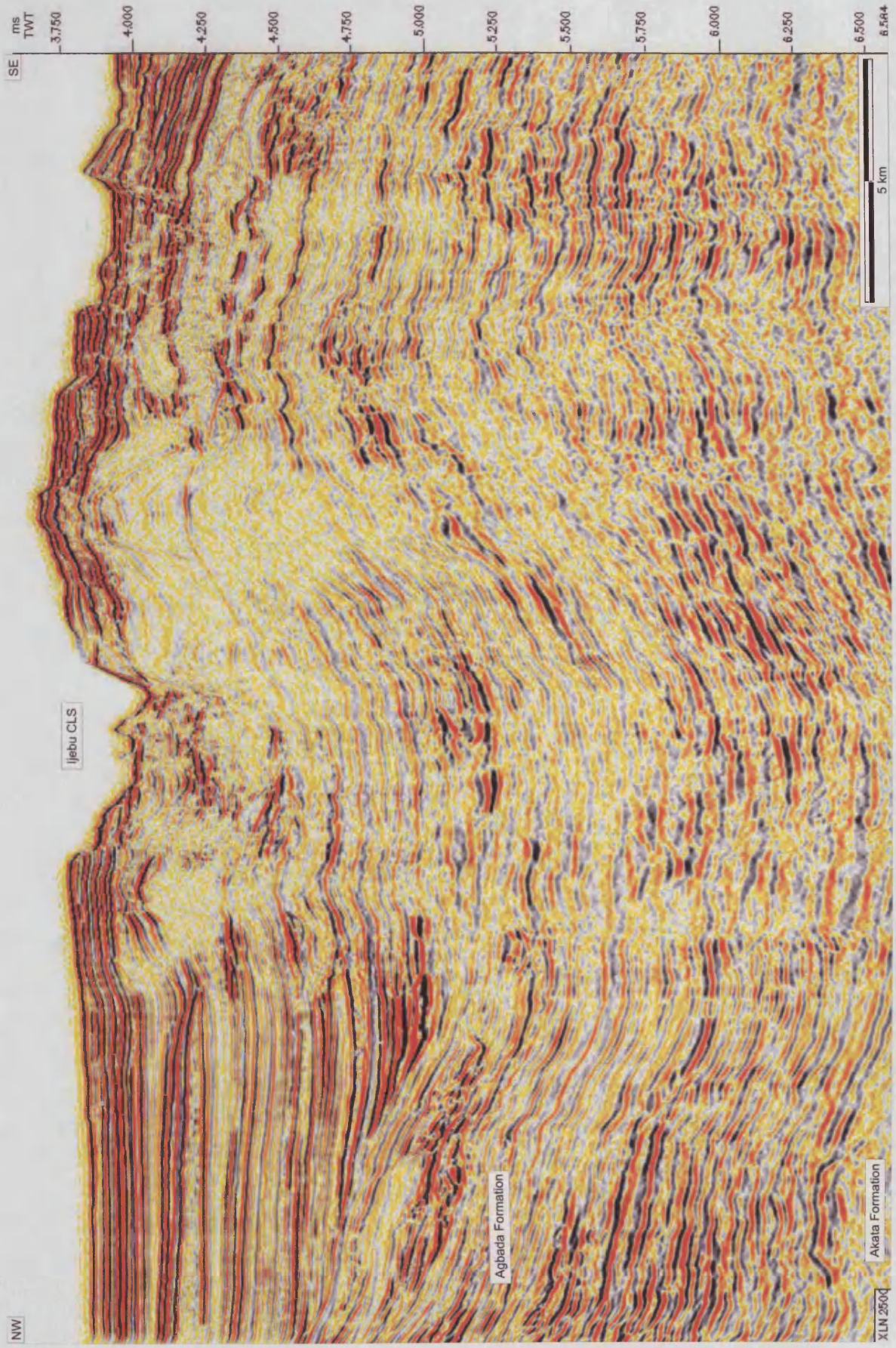
ms
TWT
3.750
4.000
4.250
4.500
4.750
5.000
5.250
5.500
5.750
6.000
6.250
6.500
8.564
SE
NW
Ijebu CLS
Agbada Formation
Akata Formation
XLN 2500
5 km

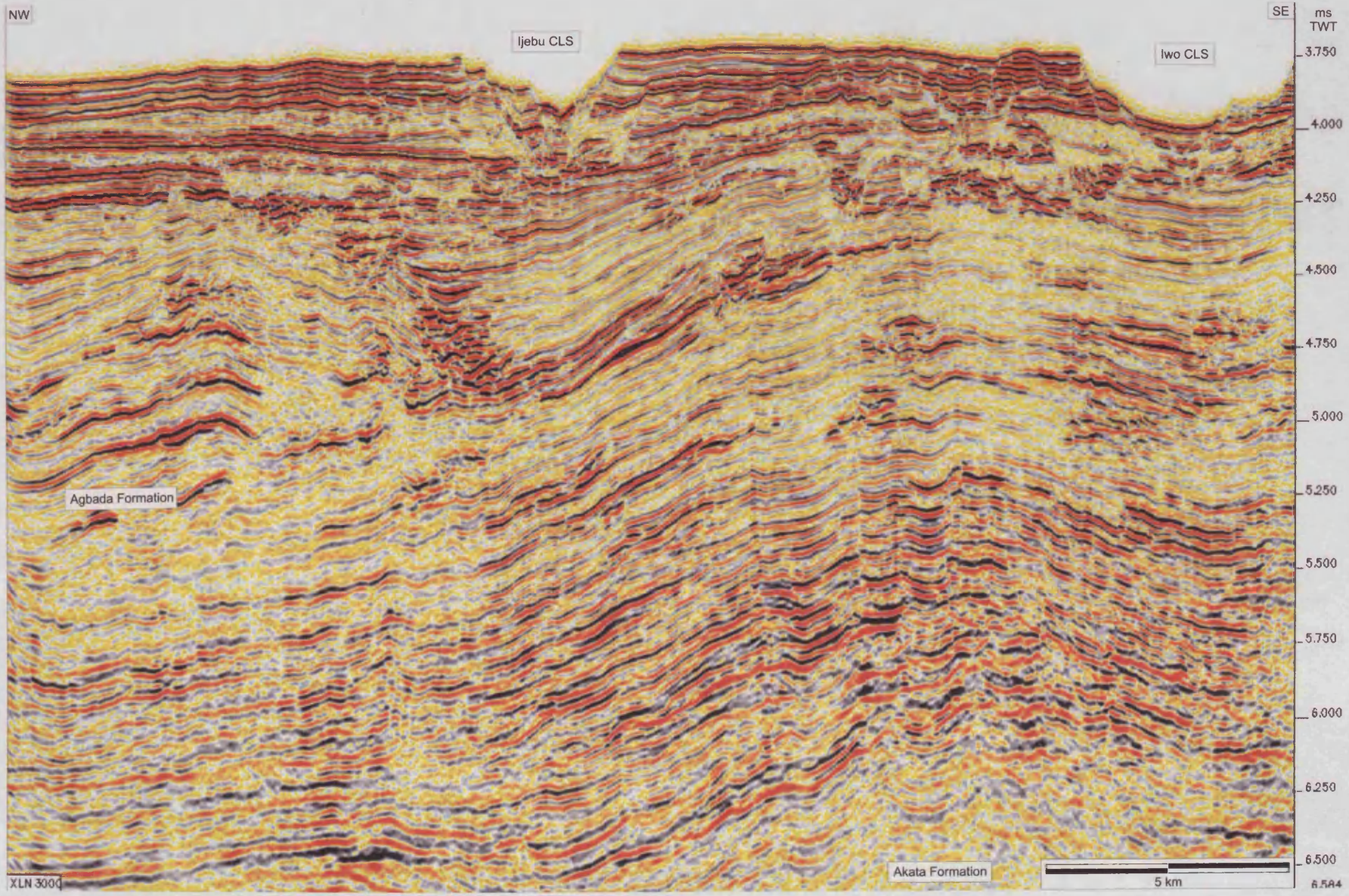
NW
SE
Ijebu CLS
Iwo CLS
ms
TWT
3.750
4.000
4.250
4.500
4.750
5.000
5.250
5.500
5.750
6.000
6.250
6.500
6.584
Agbada Formation
Akata Formation
XLN 3000
5 km

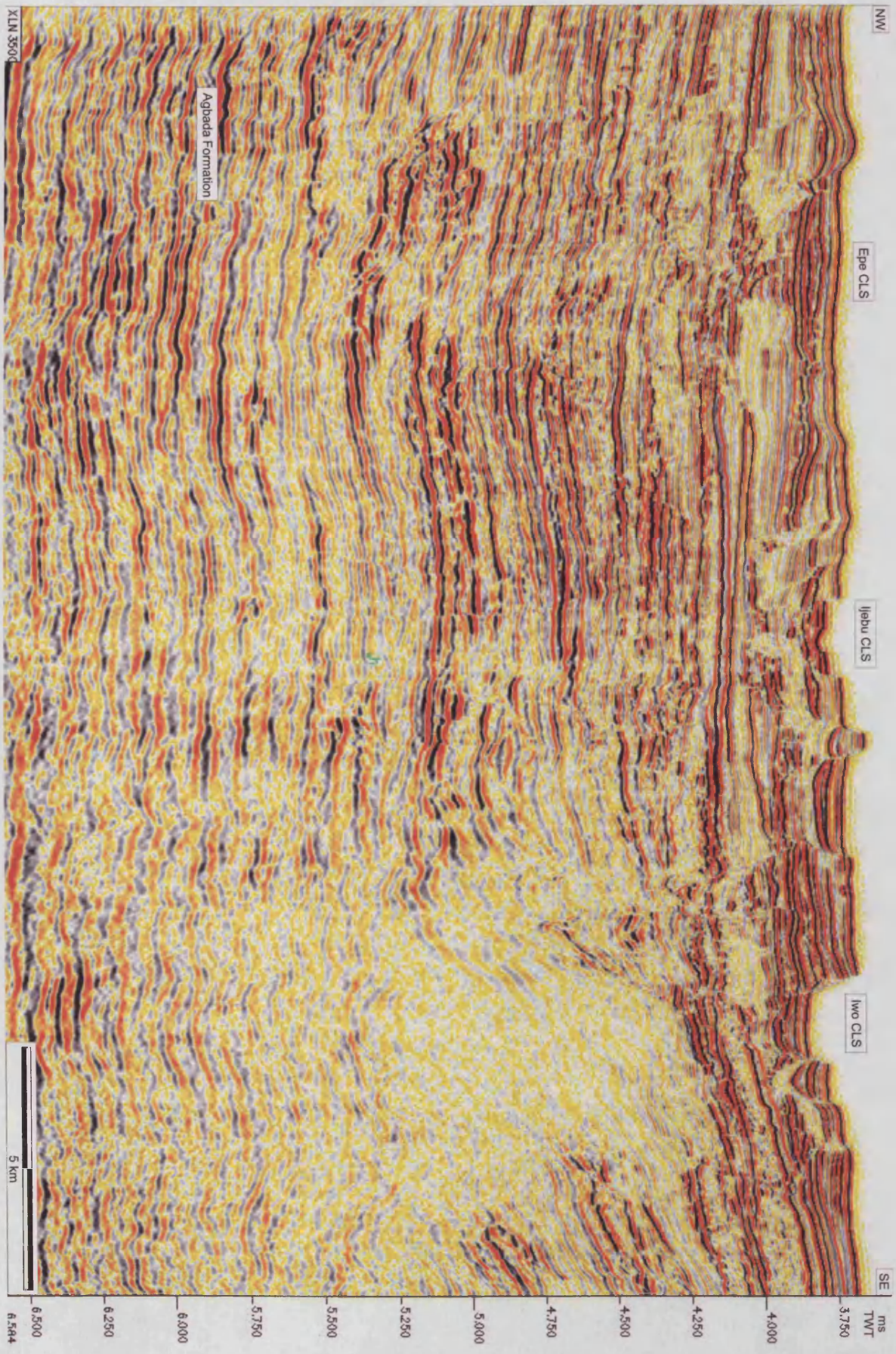

Appendix 2 *Additional images*


ms
TWT
3.750
4.000
4.250
4.500
4.750
5.000
5.250
5.500
5.750
6.000
6.250
6.500
6.544
SE
Iwo CLS
Ijebu CLS
Epe CLS
NW
Agbada Formation
5 km
XLN 4000

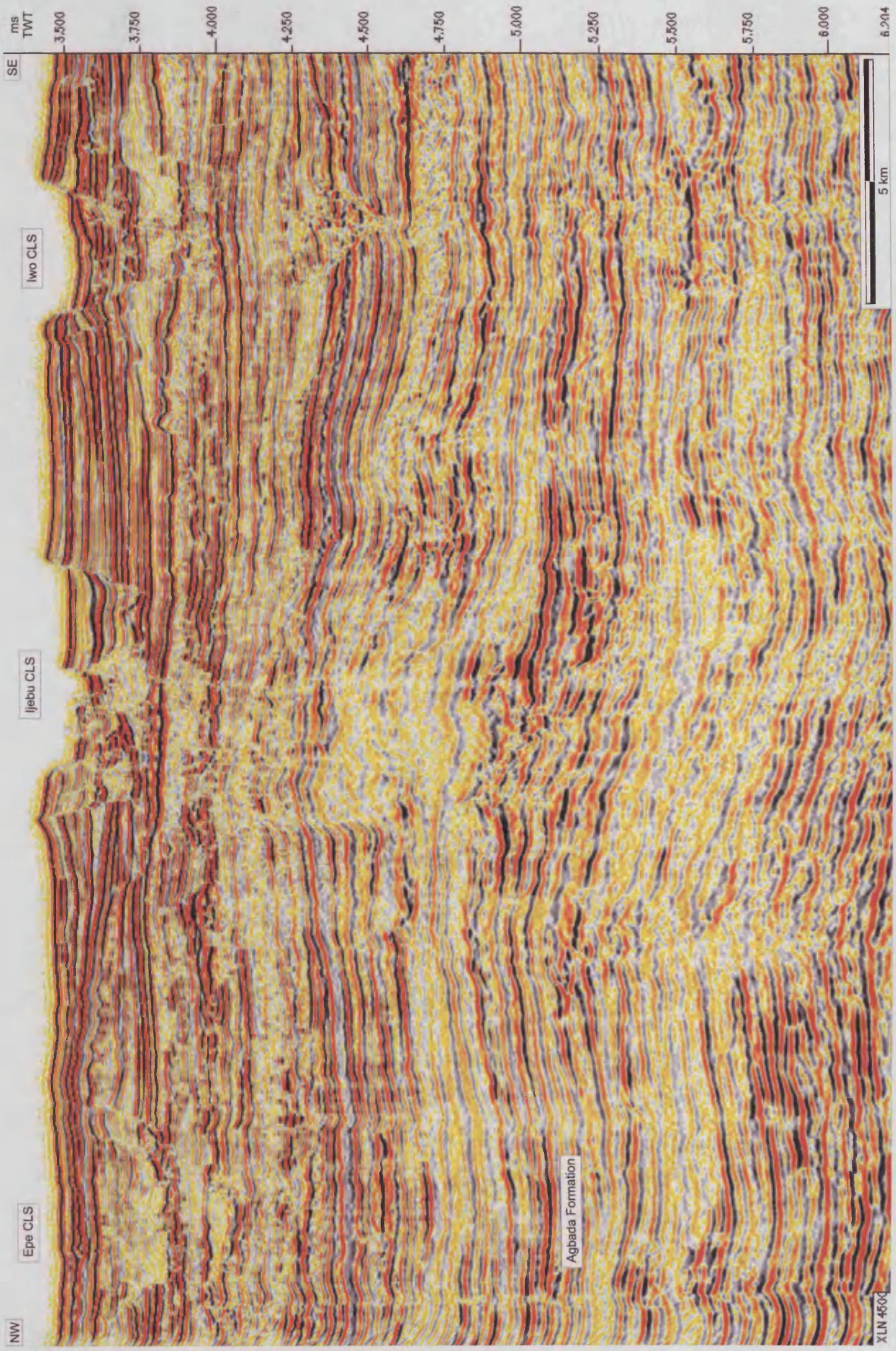
ms
TWT
3,500
3,750
4,000
4,250
4,500
4,750
5,000
5,250
5,500
5,750
6,000
6,204
SE
NW
Iwo CLS
Ijebu CLS
Epe CLS
Agbada Formation
5 km
XLN 4500

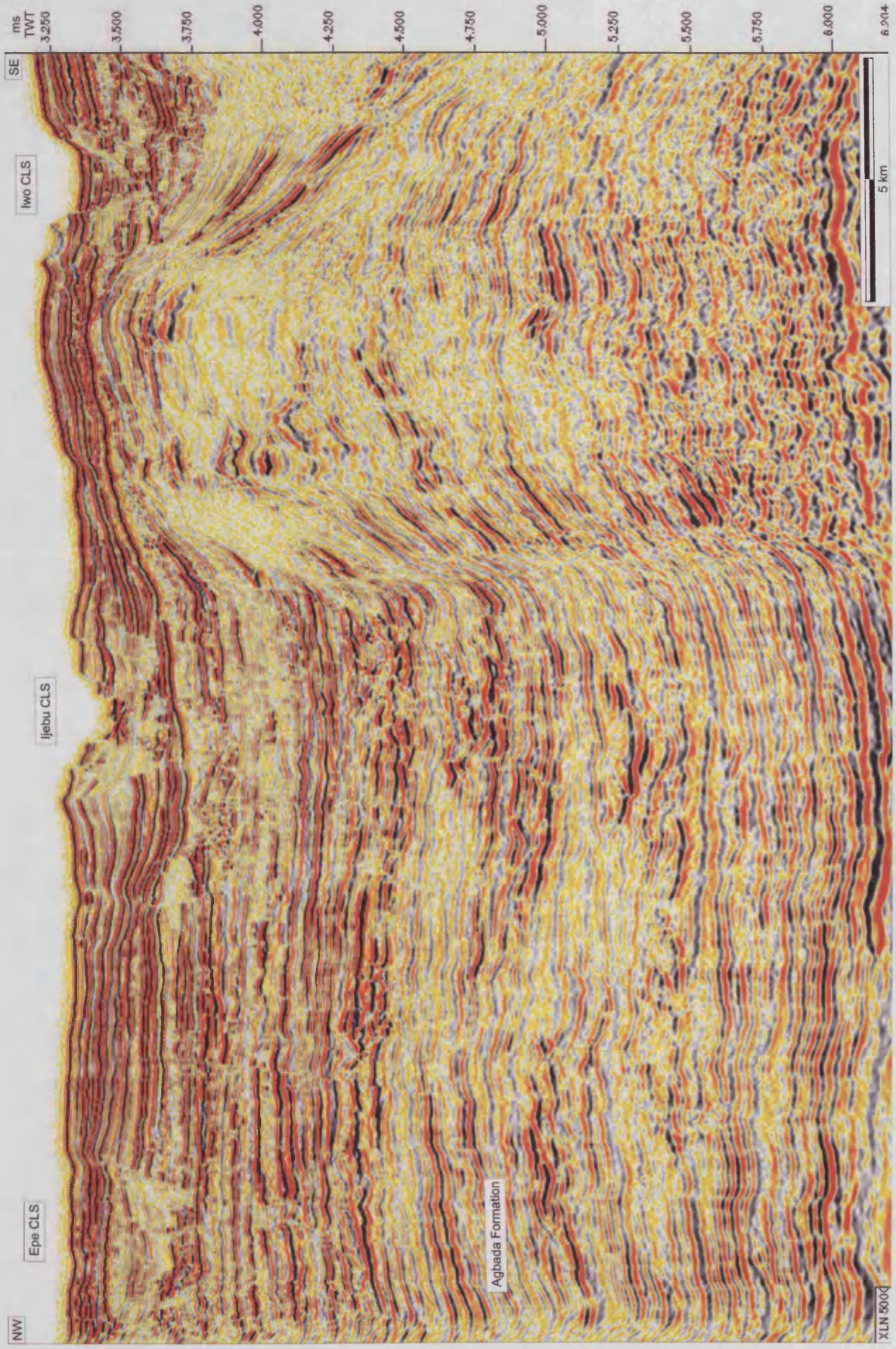
ms
TWT
3,250
3,500
3,750
4,000
4,250
4,500
4,750
5,000
5,250
5,500
5,750
6,000
SE
Iwo CLS
Ijebu CLS
Epe CLS
NW
Agbada Formation
5 km
XLN 5000

CARDIFF UNIVERSITY
PRIFYSGOL CAERDYDD